HIGH PRESSURE PHASE EQUILIBRIA OF THE SYSTEM CO_2 + *N*-DODECANE + 3,7-DIMETHYL-1-OCTANOL + 1-DECANOL

by

Carla Latsky

Dissertation presented for the Degree

of

DOCTOR OF PHILOSOPHY
CHEMICAL ENGINEERING

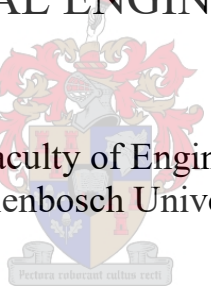

in the Faculty of Engineering
at Stellenbosch University

The financial assistance of the National Research Foundation (NRF) towards this research is hereby acknowledged. Opinions expressed and conclusions arrived at, are those of the author and are not necessarily to be attributed to the NRF.

Supervisor
Prof. C. E. Schwarz

December 2019

DECLARATION

By submitting this thesis electronically, I declare that the entirety of the work contained therein is my own, original work, that I am the sole author thereof (save to the extent explicitly otherwise stated), that reproduction and publication thereof by Stellenbosch University will not infringe any third party rights and that I have not previously in its entirety or in part submitted it for obtaining any qualification.

This dissertation includes 3 original papers published in peer-reviewed journals or books and 1 unpublished publication. The development and writing of the papers (published and unpublished) were the principal responsibility of myself and, for each of the cases where this is not the case, a declaration is included in the dissertation indicating the nature and extent of the contributions of co-authors.

Date: December 2019

PLAGIARISM DECLARATION

1. Plagiarism is the use of ideas, material and other intellectual property of another's work and to present is as my own.
2. I agree that plagiarism is a punishable offence because it constitutes theft.
3. I also understand that direct translations are plagiarism.
4. Accordingly, all quotations and contributions from any source whatsoever (including the internet) have been cited fully. I understand that the reproduction of text without quotation marks (even when the source is cited) is plagiarism.
5. I declare that the work contained in this assignment, except where otherwise stated, is my original work and that I have not previously (in its entirety or in part) submitted it for grading in this module/assignment or another module/assignment.

Student number:

Initials and surname: C. Latsky

Signature:

Date: 10/06/2019

ABSTRACT

In the detergent manufacturing industry, the product streams containing the detergent range alcohols (C_8-C_{20}) are often contaminated with unreacted alkanes. Due to similarity in the boiling and melting points of these alkanes and alcohols, traditional separation techniques such as distillation and crystallization are ineffective. Previous work has revealed that supercritical CO_2 fractionation is a viable alternative to separate detergent range alcohols and alkanes. It was however found that significant solute-solute interactions exist in mixtures containing CO_2 with detergent range alcohols and alkanes, which influences the phase behaviour and complicates thermodynamic modelling of such mixtures.

The primary aim of this study was to experimentally ***characterise the solute-solute interactions*** which occur in mixtures containing CO_2 with detergent range alkanes and alcohols, particularly ***in the quaternary system containing CO_2 with n-dodecane, 3,7-dimethyl-1-octanol and 1-decanol***. The secondary aim was to select and fit thermodynamic models within the Aspen Plus® software to determine and compare their ability to account for the interactions which occur in this system to allow prediction of phase equilibrium data for the quaternary system. Evaluation of the effect that fitting the model parameters using different data types has on the model's ability to predict phase equilibrium data forms part of the secondary aim.

The solute-solute interactions which exist in mixtures containing CO_2 with n-dodecane, 3,7-dimethyl-1-octanol and 1-decanol were characterised by analysing high pressure bubble- and dew-point and vapour-liquid-equilibrium (VLE) data of systems containing these components. To allow comprehensive analysis of the solute-solute interactions, additional phase behaviour data were required. New bubble- and dew-point data were generated for the ternary CO_2 + 3,7-dimethyl-1-octanol + n-dodecane and CO_2 + 3,7-dimethyl-1-octanol + 1-decanol systems as well as for the quaternary system. The data were measured at temperatures ranging from 308 K to 358 K and solute mass fractions ranging from 0.015 to 0.630, using the synthetic visual phase detection method. New VLE data were measured for the quaternary system. The data were measured at temperatures ranging from 308 K to 348 K and pressures up to 19.2 MPa, using an analytic-sampling method. The phase equilibrium data revealed that the solute-solute interactions which occur in these mixtures result in complex phase behaviour phenomena. The bubble- and dew-point data indicated the occurrence of ***co-***

solvency in mixtures consisting largely of n-dodecane. The relative solubility analysis revealed that the co-solvency which occurs in n-dodecane rich mixtures likely results in pinches in separation, but this can be resolved by incorporating a pressure-temperature swing setup. The ***mixtures consisting largely of 1-decanol were found to exhibit a temperature inversion***.

The RK-SOAVE, RK-ASPEN, CPA and PSRK models in Aspen Plus® were selected for the thermodynamic modelling performed in this work. These models are all based on the SRK equation of state, but they differ with regards to mixing rules and approaches to accounting for solute interactions. The ***RK-ASPEN model with solvent-solute and solute-solute BIPs (no 1-decanol + 3,7-dimethyl-1-octanol BIP) regressed from bubble- and dew-point data (HPBDP) was found to be the best suited model*** to predict bubble- and dew-point data and approximate VLE data for the quaternary system. The 1-decanol + 3,7-dimethyl-1-octanol BIP was excluded from the model as the incorporation is suspected to exaggerate the interaction between the two polar components, resulting in a decrease in model accuracy. The fact that the optimum model for the prediction of quaternary bubble- and dew-point and VLE data is based on HPBDP data is desired as the measurement technique used to obtain HPBDP data is much easier, cheaper and faster than the method used to measure VLE data. The PSRK model was found to be one of the less suited models for the prediction of quaternary phase equilibrium data and the results highlighted the need for BIPs regressed from high pressure data in regions where the solute-solute interactions significantly impacted the phase behaviour.

As the system is fully characterised experimentally, future work should be focussed on thermodynamic modelling of the system. It is suggested that the CPA model which includes a quadrupole term be investigated and other modelling tools such as the thermodynamic software package, VLXE, be evaluated.

OPSOMMING

In die skoonmaakmiddel vervaardigings-industrie word die alkohol (C_8 – C_{20}) produkstroom dikwels gekontamineer met ongereageerde alkane. Die C_8-C_{20} alkane en alkohol-isomere in die produkstrome het ooreenstemmende smelt- en kookpunte en dus kan effektiewe skeiding nie met tradisionele metodes soos distillasie en kristallisasie bewerkstellig word nie. Vorige studies het gevind dat superkritiese CO_2 fraksionering ‘n lewensvatbare alternatief is om die alkane en alkohol-isomere te skei. Die studies het wel ook gevind dat daar in mengsels wat bestaan uit, superkritiese CO_2 en C_8-C_{20} alkane en alkohol-isomere, sterk interaksies tussen die komponente is. Hierdie interaksies beïnvloed die fase-gedrag en bemoeilik termodinamiese modellering.

Die primêre doelwit van hierdie projek was om eksperimenteel die ***interaksies*** wat plaasvind in mengels wat bestaan uit superkritiese CO_2 + C_8-C_{20} alkane en alkohol-isomere te ***karakteriseer, deur te fokus op die CO_2 + n-dodekaan + 3,7-dimetiel-1-oktanol + 1-dekanol sisteem***. Die sekondêre doelwit was om termodinamiese modelle in Aspen Plus® te kies en te verfyn en om die vermoë van die modelle om die interaksies wat plaasvind in die sisteme in ag te neem, om sodoende akkurate fase-gedrag vir die kwatinêre sisteem te voorspel, te bepaal en te vergelyk. Evaluering van die effek wat die tipe regressie data wat gebruik word om die model parameters te bepaal het op die vermoë van die model om ewewigsdata te voorspel vorm ook deel van die sekondêre doelwit.

Die interaksies wat plaasvind in die CO_2 + n-dodekaan + 3,7-dimetiel-1-oktanol + 1-dekanol sisteem was ondersoek deur hoë-druk oplosbaarheidsdata en damp-vloeistof-ewewigsdata vir sisteme, wat bestaan uit hierdie komponente, te analiseer. Addisionele hoë-druk ewewigsdata was benodig om ‘n omvattende analise van die interaksies wat in die mengsels plaasvind, te doen. Nuwe hoë-druk oplosbaarheidsdata was gemeet vir die ternêre CO_2 + n-dodekaan + 3,7-dimetiel-1-oktanol en CO_2 + 3,7-dimetiel-1-oktanol + 1-dekanol sisteme, sowel as die kwatinêre sisteem. Die sintetiese visuele fase-opsporingsmetode was gebruik om die oplosbaarheidsdata van die sisteme te meet tussen 308 K en 358 K met totale alkaan en/of alkohol massafraksies tussen 0.015 tot 0.630. Nuwe damp-vloeistof-ewewigsdata was gemeet vir die kwatinêre sisteem deur gebruik te maak van ‘n analitiese metode wat damp en vloeistof monsters aanlyn geanaliseer het met gaschromatografie. Die data was gemeet tussen

temperature van 308 K en 348 K en met drukke tot 19.2 MPa. Die ewewigsdata het aangedui dat die interaksies wat plaasvind tussen die komponente komplekse fase-gedrag veroorsaak. Die oplosbaarheidsdata het aangedui dat mengsels wat ***grootliks uit n-dodekaan bestaan, verhoogde oplosbaarheid*** in CO_2 toon in vergelyking met die suiwer komponente. Die relatiewe oplosbaarheidsanalise het aangedui dat die verhoogde oplosbaarheid wat plaasvind in die n-dodekaan ryk mengsel moontlik lei tot skeidingsknyppunte, die probleem kan wel opgelos word deur die implementering van 'n druk-temperatuur omkeer stelsel. Die fase-gedrag van ***mengsels wat grootliks uit 1-dekanol bestaan het 'n temperatuur inversie*** getoon.

Die Aspen Plus® modelle wat ondersoek is in die werk is die RK-SOAVE, RK-ASPEN, CPA en PSRK modelle. Hierdie modelle is almal gebaseer op die SRK toestandsvergelyking, maar verskil ten op sigte van mengreëls en die manier waarop hul interaksies benader/beskryf. Die ***RK-ASPEN model met oplosmiddel-opgeloste stof interaksie parameters en opgeloste stof-opgeloste stof (geen 1-dekanol + 3,7-dimetiel-1-oktanol interaksie parameter) interaksie parameters bepaal deur die regressie van hoë-druk oplosbaarheidsdata, was gevind om die mees gepaste model*** te wees vir die voorspelling van oplosbaarheidsdata en die benadering van damp-vloeistof-ewewigsdata vir die kwatinêre sisteem. Die 1-dekanol + 3,7-dimetiel-1-oktanol interaksie parameter was nie in die model ingesluit nie, want dit word vermoed dat dit die interaksie tussen die twee polêre komponente oordryf wat model akkuraatheid verlaag. Die feit dat die optimum model vir die voorspelling van die kwatinêre ewewigsdata (oplosbaarheidsdata en damp-vloeistof-ewewigsdata) gebaseer is op interaksie parameters wat bepaal is deur die regressie van hoë-druk oplosbaarheidsdata is gewens aangesien die eksperimente om oplosbaarheidsdata te meet veel makliker, goedkoper en vinniger is as die eksperimente om damp-vloeistof-ewewigsdata te meet. Die PSRK model was een van die minder akkurate modelle vir die voorspelling van die kwatinêre ewewigsdata en die modelleringsresultate het die nodigheid van interaksie parameters, bepaal deur die regressie van hoë-druk data, uitgewys in areas waar die interaksies die fase-gedrag beduidend beïnvloed het.

Aangesien die sisteem ten volle eksperimenteel beskryf is, is aanbevelings vir toekomstige werk slegs gerig op termodinamiese modellering van die sisteem. Dit word voorgestel dat die CPA model wat 'n kwadrupool term insluit ondersoek word en ander modelleringsprogramme soos byvoorbeeld die termodinamiese sagteware, VLXE, evalueer word.

LIST OF CONTRIBUTIONS

Publications

The following publications have been published in international peer reviewed journals:

- C. Latsky and C.E. Schwarz, High pressure bubble- and dew-point data for a system containing supercritical CO_2 with detergent range alkanes and alcohols, The Journal of Supercritical Fluids 141 (2018) 265- 273.
- C. Latsky and C.E. Schwarz, Measurement and modelling of high pressure bubble- and dew-point data for the CO_2 + 1-decanol + 3,7-dimethyl-1-octanol system, Fluid Phase Equilibria 488 (2019) 87 – 98.
- C. Latsky, N.S. Mabena, C.E. Schwarz, High pressure phase behaviour for the CO_2 + n-dodecane + 3,7-dimethyl-1-octanol system, The Journal of Supercritical Fluids 149 (2019) 138 – 150. *[N.S. Mabena measured the bubble- and dew-point data as part of a final year project, the data processing and interpretation of the data presented in the article, as well as the writing of the article was done by the current author]*

The following publication is in preparation and will be submitted to an international peer reviewed journal:

- C. Latsky and C.E. Schwarz, Measurement and modelling of VLE data for quaternary systems containing supercritical CO_2 with n-dodecane, 1-decanol and 3,7-dimethyl-1-octanol. To be submitted to the Journal of Chemical and Engineering Data.

Conference proceedings

The work has contributed towards the following conference proceedings:

- "High Pressure Bubble- and Dew-Point Data of CO_2 with Detergent Range Alkanes and Alcohols" poster presented at the 16th European Meeting on Supercritical Fluids held in Lisbon, Portugal between the 25th and 28th of April 2017.
- "Thermodynamic modelling of systems containing supercritical CO_2 with detergent range alkanes and alcohols" oral presentation presented 30th European Symposium on Applied Thermodynamics held in Prague, Czech Republic between the 10th and 13th of June 2018.
- "Measurement and modelling of VLE data for the quaternary CO_2 + 1-decanol + n-dodecane + 3,7-dimethyl-1-octanol system" poster presented at the 17th European Meeting on Supercritical Fluids held in Ciudad Real, Spain between the 8th and 10th of April 2019.

ACKNOWLEDGEMENTS

This work is based on the research supported in part by the National Research Foundation of South Africa and Sasol Technology (Pty) Ltd. The author acknowledges that opinions, findings and conclusions or recommendations expressed in any publication generated by the supported research are that of the author, and that of the sponsors accepts no liability whatsoever in this regard. Aspen Plus® is a registered trademark of Aspen Technology Inc.

The author would like to thank the following people:

- Prof C.E. Schwarz for giving me the opportunity to conduct my postgraduate studies under her supervision and for the guidance she provided.
- Mrs H. Botha for assisting me with the analytic equipment which formed part of my experimental setup.
- Mr H. Franken and Mr R.M. Swanepoel for the expertise and assistance they provided.
- The process engineering workshop and technical staff for their assistance with equipment repairs and general laboratory maintenance problems.
- My family and friends for their support and words of encouragement.
- Theo, for being by my side and motivating me.
- Special thank you to my mother, Sonja, for always being my biggest supporter.

TABLE OF CONTENT

NOMENCLATURE

Table I: List of symbols

Symbol	Description	Symbol	Description
a	Energy parameter in cubic equations of state	R	Relative volume
a_{mn}	UNIFAC group interaction parameter	R	Universal gas constant (8.314 J/mol.K)
b	Co-volume parameter in cubic equations of state	s	UNIFAC parameter
b_{mk}	UNIFAC group interaction parameter	T	Temperature
c	Parameter in the alpha function	u	Uncertainty
c	Mathias-Copeman polar parameter	V	Vapour
c_{mk}	UNIFAC group interaction parameter	v	Molar volume
C	Critical point	$v_k^{(i)}$	Number of subgroups in a molecule of specie i
C	Constant used in the vapour pressure & density correlations	w	Weight of data group
d	Parameter in the alpha function	x	Liquid phase composition
e	UNIFAC parameter	X	Fraction of sites
F	Degrees of freedom	y	Vapour phase composition
g	Radial distribution function	Z	Measured or predicted value in the %AAD equation
g_0^E	Excess Gibbs energy at a reference state	α	Alpha function/ Relative solubility
J	UNIFAC parameter	β	Association volume (CPA)/ UNIFAC parameter (PSRK)
L	UNIFAC parameter	ε	Association energy
L	Liquid	f	Fugacity
k_a	Interaction parameter	ρ^*	Saturated molar density
k_b	Interaction parameter	ω	Acentric factor
m	Parameter in the alpha function	γ	Activity coefficient
N	Number of components	∏	Number of phases
n	Number of data points	Φ	Number of constraints/Fugacity coefficient
n_c	Number of alkyl-carbon atoms	η	Polar parameter (RK-ASPEN)/ Reduced density (CPA)
P	Pressure	Δ	Difference/Association strength
p^*	Saturated vapour pressure	θ	UNIFAC parameter
q	Relative molecular surface area	τ	UNIFAC interaction parameter
Q	Relative surface area	σ	Standard deviation
r	Relative molecular volume	μ	Chemical potential

Table II: List of subscripts

Symbol	Description	Symbol	Description
A, B, C	Component indices	mix	Mixture
A/B	Bonding sites on a molecule	n	Counter
c	Critical	i, j	Pure component indices in equations of state/ Molecule indices
C	Combinatorial	s	Solute
calc	Calculated	r	Reduced
exp	Experimental	R	Residual
k	Subgroup indices	T	Temperature
m	Counter/ Monomer	P	Pressure
max	Maximum	x	Liquid phase composition
min	Minimum	y	Vapour phase composition

Table III: List of superscripts

Symbol	Description	Symbol	Description
A_iB_j	Site A on molecule i and site B on molecule j	R	Residual
c	Critical	red	Reduced
C	Combinatorial	ref	Reference
k	Subgroup indices	sat	Saturated
l	Liquid	v	Vapour
NC	Number of components in the data group	*	Effective
NDG	Number of data groups	α, β, π	Equilibrium phases
NP	Number of data points		

Table IV: List of abbreviations

Symbol	Description	Symbol	Description
BIP	Binary interaction parameters	37DM1O	3,7-dimethyl-1-octanol
HPBDP	High pressure bubble- and dew-point	nC_{12}	n-dodecane
HPVLE	High pressure vapour-liquid-equilibrium	$C_{10}OH$	1-decanol
OF	Objective function	EoS	Equation of state
VLE	Vapour-liquid-equilibrium	EoS/G^E	Combination of equation of state and excess Gibbs energy models
%AAD	Percentage absolute average deviation		

1. INTRODUCTION

1.1. Project background and rationale

Alcohols with carbon numbers ranging from 8 to 20 are termed detergent range alcohols, as they are extensively used in the detergent and surfactant manufacturing industries [1]. Industrially, detergent range alcohols are produced by the Oxo or Ziegler processes or through high pressure hydrogenation of esters or fatty acids [2]. Amongst these process routes, the Oxo process is the most commonly used [3]. In the Oxo process, an olefin feedstock is reacted with synthesis gas in the presence of a catalyst to form aldehydes, which are then hydrogenated to form detergent range alcohol isomers [4]. The Oxo process is generally a downstream processing step in the petroleum industry. The feedstock therefore not only contains olefins, but also alkanes [5, 6]. These alkanes are inert in the Oxo process and form part of the alcohol product stream [1, 6]. The presence of the alkanes in the alcohol product stream demands post-production purification [1, 5, 7, 8], but due to the fact that the alkanes and alcohol isomers have similar and/or overlapping boiling and melting points, traditional separation techniques such as distillation and crystallization are ineffective [1, 7].

According to literature, azeotropic distillation is currently used to separate the alkanes from the alcohol isomers [1]. Drawbacks of this separation technique, including the need for an entrainer, entrainer toxicity, extreme operating conditions, entrainer regeneration and thermal degradation, has however motivated investigation into alternative separation techniques [5]. One such alternative is supercritical fluid fractionation [5]. This separation technique has gained much attention as supercritical solvents have excellent solvent properties and the solvents can be regenerated with minimal residue in the product [9, 10].

A study to evaluate the feasibility of using supercritical fractionation processes to separate detergent range alcohols and alkanes was performed by Bonthuys, et al. [7]. Although this study revealed that supercritical fluid fractionation is a viable separation method, it only investigated separation of linear alkanes and primary linear alcohols, which is not representative of the product streams found in the detergent manufacturing industry [5, 6, 11]. A follow-up study, conducted by Zamudio [5], investigated whether supercritical fractionation is feasible when considering alcohol/alkane mixtures which resemble product streams found in the detergent manufacturing industry. In order to evaluate the feasibility, the study analysed

the phase behaviour of mixtures containing detergent range alkanes and alcohols with a supercritical solvent and pilot plant tests were conducted [5]. The study by Zamudio [5] also addressed the industrial need to obtain data in a time and cost-effective manner, by developing a preliminary Aspen Plus® process model to simulate the fractionation process. The study [5] revealed that supercritical CO_2 fractionation is a feasible method to separate detergent range alcohols and alkanes. In addition to this, Zamudio [5] also found that significant solute-solute interactions occur in mixtures containing supercritical CO_2 with detergent range alcohols and alkanes, which influences the phase behaviour exhibited by these mixtures and complicates thermodynamic modelling thereof. The detection of the solute-solute interactions and the difficulty encountered to accurately account for the effect thereof when modelling systems containing supercritical CO_2 with detergent range alkanes and alcohols, prompted further investigation.

Further studies into the solute-solute interactions in mixtures containing CO_2 with detergent range alkanes and alcohols were conducted based on a model mixture containing CO_2 with n-dodecane, 1-decanol and 3,7-dimethyl-1-octanol. This system was selected as it is representative of a typical detergent manufacturing product stream, since it includes an alkane, a linear alcohol and a branched alcohol (methyl branching in 2 positions) [5, 6, 11, 12], all with similar boiling points. A study by Smith & Schwarz [13] investigated the phase behaviour of the CO_2 with n-dodecane and 1-decanol ternary subsystem, by measuring and analysing bubble- and dew-point data for mixtures containing different alkane/alcohol ratios. This was done to characterise the solute-solute interactions which exist between the linear alkane and linear alcohol in the model mixture. Furthermore, a study by Fourie [14] measured and analysed high pressure vapour-liquid-equilibrium (VLE) data for the three ternary subsystems, to determine the effect of the solute-solute interactions on the composition of co-existing phases. To the author's knowledge, no in-depth studies have thus far been conducted to measure and analyse bubble- and dew-point data for the other two ternary subsystems (i.e. CO_2 + 1-decanol + 3,7-dimethyl-1-octanol and CO_2 + 3,7-dimethyl-1-octanol + n-dodecane) and the quaternary system. A need therefore exists to determine the phase boundaries of these systems over the entire composition range. Furthermore, no studies have thus far been conducted to evaluate the effect of solute-solute interactions on the composition of the co-existing phases when all three the solutes are present, highlighting a need for VLE measurements for the quaternary CO_2 + n-dodecane + 1-decanol + 3,7-dimethyl-1-octanol system.

The identified lack or absence of sufficient data to thoroughly analyse the solute-solute interactions which exist in the quaternary system motivated the work presented here. In this study, the solute-solute interactions which exist in mixtures containing CO_2 with detergent range alkanes and alcohols is investigated by measuring and analysing high pressure bubble- and dew-point and VLE data for systems containing CO_2 with n-dodecane, 1-decanol and 3,7-dimethyl-1-octanol. This study also focusses on analysing the ability of different thermodynamic models in Aspen Plus® to predict accurate phase behaviour data for systems containing CO_2 with detergent range alkanes and alcohols, by fitting the models with system specific parameters regressed from pure component and mixture data. Where possible, the parameters are fitted using different types of data, that is bubble- and dew-point and VLE data. The purpose of this is to evaluate whether a model's ability to predict accurate phase behaviour data is affected by regressing the interaction parameters from different data types. VLE data are better suited to regress the interaction parameters as the built-in regression function in Aspen Plus® can be implemented, but the data are measured using expensive and complex equipment with meticulous and time-consuming operating procedures. On the other hand, bubble- and dew-point data require a robust, manual parameter regression approach, but the data are measured quickly and easily using relatively inexpensive equipment [15]. Seeing as money and time are limited resources, it is beneficial to determine whether the modelling results obtained when fitting the thermodynamic model using VLE data, which is easy to regress but expensive and time-consuming to measure, is comparable to the predictions obtained when fitting the model using bubble- and dew-point data, which is more tedious to regress but is significantly cheaper and faster to measure.

1.2. Aims and objectives

This study has two aims, the primary aim is to experimentally ***characterise the solute-solute interactions*** which occur in mixtures containing CO_2 with detergent range alkanes and alcohols, particularly ***in the quaternary system containing CO_2 with n-dodecane, 3,7-dimethyl-1-octanol and 1-decanol***. The secondary aim is to select and fit thermodynamic models within the Aspen Plus® software to determine and compare their ability to account for the interactions which occur in this system to allow accurate prediction of phase equilibrium data for the quaternary system. Evaluation of the effect that fitting the model using different types of data, that is bubble- and dew-point and VLE data, has on the model's ability to predict phase equilibrium data forms part of the secondary aim.

The objectives which need to be met to achieve the project aims are:

1. Measure bubble- and dew-point data for the binary, ternary and quaternary systems to compliment/complete literature data and analyse the measured data to determine how the solute-solute interactions influences the solubility of these mixtures.
2. Measure VLE data for the ternary and quaternary systems to compliment/complete literature data and analyse the measured data to determine the effect of the solute-solute interactions on the composition of co-existing equilibrium phases.
3. Evaluate the ability of models available within Aspen Plus® to predict phase equilibrium data for systems containing detergent range alkanes and alcohols by:
   3.1. Selecting thermodynamic models within the Aspen Plus® database.
   3.2. Fitting the model parameters.
   3.3. Analysing the effect that incorporating different interaction parameters and using different types of data to fit these parameters has on model accuracy.
   3.4. Comparing the different models to determine which is best suited to predict phase equilibrium data for the quaternary system.

Objectives 1 and 2 address the primary aim of this work, whilst the secondary aim is addressed by Objective 3.

1.3 Project scope

1.3.1 Chemical components

The detergent range alcohols and alkanes selected for this study are n-dodecane, 1-decanol and 3,7-dimethyl-1-octanol. This alkane/alcohol mixture represents a typical detergent alcohol product stream encountered in industry, as stated previously [5, 6, 11, 12]. The properties and molecular structure of these components are presented in Table 1 [16].

Supercritical CO_2 was selected as the solvent. The main reason for using CO_2, stems from the fact that Zamudio [5] determined that CO_2 is well suited for the supercritical fractionation of detergent range alcohols and alkanes. In addition to the findings by Zamudio [5], CO_2 also has other advantages which makes it attractive for use in supercritical fractionation processes. These advantages include the fact that CO_2 has convenient critical conditions (T_c= 304 K, P_c = 7.4 MPa), is non-toxic, non-flammable, chemically stable and cheap [17]. Furthermore, CO_2 is

abundant and it can easily be obtained as a by-product from combustion, fermentation and ammonia synthesis processes [10, 17].

Table 1: Properties of the detergent range alkanes and alcohols used in this study

Component	Molecular formula	Type	Boiling temperature (K)
n-dodecane 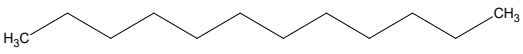	$C_{12}H_{26}$	Linear alkane	489.2
1-decanol 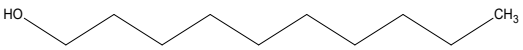	$C_{10}H_{22}O$	Linear alcohol	504.1
3,7-dimethyl-1-octanol 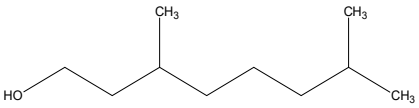	$C_{10}H_{22}O$	Branched alcohol	498.7

1.3.2 Thermodynamic region

The solubility properties of supercritical solvents are most tuneable at temperatures slightly higher than the critical temperature of the solvent [7]. Based on this and seeing as the critical temperature of CO_2 is 304 K [17], the temperature range considered in this work was limited to temperatures between 308 K and 358 K. The bubble- and dew-point data were measured using total solute mass fractions between 0.631 and 0.015, at 10 K intervals. The small temperature interval was to ensure that sufficient data exists to capture the pressure-temperature relationship. The VLE data were measured using 20 K intervals, as the data could be used without fitting correlations and the intervals allowed detection of the effect of solute-solute interaction on the composition of the co-existing phases. The intricate and time-consuming nature of the VLE experiments also motivated the use of larger temperature intervals. Based on the design specifications of the equilibrium cells used, the pressures considered in this work was limited to 27.5 MPa for the bubble- and dew-point experiments and 30 MPa for the VLE experiments.

1.3.3 Thermodynamic modelling

The modelling software used in this work was restricted to the popular process simulator, Aspen Plus®. A commercial process simulator was used instead of in-house developed software or a purely thermodynamic package, as the thermodynamic modelling performed in this work

was not only aimed at predicting phase behaviour data, but also on fitting thermodynamic models which can be used for process modelling. Furthermore, a study by Lombard [18] which investigated thermodynamic modelling of hydrocarbon-chains and light-weight supercritical solvents, using an in-house generated MATLAB code and Aspen Plus®, revealed that the results obtained using both methods were similar. This validates that Aspen Plus® is a reliable computational tool for thermodynamic modelling in the supercritical fluid extraction industry.

The thermodynamic modelling was performed using the RK-SOAVE, RK-ASPEN, CPA and PSRK models. These models are all based on the Soave-Redlich-Kwong equation of state, but they differ with regards to mixing rules and approaches to accounting for solute interactions. Chapter 3 provides a detailed discussion as to why these models were selected.

1.4 Significant contributions

This study contributes to knowledge regarding the molecular interactions which exist in mixtures containing supercritical CO_2 with detergent range alkanes and alcohols as well as the thermodynamic modelling of such systems.

The significant contributions made through the measurement and analysis of the phase behaviour data are as follows:

- New high pressure bubble- and dew-point data measured for 3 mixtures containing CO_2 + n-dodecane + 3,7-dimethyl-1-octanol. This data provides insight into and experimental evidence of the solute-solute interaction which occur in the system and the co-solvency effect which occurs as a result of the interactions.
- New high pressure bubble- and dew-point data measured for 3 mixtures containing CO_2 + 1-decanol + 3,7-dimethyl-1-octanol. This data provides insight into and experimental evidence of the solute-solute interaction which occur in the system and the temperature inversion which occurs as a result of the interactions.
- New high pressure bubble- and dew-point data measured for 4 mixtures containing CO_2 + n-dodecane + 1-decanol + 3,7-dimethyl-1-octanol. This data provides insight into and experimental evidence of the solute-solute interaction which occur in the system and the complex phase behaviour which occurs as a result of the interactions.
- New high pressure VLE data measured for 3 mixtures containing CO_2 + n-dodecane + 1-decanol + 3,7-dimethyl-1-octanol. This data provides insight into and experimental

evidence of how the composition of co-existing phases are influenced by solute-solute interactions. To the author's knowledge, no VLE data for this system is available in open literature and this work will therefore be the first to publish VLE data for the quaternary system and quantify the solute-solute interactions which exist in the system. This work will also be the first to provide experimental information on the separability of the components in the quaternary system.

The significant contributions of the work with regard to modelling in Aspen Plus® are as follows:

- Comparison of the ability of four different variations of the Soave-Redlich-Kwong (SRK) model to describe the phase equilibrium of systems containing CO_2 with n-dodecane, 1-decanol and 3,7-dimethyl-1-octanol, thus providing an outcome as to which approach is best suited for this application.
- Using the CPA model to correlate/predict data for systems containing CO_2 with n-dodecane, 1-decanol and 3,7-dimethyl-1-octanol, which to date has not been used to model data for such systems.
- An outcome as to how the type of data used to fit the model parameters influences the model accuracy. This will indicate whether a model fitted using bubble- and dew-point data, can generate phase equilibrium data and if VLE data is required. It will also provide a comparison of the degree of accuracy which can be obtained when using a predictive model based on low pressure group contribution data opposed to models regressed from high pressure data.

1.5 Publications and conference proceedings

The following publications have already been published in an international peer reviewed journal:

- C. Latsky and C.E. Schwarz, High pressure bubble- and dew-point data for a system containing supercritical CO_2 with detergent range alkanes and alcohols, The Journal of Supercritical Fluids 141 (2018) 265- 273.
- C. Latsky and C.E. Schwarz, Measurement and modelling of high pressure bubble- and dew-point data for the CO_2 + 1-decanol + 3,7-dimethyl-1-octanol system, Fluid Phase Equilibria 488 (2019) 87 – 98.

- C. Latsky, N.S. Mabena, C.E. Schwarz, High pressure phase behaviour for the CO_2 + n-dodecane + 3,7-dimethyl-1-octanol system, The Journal of Supercritical Fluids 149 (2019) 138 – 150. *[N.S. Mabena measured the bubble- and dew-point data as part of a final year project, the data processing and interpretation of the data presented in the article, as well as the writing of the article was done by the current author]*

The following publication is in preparation and will be submitted to an international peer reviewed journal:

- C. Latsky and C.E. Schwarz, Measurement and modelling of VLE data for quaternary systems containing supercritical CO_2 with n-dodecane, 1-decanol and 3,7-dimethyl-1-octanol. To be submitted to the Journal of Chemical and Engineering Data.

The work presented in this dissertation has contributed towards the following conference proceedings:

- "High Pressure Bubble- and Dew-Point Data of CO_2 with Detergent Range Alkanes and Alcohols" poster presented at the 16th European Meeting on Supercritical Fluids held in Lisbon, Portugal between the 25th and 28th of April 2017.
- "Thermodynamic modelling of systems containing supercritical CO_2 with detergent range alkanes and alcohols" oral presentation presented 30th European Symposium on Applied Thermodynamics held in Prague, Czech Republic between the 10th and 13th of June 2018.
- "Measurement and modelling of VLE data for the quaternary CO_2 + 1-decanol + n-dodecane + 3,7-dimethyl-1-octanol system" poster presented at the 17th European Meeting on Supercritical Fluids held in Ciudad Real, Spain between the 8th and 10th of April 2019.

An abstract has also been submitted for the following conference:

- "The Effect of Solute-Solute Interactions in the Presence of CO_2 on the High Pressure Thermodynamic Behaviour of CO_2 + n-Alkane + 1-Alcohol Systems" oral presentation presented at the 2019 AIChE Annual Meeting held in Orlando, USA between the 10th and 15th of November 2019.

1.6 Thesis overview

Table 2: Manuscript layout

Chapter	Description	Objective
1	Introduces the research topic and clearly defines the aim, objectives and scope of the project.	
2	Highlights the unique properties exhibited by supercritical fluids and illustrates how these properties are utilised in supercritical fractionation processes.	
3	Provides basic knowledge regarding the construction and interpretation of phase diagrams. It also reviews experimental and modelling methods available to generate high pressure phase behaviour data. Based on the information presented, the model selection is performed in this chapter.	3 (3.1)
4	Literature review which summarises and discusses the literature data, for binary, ternary and multi-component systems containing CO_2 with n-dodecane, 1-decanol and 3,7-dimethyl-1-octanol.	
5	Provides details on the experimental method used to measure the bubble- and dew-point data of the ternary and quaternary systems and presents and analyses the measured data.	1
6	Provides details on the experimental method used to measure the VLE data of the quaternary systems and presents and analyses the measured data.	2
7	Discusses the four selected thermodynamic models and fitting of the model parameters to allow the prediction of phase equilibrium data for systems containing CO_2 with detergent range alkanes and alcohols.	3 (3.2)
8	Analyses and compares the accuracy with which the fitted models can correlate/predict equilibrium data for the ternary and quaternary systems	3 (3.3 & 3.4)
9	Conclusions of the most important findings presented in this work.	

2. SUPERCRITICAL FLUIDS AND FRACTIONATION PROCESSES

This chapter defines a supercritical fluid and highlights the properties which make supercritical fluids well suited for separation processes. The advantages and disadvantages of supercritical fluid fractionation processes are also investigated, with the specific focus on replacing azeotropic distillation with supercritical fractionation as method to separate detergent range alkanes and alcohols. This chapter also briefly discusses literature findings on the technical viability of supercritical fractionation processes aimed at separating detergent range alkanes and alcohols on pilot plant scale.

2.1 Defining a supercritical fluid

A supercritical fluid is a substance which exists at a temperature and pressure above its critical temperature and pressure [19]. In the supercritical state, a fluid cannot be vaporised by isobarically increasing temperature or liquefied by isothermally increasing pressure [10, 20]. In order to illustrate this definition, a pressure-temperature diagram indicating the supercritical region is presented in Figure 1 [17].

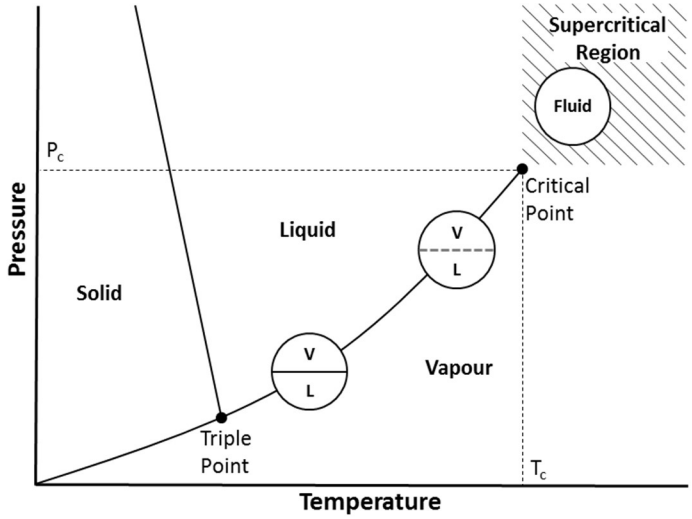

Figure 1: Schematic of a pressure-temperature diagram for a pure substance (Adapted from [17])

The disappearance of the distinction between liquid and gas in the supercritical region, illustrated in Figure 1, can be explained by analysing the effect of increasing temperature and pressure along the vapour-liquid co-existence curve. When moving along the vapour-liquid co-existence curve, the pressure and temperature increases. The increase in pressure increases the density of the gas, whilst the increase in temperature decreases the density of the liquid, due to thermal expansion. The densities of the two phases therefore approach each other. At the

critical point, the densities of the two phases become identical and the interphase between the phases disappear [10, 17].

The critical point, defined by the intersection of the critical temperature and critical pressure in Figure 1, can also be mathematically defined by investigating pressure as a function of volume at constant temperature, as illustrated in Figure 2 [17].

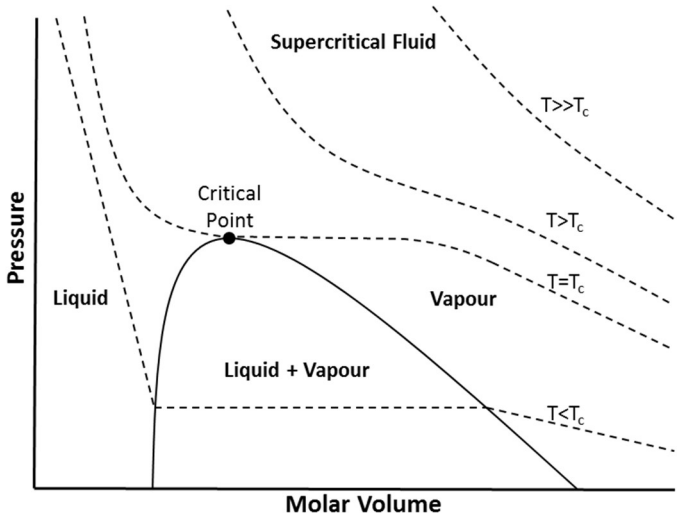

Figure 2: Schematic of a pressure-volume diagram for a pure substance (Adapted from [17])

When analysing the pressure-volume isotherms presented in Figure 2, it is seen that at temperatures much higher than the critical temperature ($T>>T_c$), the isotherm is only visible in the high molar volume region [17]. The shape of this isotherm also approximates the form $P \alpha \frac{1}{v}$, which is that of an ideal gas. As the temperature is decreased ($T>T_c$) an inflection in the isotherm becomes visible. As the temperature is lowered further, the slope of the inflection point also decreases and at the critical temperature ($T=T_c$) the slope of the inflection point is zero. The critical point can therefore be mathematically defined as follows [10, 17].

$$\left(\frac{\partial P}{\partial v}\right)_T = 0 \qquad [2.1]$$

$$\left(\frac{\partial^2 P}{\partial v^2}\right)_T = 0 \qquad [2.2]$$

2.2 Properties of supercritical fluids

Supercritical fluids exhibit properties that lie between those of a liquid and a gas [21]. In order to illustrate this, typical values for some important mass and energy rate transfer properties of gasses, liquids and supercritical fluids are compared in Table 3 [21].

Table 3: Typical properties of liquids, gasses and supercritical fluids (Adapted from [21])

Physical Property	Units	Liquid	Supercritical Fluid	Gas
Density	g/mL	1	0.05 - 1	10^{-3}
Viscosity	Pa.s	10^{-3}	10^{-4} - 10^{-5}	10^{-5}
Diffusion coefficient	m^2/s	10^{-5}	10^{-3}	10^{-1}

When analysing the density data presented in Table 3, it is noted that the density of a supercritical fluid approaches that of a liquid. However, unlike liquids the density of supercritical fluids can easily be adjusted by altering temperature and pressure, especially close to the critical point [20]. This can best be explained by referring to Figure 2. When viewing the critical temperature pressure-volume isotherm ($T=T_c$) it can be seen that close to the critical point a small variation in pressure at constant temperature can drastically increase or decrease the density. When moving away from the critical point the effect diminishes [20]. The tuneability of density is important, as the solvating power of a substance depends on the density [5, 19, 20]. This is due to the fact that solvation results from intermolecular forces. The intermolecular forces are due to the arrangement of solvent molecules around the solute molecules and thus the forces are density dependent [19]. The unique ability to manipulate the density and therefore the solvating power of supercritical fluids, makes them well suited as solvents in separation and extraction processes [5].

The next property to be analysed is viscosity. Viscosity is a transport property which describes the internal resistance of a fluid to flow [22]. From Table 3 it can be seen that the viscosity of a supercritical fluid is close to that of a gas. This characteristic improves the hydrodynamic behaviour of supercritical fluids, as it increases the ease with which the solvents can flow through the extraction or separation plant [5].

The diffusion coefficient presented in Table 3, is a measure of the rate at which a component diffuses through a medium [23]. It is seen that the diffusion properties of supercritical fluids lie between those of liquids and gasses. The diffusion in a supercritical solvent is therefore faster than in a liquid solvent [5]. This suggests that faster separation and extraction can generally be attained by using supercritical fluids, rather than normal liquid solvents [10].

Based on the properties described above, it can be said that a supercritical fluid moves like a gas, but it has solvating abilities similar to that of a liquid [19].

2.3 Principles and application

Supercritical fractionation processes separate components in mixtures by utilising both the differences in the interactions between the components and the solvent as well as the differences in volatility of the different components [24]. These processes can be operated in different modes such as single-stage or batch mode and multi-stage mode [5].The basic working principle of the different operating modes are the same and the process consists of two main sections namely, extraction and separation [5]. In these sections, the ability to adjust the solvent strength of the supercritical solvent, by manipulating temperature and pressure, is exploited [21]. The extraction section is operated at high pressure and is aimed to load the solvent with the most soluble components in the feed stream. In the separation section, the extracted products are recovered by lowering the pressure and/or increasing the temperature of the loaded solvent [21].

Single-stage or batch fractionation processes, presented in Figure 3, are mostly used to extract valuable components from solids, but it can also be used for extractions from liquids. Some industrial applications include decaffeination of coffee beans and the extraction of essential oils [25].

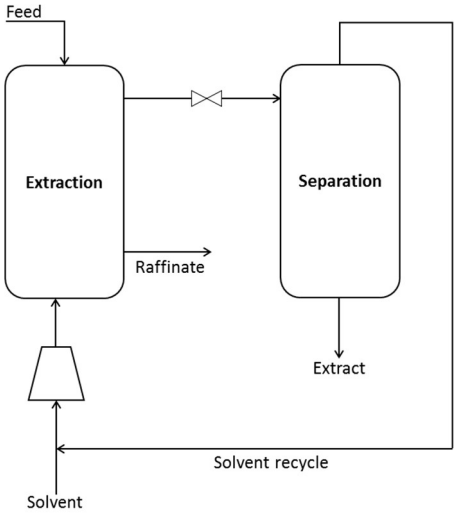

Figure 3: Schematic of a single-stage supercritical fractionation process (Adapted from [5])

If the desired separation cannot be achieved in a single stage, multi-stage processes can be used. Multi-stage processes, illustrated in Figure 4, are similar to single-stage processes, but the conditions of the extraction and/or separation units can be varied to increase extraction. Typical industrial application of multi-stage processes includes the refining of used oils and deasphalting [10].

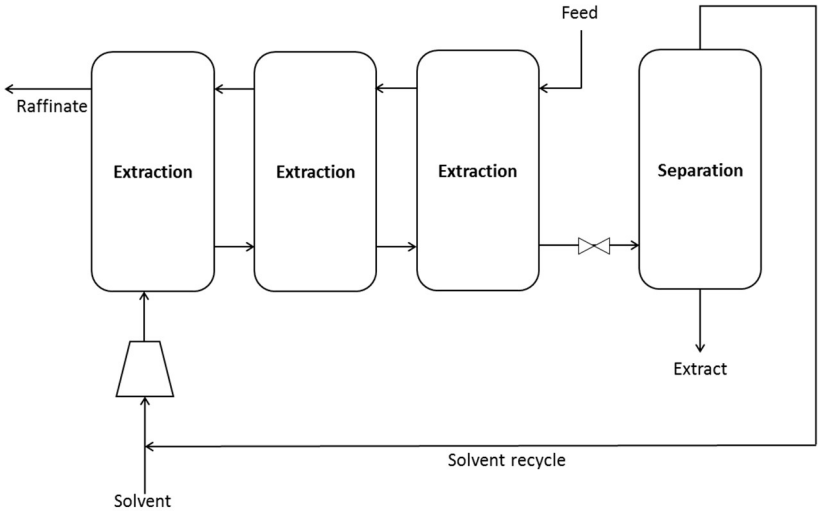

Figure 4: Schematic of a multi-stage supercritical fractionation process (Adapted from [5])

The most effective multi-stage configuration for liquid feeds is continuous counter-current contacting [25]. This type of separation process is comparable to liquid-liquid extraction and can be treated similarly [10]. Industrial applications of continuous counter-current extraction processes include the separation of fatty acid esters and the enrichment of tocotrienols and tocopherols [25].

2.4 Advantages and disadvantages of supercritical fluid fractionation

The advantages and disadvantages pertaining to supercritical fractionation processes are outlined below [10, 26].

Advantages:

- Supercritical fluids exhibit good solvent strength.
- The solvent strength of supercritical fluids can be controlled by temperature and pressure.
- The solvent strength of supercritical fluids can be manipulated to remove the dissolved product from the supercritical solvent, leaving the solvent regenerated with minimal solvent residue in the product.
- Supercritical processes are operated near the critical temperatures of the solvent. Thus, the operating temperatures of supercritical processes are generally lower than the boiling points of the low volatility solutes. This permits the extraction or separation of heat sensitive compounds.
- Supercritical fluids can replace hazardous liquid solvents.
- There are various supercritical fluids, such as CO_2, which have desirable characteristics (non-toxic, non-flammable, inert and inexpensive).

Disadvantages:

- The operating pressure of supercritical extraction processes are much higher than those of traditional extraction processes.
- Due to the high operating pressure, the phase behaviour may be complex as the system exhibits highly non-ideal behaviour in both the liquid and vapour phases.
- The capital cost of supercritical extraction processes could possibly be higher than that of traditional extraction processes as the equipment must be designed to safely operate at elevated pressures [26].

When considering the current method of separating detergent range alkanes and alcohols, namely azeotropic distillation [1], which operates under vacuum conditions with temperatures up to 473 K and requires diethylene glycol (DEG), which is a hazardous entrainer, the need to investigate alternative separation techniques is clear [1, 5]. By implementing supercritical fluid fractionation processes using CO_2 as solvent, the high temperature concern is eliminated, as supercritical fluid fractionation processes operate at temperatures just above the solvent critical temperature, that is 304 K for CO_2 [17]. The need for a hazardous entrainer is also eliminated and although an additional chemical solvent is required, CO_2 is relatively inexpensive, readily available and non-toxic, as discussed previously [10, 17]. Furthermore, unlike with azeotropic distillation where the bottoms and overheads must be chemically processed to remove the entrainer, only the overhead product of the supercritical fractionation setup must be treated to remove the solvent and this is done easily with no added materials [5]. The disadvantages of using supercritical fractionation are linked to the high pressures required, but considering that the azeotropic distillation process takes place under vacuum, both are seen as extreme operating conditions with added cost implications, risks and non-ideal phase behaviour. The information presented here indicates that supercritical CO_2 fractionation is an attractive alternative separation technique to the azeotropic distillation process currently implemented to separate detergent range alkanes and alcohols.

2.5 Separation using supercritical fluid fractionation

This section summarises the viability findings of supercritical fractionation pilot plant tests conducted to separate detergent range alkanes and alcohols.

2.5.1 Separating n-alkanes from 1-alcohols

A study conducted by Bonthuys et al., [7] investigated the feasibility of using supercritical fluid fractionation to separate linear alkanes (n-alkanes) from primary linear alcohols (1-alcohol). The components selected to represent the n-alkane and 1-alcohol in the viability study, were n-tetradecane (n-alkane) and 1-dodecanol (1-alcohol), as the close-boiling nature of these components made them the most difficult to separate within the C_{12} to C_{14} alcohol range investigated. The pilot plant tests were conducted using a single fractionation unit and CO_2 and ethane were used as supercritical solvents. Based on the results obtained from the study, Bonthuys et al., [7] concluded that supercritical fluid fractionation is a viable method to separate linear alkanes from primary linear alcohols with similar boiling points, when using either CO_2 or ethane. A follow-up study into the influence of process parameters and the size of the operating range [27] highlighted that when using CO_2 as solvent, the operating window is small. Good separation is achieved within the operating temperature range of 310 K to 317 K, but it was found that at these low temperatures the process is sensitive to temperature changes, making it difficult to control [27]. Investigation into the operating pressure range indicated that unlike ethane, CO_2 does not have an approximate linear relationship between temperature and pressure at constant composition [27], which decreases the controllability of the fractionation process. The detection of the decreased controllability of the supercritical CO_2 fractionation process within the desired operating range suggests the occurrence of complex phase behaviour, which could explain the sensitivity of the process to changes in temperature and pressure. The possibility of complex phase behaviour occurring in systems containing CO_2 with n-alkanes and 1-alcohols was further investigated by Ferreira [28]. This study [28] revealed that significant solute-solute interactions exist which results in complex phase behaviour at low temperatures close to the solvent critical temperature of 304 K [17].

2.5.2 Separating n-alkanes from 1-alcohols + branched alcohols

A study conducted by Zamudio [5], evaluated whether supercritical fluid fractionation can be used to separate linear alkanes (n-alkanes) from close-boiling primary linear alcohols (1-alcohols) and branched alcohols. The components used to represent the alkane and alcohol isomers were n-decane (n-alkane), 1-decanol (1-alcohol), 3,7-dimethyl-1-octanol and 2,6-dimethyl-2-octanol (branched alcohols). Zamudio [5] conducted pilot plant tests using a single fractionation unit and CO_2 was selected as the supercritical solvent. Based on the pilot plant results, Zamudio [5] concluded that supercritical CO_2 fractionation is a viable method to

separate detergent range alkanes and alcohols with similar boiling points. Furthermore, similar to Schwarz, et al., [27], Zamudio [5] also determined that at lower temperatures (315.9 K) better separation of the n-alkane from the alcohol isomers is attained. The significant solute-solute interactions identified by Zamudio [5] and the follow up studies by Smith & Schwarz [13] and Fourie [14], however suggest that these interaction could cause controllability issues at low temperatures. In order to fully understand the interactions which would occur if a typical detergent range alcohol product stream, containing n-alkanes with linear and branched alcohols, is fractionated using CO_2, further investigation into the phase behaviour of such mixtures is required. This supports the in-depth evaluation of the interactions which exist in the quaternary system studied in this project.

2.6 Outcome of this chapter

This chapter provided background on supercritical fluids and the basic working principle of supercritical fractionation processes. The advantages and disadvantages of using supercritical fractionation was also outlined and the progress made in testing the validity of using this technique to separate detergent range alkanes and alcohols on pilot plant scale was discussed. The information indicated that supercritical CO_2 fractionation is an attractive alternative to the azeotropic distillation process currently used to separate detergent range alkanes and alcohols. It was however highlighted that the high operating pressures of supercritical processes may result in complex phase behaviour. The viability studies also indicated controllability issues which are likely linked to complex phase behaviour which occurs within the operating range of supercritical fractionation processes. The importance of investigating high pressure phase behaviour is therefore clear. In the next chapter, basic principles regarding high pressure phase behaviour will be discussed where after focus will be shifted towards the high pressure phase behaviour of the specific system investigated in this work.

3. HIGH PRESSURE PHASE BEHAVIOUR

The basic principles pertaining to general high pressure phase behaviour, phase diagrams and the methods available to generate high pressure phase behaviour data are summarised in this chapter. The aim of this chapter is to provide the required background to allow interpretation of high pressure phase behaviour data and to provide an overview of the methods which can be used to measure phase equilibrium data. The chapter also provides background regarding thermodynamic modelling of phase equilibrium data and it outlines the thermodynamic models which will be investigated in this work, thereby addressing Objective 3.1.

3.1 General phase behaviour and phase diagrams

Phase diagrams are vital in the analysis of phase behaviour. These diagrams visually depict the phase behaviour and aid in identifying trends as well as deviations from expected phase behaviour. This section provides the basic theory required to construct and interpret phase diagrams of systems which are relevant to this study and it also discusses general phase behaviour exhibited by these systems.

3.1.1 Gibbs phase rule

A key concept to understanding equilibrium phase behaviour, is the Gibbs phase rule. The phase rule is used to determine the number of thermodynamic degrees of freedom, that is the number of intensive variables that can be independently varied to alter the equilibrium state of a system [29]. According to the Gibbs phase rule, presented in Equation 3.1, the number of degrees of freedom is the difference between the number of intensive variables and the number of equations which connect them [29, 30].

$$F = N - \Pi + 2 - \Phi \qquad [3.1]$$

Where, F is the number of degrees of freedom, N is the number of components, $\prod$ is the number of phases and ϕ accounts for constraints [29].

In order to illustrate this concept, the phase rule will be applied to a pure substance. When considering a pure substance in the one phase region, the degrees of freedom is two. Therefore, two intensive variables must be specified to fix the intensive state of the system. This means that all the equilibrium states can be represented in a two-dimensional phase diagram, as shown

in Figure 5 [29]. If the pure substance exists in a state where two phases are in equilibrium, the degrees of freedom is reduced to one and the phase behaviour is represented in the form of a curve on the pressure-temperature phase diagram, as shown in Figure 5. The degrees of freedom for the critical point of a pure substance is zero, due the additional constraints which applies to this point, as discussed in section 2.1. The critical point is therefore represented by a point [29].

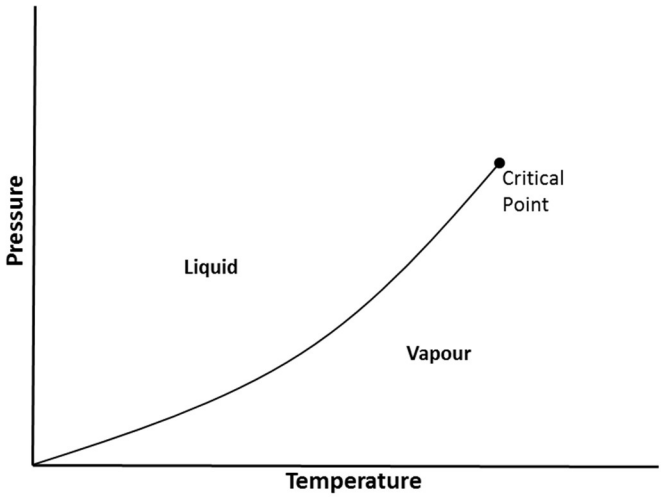

Figure 5: Schematic of a pressure-temperature diagram for a pure fluid (Adapted from [29])

3.1.2 Phase behaviour and phase diagrams for binary systems

3.1.2.1 Binary phase diagrams

When applying the Gibbs phase rule to a binary system and considering that there must be at least one phase present, the maximum degrees of freedom for a binary system is three. Therefore, three intensive variables, namely temperature, pressure and the mass or mole fraction of one component, must be specified to fix the intensive state of a binary system. This also means that a three-dimensional pressure-temperature-composition (P-T-x_A) phase diagram is required to represent all the equilibrium states of the system [30]. Three-dimensional diagrams are however often difficult to construct and interpret and therefore the dimensions are often reduced by presenting cross sections or projections. In order to illustrate this, a pressure-temperature cross section and projection of a three-dimensional phase diagram is presented in Figure 6 [29, 30].

The pressure-temperature cross section presented in Figure 6 (a) was constructed by keeping one intensive variable, namely composition (x_A), constant. Fixing one of the intensive variables increases the constraints (ϕ), thereby decreasing the degrees of freedom (F) and consequently

the dimensions required to represent all the equilibrium states of the system [29]. The pressure-temperature projection presented in Figure 6 (b) was constructed by allowing one intensive variable, namely composition (x_A), to assume all possible values, but excluding the composition axis from the diagram. The degrees of freedom therefore remain unchanged, but the dimensions of the diagram are reduced by the omission of an axis [29].

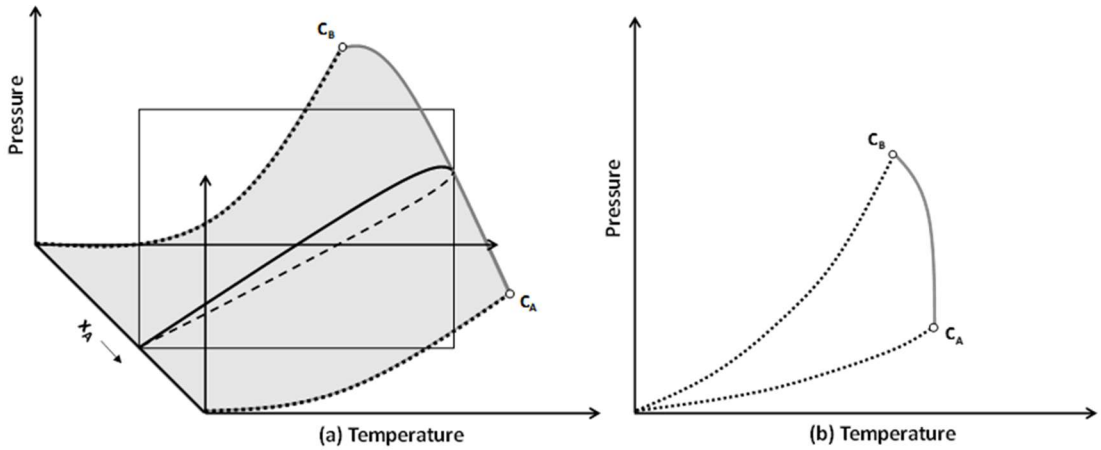

Figure 6: Schematic illustrating: (a) pressure-temperature-composition diagram of a binary mixture with a pressure-temperature cross section (b) pressure-temperature projection of the three-dimensional diagram. —— Bubble-point curve; - - - Dew-point curve; —— Critical curve; ····· Vapour pressure curve; o Pure component critical point; Grey area indicates the two phase region (Adapted from [29])

Due to the fact that cross section diagrams are constructed by fixing one or more intensive variables, the shape of the phase envelopes presented in these diagrams are dependent on the conditions at which the phase envelope is constructed. In order to illustrate this, two isothermal cross sections are compared in Figure 7.

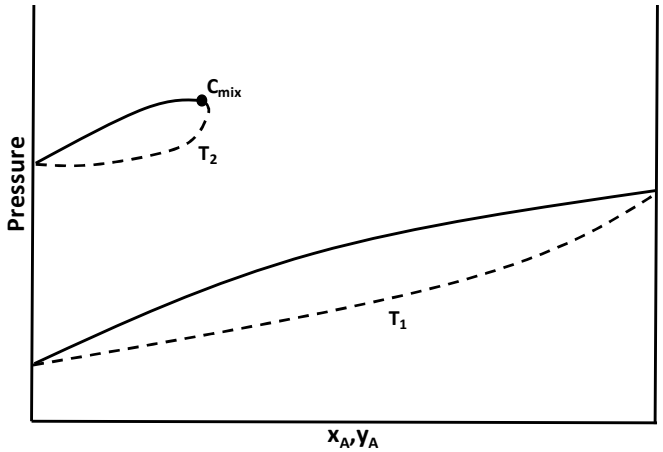

Figure 7: Schematic comparing two isothermal cross sections. —— Bubble-point curve; - - Dew-point curve (Adapted from [30])

When analysing Figure 7 it is seen that the phase envelope constructed at T_1 spans the entire x-axis. This is because T_1 is below the critical temperature of both components. The cross section constructed at T_2 does however not extend over the entire x-axis. Instead, the bubble- and dew-point curves meet at the mixture critical point (C_{mix}). This is because T_2 is above the critical temperature of component A [30].

Unlike for pure substances, the mixture critical point generally is not the highest temperature and pressure at which the vapour and liquid phase can co-exist. The critical point of a mixture is located where the nose of the pressure-temperature curve for that mixture composition is tangent to the critical curve. This concept is illustrated in Figure 8.

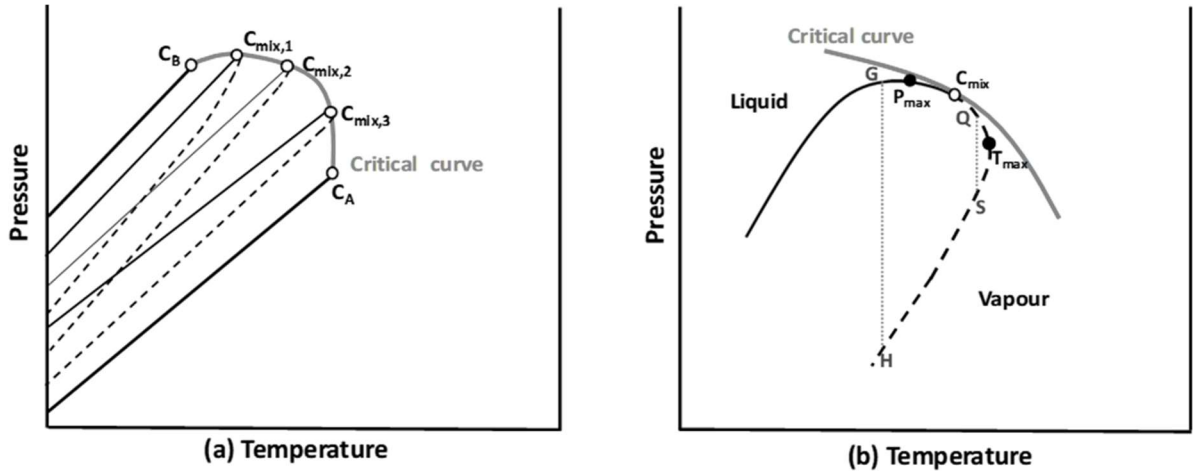

Figure 8: Schematic illustrating: (a) pressure-temperature curves for different mixtures of fixed composition (b) enlarged portion of the pressure-temperature diagram clearly illustrating the mixture critical point location (Adapted from [30])

In the pressure-temperature projection, presented in Figure 8 (a), the loops represent the pressure-temperature behaviour for different mixtures of fixed composition. From this diagram, it is clear that the mixture critical point (C_{mix}) varies with mixture composition. Figure 8 (a) does however not clearly illustrate the position of the critical point relevant to the maximum temperature and pressure points and therefore a section of the pressure-temperature projection was enlarged in Figure 8 (b). In Figure 8 (b) it is seen that the mixture critical point (C_{mix}) does not coincide with either the maximum temperature (T_{max}) or maximum pressure points (P_{max}) [30].

Further analysis of Figure 8 (b) reveals interesting phase behaviour. For mixtures which are located to the left of the mixture critical point, such as point G, a reduction of pressure along a

line such as GH results in the vaporisation of a liquid from the bubble-point to the dew-point curve. However, for a mixture located at point Q, a reduction in pressure along the line QS results in the liquefication of the saturated vapour. The amount of liquid increases until it reaches a maximum, where after vaporisation occurs until the dew-point curve is reached at point S. This phenomenon is referred to as retrograde condensation and it is often observed in mixtures containing supercritical components [29, 30].

3.1.2.2 Classification of binary phase behaviour

Seeing as the phase behaviour analysis performed in this work includes the evaluation of binary phase behaviour, a brief overview of the six types of binary fluid phase behaviour, as classified by Van Konynenburg and Scott [31], is provided below. A more in-depth discussion on the classification of binary phase behaviour is presented in work done by Dieters & Kraska [29].

Type I:

This is the simplest type of binary phase behaviour as it only contains one vapour-liquid critical curve which runs continuously between the critical points of the pure components. A schematic of type I pressure-temperature behaviour is presented in Figure 9 [29]. Examples of type I phase behaviour include binary systems containing methane + n-alkanes with carbon numbers up to 5 [32] or ethane + n-alkanes with carbon numbers up to 18 [29].

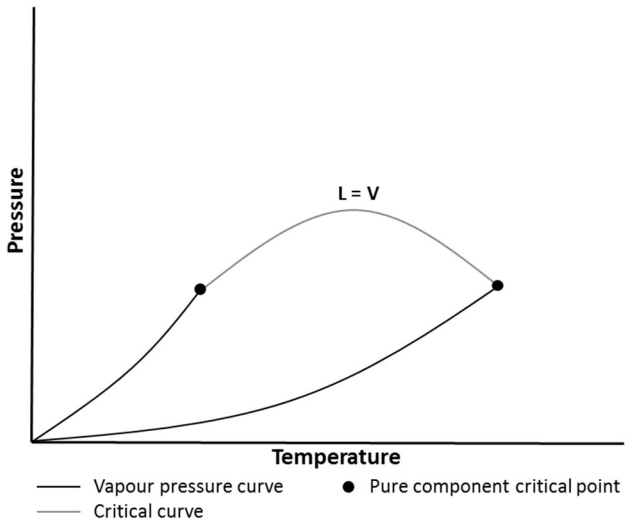

Figure 9: Schematic of a pressure-temperature projection illustrating type I binary phase behaviour (Adapted from [32])

Type II:

Similar to type I, type II phase behaviour also contains a continuous vapour-liquid critical curve which connects the pure component critical points. In additions to this, type II also has a liquid-liquid critical curve and a three-phase equilibrium curve. The critical endpoint where the liquid-liquid equilibrium curve originates is termed the upper critical endpoint. This point is termed the upper critical endpoint as it is the upper temperature limit of the three-phase equilibrium curve. At this point the two liquid phases become identical [32]. A typical type II pressure-temperature diagram is presented in Figure 10 [29]. Examples of type II phase behaviour include binary systems containing CO_2 + n-alkanes with carbon numbers between 6 and 13 [32].

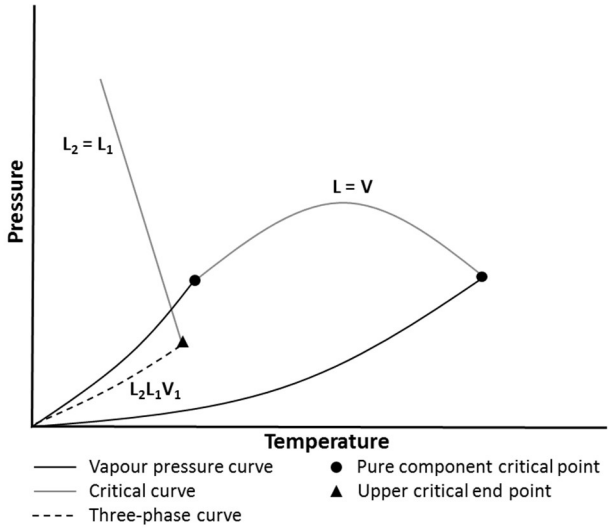

Figure 10: Schematic of a pressure-temperature projection illustrating type II binary phase behaviour (Adapted from [32])

Type III:

When analysing the type III pressure-temperature phase behaviour depicted in Figure 11, it is noted that the vapour-liquid critical curve is divided. The vapour-liquid critical curve which starts at the critical point of the more volatile component is short and ends in an upper critical endpoint. The vapour-liquid critical curve which originates at the critical point of the less volatile component changes to a liquid-liquid critical curve at higher pressures and continues to infinite pressures [29]. Examples of type III phase behaviour include CO_2 + n-tetradecane [32], CO_2 + n-hexadecane [29] and CO_2 + 1-alcohols with carbon numbers ranging from 8 to 14 [33].

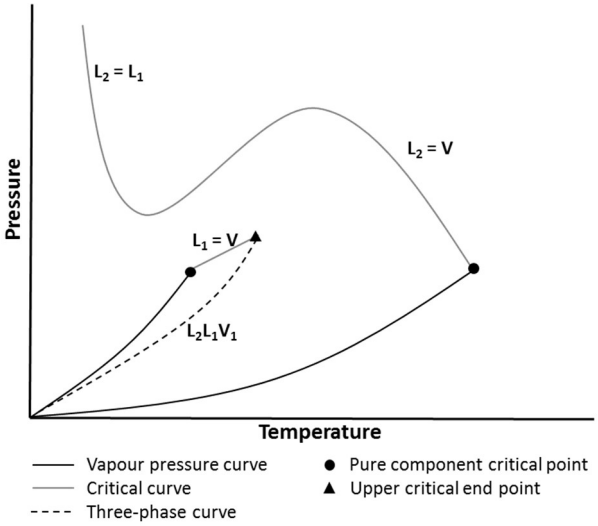

Figure 11: Schematic of a pressure-temperature projection illustrating type III binary phase behaviour (Adapted from [32])

Type IV:

From Figure 12 it can be seen that, unlike any of the previous types, type IV has a three-phase equilibrium curve which is divided into two branches. The branch which starts at the origin of the diagram is similar to the three-phase equilibrium behaviour of a type II system, as it also terminates in an upper critical endpoint from which a liquid-liquid critical curve extends. The second three-phase branch stretches between an upper critical endpoint and a lower critical endpoint. The lower critical endpoint is the low temperature limit of the three-phase equilibrium curve where the two liquid phases become identical [29, 32]. Examples of type IV phase behaviour include methane + hexane [29] and CO_2 + tridecane [32].

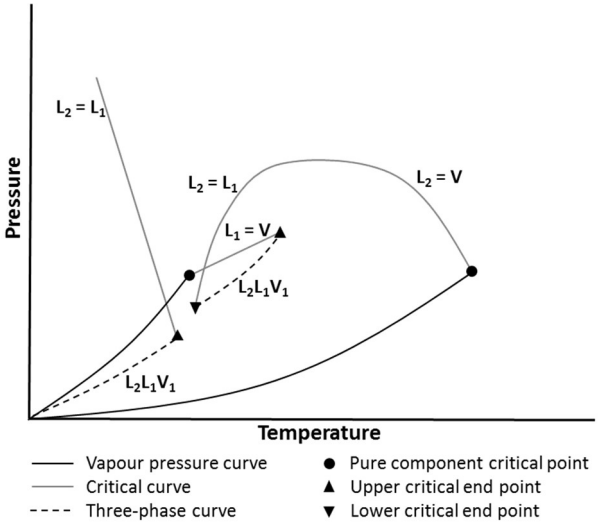

Figure 12: Schematic of a pressure-temperature projection illustrating type IV binary phase behaviour (Adapted from [32])

Type V:

A typical type V pressure-temperature diagram is presented in Figure 13 [29]. From this figure, it is seen that type V phase behaviour is characterised by a discontinuous critical curve with both branches terminating in critical endpoints [32]. When comparing Figures 12 and 13, it is noted that type V phase behaviour is similar to type IV, but no liquid-liquid critical curve is observed [29]. Examples of type V phase behaviour include methane + hexane isomers [29] and ethane + ethanol [34].

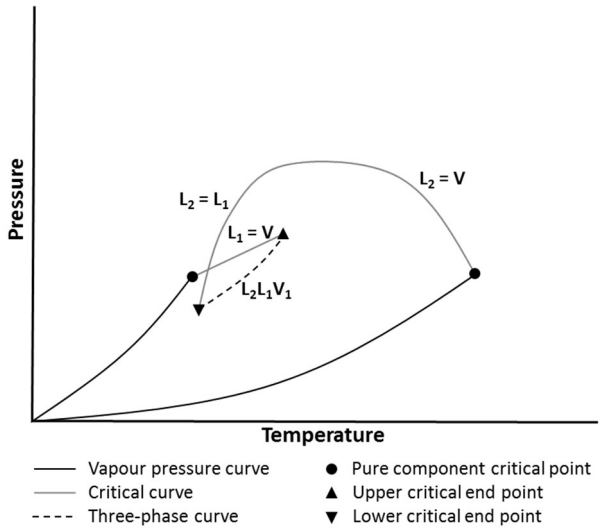

Figure 13: Schematic of a pressure-temperature projection illustrating type V binary phase behaviour (Adapted from [32])

Type VI:

A phase diagram depicting the most prominent type of VI phase behaviour is presented in Figure 14. From this figure, it can be seen that type VI phase behaviour is similar to type I, but with the addition of a liquid-liquid critical curve which has a pressure maximum. The liquid-liquid critical curve is located at low pressures and the curve terminates in an upper and lower critical endpoint [29]. Examples of type VI phase behaviour include water + n-butanol or 2-butanol [34] and water + 2-butoxyethanol [32].

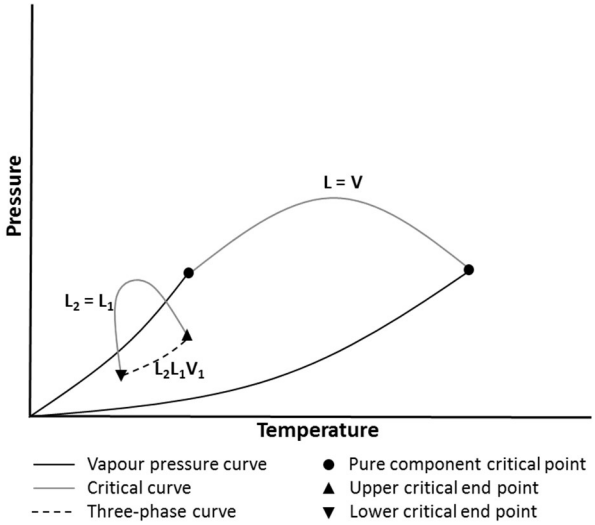

Figure 14: Schematic of a pressure-temperature projection illustrating type VI phase behaviour (Adapted from [32])

The binary phase behaviour classification presented in this section is limited to fluid phase behaviour, as solid-fluid phase equilibria is beyond the scope of this work. It should however be noted that although the formation of solid phases is not relevant to this work, solidification of components can result in the incorrect classification of fluid phase behaviour when using the phase behaviour classification scheme described in this section. This is due to the fact that the solidification may obscure the critical curves and/or critical end points, making it difficult to distinguish between the different types [10].

3.1.3 Phase behaviour and phase diagrams for ternary systems

3.1.3.1 Gibbs phase diagrams

When applying the Gibbs phase rule to a system containing three components and considering that there must be at least one phase present, the maximum degrees of freedom for a ternary system is four. Therefore, a four-dimensional pressure-temperature-composition (P-T-x_A-x_B) phase diagram is required to represent all the equilibrium states of a ternary system. Due to the fact that four-dimensional diagrams are difficult to visualise, the graphical representation of ternary phase equilibria is usually simplified by presenting it at constant pressure and temperature in a Gibbs phase triangle [32]. A Gibbs phase diagram, such as the one depicted in Figure 15, is an equilateral triangle with each corner representing a pure component [29]. The sides of the triangle represent the three binary subsystems. The method of determining the composition of a point within the diagram is visually depicted in Figure 15 [29].

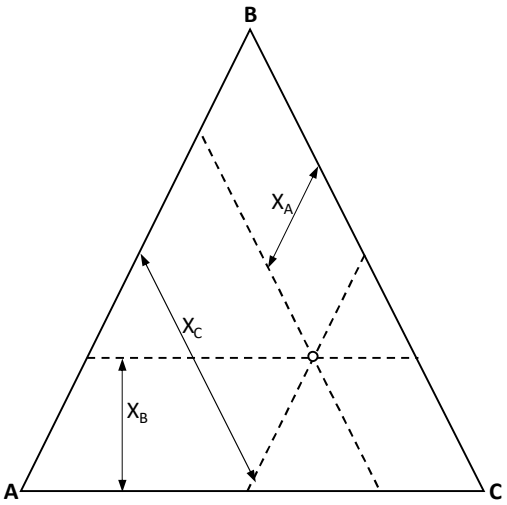

Figure 15: Gibbs diagram of a ternary system with no immiscible subsystems. The diagram also illustrates the method used to determine the composition of a point in the triangle (Adapted from [29])

The Gibbs phase diagram presented in Figure 15 represents the simplest ternary system, namely a system in which all the binary subsystems are miscible. If one of the binary subsystems are immiscible or partially immiscible, the Gibbs phase triangle in Figure 15 changes to include a two-phase vapour-liquid or liquid-liquid region, also referred to as miscibility gap. A schematic of this type of Gibbs diagram is presented in Figure 16 [29].

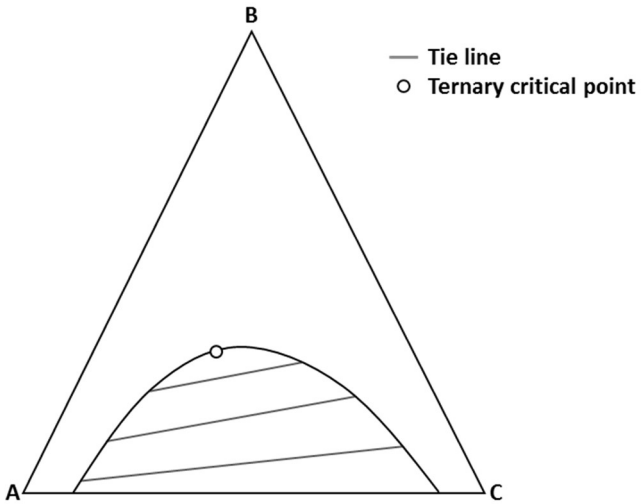

Figure 16: Gibbs diagram of a ternary system with one partially immiscible subsystem. The diagram also indicates the tie-lines and ternary critical point (Adapted from [29])

In Figure 16, it is seen that the two-phase region for the A + C subsystem starts at the edge of the triangle and moves inward. As it moves inward the size of the two-phase region decreases until it disappears. This is due to the fact that subsystems A + B and B + C are completely miscible [29]. Within the two-phase region the composition of the co-existing phases is

determined by the tie lines. From Figure 16 it is seen that the length of the tie lines decreases as the distance from the edge increases and terminate at the ternary critical point [29].

If two of the binary subsystems are immiscible, the phase behaviour can take on different forms as illustrated in Figures 17. In Figure 17 (a) it is seen that there are two two-phase regions. It can happen that the two-phase regions in Figure 17 (a) connect, as shown in Figure 17 (b) or merge, as seen in Figure 17 (c) [29]. The type of phase behaviour (a – c) obtained is however system dependent and may vary with temperature and pressure.

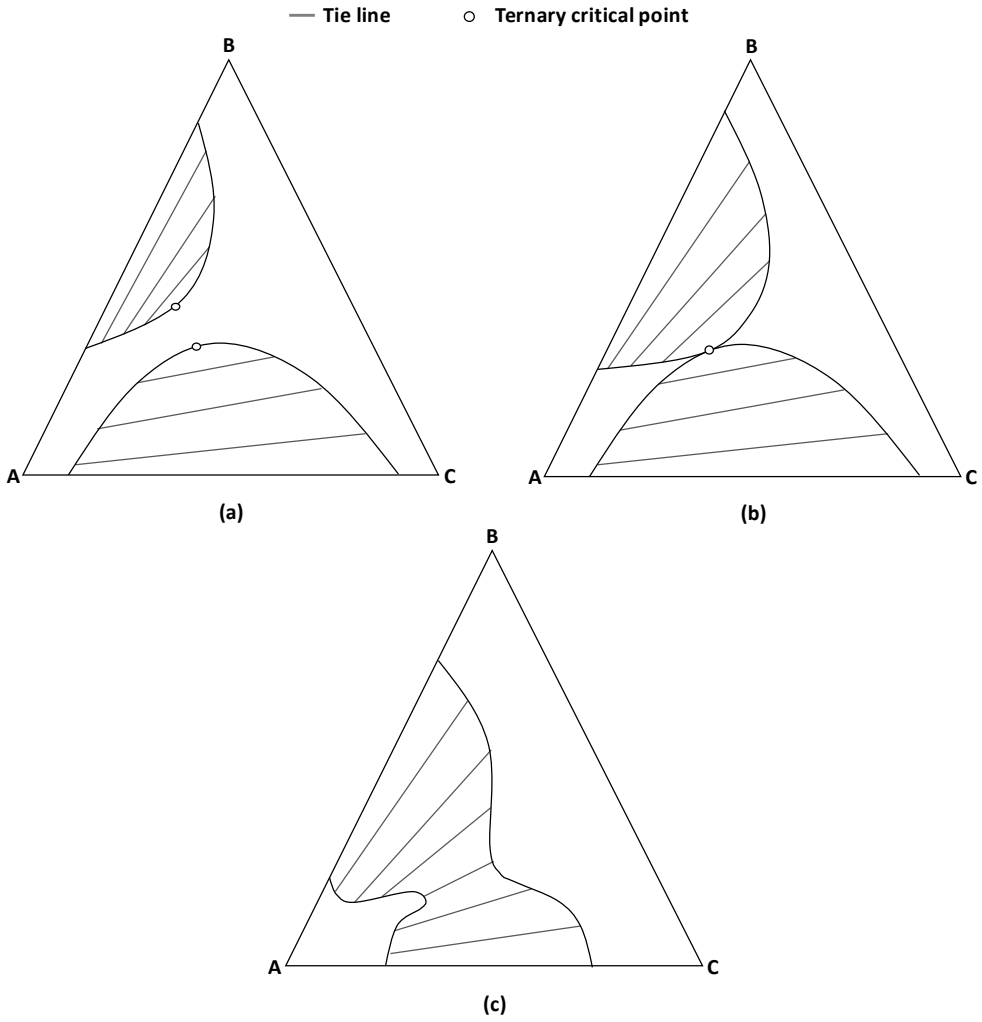

Figure 17: Gibbs triangle of a ternary system with two partially immiscible subsystems where: (a) the two-phase regions are separate (b) the two-phase regions are connected, (c) the two-phase regions are merged (Adapted from [29])

In the case were all three subsystems are immiscible, there are also various options for the phase behaviour and Figure 18 depicts three of these options. Figure 18 (a) illustrates the simplest option where none of the two-phase regions are connected. Figure 18 (b) depicts an example where two two-phase regions merge, whilst the other one remains unconnected. In

Figure 18 (c), all three of the two-phase areas are connected and this results in the formation of a three-phase triangle within the phase diagram [29]. As stated previously, the type of phase behaviour (a – c) obtained is system, temperature and pressure dependent.

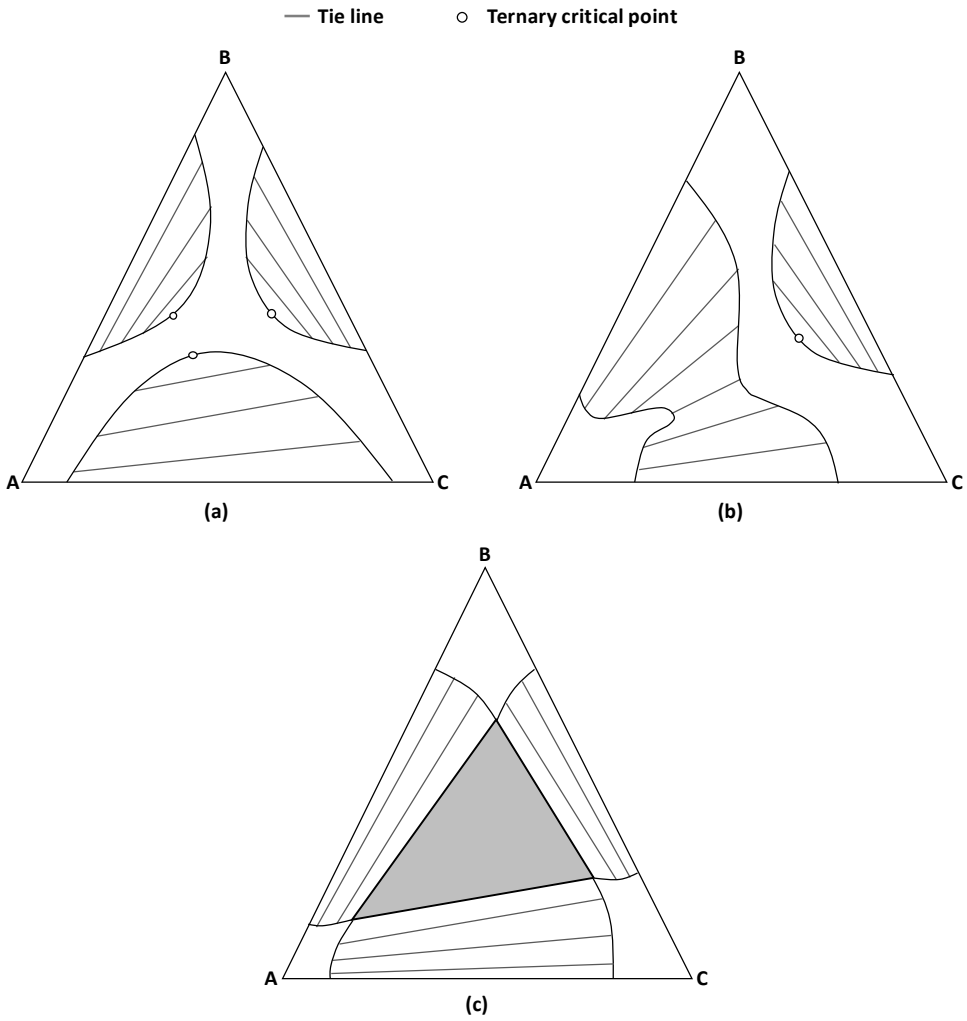

Figure 18: Gibbs triangle of a ternary system with three partially immiscible subsystems where: (a) the three two-phase regions are separate (b) two-phase regions are merged and the third is separate, (c) a three-phase region (shaded area) forms (Adapted from [29])

3.1.3.2 Three-dimensional phase diagrams

For ternary phase behaviour, two-dimensional phase diagrams are usually not sufficient to fully investigate the phase behaviour. Therefore, simplified three-dimensional phase diagrams, such as the ternary phase prism and the ternary phase cube discussed in this section, have been developed.

Ternary phase prisms:

In the previous section, it was highlighted that the size and shape of the two- and three-phase regions depicted in Gibbs phase diagrams may depend on temperature and pressure. It is therefore necessary to investigate the evolution of these Gibbs phase diagram with temperature and pressure. However, as it is difficult to visually represent both temperature and pressure, the effect of temperature and pressure is usually evaluated using isothermal or isobaric prisms. An example of an isothermal ternary phase prism is depicted in Figure 19 [29].

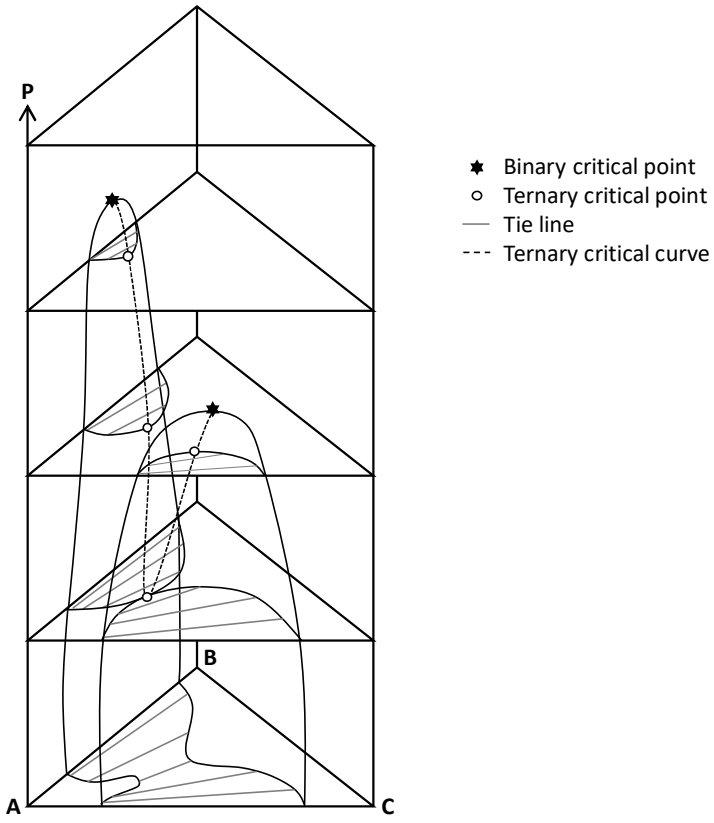

Figure 19: Isothermal ternary phase prism, illustrating the effect of pressure on ternary phase behaviour (Adapted from [29])

Figure 19 illustrates a system which changes from a cross section with two immiscible subsystems to a cross section with one immiscible subsystem, as pressure increases. At low pressures, the two immiscible subsystems are merged. As pressure increases the band connecting the two-phase region narrows and finally disintegrates into two two-phase regions. A further increase in pressure shrinks one of the two two-phase regions to a point on the prism face of the A + C subsystem. This point is referred to as a binary critical point of the A + C subsystem. At pressures above this point, only one two-phase region exists. This two-phase region eventually disappears at the binary critical point of the A + B subsystem [29].

In Figure 19, the dotted line connecting the ternary critical points is referred to as the ternary critical curve. From Figure 19 it is seen that the ternary critical curve is not a straight line. This is often the case and it usually indicates complex phase equilibria, details of which will be discussed in section 3.1.3.3.

Ternary phase cube:

The ternary phase cube is a three-dimensional representation in the P-T- x_A^{red} space, where x_A^{red} is the reduced mass fraction, defined by Equation 3.2 [29, 35].

$$x_A^{red} \equiv \frac{x_A}{x_A + x_B} \qquad [3.2]$$

In a ternary phase cube, such as the one presented in Figure 20, the ternary critical curves for all the reduced mass fractions at a specific solvent mass fraction are arranged to create a critical surface. Above the critical surface the system exists as a single phase, as the pressure in this region is high enough to allow the solvent to completely dissolve and form a homogeneous fluid mixture. At pressures below the critical surface, two phases co-exist, the solvent-rich phase is referred to as the "vapour" phase, whilst the solute-rich phase is referred to as the "liquid" phase. Often, the ternary critical surfaces are not planar and this is usually an indication of complex phase equilibria [29, 35].

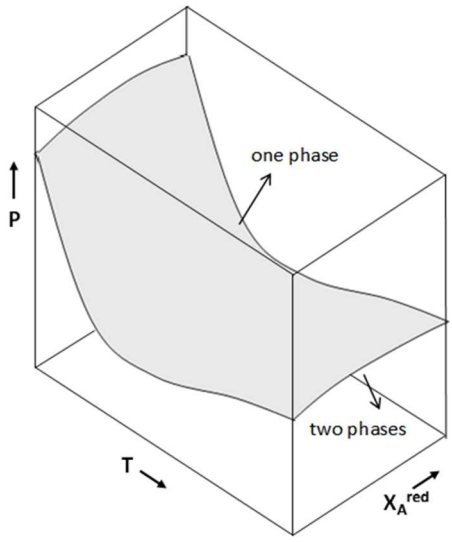

Figure 20: Schematic of a P-T- x_A^{red} ternary phase cube at a constant solvent mass fraction (x_s) (Adapted from [36])

3.1.3.3 Complex phase equilibrium phenomena in ternary systems

The classification system developed by Van Konynenburg and Scott [31] can be used to classify binary mixtures throughout the entire temperature-pressure-composition range. To

date, no equivalent classification system has been developed for ternary mixtures [37]. Bluma and Deiters [37] has developed a classification scheme, based on the classification system developed by Van Konynenburg and Scott [31], which can be used to determine the type of ternary phase behaviour, but it limited to systems with equal-sized molecules for which the Berthelot-Lorentz combining rules apply [37]. This classification scheme also requires knowledge of the type of phase behaviour exhibited by the binary subsystems, based on Van Konynenburg and Scott classification [31]. The eight types of ternary phase behaviour, classified by Bluma and Deiters [37], as defined by their constituting binary subsystems, are illustrated in Figure 21 [28, 37].

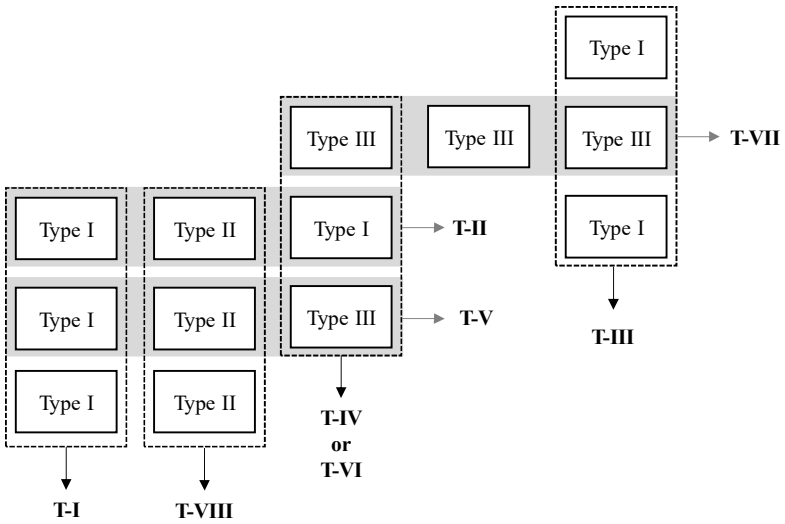

Figure 21: Ternary classification system developed by Bluma and Deiters [37] based on the type of phase behaviour exhibited by binary subsystems [31]. Diagram adapted from [28].

Although there has been limited success in finding a system to classify the phase behaviour of all ternary mixtures, the complex phase equilibria phenomena which occur in ternary mixtures has been well defined. Investigation into these phenomena is of industrial importance as they occur within the temperature, pressure and composition ranges at which super- and near-critical technology is operated [38]. In this section, the complex phase equilibria phenomena referred to as co-solvency and miscibility windows will be discussed, as it has been detected in CO_2 + 1-alcohol + n-alkane systems [38].

Co-solvency is the phenomena where the solubility of a mixture in the solvent is greater than the solubility of either of the pure constituent components in the solvent [13]. An isothermal co-solvency effect (ΔP_{min}) can numerically be defined by Equation 3.3 [36].

$$\Delta P_{min} = P^c_{AC} - P^c_{ABC,min} \quad \text{with } P^c_{AC} < P^c_{AB} \qquad [3.3]$$

Where, P^c_{AC} is the lowest binary critical pressure and $P^c_{ABC,min}$ is the pressure minimum of the isothermal ternary critical line [36].

The definition of isothermal co-solvency is visually depicted in the isothermal P- x_A^{red} cross section, presented in Figure 22 [36]. An isobaric co-solvency effect can be defined in a similar manner [36].

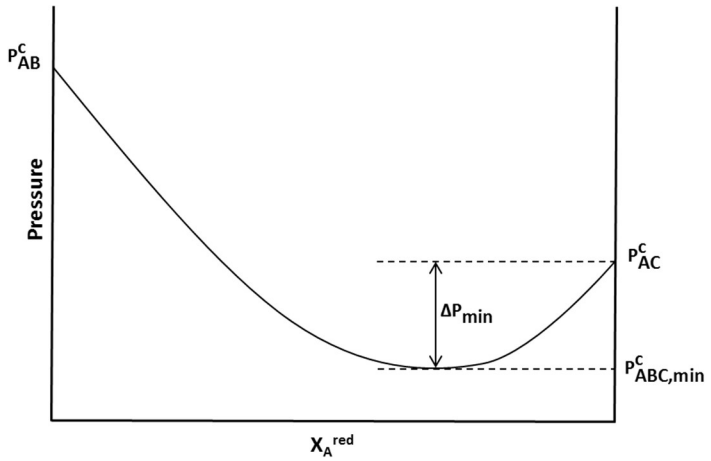

Figure 22: Isothermal P- x_A^{red} cross section of a P-T- x_A^{red} phase cube constructed at constant solvent mass fraction, used to visually illustrate the definition of co-solvency (Adapted from [36])

Under certain conditions, co-solvency can result in the formation of a miscibility window [35]. If this occurs, isobaric cross-sections taken between $P^c_{ABC,min}$and P^c_{AC}, will contain a closed one-phase loop which is surrounded by heterogeneous states. This loop is referred to as an isobaric miscibility window. Isothermal miscibility windows can be defined in a similar manner [35].

In order to visually illustrate the concept of a miscibility window, a ternary phase prism, depicting the formation of a miscibility window at constant pressure, is presented in Figure 23. When analysing Figure 23 it is seen that at high and low temperatures, the two two-phase regions are merged. The co-solvency effect however narrows the band connecting these two regions until it disintegrates into two separate two-phase regions at intermediate temperatures. The two-phase regions terminate in ternary critical points and by connecting these points an oval critical loop, known as a miscibility window, is formed. Miscibility windows are important as they indicate the possibility of altering the miscibility of a system by simply changing the composition [29]. It is also possible that an immiscible region can form in a

ternary system where all the subsystems are completely miscible. This region is referred to as a miscibility island [29].

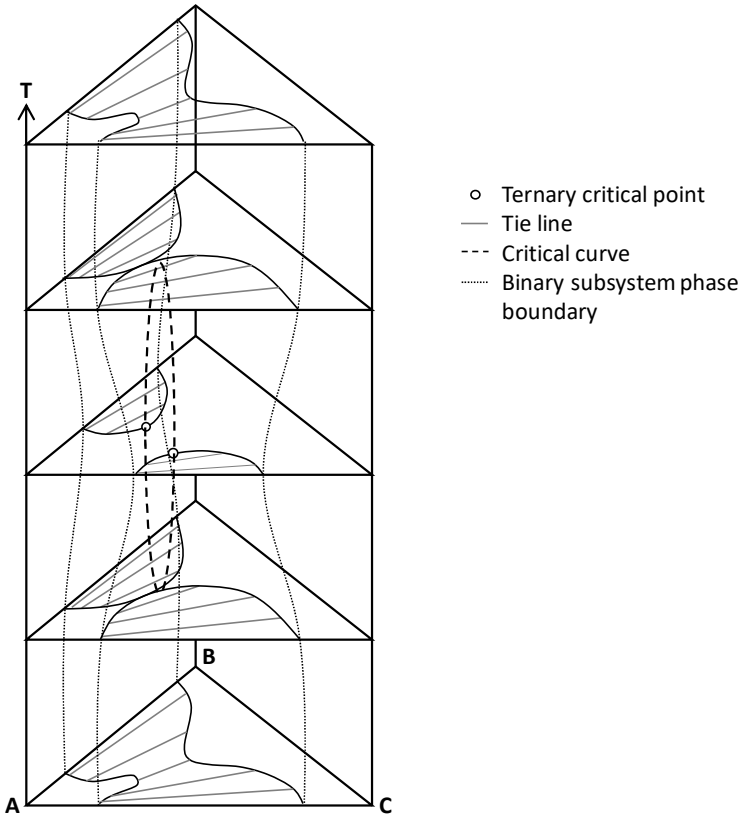

Figure 23: Isobaric ternary phase prism for a system in which the co-solvency effect results in the formation of a miscibility window (Adapted from [29])

Table 4 contains refences to studies which have detected co-solvency and related phenomena in CO_2 + 1-alcohol + n-alkane systems. From these studies it was deduced that when defining m and n as the carbon numbers of the 1-alcohol and n-alkane, respectively, co-solvency effects are most prominent in systems if $n \approx m + (7 \text{ to } 8)$ [38]. Furthermore, it was found that co-solvency effects tend to increase as the chain lengths of the n-alkanes and 1-alcohol decrease [38]. Thus far, the most distinct co-solvency effect (ΔP_{min}=14 MPa) was found in the CO_2 + 1-octanol + hexadecane system at 298 K [38].

Table 4: Occurrence of complex phase behaviour phenomena in systems containing CO_2 + 1-alcohol + alkane* systems studied by Kordikowski and Schneider [39], Phöler, et al., [40] and Scheidgen and Schneider [36].

System CO_2 +…	Ref	m	n	Co-solvency (●), Island system (■)	Closed miscibility windows, isobaric (●), isothermal (■)
1-dodecanol + tetracosane	[39]	12	24	-	-
1-dodecanol + eicosane	[39]	12	20	●	●
1-dodecanol + nonadecane	[39]	12	19	●	●/■
1-dodecanol + hexadecane	[39]	12	16	●	●
1-undecanol + octadecane	[40]	11	18	●	●
1-decanol + heptadecane	[40]	10	17	●	●
1-decanol + tetradecane	[36]	10	14	●	●
1-nonanol + hexadecane	[40]	9	16	●	●
1-nonanol + pentadecane	[40]	9	15	●	●
1-octanol + hexadecane	[36]	8	16	●	●
1-heptanol + pentadecane	[36]	7	15	●	●/■
1-hexanol + pentadecane	[36]	6	15	●	●
1-hexanol + tetradecane	[36]	6	14	●	-

*Number of the carbon atoms of the 1-alcohol (m) and 1-alkane (n)

3.1.4 Phase behaviour and phase diagrams for quaternary systems

When applying the Gibbs phase rule to a system containing four components and considering that there must be at least one phase present, the maximum degrees of freedom for a quaternary system is five. Therefore, a five-dimensional pressure-temperature-composition (P-T-x_A-x_B-x_C) phase diagram is required to represent all the equilibrium states of a quaternary system. Five-dimensional diagrams are however essentially impossible to construct and visualise and therefore quaternary VLE data are generally presented numerically [34]. The VLE data measured in this work will be tabulated and a relative solubility analysis will be performed to further evaluate the measured data.

3.2 Methods available to generate high pressure phase behaviour data

High pressure phase behaviour data can be generated through thermodynamic modelling or by conducting high pressure experiments [41]. Developing thermodynamic models to generate

high pressure data is not a trivial task, as mixtures containing a supercritical solvent exhibit highly non-ideal phase behaviour, particularly in the mixture critical region [41, 42]. Literature indicates that due to the difficulty to develop accurate thermodynamic models, experimental measurements are currently the preferred method to generate phase behaviour data [42]. Experimental measurements are however costly and time consuming and therefore the development of accurate thermodynamic models is gaining more attention [43]. In this study, both of these approaches are used and therefore this section provides background on the experimental methods and thermodynamic models which are available to generate high phase pressure behaviour data.

3.2.1 Experimental methods used to measure high pressure phase equilibrium data

There exist various methods for the measurement of high pressure phase equilibrium data. Depending on how the composition of the co-existing phases is determined, these methods can broadly be classified as either analytic methods or synthetic methods. These two main groups can be further sub-categorised, as seen in Figure 24. A brief overview of the analytic and synthetic methods is provided here, for more information the reader is referred to the work presented by Dohrn, et al. [15].

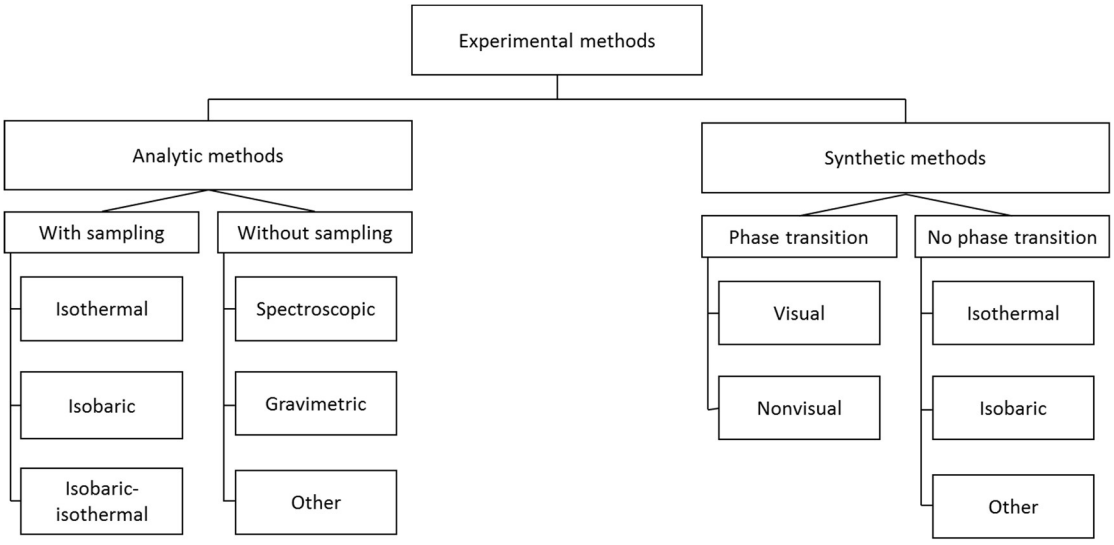

Figure 24: Classification of experimental methods (Adapted from [15])

3.2.1.1 Analytical methods

A method is classified as analytic, if the composition of the co-existing phases is determined using analytic techniques. A further distinction can be made between the different analytic

methods, based on whether or not sampling is required to determine the composition of the co-existing phases [15].

If an analytic method utilises sampling, the composition of the co-existing phases is analysed outside of the equilibrium cell, usually at atmospheric pressure conditions. A drawback of sampling methods, is that sampling can cause a pressure drop which in turn influences the phase equilibrium. Methods to reduce the pressure drop includes among others, using a variable volume cell, blocking off the sampling volume, using capillaries to withdraw samples and directly coupling the sampling valves to the analytic equipment [15].

Analytic methods which do not rely on sampling, use physiochemical methods to determine the composition of the co-existing phases. When using this approach, the composition of the phases is determined inside the pressurised equilibrium cell and therefore all problems pertaining to sampling is avoided. The physiochemical methods which are mainly used are spectroscopic and gravimetric methods [15].

The main advantage of analytic methods is that they can easily be used to measure VLE data for systems containing more than two components, as the composition of all the phases are analysed [15]. An analytic setup with sampling was therefore used in this work to measure VLE data for the quaternary system. The time-consuming measuring procedure and intricate nature of the equipment, however, limited the number of data points which could be measured.

3.2.1.2 Synthetic methods

Synthetic methods are based on the concept of synthesising a mixture of known composition and measuring equilibrium properties such as temperature and pressure. These methods can be divided into sub-classes based on whether a phase transition occurs or not [15].

In synthetic methods with a phase transition, the temperature and pressure of the system is initially set so that the mixture exists as a single phase. The phase transition point is then determined by slowly adjusting the temperature or pressure until a second phase starts to form. The phase transition point can be detected using visual or non-visual methods [15].

In synthetic methods where there is no phase transition, equilibrium properties such as temperature, pressure and density are measured and material balances are used to calculate the phase compositions. These methods can be classified as isothermal, isobaric and other synthetic methods [15].

Advantages of synthetic methods include quick and simple operating procedures and relatively inexpensive equipment when compared to analytical methods. Synthetic methods can also be used when analytic methods are not applicable, for example when the similarity in densities of co-existing phases complicates phase separation. A disadvantage of synthetic methods is that it does not provide a composition analysis of all the co-existing phases and therefore the use thereof to generate VLE data is restricted to binary systems [15]. Synthetic methods can however be used to generate bubble- and dew-point data for multi-component systems. A synthetic method with phase transition was therefore used to measure bubble- and dew-point data for the ternary and quaternary systems investigated in this work.

3.2.2 Thermodynamic modelling of high pressure phase equilibrium data

There exist various thermodynamic models and the reason for the large variety stems from the fact that to date, no single model is capable of predicting the phase behaviour of all the different systems. This section will provide general background regarding the concept of phase equilibria, classic cubic equations of state, combining of cubic equation of state models with Gibbs excess energy models (EoS/G^E) and more advanced equations of state. The section will conclude with a model selection section, where the models which are to be investigated in this work, along with the reason for their selection will be discussed. This section will therefore address Objective 3, more specifically sub-objective 3.1, as outlined in Chapter 1.

3.2.2.1 Phase equilibria

The criterion for phase equilibrium dictates that at constant temperature and pressure, different phases are in equilibrium if the chemical potential (μ) of each component is the same in all the phases [30]. Therefore, for a system at constant pressure and temperature with $\prod$ phases, equilibrium is attained if [30]:

$$\mu_i^{\alpha} = \mu_i^{\beta} = \cdots = \mu_i^{\pi} \qquad (i = 1, 2, \ldots n) \qquad [3.4]$$

Due to undesirable property characteristics associated with the chemical potential of a component the concept of fugacity (*f*) was introduced [30]. Fugacity can be seen as the 'inclination' of a molecule to move from one phase to another [44] and it is measured in units of pressure [30]. It can be shown that a system at constant temperature and pressure with $\prod$ phases is at equilibrium if the following holds true [44]:

$$f_i^{\alpha} = f_i^{\beta} = \cdots = f_i^{\pi} \qquad (i = 1, 2, \ldots n) \qquad [3.5]$$

When considering VLE ($\prod = 2$), the fugacity of a component in the vapour phase can be related to temperature, pressure and composition through the introduction of the fugacity coefficient (ϕ), defined in Equation 3.6, which can be calculated using an equation of state model [45].

$$\phi_i^v = \frac{f_i^v}{y_i P} \qquad [3.6]$$

The fugacity of a component in the liquid phase can be calculated using either the equation of state or activity coefficient approach. If the equation of state approach is used, the fugacity coefficient, defined in Equation 3.6 (based on liquid phase composition (x_i)), is used [45]. If the activity coefficient approach is used, the fugacity of the component is related to the activity coefficient (γ) through Equation 3.7 [30]. The activity coefficient can be calculated using activity coefficient models such as the Wilson [46], NRTL (non-random-two-liquid) [47], UNIQUAC (universal quasi-chemical) models [48], amongst others [45].

$$\gamma_i = \frac{f_i^l}{x_i f_i} \qquad [3.7]$$

Where f_i refers to the fugacity of an ideal solution which can be calculated using the following equation [30].

$$f_i = \phi_i^{sat} P_i^{sat} \exp\left[\frac{v_i^l (P - P_i^{sat})}{RT}\right] \qquad [3.8]$$

When considering Equation 3.5 and using the equation of state approach (Equation 3.6) to determine the fugacity of both phases, referred to as the phi-phi approach, the criterion for VLE is as follows [44].

$$\phi_i^v y_i = \phi_i^l x_i \qquad [3.9]$$

If the equation of state approach is used to determine the fugacity of the vapour phase and the activity coefficient approach is used to determine the fugacity of the liquid phase (Equation 3.7), referred to as the gamma-phi approach, the criterion for VLE is as follows [44].

$$\phi_i^v y_i P = \gamma_i x_i \phi_i^{sat} P_i^{sat} \exp\left[\frac{v_i^l (P - P_i^{sat})}{RT}\right] \quad [3.10]$$

In this work the phi-phi approach is used as equation of state based models will be employed to perform vapour and liquid phase calculations.

3.2.2.2 Classic cubic equations of state models

According to literature [44, 49, 50], classic cubic equations of state are well suited to model high pressure phase behaviour. The first cubic equation of state developed to predict vapour-liquid phase equilibria, was the van der Waals equation [51]. The van der Waals equation, presented in Equation 3.11, was developed by modifying the ideal gas law to account for repulsive and attractive forces between molecules [30].

$$P = \frac{RT}{v - b} - \frac{a}{v^2} \quad \text{with} \quad a = 0.421875 \frac{(RT_c)^2}{P_c}; \; b = 0.125 \frac{RT_c}{P_c} \quad [3.11]$$

In Equation 3.11, parameters a and b are substance specific parameters [30]. Parameter a, referred to as the energy parameter, accounts for the effect of the attractive forces between molecules. Parameter b, referred to as the co-volume parameter, accounts for the size of the molecules and it was derived based on the hard sphere model [51].

Throughout the years various studies have been conducted to improve the accuracy of the van der Waals equation [51]. Some of the most well-known cubic equations of state, namely the Redlich-Kwong [52], Soave-Redlich-Kwong [53] and Peng-Robinson equations [54] of state, were developed by modifying the van der Waals equation. Literature [44, 55] indicates that the Soave-Redlich-Kwong (SRK) and Peng-Robinson (PR) equations are the most widely used thermodynamic models for process design in the petroleum and chemical industries. To date, they are still the primary choice of models for petrochemicals, gas processing and air separation [44, 55], despite more advanced equation of state models being available.

In order to extend these cubic equations of state to mixtures, a set of mixing rules are required. The most commonly used mixing rules are the quadratic van der Waals one-fluid mixing rules, presented below [50, 56].

$$a = \sum_i \sum_j x_i x_j \sqrt{a_{ii} a_{jj}} \left(1 - k_{a,ij}\right) \quad [3.12]$$

$$b = \sum_i \sum_j x_i x_j \frac{(b_{ii} + b_{jj})}{2} \left(1 - k_{b,ij}\right) \quad [3.13]$$

3.2.2.3 EoS/G^E mixing rules for cubic equations of state

Although cubic equation of state models with classic mixing rules are generally well suited to represent high pressure phase behaviour, they are often incapable of representing the phase behaviour of systems containing highly polar and/or hydrogen bonding compounds [44, 56, 57]. Investigation into alternative mixing rules to extend the applicability of cubic equations of state, particularly mixing rules derived from excess Gibbs energy (g^E) expressions (activity coefficient models), has therefore gained much attention [57]. These mixing rules allow the inclusion of a term for excess Gibbs energy in the cubic equation of state [44]. Models derived through the combination of a cubic equation of state (most often the SRK or PR models [58]) and an excess Gibbs energy model are referred to as EoS/G^E models [44]. An EoS/G^E model thus combines the strengths of a cubic equation of state model with an activity coefficient model, thereby providing a single model which is capable of predicting high and low pressure phase equilibrium data for polar and non-polar mixtures. The advantage gained by combining these models is illustrated in a simplified manner in Figure 25 [44].

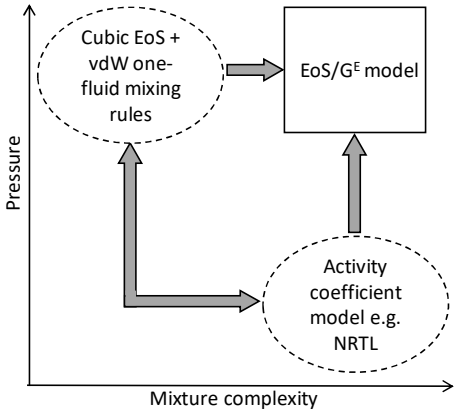

Figure 25: Simple illustration of how EoS/G^E models combine strengths of the cubic equations of state and activity coefficient models (Adapted from [44])

Most EoS/G^E models are derived by equating the excess Gibbs energies of the equation of state and the activity coefficient models, as shown below [44].

$$\left(\frac{g^E}{RT}\right)_{P^{ref}}^{EoS} = \left(\frac{g^E}{RT}\right)_{P^{ref}}^{activity\ coefficient\ model^*} \quad [3.14]$$

In Equation 3.14, P^{ref} is the reference pressure at which the excess Gibbs energies are equated. This reference pressure can be infinite pressure, as is used for the Huron-Vidal [59] and Wong-Sadler models [60] or zero pressure used for the modified Huron-Vidal (MHV2) [61] and the

predictive SRK (PRSK) [62] models [44, 58]. The specific activity coefficient models* referred to in Equation 3.14 can be the Wilson [46], NRTL, [47], UNIQUAC [48] and UNIFAC (UNIQAC Functional-group Activity Coefficients) [63] models, amongst others. Cubic equations of state models coupled with the UNIFAC model is however of particular interest as these EoS/G^E models are purely predictive [57].

3.2.2.4 Advanced equations of state models

Due to difficulty to predict phase equilibrium data for systems containing hydrogen bonding compounds, more advanced (higher-order) equation of state models, based on statistical mechanics, have been developed [64, 65]. Among them, the Statistical Associating Fluid Theory (SAFT) model [66, 67], based on Wertheim's perturbation theory [68, 69, 70, 71], and a variation thereof, namely the Perturbed Chain-SAFT (PC-SAFT) [72], are the most widely used and have been incorporated in commercial process simulators [65]. Previous studies [14, 28] have however found that when modelling the high pressure phase behaviour of systems containing CO_2 and detergent range alkanes and alcohols in Aspen Plus®, the PC-SAFT model is generally outperformed by the cubic equations of state models. Due to this finding, the SAFT and PC-SAFT models in Aspen Plus® will not be investigated in this work, as similar results are expected. Another advanced model, namely the Cubic-Plus-Association (CPA) model, has however newly been added to the Aspen Plus® (v8.8) database. This model combines the simplicity of a cubic equation of state (SRK) with a term to account for association, taken from SAFT [73]. The CPA model has previously been applied to model systems containing CO_2 with alkanes and/or alcohols [74, 75, 76, 77, 78] and it will therefore be considered in this work.

3.2.2.5 Model selection

The thermodynamic models investigated in this work are the basic Soave-Redlich-Kwong (RK-SOAVE), Redlich-Kwong-ASPEN (RK-ASPEN), Cubic-Plus-Association (CPA) and Predictive-Soave-Redlich-Kwong (PSRK) models.

The reason for selecting these models is that they are all based on one of the most widely used equations of state, namely the SRK equation of state [44, 55], but they differ with regards to mixing rules and approaches to accounting for solute interactions. Models based on the SRK equation of state were investigated rather than models based on the Peng-Robinson (PR)

equation of state, as there are more variations of the SRK model available in the Aspen Plus® software. Furthermore, only the SRK variation of the CPA model is available in Aspen Plus® and no other PR based models which can account for association are available in the software. Models based on the SRK equation of state have also been shown to better describe the phase behaviour modelled in this work than models based on the PR equation of state [5, 14].

The RK-ASPEN model allows the incorporation of one polar parameter in the mixing rules, which could account for the solute-solute interactions between the components. Previous studies [5, 14, 28] have also shown that this model is well suited to predict data for mixtures containing CO_2 with detergent range alkanes and alcohols. The PSRK model is a predictive model based on UNIFAC parameters regressed from low pressure VLE data. The model allows the incorporation of three polar parameters (Mathias-Copeman constants) [62]. The model has also been adapted for asymmetric systems [79], making it well suited for modelling supercritical systems which consist of a light gas with long chain alkanes. An initial thermodynamic model screening procedure for the modelling of systems containing CO_2 with detergent range alkanes and alcohols, conducted by Zamudio [5], indicated that the PSRK model showed promise, but development of the model was beyond the scope of the study. The CPA model does not explicitly account for polarity or quadrupole moments [73], but incorporates an association term, which in turn accounts for hydrogen bonding. To the authors' knowledge this model has not been employed to predict phase behaviour data for the ternary and quaternary systems investigated in this work.

The four models investigated in this work range from a simple version of the SRK model (RK-SOAVE) to the more complex versions and comparison of these models will allow investigation into which model is best suited to generate phase equilibrium data for the system investigated in this work. Furthermore, comparison of the performance of the models will also allow investigation into how the modelling results of a predictive model using low pressure UNIFAC parameters (PSRK) compares to the other models which are fitted using high pressure data. Comparison of the models fitted using two different data types, namely high pressure bubble- and dew-point (HPBDP) and vapour-liquid-equilibrium (HPVLE) data, will allow investigation into how model accuracy is affected by using different data types to fit the model. This will also indicate whether using HPBDP data, which is easier, faster and cheaper to generate than HPVLE data, can be used to model phase equilibrium (bubble- and dew-point and VLE) data for the system considered in this work.

3.3 Outcome of this chapter

This chapter provides the basic principles required to construct and interpret phase diagrams and it also highlights some of the complex phase behaviour which can occur in high pressure systems. In addition to this, the chapter provides background on the various techniques which are available to measure high pressure phase equilibrium data and highlights which methods will be used in this work, namely:

- Synthetic method with phase transition to measure bubble- and dew-point data
- Analytic method with sampling to measure VLE data

The chapter also provides background regarding the modelling of phase equilibrium data and Objective 3, specifically sub-objective 3.1, is addressed as the thermodynamic models used to model the phase equilibrium data in this work is identified. The four models which are to be investigated are as follows:

- Soave-Redlich-Kwong (RK-SOAVE) model
- Redlich-Kwong-ASPEN (RK-ASPEN) model
- Cubic-Plus-Association (CPA) model
- Predictive-Soave-Redlich-Kwong (PSRK) model

The principles introduced in this chapter are integral in the understanding of the following chapters in which the high phase behaviour data measured for systems containing CO_2 with detergent range alkanes and alcohols is analysed, discussed and modelled.

4. PUBLISHED PHASE BEHAVIOUR DATA FOR RELEVANT BINARY, TERNARY AND MULTI-COMPONENT SYSTEMS

This chapter summarises and discusses the literature data, available in reputable journals, for binary, ternary and multi-component systems containing supercritical CO_2 with n-dodecane, 1-decanol and 3,7-dimethyl-1-octanol. The aim of this chapter is to establish the extent of research that has been done for these systems and to determine the type of phase behaviour phenomena which can occur in these systems. This chapter also identifies whether additional phase behaviour measurements are required.

4.1 Published binary phase behaviour data

The phase equilibrium data published for binary systems containing CO_2 with n-dodecane, 1-decanol or 3,7-dimethyl-1-octanol, is summarised in Table 5. The consistency of the available data for each system, as well as phase behaviour trends identified in the previous work, is discussed in the subsequent sections.

Table 5: Summary of the published data for the binary systems CO_2 + n-dodecane, CO_2 + 1-decanol and CO_2 + 3,7-dimethyl-1-octanol

Solute	Type of data	Pressure Range (MPa)	Temperature Range (K)	Source
n-dodecane	Bubble-and dew-point	7.9 – 14.3	313 – 343	Nieuwoudt & Rand, 2002 [80]
	Bubble-and dew-point	6.4 – 15.2	308 – 348	Zamudio, 2014 [5]
	VLE	1.0 – 8.9	318	Gardeler, et al., 2002 [81]
	Solubility	0.1	298 – 318	Hayduk, et al., 1972 [82]
	LLVE*	2.0 – 2.9	254 – 268	Hottovy, et al., 1981 [83]
	Pressure-Temperature	8 – 14.4	266.8 – 289.7	Schneider, 1966 [84]
	Liquid Composition	0.01 – 81.8	313 – 393	Henni, et al., 1996 [85]

Table 5 (continued): Summary of the published data for the binary systems CO_2 + n-dodecane, CO_2 + 1-decanol and CO_2 + 3,7-dimethyl-1-octanol

Solute	Type of data	Pressure Range (MPa)	Temperature Range (K)	Source
1-decanol	VLE	7 – 19	348.2 – 453.2	Weng, et al., 1994 [86]
	VLE	2.1 – 15.2	308.1 – 328.2	Chang, et al., 1998 [87]
	VLE	1 – 5	348.2 – 453.2	Lee & Chen, 1994 [88]
	VLE	0.3 – 20.1	357.3 – 422.1	Gardeler & Gmehling, 2004 [89]
	VLE	7.6 – 39.8	308 – 348	Zamudio, 2014 [5]
	LLVE*	3.2 – 7.8	270.5 – 307.2	Lam, et al., 1990 [90]
	Solubility	0.1	284 – 313.5	Wilcock, et al., 1978 [91]
	VLE	16 – 19	313.2 – 343.2	Pöhler, 1994 [92]
	Pressure-Temperature	21.1 – 97.1	305.1 – 393.6	Scheidgen, 1997 [93]
	Vapour composition	9 – 18	323	Ghaziaskar, et al., 2005 [94]
	Liquid Composition	1.9 – 15.1	303 – 343	Ioniță, et al., 2013 [95]
	Liquid Composition	0.01 – 3.2	271 – 279.6	Patton & Luks, 1994 [96]
3,7-dimethl-1-octanol	VLE	7.5 – 17.9	308 – 348	Zamudio, 2014 [5]

*LLVE = Liquid-Liquid-Vapour Equilibria

4.1.1 Binary system: CO_2 + n-dodecane

The consistency of the literature data, measured within the temperature (308 K – 358 K) and pressure (up to 30 MPa) range applicable to this work, was evaluated by comparing the data obtained from the different sources. In Figure 26, two isothermal pressure-composition diagrams were constructed to accommodate the different temperatures at which the data were measured. Furthermore, from Figure 26 it is noted that the data presented by Zamudio [5] is used for comparison in both pressure-composition diagrams. This is because the pressure-

temperature correlations, presented by Zamudio [5], can be used to adjust the data to any temperature between 308 K and 348 K. When analysing the diagrams in Figure 26, it can be concluded that there is generally a good correlation between the data obtained from the different sources and therefore the literature data is deemed reliable.

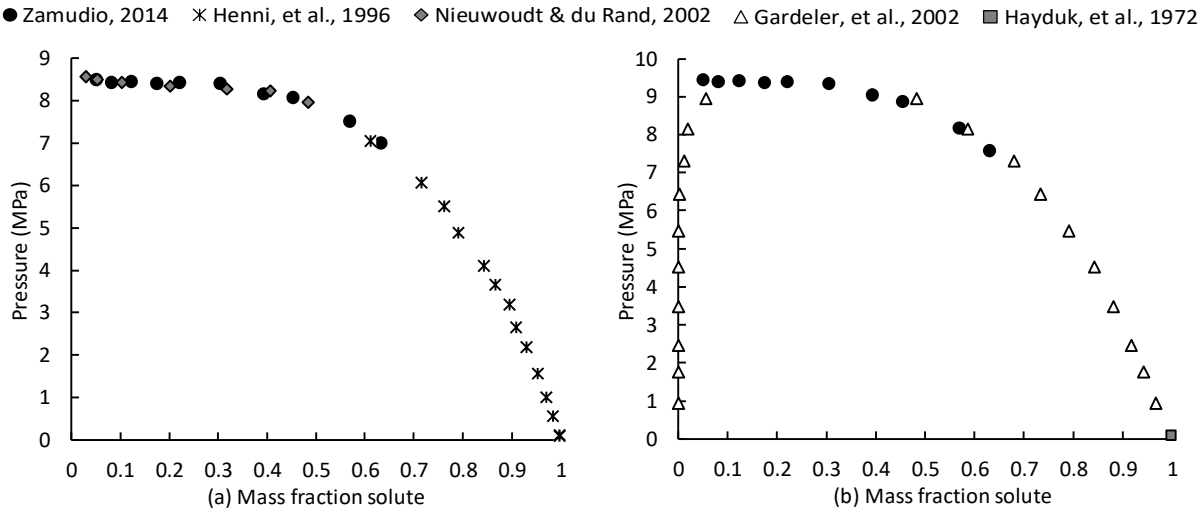

Figure 26: Pressure-composition diagrams comparing the phase behaviour data of the CO_2 + n-dodecane system obtained from different literature sources at: (a) 313 K and (b) 318 K.

Analysis of the phase behaviour presented by the different sources did not reveal deviations from the general expected trend which dictates that an increase in temperature results in an increase in phase transition pressure. The study by Zamudio [5] did however find that the phase behaviour measured at 308 K indicates the possibility of a three-phase region occurring at low solute mass fractions. This study also speculated that the phase behaviour of the CO_2 + n-dodecane system could be classified as type II, but stated that more data would be required to confirm the type [5]. The classification type suspected by Zamudio [5] was found to be in agreement with literature, which reported that binary systems consisting of CO_2 with C7 to C12 n-alkanes display type II phase behaviour [32, 97].

4.1.2 Binary system: CO_2 + 1-decanol

The literature data available for the CO_2 + 1-decanol system, measured within the temperature and pressure range considered in this work, are compared in Figure 27. The pressure-composition diagrams, presented in Figure 27, were constructed at three different temperatures to accommodate the different temperatures at which the literature data were measured. Unfortunately, the data presented by Gardeler & Gmehling [89] could not be compared as the temperature at which the data were measured was outside the temperature range of the other

studies and the pressure-temperature correlations presented by Zamudio [5] are not suited for extrapolation. The trends presented by Gardeler & Gmehling [89] are however consistent with literature and if other data at 357 K were available it would likely be comparable. The data presented by Wilcock, et al., [91] is also not compared in Figure 27, as Wilcock , et al., [91] only measured one solubility point at a pressure of 0.1 MPa and solute mass fraction of 0.998, which is outside the composition range investigated by Zamudio [5], the only source which reported data at the same temperature as Wilcock , et al., [91]. The point measured by Wilcock, et al., [91] is however consistent with the general phase behaviour trend depicted in Figure 27 (as the solute mass fraction approaches 1, pressure approaches 0 MPa [87, 88, 95]).

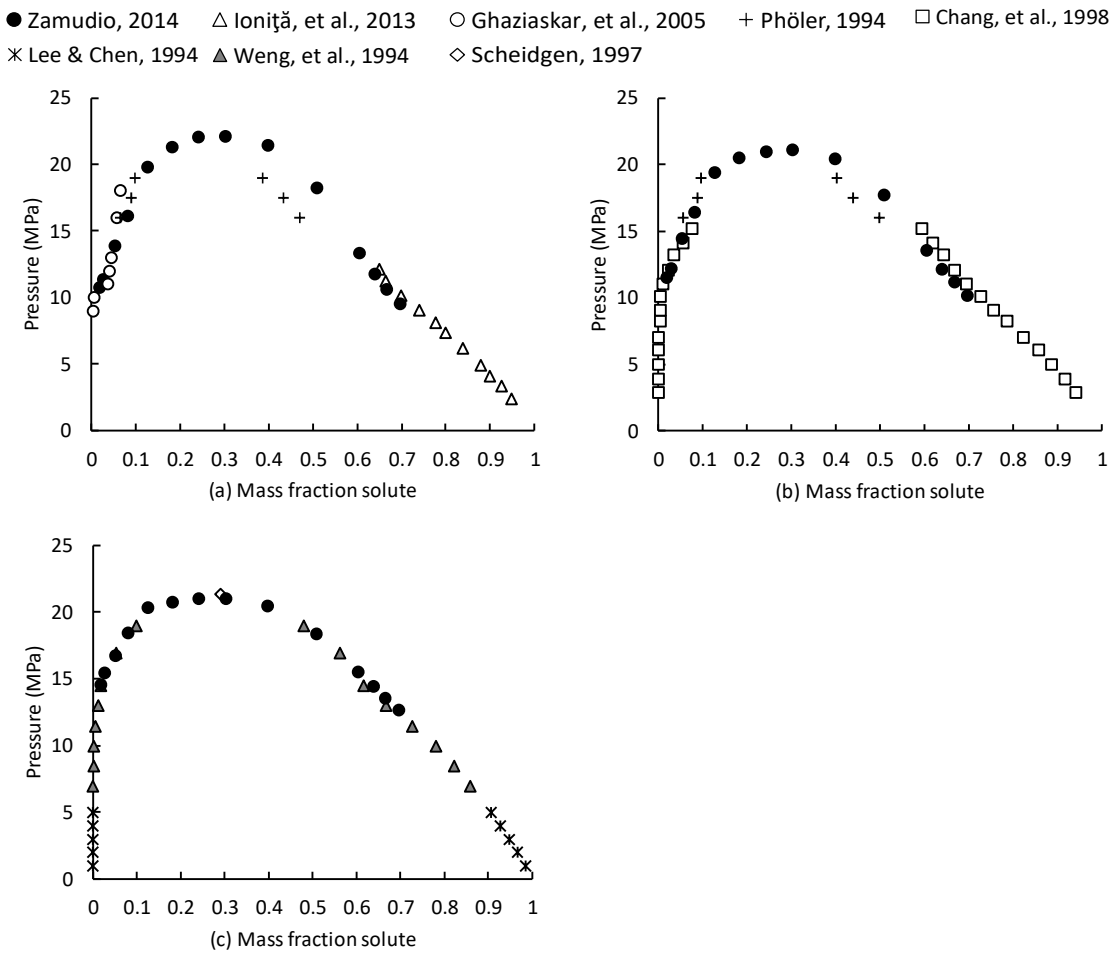

Figure 27: Pressure-composition diagrams comparing the phase behaviour data of the CO_2 + 1-decanol system obtained from different literature sources at: (a) 323, (b) 328 K and (c) 348 K

Comparison of the data sets in Figure 27 reveals that the data obtained from the different sources generally correlate fairly well. The only significant deviation is observed in the high solute concentration region, where the data presented by Phöler [40] deviates from the data measured by Zamudio [5]. The data measured by Zamudio [5] in this region is however in agreement with the other sources, creating doubt in the data presented by Phöler [40]. A study

by Schwarz [33] raised similar concerns regarding the data presented by Phöler [40]. Furthermore, although the data measured by Ghaziaskar, et al., [94] generally corresponds to the other data sets, there is a small discrepancy between the data measured by Ghaziaskar, et al., [94] at solute mass fraction above 0.1 and other sources. This was also detected by Schwarz [33] and can likely be explained by the method used by Ghaziaskar, et al., [94]. Based on the correlation of the data and explanation of the deviations, it can be concluded that sufficient reliable literature data exists for this system.

Phase behaviour analyses performed by Zamudio [5], Ioniţă, et al., [95] and Scheidgen [93] found that the CO_2 + 1-decanol system exhibits type III phase behaviour. This is in accordance with findings presented by Schwarz [33], which states that CO_2 + 1-alcohol systems with carbon numbers from 8 to 14 exhibit type III phase behaviour. Zamudio [5] also found that between 1-decanol mass fractions of 0.07 and 0.64, the CO_2 + 1-decanol system exhibits a temperature inversion. The data presented by Ioniţă, et al., [95] also suggests the occurrence of a temperature inversion. A temperature inversion is the phenomenon where the phase behaviour of a system contradicts the normal phase behaviour trends with regards to temperature [98]. Normal phase behaviour dictates that an increase in temperature results in a decrease in solubility (increase in phase transition pressures). The presence of a temperature inversion is therefore noted if there is a region where the solubility of a system increases (lower phase transition pressures) with an increase in temperature. According to literature, temperature inversions are a common occurrence for CO_2 + 1-alcohol systems [5, 33, 93]. Pressure-temperature curves of CO_2 + 1-alcohol systems, measured by Scheidgen [93], are presented in Figure 28, to illustrate the effect of a temperature inversion.

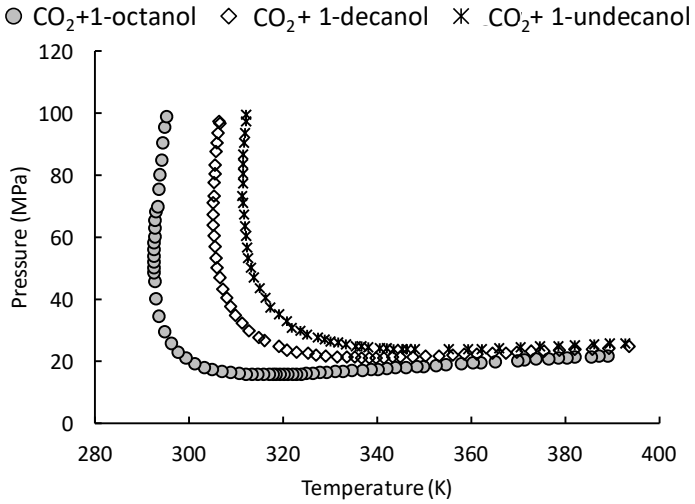

Figure 28: Pressure-temperature diagrams for CO_2 + 1-octanol, CO_2 + 1-decanol and CO_2 + undecanol systems constructed with data obtained from Scheidgen [93]

When analysing points on the CO_2 + 1-decanol [93] curve at 310 K and 340 K one would expect to see the that the solubility pressure at 340 K is higher than the pressure at 310 K, according to the normal phase behaviour trend. This is however not the case, as at 310 K the solubility pressure (≈35 MPa) is higher than at 340 K (≈21 MPa), due to the temperature inversion. It is proposed that strong solute-solvent and solute-solute interactions could likely explain the occurrence of a temperature inversion. Zamudio [5] suggests that in primary linear alcohols the hydroxyl group forms multimer hydrogen bonds which results in a more compact alcohol structure [99]. At low temperatures, high pressures are required to form a homogenous phase as the kinetic energy of the alcohol molecules cannot overcome the multimer bonds. An increase in temperature results in an increase in the kinetic energy of the alcohol molecules, which in turn increases the ease with which the CO_2 molecules can disrupt the multimer bonds and therefore lower pressure is required to form a homogenous mixture. Once the kinetic energy of the alcohol molecules overcome the multimer bonds, the normal phase behaviour resumes [5]. A similar theory regarding the occurrence of a temperature inversion in CO_2 + 1-alcohol systems is postulated by Schwarz [33].

4.1.3 Binary system: CO_2 + 3,7-dimethyl-1-octanol

The phase behaviour for the CO_2 + 3,7-dimethyl-1-octanol system is the least researched, with only one study reporting phase behaviour data for the system. Due to the lack of data, the phase behaviour data presented by Zamudio [5] for the CO_2 + 3,7-dimethyl-1-octanol system cannot be verified. The data is however assumed to be reliable as the data obtained from this study for the CO_2 + n-dodecane and CO_2 + 1-decanol systems were found to be consistent with other literature sources, as discussed in sections 4.1.1 and 4.1.2.

The phase behaviour analysis performed by Zamudio [5] for the CO_2 + 3,7-dimethyl-1-octanol system did not reveal any unexpected trends. Furthermore, the study could also not classify the type of phase behaviour exhibited by this system.

4.2 Published ternary phase behaviour data

The bubble- and dew-point and VLE data published for ternary systems containing CO_2 with n-dodecane, 1-decanol, 3,7-dimethyl-1-octanol, are summarised in Table 6. It is noted that data for the ternary subsystems are limited. Furthermore, due to the fact that the composition of the mixtures investigated in each study differs, the consistency of the data could not be compared

by comparing the different data sets, as was done in section 4.1. Each of the studies did however verify their method and results and therefore the data is deemed reliable. In the subsequent sections the phase behaviour trends identified in these studies will be discussed.

Table 6: Summary of the published data for the ternary systems CO_2 + n-dodecane + 1-decanol, CO_2 + n-dodecane + 3,7-dimethyl-1-octanol and CO_2 + 1-decanol + 3,7-dimethyl-1-octanol

Mixture CO_2 +	Type of data	Pressure Range (MPa)	Temperature Range (K)	Source
n-dodecane + 1-decanol	Bubble- and dew-point	6.3 – 29.7	308 – 348	Zamudio, 2014 [5]
	Bubble- and dew-point	6.4 – 17	308 – 348	Smith & Schwarz, 2015 [13]
	VLE	6.8 – 20	308 – 348	Fourie, 2018 [14]
n-dodecane + 3,7-dimethyl-1-octanol	Bubble- and dew-point	6.3 – 29.67	308 – 348	Zamudio, 2014 [5]
	VLE	6.8 – 15.7	308 – 348	Fourie, 2018 [14]
1-decanol + 3,7-dimethyl-1octanol	Bubble- and dew-point	6.3 – 29.67	308 – 348	Zamudio, 2014 [5]
	VLE	6.8 – 23.7	308 – 348	Fourie, 2018 [14]

4.2.1 Ternary system: CO_2 + n-dodecane + 1-decanol

The study by Zamudio [5] was the first to evaluate the phase behaviour of a ternary mixture containing CO_2, n-dodecane and 1-decanol. Zamudio [5] however only investigated the phase behaviour of a ternary mixture rich in 1-decanol (0.778 mass fraction 1-decanol). Due to the large quantity of 1-decanol, the phase behaviour of the ternary mixture exhibited a temperature inversion, which is a prominent feature of the CO_2 + 1-decanol system. The temperature and composition range of the temperature inversion present in the ternary system was however found to be smaller compared to that of the CO_2 + 1-decanol system. Furthermore, the presence of n-dodecane in the mixture was also found to significantly lower the phase transition pressure compared to the CO_2 + 1-decanol system. This was stated to be due to the fact that the non-polar n-dodecane disrupts the multimer formation of the alcohol molecules [5].

In order to further investigate the phase behaviour of this system, Smith & Schwarz [13] measured the phase behaviour of three mixtures containing CO_2 with 1-decanol and n-dodecane. The mixtures were prepared so the 1-decanol mass fraction in each was 0.10, 0.20 and 0.60. The results obtained from the study found that although the 1-decanol rich mixture showed indications of a temperature inversion, the phase behaviour of the mixture was dominated by the presence of n-dodecane [13]. This agrees with the results obtained by Zamudio [5]. Furthermore, the results for systems rich in n-dodecane revealed that co-solvency is likely to occur, but that it is not a prominent characteristic [13].

Fourie [14] measured VLE data for three mixtures containing CO_2 with n-dodecane and 1-decanol. The mixtures were prepared so that the 1-decanol mass fraction in each was 0.25, 0.50 and 0.75. Analysis of the data revealed the occurrence of co-solvency in mixtures consisting mainly of n-dodecane. This finding agrees with the results presented by Smith & Schwarz [13] and Zamudio [5]. In addition, Fourie [14] also reported that a density inversion, also known as a barotropic phenomenon, occurred in certain mixtures at low temperatures and high pressures. Fourie [14] also investigated the fractionation sharpness of the components by calculating the relative solubility, defined as follows [21]:

$$\alpha_{i,j} = \frac{\left(\frac{y_i}{x_i}\right)}{\left(\frac{y_i}{x_i}\right)} \qquad [4.1]$$

Where y and x represent the vapour and liquid fractions of solutes i and j, respectively. In order to achieve separation, relative solubility values should be higher than 1.05 or lower than 0.95 [28]. Impractical/ineffective separation is attained at values closer to 1.00 [100]. The relative solubility results obtained by Fourie [14] revealed that within the composition and temperature range of the study, n-dodecane and 1-decanol can be separated using CO_2 as solvent. Fourie [14] however also found that separability decreases with an increase in bulk n-dodecane content. Based on this and the identified co-solvency in the system, it can be postulated that separation might be more difficult for mixtures containing more than 75 wt% n-dodecane.

4.2.2 Ternary system: CO_2 + n-dodecane + 3,7-dimethyl-1-octanol

The phase behaviour of the ternary system containing CO_2 with n-dodecane and 3,7-dimethyl-1-octanol was investigated in two separate studies. In the first study, conducted by Zamudio [5], the phase behaviour of a mixture rich in n-dodecane (0.667 mass fraction n-dodecane) was investigated. The results of this study revealed signs of a three-phase region at 308 K and low

solute mass fractions. Due to the fact that the mixture mainly consisted of n-dodecane and that the binary system of CO_2 + n-dodecane also showed an indication of a three-phase region, the occurrence was deemed possible. Further investigation into the phase behaviour revealed the mixture to be co-solvent, as the mixture displayed a higher solubility in supercritical CO_2 than either of the pure components [5].

In the second study, conducted by Fourie [14], the VLE data of three mixtures containing CO_2 with n-dodecane and 3,7-dimethyl-1-octanol were measured. The mixtures were prepared so the n-dodecane mass fraction in each was 0.25, 0.50 and 0.75. The results obtained from this study also indicated co-solvency in mixtures consisting mainly of n-dodecane, but no reference was made to a possible three phase region [14]. Fourie [14] also investigated the fractionation sharpness of the components by calculating the relative solubility, using Equation 4.1. The results indicated that n-dodecane and 3,7-dimethyl-1-octanol can be separated in the mixtures containing 0.25 and 0.50 mass fraction n-dodecane, but in the system containing 0.75 mass fraction n-dodecane separation is ineffective when using CO_2 as solvent. The ineffective separation of the components in the n-dodecane rich, co-solvent mixture is in agreement with the results for the CO_2+ n-dodecane + 1-decanol system discussed previously.

4.2.3 Ternary system: CO_2 + 1-decanol + 3,7-dimethyl-1-octanol

Zamudio [5] investigated the phase behaviour of the CO_2 + 1-decanol + 3,7-dimethyl-1-octanol system by measuring the bubble- and dew-point data for a mixture containing 0.875 mass fraction 1-decanol. The study found that the ternary mixture exhibited a temperature inversion with similar temperature and pressure ranges to the temperature inversion observed for the CO_2 + 1-decanol system. Furthermore, it was noted that the phase transition pressures of the ternary system were similar to that of the CO_2 + 1-decanol system. The similarity in the phase transition pressure was stated to be due to the fact that 3,7-dimethyl-1-octanol does not disrupt the formation of multimers by the 1-decanol molecules, instead it contributes to multimer formation as it is also a polar molecule with a hydroxyl group in a prominent position [5].

Fourie [14] measured VLE data for three mixtures containing CO_2 with 1-decanol and 3,7-dimethyl-1-octanol. The mixtures were prepared so the 1-decanol mass fraction in each was 0.25, 0.50 and 0.75. Similar to the CO_2 + n-dodecane + 1-decanol system, a density inversion also occurred in certain mixtures at low temperatures and high pressures. Fourie [14] also

investigated the fractionation sharpness of the components by calculating the relative solubility, using Equation 4.1. The results indicated that the two alcohols can be separated within the ranges investigated, but the relative solubility values were close to 1, indicating less effective separation.

4.3 Published multi-component phase behaviour data

The literature review on published data revealed only one study that investigated the phase behaviour of multi-component mixtures containing CO_2 with n-dodecane, 3,7-dimethyl-1-octanol and 1-decanol. The study, conducted by Zamudio [5], measured bubble- and dew-point data for a mixture consisting of 20 wt% n-dodecane + 10 wt% 3,7-dimethyl-1-octanol + 70 wt% 1-decanol, at temperatures between 308 K and 348 K and with pressures ranging from 6.3 MPa to 15.6 MPa. The study did not provide an in-depth analysis of phase behaviour, but it was noted that the phase behaviour exhibited a temperature inversion, which was to be expected as the system mainly consisted of 1-decanol [5].

No published VLE data was found for the quaternary systems containing CO_2 with n-dodecane, 3,7-dimethyl-1-octanol and 1-decanol.

4.4 Published phase behaviour data for the solute + solute systems

To the author's knowledge, no data has been published for the 1-decanol + n-dodecane, 1-decanol + 3,7-dimethyl-1-octanol or n-dodecane + 3,7-dimethyl-1-octanol systems [101, 102]. Due to the high boiling points of the components (that is 489.2 K for n-dodecane, 504.1 K for 1-decanol and 498.7 K for 3,7-dimethyl-1-octanol [16]), phase equilibrium data for these systems must be measured at sub-atmospheric pressures [28]. Furthermore, to measure phase equilibrium data for the analysis of the interactions which occur in these systems within the temperature range considered in this work (308 K – 358 K), very low pressures are required. Measuring of low pressure phase equilibrium data is however beyond the scope of this study. Furthermore, the results obtained from Ferreira [28] suggests that low pressure data does not significantly contribute to high pressure phase equilibrium analysis or modelling.

4.5 Outcome of this chapter

In this chapter, a literature review was conducted to establish the amount of published data available for systems containing CO_2 with n-dodecane, 1-decanol and 3,7-dimethyl-1-octanol

and to determine the type of phase behaviour phenomena which has been reported for these systems.

The following conclusions can be drawn from the literature review:

- Mixtures containing large amounts of 1-decanol generally exhibit signs of a temperature inversion [5, 13].
- Mixtures consisting largely of n-dodecane are likely to be co-solvent and can possibly exhibit a three-phase region at low temperature and solute mass fractions [5, 13, 103].
- Co-solvency which occurs in n-dodecane rich mixtures could lead to more difficult separation and even pinches in separation.
- There is sufficient binary phase behaviour data available for analysis and modelling purposes.
- Although there exists sufficient bubble- and dew-point data for the CO_2 + n-dodecane + 1-decanol system, the amount of bubble- and dew-point data available for the CO_2 + n-dodecane + 3,7-dimethyl-1-octanol and CO_2 + 1-decanol + 3,7-dimethyl-1-octanol systems is inadequate.
- Sufficient VLE data exists for all three ternary systems.
- There is a lack of bubble- and dew-point as well as VLE data for the quaternary system.

In order to address the lack of phase behaviour data identified in this chapter, the following additional data were measured:

- Bubble- and dew-point for the CO_2 + n-dodecane + 3,7-dimethyl-1-octanol system
- Bubble- and dew-point for the CO_2 + 1-decanol + 3,7-dimethyl-1-octanol system
- Bubble- and dew-point and VLE data for the quaternary system

The measured bubble- and dew-point and VLE data, along with details regarding the methods used to measure the data are provided in the subsequent chapters.

5. EXPERIMENTAL BUBBLE- AND DEW-POINT DATA

The simplest approach to characterising the solute-solute interactions which exist in mixtures comprising of CO_2, n-dodecane, 3,7-dimethyl-1-octanol and 1-decanol is by evaluating bubble- and dew-point data for mixtures containing these components. Due to a lack of published bubble- and dew-point data, as discussed in Chapter 4, additional bubble- and dew-point data were required to thoroughly analyse and model the phase behaviour of the ternary CO_2 + n-dodecane + 3,7-dimethyl-1-octanol and CO_2 + 1-decanol + 3,7-dimethyl-1-octanol systems as well as the quaternary CO_2 + n-dodecane + 3,7-dimethyl-1-octanol + 1-decanol system.

Due to time constraints, only the bubble- and dew-point data for the quaternary system could be measured in this study. The bubble- and dew-point data for the other two systems however formed an integral part of the work presented in this study and therefore the data for the two ternary systems were internally generated by well-trained, competent undergraduate BEng (Chemical) students. The bubble- and dew-point data for the ternary CO_2 + n-dodecane + 3,7-dimethyl-1-octanol system was measured by Ms. N.S. Mabena and the data for the ternary CO_2 + 3,7-dimethyl-1-octanol +1-decanol system was measured by Mr. N. Schonegevel. The analysis of the ternary bubble- and dew-point data however formed part of this study and is the work of the current author.

The aim of this chapter is to (i) provide details on the experimental method used to measure the bubble- and dew-point data of the ternary and quaternary systems and to (ii) present and (iii) analyse the phase behaviour of these systems. This chapter therefore addresses Objective 1, as it presents bubble- and dew-point data, generated to address a lack of literature data and it also provides an analysis of the data to determine the effect of the solute-solute interactions on the solubility of the mixtures.

5.1 Methodology

The ternary and quaternary bubble- and dew-point data presented in this chapter were generated using the same method. A brief overview of this method is given by providing details regarding the experimental setup, the experimental procedure followed, the equipment calibration and accuracy, the materials used and the data processing steps required. This section will also evaluate the validity of the experimental data obtained using this method.

5.1.1 Experimental setup

The bubble- and dew-point data presented in this study were measured using the synthetic visual phase detection method. The experiments were conducted using two previously constructed variable volume view cells. The design and operating procedures of these two cells are similar, with the main difference between them being their size. The internal volume of the larger cell is 80 cm^3, whilst that of the smaller cell is only 45 cm^3. Both cells have been designed to withstand operating temperatures and pressures up to 473 K and 27.5 MPa, respectively [10, 104]. A schematic of the basic design of the cells is presented in Figure 29 [105].

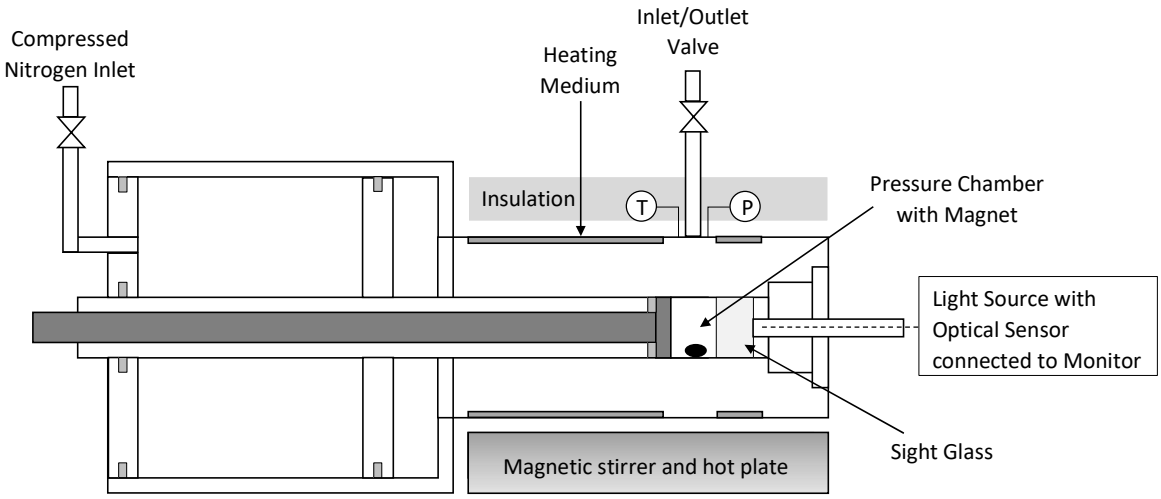

Figure 29: Schematic illustrating the basic design of a variable volume view cell (Adapted from [105])

It is seen that the design of these cells is based on a movable piston-cylinder setup [10]. The pressure within the cells are controlled by adjusting the position of the piston and the temperature is regulated by means of a heating jacket through which a heating medium is circulated [105]. The pressure and temperature within the cells are measured using ONEhalf20 pressure transducers and 4-wire-Pt-100-probes, respectively [13]. In order to maintain a homogenous mixture within the cells, a magnetic stirrer is used and to reduce heat losses the cells are insulated. An optical sensor with a light source is used to project the cell content onto a monitor in order to visually detect the phase transition [105]. For more details regarding the design of these variable volume view cells, the reader is referred to work done by Schwarz [33] and Fourie, et al. [104].

5.1.2 Experimental procedure

The experimental procedure consists of three separate parts namely loading the cell, measuring the data and unloading the cell.

During the loading procedure, a known amount of solute is added to the cell, along with a magnetic stirrer bar. The cell is then securely closed, evacuated and flushed with CO_2. Thereafter, a known amount of CO_2 is loaded [105]. Once the cell is loaded, the heating bath is set to the first temperature, the magnetic stirrer is turned on and the cell content is pressurised to the one-phase region [104].

Once thermal equilibrium is reached, the measuring procedure can commence. During this procedure, the phase transition is visually detected by slowly reducing the pressure in the cell until a second phase starts to form. At this transition point the pressure and temperature is recorded. The cell content is then re-pressurised to the one-phase region and the process is repeated until the phase transition pressure is accurately determined to within 0.02 MPa. After establishing the phase transition pressure, the heating bath is set to the next temperature and the cell content is again pressurised to the one-phase region. This procedure is repeated at each set temperature [104].

Once the measuring procedure has been completed, the cell must be unloaded and cleaned. During the unloading procedure, the CO_2 is vented to the atmosphere and the solute is collected and discarded in the appropriate waste container. The cell is then cleaned by rinsing it with isopropanol and methanol [104].

Further details regarding the experimental procedure and safety requirements which need to be considered when performing the experiments are provided in Appendix A.

5.1.3 Equipment calibration and accuracy

The accuracy of data obtained through experimental work is always affected by human error and equipment faults. In this work, human errors mainly include solute and solvent losses whilst loading the cell and mistakes made when visually determining the phase transition. Equipment faults refer to the inaccuracy of the measuring equipment. The effect of equipment inaccuracies can partially be accounted for through calibration. The pressure transmitter was therefore calibrated using a dead weigh tester and the calibration data is presented in Appendix A. The Pt100 probe was calibrated by Thermon South Africa (Pty) Ltd., which is a South African National Accreditation System (SANAS) approved institute and the calibration certificate and correlations developed using the calibration data are provided in Appendix A.

Based on the uncertainty analysis method presented by Schwarz & Nieuwoudt [105], the work done by Smith & Schwarz [13] and the most recent calibration data gathered, the measurement uncertainties in this work has been determined to be as follows:

- Based on the calibration certificate, the standard uncertainty in temperature is deemed to be better than 0.1 K (i.e. u(T) = 0.1) over the temperature range of interest.
- Accounting for inaccuracies when visually detecting the phase transition pressure (0.05 MPa), and considering the accuracy of the calibration curves and hysteresis effects (0.02 MPa), the standard uncertainty in pressure is deemed to be better than 0.07 MPa (i.e. u(P) = 0.07) [13, 105].
- Based on the accuracy of the balances, the maximum relative uncertainty in mass fraction is deemed to be 0.01 of the mass fraction value (i.e. u(x) = 0.01x) [105].

5.1.4 Materials used

The materials used in the experiments, along with their CAS number, supplier information and purity data are presented in Table 7. The purity of the components listed in Table 7 was verified using GC analysis and all the components were used without further purification.

Table 7: Purity data and supplier information of the materials used in experiments

Material	CAS number	Supplier	Product number	Purity
1-decanol	112-30-1	Sigma-Aldrich	150584	>99%
n-dodecane	112-40-3	Sigma-Aldrich	297879	>99%
3,7-dimethyl-1-octanol	106-21-8	Sigma-Aldrich	W239100	>98%
CO_2	124-38-9	Air Products	K243C	99.995%

5.1.5 Temperature correction of the data

Due to changes in ambient conditions, slight differences between the set point temperatures and actual measurement temperatures are inevitable [13, 104]. In order to generate isothermal data, pressure-temperature correlations at constant composition were therefore fitted to the experimental data [10]. This method has been used by various studies [33, 106, 107, 108] and from literature it was found that generally, linear correlations are adequate to describe the pressure-temperature relationship [10, 13, 43, 104]. Linear correlation curves were therefore initially fitted to the pressure-temperature data. The predictions made by the linear correlations were then analysed using the acceptance criteria presented below and if the predictions violated

any of the criteria a higher order polynomial correlation was used [13]. Higher order polynomials were particularly required for systems containing CO_2 + 1-decanol, in order to capture the curvature of the solubility curve resulting from the temperature inversion. To ensure that sufficient data were available to fit these higher order polynomials, bubble- and dew-point data for systems containing 1-decanol were measured at six temperatures (308 K – 358 K), whereas data for systems which did not contain 1-decanol were only measured at five temperatures (308 K – 348 K).

$$R^2 > 0.98 \quad [5.1]$$

$$\left|P_{predicted} - P_{measured}\right| = 0.2\ MPa \quad [5.2]$$

$$\frac{\left|P_{predicted} - P_{measured}\right|}{P_{measured}}\ x\ 100 \leq 2\% \quad [5.3]$$

5.1.6 Validation of experimental data

In order to validate the results presented in this section, the reproducibility of the data and the accuracy of the experimental method was investigated.

Reproducibility

Since the data presented in this section was measured by different operators, the reproducibility of each data set was analysed separately. In addition to investigating the reproducibility of the data, this approach will also determine whether the data measured by the different operators is reliable. The reproducibility of each data set was evaluated by repeating an experiment under different ambient conditions and with a slight change in composition and the results are presented in Figures 30 to 32.

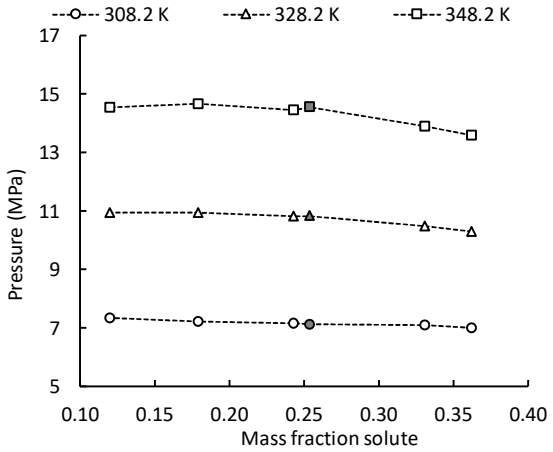

Figure 30: Pressure-composition diagram comparing the phase transition pressures measured at solute mass fractions of 0.243 and 0.254 for the system CO_2 + (85% n-dodecane + 15% 3,7-dimethyl-1-octanol), with the grey filled marker illustrating the repeated experiment

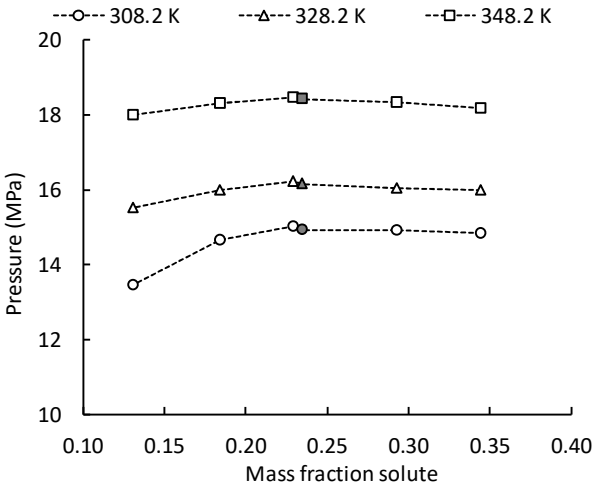

Figure 31: Pressure-composition diagram comparing the phase transition pressures measured at solute mass fractions of 0.229 and 0.235 for the system CO_2 + (25% 1-decanol + 75% 3,7-dimethyl-1-octanol), with the grey filled marker illustrating the repeated experiment

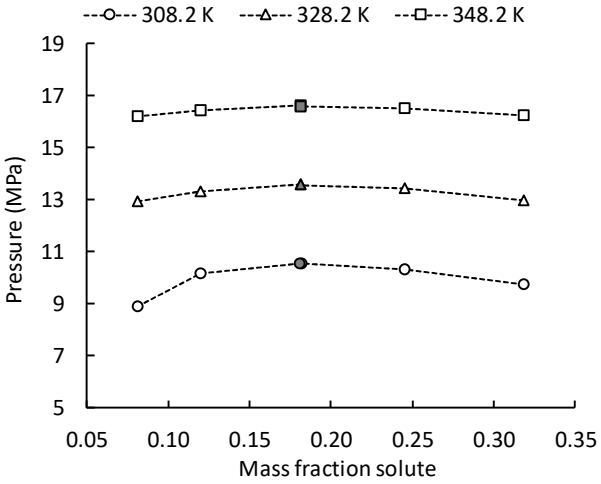

Figure 32: Pressure-composition diagram comparing the phase transition pressures measured at solute mass fractions of 0.181 and 0.182 for the system CO_2 + (33.3% n-dodecane + 33.3% 1-decanol + 33.3% 3,7-dimethyl-1-octanol), with the grey filled marker illustrating the repeated experiment

When analysing Figures 30 to 32 it is noted that there is generally a good correlation between the repeated measurements, with only slight deviations in pressure. The small pressure differences are within the measurement accuracy and therefore it can be concluded that the bubble- and dew-point data presented in this study is reproducible and that the data sets measured by the different operators are reliable.

Verification of the experimental method

Generally, the accuracy of the experimental method is investigated by comparing data measured using the method to literature data. Due to the fact that the compositions of the mixtures investigated in this study differs from that measured in literature, this approach could

not be followed. Literature however shows that the experimental method used in this work has been verified in several previous studies [5, 104, 105]. Based on this, the experimental method employed in this work is deemed accurate.

5.2 Results for the CO_2 + n-dodecane + 3,7-dimethyl-1-octanol system

The aim of the experimental work conducted for the system containing CO_2 with n-dodecane (nC_{12}) and 3,7-dimethyl-1-octanol (37DM1O) was to evaluate the effect of solute-solute interactions on the solubility of the system and to determine whether the system exhibits complex phase behaviour, with particular focus on the occurrence of co-solvency. The motivation for focussing on co-solvency stems from the fact that previous studies conducted for the CO_2 + n-dodecane + 3,7-dimethyl-1-octanol system reported the of occurrence of this phenomena [5, 103]. The experimental work conducted in this study therefore serves to expand this finding by conducting supplementary bubble- and dew-point experiments to generate data within the co-solvency region.

According to literature, n-dodecane rich mixtures are likely to exhibit co-solvency and therefore bubble- and dew-point data for mixtures containing large amounts of n-dodecane were measured [5, 103]. The specific solute ratios of the three mixtures investigated are as follows:

- Mixture 1: 50 wt% n-dodecane + 50 wt% 3,7-dimethyl-1-octanol
- Mixture 2: 75 wt% n-dodecane + 25 wt% 3,7-dimethyl-1-octanol
- Mixture 3: 85 wt% n-dodecane + 15 wt% 3,7-dimethyl-1-octanol

The data for each of the mixtures were measured between 308 K and 348 K with total solute mass fractions ranging between 0.625 and 0.016. The experimental data were measured by Ms. N.S. Mabena, but all data processing and interpretation thereof is the work of the current author. The experimental data are provided in Appendix B.

5.2.1 Isothermal data

The isothermal data generated for the three ternary mixtures, along with the pressure-temperature correlations used to generate the data, are presented in Tables 8 to 10.

Table 8: Isothermal data and pressure-temperature correlations for Mixture 1 consisting of CO_2 + (50 wt% n-dodecane + 50 wt % 3,7-dimethyl-1-octanol)

Mass Fraction Solute (g/g)	Pressure-Temperature Correlations						Isothermal P-xy Data, with P in MPa				
	$P = A \times T^4 + B \times T^3 + C \times T^2 + D \times T + E$, with P in MPa and T in K						Temperature (K)				
	A	B	C	D	E	R^2	308.2	318.2	328.2	338.2	348.2
0.625	0	0	0	0.12307	-31.426	0.998	6.50	7.73	8.96	10.19	11.42
0.530	0	0	0	0.14469	-37.607	1.000	6.98	8.43	9.87	11.32	12.77
0.453	0	0	0	0.16816	-44.793	1.000	7.03	8.71	10.39	12.07	13.75
0.380	0	0	0	0.18492	-49.974	1.000	7.01	8.86	10.71	12.56	14.41
0.290	0	0	0	0.19653	-53.225	0.999	7.34	9.30	11.27	13.23	15.20
0.235	0	0	0	0.19752	-53.423	0.999	7.44	9.42	11.39	13.37	15.34
0.173	0	0	0	0.19744	-53.373	0.998	7.47	9.44	11.42	13.39	15.37
0.131	0	0	0	0.19021	-50.934	0.996	7.68	9.58	11.48	13.38	15.29
0.0781	0	0	0	0.18117	-48.157	0.997	7.67	9.48	11.29	13.11	14.92
0.0515	0	0	-9.4447E-04	0.78058	-143.293	1.000	7.56	9.45	11.15	12.67	13.99
0.0303	0	0	-1.0319E-03	0.81927	-146.787	1.000	7.69	9.42	10.94	12.26	13.37
0.0158	0	0	-1.5872E-03	1.1574	-198.363	1.000	7.56	9.20	10.51	11.51	12.19

Table 9: Isothermal data and pressure-temperature correlations for Mixture 2 consisting of CO_2 + (75 wt% n-dodecane + 25 wt % 3,7-dimethyl-1-octanol)

Mass Fraction Solute (g/g)	Pressure-Temperature Correlations						Isothermal P-xy Data, with P in MPa				
	$P = A \times T^4 + B \times T^3 + C \times T^2 + D \times T + E$, with P in MPa and T in K						Temperature (K)				
	A	B	C	D	E	R^2	308.2	318.2	328.2	338.2	348.2
0.620	0	0	0	0.11321	-28.555	1.000	6.33	7.46	8.59	9.73	10.86
0.537	0	0	0	0.12738	-32.572	1.000	6.68	7.95	9.23	10.50	11.77
0.448	0	0	0	0.14709	-38.463	1.000	6.86	8.33	9.81	11.28	12.75
0.384	0	0	0	0.16011	-42.331	1.000	7.01	8.61	10.21	11.81	13.41
0.243	0	0	0	0.18409	-49.610	1.000	7.12	8.96	10.80	12.64	14.48
0.197	0	0	0	0.18614	-50.147	0.999	7.21	9.07	10.93	12.79	14.66
0.135	0	0	0	0.18149	-48.609	0.999	7.32	9.13	10.95	12.76	14.58
0.0883	0	0	0	0.17872	-47.688	0.999	7.38	9.17	10.96	12.74	14.53
0.0527	0	0	0	0.16303	-42.599	0.998	7.64	9.27	10.90	12.53	14.16
0.0310	0	0	-1.0583E-03	0.82492	-146.111	1.000	7.60	9.22	10.63	11.83	12.81
0.0155	0	0	-8.2717E-04	0.64432	-112.295	0.998	7.71	8.97	10.07	11.00	11.76

Table 10: Isothermal data and pressure-temperature correlations for Mixture 3 consisting of CO_2 + (85 wt% n-dodecane + 15 wt % 3,7-dimethyl-1-octanol)

Mass Fraction Solute (g/g)	Pressure-Temperature Correlations						Isothermal P-xy Data, with P in MPa				
	$P = A \times T^4 + B \times T^3 + C \times T^2 + D \times T + E$, with P in MPa and T in K						Temperature (K)				
	A	B	C	D	E	R^2	308.2	318.2	328.2	338.2	348.2
0.573	0	0	0	0.11004	-27.603	0.999	6.30	7.40	8.51	9.61	10.71
0.493	0	0	0	0.13640	-35.292	1.000	6.74	8.10	9.47	10.83	12.19
0.363	0	0	0	0.16431	-43.626	1.000	7.01	8.65	10.29	11.94	13.58
0.331	0	0	0	0.17016	-45.353	0.999	7.08	8.78	10.49	12.19	13.89
0.254	0	0	0	0.18553	-50.059	1.000	7.11	8.97	10.82	12.68	14.53
0.243	0	0	0	0.18237	-49.040	0.999	7.16	8.98	10.80	12.63	14.45
0.179	0	0	0	0.18545	-49.920	1.000	7.22	9.08	10.93	12.79	14.64
0.120	0	0	0	0.17975	-48.046	0.999	7.34	9.14	10.94	12.74	14.54
0.0901	0	0	0	0.17942	-47.950	0.999	7.34	9.13	10.93	12.72	14.52
0.0468	0	0	0	0.15094	-38.928	0.998	7.58	9.09	10.60	12.11	13.62
0.0169	0	0	-1.1034E-03	0.82892	-143.029	0.999	7.63	9.01	10.16	11.10	11.82

5.2.2 Effect of temperature

The effect of temperature on the phase behaviour was analysed by constructing pressure-composition diagrams for the three mixtures investigated. It was determined that the phase behaviour of all three mixtures conformed to the normal trend, where an increase in temperature results in an increase in phase transition pressure. In order to illustrate this, the pressure-composition diagrams constructed for Mixtures 1 and 3 are presented in Figure 33.

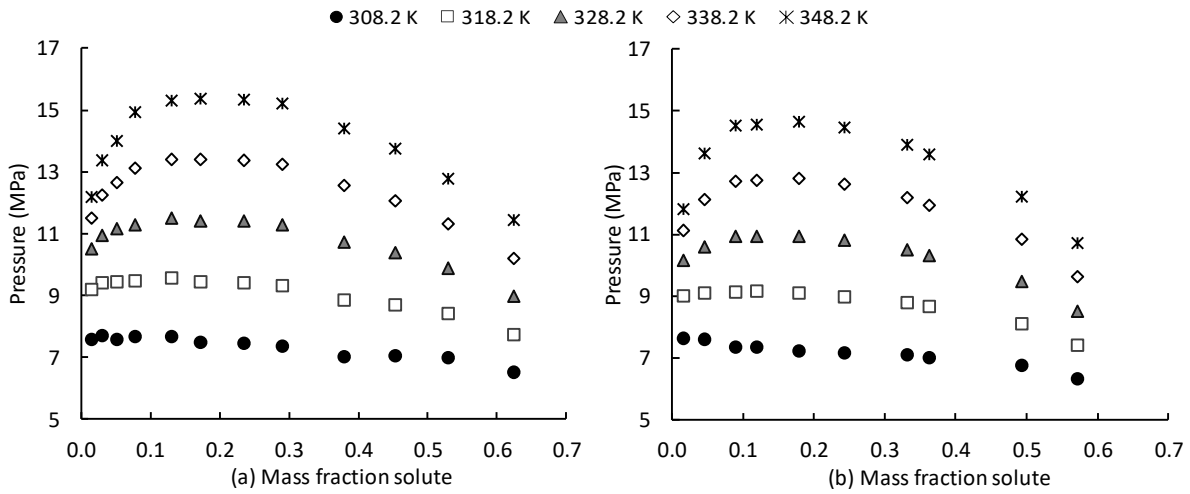

Figure 33: Pressure-composition diagrams illustrating the phase behaviour of (a) Mixture 1: 50 wt% nC_{12} + 50 wt% 37DM1O and (b) Mixture 3: 85 wt% nC_{12} + 15 wt% 37DM1O

5.2.3 Effect of solute composition

In order to evaluate the effect of solute composition on phase transition pressure, three-dimensional P-x_s-x_A^{red} phase cubes were constructed at different temperatures within the temperature range investigated.

Figure 34 and 35 illustrate the P-x_s-x_A^{red} diagrams constructed at 308 K and 348 K, respectively. In these diagrams, the phase transition pressure (P) is plotted against the mass fraction total solute (x_s) at different mixture compositions [13, 98]. The compositions of the different mixtures are represented by the reduced n-dodecane mass fraction (x_A^{red}), which is mathematically defined as $x_A^{red} \equiv \frac{x_A}{x_A + x_B}$, where A refers to n-dodecane and B refers to 3,7-dimethyl-1-octanol. The boundary conditions where $x_A^{red} = 0$ and $x_A^{red} = 1$, represent the phase behaviour of the binary systems CO_2 + 3,7-dimethyl-1-octanol and CO_2 + n-dodecane, respectively and this data, along with data at $x_A^{red} = 0.667$, were sourced from literature [5].

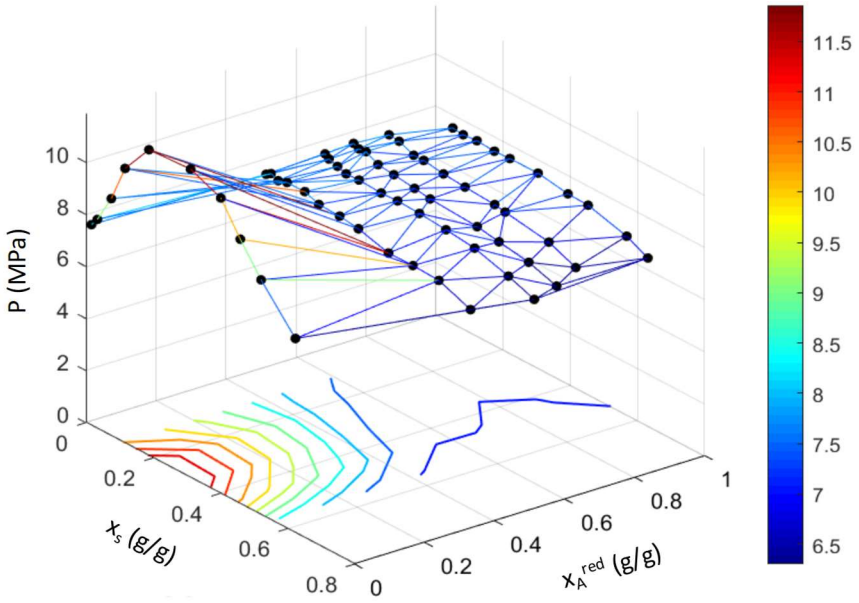

Figure 34: Ternary phase cube where phase transition pressure (P) is plotted as a function of total solute mass fraction (x_s) and reduced n-dodecane mass fraction (x_A^{red}) at 308.2 K. Data at $x_A^{red} = 0$, $x_A^{red} = 0.667$ and $x_A^{red} = 1$ obtained from literature [5].

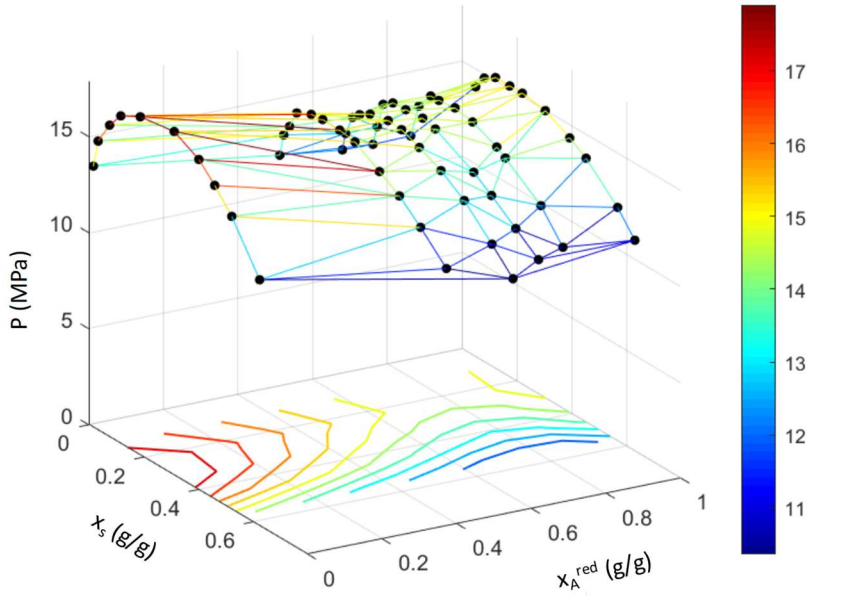

Figure 35: Ternary phase cube where phase transition pressure (P) is plotted as a function of total solute mass fraction (x_s) and reduced n-dodecane mass fraction (x_A^{red}) at 348.2 K. Data at $x_A^{red} = 0$, $x_A^{red} = 0.667$ and $x_A^{red} = 1$ obtained from literature [5].

When analysing Figure 34 and 35, it is noted that the phase transition pressure of the CO_2 + 3,7-dimethyl-1-octanol system ($x_A^{red} = 0$) is always higher than that of the CO_2 + n-dodecane system ($x_A^{red} = 1$). According to Zamudio [5], this can be explained by the increased polarity of 3,7-dimethyl-1-octanol relative to n-dodecane. Zamudio [5] proposes that the polar hydroxyl groups of the 3,7-dimethyl-1-octanol molecules form hydrogen bonded multimers which results in a dense alcohol structure. This alcohol structure is difficult to penetrate and high pressure is required to force CO_2 molecules between the alcohol molecules to dissolve it into

one phase. In contrast to this, the n-dodecane molecules are non-polar and cannot form multimers. Therefore, the CO_2 molecules can more easily gain access to the n-dodecane molecules and thus lower pressure is required for solubility [5]. This theory is supported by a study conducted by Schwarz, et al. [109] which found that polarity influences solubility and concluded that alkanes are more soluble in non-polar solvents than their corresponding alcohols.

Due to the higher solubility of n-dodecane, it is expected that the addition thereof to a mixture will result in a constant linear decrease in phase transition pressure [98]. However, from Figures 34 and 35 it can be seen that although the phase transition pressure does decrease with an increase in n-dodecane (x_A^{red} -> 1), the trend is not linear. This non-linear decrease is due to solute-solute interactions which exists in the mixtures and it is better illustrated in the P-x_A^{red} diagram, presented in Figure 36. The P-x_A^{red} diagram presented in Figure 36, was constructed by combining isothermal P-x_A^{red} sections of the P-x_s-x_A^{red} diagrams at a constant total solute mass fraction (x_s) of 0.5 (the diagram is however representative of the entire solute mass fraction range investigated) [98]. Since the experiments for the different mixtures were not conducted at the exact same solute mass fractions, polynomial pressure-composition curves were fitted to the isothermal data to allow interpolation at specific solute mass fractions [13].

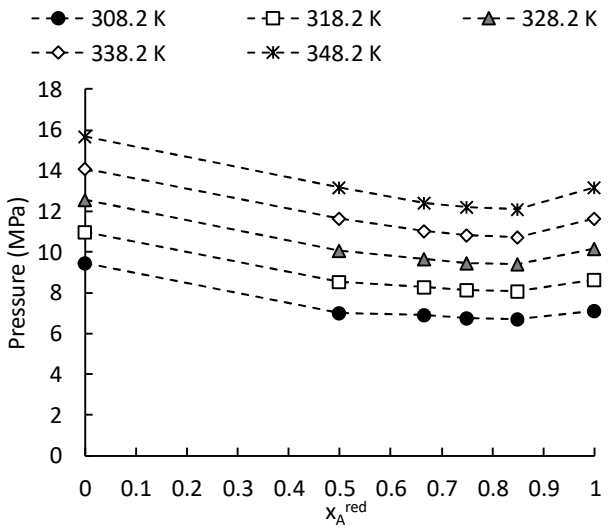

Figure 36: Phase transition pressure plotted as a function of reduced n-dodecane mass fraction (x_A^{red}) at constant total solute mass fraction of 0.5 for temperatures ranging from 308.2 K to 348.2 K. Data at $x_A^{red} = 0$, $x_A^{red} = 0.667$ and $x_A^{red} = 1$ obtained from literature [5].

Analysis of Figure 36 not only illustrates the non-linear decrease in phase transition pressure, but it also reveals a pressure minimum in the isothermal P-x_A^{red} curves. The presence of a

pressure minimum in the curves shows that some mixtures containing n-dodecane and 3,7-dimethyl-1-octanol are more soluble in CO_2 than either of the pure components [98]. This indicates the occurrence of co-solvency, which is caused by specific solute-solute interactions between the molecules in a mixture [5].

5.2.4 Occurrence of co-solvency

In order to determine which of the mixtures investigated in this work (Mixtures 1 to 3) are co-solvent, the phase behaviour of each ternary mixture was compared to the phase behaviour of its constituent binary subsystems at a specific temperature, as shown in Figure 37. The co-solvency which occurs in the system measured by Zamudio [5], containing 66.7 wt% n-dodecane, is also illustrated in this figure.

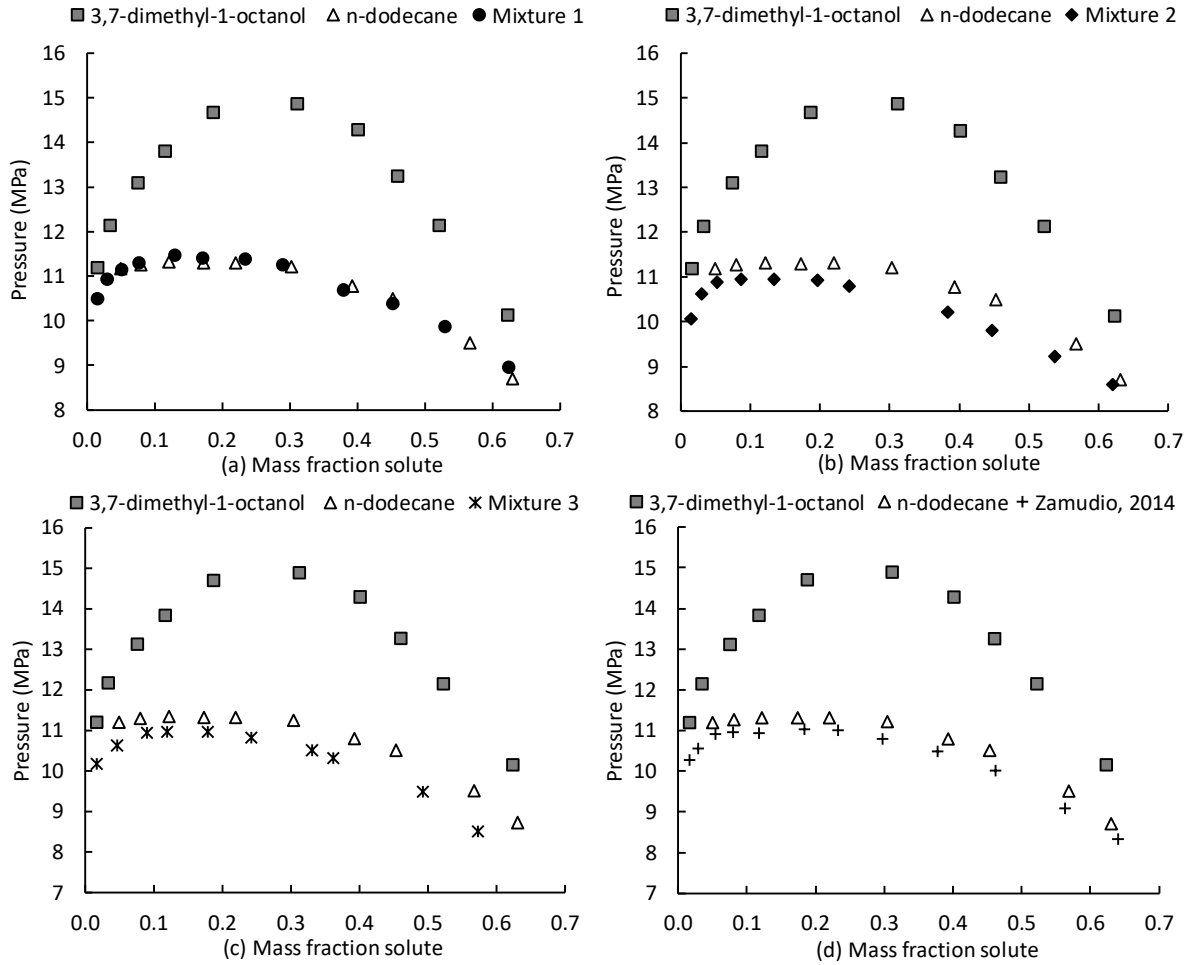

Figure 37: Pressure-composition diagrams comparing the phase behaviour of CO_2 + 3,7-dimethyl-1-octanol [5] and CO_2 + n-dodecane [5] systems at 328.2 K to (a) Mixture 1: 50 wt% nC_{12} + 50 wt% 37DM1O, (b) Mixture 2: 75 wt% nC_{12} + 25 wt% 37DM1O, (c) Mixture 3: 85 wt% nC_{12} + 15 wt% 37DM1O and (d) Zamudio mixture: 66.7 wt% nC_{12} + 33.3 wt% 37DM1O (Zamudio, 2014 [5])

From this analysis, it was found that although the phase transition curve of Mixture 1, presented in Figure 37 (a), closely resembles that of the CO_2 + n-dodecane system, the mixture does not show clear signs of enhanced solubility. On the other hand, the phase transition curves of Mixture 2 and 3, presented in Figure 37 (b) and (c), were found to be located at pressures well below that of comprising binary subsystems, indicating that these mixtures are co-solvent. Seeing as Mixtures 2 and 3 consist of 75 wt% and 85 wt% n-dodecane, respectively, it can be concluded that CO_2 + n-dodecane + 3,7-dimethyl-1-octanol systems consisting largely of n-dodecane are likely to be co-solvent. This agrees with the findings reported by Zamudio [5] and Fourie et al., [103].

The effect of co-solvency can be better illustrated using Gibbs phase diagrams. Since Gibbs phase diagrams are constructed at constant temperature and pressure, interpolation is however required to construct these diagrams. The fitted pressure-composition curves used to construct the P-x_A^{red} diagrams in section 5.2.3 were therefore re-applied, but instead of determining the pressure at a specific composition, the curves were used to determine the composition at a specific pressure. In Figure 38, two Gibbs phase diagrams constructed using this approach are presented. The diagrams in Figure 38 were constructed at a temperature of 348 K and (a) 14.06 MPa and (b) 14.60 MPa.

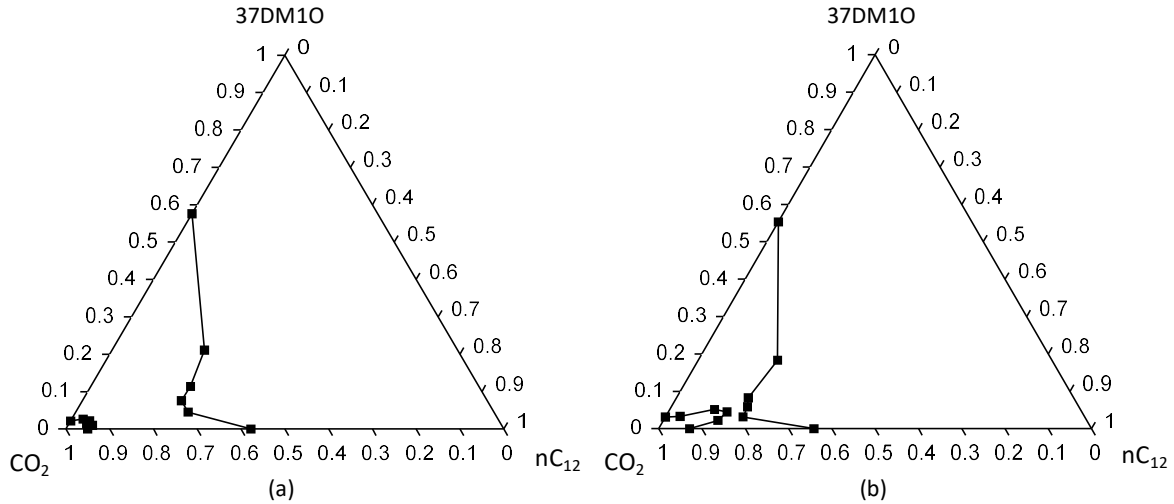

Figure 38: Gibbs phase diagrams for the CO_2 + n-dodecane + 3,7-dimethyl-1-octanol system at a temperature of 348.2 K at pressures of: (a) 14.06 MPa and (b) 14.60 MPa. Binary boundary conditions and data at x_A^{red} = 0.667 obtained from literature [5].

These diagrams clearly illustrate how the co-solvency effect narrows the band connecting the two two-phase regions. As the band narrows with an increase in pressure, the solubility curves approach each other. From the data measured in this work, no clear separation of the two two-

phase regions is seen, but the data suggest the presence thereof. Separation might thus occur, but the separation gap is likely to be small. The data did not reveal signs of other complex phase behaviour phenomena resulting from the co-solvency effect such as liquid-liquid gas holes and miscibility windows, but such phenomena may occur at conditions not considered here.

5.2.5 Section outcome

Conclusion on the phase behaviour

Analysis of the measured phase behaviour data for the CO_2 + n-dodecane + 3,7-dimethyl-1-octanol system, with regards to temperature, did not reveal any sign of complex phase behaviour. The phase behaviour of all the mixtures conformed to the normal trend, where an increase in temperature results in decreased solubility. Analysis of the effect of mixture composition revealed that the phase behaviour of the system is influenced by solute-solute interactions. These interactions were found to result in the occurrence of co-solvency in the mixtures containing 75 wt% and 85 wt% n-dodecane. The co-solvency effect does however not result in phenomena such as liquid-liquid gas holes and miscibility windows within the temperature and composition ranges considered in this work.

Significant contribution

New high pressure bubble- and dew-point data were measured for 3 mixtures containing CO_2 + n-dodecane + 3,7-dimethyl-1-octanol. The data provided insight into the solute-solute interactions which occur in the system and the co-solvency effect which occurs as a result of the interactions. It should be noted that the data were measured using solute compositions which had not been measured previously.

Publications

The work presented in this section contributed to the following publication:

- C. Latsky, N.S. Mabena, C.E. Schwarz, *High pressure phase behaviour for the CO_2 + n-dodecane + 3,7-dimethyl-1-octanol system*. The Journal of Supercritical Fluids 149 (2019) 138 – 150.

5.3 Results for the ternary system: CO_2 + 3,7-dimethyl-1-octanol + 1-decanol

The aim of the experimental work conducted for the system containing CO_2 with 3,7-dimethyl-1-octanol system (37DM1O) and 1-decanol ($C_{10}OH$) was to evaluate the effect of solute-solute interactions on the solubility of the system and to determine whether the system exhibits complex phase behaviour, with particular focus on the occurrence of temperature inversions. The motivation for focussing on the occurrence of temperature inversions stem from the fact that phase behaviour data for the CO_2 + 3,7-dimethyl-1-octanol + 1-decanol system measured in previous studies [5, 14] exhibited this phenomena or signs thereof. The experimental work conducted in this study serves to elaborate on this finding. The additional data measured in this work allows investigation into the interaction which exist between the linear and branched alcohol and the dependence of this interaction on mixture composition, which has not been evaluated previously. It also allows investigation into how the addition of 3,7-dimethyl-1-octanol influences the phase behaviour of the ternary system and whether the 3,7-dimethyl-1-octanol, if present in significant amounts, disrupts the 1-decanol multimer formation as much as n-dodecane [13] or whether it aids multimer formation, as it is also a polar molecule capable of forming hydrogen bonds similar to 1-decanol.

In order to roughly determine when the system starts to exhibit a temperature inversion, experiments were conducted using mixtures containing low, medium and high concentrations of 1-decanol. The specific solute ratios of the three mixtures investigated are as follows:

- Mixture 4: 75 wt% 3,7-dimethyl-1-octanol + 25 wt% 1-decanol
- Mixture 5: 50 wt% 3,7-dimethyl-1-octanol + 50 wt% 1-decanol
- Mixture 6: 25 wt% 3,7-dimethyl-1-octanol + 75 wt% 1-decanol

The bubble- and dew-point data of each mixture was measured between 308 K and 358 K with solute mass fractions ranging from 0.605 to 0.015. The experimental data were measured by Mr. N. Schonegevel under supervision of the current author. All data processing and interpretation thereof is also the work of the current author. The experimental data are provided in Appendix B.

5.3.1 Isothermal data

The isothermal data generated for the three ternary mixtures, along with the pressure-temperature correlations used to generate the data, are presented in Tables 11 to 13.

Table 11: Isothermal data and pressure-temperature correlations for Mixture 4 consisting of CO_2 + (75 wt% 3,7-dimethyl-1-octanol + 25 wt% 1-decanol)

Mass Fraction Solute (g/g)	Pressure-Temperature Correlations: $P = A \times T^4 + B \times T^3 + C \times T^2 + D \times T + E$, with P in MPa and T in K						Isothermal P-xy Data, with P in MPa: Temperature (K)					
	A	B	C	D	E	R^2	308.2	318.2	328.2	338.2	348.2	358.2
0.605	0	0	-8.9904E-04	0.7442	-136.440	1.000	7.53	9.34	10.97	12.43	13.70	14.79
0.497	0	0	1.0432E-03	-0.5816	91.972	0.996	11.82	12.54	13.47	14.60	15.95	17.50
0.412	0	0	1.1394E-03	-0.6588	108.721	0.994	13.90	14.45	15.22	16.23	17.46	18.92
0.345	0	0	1.2837E-03	-0.7595	126.977	0.990	14.85	15.29	16.00	16.95	18.17	19.64
0.293	0	0	1.4989E-03	-0.8985	149.472	0.990	14.93	15.33	16.03	17.04	18.34	19.94
0.229	0	0	1.2789E-03	-0.7535	125.768	0.991	15.02	15.50	16.23	17.21	18.46	19.95
0.184	0	0	1.1862E-03	-0.6874	113.841	0.993	14.65	15.21	16.00	17.03	18.30	19.80
0.131	0	0	5.5027E-04	-0.2477	37.532	0.998	13.47	14.44	15.52	16.71	18.01	19.42
0.0850	0	0	0	0.14542	-33.650	0.996	11.16	12.62	14.07	15.52	16.98	18.43
0.0540	0	0	-9.1601E-04	0.772	-141.822	1.000	8.98	10.95	12.75	14.36	15.79	17.04
0.0320	0	0	-1.6843E-03	1.279	-226.427	1.000	7.81	10.05	11.95	13.52	14.76	15.65
0.0166	0	0	-1.6360E-03	1.220	-212.972	1.000	7.69	9.64	11.27	12.57	13.55	14.19

Table 12: Isothermal data and pressure-temperature correlations for Mixture 5 consisting of CO_2 + (50 wt% 3,7-dimethyl-1-octanol + 50 wt% 1-decanol)

Mass Fraction Solute (g/g)	Pressure-Temperature Correlations: $P = A \times T^4 + B \times T^3 + C \times T^2 + D \times T + E$, with P in MPa and T in K						Isothermal P-xy Data, with P in MPa: Temperature (K)					
	A	B	C	D	E	R^2	308.2	318.2	328.2	338.2	348.2	358.2
0.596	0	0	0	0.1276	-30.068	0.999	9.24	10.52	11.80	13.07	14.35	15.62
0.499	0	-6.2632E-05	0.06415	-21.772	2463.886	0.999	13.91	13.71	14.39	15.56	16.86	17.91
0.414	0	-9.5613E-05	0.09854	-33.735	3854.052	0.996	18.11	16.63	16.60	17.46	18.63	19.53
0.350	0	-1.0721E-04	0.11055	-37.876	4330.904	0.994	19.37	17.53	17.33	18.13	19.29	20.16
0.266	0	-1.1224E-04	0.11577	-39.687	4540.339	0.993	19.91	17.90	17.62	18.40	19.56	20.42
0.217	0	-1.1022E-04	0.11364	-38.933	4451.509	0.993	19.59	17.68	17.47	18.27	19.45	20.33
0.185	0	-1.0401E-04	0.10713	-36.662	4186.921	0.994	19.11	17.45	17.37	18.23	19.42	20.31
0.147	0	-8.8606E-05	0.09114	-31.119	3545.668	0.997	17.67	16.58	16.80	17.80	19.05	20.03
0.116	0	-5.3355E-05	0.05485	-18.673	2122.416	0.999	15.74	15.57	16.19	17.27	18.50	19.55
0.0759	0	0	0	0.1224	-25.446	0.997	12.28	13.50	14.73	15.95	17.18	18.40
0.0502	0	0	-1.0285E-03	0.8306	-148.610	1.000	9.67	11.53	13.19	14.64	15.89	16.93
0.0315	0	0	-1.5143E-03	1.1564	-204.404	0.998	8.14	10.22	12.00	13.47	14.64	15.51
0.0164	0	0	-1.4872E-03	1.1174	-195.333	0.999	7.78	9.64	11.20	12.47	13.44	14.11

Table 13: Isothermal data and pressure-temperature correlations for Mixture 6 consisting of CO_2 + (25 wt% 3,7-dimethyl-1-octanol + 75 wt% 1-decanol)

Mass Fraction Solute (g/g)	Pressure-Temperature Correlations						Isothermal P-xy Data, with P in MPa					
	$P = A \times T^4 + B \times T^3 + C \times T^2 + D \times T + E$, with P in MPa and T in K						Temperature (K)					
	A	B	C	D	E	R^2	308.2	318.2	328.2	338.2	348.2	358.2
0.585	0	0	0	0.11609	-26.370	0.997	9.40	10.56	11.72	12.88	14.05	15.21
0.479	0	-1.4462E-04	0.14913	-51.143	5850.54	0.989	19.89	16.96	16.24	16.88	18.00	18.74
0.401	5.7400E-06	-7.8506E-03	4.0272	-918.293	78548.06	0.999	25.90	20.29	18.83	18.95	19.43	20.45
0.341	6.0731E-06	-8.3129E-03	4.2676	-973.840	83357.37	0.999	26.93	20.90	19.34	19.47	19.98	20.99
0.293	5.7259E-06	-7.8613E-03	4.0479	-926.416	79527.01	0.999	27.09	21.00	19.45	19.66	20.26	21.24
0.230	6.0037E-06	-8.2354E-03	4.2366	-968.635	83065.63	0.993	27.00	20.88	19.36	19.60	20.17	21.13
0.177	5.3165E-06	-7.2862E-03	3.7449	-855.424	73288.76	1.000	25.13	20.05	18.94	19.32	19.99	21.01
0.121	0	-1.2895E-04	0.13301	-45.6185	5220.74	0.997	20.68	18.16	17.64	18.32	19.45	20.24
0.0806	0	-7.0943E-05	0.07239	-24.488	2762.92	1.000	15.20	14.99	15.72	16.96	18.28	19.26
0.0503	0	0	0	0.13991	-32.376	0.996	10.74	12.14	13.54	14.94	16.34	17.73
0.0302	0	0	-1.5948E-03	1.2255	-218.079	1.000	8.12	10.39	12.33	13.96	15.27	16.26
0.0154	0	0	-1.5529E-03	1.1788	-208.204	1.000	7.57	9.63	11.38	12.82	13.95	14.77

5.3.2 Effect of solute composition

The effect of solute composition on phase transition pressure was evaluated by constructing three-dimensional P-x_s-x_B^{red} phase cubes at different temperatures within the temperature range investigated.

Figure 39 and 40 illustrate the P-x_s-x_B^{red} diagrams constructed at 308 K and 348 K, respectively. In these diagrams, the phase transition pressure (P) is plotted against the mass fraction total solute (x_s) at different mixture compositions. The compositions of the different mixtures are represented by the reduced 3,7-dimethyl-1-octanol mass fraction (x_B^{red}), which is mathematically defined as $x_B^{red} \equiv \frac{x_B}{x_B + x_C}$, where B refers to 3,7-dimethyl-1-octanol and C refers to 1-decanol. The boundary conditions where $x_B^{red} = 0$ and $x_B^{red} = 1$ represent the phase behaviour of the binary systems CO_2 + 1-decanol and CO_2 + 3,7-dimethyl-1-octanol, respectively and this data, along with data at $x_B^{red} = 0.125$, were sourced from literature [5].

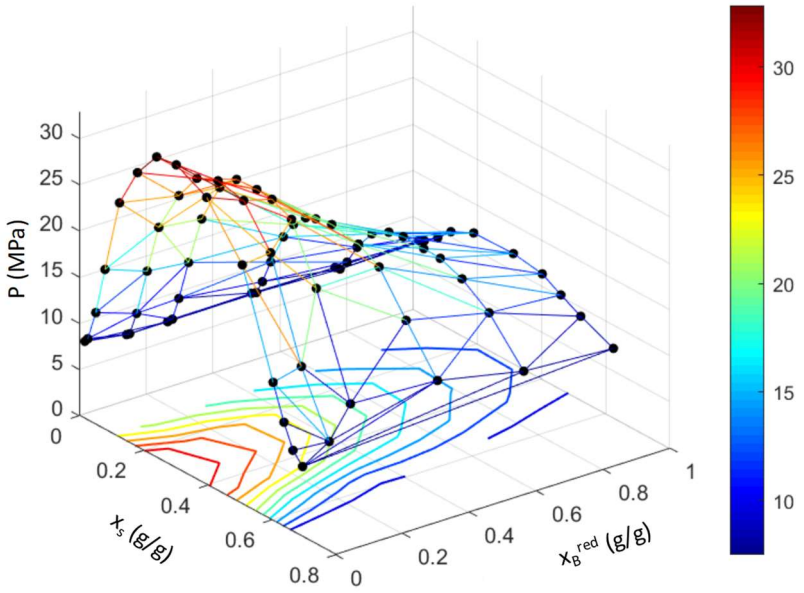

Figure 39: Ternary phase cube where phase transition pressure (P) is plotted as a function of solute mass fraction (x_s) and reduced 3,7-dimethyl-1-octanol mass fraction (x_B^{red}) at 308.2 K. Data at $x_B^{red} = 0$, $x_B^{red} = 0.125$ and $x_B^{red} = 1$ obtained from literature [5].

When viewing the P-x_s-x_B^{red} diagrams presented in Figure 39 and 40, it is noted that throughout the temperature range the phase transition pressure of the CO_2 + 1-decanol system ($x_B^{red} = 0$) is always higher than that of the CO_2 + 3,7-dimethyl-1-octanol system ($x_B^{red} = 1$). This indicates that 3,7-dimethyl-1-octanol is more soluble in CO_2 than 1-decanol. According to Zamudio [5], the increased solubility of 3,7-dimethyl-1octanol can be explained by the fact that 3,7-

dimethyl-1-octanol has a shorter hydrocarbon backbone than 1-decanol and/or it can be attributed to the shielding effect of the methyl branches which decreases the polarity of 3,7-dimethyl-1-octanol relative to 1-decanol. The hydrogen bonds formed between 3,7-dimethyl-1-octanol molecules are thus weaker than those formed between the 1-decanol molecules. Due to the higher solubility of 3,7-dimethyl-1-octanol, the addition thereof lowers the phase transitions pressure of a mixture. This effect is more clearly illustrated in the P- x_B^{red} diagram presented in Figure 41.

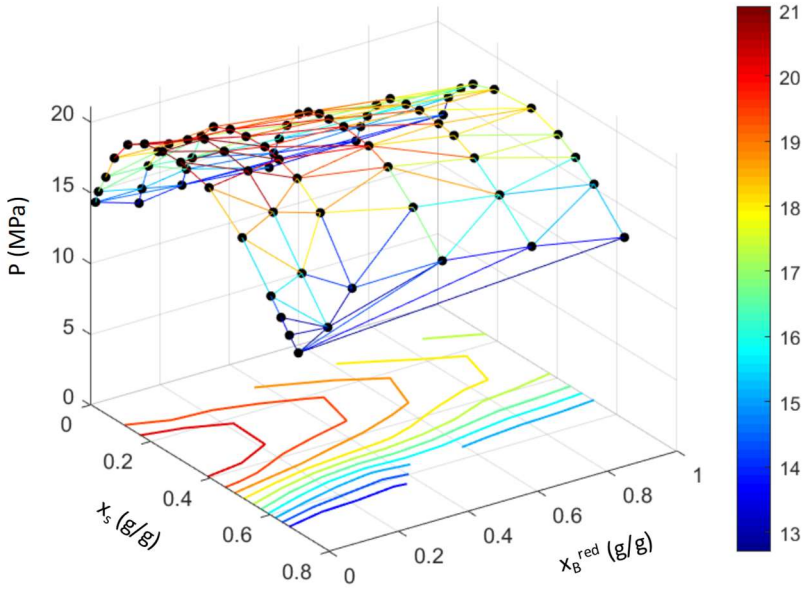

Figure 40: Ternary phase cube where phase transition pressure (P) is plotted as a function of solute mass fraction (x_s) and reduced 3,7-dimethyl-1-octanol mass fraction (x_B^{red}) at 348.2 K. Data at $x_B^{red} = 0$, $x_B^{red} = 0.125$ and $x_B^{red} = 1$ obtained from literature [5].

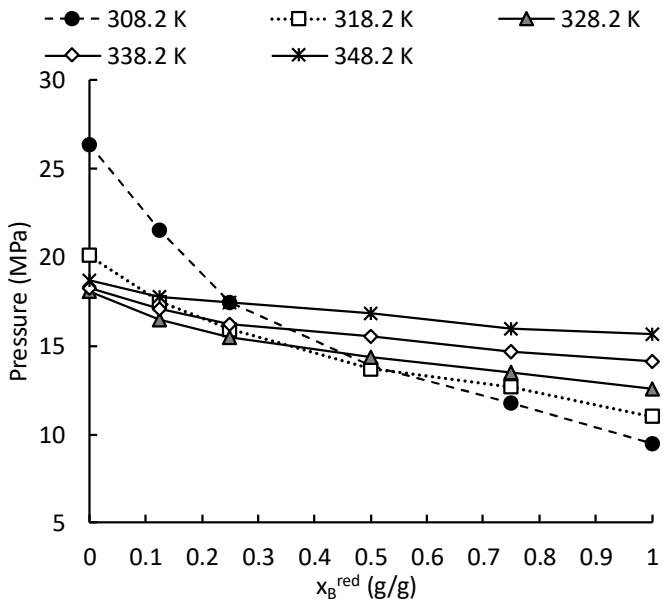

Figure 41: Phase transition pressure plotted as a function of reduced 3,7-dimethyl-1-octanol mass fraction (x_B^{red}) at constant total solute mass fraction of 0.5 for temperatures ranging from 308.2 K to 348.2 K. Data at $x_B^{red} = 0$, $x_B^{red} = 0.125$ and $x_B^{red} = 1$ obtained from literature [5].

It can be seen that as the amount of 3,7-dimethyl-1-octanol increases, the phase transition pressure continuously decreases. The decrease observed does however not follow a linear trend, indicating that solute-solute interactions exists within the mixtures. The absence of a pressure minimum in the curves indicates that these interactions are not sufficient to result in co-solvency. The phase behaviour does however reveal another phenomenon, namely a temperature inversion.

5.3.3 Effect of temperature and the occurrence of temperature inversions

In general, it is expected that an increase in temperature will result in an increase in phase transition pressure. The previous section however highlighted that the phase behaviour of some ternary mixtures containing CO_2 with 3,7-dimethyl-1-octanol and 1-decanol exhibits a temperature inversion, which contradicts the normal phase behaviour [98]. Literature [5, 7, 33, 39, 40, 93, 104, 110] indicates that a temperature inversion is a prominent feature of the phase behaviour exhibited by a certain range of the CO_2 + 1-alcohol homologous series. As stated previously, Zamudio [5] postulates that the temperature inversion observed for the CO_2 + 1-decanol system is due to the fact that at low temperatures the kinetic energy of the 1-decanol molecules cannot overcome the multimer bonds formed between the 1-decanol molecules and therefore high pressure is required for total solubility. It is therefore expected that a temperature inversion will occur in systems where 1-decanol dominates the phase behaviour. In order to determine which of the mixtures investigated in this section displays a temperature inversion, pressure-composition diagrams for the three ternary mixtures were constructed. These diagrams, along with a pressure-composition diagram constructed using data measured by Zamudio [5] for a mixture containing 87.5 wt% 1-decanol, are presented in Figure 42.

When analysing Figure 42 (a), it is noted that the phase behaviour of the system comprising of 25 wt% 1-decanol, does not exhibit a temperature inversion in the temperature range considered. The amount of 1-decanol present in the system is too low to dominate the phase behaviour of the mixture. The presence of 1-decanol in the mixture does however increase the phase transition pressure of the mixture relative to the CO_2 + 3,7-dimethyl-1-octanol system, especially at 308 K and 318 K.

When viewing Figure 42 (b) and (c) it is noted that both mixtures exhibit a temperature inversion. Further analysis however reveals that the temperature and composition ranges of the

temperature inversion displayed by the two mixtures differ. It is seen that the phase behaviour of the mixture containing 50 wt% 1-decanol displays a temperature inversion between solute mass fractions of approximately 0.11 and 0.51. The temperature inversion for the mixture containing 75 wt% 1-decanol occurs between solute mass fractions of approximately 0.08 and 0.55. The increase of 1-decanol from 50 wt% to 75 wt% therefore drives the phase behaviour towards that of the CO_2 + 1-decanol system in which the temperature inversion occurs between solute mass fractions of approximately 0.07 and 0.64 [5]. This is in agreement with the data presented by Zamudio [5] where a mixture containing 87.5 wt% 1-decanol exhibits a temperature inversion between solute mass fractions of 0.08 and 0.61 [5].

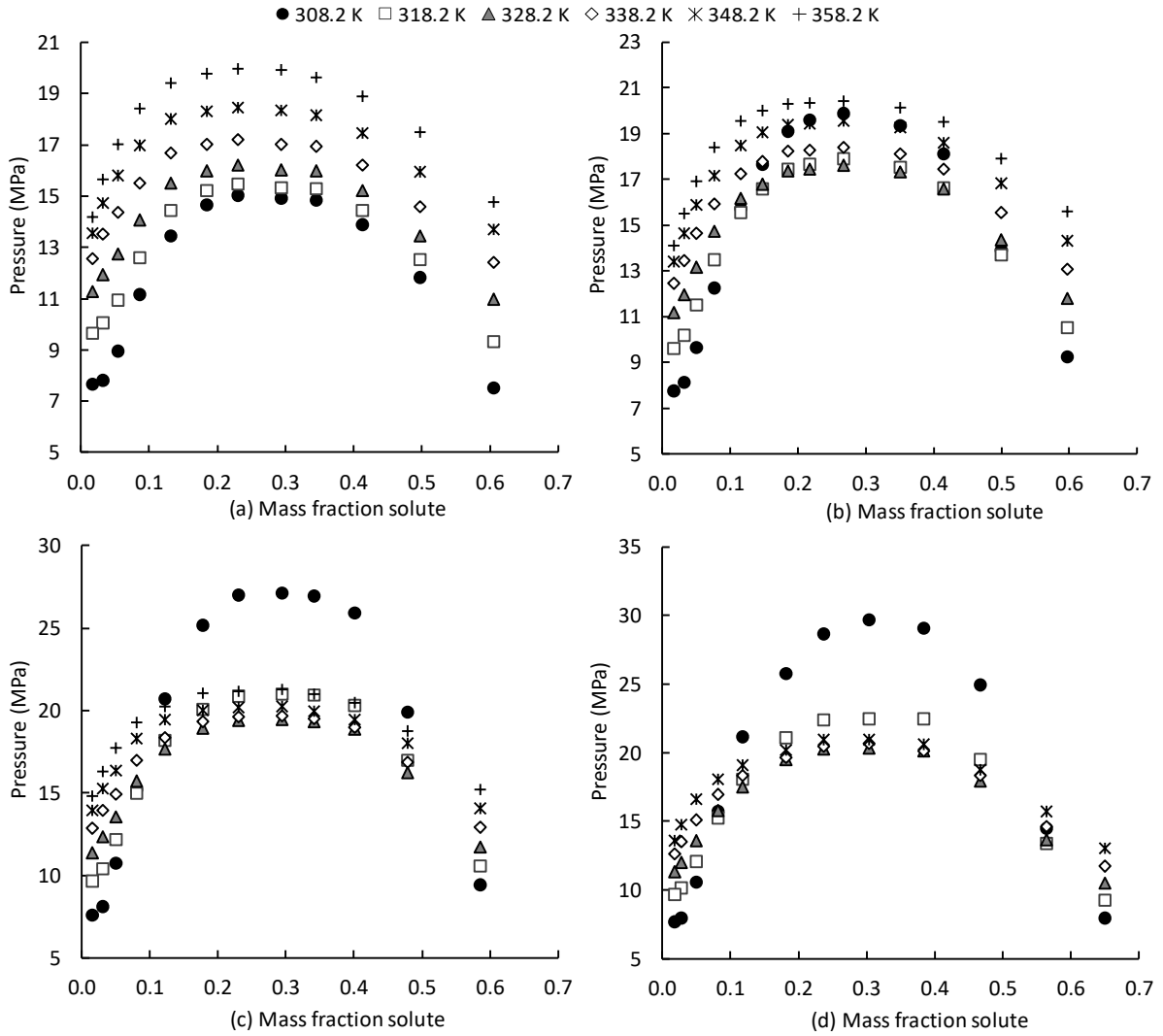

Figure 42: Pressure-composition diagrams illustrating the phase behaviour of (a) Mixture 4: 75 wt% 37DM1O + 25 wt% $C_{10}OH$, (b) Mixture 5: 50 wt% 37DM1O + 50 wt% $C_{10}OH$, (c) Mixture 6: 25 wt% 37DM1O + 75 wt% $C_{10}OH$ and (d) Zamudio mixture: 12.5 wt% 37DM1O + 87.5 wt% $C_{10}OH$ [5]

The findings presented here suggest that the 3,7-dimethyl-1-octanol does not aid 1-decanol multimer formation, but rather disrupts it. The 3,7-dimethyl-1-octanol molecules do however not impede the 1-decanol multimer formation as much as non-polar n-dodecane does [13].

5.3.4 Section outcomes

Conclusion on the phase behaviour

Analysis of the generated phase behaviour data for the CO_2 + 3,7-dimethyl-1-octanol + 1-decanol system revealed that significant solute-solute interactions occur in the system, which influences the solubility thereof. The phase behaviour for the mixtures consisting of 50 wt% and 75 wt% 1-decanol revealed that the solute-solute interactions which exist in these mixtures result in the occurrence of a temperature inversion. The phase behaviour of the mixture containing only 25 wt% 1-decanol did not exhibit a temperature inversion, as the 1-decanol content in the mixture was too low to dominate the phase behaviour of the mixture. The presence of 1-decanol in this mixture was however found to increase the phase transition pressure of the mixture relative to the CO_2 + 3,7-dimethyl-1-octanol system, especially at 308 K and 318 K. The 3,7-dimethyl-1-octanol was found to disrupt 1-decanol multimer formation, but it does not impede it as much as n-dodecane does.

Significant contribution

New high pressure bubble- and dew-point data were measured for 3 mixtures containing CO_2 + 1-decanol + 3,7-dimethyl-1-octanol. The data provided insight into the solute-solute interaction which occur in the system and the temperature inversion which occurs as a result of the interactions. It should be noted that the data were measured over a wide range of solute compositions which had not been measured previously.

Publications

The work presented in this section contributed to the following publication:

- C. Latsky and C.E. Schwarz, *Measurement and modelling of high pressure bubble- and dew-point data for the CO_2 + 1-decanol + 3,7-dimethyl-1-octanol system*, Fluid Phase Equilibria 488 (2019) 87 – 98.

5.4 Results for the quaternary system

The aim of the experimental work conducted for the quaternary system was to evaluate the effect of solute-solute interactions on the solubility of the system and to determine whether the system exhibits complex phase behaviour.

Due to the fact that limited bubble- and dew-point data exists for the quaternary system, literature findings for the binary and ternary subsystems, as well as the findings presented in sections 5.2 and 5.3, were used to establish the quaternary mixture compositions which were to be investigated in this work [5, 13, 103]. The main phase behaviour phenomena reported for the subsystems were co-solvency and temperature inversions and therefore the experimental mixtures were selected to allow investigation into the occurrence of such phenomena. The possible occurrence of co-solvency was addressed by selecting a mixture consisting largely of n-dodecane and the possibility of a temperature inversion was investigated by selecting 1-decanol rich mixtures. A mixture consisting of equal weight amounts of all the components was also selected. This was done to determine the effect of solute-solute interactions on phase behaviour when none of the components dominate the mixture composition. The specific solute ratios of the four mixtures investigated are as follows:

- Mixture 7: 33.3 wt% n-dodecane+33.3 wt% 3,7-dimethyl-1-octanol+33.3 wt% 1-decanol
- Mixture 8: 5 wt% n-dodecane + 10 wt% 3,7-dimethyl-1-octanol + 85 wt% 1-decanol
- Mixture 9: 84.2 wt% n-dodecane + 10.5 wt% 3,7-dimethyl-1-octanol + 5.3 wt% 1-decanol
- Mixture 10: 10.1 wt% n-dodecane + 30 wt% 3,7-dimethyl-1-octanol + 59.9 wt% 1-decanol

The bubble- and dew-point data were measured between 308 K and 358 K with solute mass fractions ranging from 0.631 to 0.015. The data presented in this section and the analysis thereof is the work of the current author. The experimental data are presented in Appendix B.

5.4.1 Measured data and isothermal data

The bubble- and dew-point data generated for the four quaternary mixtures is presented in this section. Tables 14 (a), 15 (a), 16 (a) and 17 (a) provide the measured data for each mixture, whilst Tables 14 (b), 15 (b), 16 (b) and 17 (b) provide the corresponding isothermal data, along with the pressure-temperature correlations used to generate the data.

Table 14 (a): Measured data for Mixture 7 consisting of CO_2 + (33.3 wt% n-dodecane + 33.3 wt% 3,7-dimethyl-1-octanol + 33.3 wt% 1-decanol)

Mass Fraction Solute (g/g)	Temperature (K)						Pressure (MPa)					
	T_1	T_2	T_3	T_4	T_5	T_6	P_1	P_2	P_3	P_4	P_5	P_6
0.631	309.2	318.6	328.1	338.0	347.4	357.1	7.16	8.39	9.66	10.88	12.01	13.02
0.545	309.2	318.7	328.4	338.0	347.1	357.0	7.57	9.15	10.64	12.13	13.49	14.73
0.456	309.2	318.8	328.6	338.2	347.7	357.4	8.30	10.05	11.85	13.49	15.01	16.34
0.392	309.2	318.8	328.2	338.0	347.4	357.1	9.01	10.60	12.31	13.97	15.50	16.85
0.318	309.1	318.4	328.1	337.5	347.0	356.6	9.89	11.30	12.98	14.61	16.13	17.49
0.245	309.0	318.5	327.8	337.7	347.0	356.8	10.47	11.80	13.40	14.96	16.44	17.77
0.181	308.8	318.1	327.8	337.2	346.4	355.7	10.72	11.93	13.46	15.01	16.44	17.74
0.120	309.0	318.5	328.3	337.9	347.3	357.0	10.22	11.76	13.40	14.96	16.40	17.65
0.0810	309.0	318.4	327.9	337.2	347.0	356.6	9.09	11.05	12.86	14.59	16.01	17.36
0.0499	309.2	318.6	328.4	337.9	347.4	357.0	8.16	10.36	12.23	13.81	15.16	16.24
0.0300	308.9	318.2	327.8	337.7	347.2	356.2	7.90	9.96	11.63	13.11	14.21	15.11
0.0146	308.8	318.3	327.7	337.2	346.7	356.0	7.87	9.66	11.07	12.27	13.12	13.70

Table 14 (b): Pressure-temperature correlations and isothermal data generated for Mixture 7

Mass Fraction Solute (g/g)	Pressure-Temperature Correlations						Isothermal P-xy Data, with P in MPa					
	$P = A \times T^4 + B \times T^3 + C \times T^2 + D \times T + E$, with P in MPa and T in K						Temperature (K)					
	A	B	C	D	E	R^2	308.2	318.2	328.2	338.2	348.2	358.2
0.631	0	0	0	0.12315	-30.827	0.998	7.12	8.35	9.58	10.81	12.05	13.28
0.545	0	0	0	0.15053	-38.851	0.998	7.54	9.04	10.55	12.05	13.56	15.06
0.456	0	0	0	0.16797	-43.479	0.997	8.28	9.96	11.64	13.32	15.00	16.68
0.392	0	0	0	0.16581	-42.193	0.999	8.90	10.56	12.22	13.88	15.53	17.19
0.318	0	0	0	0.16263	-40.385	0.999	9.73	11.36	12.98	14.61	16.24	17.86
0.245	0	0	0	0.15542	-37.581	0.999	10.31	11.87	13.42	14.97	16.53	18.08
0.181	0	0	0	0.15246	-36.448	0.999	10.53	12.06	13.58	15.11	16.63	18.16
0.120	0	0	0	0.15664	-38.096	0.998	10.17	11.74	13.31	14.87	16.44	18.01
0.0810	0	0	-1.0187E-03	0.85132	-156.710	1.000	8.89	11.02	12.95	14.68	16.20	17.52
0.0499	0	0	-1.5486E-03	1.1988	-214.425	1.000	7.93	10.22	12.20	13.87	15.23	16.28
0.0300	0	0	-1.7294E-03	1.2985	-228.178	1.000	7.75	9.90	11.71	13.18	14.29	15.06
0.0146	0	0	-1.6592E-03	1.2259	-212.474	1.000	7.75	9.62	11.15	12.36	13.23	13.77

Table 15 (a): Measured data for Mixture 8 consisting of CO_2 + (5 wt% n-dodecane + 10 wt% 3,7-dimethyl-1-octanol + 85 wt% 1-decanol)

Mass fraction solute (g/g)	Temperature (K)						Pressure (MPa)					
	T_1	T_2	T_3	T_4	T_5	T_6	P_1	P_2	P_3	P_4	P_5	P_6
0.625	309.1	318.5	328.1	337.6	347.1	356.5	9.50	10.37	11.70	12.94	14.10	15.10
0.531	309.1	318.5	328.1	337.8	347.2	356.7	17.05	15.07	15.10	15.84	16.81	17.77
0.433	309.1	318.5	328.1	337.3	346.6	356.2	24.10	19.28	18.27	18.50	19.12	19.92
0.376	308.9	318.4	327.9	337.5	346.9	356.4	26.20	20.22	18.95	19.08	19.73	20.55
0.302	309.1	318.5	328.1	337.7	347.1	356.7	27.37	20.93	19.37	19.48	20.15	20.98
0.235	309.0	318.5	328.1	337.7	347.2	356.8	27.48	21.17	19.67	19.65	20.26	21.09
0.182	309.1	318.6	328.2	337.8	347.3	357.0	25.67	20.30	19.16	19.35	20.06	20.90
0.118	309.0	318.6	328.2	337.8	347.4	357.1	20.16	17.54	17.42	18.12	19.07	20.01
0.0805	308.9	318.5	328.2	337.7	347.4	356.8	15.10	14.72	15.47	16.57	17.67	18.67
0.0492	308.9	318.3	327.8	337.4	346.9	356.3	10.31	11.94	13.56	15.07	16.43	17.42
0.0291	309.0	318.6	328.2	337.5	347.4	357.2	8.43	10.50	12.35	13.92	15.19	16.11
0.0147	308.9	318.6	328.3	337.9	347.4	357.0	7.82	9.77	11.39	12.67	13.65	14.36

Table 15(b): Pressure-temperature correlations and isothermal data generated for Mixture 8

Mass Fraction Solute (g/g)	Pressure-Temperature Correlations $P = A \times T^4 + B \times T^3 + C \times T^2 + D \times T + E$, with P in MPa and T in K						Isothermal P-xy Data, with P in MPa Temperature (K)					
	A	B	C	D	E	R^2	308.2	318.2	328.2	338.2	348.2	358.2
0.625	0	0	0	0.12159	-28.180	0.997	9.29	10.50	11.72	12.94	14.15	15.37
0.531	0	-1.2253E-04	0.1260	-43.073	4910.356	0.993	17.28	15.24	15.00	15.83	17.01	17.80
0.433	6.0993E-06	-8.3435E-03	4.2801	-975.79	83433.929	1.000	24.87	19.40	18.23	18.59	19.19	20.21
0.376	7.4168E-06	-1.0139E-02	5.1978	-1184.20	101182.603	0.992	26.92	20.35	18.87	19.19	19.77	20.85
0.302	7.2512E-06	-9.9454E-03	5.1153	-1169.27	100240.113	1.000	28.36	21.09	19.31	19.57	20.19	21.20
0.235	7.2800E-06	-9.9627E-03	5.1131	-1166.32	99784.076	0.993	28.33	21.34	19.59	19.75	20.28	21.33
0.182	6.1978E-06	-8.4975E-03	4.3690	-998.34	85556.252	1.000	26.50	20.48	19.09	19.44	20.08	21.08
0.118	0	-1.4859E-04	0.1527	-52.186	5949.329	0.990	20.42	17.77	17.29	18.09	19.29	19.99
0.0805	0	-7.5174E-05	0.0767	-25.954	2929.606	0.998	15.14	14.78	15.41	16.58	17.84	18.73
0.0492	0	0	-8.4448E-04	0.71359	-129.576	1.000	10.13	11.97	13.65	15.16	16.50	17.67
0.0291	0	0	-1.6125E-03	1.2345	-219.086	1.000	8.21	10.45	12.37	13.97	15.25	16.21
0.0147	0	0	-1.6548E-03	1.2374	-216.489	1.000	7.67	9.68	11.36	12.71	13.72	14.41

Table 16 (a): Measured data for Mixture 9 consisting of CO_2 + (84.2 wt% n-dodecane + 10.5 wt% 3,7-dimethyl-1-octanol + 5.3 wt% 1-decanol)

Mass fraction solute (g/g)	Temperature (K)						Pressure (MPa)					
	T_1	T_2	T_3	T_4	T_5	T_6	P_1	P_2	P_3	P_4	P_5	P_6
0.615	308.8	318.5	328.0	337.6	347.2	356.7	6.24	7.39	8.52	9.71	10.81	11.93
0.508	308.7	318.1	327.6	337.1	346.4	355.9	6.86	8.26	9.65	11.06	12.51	13.81
0.412	309.0	318.5	328.0	337.6	347.0	356.7	7.18	8.75	10.36	12.01	13.61	15.06
0.352	308.8	318.3	328.0	337.6	347.1	356.8	7.21	8.85	10.60	12.38	14.06	15.57
0.290	309.0	318.2	327.9	337.5	346.6	356.0	7.32	9.03	10.85	12.71	14.41	15.94
0.221	309.2	318.8	328.4	338.0	347.6	357.2	7.50	9.27	11.19	13.03	14.65	16.18
0.172	308.2	318.7	328.4	337.9	347.5	357.1	7.34	9.29	11.23	13.04	14.65	16.11
0.121	309.2	318.8	328.3	338.1	347.6	357.1	7.65	9.41	11.23	13.00	14.56	15.94
0.0792	309.1	318.6	328.1	337.8	347.3	356.9	7.59	9.31	11.01	12.68	14.11	15.31
0.0497	308.9	318.4	327.9	337.4	346.9	356.4	7.70	9.30	10.89	12.36	13.55	14.55
0.0304	309.0	318.4	327.7	337.5	346.9	356.7	7.81	9.26	10.72	11.98	12.97	13.73
0.0151	309.0	318.6	328.2	337.8	347.5	356.5	7.76	9.10	10.28	11.16	11.80	12.17

Table 16 (b): Pressure-temperature correlations and isothermal data generated for Mixture 9

Mass Fraction Solute (g/g)	Pressure-Temperature Correlations						Isothermal P-xy Data, with P in MPa					
	$P = A \times T^4 + B \times T^3 + C \times T^2 + D \times T + E$, with P in MPa and T in K						Temperature (K)					
	A	B	C	D	E	R^2	308.2	318.2	328.2	338.2	348.2	358.2
0.615	0	0	0	0.11901	-30.508	1.000	6.16	7.35	8.54	9.74	10.93	12.12
0.508	0	0	0	0.14796	-38.809	1.000	6.79	8.27	9.75	11.23	12.70	14.18
0.412	0	0	0	0.16655	-44.261	1.000	7.06	8.73	10.39	12.06	13.72	15.39
0.352	0	0	0	0.17604	-47.132	0.999	7.11	8.87	10.63	12.39	14.16	15.92
0.290	0	0	0	0.18518	-49.865	0.999	7.20	9.05	10.90	12.75	14.61	16.46
0.221	0	0	0	0.18264	-48.883	0.998	7.40	9.22	11.05	12.88	14.70	16.53
0.172	0	0	0	0.18130	-48.420	0.998	7.45	9.26	11.07	12.89	14.70	16.51
0.121	0	0	0	0.17475	-46.256	0.998	7.59	9.34	11.09	12.84	14.58	16.33
0.0792	0	0	0	0.16310	-42.638	0.996	7.62	9.25	10.88	12.52	14.15	15.78
0.0497	0	0	-9.0518E-04	0.74795	-137.011	1.000	7.52	9.33	10.96	12.41	13.67	14.76
0.0304	0	0	-1.1019E-03	0.85917	-152.506	0.999	7.61	9.31	10.78	12.03	13.05	13.86
0.0151	0	0	-1.3448E-03	0.98805	-169.151	1.000	7.62	9.08	10.27	11.19	11.84	12.22

Table 17 (a): Measured data for Mixture 10 consisting of CO_2 + (10.1 wt% n-dodecane + 30 wt% 3,7-dimethyl-1-octanol + 59.9 wt% 1-decanol)

Mass fraction solute (g/g)	Temperature (K)						Pressure (MPa)					
	T_1	T_2	T_3	T_4	T_5	T_6	P_1	P_2	P_3	P_4	P_5	P_6
0.621	308.8	318.2	327.6	337.0	346.4	355.9	7.52	9.22	10.71	12.09	13.19	14.27
0.533	309.2	318.8	328.3	338.0	347.5	357.2	11.63	11.96	13.03	14.32	15.54	16.66
0.455	309.6	318.3	328.1	337.7	347.5	357.3	15.28	14.55	15.02	16.02	17.06	18.19
0.410	307.4	317.4	327.0	336.3	346.4	355.7	16.33	14.92	15.31	16.25	17.43	18.57
0.307	309.0	318.6	328.4	337.9	347.6	357.4	18.32	16.55	16.75	17.57	18.63	19.73
0.241	308.8	318.4	328.1	337.8	347.4	357.2	18.85	16.91	16.92	17.69	18.72	19.82
0.192	308.7	318.3	328.0	337.6	347.4	357.2	18.88	16.98	17.01	17.77	18.81	19.86
0.122	308.7	318.3	328.0	337.6	347.3	357.0	16.32	15.59	16.18	17.20	18.31	19.40
0.0784	308.8	318.4	328.1	337.7	347.4	357.1	12.79	13.45	14.61	15.94	17.24	18.42
0.0480	308.7	318.4	328.1	337.7	347.4	357.2	9.42	11.34	13.11	14.72	16.08	17.17
0.0309	308.7	318.4	327.9	337.8	347.0	356.3	8.29	10.51	12.36	13.92	15.23	16.26
0.0151	309.4	318.9	328.4	337.8	347.3	356.6	7.61	9.53	11.11	12.35	13.61	14.24

Table 17 (b): Pressure-temperature correlations and isothermal data generated for Mixture 10

Mass Fraction Solute (g/g)	Pressure-Temperature Correlations						Isothermal P-xy Data, with P in MPa					
	$P = A \times T^4 + B \times T^3 + C \times T^2 + D \times T + E$, with P in MPa and T in K						Temperature (K)					
	A	B	C	D	E	R^2	308.2	318.2	328.2	338.2	348.2	358.2
0.621	0	0	-9.3592E-04	0.76484	-139.402	1.000	7.41	9.20	10.80	12.21	13.44	14.48
0.533	0	-5.3649E-05	0.05449	-18.307	2048.681	1.000	11.62	11.97	12.97	14.32	15.67	16.72
0.455	0	-7.7252E-05	0.07947	-27.126	3088.351	0.997	15.46	14.64	14.97	15.99	17.23	18.22
0.410	0	-9.9857E-05	0.10238	-34.851	3956.010	0.996	16.13	15.01	15.31	16.43	17.75	18.70
0.307	0	-1.1134E-04	0.11468	-39.243	4479.765	0.993	18.51	16.73	16.63	17.54	18.80	19.74
0.241	0	-1.1203E-04	0.11559	-39.629	4532.643	0.995	19.00	17.05	16.83	17.67	18.90	19.85
0.192	0	-1.1209E-04	0.11551	-39.555	4519.070	0.995	19.00	17.11	16.93	17.78	18.99	19.88
0.122	0	-7.9685E-05	0.08171	-27.797	3155.094	0.998	16.37	15.68	16.13	17.22	18.49	19.46
0.0784	0	0	5.8964E-04	-0.2719	40.415	0.997	12.62	13.59	14.69	15.90	17.22	18.67
0.0480	0	0	-1.1143E-03	0.9028	-163.123	1.000	9.28	11.33	13.15	14.76	16.14	17.30
0.0309	0	0	-1.4995E-03	1.1639	-208.084	1.000	8.18	10.43	12.38	14.03	15.38	16.42
0.0151	0	0	-1.5128E-03	1.1486	-202.929	0.999	7.36	9.37	11.08	12.48	13.59	14.39

5.4.2 Occurrence of a temperature inversion

In order to determine whether the mixtures investigated in this work exhibit a temperature inversion, the pressure-composition diagrams presented in Figure 43 were constructed. A pressure-composition diagram constructed using quaternary data measured by Zamudio [5] is also included in the figure for comparison.

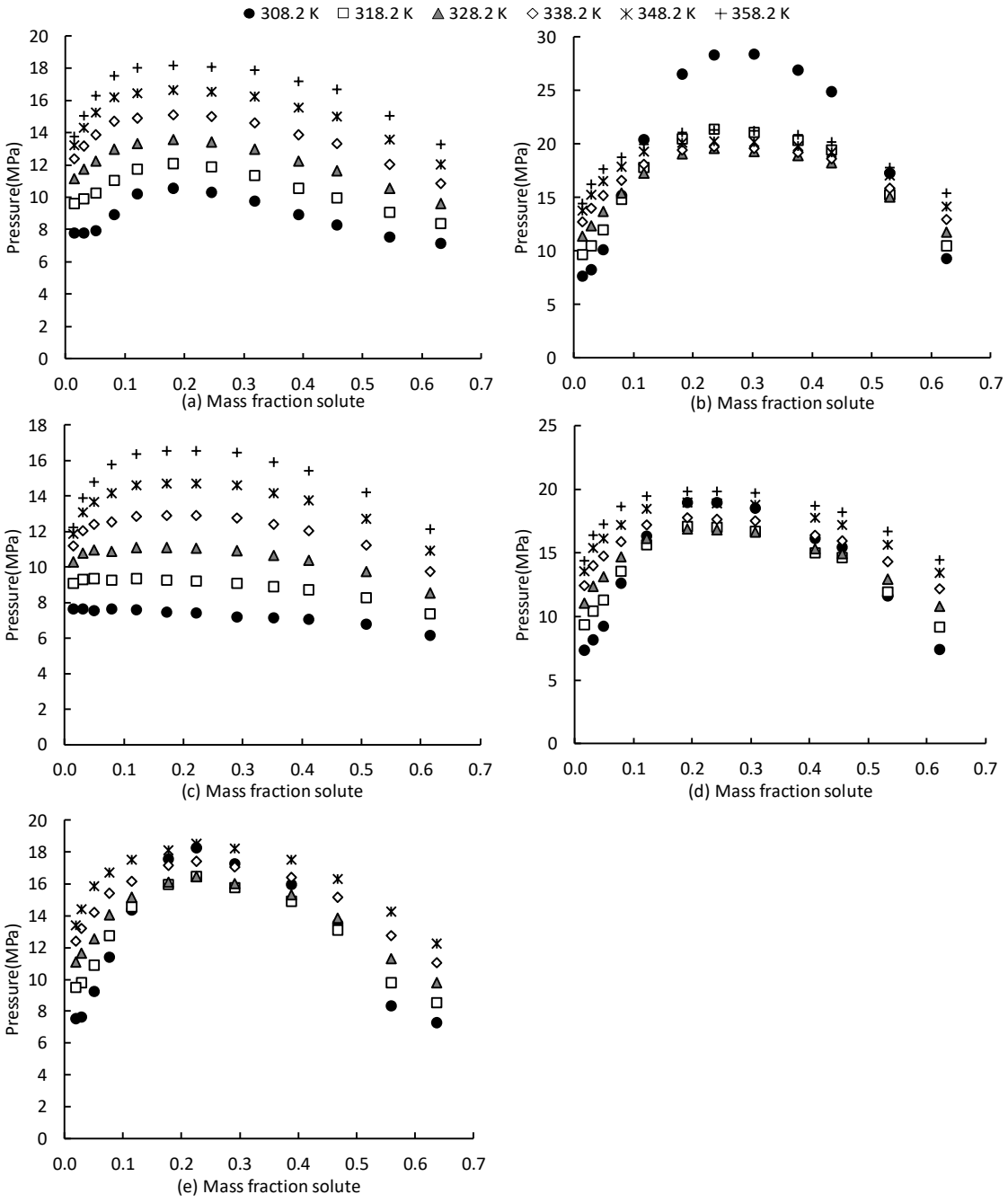

Figure 43: Pressure-composition diagrams illustrating the phase behaviour of: (a) Mixture 7: 33.3 wt% nC_{12}+33.3 wt% 3,7DM1O+33.3 wt% $C_{10}OH$, (b) Mixture 8: 5 wt% nC_{12}+10 wt% 3,7DM1O+85 wt% $C_{10}OH$, (c) Mixture 9: 84.2 wt% nC_{12}+10.5 wt% 3,7DM1O+5.3 wt% $C_{10}OH$, (d) Mixture 10: 10.1 wt% nC_{12}+30 wt% 3,7DM1O+59.9 wt% $C_{10}OH$ and (e) Zamudio mixture: 20 wt% nC_{12}+ 10 wt% 3,7DM1O+ 70 wt% $C_{10}OH$ [5]

When analysing Figure 43 it is seen that the phase behaviour of Mixtures 7 and 9, presented in Figure 43 (a) and (c), conform to the normal trend where an increase in temperature results in an increase in phase transition pressure. This is however not true for the phase behaviour of Mixtures 8 and 10, presented in Figure 43 (b) and (d). Within a specific solute mass fractions range, the phase behaviour presented in Figure 43 (b) and (d) contradicts the normal trend, thus indicating that these mixtures exhibit a temperature inversion. Seeing as both these mixtures consist largely of 1-decanol and that the phase behaviour of the binary CO_2 + 1-decanol subsystem, as well as the ternary subsystems rich in 1-decanol also exhibited temperature inversions, this is to be expected [5]. Further analysis of Figure 43 (b) and (d), reveals that the temperature and composition range of the temperature inversion exhibited by Mixture 8, is closer to that of the CO_2 + 1-decanol system than the temperature inversion displayed by Mixture 10. This can be explained by the fact that Mixture 10 consists of less 1-decanol and/or that it contains more n-dodecane compared to Mixture 8. The lower quantity of 1-decanol in Mixture 10 decreases its ability to dominate the phase behaviour and the addition of n-dodecane disrupts the formation of multimers between the 1-decanol molecules. These findings are in agreement with the data presented by Zamudio [5].

5.4.3 Occurrence of a co-solvency

In order to evaluate if any of the quaternary mixtures investigated in this work are co-solvent, the phase behaviour of each mixture was compared to the binary phase behaviour of its constituent components. This analysis revealed that only Mixture 9 showed signs of co-solvency. The co-solvency effect in this mixture was however not very prominent, especially at lower temperatures. To illustrate this, two comparative pressure-composition diagrams constructed at (a) 318 K and (b) 348 K are presented in Figure 44.

Seeing as the ternary subsystems consisting largely of n-dodecane were found to be co-solvent, it is likely that Mixture 9, consisting of 84.2 wt% n-dodecane, would also be co-solvent [5, 13]. However, to ensure that the trend identified is due to the phase behaviour exhibited by the mixture and not experimental error, the pressure-composition curves of Mixture 9 and n-dodecane were isolated and error bars of 0.07 MPa were added, as shown in Figure 45. It is seen that even with the inclusion of the error bars, the phase transition curve of the mixture is located at pressures below that of n-dodecane and therefore it can be concluded that co-solvency does occur in this mixture.

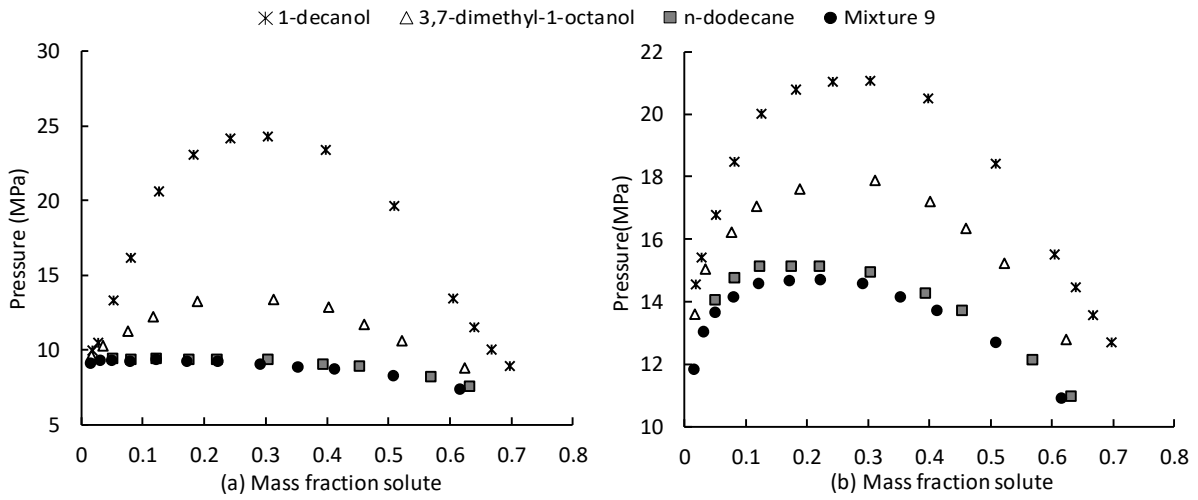

Figure 44: Pressure composition diagrams comparing the phase behaviour of the binary CO_2 + n-dodecane [5], CO_2 + 3,7-dimethyl-1-octanol [5] and CO_2 + 1-decanol [5] systems to that of Mixture 9: 84.2 wt% nC_{12}+10.5 wt% 3,7DM1O+5.3 wt% $C_{10}OH$ at (a) 318.2 K and (b) 348.2 K

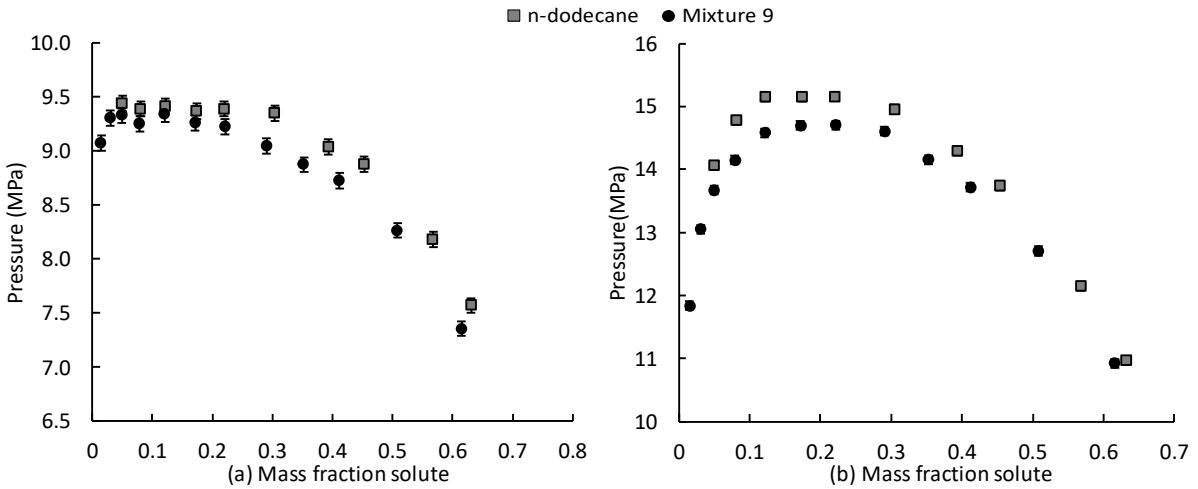

Figure 45: Pressure composition diagrams comparing the phase behaviour of the binary CO_2 + n-dodecane [5] system to that of Mixture 9: 84.2 wt% nC_{12}+10.5 wt% 3,7DM1O+5.3 wt% $C_{10}OH$ at (a) 318.2 K and (b) 348.2 K

5.4.4 Section outcomes

Conclusion on the phase behaviour

Analysis of the phase behaviour data measured for the CO_2 + n-dodecane + 3,7-dimethyl-1-octanol + 1-decanol system revealed that the mixtures consisting of 85 wt% and 59.9 wt% 1-decanol displayed a temperature inversion. The analysis also revealed that the mixture consisting of 84.2 wt% n-dodecane was co-solvent. Furthermore, the analysis revealed that no complex phase behaviour was exhibited by the mixture containing equal amounts of all the components. Based on these findings it can be concluded that in quaternary mixtures where the composition consists largely of one component, the solute-solute interactions which occur in

the mixture will result in the formation of complex phase behaviour phenomena associated with that component.

Significant contribution

New high pressure bubble- and dew-point data were measured for 4 mixtures containing CO_2 + n-dodecane + 1-decanol + 3,7-dimethyl-1-octanol. The data provided insight into the solute-solute interaction which occur in the system and the complex phase behaviour which occurs as a result of the interactions. It should be noted that the data were measured using solute compositions which had not been measured previously.

Publications

The work presented in this section contributed to the following publications:

- C. Latsky and C.E. Schwarz, *High pressure bubble- and dew-point data for a system containing supercritical CO_2 with detergent range alkanes and alcohols*, The Journal of Supercritical Fluids 141 (2018) 265- 273.

5.5 Outcome of this chapter

In this chapter, Objective 1 of the project was addressed by measuring and analysing bubble- and dew-point data for the ternary CO_2 + n-dodecane + 3,7-dimethyl-1-octanol and CO_2 + 1-decanol + 3,7-dimethyl-1-octanol systems as well as the quaternary CO_2 + n-dodecane + 3,7-dimethyl-1-octanol + 1-decanol system.

The main findings of the phase behaviour analysis for the different systems are as follows:

- Significant solute-solute interactions exist in all systems investigated and these interactions result in complex phase behaviour.
- The phase behaviour of the ternary system containing CO_2 with n-dodecane and 3,7-dimethyl-1-octanol, revealed that co-solvency occurs if mixtures comprising of these components are n-dodecane rich. The co-solvency effect does however not result in phenomena such as miscibility windows, within the temperature and composition range investigated in this work.
- The phase behaviour of the ternary system consisting of CO_2 with 1-decanol and 3,7-dimethyl-1-octanol, was found to exhibit a temperature inversion when mixtures containing these components consist of significant (50 wt% or more) amounts of

1-decanol. The addition of 3,7-dimethyl-1-octanol was found to disrupt 1-decanol multimer formation, but it does not impede it as much as n-dodecane.

- The phase behaviour of the quaternary system revealed that if the composition of a mixture largely comprises of one component, the solute-solute interactions which occur in the mixture will result in the formation of complex phase behaviour phenomena associated with that component. The quaternary mixture consisting largely of n-dodecane was therefore found to be co-solvent, whilst the mixtures rich in 1-decanol exhibited temperature inversions.

While bubble- and dew-point data and analysis thereof has provided information regarding solute-solute interactions and the effect thereof on the solubility of mixtures, it cannot provide information regarding the effect of the solute-solute interactions on the composition of co-existing equilibrium phases. In order to analyse this, VLE data is required and this is addressed in Chapter 6.

6. EXPERIMENTAL VAPOUR-LIQUID-EQUILIBRIUM DATA

VLE data and how it is affected by molecular interactions is of great importance to the development of thermodynamic models and the design of supercritical extraction plants. Based on a literature review, it is known that there exists sufficient VLE data for all the ternary subsystems containing CO_2 with n-dodecane, 3,7-dimethyl-1-octanol and 1-decanol [14]. However, to the author's knowledge, no VLE data has been published for the quaternary CO_2 + n-dodecane + 3,7-dimethyl-1-octanol + 1-decanol system.

Experiments were therefore conducted to quantify the composition of co-existing phases in mixtures containing CO_2 with n-dodecane, 3,7-dimethyl-1-octanol and 1-decanol. The aim of this chapter is to (i) provide details regarding the experimental method employed to measure the data and to (ii) present and (iii) analyse the data generated for the system. This chapter therefore addresses Objective 2, as it presents and analyses VLE data which was generated to address a lack of literature data.

6.1 Methodology

This section provides an overview of the approach followed to measure the VLE data presented in this chapter and it also provides details regarding the validity of the experimental data.

6.1.1 Experimental range

In this work, VLE data were measured for three quaternary systems containing CO_2 with n-dodecane, 3,7-dimethyl-1-octanol and 1-decanol. The VLE experiments were conducted using mixtures with similar overall compositions to the mixtures used for the quaternary bubble- and dew-point measurements, for the same reasons mentioned in Chapter 5. Experiments were however not conducted using a mixture containing equal amounts of the components, as the bubble- and dew-point data for this mixture did not indicate the occurrence of any complex phase behaviour. The solute ratios of the three mixtures investigated are as follows:

- Mixture 11: 5 wt% n-dodecane + 12 wt% 3,7-dimethyl-1-octanol + 83 wt% 1-decanol
- Mixture 12: 85 wt% n-dodecane + 10 wt% 3,7-dimethyl-1-octanol + 5 wt% 1-decanol
- Mixture 13: 10 wt% n-dodecane + 30 wt% 3,7-dimethyl-1-octanol + 60 wt% 1-decanol

The mixtures were synthesized using the same materials as those used for the bubble- and dew-point experiments, presented in Table 7. For each mixture, at least 15 VLE points were measured and the temperature and pressure ranges for the experiments are presented in Table 18. These temperature and pressure ranges were selected based on work done by Fourie [14] as well as the results obtained from the bubble- and dew-point data presented in Chapter 5.

Table 18: Temperature and pressure ranges for the VLE experiments

Mixture	Pressure Range (MPa)*		
	308 K	328 K	348 K
11	10.4 – 19.2	12.3 – 18.2	14.0 – 19.2
12	6.0 – 7.2	8.5 – 10.8	11.0 – 14.2
13	9.4 – 17.0	9.4 – 15.7	12.3 – 18.2

*Data measured at a minimum of 5 pressures at each temperature for each mixture

6.1.2 Experimental setup

The VLE data were measured using a previously constructed static-analytic setup which consists of an equilibrium cell, sample transfer area and sample analysis section [111]. The variable volume equilibrium cell (which operates similarly to the cells used for the bubble- and dew-point measurements, except that the phases are analysed through sampling) has a volume of between 75 cm^3 and 125 cm^3. The temperature in the setup is monitored using 12 Pt100 probes and the maximum operating temperature is restricted to 423 K. The pressure is measured using an ONEhalf20 melt transmitter and the maximum operating pressure is 30 MPa [111]. For more information regarding temperature and pressure control and monitoring, the reader is referred to work of Fourie [111].

In order to illustrate the working principle of the experimental setup, a cross-section of the equipment is provided in Figure 46 [111]. From this diagram it is seen that the temperature is controlled using two methods. A Julabo ME-6 circulation bath is used to circulate liquid through the heating jacket surrounding the equilibrium cell. A forced convection oven is used to control the temperature in the area around the equilibrium cell and the pressure intensifier [111]. The pressure within the system is regulated by adjusting the piston position. In order to view the cell content, the equipment includes an endoscope and high definition camera. Furthermore, to ensure homogenous mixing, the setup is also equipped with a magnetic stirrer. In order to withdraw samples, the equilibrium cell is equipped with two electromagnetic rapid

on-line sampler injectors (ROLSI^{TM}). The ROLSI^{TM} capillary penetrates the equilibrium cell and a moveable piston seals the top [111]. A manual displacement device allows the adjustment of the height of the samplers whilst maintaining system pressure. The samples withdrawn from the equilibrium cell are analysed through online gas chromatography (GC) analysis.

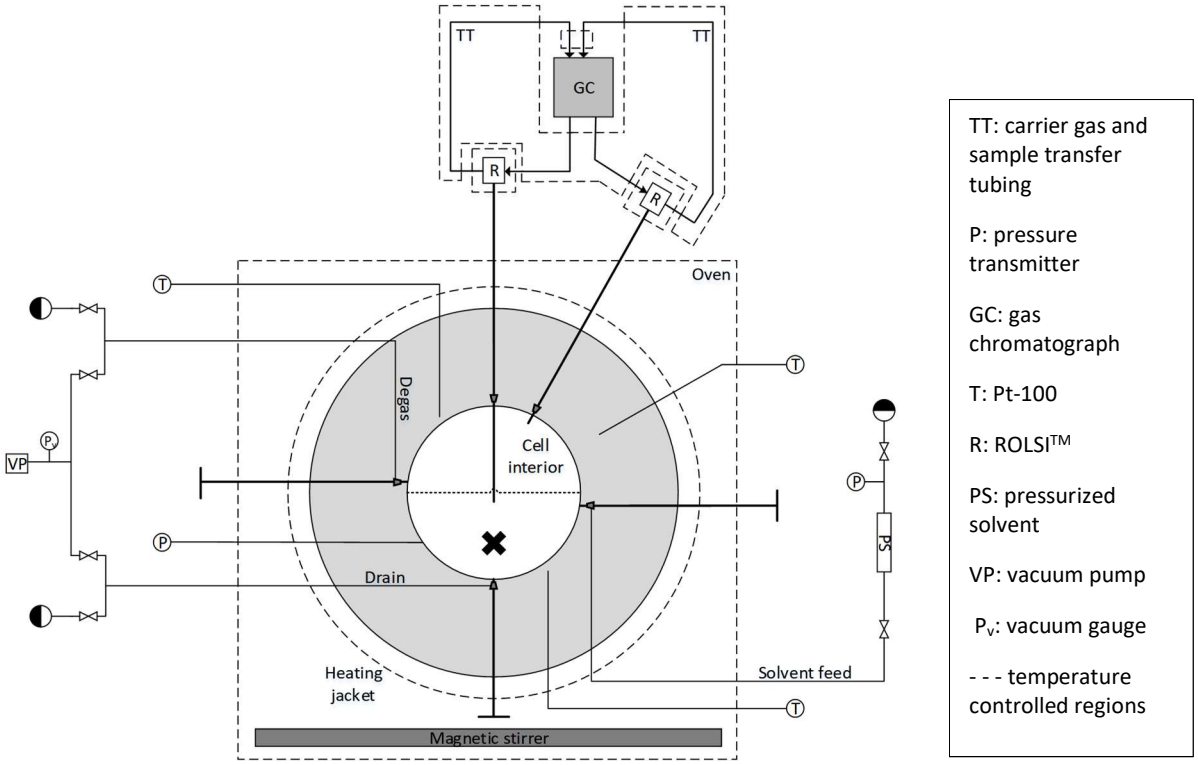

Figure 46: Cross section of the high-pressure analytic phase equilibria setup (Adapted from [111])

A schematic illustrating the configuration of the GC which forms part of the experimental setup is provided in Figure 47 [111]. From this diagram, it is seen that the GC hardware is arranged in two parallel pathways to allow concurrent analysis of the extracted samples [111]. Furthermore, it is noted that the GC is equipped with flame ionisation detectors (FID) and a thermal conductivity detector (TCD). The reason for using two different types of detectors is due to the fact that the superior detection limits of an FID makes it the preferred detector for solute analysis, but it cannot detect CO_2. TCD analysis is therefore used to quantify the amount of CO_2 present in each sample [112].

Referring to Figure 47, the sample analysis path followed can be described as follows: The vapour and liquid samplers (R_1 and R_2) simultaneously extract samples from the equilibrium cell. The samples are then vaporised and transported to the GC inlets (SSL_1 and SSL_2) via heated transfer tubing, through which helium carrier gas is circulated. Upon entering the GC,

the samples pass through columns C_1 and C_2. These columns allow the CO_2 in each sample to pass, but retains and separates the higher-boiling solutes. Valves V_1 and V_2 then direct the CO_2 towards columns C_3 and C_4. The outlets of these columns are joined and the CO_2 content of both samples are analysed using the same TCD. In order to enable the analysis of two separate peaks on one TCD, columns C_3 and C_4 differ in length by a factor of two. Once all the CO_2 has passed V_1 and V_2, the valves switch and the solutes which were retained and separated in columns C_1 and C_2 are directed towards the FIDs [112].

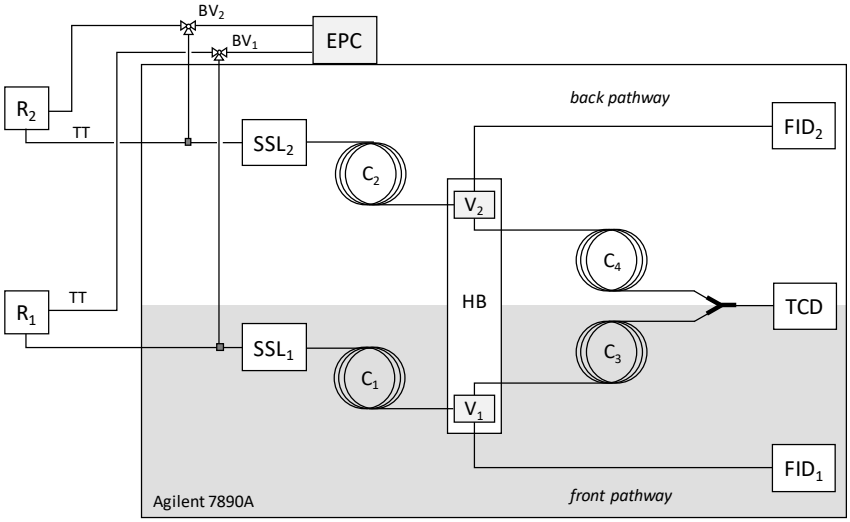

Figure 47: Schematic of the GC configuration: R – ROLSI™; TT – transfer tubing; BV – ball valve; SSL – split-splitless inlet; EPC – carrier gas control; C – columns; V – 4-port valve; HB – heated valve box, TCD – thermal conductivity detector, FID – flame ionization detector (Adapted from [111])

For more information regarding the experimental setup, the reader is referred to work of Fourie, et al. [111, 112].

6.1.3 Experimental procedure

The experimental method used to measure the VLE data is based on a procedure developed by Fourie, et.al [111]. This section briefly describes the loading, measuring and unloading steps in the experimental procedure and further details regarding the procedure are provided in Appendix C.

Prior to starting the loading procedure, the magnetic stirrer must be added to the cell and the pressure intensification section must be attached. During the loading procedure, the liquid solute is added to the cell using a needle syringe. The cell is then evacuated and flushed with CO_2 to remove air from the system. Thereafter, the CO_2 is added to the cell. Upon completion

of the loading procedure, the oven panelling is installed, the magnetic stirrer is turned on and the temperature of the heating bath and oven is set to the first measuring temperature. When the temperature approaches the set point, the pressure in the cell is adjusted by manipulating the piston position. The dense-phase ROLSI^{TM} is then lowered to ensure that the capillary tip is submerged in the liquid phase. Once the temperature and pressure reach the set point values, mixing is continued until the system is visually stable and equilibrium is attained. The mixing is then stopped and a period is allowed for the system to stabilize before sampling commences [111].

The sampling procedure consists of two parts. The first part is a slow purge run, during which consecutive samples are extracted from both phases until the peak heights are stable. The aim of this slow purge run is to clear the ROLSI^{TM} capillaries and transfer lines, this can take up to 90 minutes [112]. The second part of the procedure consists of interchanging fast purge and analysis runs which are repeated until a set of at least three samples of acceptable repeatability are withdrawn. The repeatability of a set of samples is deemed to be acceptable if the maximum standard deviation in the mass fractions of the different components is less than 0.009 [111]. The entire sampling procedure can last up to 4 hours and during this time the pressure is manually controlled to ensure that it does not fluctuate more than ± 0.01 MPa [111].

Once the sampling of all temperature-pressure combinations for a mixture is complete, the cell is unloaded. This is done by venting the solvent to the atmosphere and draining the liquid solute. Upon completion of the unloading procedure, the cell is opened and cleaned with acetone.

6.1.4 Equipment calibration and accuracy

The experimental setup used to measure the VLE data requires temperature, pressure and GC calibration to accurately quantify the composition of the co-existing phases.

The equipment used to measure temperature and pressure was calibrated to account for equipment inaccuracies which result in deviations between the displayed and actual measurements. The pressure transmitter was calibrated using a dead weigh tester and the calibration data along with the temperature-specific correlation which were developed are presented in Appendix C. The Pt100 probe used to measure the temperature inside the

equilibrium cell was calibrated by Thermon South Africa (Pty) Ltd., which is a South African National Accreditation System (SANAS) approved institute. The calibration certificate and the temperature correlations developed using the calibration data is provided in Appendix C. The standard uncertainty in the pressure and temperature measurements is deemed to be better than 0.04 MPa and 0.1 K, respectively [111].

The GC was calibrated not only to account for equipment inaccuracies, but also to develop component-specific calibration curves which were used to quantify the composition of the sampled phases. The GC was calibrated according to a procedure developed by Fourie, et al., [112] which entailed manually injecting a known mass of liquid or gas directly into the GC inlet and then relating the mass to the detector peak area. Calibration data for each component was generated at four or five dilution concentrations, with two replicate injections per concentration. The relative standard deviation between the replicate injections were smaller than 2 % and the linear calibration curves, presented in Appendix C, which were developed using the calibration data have R^2 values greater than 0.9995 [112]. In order to determine the uncertainty in the mass fractions reported in this work, the "Guide to the expression of uncertainty in measurement" [113] was used. This accuracy analysis determines the combined standard uncertainty in the mass fractions, based on the calibration, GC and sampling accuracy. The maximum standard uncertainty for the mass fractions reported in this work are presented in Table 19, and details regarding the method employed to determine this is presented in Appendix C. The assistance of Mr. R.M. Swanepoel, a PhD candidate in Chemical Engineering, with this accuracy analysis is acknowledged here.

Table 19: Maximum standard uncertainty in the mass fractions reported for each component

Component	Maximum Standard Uncertainty u(x,y)	
	Liquid Phase	Vapour Phase
1-decanol	0.004	0.006
n-dodecane	0.003	0.008
3,7-dimethyl-1-octanol	0.003	0.006
CO_2	0.005	0.011

6.1.5 Validation of the experimental results

In order to validate the VLE data presented in this chapter, the repeatability and reproducibility of the data was evaluated and the accuracy of the experimental method was investigated.

Repeatability and Reproducibility

The experimental procedure used to generate the VLE data dictates that sampling for each temperature-pressure combination must be continued under the same conditions until at least three samples of acceptable repeatability are withdrawn. Therefore, the repeatability of the data is ensured in each experimental run.

The reproducibility of the VLE data was investigated by comparing the results obtained from two experiments which were conducted three days apart, under different ambient conditions and with slight changes in the equilibrium conditions. From the reproducibility results, presented in Table 20, it is seen that there is generally good correlation between the results obtained from the different experiments, with the maximum deviation in mass fraction being 0.004. The deviations observed are within the experimental accuracy, as outlined in Table 19. The VLE data presented in this chapter is therefore deemed reproducible.

Table 20: Comparison of the liquid and vapour compositions results, based on a mass fraction basis, obtained for two experiments repeated under slightly different conditions

T (K)	P (MPa)	Liquid				Vapour			
		CO_2	37DM1O	nC_{12}	$C_{10}OH$	CO_2	37DM1O	nC_{12}	$C_{10}OH$
308.6	6.01	0.327	0.065	0.571	0.037	0.961	0.006	0.029	0.004
308.6	6.03	0.326	0.066	0.571	0.037	0.965	0.006	0.026	0.004

Verification of the experimental method:

Seeing as no literature data exists for the quaternary system measured in this work, the accuracy of the experimental method was verified by replicating literature data, measured by Fourie [14], for the ternary CO_2 + n-dodecane + 1-decanol system with a bulk n-dodecane to 1-decanol mass fraction ratio of 25:75. The measured and literature data [14] are compared in the Gibbs phase diagrams presented in Figure 48 at (a) 308 K and 6.8 MPa and (b) 328 K and 12.3 MPa.

From the diagrams it can be seen that the measured data correlates well with the literature data [14]. The slight deviations can be attributed to small differences in experimental conditions such as temperature, pressure and overall mixture composition. Based on the agreement between the data sets the experimental method used to measure the VLE data in this work is deemed to be accurate.

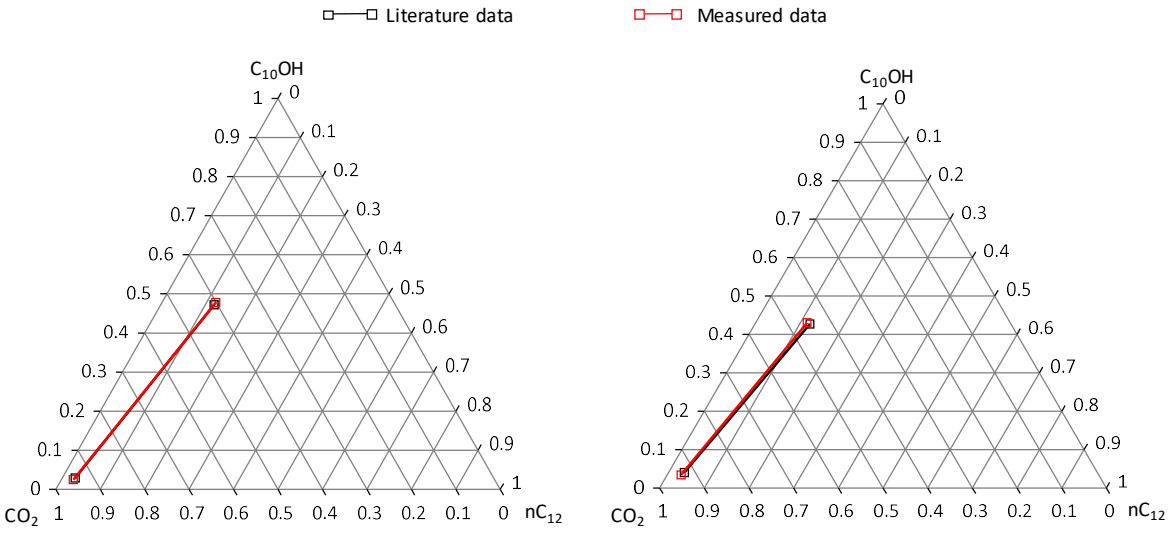

Figure 48: Gibbs phase diagram constructed to compare literature data [14] for the ternary CO_2 + n-dodecane + 1-decanol system with a bulk n-dodecane to 1-decanol mass fraction ratio of 25:75 to experimental data measured in this work at (a) 308 K and 6.8 MPa and (b) 328 K and 12.3 MPa

6.2 Experimental difficulties and observations

In this work, experimental difficulties similar to those experienced by Fourie [14] were encountered. The difficulties, which disrupted the equilibrium conditions and complicated sampling, were mainly encountered when measuring 1-decanol rich mixtures at low temperatures. These systems were found to be highly sensitive to sampling and withdrawing a sample often affected the system pressure. Continuous pressure control was therefore required to maintain the pressure within ± 0.01 MPa. In some of these systems, sampling also resulted in localised mist formation. Although localised mist formation disrupts the equilibrium conditions, literature indicated that accurate VLE data could be generated even if localised mist formation occurs [112]. Sampling was therefore not interrupted by the occurrence of localised mist formation.

In addition to sampling-related disturbances, stirring the 1-decanol rich mixtures at low temperatures resulted in finely dispersed bubbles forming in the liquid phase and/or liquid droplets being suspended in the vapour phase, as shown in Figure 49. Fourie et. al., [112] referred to this as “turbulent mixing”. The formation of these bubbles and/or droplets delayed the sampling procedure as the system required several hours to reach visual stability. If the suspended droplets coagulated on the vapour capillary cone to form a drop, as is the case in Figure 49 (b), vapour-phase sampling could not commence until the drop separated from the vapour capillary tip. In order to prevent these mixing-related problems, the stirrer speed was

reduced and stirring was performed in a start-stop fashion, as suggested in literature [112]. This reduced the stirring efficiency, which in turn resulted in the transitional phase requiring more time to fully develop, once again delaying sampling. The delays imposed by reducing the stirrer speed were however shorter than the delays brought about by mixing-related problems.

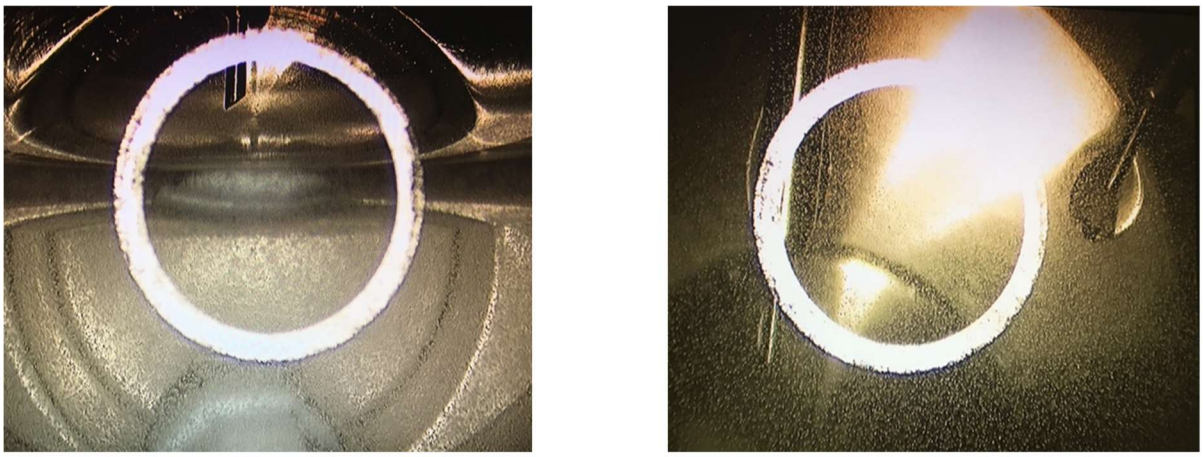

(a) (b)

Figure 49: Stirring a quaternary mixture containing 85 wt% 1-decanol at 308.6 K and 18.2 MPa causes turbulent mixing which results in the formation of (a) bubbles in the liquid phase and (b) suspended droplets in the vapour phase

Based on the findings reported by Zamudio [5] for the CO_2 + 1-decanol system, it is suspected that the difficulties which were encountered whilst measuring VLE data for the 1-decanol rich systems, are related to the strong associative solute-solute interactions which exist between the 1-decanol molecules at low temperatures. Zamudio [5] suggested that the hydroxyl group of the 1-decanol molecules form multimer hydrogen bonds and that these bonds result in a more compact alcohol structure [5]. The intermolecular forces associated with the more compact alcohol structure are suspected to increase the density, viscosity and surface tension of the liquid phase in 1-decanol rich systems. Sampling and mixing a denser and more viscous phase with a higher surface tension is likely to have greater disruptive effects on a system, thus providing a possible explanation for the difficulties encountered.

6.3 Vapour-liquid-equilibrium results for the quaternary system

6.3.1 Measured data

The VLE data measured for the three quaternary systems are provided in Tables 21 to 23.

Table 21: VLE data measured for Mixture 11 consisting of 5 wt% n-dodecane + 12 wt% 3,7-dimethyl-1-octanol + 83 wt% 1-decanol

T (K)	P(MPa)	Liquid				Vapour			
		CO_2	37DM1O	nC_{12}	$C_{10}OH$	CO_2	37DM1O	nC_{12}	$C_{10}OH$
308.6	10.41	0.368	0.069	0.024	0.540	0.950	0.008	0.009	0.033
	12.31	0.387	0.066	0.023	0.525	0.932	0.010	0.010	0.049
	14.00	0.403	0.064	0.022	0.510	0.899	0.013	0.011	0.076
	15.69	0.415	0.062	0.020	0.502	0.886	0.015	0.011	0.088
	17.00	0.421	0.062	0.021	0.496	0.881	0.015	0.012	0.092
	19.21[1]	0.877	0.015	0.011	0.098	0.485	0.056	0.020	0.439
328.8	12.31	0.379	0.068	0.026	0.526	0.962	0.006	0.007	0.025
	14.01	0.419	0.063	0.023	0.495	0.936	0.009	0.009	0.046
	15.70	0.458	0.058	0.020	0.464	0.904	0.013	0.010	0.073
	17.02	0.490	0.055	0.020	0.434	0.870	0.016	0.012	0.102
	18.20	0.534	0.050	0.018	0.398	0.836	0.020	0.012	0.133
348.9	14.00	0.351	0.070	0.028	0.550	0.976	0.004	0.005	0.015
	15.71	0.407	0.064	0.025	0.504	0.955	0.007	0.006	0.032
	17.01	0.449	0.059	0.023	0.469	0.929	0.009	0.008	0.053
	18.21	0.501	0.054	0.020	0.426	0.909	0.012	0.009	0.070
	19.22	0.549	0.049	0.018	0.384	0.862	0.017	0.011	0.110

[1] Barotropy/Density inversion

Table 22: VLE data measured for Mixture 12 consisting of 85 wt% n-dodecane + 10 wt% 3,7-dimethyl-1-octanol + 5 wt% 1-decanol

T (K)	P(MPa)	Liquid				Vapour			
		CO_2	37DM1O	nC_{12}	$C_{10}OH$	CO_2	37DM1O[1]	nC_{12}	$C_{10}OH$[1]
308.6	6.03	0.326	0.066	0.571	0.037	0.965	0.0059	0.026	0.0036
	6.59	0.401	0.058	0.507	0.033	0.990	0.0033	0.004	0.0022
	6.82	0.452	0.054	0.459	0.035	0.976	0.0046	0.016	0.0029
	7.05	0.527	0.047	0.395	0.031	0.991	0.0030	0.005	0.0020
	7.20	0.579	0.042	0.351	0.027	0.991	0.0029	0.004	0.0019
328.8	8.51	0.363	0.061	0.540	0.037	0.990	0.0027	0.006	0.0016
	9.52	0.461	0.052	0.453	0.035	0.987	0.0028	0.009	0.0017
	10.00	0.518	0.047	0.407	0.029	0.983	0.0032	0.012	0.0018
	10.31	0.564	0.042	0.367	0.027	0.980	0.0034	0.015	0.0019
	10.60	0.616	0.037	0.322	0.025	0.971	0.0045	0.022	0.0023
	10.79	0.664	0.033	0.280	0.024	0.958	0.0058	0.033	0.0030
348.9	11.02	0.388	0.057	0.517	0.038	0.984	0.0030	0.012	0.0017
	12.49	0.477	0.049	0.443	0.032	0.973	0.0041	0.021	0.0021
	13.51	0.560	0.041	0.372	0.027	0.958	0.0057	0.034	0.0027
	13.69	0.582	0.039	0.354	0.024	0.949	0.0066	0.041	0.0032
	13.99	0.612	0.037	0.327	0.024	0.937	0.0078	0.051	0.0038
	14.20	0.634	0.035	0.307	0.025	0.927	0.0089	0.060	0.0043

[1] Due to the low mass fractions of these components present in the vapour phase an additional decimal was added to allow analysis of the changes in bubble- and dew-point with pressure and temperature.

Table 23: VLE data measured for Mixture 13 consisting of 10 wt% n-dodecane + 30 wt% 3,7-dimethyl-1-octanol + 60 wt% 1-decanol

T(K)	P(MPa)	Liquid				Vapour			
		CO_2	37DM1O	nC_{12}	$C_{10}OH$	CO_2	37DM1O	nC_{12}	$C_{10}OH$
308.6	9.40	0.408	0.172	0.050	0.371	0.945	0.016	0.015	0.024
	10.41	0.423	0.166	0.044	0.367	0.935	0.019	0.016	0.030
	12.31	0.454	0.156	0.044	0.346	0.888	0.032	0.022	0.057
	14.02	0.482	0.148	0.041	0.328	0.855	0.042	0.024	0.079
	15.70	0.515	0.138	0.042	0.305	0.838	0.047	0.025	0.090
	17.01	0.548	0.129	0.038	0.286	0.817	0.054	0.025	0.105
328.8	9.41	0.305	0.200	0.071	0.424	0.990	0.003	0.004	0.003
	10.44	0.354	0.186	0.065	0.396	0.985	0.005	0.005	0.005
	12.30	0.428	0.163	0.053	0.356	0.955	0.013	0.012	0.020
	14.01	0.485	0.147	0.047	0.321	0.906	0.027	0.019	0.048
	15.70	0.551	0.127	0.042	0.280	0.848	0.044	0.023	0.085
348.9	12.30	0.325	0.193	0.070	0.412	0.984	0.005	0.005	0.006
	14.00	0.395	0.173	0.063	0.369	0.972	0.008	0.008	0.012
	15.70	0.455	0.155	0.052	0.337	0.943	0.017	0.012	0.028
	17.00	0.512	0.139	0.045	0.305	0.911	0.026	0.016	0.047
	18.20	0.592	0.117	0.036	0.256	0.845	0.045	0.022	0.088

6.3.2 Analysis of the quaternary vapour-liquid-equilibrium data

The complexity associated with constructing phase behaviour diagrams for quaternary systems prevented visual analysis of the quaternary VLE data, thus making it more difficult to identify trends. The phase behaviour results obtained from the bubble- and dew-point data measured for the quaternary system, presented in Chapter 5, were therefore used to aid analysis of the VLE data.

For bubble- and dew-point measurements, general phase behaviour dictates that an increase in temperature results in an increase in phase transition pressure. The increase of phase transition pressure indicates a decrease in solubility, where solubility is defined as the amount of solvent in the liquid phase and the amount of solutes in the vapour phase. Translating this to VLE data, which is measured at constant temperature and pressure, would therefore suggest that if a system exhibits normal phase behaviour with regard to temperature, an increase in temperature at constant pressure would result in decreased solubility. This would also mean that below the phase transition point, an increase in pressure at constant temperature would result in an increase in solubility. The change in solubility of VLE data can be analysed by investigating the relative amounts of solute and solvent reporting to the different phases. A decrease in

solubility would result in more solvent and less solute reporting to the vapour phase whilst less solvent and more solute would report to the liquid phase. The opposite also holds true.

Based on the bubble- and dew-point data presented in Chapter 5, is it expected that Mixtures 11 and 13, which consists largely of 1-decanol, will exhibit a temperature inversion. When evaluating the VLE data for Mixture 11, presented in Table 21, it reveals that as temperature increases from 308 K to 328 K at constant pressure of 17 MPa, the amount of CO_2 in the liquid phase increases and the amount of solute decreases whilst in the vapour phase the amount of CO_2 decreases and the amount of solute increases. This deviates from the normal VLE behaviour previously discussed and therefore confirms the presence of a temperature inversion. Although less prominent, analysis of the VLE data for Mixture 13, presented in Table 23, reveals similar trends when evaluating the change in liquid composition as the temperature increases from 308 K to 328 K at constant pressure of 15.7 MPa. In addition to the temperature inversion displayed by Mixture 11, barotropy was also observed for this mixture at 308.6 K and 19.21 MPa. This is in correlation with findings presented by Fourie [14].

From the bubble- and dew-point results for the quaternary system, it is also known that Mixture 12, which consists largely of n-dodecane, is likely to be co-solvent. Analysis of the VLE data for Mixture 12, presented in Table 22, reveals that the vapour composition data measured at 308 K deviates from the normal VLE behaviour, which suggests complex phase behaviour (data was re-measured to confirm deviation). The detection of complex phase behaviour is likely, seeing as the measurements were recorded close to the critical temperature and pressure of the solvent, where behavioural complexities are known to occur [103]. This can however not confirm that the mixture is co-solvent.

6.4 Relative solubility analysis

The relative solubilities of the comprising components of the quaternary system were determined for each mixture using Equation 4.1 $\left(\alpha_{i,j}= \left(\frac{y_i}{x_i}\right) / \left(\frac{y_j}{x_j}\right)\right)$, along with the experimental data presented in Tables 21 to 23. The results of the relative solubilities, $\alpha_{37DM1O,C10OH}$, $\alpha_{nC12,C10OH}$ and $\alpha_{nC12,37DM1O}$, are presented in Figures 50, 51 and 52, respectively. In these diagrams the relative solubility of each mixture is plotted against pressure at constant temperatures of (a) 308.6 K, (b) 328.8 K and (c) 348.9 K. The diagrams also indicate the region in which separation is impractical/ineffective ($0.95 < \alpha_{i,j} < 1$), discussed previously [28, 100].

When analysing the diagrams presented in Figures 50 to 52, it is noted that the relative solubilities of (3,7-dimethyl-1-octanol and 1-decanol), (n-dodecane and 1-decanol) and (n-dodecane and 3,7-dimethyl-1-octanol) for Mixtures 11 and 13, which are rich in 1-decanol, are negatively correlated with pressure at all temperatures. This indicates that for these mixtures, an increase in pressure will favour the relative solubility of the less soluble component [14]. The relative solubility for the alkane rich mixture, Mixture 12, however tends to generally be positively correlated with pressure, at 328.8 K and 348.9 K. This indicates that an increase in pressure at these temperatures will enhance the solubility of the more soluble component. No clear distinction can be made with regards to the solubility trends at 308.8 K for Mixture 12. This is due to the sensitivity of the relative solubility to the vapour phase composition at lower pressures, due to composition inaccuracies at low temperature and pressure [14].

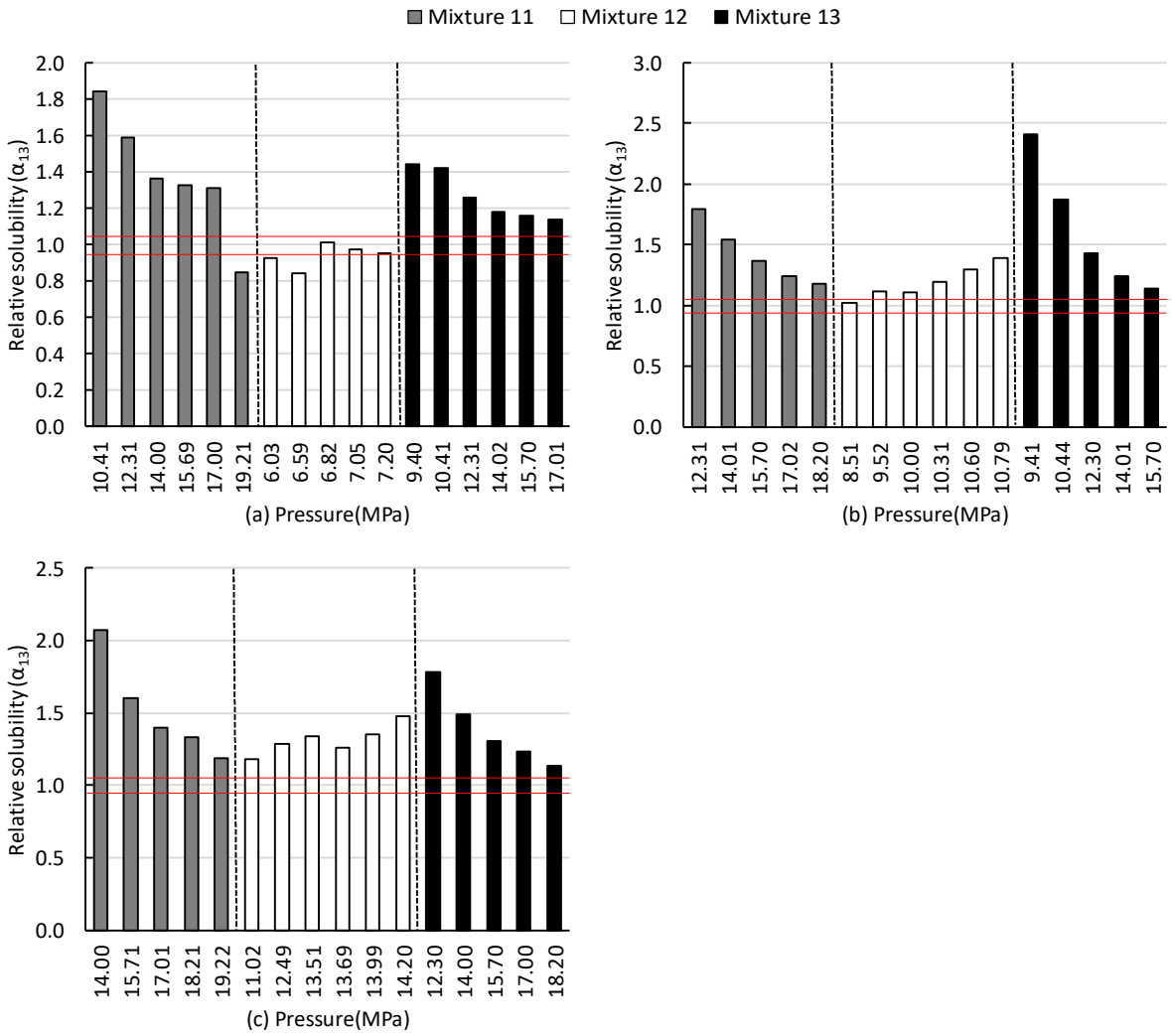

Figure 50: Comparison of relative solubility of 3,7-dimethyl-1-octanol and 1-decanol in three quaternary mixtures at (a) 308.6 K, (b) 328.8 K and (c) 348.9 K

From Figure 50 it is seen that for the 1-decanol rich mixtures, Mixtures 11 and 13, 3,7-dimethyl-1-octanol and 1-decanol are separable at all temperatures considered. Furthermore, with the exception of Mixture 11 at 308.6 K and 19.21 MPa, separation of these mixtures will generally favour the more soluble component, namely 3,7-dimethyl-1-octanol. For the n-dodecane rich mixture, Mixture 12, the separability of the components is seen to improve with temperature. At 308 K, the components are generally inseparable, except at low pressures, where the solubility analysis is less reliable, as discussed previously. At 328 K, the components can be separated but higher pressures are required. At 348 K, the components can be separated and the separation will favour the more soluble component (3,7-dimethyl-1-octanol).

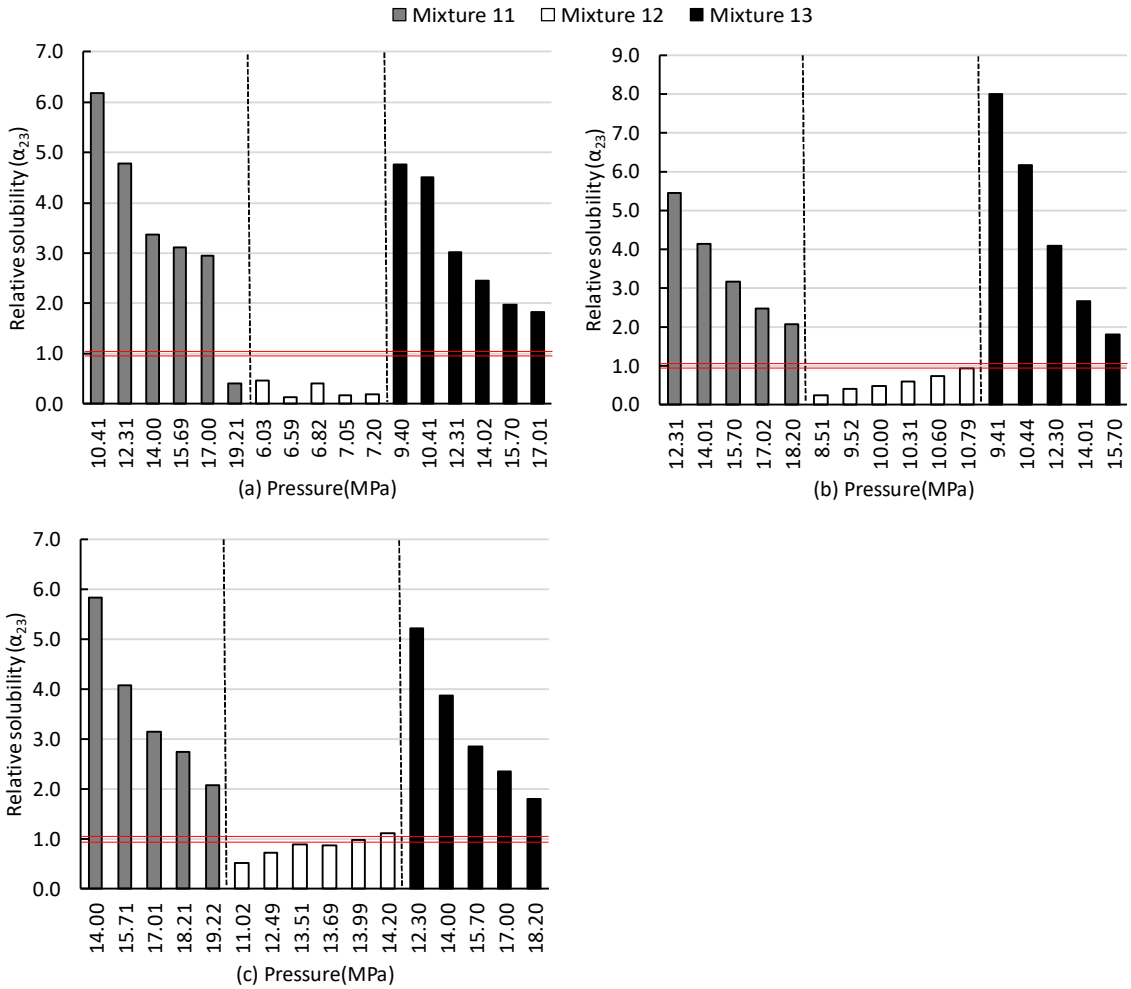

Figure 51: Comparison of relative solubility of n-dodecane and 1-decanol in three quaternary mixtures at (a) 308.6 K, (b) 328.8 K and (c) 348.9 K

Analysis of Figure 51 reveals that separability of n-dodecane and 1-decanol in the 1-decanol rich mixtures, Mixtures 11 and 13, show the same trends as those identified for the separation of 3,7-dimethyl-1-octanol and 1-decanol, discussed previously. For the n-dodecane rich

mixture, Mixture 12, the separability of n-dodecane and 1-decanol is seen to decrease with an increase in temperature. At 308 K, n-dodecane and 1-decanol can be separated at all the pressures considered, but at 348 K the relative solubility values at pressures above 12.49 MPa are generally bordering the region where separation is impractical/ineffective. Furthermore, where separation of n-dodecane and 1-decanol is possible for the n-dodecane rich mixture, separation will generally favour the less soluble component, namely 1-decanol.

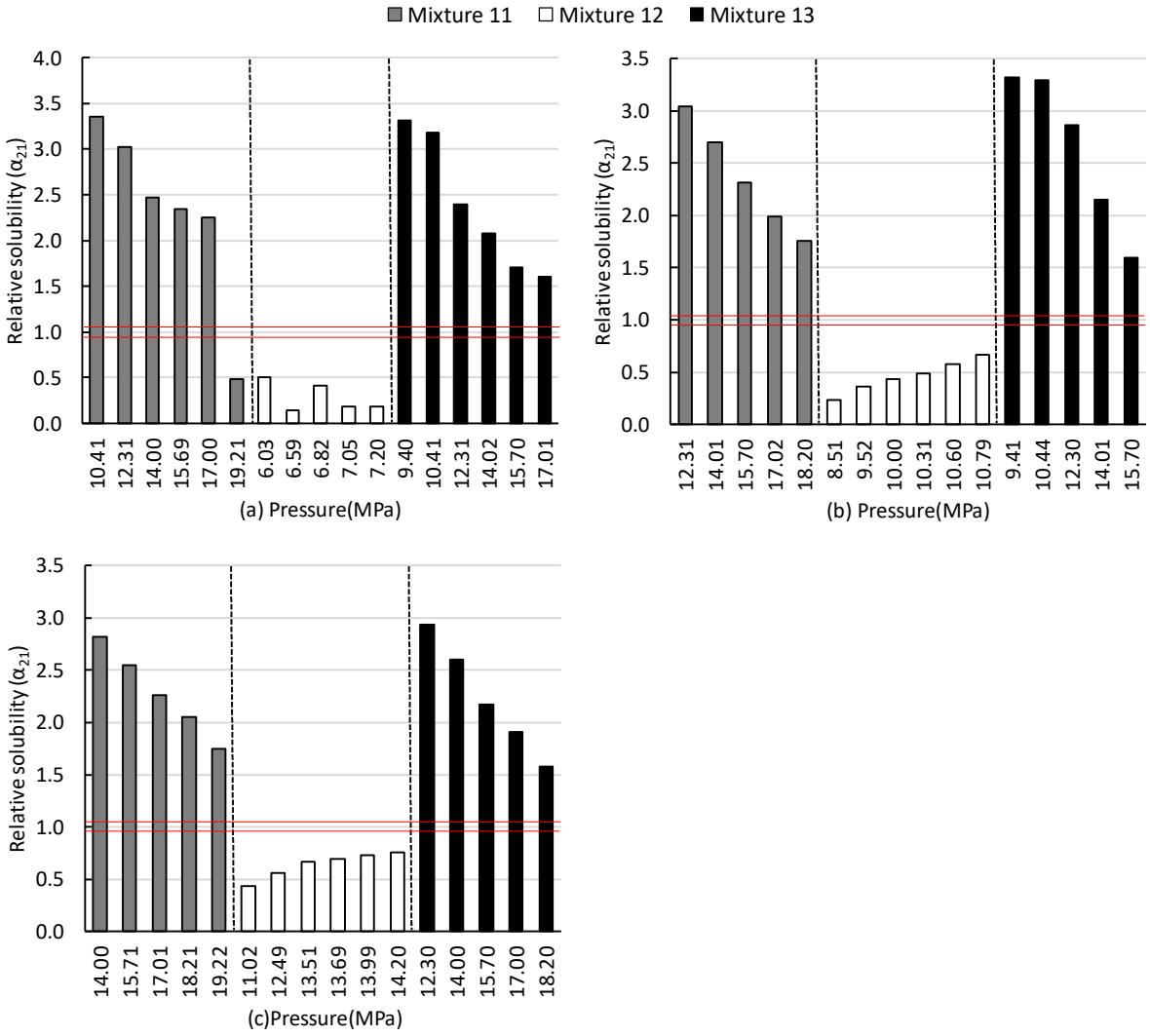

Figure 52: Comparison of relative solubility of n-dodecane and 3,7-dimethyl-1-octanol in three quaternary mixtures at (a) 308.6 K, (b) 328.8 K and (c) 348.9 K

The separability analysis of n-dodecane and 3,7-dimethyl-1-octanol presented in Figure 52 reveals that these components can be separated in all the mixtures and at all temperatures. For the 1-decanol rich mixtures, Mixture 11 and 13, the separation will generally favour the more soluble components, namely n-dodecane. For the n-dodecane rich mixture, Mixture 12, separation will however favour the less soluble component, that is 3,7-dimethyl-1-octanol.

Based on the findings presented here it is evident that the components in the 1-decanol rich mixtures, Mixtures 11 and 13, can be separated with greater ease than the components in the n-dodecane rich mixture, Mixtures 12. For Mixtures 11 and 13, all of the components are separable and separation generally favours the more soluble component. For Mixture 12, only n-dodecane and 3,7-dimethyl-1-octanol can be separated at all the conditions investigated. Separation of n-dodecane from 1-decanol and 1-decanol from 3,7-dimethyl-1-octanol, although possible, is dependent on specific temperature and pressure conditions and the component which will preferentially be extracted also varies. The greater difficulty to separate the components in the n-dodecane rich mixture is likely linked to the co-solvency which occurs in the system that may lead to pinches in separation. The separation difficulties could be resolved by incorporating a pressure-temperature swing setup, that is using more than one column at different temperature and pressure combinations (analogous to pressure-swing distillation).

6.5 Outcome of this chapter

This chapter addresses Objective 2, as it presents and analyses VLE data for the quaternary CO_2 + n-dodecane + 3,7-dimethyl-1-octanol + 1-decanol system.

The main outcomes of this chapter are:

- The inclusion of the experimental difficulties and observation section provided a practical example of how the solute-solute interaction influences not only phase behaviour, but also fluid properties. It was postulated that strong associative solute-solute interactions which exist between the 1-decanol molecules at low temperatures complicated the measurement of VLE data for mixtures consisting largely of 1-decanol, as it altered the fluid properties (viscosity and surface tension) of the mixtures at low temperature.
- In mixtures containing large amounts of 1-decanol, the composition of the co-existing vapour and liquid phases indicated the occurrence of temperature inversions.
- The VLE data for the n-dodecane rich mixture suggested behavioural complexities, but it could not confirm whether or not the mixture is co-solvent.
- Components in the 1-decanol rich mixtures were found to be separable at all the conditions considered in this work and separation generally favours the more soluble component.
- Separation of components in the n-dodecane rich mixture was found to be temperature and pressure dependent and the component which is preferentially extracted varies. The greater

difficulty associated with separating components in the n-dodecane rich mixture is likely linked to co-solvency effects which possibly causes pinches in separation.

The experimental bubble- and dew-point and VLE data presented in Chapter 5 and Chapter 6 provide valuable insight into the effect that solute-solute interactions have on the phase behaviour exhibited by mixtures containing CO_2 with n-dodecane, 3,7-dimethyl-1-octanol and 1-decanol. Conducting experiments to generate phase behaviour data, particularly VLE data, are however costly and time-consuming and therefore the possibility of predicting accurate phase behaviour data using thermodynamic models is investigated in Chapters 7 and 8.

Significant contribution

New high pressure VLE data were measured for 3 mixtures containing CO_2 + n-dodecane + 1-decanol + 3,7-dimethyl-1-octanol. This data provided insight into how the composition of co-existing phases is influenced by solute-solute interactions. It should be noted that to the author's knowledge there exists no VLE data for this system in open literature and this work will therefore be the first to publish VLE data for the quaternary system.

Publications

The work presented in this chapter has contributed to the following publication:

- C. Latsky and C.E. Schwarz, *Measurement and modelling of VLE data for quaternary systems containing supercritical CO_2 with n-dodecane, 1-decanol and 3,7-dimethyl-1-octanol*. To be submitted to the Journal of Chemical and Engineering Data.

7. THERMODYNAMIC MODELLING: MODELS AND MODEL PARAMETERS

Process modelling plays a key role in the design and optimisation of supercritical fractionation processes. The success of process modelling is however dependent on amongst others the accuracy of the thermodynamic model employed to describe the phase behaviour and thermodynamic properties of the system [55].

The aim of this chapter is to fit the model parameters of the selected thermodynamic models, in Aspen Plus®, to allow accurate prediction of phase equilibrium data for systems containing CO_2 with detergent range alkanes and alcohols. This chapter therefore addresses Objective 3.2.

7.1 Thermodynamic models

The thermodynamic modelling is performed in Aspen Plus® with four different variations of the SRK equation of state, namely the RK-SOAVE, RK-ASPEN, CPA and PSRK models. The reasons for selecting these models were addressed in Chapter 3. In this section, details regarding the four models will be provided in accordance to their format within the Aspen Plus® software.

7.1.1 RK-SOAVE model

The RK-SOAVE model is the based on the original Soave-Redlich-Kwong equation of state [53], presented in Equations 7.1 to 7.5, which was developed from the Redlich-Kwong [52] equation of state, by modifying the temperature dependence of the energy parameter to make it more general [53].

$$P = \frac{RT}{v-b} - \frac{a(T)}{v\,(v+b)} \quad [7.1]$$

$$a(T) = 0.42748\frac{(RT_c)^2}{P_c}\,\alpha(T) \quad [7.2]$$

$$\alpha(T) = \left[1 + m\left(1 - \sqrt{T_r}\right)\right]^2 \quad [7.3]$$

$$m = 0.48 + 1.574\omega - 0.176\omega^2 \quad [7.4]$$

$$b = 0.08664\frac{RT_c}{P_c} \quad [7.5]$$

In order to extend the model to mixtures, the energy and co-volume parameters must be estimated using a set of mixing rules. The most commonly used mixing rules are the van der

Waals one-fluid mixing rules, presented in Equations 7.6 and 7.7. The one-fluid mixing rules assume that the properties of a mixture can be represented by a hypothetical pure fluid. This implies that the thermodynamic properties of a constant composition mixture are isomorphic to that of a one-component fluid [114].

$$a = \sum_i \sum_j x_i x_j a_{ij} \quad [7.6]$$

$$b = \sum_i \sum_j x_i x_j b_{ij} \quad [7.7]$$

The cross coefficients, namely a_{ij} and b_{ij}, in Equations 7.6 and 7.7 are determined by applying the following combining rules [50, 115].

$$a_{ij} = \sqrt{a_{ii} a_{jj}}\,(1 - k_{a,ij}) \quad [7.8]$$

$$b_{ij} = \frac{(b_{ii} + b_{jj})}{2}\left(1 - k_{b,ij}\right) \quad [7.9]$$

Where, $k_{a,ij}$and $k_{b,ij}$ are binary interaction parameters which can be regressed from experimental data [45]. For the RK-SOAVE model, the $k_{a,ij}$ parameter is temperature dependent, as shown in Equation 7.10 [16], whilst $k_{b,ij} = 0$.

$$k_{a,ij} = {k_{a,ij}}^0 + {k_{a,ij}}^1 T + \frac{{k_{a,ij}}^2}{T} \quad [7.10]$$

Due to the fact that $k_{b,ij} = 0$, Equation 7.7 reduces to Equation 7.11 [16, 53, 114].

$$b = \sum_i x_i b_i \quad [7.11]$$

7.1.2 RK-ASPEN model

The RK-ASPEN model is based on the SRK equation of state [53], but the energy parameter is modified to include the Mathias (Equations 7.12 and 7.13) and Boston-Mathias (Equations 7.13 to 7.16) alpha functions for sub- and supercritical components, respectively [116]. The reason for using two different alpha functions stems from the fact that the Mathias alpha function was only derived for reduced temperatures below 1 and therefore the Boston-Mathias extrapolation is required at supercritical conditions ($T_r > 1$) [116]. Inclusion of these alpha functions extends the SRK equation to polar systems by introducing a polar parameter, η_i. This polar parameter is highly empirical and can only be determined by regressing pure component vapour pressure data [116].

$$\alpha_i(T) = [1 + m_i\left(1 - \sqrt{T_{ri}}\right) - \eta_i(1 - T_{ri})(0.7 - T_{ri})]^2 \quad [7.12]$$

$$m_i = 0.48508 + 1.55171\omega_i - 0.15613\omega_i^2 \quad [7.13]$$

$$\alpha_i(T) = \left[exp(c_i\left(1 - T_r^{di}\right))\right]^2 \quad [7.14]$$

$$d_i = 1 + \frac{m_i}{2} + 0.3\eta_i \quad [7.15]$$

$$c_i = 1 - \frac{1}{d_i} \quad [7.16]$$

The model is extended to mixtures by using the quadratic van der Waals one-fluid mixing rules presented in Equations 7.6 to 7.9 [116]. Unlike the normal SRK model, the mixing rules for the RK-ASPEN model allows the inclusion of two temperature dependent binary interaction parameters, namely $k_{a,ij}$, $k_{b,ij}$, as presented in Equations 7.17 and 7.18 [5, 16].

$$a = \sum_i \sum_j x_i x_j \sqrt{a_{ii} a_{jj}}\,(1 - k_{a,ij}) \quad \text{with} \quad k_{a,ij} = k_{a,ij}^o + k_{a,ij}^1 \frac{T}{1000} \quad [7.17]$$

$$b = \sum_i \sum_j x_i x_j \frac{(b_{ii} + b_{jj})}{2}\left(1 - k_{b,ij}\right) \quad \text{with} \quad k_{b,ij} = k_{b,ij}^o + k_{b,ij}^1 \frac{T}{1000} \quad [7.18]$$

7.1.3 CPA model

The CPA model, developed by Kontogeorgis et al. [73], combines the SRK equation of state [53] with an association term similar to that of SAFT [66]. The physical interactions between the molecules are accounted for by the SRK model, whilst specific site-site interactions due to hydrogen bonding between like and unlike molecules are accounted for by the association term. The CPA model in Aspen Plus® does not explicitly account for polarity and quadrupolar moments. Due to the incorporation of the association term, assumptions made in the development of the SAFT model, also apply to the CPA model. This allows steric hindrance and cooperativity effects to be neglected, as the activity of each bonding site on a specific molecule is assumed to be independent of bonding on the other sites [117]. The CPA model applied to mixtures can be expressed in terms of pressure as follows [117].

$$P = \underbrace{\frac{RT}{v-b} - \frac{a_o\left[1 + c_1\left(1 - \sqrt{T_r}\right)\right]^2}{v(v+b)}}_{\text{Physical term}} + \underbrace{\frac{RT}{2v}\left(1 + \frac{1}{v}\frac{\partial \ln g}{\partial\left(\frac{1}{v}\right)}\right)\sum_i x_i \sum_{Ai}(1 - X_{Ai})}_{\text{Association term}} \quad [7.19]$$

The term X_{Ai} in Equation 7.19 represents the fraction of A-sites on molecule i which do not bond with other active sites. The value of X_{Ai} is found by solving the following equations [117].

$$X_{Ai} = \frac{1}{1 + \left(\frac{1}{v}\right)\sum_j x_j \sum_{Bj} X_{Bj} \Delta^{A_i B_j}} \quad [7.20]$$

Where $\Delta^{A_iB_j}$ is the association strength between two sites belonging to two different molecules (e.g. site A on molecule i and site B on molecule j) and it is calculated according to Equation 7.21 [44, 117].

$$\Delta^{A_iB_j} = g(v)^{ref}\left[exp\left(\frac{\epsilon^{A_iB_j}}{RT}\right) - 1\right] b_{ij}\beta^{A_iB_j} \qquad [7.21]$$

The $g(v)^{ref}$ term refers to the radial distribution function and it is calculated as follows [117].

$$g(v)^{ref} = \frac{1}{1-1.9\eta} \quad \text{with} \quad \eta = \frac{b}{4v} \quad \text{while} \quad b_{ij} = \frac{b_i + b_j}{2} \qquad [7.22]$$

Prior to calculating the association term, the association scheme of each associating component must be determined. The association scheme determines the number and type of association sites on a molecule [44]. Huang and Radosz [66], developed eight association schemes. The schemes available in the Aspen Plus® software is presented in Table 24 [16, 66, 117].

Table 24: Association schemes available in Aspen Plus® [16] based on the terminology of Huang and Radosz [66]

Type	Sites	Species	Formula	X^A approximations
1A	1 electron donor/ acceptor	Acids	Acids: 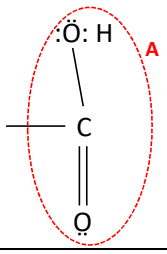	X^A
2B	1 electron donor 1 electron acceptor	Alcohols	Alcohols: 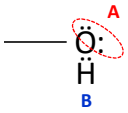	$X^A = X^B$
3B	2 electron donors 1 electron acceptor	Alcohols, Ammonia	Alcohols: 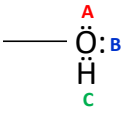	$X^A = X^B$ $X^C = 2X^A - 1$
4C	2 electron donors 2 electron acceptors	Water, Glycols	Water: 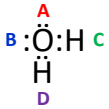	$X^A = X^B = X^C = X^D$

The van der Waals one-fluid mixing rules, presented in Equations 7.6 to 7.9, are applied to calculate the mixture energy and co-volume parameters for the SRK component of the model [44, 117]. The mixing rule for the energy parameter allows the incorporation of a temperature

dependent binary interaction term with a reference temperature of 298.15 K [16]. No interaction parameter is incorporated for the co-volume parameter [44]. The mixing rules for the energy parameter in this model is presented in Equation 7.23, whilst the co-volume parameter is determined using the simplified mixing rule presented in Equation 7.11.

$$a = \sum_i \sum_j X_i X_j \sqrt{a_{ii} a_{jj}} \, (1 - k_{a,ij}) \quad \text{with} \quad k_{a,ij} = k^o_{a,ij} + k^1_{a,ij} \frac{T}{298.15} \qquad [7.23]$$

No mixing rules are required for the association term, but CR-1 combining rules, presented in Equations 7.24 and 7.25, are employed to calculate the cross-association energy (ε^{AiBj}) and volume (β^{AiBj}) parameters between two different associating molecules [16, 44, 117].

$$\varepsilon^{A_i B_j} = \frac{\varepsilon^{A_i B_i} + \varepsilon^{A_j B_j}}{2} \qquad [7.24]$$

$$\beta^{A_i B_j} = \sqrt{\beta^{A_i B_i} \beta^{A_j B_j}} \qquad [7.25]$$

7.1.4 PSRK model

The PSRK model [62] is an EoS/G^E model based on the SRK [53] cubic equation of state, but the energy parameter is adapted to include the Mathias and Copeman [118] alpha function, presented in Equation 7.26.

$$\alpha(T) = [1 + c_1(1 - T_r^{0.5}) + c_2(1 - T_r^{0.5})^2 + c_3(1 - T_r^{0.5})^3]^2 \qquad [7.26]$$

Where c_1, c_2 and c_3 are adjustable polar parameters [16], regressed from pure component vapour pressure data over a wide range of temperatures, typically between $0.5 < T_R < 1$ [119]. At supercritical conditions ($T_R > 1$), parameters c_2 and c_3 are set to zero and c_1 is calculated using the acentric factor [53] i.e. $c_1 = m = 0.48 + 1.574\omega_i - 0.176\omega_i^2$ (see Equation 7.4).

The model is extended to mixtures by employing the PSRK mixing rules [120]. The PSRK mixing rules allow the energy parameter (a) in the SRK model, to incorporate an expression for excess Gibbs energy (g_0^E) at a suitable reference pressure [44, 62]. The reference state for the PSRK mixing rules is the liquid state at atmospheric pressure. The inverse packing fraction is assumed to be constant at an optimised value of 1.1 and the excess molar volume is neglected. Considering this, the following relation is attained [62, 120]:

$$\frac{a(T)}{bRT} = \sum x_i \frac{a_i(T)}{b_i RT} + \frac{1}{-0.64663} \left(\frac{g_0^E}{RT} + \sum x_i \, ln \frac{b}{b_i} \right) \qquad [7.27]$$

Where $a_i(T)$ and b_i are calculated using the SRK derived Equations 7.2 (with the Mathias-Copeman [118] alpha function) and 7.5. The mixture co-volume parameter (b) is calculated using the linear mixing rule presented in Equation 7.11 [120]. The excess Gibbs energy (g_0^E)

is determined by applying Equation 7.28 [44] and using the UNIFAC [63] group contribution model to determine the activity coefficient [62].

$$\frac{g_0^E}{RT} = \sum x_i ln\gamma_i \qquad [7.28]$$

The UNIFAC method [63], is a group contribution method implying that the activity coefficients are not estimated considering the liquid mixture as a solution of molecules, but rather as a solution of structural units from which the molecules are formed. The UNIFAC method [63] is based on the UNIQUAC method [48] and the activity coefficient is calculated using Equation 7.29 [30].

$$\ln\gamma_i = ln\gamma_i^C + ln\gamma_i^R \quad \text{with} \quad ln\gamma_i^C = 1 - J_i + \ln J_i - 5q_i\left(1 - \frac{J_i}{L_i} + \ln\frac{J_i}{L_i}\right) \quad \text{and}$$
$$ln\gamma_i^R = q_i\left[1 - \sum_k\left(\theta_k\frac{\beta_{ik}}{s_k} - e_{ki}\ln\frac{\beta_{ik}}{s_k}\right)\right] \qquad [7.29]$$

Equation 7.29 is solved by applying the following equations and using published data to determine the relative volume (R_k) and relative surface area (Q_k) for each subgroup/structural unit, k, as well as the group interaction parameter (a_{mn}) [30].

$$J_i = \frac{r_i}{\sum_j r_j x_j} \quad \text{with} \quad r_i = \sum_k v_k^{(i)} R_k \qquad [7.30]$$

$$L_i = \frac{q_i}{\sum_j q_j x_j} \quad \text{with} \quad q_i = \sum_k v_k^{(i)} Q_k \qquad [7.31]$$

$$e_{ki} = \frac{v_k^{(i)} Q_k}{q_i} \qquad [7.32]$$

$$\beta_{ik} = \sum_m e_{mi}\tau_{mk} \qquad [7.33]$$

$$\theta_k = \frac{\sum_i x_i q_i e_{ki}}{\sum_j x_j q_j} \qquad [7.34]$$

$$s_k = \sum_m \theta_m \tau_{mk} \qquad [7.35]$$

$$\tau_{mk} = exp\left(\frac{-a_{mn}}{T}\right) \qquad [7.36]$$

Where i and j represents the species index, k identifies the subgroup and m represents an index for the different subgroups. The number of subgroups k in a molecule of specie i is represented by $v_k^{(i)}$ [30].

The UNIFAC model employed in the PSRK model, is revised from the original in that the group interaction parameters allow the incorporation of temperature dependency and therefore Equation 7.36 is reformulated as shown in Equation 7.37 [62]. The UNIFAC groups are also

extended for the PSRK model to include roughly 30 light gasses, amongst these are CO_2 which is applicable to this work.

$$\tau_{mk} = exp\left(-\frac{a_{mn} + b_{mn}T + c_{mn}T^2}{T}\right) \quad [7.37]$$

Where b_{mn} and c_{mn} are set to zero for all UNIFAC main groups up to 44 [62]. The incorporation of temperature dependence allows the UNIFAC method in the PSRK model to be used at higher temperatures and pressures, even at supercritical conditions [120].

In order to extend the PSRK model to highly asymmetric systems, such as the CO_2 + alkane + 1-alcohol systems considered in this work, the Li-correction [79] is applied. The Li-correction is based on the concept of effective R_k and Q_k parameters, as shown in Equations 7.38 and 7.39. The effective parameters for CH_3, CH_2, CH and C depend on the number of carbon atoms in a molecule, calculated using Equation 7.40 [79].

$$R_k^* = f(n_c)R_k \quad [7.38]$$

$$Q_k^* = f(n_c)Q_k \quad [7.39]$$

$$f(n_c) = 1.0 - 0.36983n_c^{\frac{1}{2}} + 1.0287n_c^{\frac{3}{4}} - 1.0199n_c + 0.41645\,n_c^{\frac{5}{4}} - 0.05536n_c^{\frac{3}{2}} \quad [7.40]$$

Where R_k and Q_k are the original UNIFAC parameters and n_c refers to the number of alkyl-carbon atoms. Equation 7.40 is only valid for n_c values smaller than 45 [79].

7.2 Pure component parameters

7.2.1 Critical parameters and acentric factors

The critical temperatures ($T_{c,i}$), critical pressures ($P_{c,i}$) and acentric factors (ω) used in this work, are provided in Table 25. These values were obtained from the built-in Aspen Plus® database [16] and used for all models investigated. These values correspond well to other literature sources [21, 121, 122].

Table 25: Critical properties and acentric factors for the components [16]

Component	$T_{c,i}$ (K)	$P_{c,i}$ (MPa)	ω_i
n-dodecane	658	1.82	0.576
3,7-dimethyl-1-octanol	667	2.55	0.779
1-decanol	688	2.31	0.607
CO_2	304	7.38	0.224

7.2.2 Saturation properties

In order to regress some of the pure component parameters, saturation properties such as vapour pressure and liquid density data are required. The saturated vapour pressure data used in this work were generated using empirical correlations. Depending on the parameters available in the Aspen Plus® database, the vapour pressure data were either calculated using the extended Antoine correlation, presented in Equation 7.41, or the NIST Wagner 25 liquid vapour pressure correlation, presented in Equation 7.42 [16]. The parameters for these equations are provided in Appendix E.1.

$$\ln p_i^* = C_{1,i} + \frac{C_{2,i}}{T + C_{3,i}} + C_{4,i}T + C_{5,i}\ln T + C_{6,i}T^{C_{7,i}} \quad \text{for } C_{8,i} \leq T \leq C_{9,i} \quad [7.41]$$

$$\ln p_i^* = \ln p_{c,i} + \frac{C_{1,i}(1-T_{ri}) + C_{2,i}(1-T_{ri})^{1.5} + C_{3,i}(1-T_{ri})^{2.5} + C_{4,i}(1-T_{ri})^{5}}{T_{ri}} \quad \text{for } C_{5,i} \leq T \leq C_{6,i} \quad [7.42]$$

The saturated molar liquid density data were also generated using empirical correlations available within Aspen Plus® [16]. Depending on the parameters available in the Aspen Plus® database, the liquid density data were either calculated using the DIPPR 105 correlation, presented in Equation 7.43, or the NIST TDE Expansion correlation, presented in Equation 7.44 [16]. The parameters for these equations are provided in Appendix E.1.

$$\rho_i^{*,l} = \frac{C_{1,i}}{C_{2,i}^{1+\left(1-\frac{T}{C_{3,i}}\right)^{C_{4,i}}}} \quad \text{for } C_{6,i} \leq T \leq C_{7,i} \quad [7.43]$$

$$\rho_i^{*,l} = \rho_{c,i} + C_{1,i}^{0.35} + \sum_{m=2}^{n} C_{m,i}\left(1 - \frac{T}{T_{c,i}}\right)^{m-1} \quad \text{for } 0 \leq T\,(K) \leq 1000 \quad [7.44]$$

7.2.3 RK-SOAVE

Apart from the pure component critical properties and acentric factors presented in Table 25, the RK-SOAVE model (basic SRK equation of state) does not include any other pure component parameters which needed to be regressed.

7.2.4 RK-ASPEN

In addition to the pure component parameters listed in Table 25, the RK-ASPEN model also incorporates pure component polar parameters. Unlike the critical properties and acentric factors, the pure component polar parameters were not available in the built-in Aspen Plus® database. Therefore, these parameters needed to be regressed from vapour pressure data.

The polar parameters were regressed from generated vapour pressure data (Equations 7.41 and 7.42), using the built-in regression function in Aspen Plus®. The Britt-Luecke minimization algorithm was employed to perform a maximum-likelihood estimation based on the objective function presented in Equation 7.45 [16, 18].

$$OF = \sum_{i=1}^{NP} \frac{\left|P_{exp,i}^{sat} - P_{calc,i}^{sat}\right|}{P_{exp,i}^{sat}} \qquad [7.45]$$

The regressed polar parameters are presented in Table 26. From Table 26 it is seen that the polar parameter for CO_2 is regressed at temperatures between 250 K – 300 K [14] and not over the temperature range considered in this work. This is due to the fact that the critical temperature of CO_2 is 304 K [16] and therefore vapour pressure data for the solvent could not be generated within the same temperature range as for the solutes. The polar parameter for CO_2 is therefore extrapolated to the temperature range considered in this work.

Table 26: RK-ASPEN pure component polar parameters (η_i) regressed in this work

Component	T-range (K)	η_i
n-dodecane	300 – 360	0.0095
1-decanol	300 – 360	-0.4197
3,7-dimethyl-1-octanol	300 – 360	0.5016
CO_2	250 – 300	0.0503

The polar parameters determined for n-dodecane and 1-decanol correlate well with parameters presented by Zamudio [5], but there is a large deviation between the 3,7-dimethyl-1-octanol polar parameter determined in this work and that reported by Zamudio [5]. The 3,7-dimethyl-1-octanol polar parameter regressed in this work is however deemed to be accurate, as a study conducted by Fourie, et al., [14] reported a 3,7-dimethyl-1-octanol polar parameter of 0.5008, which corresponds closely to the polar parameter determined in this work. The CO_2 polar parameter regressed in this work also correlates well with the CO_2 polar parameter presented by Fourie, et al., [14].

7.2.5 CPA

The CPA model has three pure component parameters (a_o, b, c_1) for non-associating components and five pure component parameters (a_o, b, c_1, ε^{AiBi}, β^{AiBi}) for associating components. In Aspen Plus®, the a_o, b and c_1 parameters are determined by fitting vapour pressure and saturated molar liquid density data to monomer parameters (T_{cm}, P_{cm}, m_m). The

monomer parameters are then related to the a_o, b and c_1 parameters using Equations 7.46 to 7.48 [16, 44].

$$m_m = c_1\sqrt{\frac{a_o\Omega_b}{\Omega_a\, b\, R\, T_c}} \qquad \text{with} \quad \Omega_a = 0.42748, \quad \Omega_b = 0.08664 \qquad [7.46]$$

$$T_{cm} = \left(\frac{1+c_1}{c_1}\,\frac{m_m}{1+m_m}\right)^2 T_c \qquad [7.47]$$

$$P_{cm} = \Omega_b \frac{RT_{cm}}{b} \qquad [7.48]$$

The association energy (ε^{AiBi}) and association volume (β^{AiBi}) parameters are also fitted to vapour pressure and saturated molar liquid density data and the association type is selected based on the number of active sites (see Table 24).

The pure component parameters for n-dodecane, 1-decanol and CO_2 were regressed with the built-in regression function in Aspen Plus®, using vapour pressure and saturated liquid density data generated over a reduced temperature range (T_r) of 0.5 to 0.9 using Equations 7.41 to 7.44 [44]. Initial values for the parameters were obtained from literature [73, 76]. These initial estimates were input into Aspen Plus® to allow convergence at a unique set of parameters. A maximum-likelihood estimation, based on the objective function in Equation 7.49 [18], was performed using the Britt-Luecke minimization algorithm to regress the parameters [16].

$$OF = \sum_{i=1}^{NP}\frac{\left|P_{exp,i}^{sat} - P_{calc,i}^{sat}\right|}{P_{exp,i}^{sat}} + \sum_{i=1}^{NP}\frac{\left|\rho_{exp,i}^{sat} - \rho_{calc,i}^{sat}\right|}{\rho_{exp,i}^{sat}} \qquad [7.49]$$

Due to the absence of literature parameters for 3,7-dimethyl-1-octanol, the approach to regress the pure component parameters needed to be adapted, as initial estimates must be provided in order to regress the parameters and obtain a unique set of parameters. The regression data sets for the 3,7-dimethyl-1-octanol parameter estimation therefore included a set of high pressure VLE data for a system containing 3,7-dimethyl-1-octanol + ethane [123], along with the saturated liquid density and vapour pressure data. This was done as Fourie [14] indicated that this approach allows the regression of a unique set of parameters capable of predicting pure component as well as mixture data. The pure component parameters for ethane were regressed using the same procedure as for n-dodecane, 1-decanol and CO_2, explained above. Due to the inclusion of the high pressure data in the regression, the saturated liquid density and vapour pressure data were generated over a reduced temperature range (T_r) of 0.7 to 0.95 [44]. The Britt-Luecke minimization algorithm was employed to perform a maximum-likelihood

estimation based on the objective function presented in Equation 7.50 [16, 18, 124] . In order to ensure that the model predicts accurate pure component and mixture data, the weight contribution of the data sets to the regression was adapted to allow the pure component data to weigh more than the mixture VLE data ($w_1 = w_2 = 2$; $w_n = 0.1$).

$$OF = w_1 \sum_{i=1}^{NP} \frac{\left|P_{exp,i}^{sat} - P_{calc,i}^{sat}\right|}{P_{exp,i}^{sat}} + w_2 \sum_{i=1}^{NP} \frac{\left|\rho_{exp,i}^{sat} - \rho_{calc,i}^{sat}\right|}{\rho_{exp,i}^{sat}} + \sum_{n=1}^{NDG} w_n \sum_{i=1}^{NP} \left[\left(\frac{T_{exp,i} - T_{calc,i}}{\sigma_{T,i}}\right)^2 + \left(\frac{P_{exp,i} - P_{calc,i}}{\sigma_{P,i}}\right)^2 + \sum_{j=1}^{NC-1}\left(\frac{x_{exp,i,j} - x_{calc,i,j}}{\sigma_{x,i,j}}\right)^2 + \sum_{j=1}^{NC-1}\left(\frac{y_{exp,i,j} - y_{calc,i,j}}{\sigma_{y,i,j}}\right)^2\right] \quad [7.50]$$

The alcohols (1-decanol and 3,7-dimethyl-1-octanol) were modelled using the 2B association scheme, which is in accordance with literature [44, 75, 117]. Due to the fact that CO_2 has a very large quadrupole moment, which is not accounted for by the CPA model available within Aspen Plus®, literature approaches to modelling CO_2 using the CPA model were reviewed. Various literature sources [75, 76, 77, 125] have investigated different approaches to model CO_2 using CPA, but no consensus as to which approach is best has been reached. Therefore, in this work, 4 different scenarios were tested, that is modelling CO_2 as non-associating (n.a.) and associating with type 2B, 3B and 4C schemes, in order to determine which is best suited for this application of the CPA model. The accuracy of each approach was analysed by determining the percentage average absolute deviation (%AAD) between the predicted and experimental data. The percentage absolute average deviation (%AAD), calculated using Equation 7.51 [5], was only used as a comparative quantity in this work and not an absolute error measurement.

$$\%AAD = \frac{1}{n} \sum_{i=1}^{n} \left|\frac{Z_{measured} - Z_{predicted}}{Z_{measured}}\right| x\ 100 \quad [7.51]$$

The accuracy with which the phase transition pressures are predicted at 338 K and 348 K for the three binary systems using the different approaches is analysed in Table 27. The model used to obtain the pressure predictions for the accuracy analysis included solvent-solute binary interaction parameters, the method to regress these parameters and the final values will be presented in section 7.3.2. The accuracy analysis was performed at 338 K and 348 K to reduce error introduced due to the model's inability to predict data close to the solvent critical point [10].

Table 27: Comparison of the accuracy of phase transition pressure predictions obtained when using different approaches to model CO_2

	CO_2 + n-dodecane			CO_2 + 1-decanol			CO_2 + 3,7-dimethyl-1-octanol			Combined overall %AAD[3]
	%AAD			%AAD			%AAD			
	P_{338K}	P_{348K}	Overall[2]	P_{338K}	P_{348K}	Overall[2]	P_{338K}	P_{348K}	Overall[2]	
n.a.[1]	1.4	1.0	1.2	23.0	22.7	22.9	7.2	8.3	7.7	10.6
2B	3.0	2.4	2.7	3.6	5.1	4.4	7.1	9.6	8.3	5.1
3B	3.1	2.5	2.8	4.1	5.7	4.9	6.5	9.4	8.0	5.2
4C	3.0	2.4	2.7	4.5	6.0	5.2	6.6	9.6	8.1	5.4

[1]Non-asssociating
[2]Average of $\%AAD_{P338K}$ and $\%AAD_{P348K}$
[3]Average of the overall %AAD for the two binary systems

When analysing the %AAD values for the CO_2 + n-dodecane system it is noted that although there is little difference in accuracy when modelling CO_2 as an inert or associating compound, modelling of CO_2 as a self-associating compound does slightly decrease model accuracy, regardless of the association scheme used. The %AAD values for the CO_2 + 1-decanol system reveals that modelling CO_2 as a non-associating component results in large deviations between the experimental and predicted data. This is corrected by modelling CO_2 as an associating component. When analysing the %AAD values for the CO_2 +3,7-dimethyl-1-octanol system, presented in Table 27, it is noted that there is not much difference in accuracy when modelling CO_2 as an inert or associating compound, regardless of the association scheme used.

From the results presented here it is clear that CO_2 must be modelled as an associating compound when predicting data for systems containing 1-decanol. When considering the %AAD values presented in Table 27, the difference between the different schemes are marginal, with the 2B scheme performing slightly better than the 3B and 4C schemes. Based on the this and the fact that the approach to modelling CO_2 as a self-associating compound is not theoretically correct (CO_2 is not self-associating), the least rigorous approach, that is the simplest relevant association scheme, namely the 2B scheme (illustrated in Figure 53), will be applied to model CO_2. The approach to modelling CO_2 as a 2B associating compound will be consistent whether or not a system contains 1-decanol. The final pure component parameters for the CPA model are presented in Table 28.

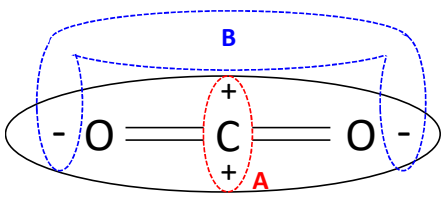

Figure 53: Modelling CO_2 using the 2B scheme simplifies it to have one-positive and one-negative site

Table 28: Pure component CPA parameters regressed in this work

Component	T_{cm} (K)	P_{cm} (Pa)	m_m	ε/R (K)	β	Association type
n-dodecane	677.74	2261043	1.23967	-	-	-
1-decanol	705.34	2760248	1.072324	3373.58	0.000391	2B
3,7-dimethyl-1-octanol	673.33	2663621	1.524217	2881.49	0.000110	2B
CO_2	299.75	7792082	0.729683	451.97	0.049187	2B

7.2.6 PSRK

Along with the pure component critical parameters and acentric factors, the PSRK model also incorporates a set of Mathias-Copeman parameters for each pure component. The Mathias-Copeman parameters, presented in Table 29, were regressed from vapour pressure data generated using the empirical correlations presented in Equations 7.41 and 7.42. The objective function employed in the regression is presented in Equation 7.45.

Table 29: Mathias-Copeman parameters regressed in this work using vapour pressure data

Component	T-range (K)	c_1	c_2	c_3
n-dodecane	329 – 658	1.4296	-0.9329	1.9714
1-decanol	344 – 688	1.4389	-1.2910	5.4653
3,7-dimethyl-1-octanol	334 – 667	1.6742	0.0534	-3.1156
CO_2	217 – 304*	0.8863	-0.9120	3.2543

*Smaller temperature range as empirical correlation cannot be used below 216.58 K [16].

The PSRK model also requires the van der Waals relative volume (R_k) and relative surface area (Q_k), for each structural unit from which the molecules of the different components are formed. Based on the molecular formula of each component and the van der Waals group assignments, the relevant R_k and Q_k values, presented in Table 30, were obtained from literature [16, 120].

Table 30: Group assignment and van der Waals relative volume (R_k) and surface area (Q_k) parameters, obtained from literature [16, 120], for the structural units applicable to this work

Main group	Sub group	k	Aspen Plus® group number	R_k	Q_k
1 CH_2	CH_3	1	1015	0.9011	0.848
	CH_2	2	1010	0.6744	0.540
	CH	3	1005	0.4469	0.228
5 OH	OH	14	1200	1.0000	1.200
56 CO_2	CO_2	117	3850	1.3000	0.982

7.3 Interaction parameters

7.3.1 UNIFAC group interaction parameters for the PSRK model

The PSRK model incorporates parameters to account for interactions between the different structural units in a mixture. These interaction parameters are determined from low pressure VLE data [119] and are specified in terms of main group interactions, as the group interaction between all subgroups belonging to the same main group are considered identical [30]. The group interaction parameters applicable to this work were obtained from literature [120] and are presented in Table 31.

Table 31: Group interaction parameters obtained from literature [120] for the PSRK model (group m and n refer to main groups)

Group m	Group n	a_{mn} (K)	b_{mn}	$c_{mn}(K^{-1})$	a_{nm}(K)	b_{nm}	$c_{nm}(K^{-1})$
1 "CH_2"	5 "OH"	986.5			156.4		
1 "CH_2"	56 "CO_2"	919.8	-3.9132	4.63E-03	-38.672	0.8615	-1.79E-03
5 "OH"	56"CO_2"	510.64			148.16		

7.3.2 Binary solvent-solute interaction parameters for the RK-SOAVE, RK-ASPEN and CPA models

The RK-SOAVE, RK-ASPEN and CPA models also incorporate interaction parameters, but unlike the PSRK model these parameters are regressed from high pressure phase behaviour data for specific molecule-molecule interactions. The interaction parameters presented in this section are employed to account for interactions between the solvent and solute molecules.

The binary solvent-solute interaction parameters presented here were regressed using the built-in regression function in Aspen Plus®. In order to perform the regressions, experimental VLE data for the CO_2 + n-dodecane, CO_2 + 3,7-dimethyl-1-octanol and CO_2 + 1-decanol systems were required. Literature data published by Zamudio [5] was used for the regressions. Zamudio [5] however measured bubble- and dew-point data and therefore the data needed to be converted to VLE data, prior to performing the regressions. This was done by fitting pressure-composition curves to the bubble- and dew-point data and using the correlations to calculate the composition of the co-existing phases in 0.2 MPa intervals [5]. This approach to convert bubble- and dew-point data to VLE data worked well for the CO_2 + 3,7-dimethyl-1-octanol and CO_2 + 1-decanol systems, but was less successful for the CO_2 + n-dodecane system. The conversion of data for the CO_2 + n-dodecane system was complicated by the fact that the

bubble- and dew-point curves for the system are very flat (little curvature). Due to this only a limited number of VLE data points could be generated.

The built-in regression function in Aspen Plus® uses the VLE data as input and employs the Britt-Luecke minimization algorithm to perform a maximum-likelihood estimation based on the objective function presented in Equation 7.52 [16, 18, 124] to regress the interaction parameters.

$$OF = \sum_{n=1}^{NDG} w_n \sum_{i=1}^{NP} \left[\left(\frac{T_{exp,i} - T_{calc,i}}{\sigma_{T,i}} \right)^2 + \left(\frac{P_{exp,i} - P_{calc,i}}{\sigma_{P,i}} \right)^2 + \sum_{j=1}^{NC-1} \left(\frac{x_{exp,i,j} - x_{calc,i,j}}{\sigma_{x,i,j}} \right)^2 + \sum_{j=1}^{NC-1} \left(\frac{y_{exp,i,j} - y_{calc,i,j}}{\sigma_{y,i,j}} \right)^2 \right] \quad [7.52]$$

The binary solvent-solute interaction parameters regressed for the three different models, which incorporate these parameters, are presented in Table 32. It is noted that the solvent-solute BIPs were only regressed using data between 338 K to 348 K. This was done to reduce the error introduced due to the model's inability to regress data close to the solvent critical point. Data points within the critical region, which caused convergence errors, were removed from the data sets and excluded from the regression procedure [5, 126].

Table 32: Binary solvent-solute interaction parameters regressed in this work for the RK-SOAVE, CPA and RK-ASPEN models

Solvent-solute BIP CO_2 + ...	T-range (K)	RK-SOAVE	CPA	RK-ASPEN		
		$k_{a,ij}^0$	$k_{a,ij}^0$	$k_{a,ij}^0$	$k_{a,ij}^1$	$k_{b,ij}^0$
n-dodecane	338 – 348	0.09182	0.07760	0.08910		0.04398
1-decanol	338 – 348	0.10630	0.14732	0.20307	-0.34900	-0.03063
3,7-dimethyl-1-octanol	338 – 348	0.06122	0.09756	0.22401	-0.43828	

From the table it is also noted that temperature dependence was only incorporated in the RK-ASPEN model. The reason for this is that the inclusion of temperature dependence in the RK-ASPEN model improved the model accuracy to such a degree that the decrease in model robustness could be justified. In order to illustrate this, the %AAD regression results with and without the inclusion of temperature dependence for the CO_2 + 1-decanol and CO_2 + 3,7-dimethyl-1-octanol interaction parameters are presented in Appendix E.2.

7.3.3 Binary solute-solute interaction parameters for the RK-SOAVE, RK-ASPEN and CPA models

In addition to solvent-solute interaction parameters, binary interaction parameters which account for interactions between the different solutes in a mixture can also be incorporated in the RK-SOAVE, RK-ASPEN and CPA models. In this section, two sets of binary interaction parameters, regressed to account for solute-solute interactions in mixtures containing CO_2 with n-dodecane, 3,7-dimethyl-1-octanol and 1-decanol, are presented. The one set of solute-solute interaction parameters was regressed using ternary bubble- and dew-point data whilst the other was regressed using ternary VLE data. This was done to allow investigation of the effect that using different data types to regress interaction parameters has on the accuracy of the model.

7.3.3.1 Interaction parameters regressed using bubble- and dew-point data

When using bubble- and dew-point data to determine binary interaction parameters (BIPs), the built-in Aspen Plus® regression function cannot be used, as the regression function requires VLE input data. The binary solute-solute interaction parameters presented in this section were therefore determined by manually regressing bubble- and dew-point data for ternary systems containing CO_2 with n-dodecane, 3,7-dimethyl-1-octanol and 1-decanol [5, 13].

This approach entailed using a two-outlet flash drum in an Aspen Plus® flowsheet to predict the phase transition pressures of the different mixtures. The feed temperature, pressure and composition along with the operating temperature and vapour fraction of the flash drum were specified to resemble experimental conditions [9, 13]. In the high solute concentration region, bubble-point data were simulated by setting the vapour fraction equal to zero, whilst in the low solute concentration region, dew-point data were simulated by setting the vapour fraction equal to one. The pure component parameters and binary solvent-solute interaction parameters, regressed in this work, were incorporated in the models along with manually selected BIPs values (ka_{ij}^0 for RK-SOAVE, ka_{ij}^0 and kb_{ij}^0 for RK-ASPEN, ka_{ij}^0 for CPA) [13]. The phase transition pressure was then predicted with the Gibbs flash convergence algorithm. The percentage absolute average deviation (%AAD) between the predicted and measured phase transition pressure was calculated [9, 13]. If a data point resulted in a convergence error, it was excluded from the %AAD calculation. The simulation runs were repeated using different BIP values to determine which BIPs, within the range investigated, resulted in the lowest overall percentage absolute average deviation (%AAD) [13].

The ternary bubble- and dew-point data for the CO_2 + n-dodecane + 3,7-dimethyl-1-octanol and CO_2 + 3,7-dimethyl-1-octanol + 1-decanol systems, measured in this work, was used to regress the n-dodecane + 3,7-dimethyl-1-octanol and 3,7-dimethyl-1-octanol + 1-decanol solute-solute interaction parameters. The n-dodecane + 1-decanol solute-solute interaction parameter was regressed using bubble- and dew-point data obtained from literature [13]. For each ternary system, binary solute-solute interaction parameters were regressed for three different mixtures at 338 K and 348 K. These temperatures were selected to reduce the error introduced by the inability of the model to predict data close to the solvent critical temperature, as discussed previously [5]. All possible BIP values could not be investigated and regression limits were therefore imposed. These limits were set at BIP values beyond which further expansion of the regression range did not significantly improve the model fit or worsened it. The results of the regressions performed for each model, along with the limits within which the regressions were performed, are presented in Appendix E.3. The final interaction parameter values for each system were selected based on the interaction parameters which resulted in the lowest combined %AAD for all three mixtures at 338 K and 348 K and the results for each model is presented in Table 33.

Table 33: RK-SOAVE, CPA and RK-ASPEN binary solute-solute interaction parameters regressed in this work using HPBDP data

Solute-solute BIP CO_2 + ...	RK-SOAVE	CPA	RK-ASPEN	
	$k_{a,ij}^0$	$k_{a,ij}^0$	$k_{a,ij}^0$	$k_{b,ij}^0$
n-dodecane + 37DM1O	0.050	0.060	0.105	0.150
1-decanol + n-dodecane	0.030	0.010	0.075	0.075
37DM1O + 1-decanol	0.020	0.030	0.015	0.015

It should be noted that the interaction parameter values presented in Table 33 are the optimum interaction parameters within the regression range investigated and the data used. Investigation beyond these limits could however reveal interaction parameters better suited to account for solute-solute interactions, but the use of the manual regression procedure prohibits investigation of all the different combinations. The low resolution (relatively large parameter intervals and limited temperature range) of the manual regression approach also prevents investigation into the effect of incorporating temperature dependency when determining the interaction parameters [5]. The inclusion of the interaction parameters presented in Table 33 could therefore improve the model fit, but it might not result in the best fit.

7.3.3.2 Interaction parameters regressed from vapour-liquid-equilibrium data

Binary solute-solute interaction parameters were also regressed from ternary VLE data, using the built-in Aspen Plus® regression function. The same objective function used for the regression of the solvent-solute interaction parameters, presented in Equation 7.52, was employed to regress the solute-solute interaction parameters presented in this section [16, 18, 124]. The ternary VLE data used for the regressions were obtained from literature [14]. Due to the inability of the models to regress data at temperatures close to the solvent critical and within the mixture critical region, all data sets measured at 308 K as well as data points located within the mixture critical region which resulted in convergence errors were excluded from the regression procedure. The solute-solute interaction parameters regressed for the RK-SOAVE, CPA and RK-ASPEN models are presented in Table 34.

Table 34: RK-SOAVE, CPA and RK-ASPEN binary solute-solute interaction parameters regressed in this work using VLE data obtained from literature [14]

Solute-solute BIP CO_2 + ...	RK-SOAVE	CPA	RK-ASPEN	
	$k_{a,ij}^0$	$k_{a,ij}^0$	$k_{a,ij}^0$	$k_{b,ij}^0$
n-dodecane + 37DM1O	0.0224	0.0246	0.1121	0.1498
1-decanol + n-dodecane	0.0101	-0.0220	0.0827	0.1002
37DM1O + 1-decanol	-0.0325	-0.0542	0.0355	0.0637

When analysing the binary solute-solute interaction parameters, presented in Table 34, it is noted that none of the interaction parameters are temperature dependent, although the built-in regression method in Aspen Plus® allows the incorporation of temperature dependency. This is to allow fair comparison between the interaction parameters regressed from bubble- and dew-point and VLE data, since the low resolution of the bubble- and dew-point manual regression procedure prevents the incorporation of temperature dependence, as stated previously. In order to determine the effect of this limitation on model accuracy, the model fit of the VLE regressed solute-solute interaction parameters, with and without temperature dependency for all three models is compared in Appendix E.3.

7.4 Outcome of this chapter

The aim of this chapter was to fit the model parameters of the RK-SOAVE, RK-ASPEN, CPA and PSRK models in Aspen Plus® to allow accurate prediction of phase equilibrium data for systems containing CO_2 with detergent range alkanes and alcohols.

The main outcomes of this chapter are:

- The parameters for each of the models were determined to be as follow.
  - *RK-SOAVE*

    Pure component parameters: T_c, P_c, ω

    Interaction parameters: $k_{a,ij}^0$, $k_{a,ij}^1$, $k_{a,ij}^2$
  - *RK-ASPEN*

    Pure component parameters: T_c, P_c, ω, η_i

    Interaction parameters: $k_{a,ij}^0$, $k_{a,ij}^1$ and $k_{b,ij}^0$, $k_{b,ij}^1$
  - *CPA*

    Pure component parameters: a_0, b, c_1, ε, β

    Interaction parameters: $k_{a,ij}^0$, $k_{a,ij}^1$
  - *PSRK*

    Pure component parameters: T_c, P_c, ω, c_1, c_2, c_3

    Parameters for structural units: R_k, Q_k

    Group interaction parameters: a_{mn}, b_{mn}, c_{mn} and a_{nm}, b_{nm}, c_{nm}
- The pure component parameters were obtained from literature or regressed.
- The UNIFAC parameters were obtained from literature.
- Solvent-solute interaction parameters and two sets of solute-solute interaction parameters were also regressed. The one set of solute-solute BIPs was regressed using bubble- and dew-point data (manual regression) and the other was regressed using VLE data (built-in regression function).

By achieving the aim of this chapter, Objective 3, in particular sub-objective 3.2, of the project was addressed. In the next chapter, the effect of incorporating the interaction parameters regressed in this chapter on model accuracy will be analysed. The performance of the different models will also be compared to determine which is best suited to predict equilibrium data for systems containing CO_2 with detergent range alkanes and alcohols.

Publications

The model parameters and modelling techniques presented in this section formed/will form part of all the publications as all articles presenting measured data (4 articles) includes modelling.

8. THERMODYNAMIC MODELLING: TERNARY AND QUATERNARY SYSTEMS

The RK-SOAVE, RK-ASPEN, CPA and PSRK thermodynamic models were selected to generate phase equilibrium data for systems containing CO_2 with detergent range alkanes and alcohols and the model parameters were fitted in the previous chapter. The aims of this chapter are to:

(i) Evaluate the accuracy with which these models can generate phase equilibrium data when incorporating the fitted interactions parameters.

(ii) Investigate the effect of using different data types to regress the solute-solute interaction parameters on model accuracy.

(iii) Compare the performance of the different models, when including the optimum parameters, to determine which model is best suited to generate phase equilibrium data for the systems.

This chapter will therefore address Objective 3, specifically sub-objectives 3.3 and 3.4. In the first section of this chapter, section 8.1, the phase equilibrium data of the ternary subsystems are modelled using the four fitted models. This section will provide insight into the accuracy with which the models can correlate data and how the fitted parameters influence model accuracy (*sub-objective 3.3*). The results of this section will provide insight into which BIPs are required to improve model accuracy when predicting the quaternary phase equilibrium data in the second section. In section 8.2, the predictive capability of the fitted models will be evaluated and compared to determine which is best suited to predict data for the quaternary system, which is the main focus of the modelling (*sub-objective 3.4*). Both sections will also provide an outcome as to how the type of data used to fit the model parameters influences the model's ability to correlate (ternary) and predict (quaternary) phase equilibrium data for these systems (*sub-objective 3.3*).

8.1 Modelling ternary phase equilibrium data

In this section the ability of the RK-SOAVE, RK-ASPEN, CPA and PSRK models to generate equilibrium data for the ternary subsystems will be evaluated and compared. The bubble- and dew-point data were modelled by implementing the flash algorithm in Aspen Plus® and specifying the flash drum feed and operating conditions to resemble the experimental

conditions at which the data were measured [9]. The VLE data were modelled using the built-in evaluation function in Aspen Plus® [14].

The accuracy of the models was evaluated and compared by performing %AAD analyses as well as constructing and analysing pressure-composition diagrams for the bubble- and dew-point data and Gibbs phase diagrams for the VLE data. In the Gibbs phase diagrams, the tie-lines were constructed using data obtained from Fourie [14] and data obtained from Zamudio [5] were used to define the binary boundary conditions.

8.1.1 CO_2 + n-dodecane + 1-decanol

The ability of the four models to correlate phase equilibrium data for ternary CO_2 + n-dodecane + 1-decanol mixtures, is evaluated and compared in this section. The bubble- and dew-point data modelled here was obtained from literature [5, 13]. To allow ease of reference, the mixtures containing 0.90, 0.80, 0.40 [13] and 0.222 [5] mass fraction n-dodecane, will be referred to as mixtures SS1, SS2, SS3 and Z4, respectively. The VLE data modelled in this section was obtained from work done by Fourie [14].

8.1.1.1 RK-SOAVE

High pressure bubble- and dew-point data

Figure 54 indicates the accuracy with which the RK-SOAVE model can correlate bubble- and dew-point data for this system. The diagrams clearly illustrate the significant improvement in model fit when incorporating the solvent-solute BIPs. This improvement is deemed to be due to the fact that the regressed BIPs account for the large quadruple moment of CO_2, which causes complex phase behaviour in the mixtures [125] and cannot be accounted for by the model itself.

The effect of including the solute-solute BIP on model accuracy it is seen to be mixture dependent. As the 1-decanol content in the mixture increases, the necessity of including the solute-solute BIP becomes more apparent. From Figures 54 (b) to (d) it is noted that the inclusion of the solute-solute BIP reduces the degree of overprediction in the mixture critical region at temperatures above 318 K, regardless of the type of data used to regress it. For the mixtures consisting largely of 1-decanol, presented in Figure 54 (c) and (d), the inclusion of the solute-solute BIP is also seen to improve the model fit in the high solute concentration region at higher temperatures. This is likely due to the fact that as the amount of 1-decanol in

the overall mixture composition increases, the mixtures become more polar and interactions between the solutes become more apparent. The RK-SOAVE model is best suited for non-polar or slightly polar mixtures [16] and therefore as the polarity of the mixture increases, fitted solute-solute BIPs are required to account for the complex behaviour which occur due to solute-solute interactions in the mixtures.

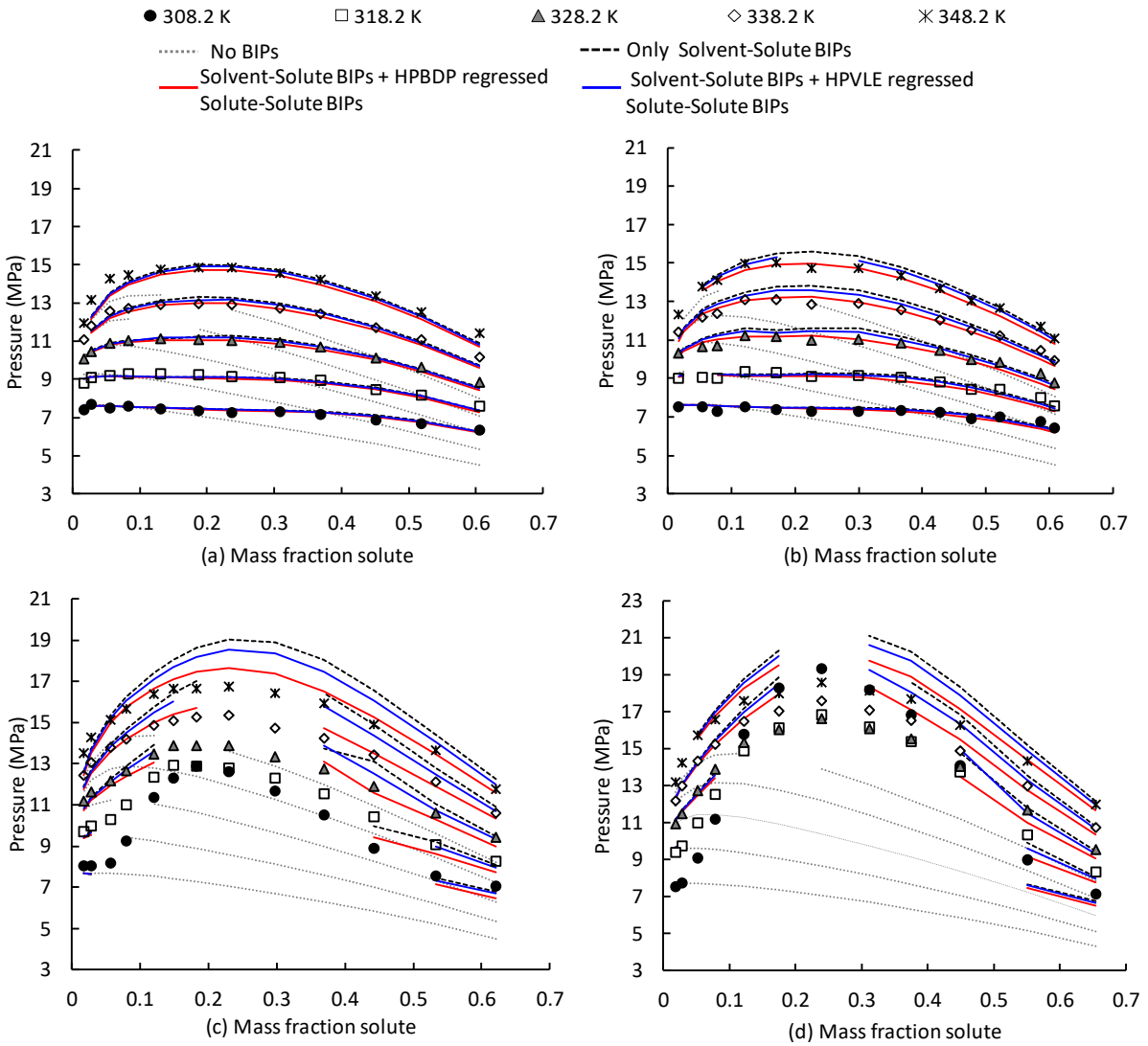

Figure 54: Pressure-composition diagrams comparing experimental data to data generated using the RK-SOAVE model for (a) Mixture SS1: 90wt% nC_{12} + 10 wt% $C_{10}OH$ [13], (b) Mixture SS2: 80wt% nC_{12} + 20 wt% $C_{10}OH$ [13], (c) Mixture SS3: 40wt% nC_{12} + 60 wt% $C_{10}OH$ [13] and (d) Mixture Z4: 22.2wt% nC_{12} + 77.8 wt% $C_{10}OH$ [5]

It is noted that for Mixture SS1 (90 wt% n-dodecane) there is little difference in the model fit obtained when incorporating the BIPs regressed from HPBDP and HPVLE data. For the other mixtures, containing more 1-decanol, the fit obtained using the solute-solute BIP regressed from HPBDP data is however generally more accurate.

Analysis of the model fit attained when incorporating the solute-solute BIP regressed from HPBDP data (more accurate BIP) reveals that there is generally good correlation between the experimental and predicted data for Mixtures SS1 and SS2 (n-dodecane rich). For Mixtures SS3 (40 wt% n-dodecane) and Z4 (22 wt% n-dodecane), a decrease in model accuracy is however noted. The decrease in model accuracy with an increase in 1-decanol content is likely linked to the increased polarity and complexity of the mixtures and the inability of the RK-SOAVE model to account for this, as discussed previously. For these mixtures there also exists a large range of compositions for which the model cannot correlate phase transition data at lower temperatures. The correlated data at these conditions are also seen to be fairly inaccurate. This is likely due to the fact that the model cannot account for the temperature inversion which occurs in the system. At higher temperatures there are also regions within the mixture critical region where the model cannot correlate phase transition pressures. This is due to inherent model flaws, as equations of state based models are known to struggle to predict accurate data within the mixture critical region [127].

High pressure vapour-liquid-equilibrium data

The accuracy with which the RK-SOAVE model can correlate VLE data for this system is evaluated in Figure 55. It is noted that the inclusion of the solvent-solute BIPs significantly improves model accuracy at 328 K and 348 K. At 308 K, however, the incorporation of this parameter only improves the accuracy of the liquid phase correlations and slightly decreases the accuracy of the vapour phase correlations. The addition of the solute-solute BIPs, regardless of the type of data used to regress the parameter, does not improve model accuracy at 308 K and the %AAD values reported at this temperature are very large. The inability of the BIPs to improve model accuracy at 308 K could be due to the fact that the low temperature data sets were not included when regressing these parameters. The large errors could also be due to the fact that the model cannot account for the temperature inversion which occurs in the system. Another contributing factor could also be inherent model flaws, as equations of state based model have been reported to struggle to predict phase behaviour data close to the solvent critical point [126].

Comparison of the model accuracy attained when incorporating the solute-solute BIPs regressed using different data types reveals that at 328 K, the model which incorporates the HPVLE regressed BIP is better suited to correlate VLE data. At 348 K, both sets of solute-solute BIPs perform similarly. Furthermore, it is noted that regardless of the type of BIP

included in the model, there still exist significant deviations between the experimental data and the correlated data.

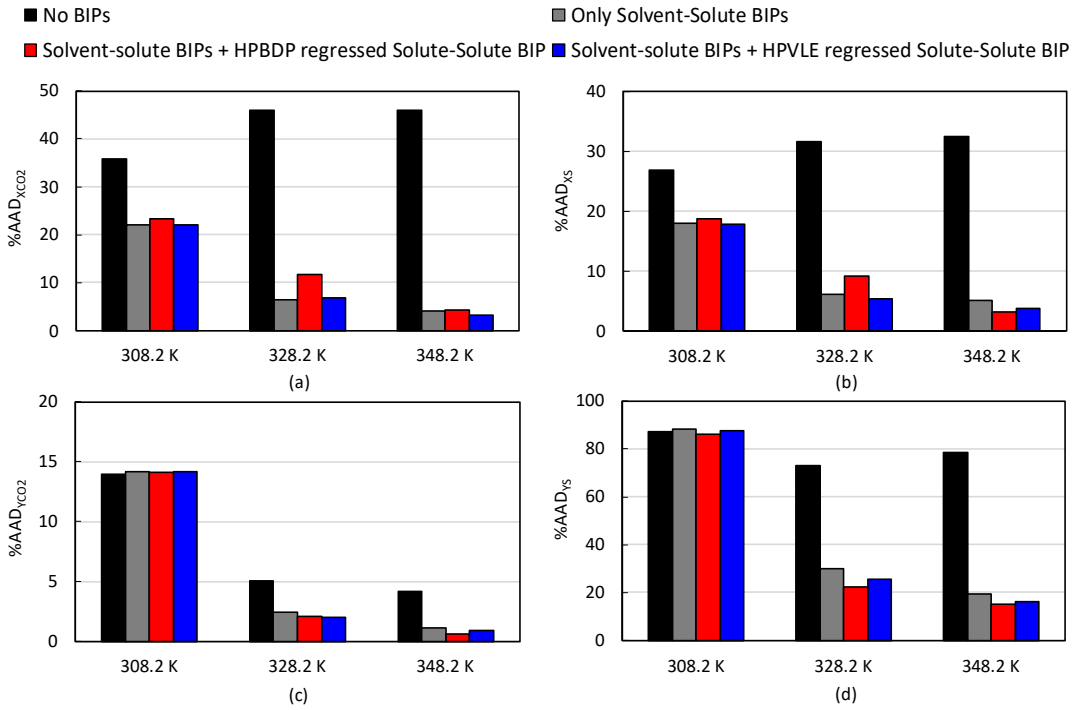

Figure 55: Evaluation of the accuracy with which the RK-SOAVE model can correlate VLE data by comparing the %AAD values for the correlation of (a) liquid and (c) vapour phase CO_2 composition and (b) liquid and (d) vapour phase solute composition (average %AAD for nC_{12} and $C_{10}OH$)

The model fit is analysed in Figures 56 and 57. Due to the inability of the model to correlate accurate data at 308 K, Gibbs phase diagrams were not constructed at this temperature. From the diagrams it is noted that although the model generally struggles to correlate the exact composition of the equilibrium phases, the model is capable of correlating fairly accurate tie-line slopes, regardless of the type of BIPs incorporated. This indicates that the model is capable of describing the ratio of the solutes correctly, but it does not model the total solubility in CO_2 accurately.

The incorporation of the solute-solute BIP regressed from HPBDP data generally improves the accuracy of the vapour compositions (Figure 56 (b) and 57 (b)), which is the region of interest in supercritical fluid fractionation processes [5]. It also improves the ability of the model to correlate the curvature of the liquid phase curve within the n-dodecane rich region at moderate pressures. The incorporation of the solute-solute BIP regressed from HPVLE data improves both liquid and vapour phase correlations. These parameters should therefore be included in the respective models (that is the model regressed from HPBDP and HPVLE data).

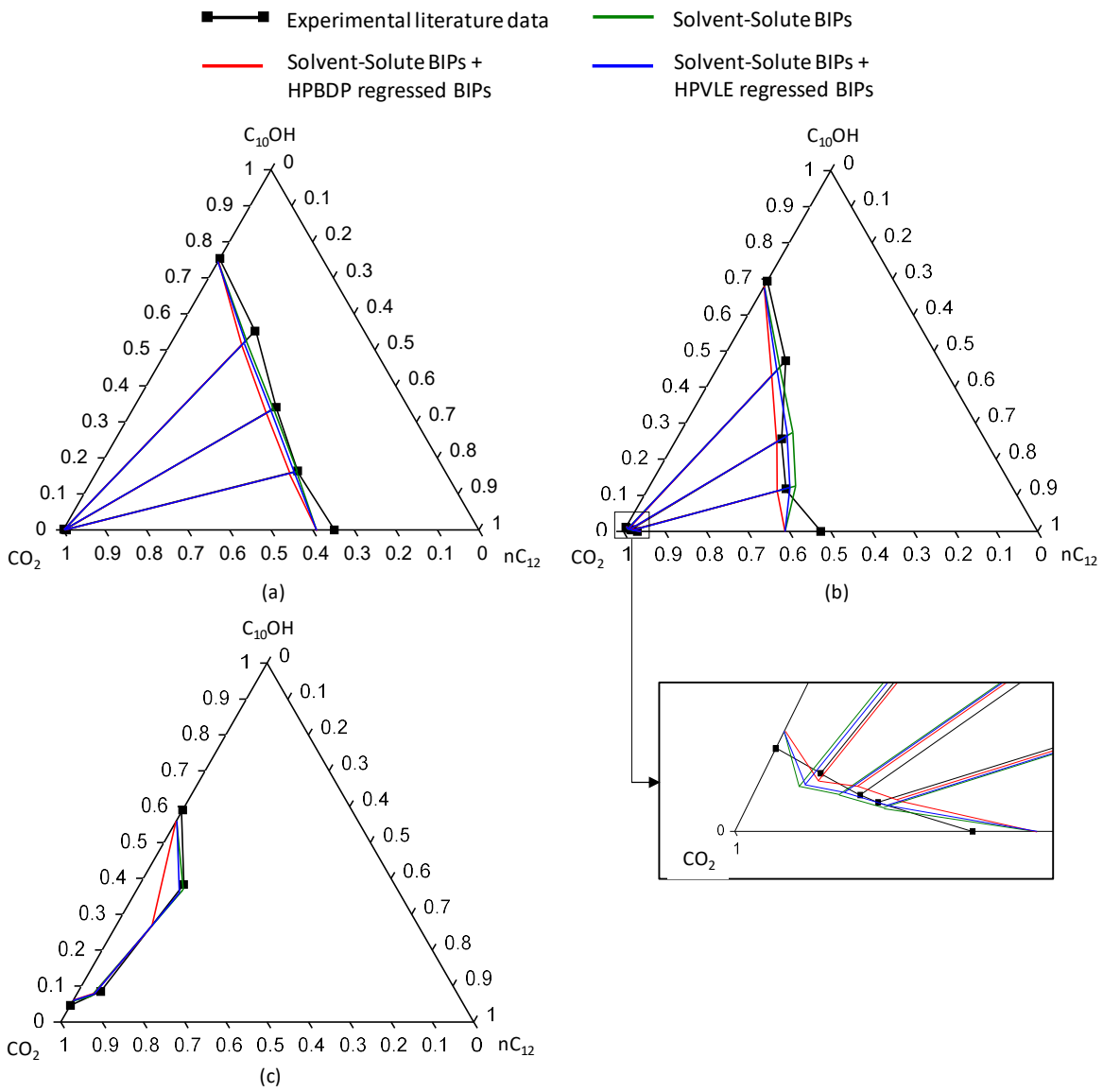

Figure 56: Gibbs phase diagram constructed at 328.2 K and (a) 8.3 MPa, (b)10.4 MPa and (c) 14.0 MPa, comparing experimental literature data [5, 14] to RK-SOAVE correlations obtained when using incorporating different parameters

At lower pressures, illustrated in Figures 56 (a) and 57 (a), the correlations are fairly similar and the model struggles to correlate the slightly convex-to-concave nature of the liquid curve. At slightly higher pressures, presented in Figure 56 (b) and 57 (b), the ability of the model which includes the solute-solute BIP regressed from HPBDP data to correlate the convex-to-concave nature of the liquid curve is improved. The model can however not accurately correlate the s-shaped liquid curve, which exists due to the narrowing of the band connecting the two two-regions, due to co-solvency [103]. The incorporation of the solute-solute BIP regressed from HPVLE data does not improve the model's ability to correlate the curvature of the liquid phase curve, as the curves still have a convex-type shape. The inability of the model to correlate the correct curvature, particularly in the n-dodecane rich region, can partially be

attributed to the fact that the model cannot correlate accurate binary phase equilibrium data (discussed in Appendix F). From the results presented here it can be concluded that the RK-SOAVE model cannot quantitatively or qualitatively correlate the occurrence of co-solvency.

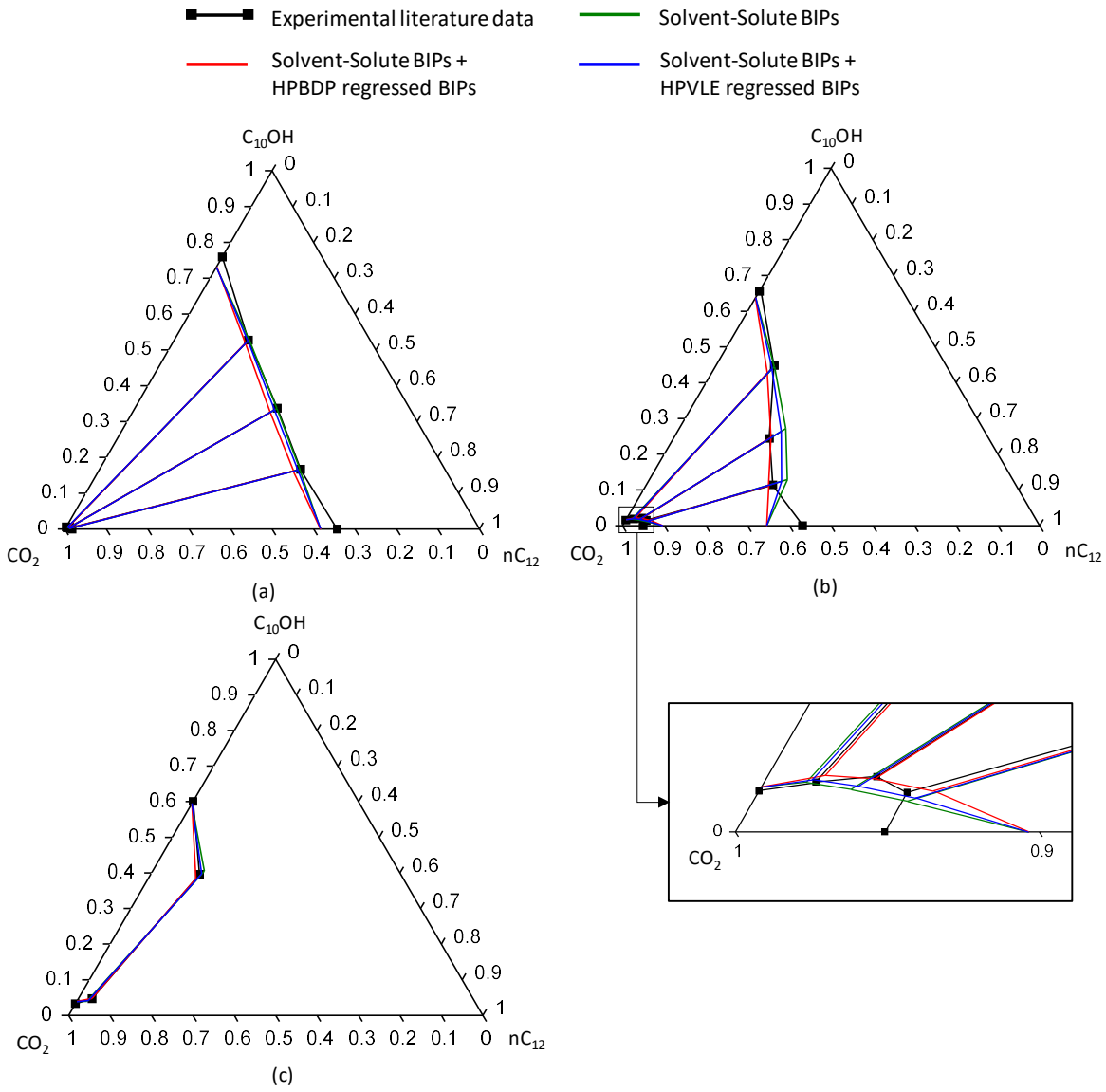

Figure 57: Gibbs phase diagram constructed at 348.2 K and (a) 10.4 MPa, (b)14 MPa and (c) 15.7 MPa, comparing experimental literature data [5, 14] to RK-ASPEN correlations obtained when using incorporating different parameters

Conclusion

With the inclusion of solvent-solute BIPs and a solute-solute BIP the RK-SOAVE model can correlate fairly accurate phase transition pressures for n-dodecane rich ternary mixtures. The model accuracy is however seen to decrease with an increase in 1-decanol content, particularly at lower temperatures. The model also cannot correlate the exact composition of co-existing equilibrium phases and can only generate fairly accurate tie-line slopes. Furthermore, although the inclusion of the different solute-solute BIPs are deemed necessary, the phase transition

pressure correlations obtained when incorporating the solute-solute BIP regressed from HPBDP data was found to be more accurate. For the VLE data however, the compositions correlated when using the solute-solute BIP regressed from HPVLE data was found to be generally more accurate.

8.1.1.2 RK-ASPEN

High pressure bubble- and dew-point data

Figure 58 illustrates the ability of the RK-ASPEN model to correlate phase transition pressures for this system.

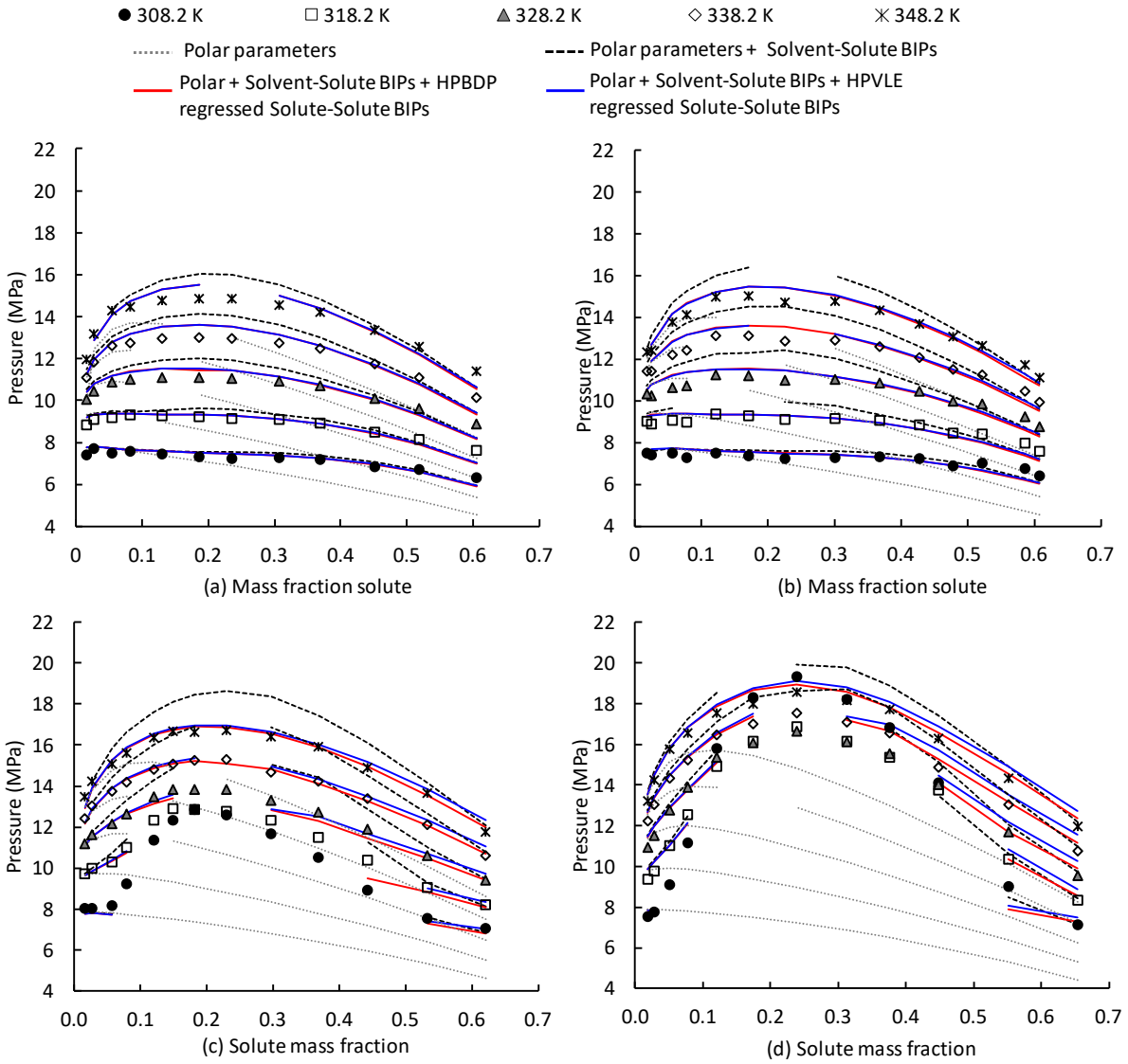

Figure 58: Pressure-composition diagrams comparing experimental data to data generated using the RK-ASPEN model for (a) Mixture SS1: 90wt% nC_{12} + 10 wt% $C_{10}OH$ [13], (b) Mixture SS2: 80wt% nC_{12} + 20 wt% $C_{10}OH$ [13], (c) Mixture SS3: 40wt% nC_{12} + 60 wt% $C_{10}OH$ [13] and (d) Mixture Z4: 22.2wt% nC_{12} + 77.8 wt% $C_{10}OH$ [5]

It is seen that the inclusion of the solvent-solute BIPs significantly improves the model fit. There is also generally little difference between the model correlations obtained when using the different solute-solute BIPs. The largest deviation is noted within the high solute concentration region of the 1-decanol rich mixtures, where the model which incorporates the solute-solute BIP regressed from HPBDP data tends to provide slightly more accurate correlations.

With the inclusion of the solute-solute BIPs, the models generally fit the experimental data fairly well, especially in the low solute concentration region. For the n-dodecane rich mixtures, both models however tend to slightly overpredict data within the mixture critical region and slightly underestimate data in the high solute mass fraction region. The model fit for the 1-decanol rich mixtures reveals that even with the inclusion of the solute-solute BIPs the model is still unable to correlate a wide range of phase transition pressures at temperatures below 328 K. There are also areas within/or close to the mixture critical region where the model is unable to correlate phase transition data. Possible reasons for these discrepancies are addressed in section 8.1.1.1.

High pressure vapour-liquid-equilibrium data

Results indicating the accuracy with which the RK-ASPEN model can correlate VLE data for this system is presented in Figure 59. It is noted that at 308 K and 328 K the incorporation of the solvent-solute BIPs improves the model's ability to correlate liquid phase compositions, but decreases the accuracy of the vapour phase compositions correlations. At 348 K, the inclusion of these parameters improves the accuracy of both liquid and vapour phase correlations.

Analysis of the effect of including the different solute-solute BIPs reveals that these parameters only improve the model's ability to correlate VLE data at temperatures above 308 K. At 328 K, the incorporation of the solute-solute BIP regressed from HPBDP data is seen to slightly decrease the model's ability to correlate liquid phase compositions, but it improves the accuracy of the vapour phase composition correlations. At 348 K, it improves the accuracy of both liquid and vapour phase composition correlations. The solute-solute BIP regressed from HPVLE data, is seen to generally improve model accuracy. The poorer performance of the BIPs at low temperatures as well as the large %AAD values reported at 308 K have been addressed in the previous section.

Comparison of the model accuracy when incorporating the solute-solute BIPs regressed from HPBDP and HPVLE data reveals that at 328 K, the correlations obtained when using the BIP regressed from HPVLE data are slightly more accurate. At 348 K, there is very little difference in the accuracy obtained.

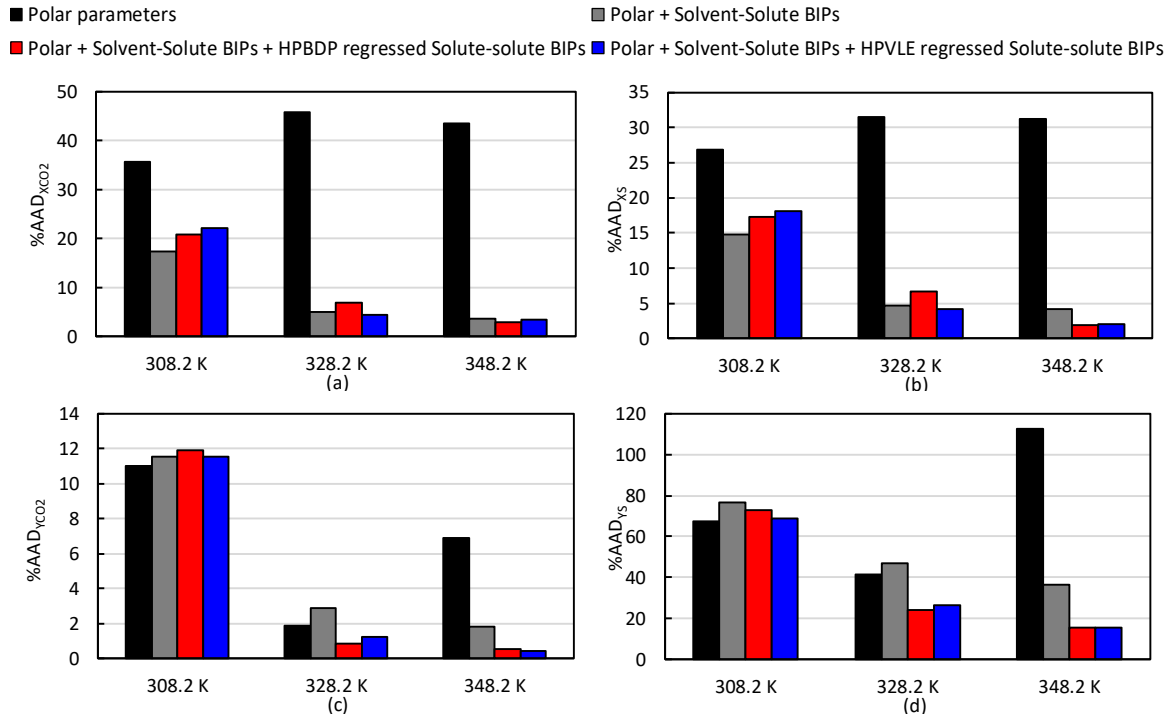

Figure 59: Evaluation of the accuracy with which the RK-ASPEN model can correlate VLE data by comparing the %AAD values for the correlation of (a) liquid and (c) vapour phase CO_2 composition and (b) liquid and (d) vapour phase solute composition (average %AAD for nC_{12} and $C_{10}OH$)

The Gibbs phase diagrams presented in Figures 60 and 61, were constructed to analyse the model fit. From these diagrams it is noted that although the model cannot always correlate the exact composition of the co-existing phases, it can generate accurate tie-line slopes. Further analysis reveals that even with the incorporation of the solute-solute BIPs, the model struggles to correlate the slightly convex-to-concave nature of the liquid curve at low pressures. However, as the pressure increases the model's ability to correlate the convex-to-concave nature of the liquid curve is improved. The models can be seen to qualitatively correlate the occurrence of co-solvency, but cannot account for the quantitative effect thereof, as the correlations within the pinch point and n-dodecane rich regions deviate from the experimental data. As stated previously, this is partially due to the fact that the model cannot correlate accurate binary phase equilibrium data (discussed in Appendix F).

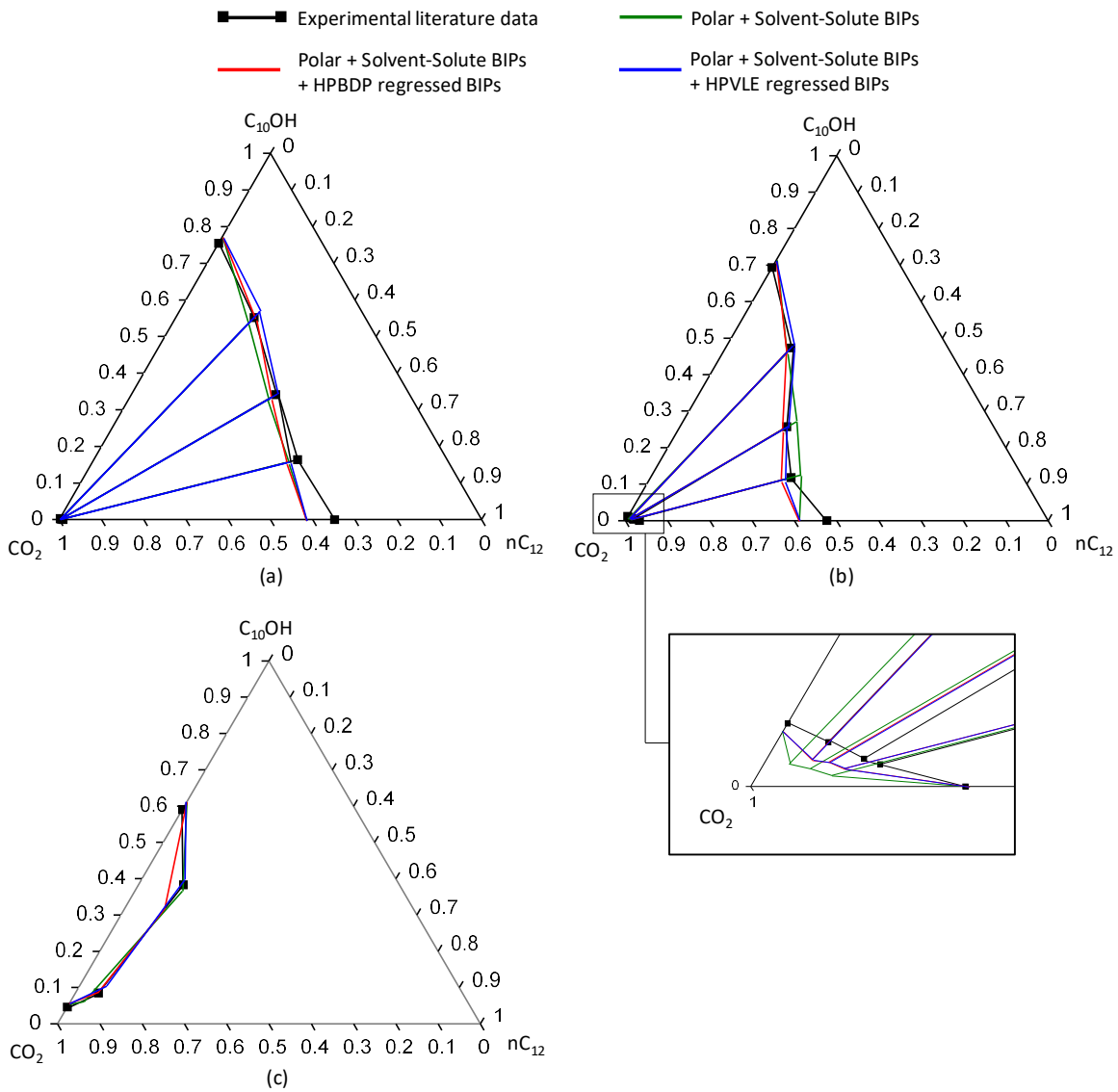

Figure 60: Gibbs phase diagram constructed at 328.2 K and (a) 8.3 MPa, (b)10.4 MPa and (c) 14.0 MPa, comparing experimental literature data [5, 14] to RK-ASPEN correlations obtained when using incorporating different parameters

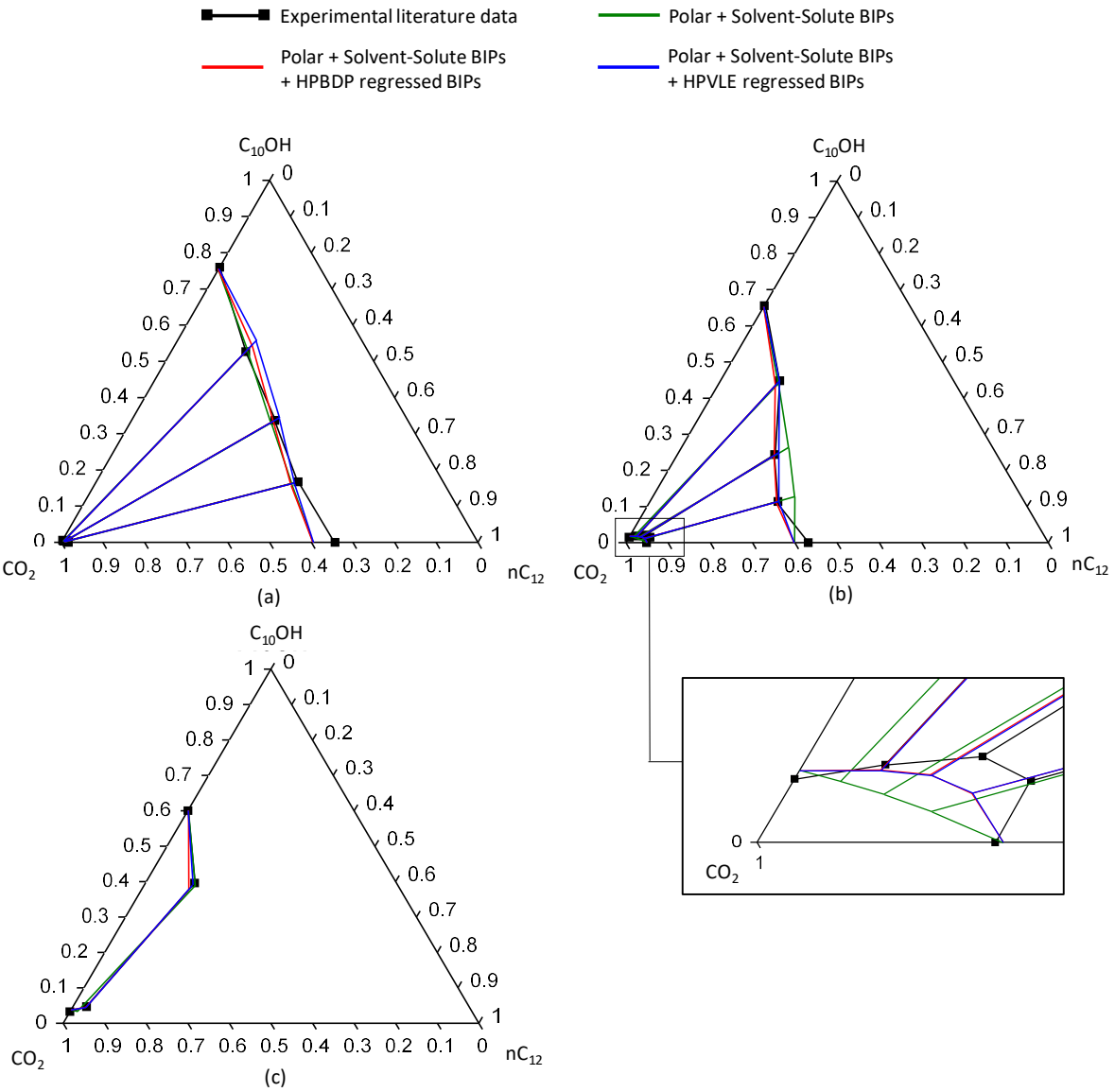

Figure 61: Gibbs phase diagram constructed at 348.2 K and (a) 10.4 MPa, (b)14 MPa and (c) 15.7 MPa, comparing experimental literature data [5, 14] to RK-ASPEN correlations obtained when using incorporating different parameters

Conclusion

With the inclusion of polar parameters, solvent-solute BIPs and a solute-solute BIP, the RK-ASPEN model correlates fairly accurate bubble- and dew-point data for this ternary system. The model can however not correlate the exact composition of co-existing equilibrium phases, but it can generate fairly accurate tie-line slopes. Furthermore, although there was generally little difference between the phase transition pressure obtained when using the different solute-solute BIPs, the model which incorporated the solute-solute BIP regressed from HPBDP data performed slightly better. For the VLE data however, the correlations obtained using the solute-solute BIP regressed from HPVLE data were generally slightly more accurate.

8.1.1.3 CPA

High pressure bubble- and dew-point data

Pressure-composition diagrams illustrating the accuracy with which the CPA model can correlate bubble- and dew-point data for this system, are presented in Figure 62.

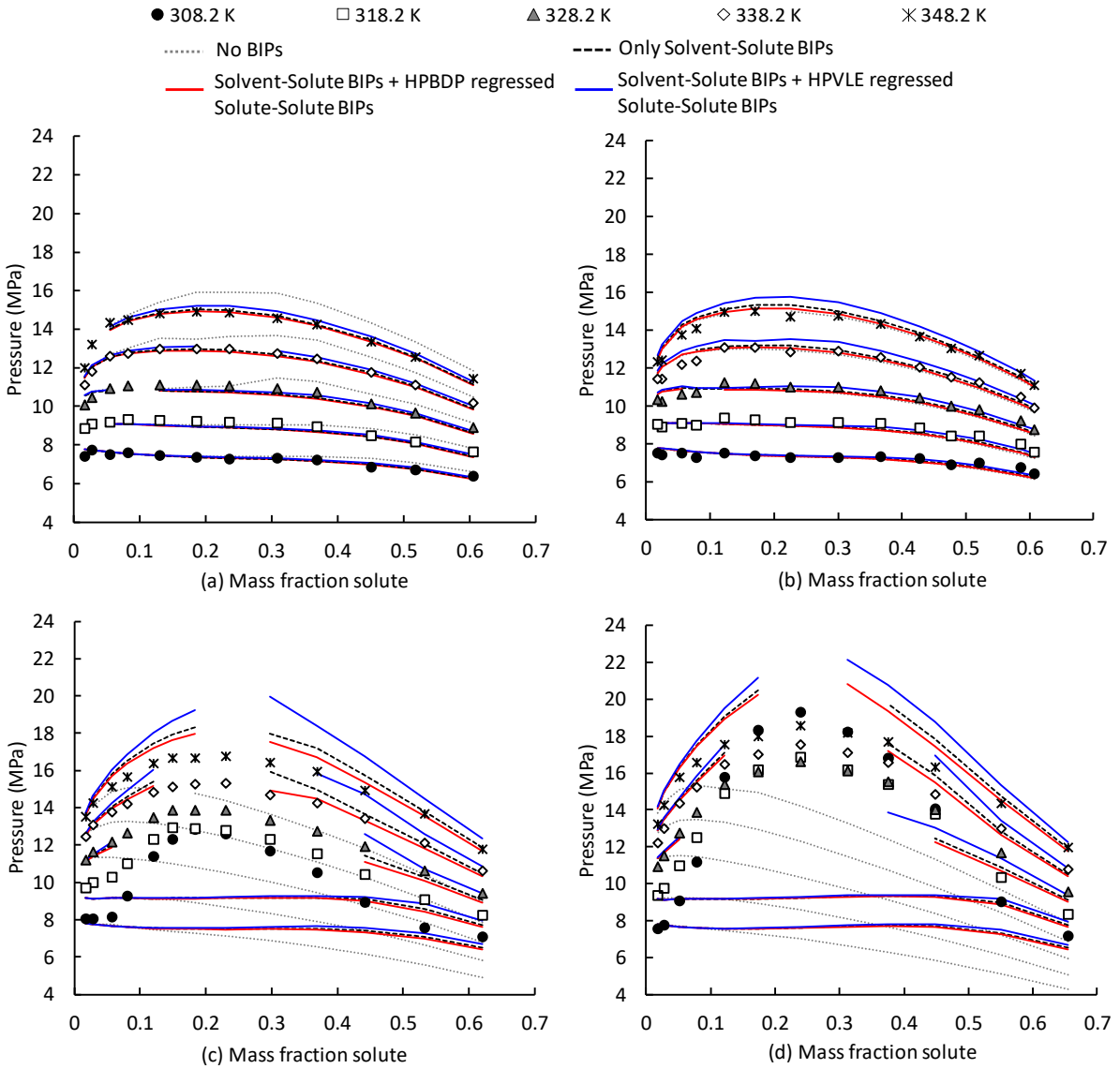

Figure 62: Pressure-composition diagrams comparing experimental data to data generated using the CPA model for (a) Mixture SS1: 90wt% nC_{12} + 10 wt% $C_{10}OH$ [13], (b) Mixture SS2: 80wt% nC_{12} + 20 wt% $C_{10}OH$ [13], (c) Mixture SS3: 40wt% nC_{12} + 60 wt% $C_{10}OH$ [13] and (d) Mixture Z4: 22.2wt% nC_{12} + 77.8 wt% $C_{10}OH$ [5]

The incorporation of the solvent-solute BIPs is seen to generally improve model fit for all the mixtures. The model, however, overestimates the phase transition pressures as the mixture critical region is approached. There are also areas within the mixture critical region where the model cannot correlate phase transition pressures and this results in an incomplete phase

diagram. According to literature [128], problems regarding predictions in the mixture critical region are known to be a shortcoming of the CPA model and have been encountered in previous work [129, 130]. The reasons for the poor performance at low temperatures are linked to the reasons discussed for the previous models.

Analysis of the effect of incorporating the solute-solute BIPs reveals that the inclusion of the parameters either has no effect on model fit or it decreases model fit. The model fit attained for Mixtures SS1and SS2 with and without the inclusion of the solute-solute BIP regressed from HPBDP data are fairly similar. For these mixtures the inclusion of the solute-solute BIP regressed from HPVLE data generally worsens the model fit, as it results in a noticeable overprediction of transition pressures at higher temperatures. The general ability of the model to correlate data for this system is seen to decrease if 1-decanol is present in significant amounts. For Mixtures SS3 and Z4, the inclusion of the solute-solute BIP regressed from HPBDP data is seen to slightly improve the model fit at higher temperatures. For these mixtures, the inclusion of the solute-solute BIP regressed from HPVLE data slightly improves the model fit within the liquid region at temperatures below 328 K, but considering the small range over which the model can correlate accurate data, this improvement is not seen as substantial. The inclusion of this parameter also causes a significant degree of overprediction within the mixture critical region at higher temperatures. From this it is concluded that the inclusion of a solute-solute BIP does not significantly improve the model's ability to correlate bubble- and dew-point data for this system, regardless of the data used to regress it.

High pressure vapour-liquid-equilibrium data

An accuracy analysis indicating the ability of the CPA model to correlate VLE data for this system is presented in Figure 63. It is noted that the inclusion of the solvent-solute BIPs generally improves model accuracy. Further addition of the solute-solute BIP regressed from HPBDP data only slightly improves the accuracy of the vapour phase correlations at 348 K. The solute-solute BIP regressed from HPVLE data only improves the accuracy of the liquid phase correlations at 328 K. Furthermore, the %AAD values reported at 308 K are large compared to the other temperatures, regardless of the BIPs incorporated in the model. The same reasoning with regards to poor performance at low temperatures presented in the previous section applies here.

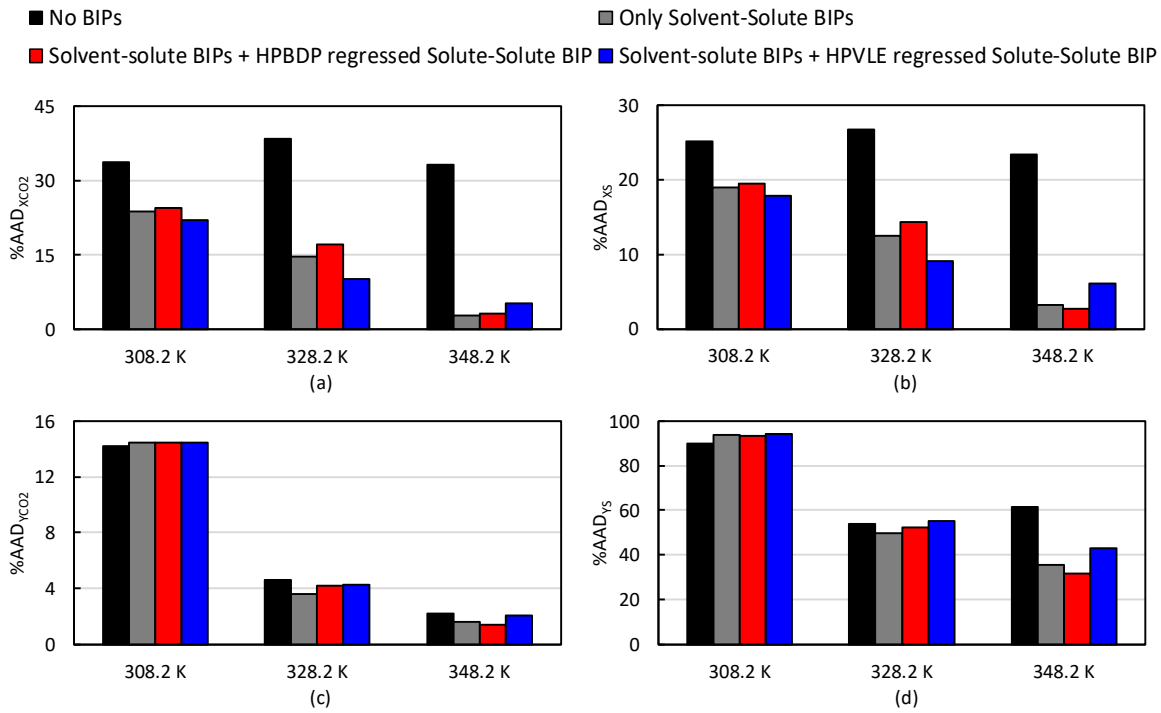

Figure 63: Evaluation of the accuracy with which the CPA model can correlate VLE data by comparing the %AAD values for the correlation of (a) liquid and (c) vapour phase CO_2 composition and (b) liquid and (d) vapour phase solute composition (average %AAD for nC_{12} and $C_{10}OH$)

Figures 64 and 65 illustrate the fit of the CPA model. From these diagrams it is noted that although the model correlations tend to deviate from the experimental data, the CPA model can correlate fairly accurate tie-line slopes. Furthermore, at lower pressures the model struggles to predict the slightly convex-to-concave nature of the liquid curve at 328 K, regardless of the BIPs incorporated. At higher pressures, the curvature of the liquid phase curve correlated by the model which only incorporates the solvent-solute BIPs and the model which also includes the solute-solute BIP regressed from HPBDP data, is improved. These two model variations can qualitatively correlate the occurrence of co-solvency, but cannot accurately account for the quantitative effect thereof. This can partially be attributed to the poor performance of the model when correlating the binary phase equilibrium data, highlighted previously (discussed in Appendix F). At these pressures, the incorporation of the solute-solute BIP regressed from HPVLE data decreases the model's ability to correlate the curvature of the liquid phase and it also decreases the accuracy of the vapour phase composition correlations.

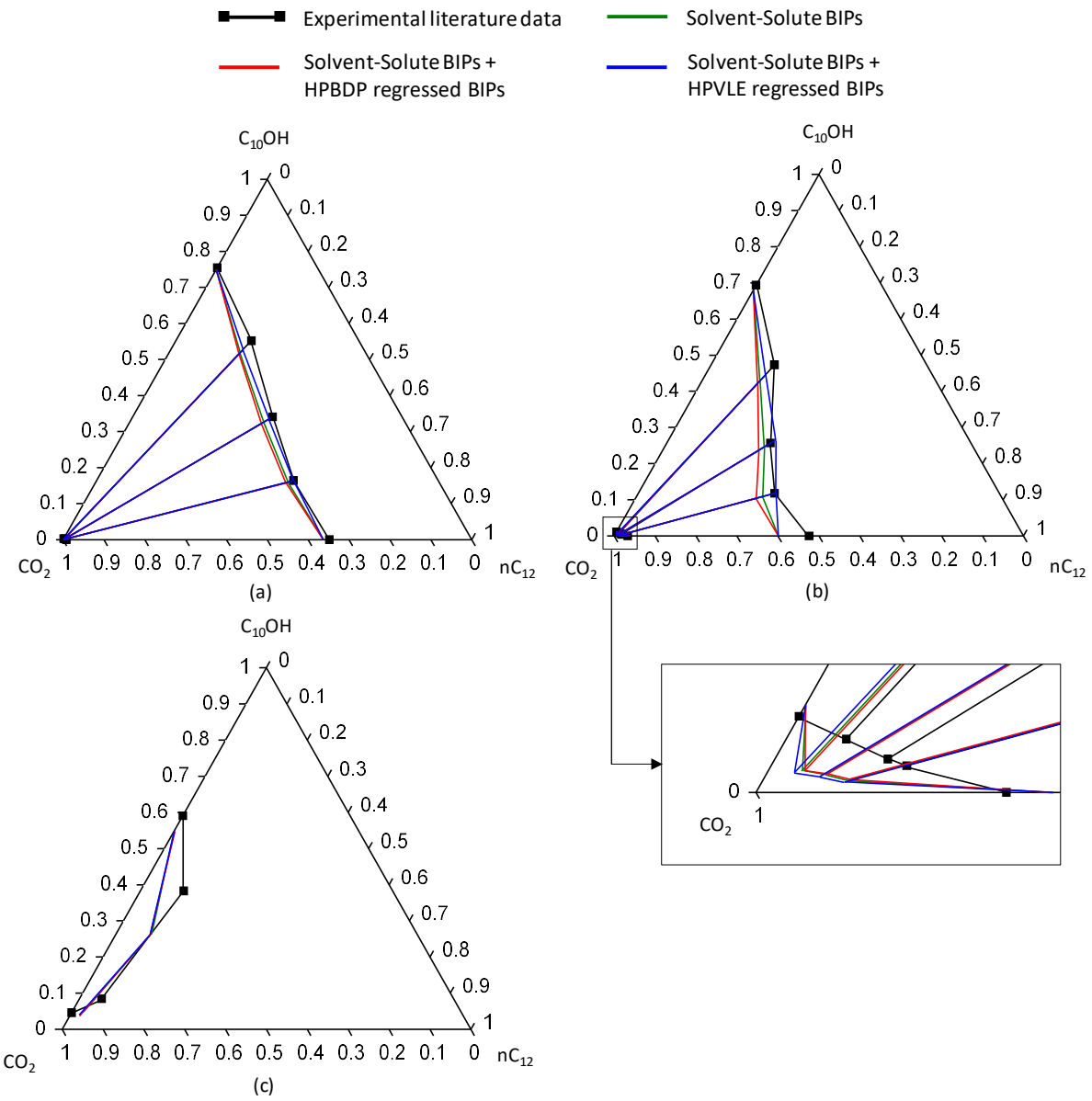

Figure 64: Gibbs phase diagram constructed at 328.2 K and (a) 8.3 MPa, (b)10.4 MPa and (c) 14.0 MPa, comparing experimental literature data [5, 14] to CPA correlations obtained when using incorporating different parameters

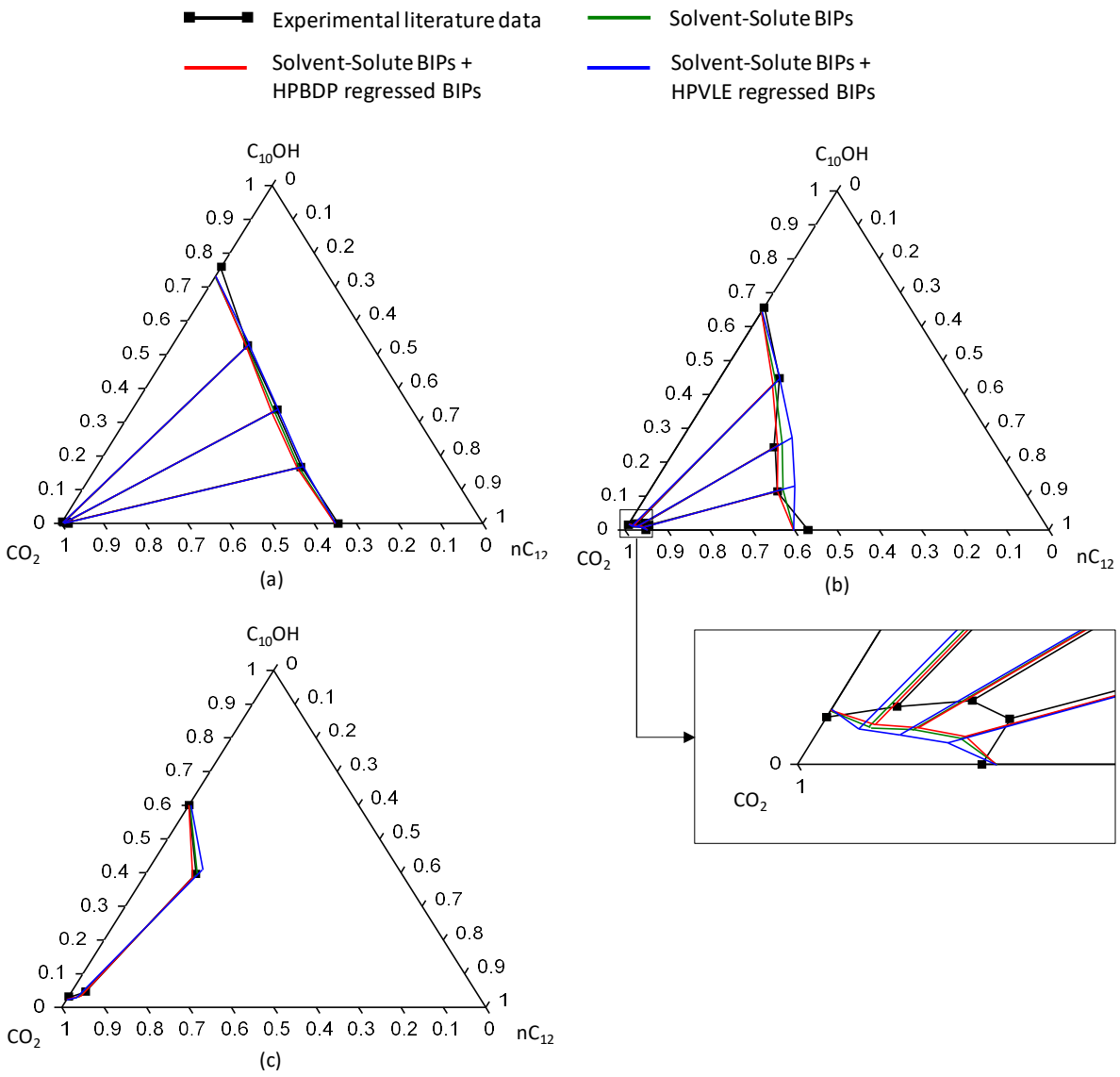

Figure 65: Gibbs phase diagram constructed at 348.2 K and (a) 10.4 MPa, (b)14 MPa and (c) 15.7 MPa, comparing experimental literature data [5, 14] to CPA correlations obtained when using incorporating different parameters

Conclusion

With the inclusion of solvent-solute BIPs, the CPA model can correlate fairly accurate bubble- and dew-point data for the ternary system consisting largely of n-dodecane. The accuracy is however seen to decrease if 1-decanol is present in significant amounts. Furthermore, the model cannot correlate the exact composition of co-existing equilibrium phases, but it can generate fairly accurate tie-line slopes. The incorporation of a solute-solute BIP did not have a consistent impact on model performance and in some instances it resulted in a noticeable decrease in model accuracy. Hence, the inclusion of a solute-solute BIP, regardless of the type of data used to regress it, is cautioned.

8.1.1.4 PSRK

High pressure bubble- and dew-point data

In Table 35, the accuracy with which the PSRK model can predict bubble- and dew-point data for this system is analysed. It is noted that the %AAD values for Mixtures SS1 and SS2, are generally smaller than the %AAD values reported for Mixtures SS3 and Z4. This indicates that the PSRK model predicts more accurate bubble- and dew-point data for mixtures consisting largely of n-dodecane, than it does for mixtures comprising largely of 1-decanol.

Table 35: Analysis of the accuracy with which the PSRK model can predict phase transitions pressures between 308.2 K and 348.2 K

Mix no	Mixture solute composition	%AAD between experimental and PSRK predicted phase transition pressures				
		Temperature (K)				
		308.2	318.2	328.2	338.2	348.2
SS1	90 wt% nC_{12} + 10 wt% $C_{10}OH$	1.3	2.0	1.7	1.5	2.4
SS2	80 wt% nC_{12} + 20 wt% $C_{10}OH$	1.7	2.2	1.7	1.8	1.0
SS3	40 wt% nC_{12} + 60 wt% $C_{10}OH$	5.1	3.5	2.6	4.1	4.8
Z4	22.2 wt% nC_{12} + 77.8 wt% $C_{10}OH$	6.9	8.5	5.4	3.7	4.9

When analysing the diagrams presented in Figure 66 it is noted that the PSRK model is capable of predicting fairly accurate phase transition curves for Mixtures SS1 and SS2. Analysis of the model predictions attained for Mixtures SS3 and Z4, reveals that the model is incapable of predicting phase transitions pressures over a large range of compositions at temperatures below 328 K. The reasons for this are the same as for the previous three models. The accuracy of the model predictions generally improves at higher temperatures, but the model tends to overestimate the phase transition pressures within/close to the mixture critical region. The deviation between the predicted and experimental data observed for these mixtures is likely linked to the large quadrupole moment of CO_2 (particularly in the low solute concentration region), hydrogen bonding between the 1-decanol molecules (significant in the high solute concentration region) and complex phase behaviour which occurs at high pressures (mixture critical region), which is not accounted for in the predictive model based on low pressure VLE data.

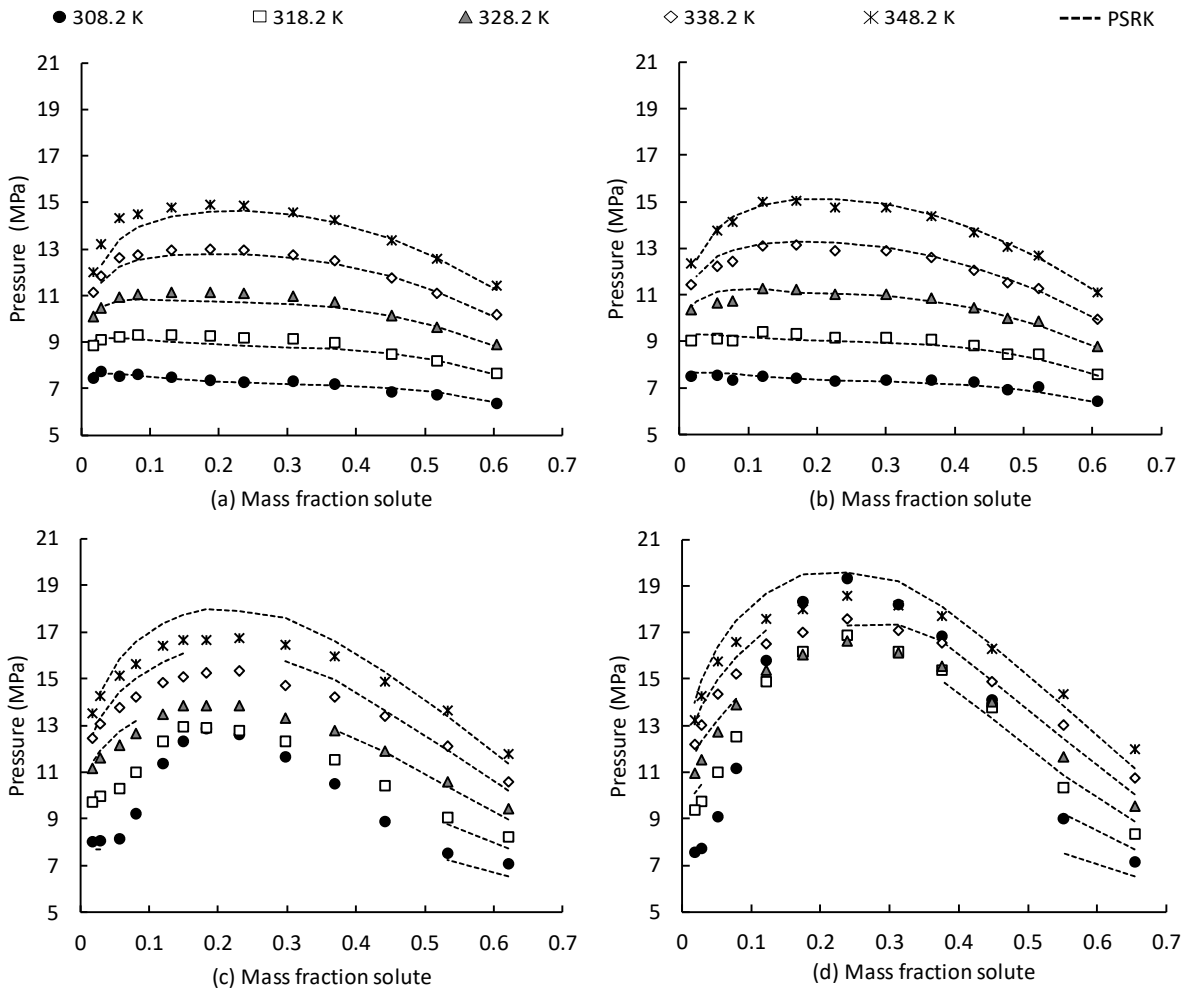

Figure 66: Pressure-composition diagrams comparing experimental data to data generated using the PSRK model for (a) Mixture SS1: 90wt% nC_{12} + 10 wt% $C_{10}OH$ [13], (b) Mixture SS2: 80wt% nC_{12} + 20 wt% $C_{10}OH$ [13], (c) Mixture SS3: 40wt% nC_{12} + 60 wt% $C_{10}OH$ [13] and (d) Mixture Z4: 22.2wt% nC_{12} + 77.8 wt% $C_{10}OH$ [5]

High pressure vapour-liquid-equilibrium data

The accuracy with which the PSRK model can predict VLE data for this system is presented in Table 36. It is noted that very large %AAD values are reported at 308 K, indicating that the model cannot predict VLE data at this temperature, due to reasons discussed previously.

Table 36: Analysis of the accuracy with which the PSRK model can predict VLE data between 308.2 K and 348.2 K

Temperature (K)	%AAD			
	x_{CO2}	x_s^*	y_{CO2}	y_s^*
308.2	22.6	18.2	14.3	88.5
328.2	11.2	8.3	2.8	36.5
348.2	5.5	3.9	1.1	24.8

*Average %AAD of the n-dodecane and 1-decanol mass fractions in the phase

As the temperature increases, the %AAD values are seen to decrease. This indicates that model accuracy improves with an increase in temperature. This is likely due to the fact that an increase in temperature increases the kinetic energy of the 1-decanol molecules, which disrupts the ability of these molecules to form multimers, thereby reducing the degree of solute-solute interaction in the system. The predictive model therefore performs better at higher temperatures, as the complex phase behaviour which is introduced by solute-solute interaction is reduced at these conditions.

Figures 67 and 68 illustrate the ability of the PSRK model to predict VLE data for the system. From these diagrams it is noted that the model predicts fairly accurate tie-line slopes, but there are generally significant deviations between the experimental and predicted compositions.

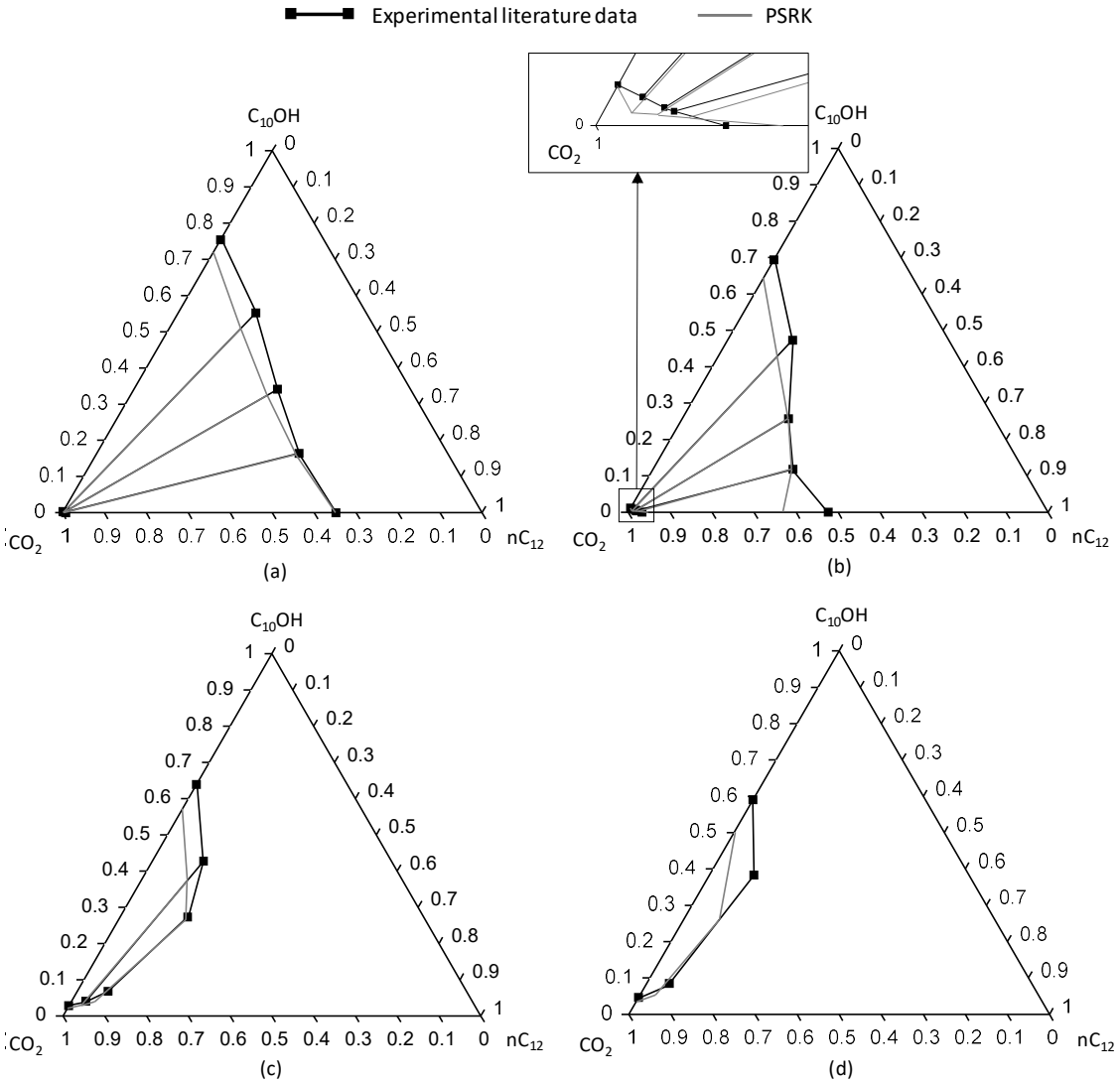

Figure 67: Gibbs phase diagram constructed at 328.2 K and (a) 8.3 MPa, (b)10.4 MPa, (c) 12.3 MPa and (d) 14.0 MPa, comparing experimental literature data [5, 14] to PSRK predictions

At the lowest pressures there is generally a significant deviation between the experimental and predicted liquid phase composition data within the 1-decanol rich region. The correlation between the experimental and predicted data is seen to improve within the n-dodecane rich region and the model is capable of accounting for the concavity of the liquid curve in this region. The predictive model likely performs better in the n-dodecane rich region, as the complex phase behaviour which is introduced by solute-solute interaction is reduced at these conditions.

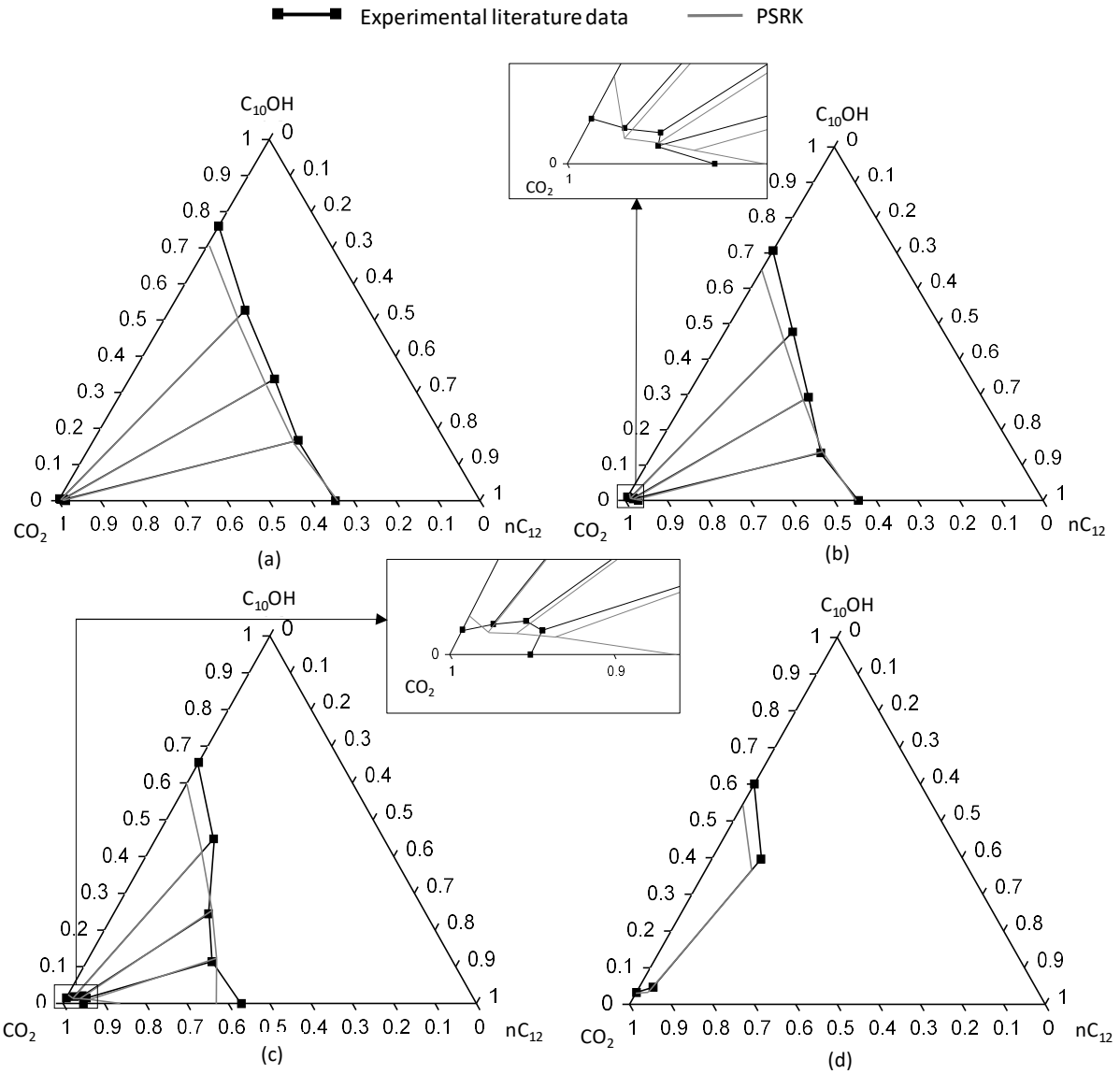

Figure 68: Gibbs phase diagram constructed at 348.2 K and (a) 10.4 MPa, (b)12.3 MPa, (c) 14.0 MPa and (d) 15.7 MPa, comparing experimental literature data [5, 14] to PSRK predictions

At higher pressures where co-solvency results in a s-shape liquid phase curve, presented in Figures 67 (b) and 68 (c), the model predicts fairly accurate liquid phase composition data within the pinch point region, but there is a significant deviation between the experimental and

predicted data within the n-dodecane rich region. The deviation in the n-dodecane region is due to the fact that the model cannot predict accurate CO_2 + n-dodecane binary data at higher pressures approaching the binary mixture critical point (discussed in Appendix F). The deviation in the predictions in the n-dodecane rich region prevents the model from predicting the correct convex-to-concave shape of the liquid curve. The curvature of the vapour phase predictions at these pressures is also seen to vary significantly from the experimental data. The PSRK model can therefore not quantitatively or qualitatively predict the occurrence of co-solvency.

Conclusion

The PSRK predicts fairly accurate bubble- and dew-point data for the ternary mixtures rich in n-dodecane, but the accuracy of the predictions noticeably decreases with an increase in 1-decanol mass fraction, particularly at lower temperatures. Furthermore, the model cannot predict the exact composition of co-existing equilibrium phases and can only generate fairly accurate tie-line slopes.

8.1.1.5 Model comparison

In this section the performance of the different models will be compared. Due to the detection of inaccuracies at lower temperatures, the model comparison will only be conducted at temperatures above 328 K. Only the optimum BIPs, as identified in the previous sections, will be included in the models in this section. The fitted models used for the comparison are therefore as follows:

Bubble- and dew-point data:

- RK-SOAVE + solvent-solute + solute-solute BIP regressed from HPBDP data
- RK-ASPEN + solvent-solute + solute-solute BIP regressed from HPBDP data
- CPA + solvent-solute BIPs
- PSRK

Vapour-liquid-equilibrium data:

- RK-SOAVE + solvent-solute + solute-solute BIP regressed from HPVLE data
- RK-ASPEN + solvent-solute + solute-solute BIP regressed from HPVLE data
- CPA + solvent-solute BIPs
- PSRK

High pressure bubble- and dew-point data

The accuracy with which the four models can generate bubble- and dew-point data for this system is compared in Figure 69.

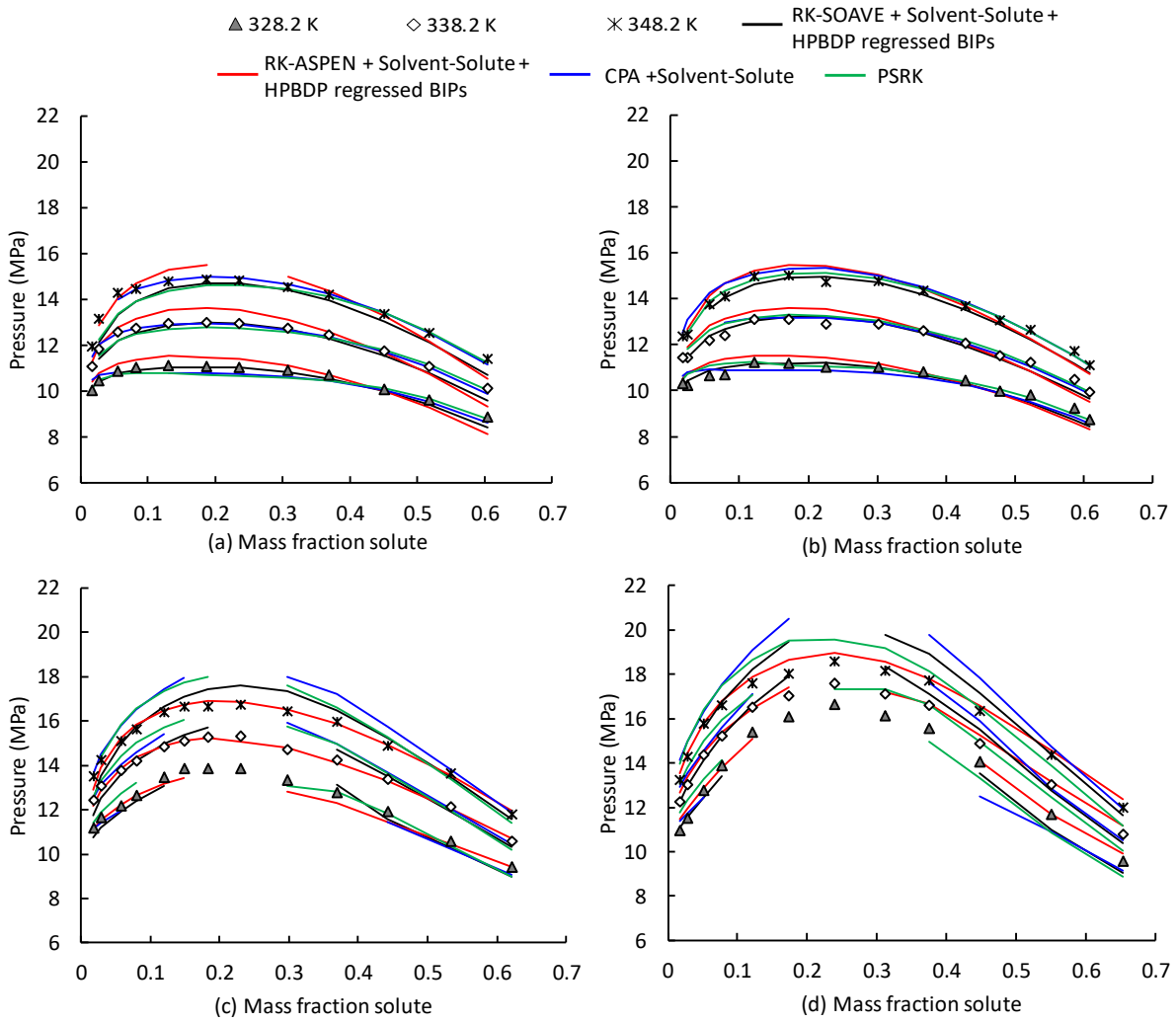

Figure 69: Pressure-composition diagrams comparing experimental data to modelled data for (a) Mixture SS1: 90wt% nC_{12} + 10 wt% $C_{10}OH$ [13], (b) Mixture SS2: 80wt% nC_{12} + 20 wt% $C_{10}OH$ [13], (c) Mixture SS3: 40wt% nC_{12} + 60 wt% $C_{10}OH$ [13] and (d) Mixture Z4: 22.2wt% nC_{12} + 77.8 wt% $C_{10}OH$ [5]

From the diagrams it is not explicitly clear as to which model is most suited to correlate/predict bubble- and dew-point data for this system. Upon further analysis it is however deemed that the RK-ASPEN model is best suited. The reason for this is motivated by the fact that although the model is slightly less accurate for n-dodecane rich mixtures, it can still correlate accurate phase transition trends and vapour phase data, which is the region of importance. The model can also correlate accurate data for mixtures consisting of larger quantities of 1-decanol. The RK-SOAVE model is the second-best option, as it can also generally correlate fairly accurate trends and data, particularly in the vapour phase region. The model is however less suited to correlate the bubble- and dew-point data of 1-decanol rich mixtures. The CPA and PSRK models can be applied with much success for n-dodecane rich mixtures, but they are the least suited models for 1-decanol rich mixtures.

High pressure vapour-liquid-equilibrium data

The accuracy with which the four models can generate VLE data for this system is analysed in Figure 70 and the fit of the different models are compared in Figures 71 and 72.

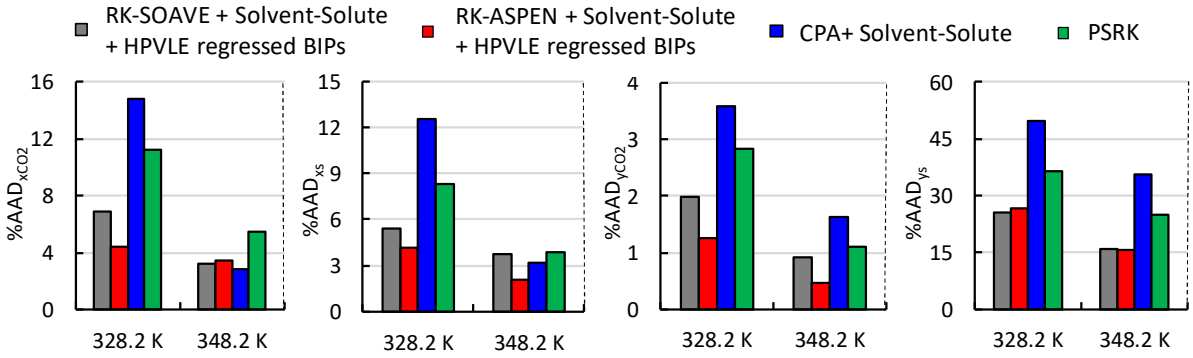

Figure 70: Comparison of the accuracy with which the models can correlate/predict the liquid and vapour phase CO_2 composition as well as the liquid and vapour phase solute composition (average %AAD for nC_{12} and $C_{10}OH$)

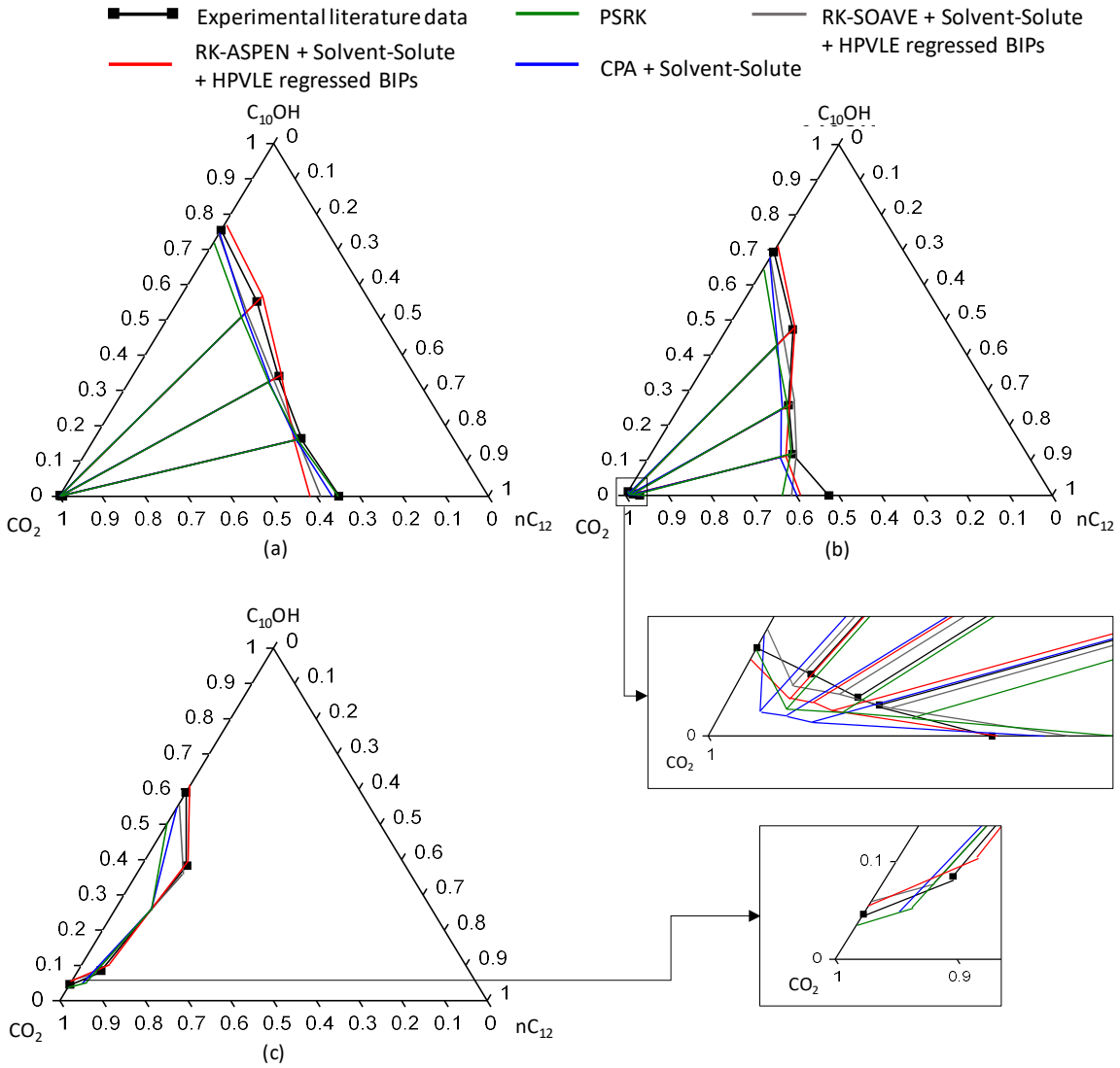

Figure 71: Gibbs phase diagram constructed at 328.2 K and (a) 8.3 MPa, (b)10.4 MPa and (c) 14.0 MPa, comparing experimental literature data [5, 14] to modelled data

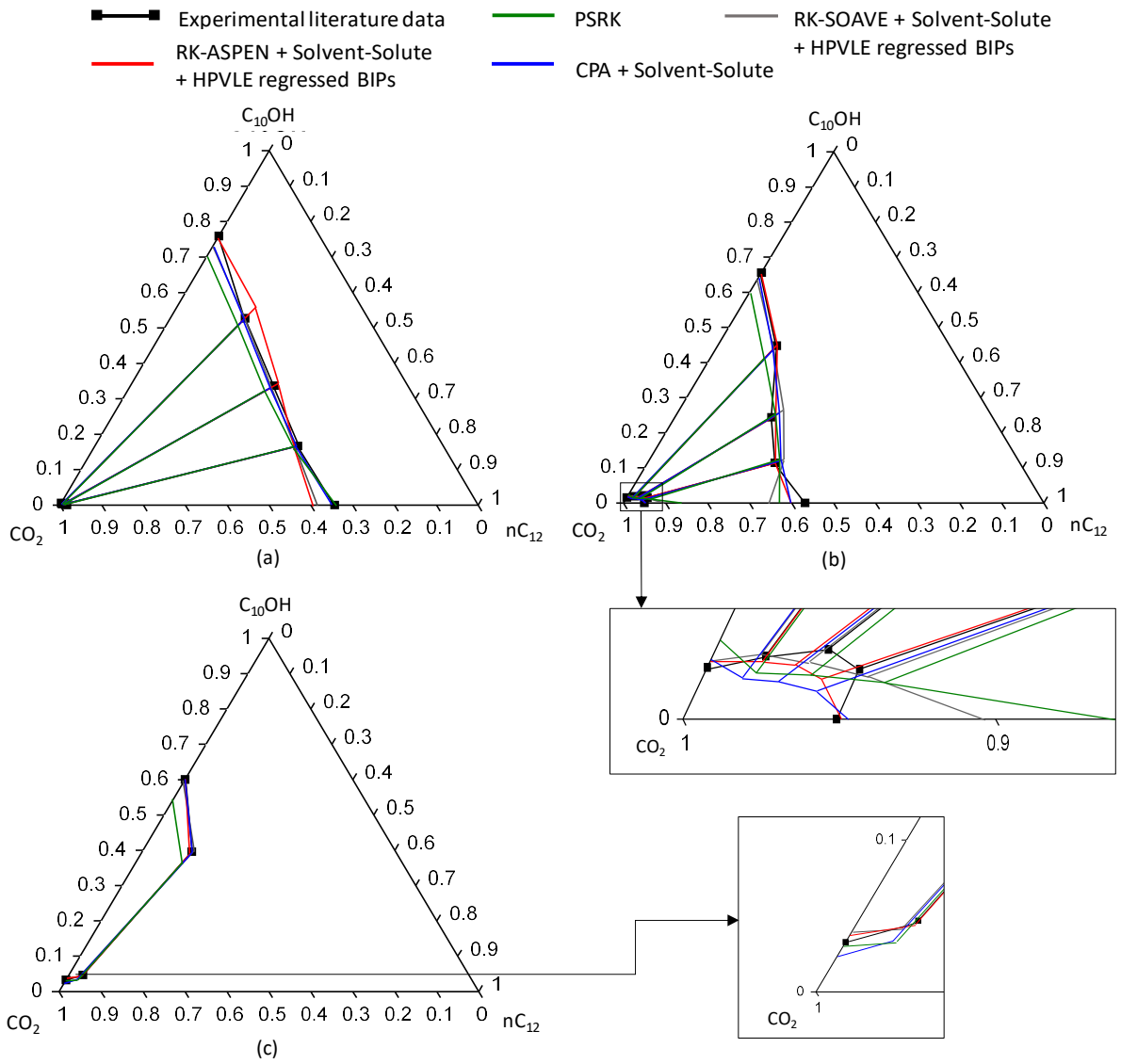

Figure 72: Gibbs phase diagram constructed at 348.2 K and (a) 10.4 MPa, (b)14 MPa and (c) 15.7 MPa, comparing experimental literature data [5, 14] to modelled

From Figures 70 to 72 it is clear that the RK-SOAVE and the RK-ASPEN models are better suited to correlate VLE data for this system, than the PSRK and CPA models. Comparison of the %AAD reveals that the RK-ASPEN model is generally more accurate than the RK-SOAVE model. Analysis of Figures 71 and 72 shows that with the exception of the correlations at the lowest pressure, the fit obtained using the RK-ASPEN model better corresponds to the experimental data than the other models. The RK-ASPEN model can also qualitatively correlate the occurrence of co-solvency, although it cannot account for the quantitative effect thereof. It can therefore be concluded that the RK-ASPEN model is best suited to correlate VLE data for this system. With that said it should be noted that although the model is the most accurate of the models investigated, there is still deviation between the experimental and

correlated data indicating that the model cannot correlate the exact composition of co-existing equilibrium phases and can only be used to approximate VLE data.

8.1.1.6 Section outcomes

The main outcomes of this section are:

- The models were found to generate fairly accurate ternary bubble- and dew-point data for the system above 328 K. The accuracy of the RK-ASPEN was however found to increase with an increase in 1-decanol fraction, whilst the accuracy of the other models decreased.
- None of the models were capable of correlating the exact composition of the co-existing equilibrium phases, but could generate accurate tie-line slopes.
- The inclusion of the solvent-solute BIPs generally significantly improved model accuracy. With the exception of the CPA model, the incorporation of the regressed solute-solute BIPs were also seen to improve model accuracy.
- The RK-ASPEN model including the solvent-solute BIP and solute-solute BIP regressed from HPBDP data and HPVLE data were found to be best suited to generate bubble- and dew-point and VLE data for this system, respectively.

8.1.2 CO_2 + n-dodecane + 3,7-dimethyl-1-octanol

In this section, the ability of the four models to generate equilibrium data for ternary CO_2 + n-dodecane + 3,7-dimethyl-1-octanol mixtures, is evaluated and compared. The experimental bubble- and dew-point data measured in this work (Mixtures 1 – 3) as well as data obtained from literature (Mixture Z5) [5] is modelled in this section. The VLE data modelled in this section was obtained from work done by Fourie [14].

8.1.2.1 RK-SOAVE

High pressure bubble- and dew-point data

Figure 73 illustrates the ability of the RK-SOAVE model to correlate bubble- and dew-point data for this system. Similar to the previous system, the incorporation of the solvent-solute BIPs significantly improves model fit. The inclusion of the solute-solute BIP, regardless of the type of data used to regress it, further improves model accuracy as it reduces the degree of overprediction within the mixture critical and lower solute concentration regions. This improvement in model fit is however accompanied by a decrease in model accuracy in the high solute concentration region for Mixtures 1, 2 and Z4, indicating that the model cannot

accurately account for the solute-solute interactions which occur in this region for mixtures containing larger quantities of 3,7-dimethyl-1-octanol.

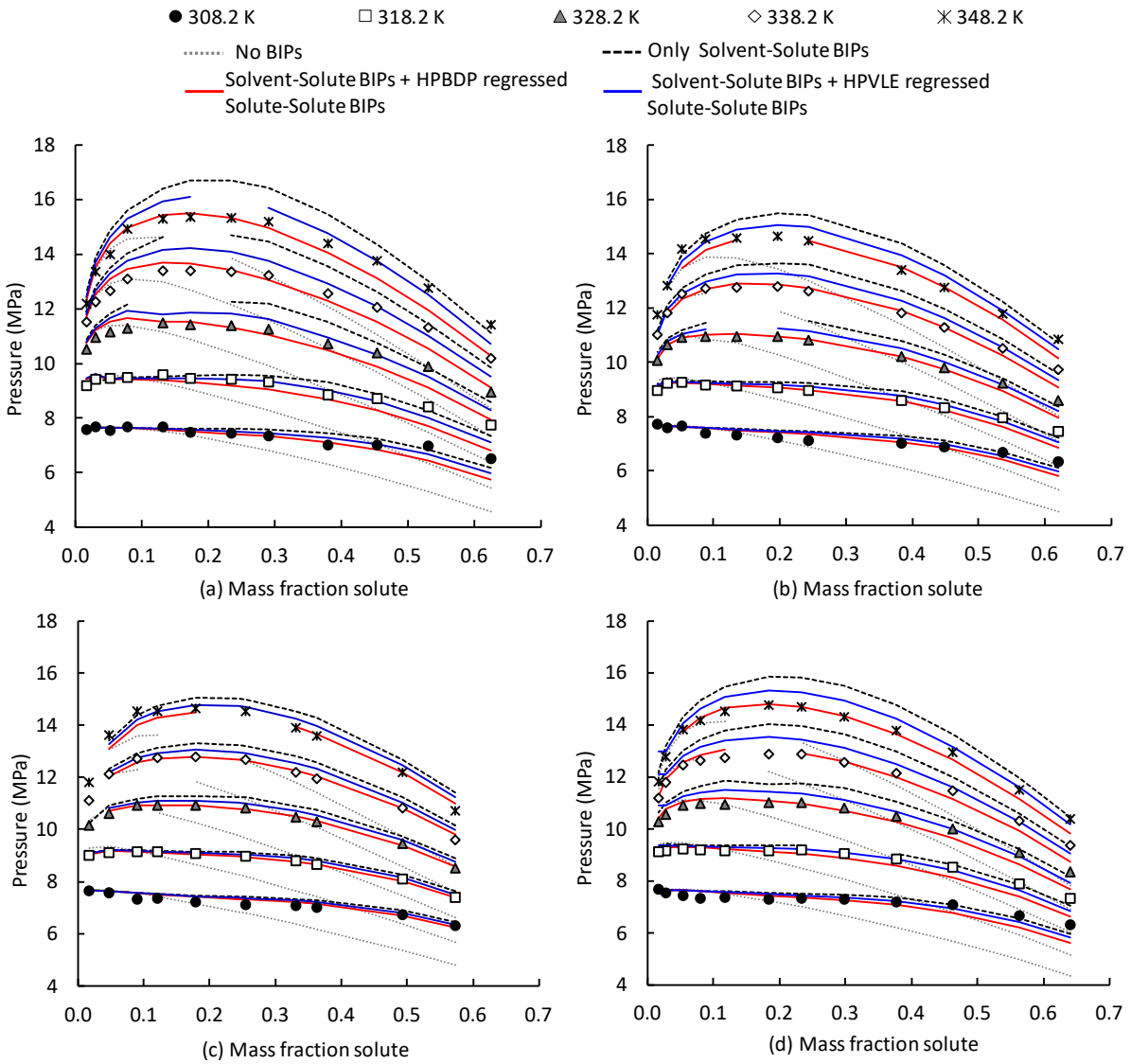

Figure 73: Pressure-composition diagrams comparing experimental data to data generated using the RK-SOAVE model for (a) Mixture 1: 50 wt% nC_{12} + 50 wt% 37DM1O, (b) Mixture 2: 75 wt% nC_{12}+ 25 wt% 37DM1O, (c) Mixture 3: 85 wt% nC_{12}+ 15 wt% 37DM1O and (d) Mixture Z5: 66.7 wt% nC_{12}+ 33.3 wt% 37DM1O [5]

Comparison of the model fit obtained when incorporating the different solute-solute BIPs reveals that within the critical region and lower solute concentration region, the model which incorporates the solute-solute BIP regressed from HPBDP data is generally more accurate. The model which incorporates the solute-solute BIP regressed from HPVLE data is only more accurate in the high solute concentration region for the mixtures consisting of larger amounts of 3,7-dimethyl-1-octanol. Seeing as the lower solute concentration region is the region of importance [5], the solute-solute BIP regressed from HPBDP data is favoured for application

in this model. The convergence errors identified in the mixture critical region has been addressed previously.

High pressure vapour-liquid-equilibrium data

Figure 74 illustrates the accuracy with which the RK-SOAVE model can correlate VLE data for this system. The inclusion of the solvent-solute BIPs generally improves model accuracy. At 308 K, the inclusion of a solute-solute BIP does not significantly improve model accuracy or even decreases it. The poor performance at this temperature has been discussed previously. With the exception of the liquid phase composition correlations obtained from the model incorporating the solute-solute BIP regressed from HPBDP data at 328 K, the incorporation of a solute-solute BIP is seen to improve model accuracy, regardless of the data type used to regress it. Comparison of the model performance at 328 K and 348 K, indicates that the model which incorporates the solute-solute BIP regressed from HPBDP data tends to outperform the model which incorporates the solute-solute BIP regressed from HPVLE data.

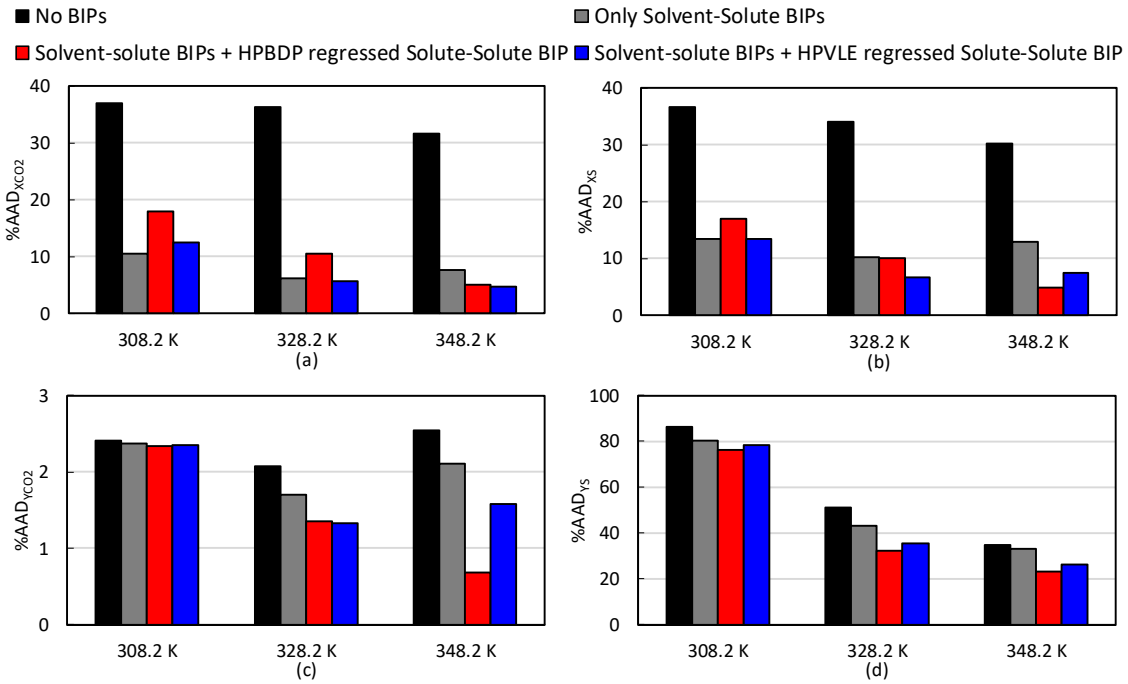

Figure 74: Evaluation of the accuracy with which the RK-SOAVE model can correlate VLE data by comparing the %AAD values for the correlation of (a) liquid and (c) vapour phase CO_2 composition and (b) liquid and (d) vapour phase solute composition (average %AAD for nC_{12} and 37DMO)

The model fit is analysed in Figures 75 and 76. Analysis of the diagrams reveals that the model struggles to correlate accurate VLE data for the system, but as seen previously, it generates fairly accurate tie-line slopes. The inclusion of the solute-solute BIP regressed from HPBDP data improves the model's ability to correlate vapour phase composition data and the curvature

of the liquid phase boundary. The solute-solute BIP regressed from HPVLE data also slightly improves the model's ability to correlate the curvature of the phase boundaries when it is influenced by co-solvency. These parameters should therefore be incorporated in the respective models.

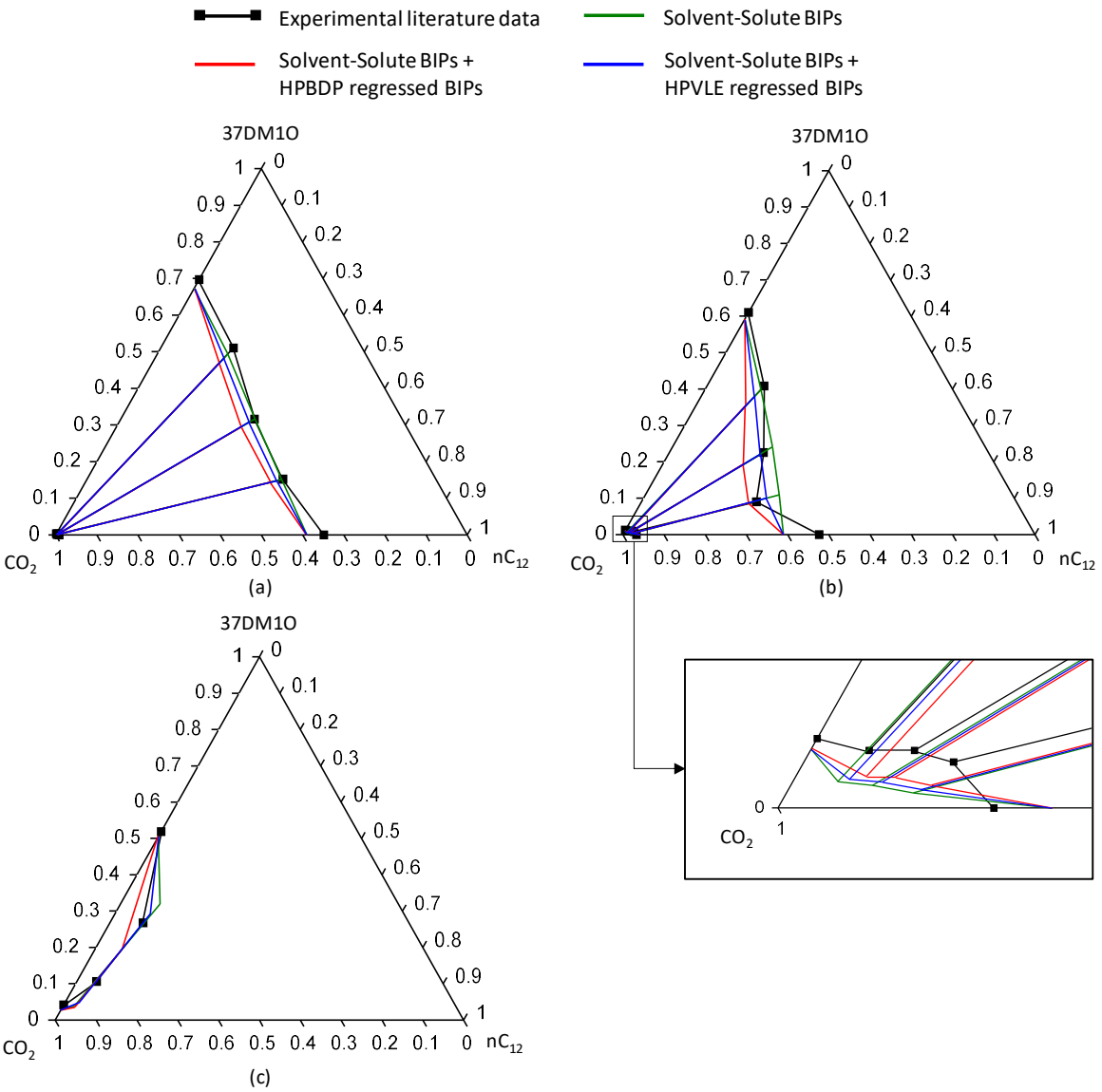

Figure 75: Gibbs phase diagram constructed at 328.2 K and (a) 8.3 MPa, (b)10.4 MPa and (c) 12.3 MPa, comparing experimental literature data [5, 14] to RK-SOAVE correlations obtained when using incorporating different parameters

At the lower pressures, the model struggles to correlate the slightly convex-to-concave nature of the liquid curve. At slightly higher pressures, the ability of the model to correlate the convex-to-concave nature of the liquid curve is improved, regardless of the type of data used to regress the solute-solute BIP. The curvature modelled using the solute-solute BIP regressed from HPBDP data is however more accurate. When incorporating the solute-solute BIP regressed from HPBDP data the model can qualitatively correlate the occurrence of co-solvency but it

cannot account for the quantitative effect thereof. As stated previously, this can partially be attributed to the model performance when predicting binary data.

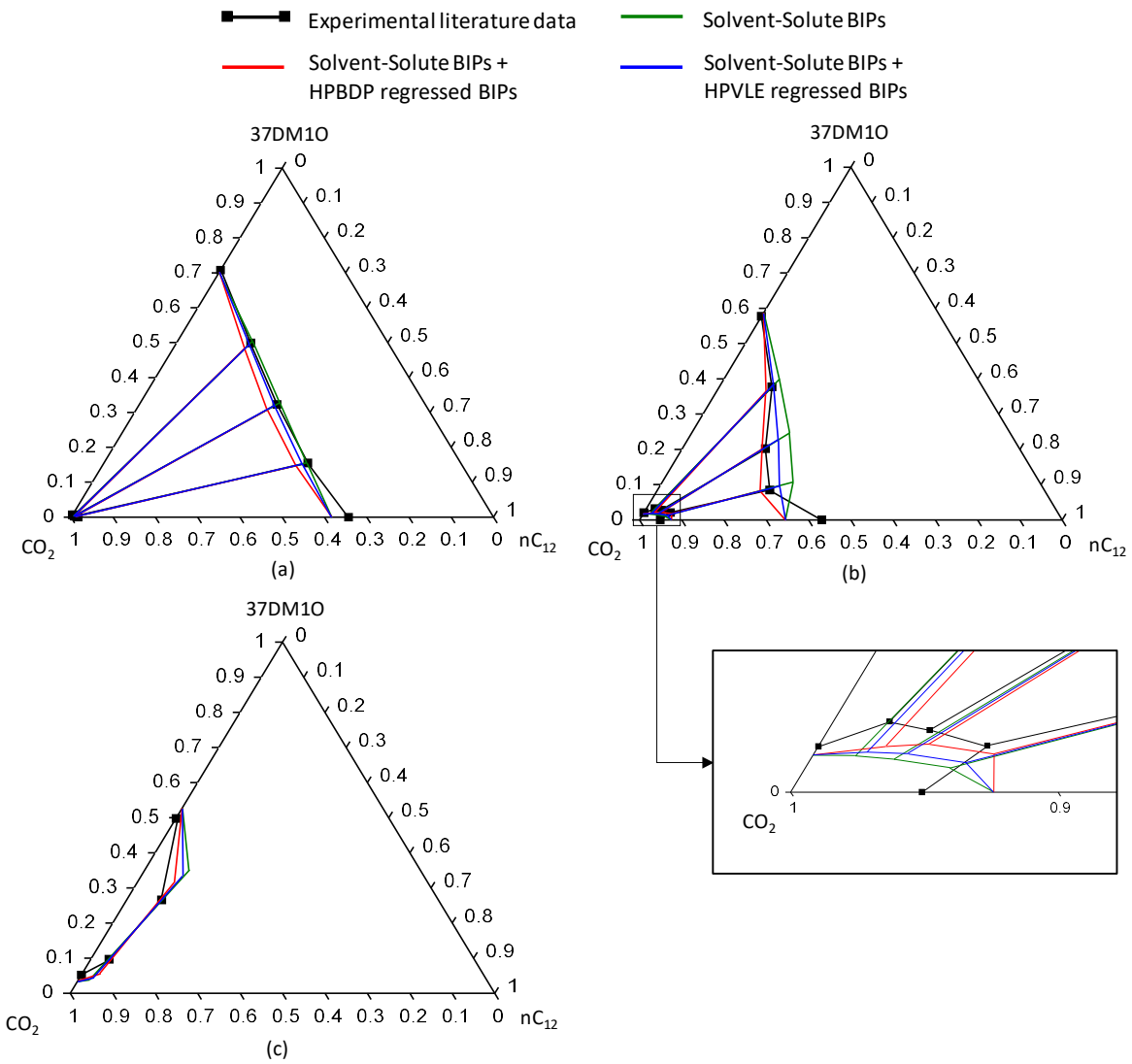

Figure 76: Gibbs phase diagram constructed at 348.2 K and (a) 10.4 MPa, (b)14.0 MPa and (c) 15.7 MPa, comparing experimental literature data [5, 14] to RK-SOAVE correlations obtained when using incorporating different parameters

Conclusion

With the inclusion of the solvent-solute BIPs and a solute-solute BIP the RK-SOAVE model can generate fairly accurate bubble- and dew-point data for n-dodecane rich ternary mixtures, but the model accuracy decreases with an increase in 3,7-dimethyl-1-octanol content. Furthermore, the model cannot correlate the exact composition of co-existing equilibrium phases and can only generate accurate tie-line slopes. The inclusion of a solute-solute BIP is deemed necessary, regardless of the type of data used to regress it, but the model which included the solute-solute BIP regressed from HPBDP data was found to be more accurate.

8.1.2.2 RK-ASPEN

High pressure bubble- and dew-point data

Figure 77 illustrates the accuracy with which the RK-ASPEN model can correlate bubble- and dew-point data for this system. As seen previously, the inclusion of the solvent-solute BIPs significantly improves the model fit, particularly in the high solute concentration region.

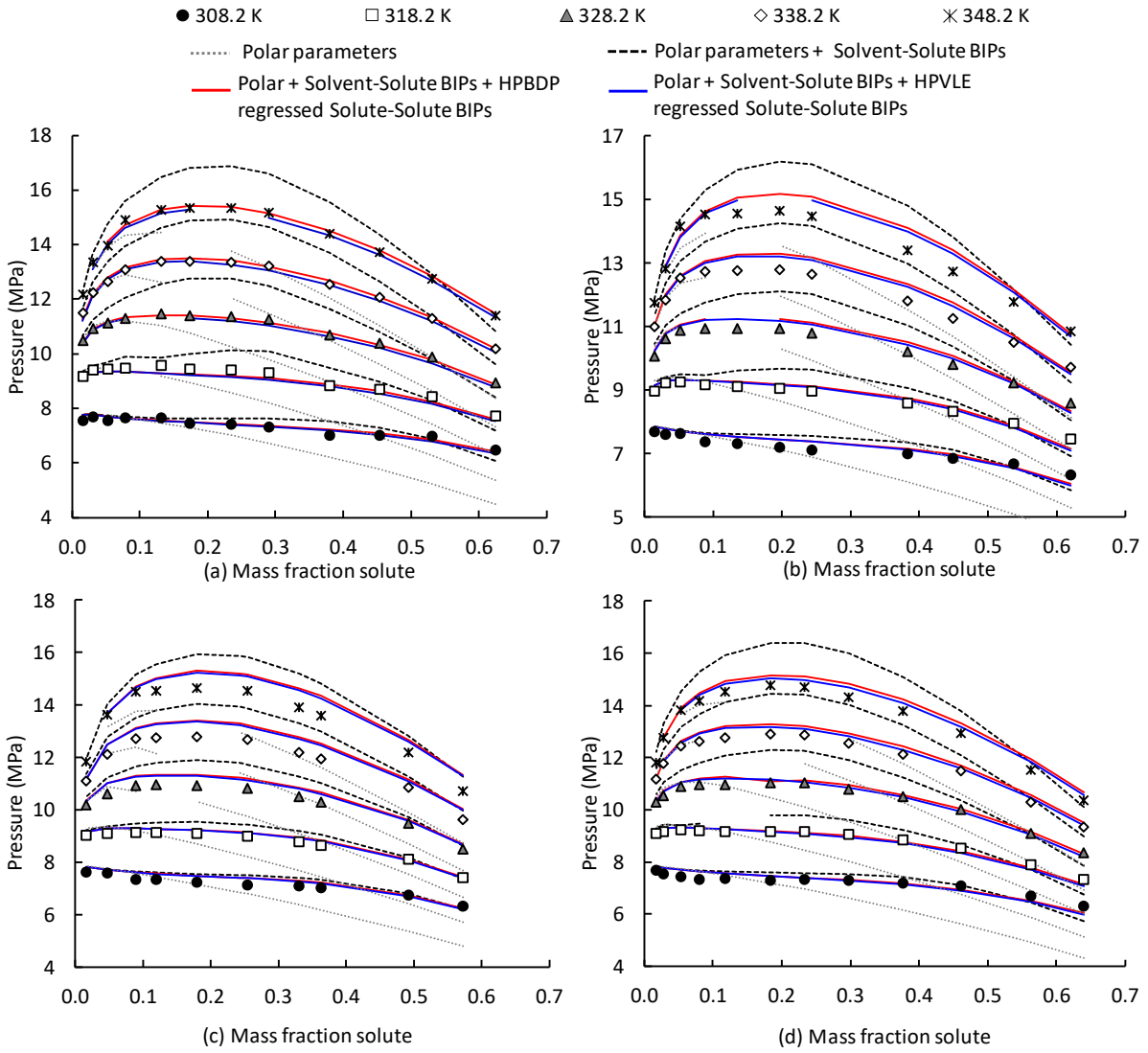

Figure 77: Pressure-composition diagrams comparing experimental data to data generated using the RK-ASPEN model for (a) Mixture 1: 50 wt% nC_{12} + 50 wt% 37DM1O, (b) Mixture 2: 75 wt% nC_{12}+ 25 wt% 37DM1O, (c) Mixture 3: 85 wt% nC_{12}+ 15 wt% 37DM1O and (d) Mixture Z5: 66.7 wt% nC_{12}+ 33.3 wt% 37DM1O [5]

With the exception of the high solute concentration region in Figures 77 (a), (b) and (d), the model which incorporates the solvent-solute BIPs generally overpredicts the phase transition pressures. This deviation is however seen to be reduced with the incorporation of the solute-solute BIP. Furthermore, it is noted that there is little difference between the model correlations

obtained when using the solute-solute BIP regressed from HPBDP and HPVLE data. With the incorporation of the solute-solute BIP, the model correlates fairly accurate phase transition pressures, but the model still tends to slightly overpredict the phase transition pressures as the mixture critical region is approached. There are also areas within/or close to the mixture critical region where the models are unable to correlate phase transition data. The reasons for this have been discussed previously.

High pressure vapour-liquid-equilibrium data

Figure 78 analyses the accuracy with which the RK-ASPEN model can correlate VLE data for this system. This figure reveals that, with the exception of the vapour phase composition correlations at 328 K, the incorporation of the solvent-solute BIPs improves model accuracy. Incorporation of a solute-solute BIP, regardless of the type of data used to regress it, generally further improves model accuracy.

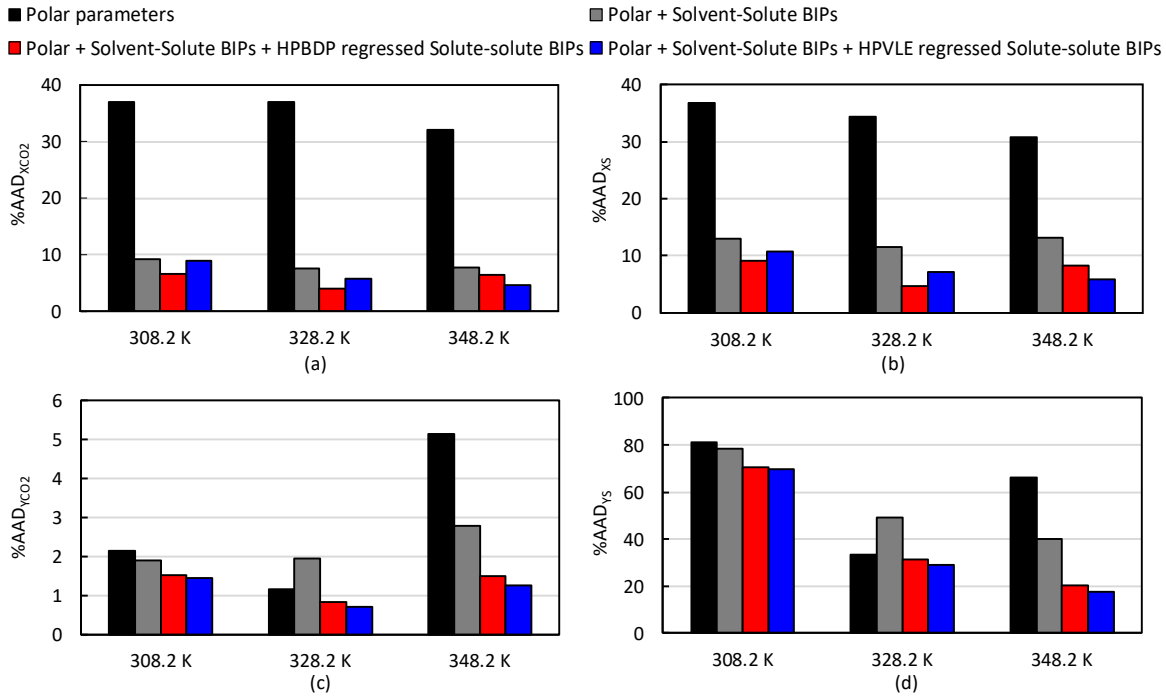

Figure 78: Evaluation of the accuracy with which the RK-ASPEN model can correlate VLE data by comparing the %AAD values for the correlation of (a) liquid and (c) vapour phase CO_2 composition and (b) liquid and (d) vapour phase solute composition (average %AAD for nC_{12} and 37DMO)

Figures 79 and 80, illustrate the model fit. From these diagrams it is noted that the model is generally capable of correlating fairly accurate tie-line slopes. The incorporation of the solute-solute BIP generally improves model fit, regardless of the type of data used to regress it. The improvement is particularly prominent within the pinch point region. These parameters should

therefore be incorporated in the model. Furthermore, it is noted that there is usually little difference between the correlations obtained when including the solute-solute BIPs regressed using different data types.

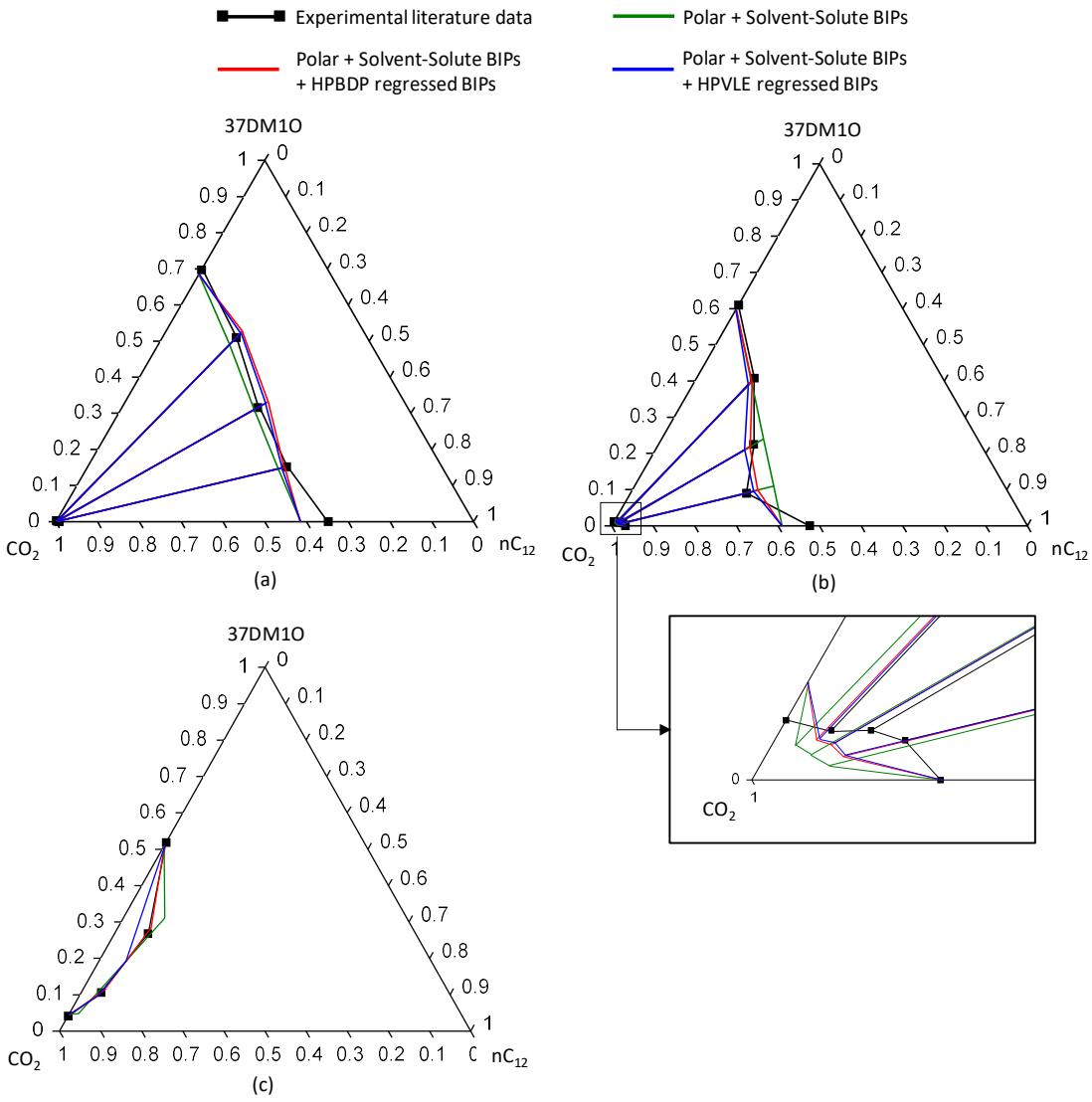

Figure 79: Gibbs phase diagram constructed at 328.2 K and (a) 8.3 MPa, (b)10.4 MPa and (c) 12.3 MPa, comparing experimental literature data [5, 14] to RK-ASPEN correlations obtained when using incorporating different parameters

At the lower pressures, the model battles to correlate the concavity of the liquid curve within the n-dodecane rich region. At slightly higher pressures, this is improved. The model correlates an s-shaped liquid curve, but within the pinch point and n-dodecane rich regions, the model struggles to generate accurate phase composition data for both the liquid and vapour phases. The model can therefore qualitatively correlate the occurrence of co-solvency, but it cannot quantitatively accurately account for the effect thereof. As stated previously, this is partially attributed to the accuracy of the CO_2 + n-dodecane correlations.

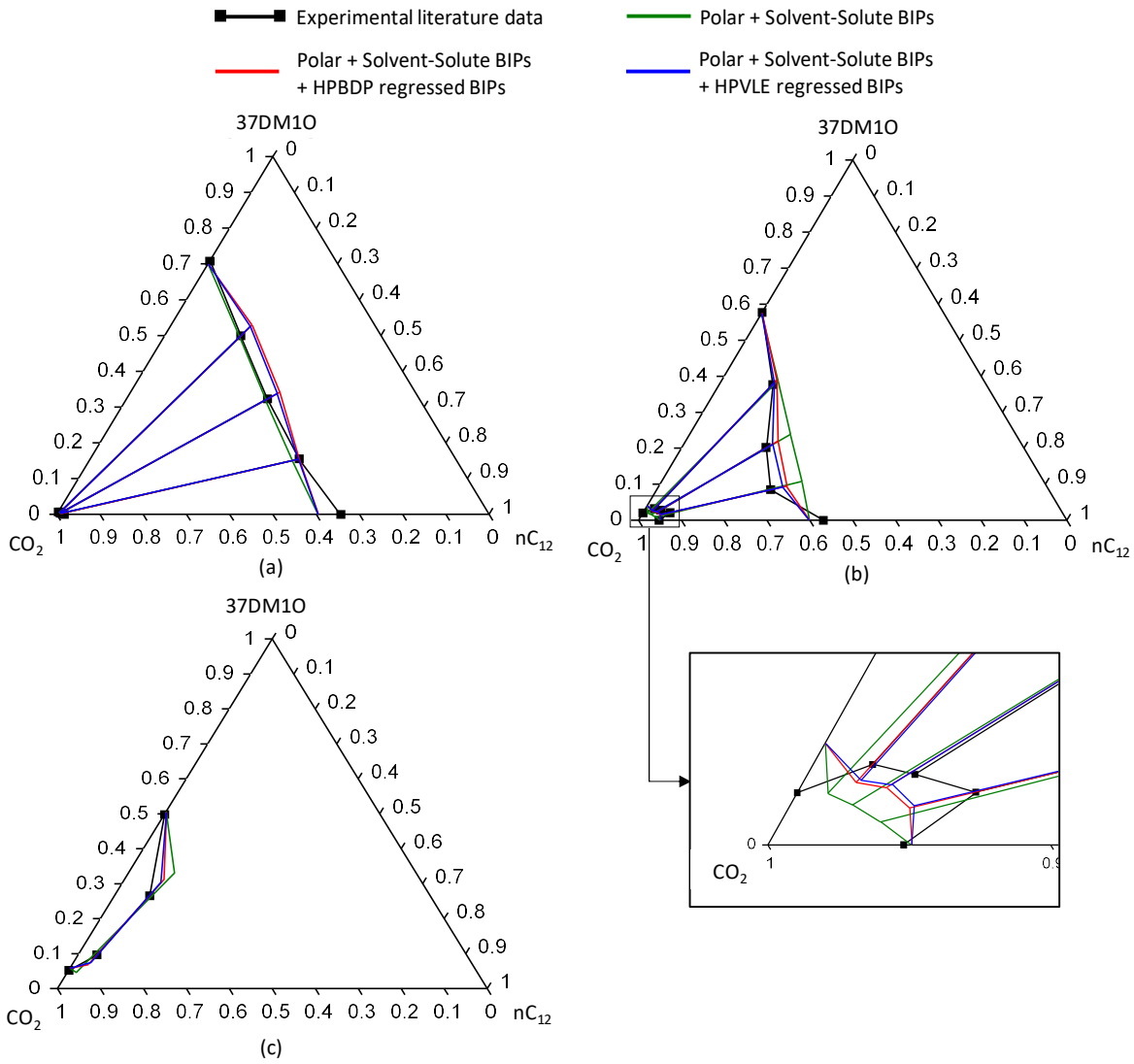

Figure 80: Gibbs phase diagram constructed at 348.2 K and (a) 10.4 MPa, (b)14.0 MPa and (c) 15.7 MPa, comparing experimental literature data [5, 14] to RK-ASPEN correlations obtained when using incorporating different parameters

Conclusion

With the inclusion of the polar parameters, solvent-solute BIPs and solute-solute BIP the RK-ASPEN model is well suited to correlate bubble- and dew-point data for this ternary system, particularly for mixtures containing larger amounts of 3,7-dimethyl-1-octanol. The model can however not correlate the exact composition of co-existing equilibrium phases and can only generate fairly accurate tie-line slopes. Furthermore, there was very little difference between the equilibrium correlations obtained when incorporating the solute-solute BIP regressed from HPBDP and HPVLE data.

8.1.2.3 CPA

High pressure bubble- and dew-point data

The bubble- and dew-point correlations obtained when using the CPA model, are presented in Figure 81.

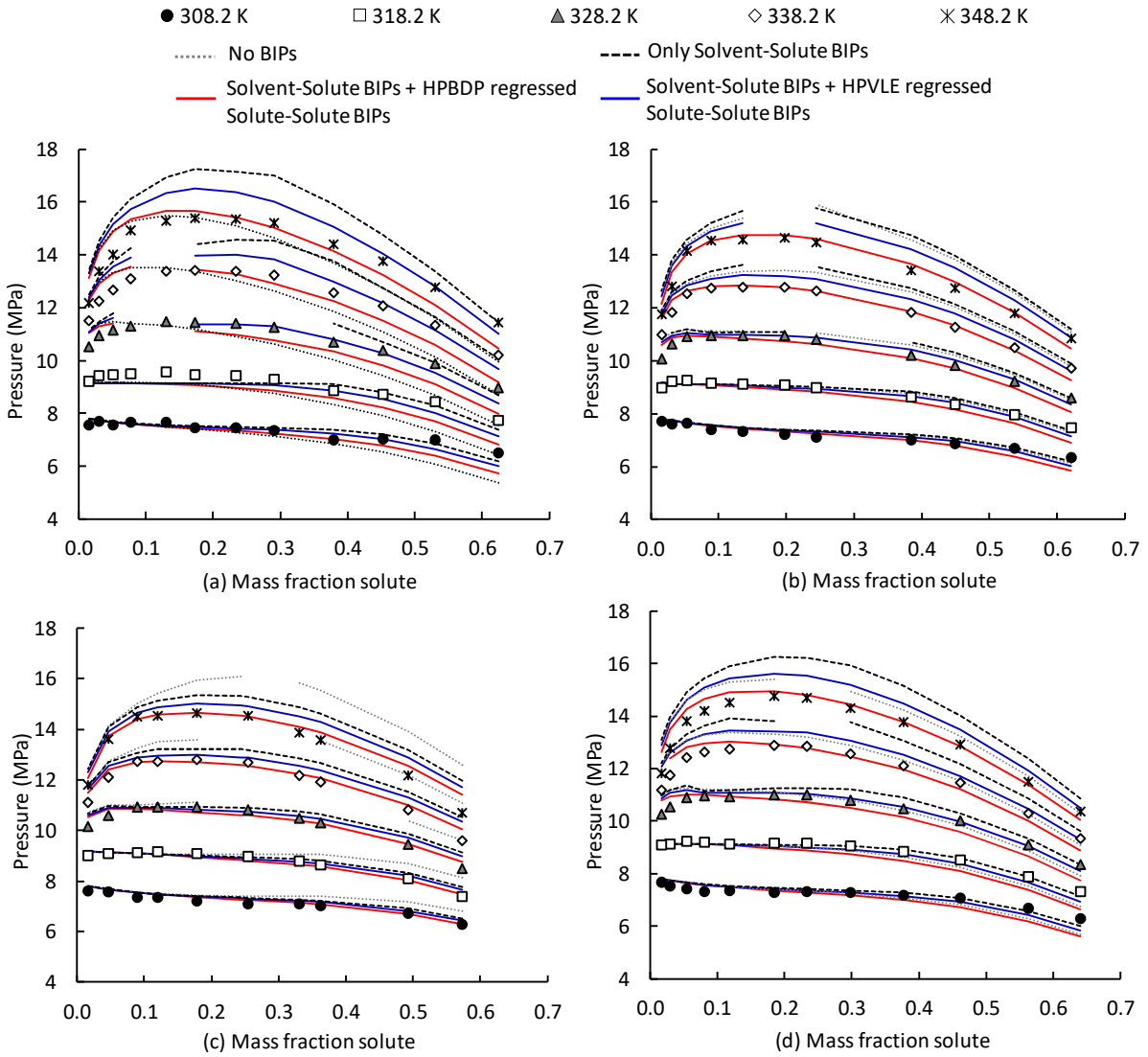

Figure 81: Pressure-composition diagrams comparing experimental data to data generated using the CPA model for (a) Mixture 1: 50 wt% nC_{12} + 50 wt% 37DM1O, (b) Mixture 2: 75 wt% nC_{12}+ 25 wt% 37DM1O, (c) Mixture 3: 85 wt% nC_{12}+ 15 wt% 37DM1O and (d) Mixture Z5: 66.7 wt% nC_{12}+ 33.3 wt% 37DM1O [5]

The effect of including the solvent-solute BIPs on model fit is seen to vary depending on the mixture composition. The inability of the solvent-solute BIPs to improve model accuracy for all the mixtures at all temperatures is deemed to be due to the fact that CO_2 is modelled as a self-associating component. The decision to model CO_2 as a self-associating component was based on the significant improvement in model accuracy if a mixture contains 1-decanol. The system investigated in this section does however not contain 1-decanol. From Table 27,

presented in section 7.2.5, a slight decrease in model accuracy is seen for the CO_2 + n-dodecane and CO_2 + 3,7-dimethyl-1-octanol systems when modelling CO_2 as a self-associating compound. Therefore, for the 50 wt% n-dodecane mixture modelled in this section, the inaccuracy introduced by modelling CO_2 as a self-associating component is enhanced by incorporating both the CO_2 + n-dodecane and CO_2 + 3,7-dimethyl-1-octanol BIPs, as both components are present in significant amounts. For the 85 wt% n-dodecane mixture, the composition is dominated by n-dodecane and therefore the error introduced by modelling CO_2 as a self-associating component mainly stems from the CO_2 + n-dodecane BIP and it is not significantly enhanced by the CO_2 + 3,7-dimethyl-1-octanol BIP, as less CO_2 with 3,7-dimethyl-1-octanol interactions exist. This likely explains the improved model fit for the 85 wt% n-dodecane mixture compared to the 50 wt% n-dodecane mixture.

When analysing the effect of incorporating the solute-solute BIP regressed from HPBDP data it is noted that for Mixtures 1, 2 and Z5, the inclusion of this parameter reduces the overprediction of pressure within the low solute concentration and mixture critical regions at higher temperatures. This improvement in model fit is however accompanied by an underestimation of the pressures in the high solute concentration region. For the n-dodecane rich mixture, Mixture 3, the inclusion of this parameter generally improves the model fit. Incorporation of the solute-solute BIP regressed from HPVLE data generally also reduces the degree of overprediction in the low solute concentration and mixture critical regions. The improvement in model fit within these regions are however less than that seen when incorporating the BIP regressed from HPBDP data.

High pressure vapour-liquid-equilibrium data

The accuracy with which the CPA model can correlate VLE data for this system is presented in Figure 82. The inclusion of the solvent-solute BIPs is seen to improve the accuracy of the liquid phase correlations, but it slightly decreases the accuracy of the vapour phase correlations. Reasons for the large %AAD values reported at 308 K, particularly for the correlation of the vapour phase solute compositions at 308 K, has been discussed previously. At 328 K and 348 K, both solute-solute BIPs generally improve model accuracy, but the correlations obtained when including the solute-solute BIP regressed from HPBDP data are however more accurate.

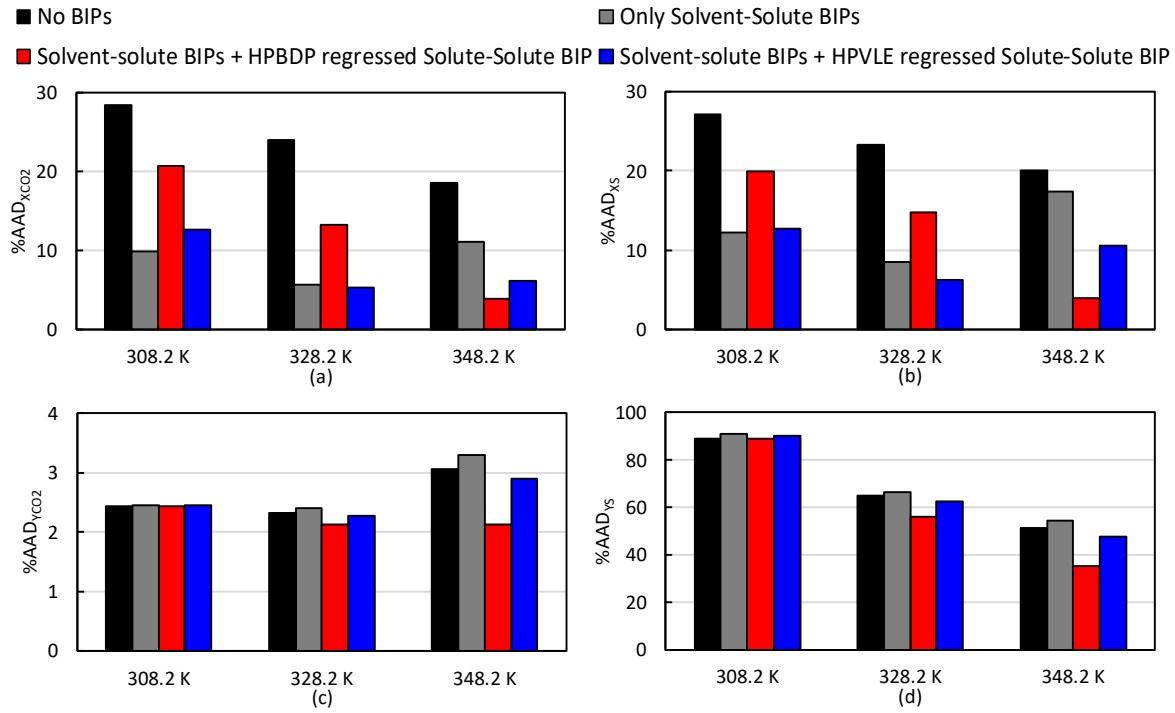

Figure 82: Evaluation of the accuracy with which the CPA model can correlate VLE data by comparing the %AAD values for the correlation of (a) liquid and (c) vapour phase CO_2 composition and (b) liquid and (d) vapour phase solute composition (average %AAD for nC_{12} and 37DMO)

The model fit is analysed in Figures 83 and 84. It is seen that similar to the previous models, the CPA model is capable of generating fairly accurate tie-line slopes, regardless of the type of BIPs included. At low and moderate pressures, the inclusion of the solute-solute BIP improves the model's ability to correlate the concavity of the liquid phase curve, regardless of the data type used to regress it. The model which incorporates the solute-solute BIP regressed from HPBDP data is however generally capable of correlating a more accurate convex-to-concave shape. The composition correlations however deviate from the experimental data and the model can therefore qualitatively account for co-solvency effects, but it cannot account for the quantitative effect thereof. This is partially due to the accuracy of the binary correlations, as discussed previously. The model which incorporates the solute-solute BIP regressed from HPVLE data cannot qualitatively or quantitatively account for co-solvency. Furthermore, the model fit within the vapour phase region obtained when incorporating the solute-solute BIP regressed from HPBDP data is also more accurate.

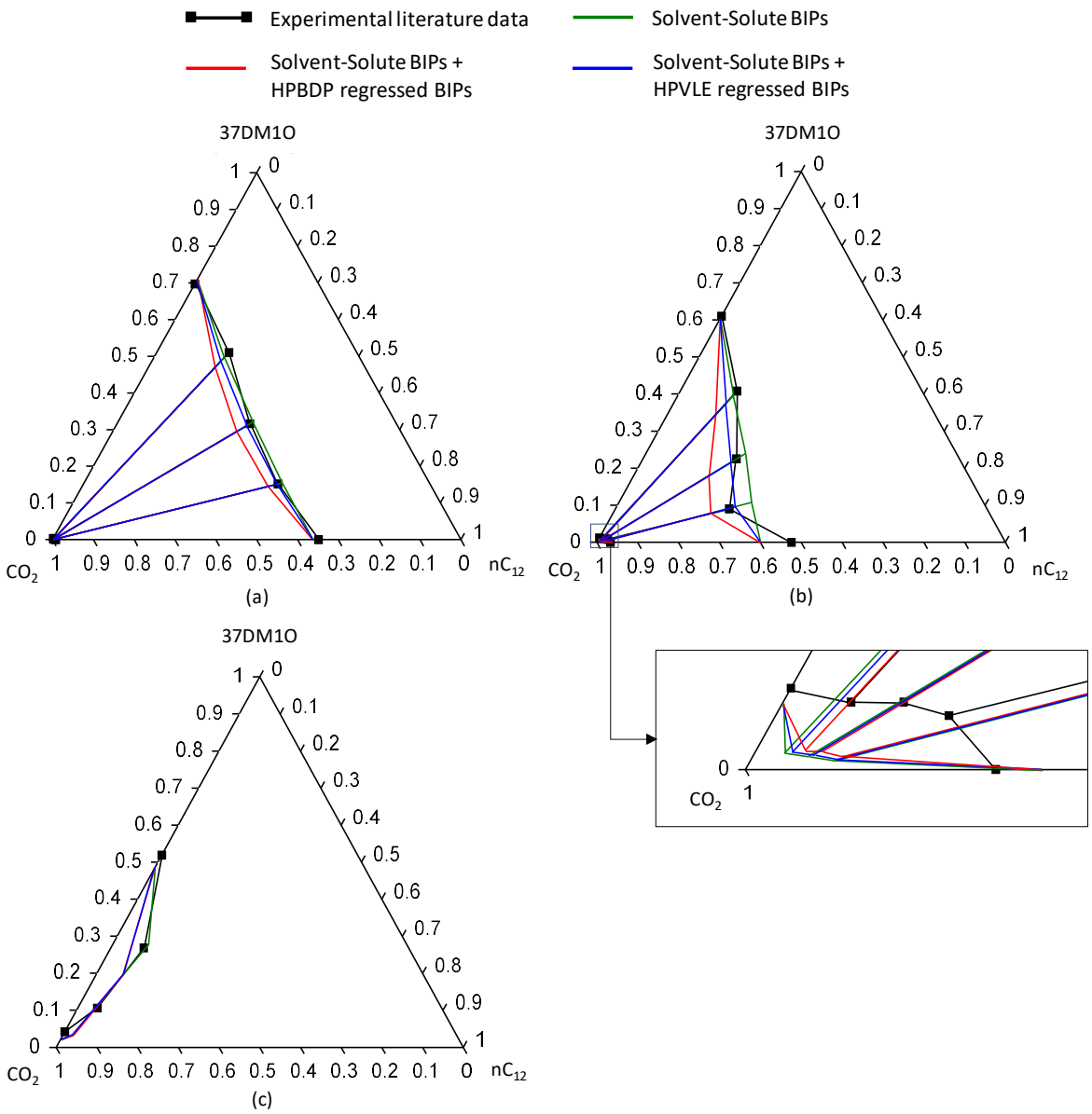

Figure 83: Gibbs phase diagram constructed at 328.2 K and (a) 8.3 MPa, (b)10.4 MPa and (c) 12.3 MPa, comparing experimental literature data [5, 14] to CPA correlations obtained when using incorporating different parameters

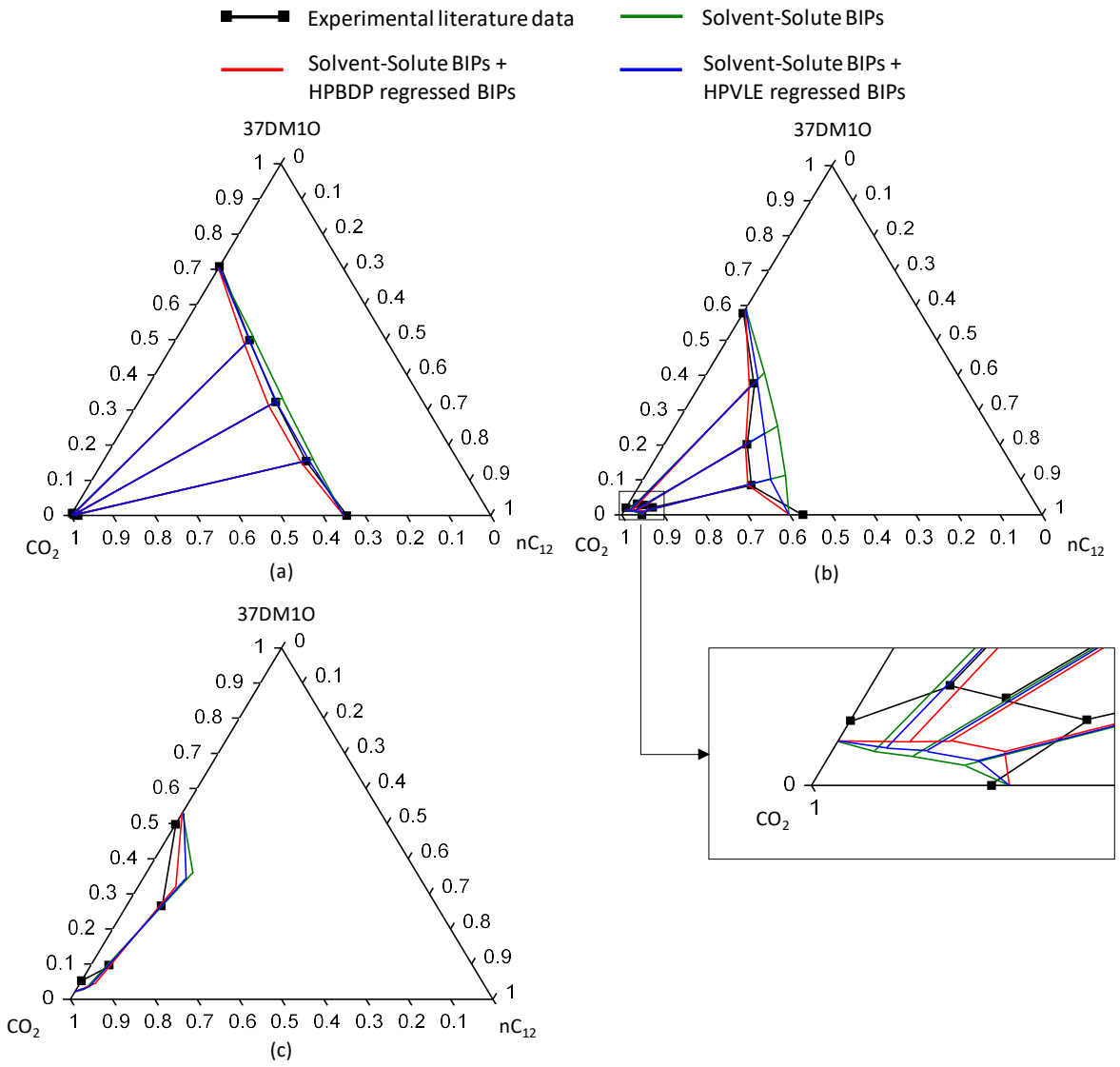

Figure 84: Gibbs phase diagram constructed at 348.2 K and (a) 10.4 MPa, (b)14.0 MPa and (c) 15.7 MPa, comparing experimental literature data [5, 14] to CPA correlations obtained when using incorporating different parameters

Conclusion

With the inclusion of the solvent-solute BIPs and solute-solute BIP the CPA model can correlate fairly accurate bubble- and dew-point data for n-dodecane rich ternary mixtures, but the model accuracy is seen to decrease with an increase in 3,7-diemthyl-1-octanol content. Furthermore, the model cannot correlate the exact composition of co-existing equilibrium phases and can only generate fairly accurate tie-line slopes. The inclusion of the solute-solute BIP improves model accuracy, regardless of the data type used to regress it, but the correlations obtained when incorporating the solute-solute BIP regressed from HPBDP data are generally more accurate.

8.1.2.4 PSRK

High pressure bubble- and dew-point data

The ability of the PSRK model to predict bubble- and dew-point data for this system is analysed in Table 37 and Figure 85. From the table it is noted that the %AAD values are generally rather low, indicating that the PSRK model predicts fairly accurate phase transition pressures.

Table 37: Analysis of the accuracy with which the PSRK model can predict transitions pressures between 308.2 K and 348.2 K

Mix no	Mixture solute composition	%AAD between experimental and PSRK predicted phase transition pressures				
		Temperature (K)				
		308.2	318.2	328.2	338.2	348.2
1	50 wt% nC_{12} + 50 wt% 37DM1O	2.4	3.2	2.3	2.7	2.7
2	75 wt% nC_{12} + 25 wt% 37DM1O	1.5	1.1	1.0	1.6	2.4
3	85 wt% nC_{12}+ 15 wt% 37DM1O	1.0	1.3	1.7	1.9	3.0
Z5	66.7 wt% nC_{12}+ 33.3 wt% 37DM1O	2.7	2.1	1.3	1.8	1.9

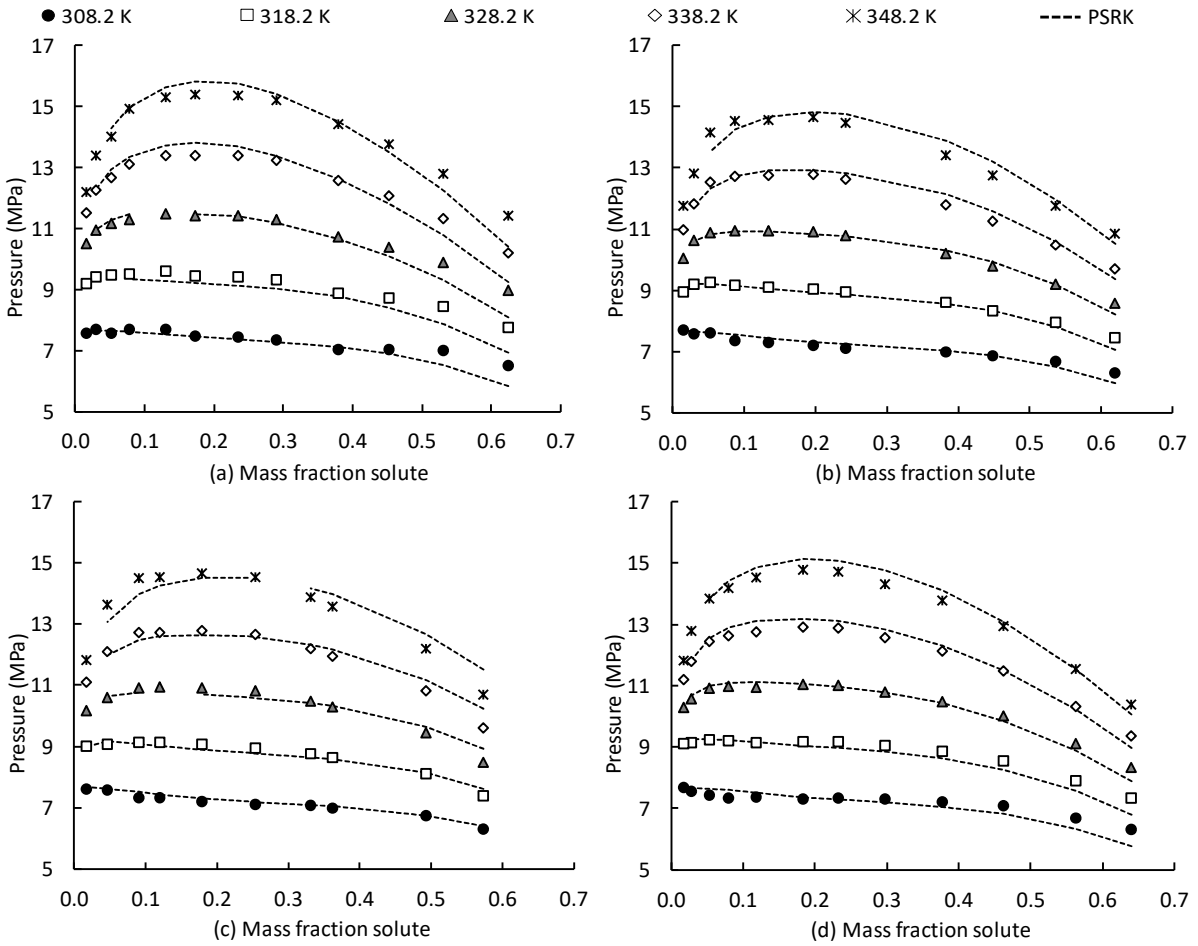

Figure 85: Pressure-composition diagrams comparing experimental data to predicted data generated using the PSRK model for (a) Mixture 1: 50 wt% nC_{12} + 50 wt% 37DM1O, (b) Mixture 2: 75 wt% nC_{12}+ 25 wt% 37DM1O, (c) Mixture 3: 85 wt% nC_{12}+ 15 wt% 37DM1O and (d) Mixture Z5: 66.7 wt% nC_{12}+ 33.3 wt% 37DM1O [5]

From Figure 85 it is seen that the model generally predicts fairly accurate phase transition trends which correspond to the experimental data. It is however noted that for Mixture 1, containing the largest amount of 3,7-dimethyl-1-octanol, the model tends to underestimate the phase transition pressures within the high solute concentration region. This suggests that the predictive model is slightly less accurate for 3,7-dimethyl-1-octanol rich mixtures in which the solute-solute interactions are more prominent.

High pressure vapour-liquid-equilibrium data

The accuracy of the VLE predictions obtained when using the PSRK model is presented in Table 38. The large %AAD values reported at 308 K has been addressed previously. Furthermore, similar to the CO_2 + n-dodecane + 1-decanol system, the accuracy of the PSRK model is seen to improve with temperature.

Table 38: Analysis of the accuracy with which the PSRK model can predict VLE data between 308.2 K and 348.2 K

Temperature (K)	%AAD			
	x_{CO2}	x_s*	y_{CO2}	y_s*
308.2	18.9	18.2	2.3	73.2
328.2	9.0	8.4	1.2	27.4
348.2	5.3	6.6	1.1	20.7

*Average %AAD of the n-dodecane and 3,7-dimethyl-1-octanol in the phase

The model fit attained is analysed in Figure 86 and 87. From these diagrams it is seen that similar to the other models, the PSRK model is capable of predicting fairly accurate tie-line slopes. Furthermore, at the lowest pressures, the model generally predicts fairly accurate liquid phase compositions within the n-dodecane rich region. Noticeable deviations are however seen between the experimental and predicted data with an increase in 3,7-dimethyl-1-octanol content. This was also noted for the bubble- and dew-point predictions. At slightly higher pressures, the deviation within the 3,7-dimethyl-1-octanol rich region is still noticeable. In addition to this, the model's ability to predict accurate data and the correct curvature within the n-dodecane rich region is seen to decrease. The reason for this is related to the accuracy of the binary predictions, discussed previously. The model does however predict fairly accurate data within the pinch point region, and the liquid curve tends to form a s-shaped curve. The vapour phase composition predictions are however seen to deviate significantly from the experimental data. The PSRK model can therefore only suggest the occurrence of co-solvency.

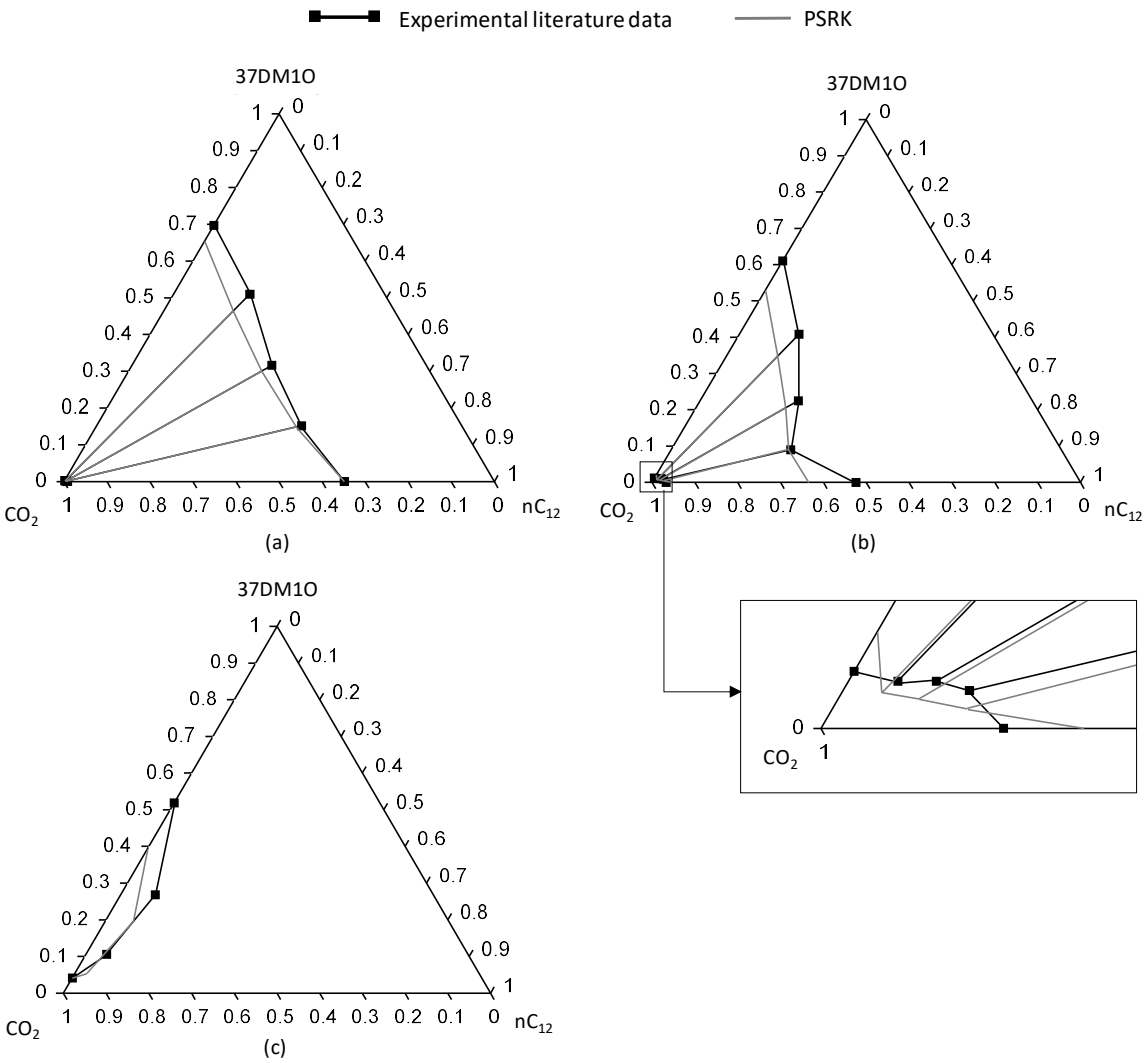

Figure 86: Gibbs phase diagram constructed at 328.2 K and (a) 8.3 MPa, (b)10.4 MPa and (c) 12.3 MPa, comparing experimental literature data [5, 14] to PSRK predictions

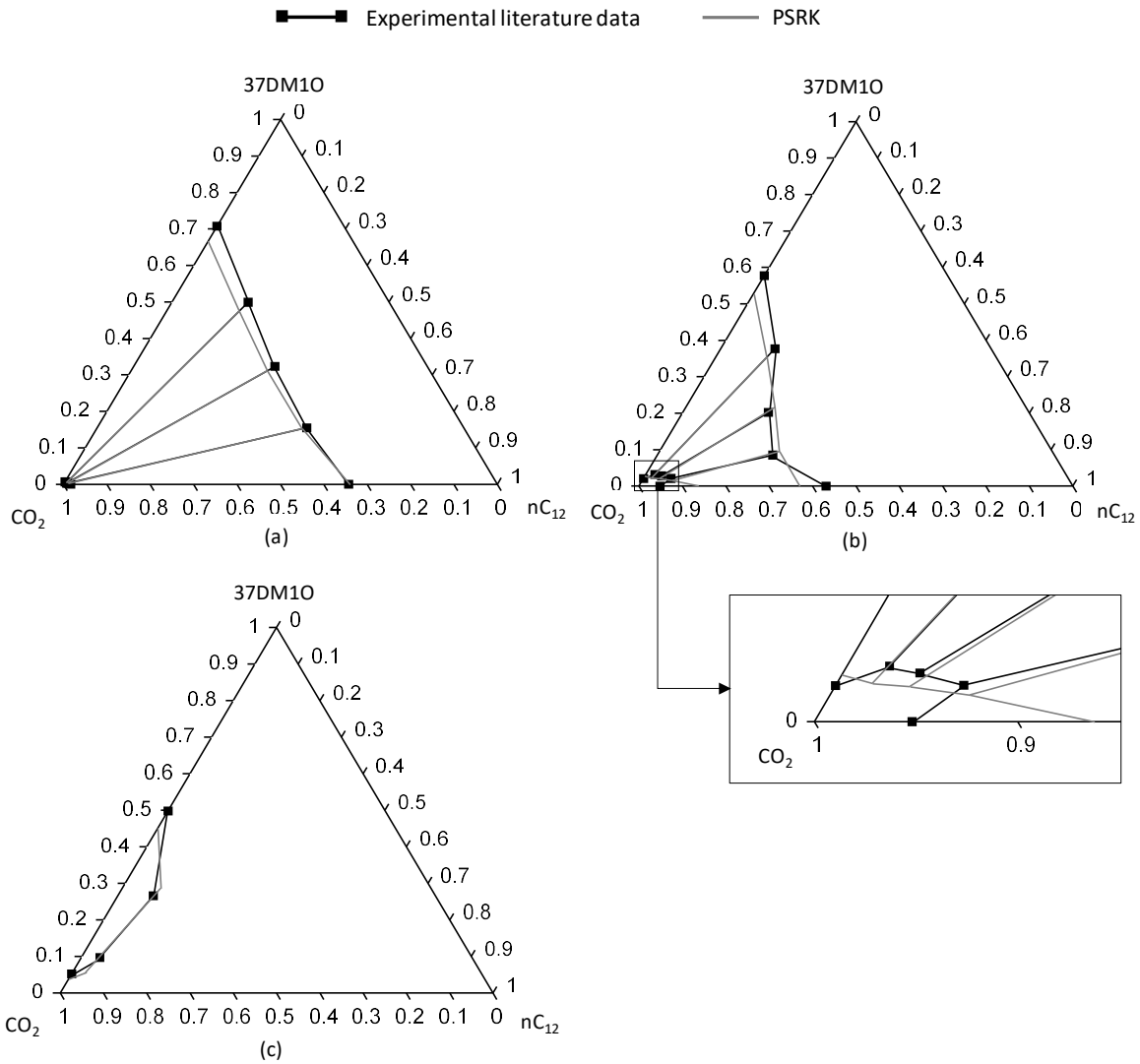

Figure 87: Gibbs phase diagram constructed at 348.2 K and (a) 10.4 MPa, (b)14.0 MPa and (c) 15.7 MPa, comparing experimental literature data [5, 14] to PSRK predictions

Conclusion

The PSRK model predicts fairly accurate bubble- and dew-point data for this ternary system, but the model accuracy tends to decrease when 3,7-dimethyl-1-octanol starts to dominate the mixture composition. Furthermore, the model cannot predict the exact composition of co-existing phases and can only generate fairly accurate tie-line slopes.

8.1.2.5 Model comparison

In this section the performance of the different models at temperatures above 328 K will be compared. Only the optimum BIPs, as identified in the previous sections, will be included in the models in this section. The fitted models used for the comparison are therefore as follows:

Bubble- and dew-point data:	Vapour-liquid-equilibrium data:
• RK-SOAVE + solvent-solute + solute-solute BIP regressed from HPBDP data • RK-ASPEN + solvent-solute + solute-solute BIP regressed from HPBDP data • CPA + solvent-solute + solute-solute BIP regressed from HPBDP data • PSRK	• RK-SOAVE + solvent-solute + solute-solute BIP regressed from HPBDP data • RK-ASPEN + solvent-solute + solute-solute BIP regressed from HPBDP data • CPA + solvent-solute + solute-solute BIP regressed from HPBDP data • PSRK

It is interesting to note that all the optimum solute-solute BIPs incorporated in the models are regressed from HPBDP data. This differs from the previous system in which the optimum parameters were found to correspond to the type of data being correlated. It is however preferred to incorporate BIPs regressed from HPBDP data, as the experiments required to generate this data are simpler, faster and cheaper to conduct.

High pressure bubble- and dew-point data

The accuracy with which the four models can correlate/predict bubble- and dew-point data for this system is compared in Figure 88.

The diagrams do not clearly indicate the superiority of one model with regards to its ability to model phase transition pressures for this system. For the n-dodecane rich mixtures, the general phase behaviour correlated/predicted by the RK-SOAVE, CPA and PSRK models are seen to be more accurate than that of the RK-ASPEN model, although the RK-ASPEN model still correlates fairly accurate data and the correct trends. For the mixtures consisting of larger amounts of 3,7-dimethyl-1-octanol, the RK-ASPEN model is seen to be the most accurate. Different models can therefore be selected based on the composition of a mixture, but the aim is however to determine the best suited model over the entire composition range. In order to determine the best suited model for supercritical fractionation processes, focus is shifted to the ability of the models to correlate/predict data in the low solute concentration (vapour phase) regions. From this analysis it is deemed that the RK-ASPEN model is the most suited model, as it generally provides more accurate vapour phase transition pressures and also converges in the very low solute concentration region where the other models tend to fail.

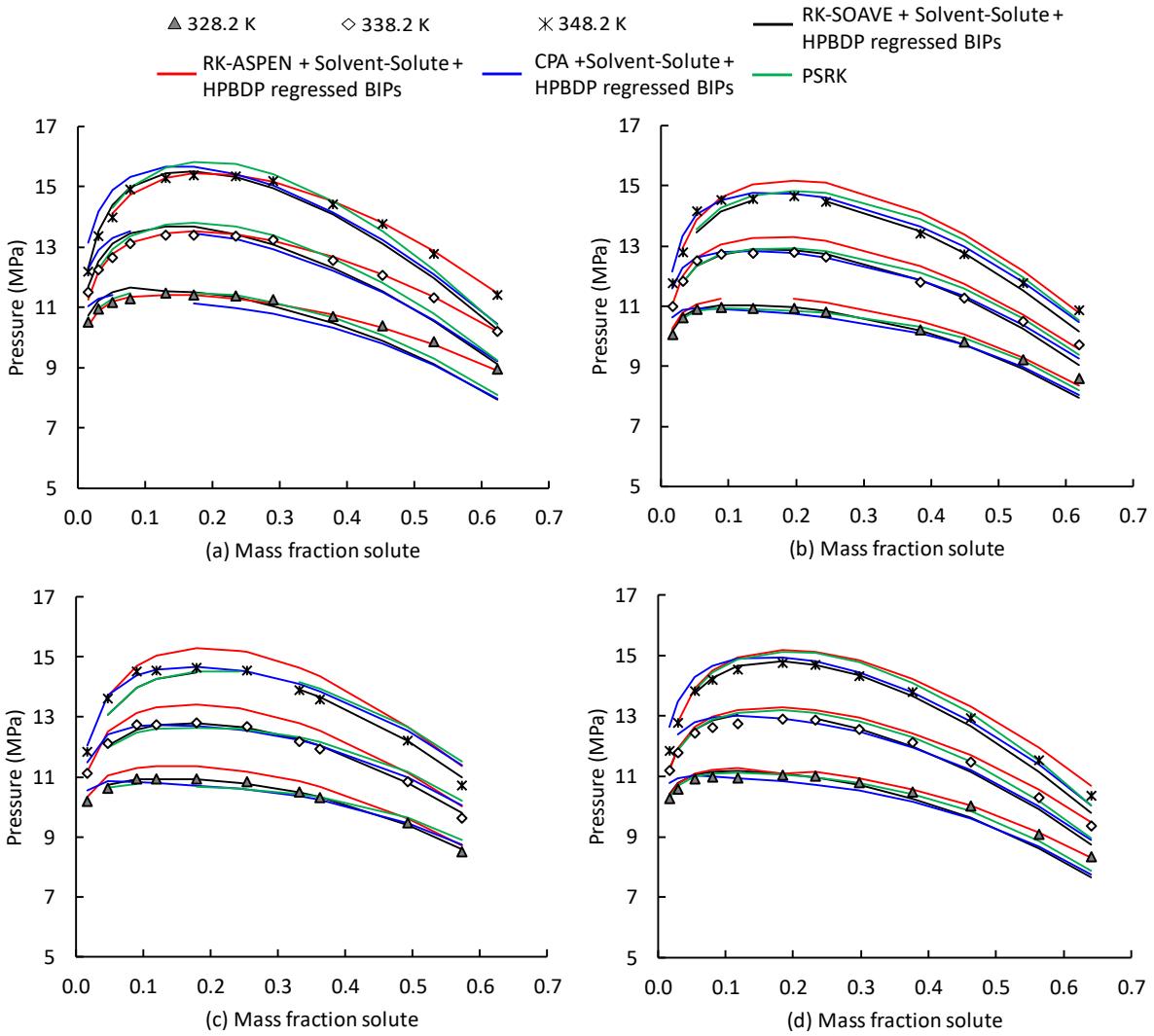

Figure 88: Pressure-composition diagrams comparing experimental data to modelled data for (a) Mixture 1: 50 wt% nC_{12} + 50 wt% 37DM1O, (b) Mixture 2: 75 wt% nC_{12}+ 25 wt% 37DM1O, (c) Mixture 3: 85 wt% nC_{12}+ 15 wt% 37DM1O and (d) Mixture Z5: 66.7 wt% nC_{12}+ 33.3 wt% 37DM1O [5]

High pressure vapour-liquid-equilibrium data

Figure 89 indicates the accuracy with which the four models can correlate/predict VLE data for this system. At 328 K, the RK-ASPEN model generally provides the most accurate correlations. At 348 K, the liquid correlations obtained using the CPA model is seen to be the most accurate, but the corresponding vapour correlations are the least accurate of all four models. No clear conclusion as to which model is best suited to generate VLE data for this system at 348 K can be drawn from the %AAD analysis. The fit of the different models at this temperature is therefore compared in Figure 90.

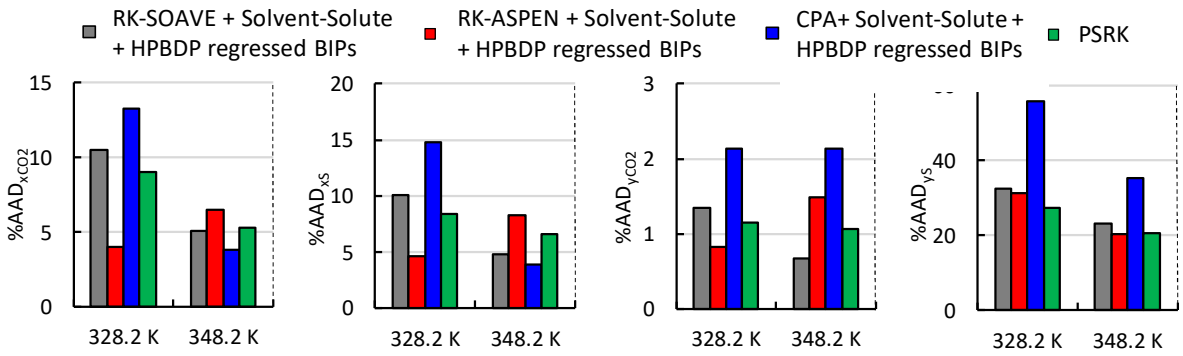

Figure 89: Comparison of the accuracy with which the models can correlate/predict the liquid and vapour phase CO_2 composition as well as the liquid and vapour phase solute composition (average %AAD for nC_{12} and 37DM1O)

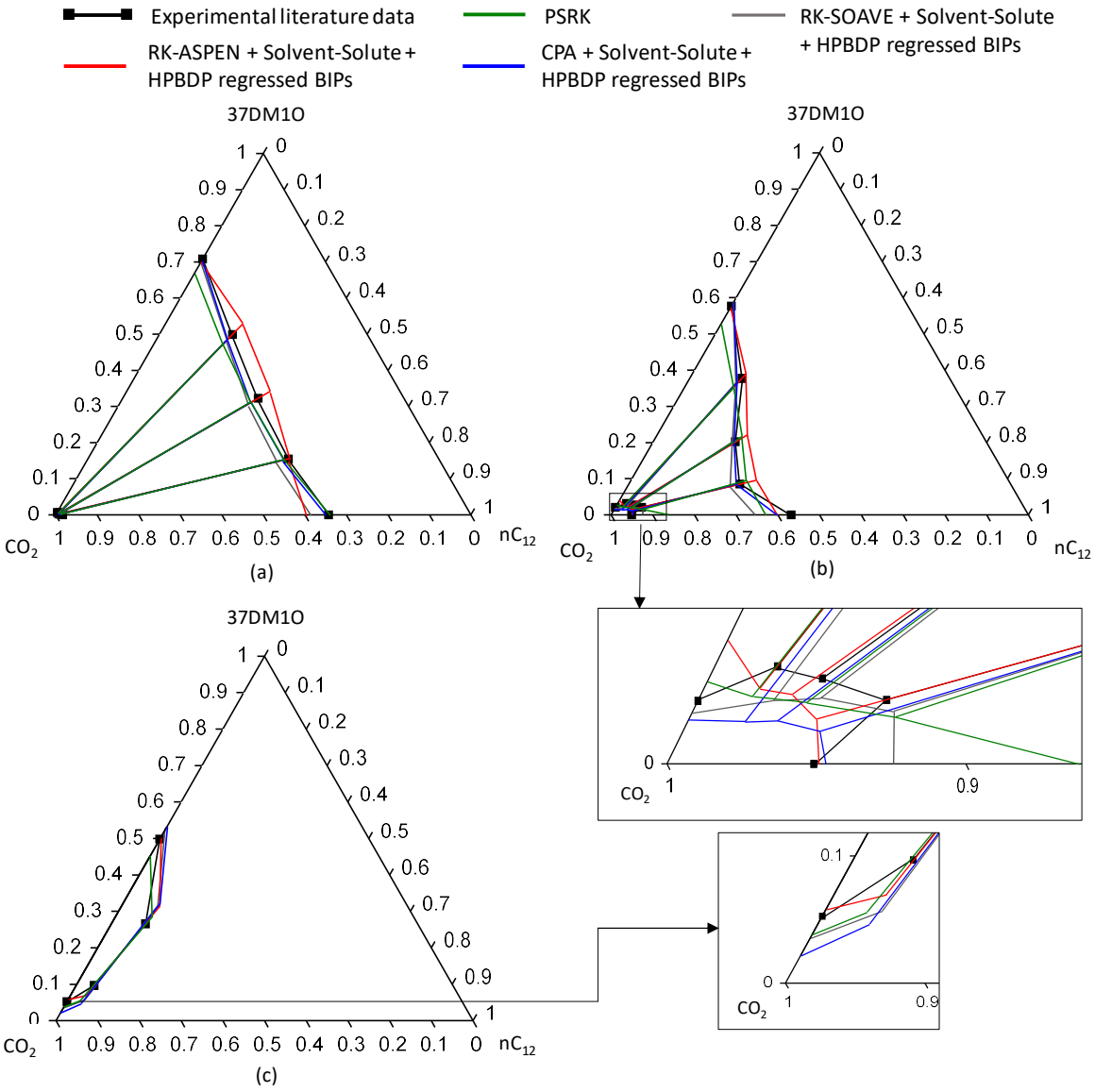

Figure 90: Gibbs phase diagram constructed at 348.2 K and (a) 10.4 MPa, (b)14.0 MPa and (c) 15.7 MPa, comparing experimental literature data [5, 14] to modelled data

The focus of model performance for supercritical fluid fractionation applications is shifted to the vapour phase region. The vapour phase curvature obtained from the RK-ASPEN model generally corresponds better to the experimental curve than the other models. Based on this and the fact that the RK-ASPEN model generally outperforms the other models at 328 K, the RK-ASPEN model is deemed to be most suited to correlate VLE data for this system. The model still however cannot correlate the exact composition of co-existing equilibrium phases and can only be used to approximate VLE data.

8.1.2.6 Section outcomes

The main outcomes of this section are:

- The models were found to correlate/predict fairly accurate bubble- and dew-point data for the ternary system. The accuracy of the RK-ASPEN model was however found to increase with an increase in 3,7-dimethyl-1-octanol fraction, whilst the accuracy of the other models decreased.
- None of the models were capable of correlating the exact composition of the co-existing equilibrium phases and could only generate accurate tie-line slopes.
- The RK-ASPEN model including the fitted solvent-solute BIPs and solute-solute BIP regressed from HPBDP data was found to be the best suited model to generate equilibrium data for this system.

8.1.3 CO_2 + 1-decanol + 3,7-dimethyl-1-octanol

In this section, the ability of the four models to generate equilibrium data for ternary CO_2 + 3,7-dimethyl-1-octanol + 1-decanol mixtures, are evaluated and compared. The experimental bubble- and dew-point data measured in this work (Mixtures 4 – 6), along with data obtained from literature (Mixture Z6) [5] is modelled here. The VLE data modelled in this section was obtained from work done by Fourie [14].

8.1.3.1 RK-SOAVE

High pressure bubble- and dew-point data

In order to analyse the ability of the RK-SOAVE model to correlate bubble- and dew-point data for this system, two sets of pressure-composition diagrams were constructed. The first, presented in Figure 91, was constructed at 308 K and 318 K. From this figure it is seen that there exists a wide range of compositions for which the model cannot correlate phase transition

pressures, regardless of the BIPs incorporated. Furthermore, the pressures which can be correlated deviate significantly from the experimental data. The inability of the model to correlate data at the lower temperatures is linked to the inherent model flaws, complex phase behaviour and regression techniques, as discussed previously.

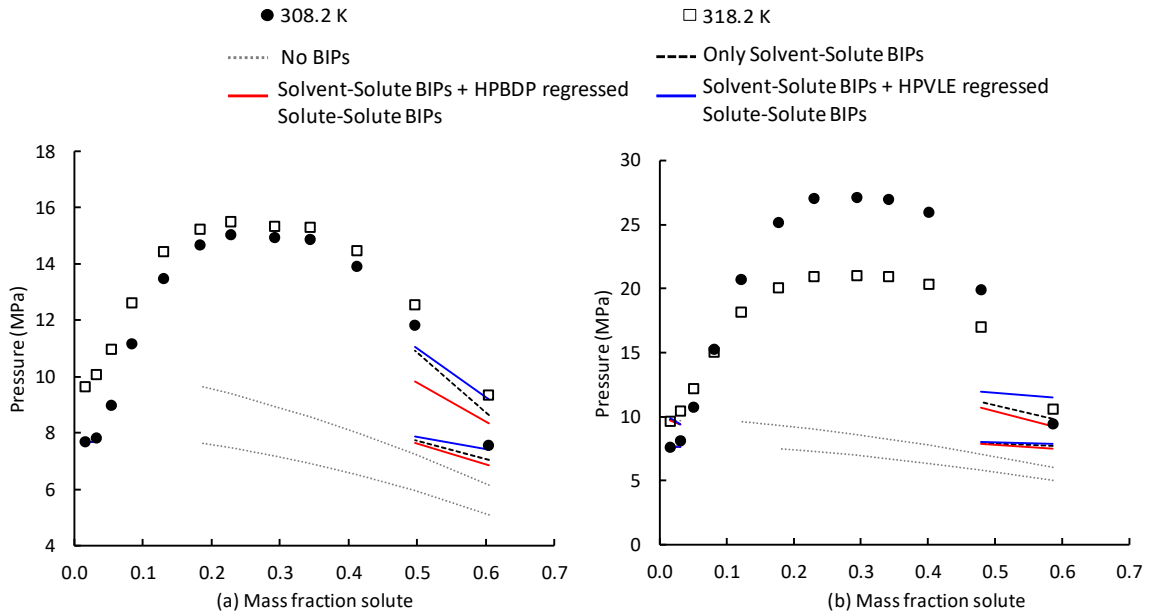

Figure 91: Pressure-composition diagrams comparing experimental data to data generated using the RK-SOAVE model for (a) Mixture 4: 75 wt% 37DM1O + 25 wt% C_{10}OH and (b) Mixture 6: 25 wt% 37DM1O + 75 wt% C_{10}OH at temperatures below 328.2 K

The second set of pressure-composition diagrams, constructed at temperatures above 328 K, are presented in Figure 92. The gaps that still exist in these transition curves, are due to the inability of the model to convergence in the mixture critical region, as explained previously. Similar to the previous systems, the incorporation of the solvent-solute BIPs is seen to significantly improve the model fit. The inclusion of the solvent-solute BIPs, allows the model to correlate the correct bubble- and dew-point trends, but there is usually some deviation between the modelled and measured data. The incorporation of the solute-solute BIP regressed from HPBDP data is seen to generally reduce the degree of overprediction in the mixture critical region. However, within the low solute concentration region, which is the region of interest, the inclusion of this solute-solute BIP has a tendency to decrease model accuracy. The incorporation of this BIP also does not allow for accurate correlation of transition pressures in the high solute concentration region. The inclusion of the solute-solute BIP regressed from HPVLE data is seen to generally only decrease model accuracy. Based on the inability of the

solute-solute BIPs to consistently improve model accuracy, the incorporation thereof is not recommended, regardless of the type of data used to regress it.

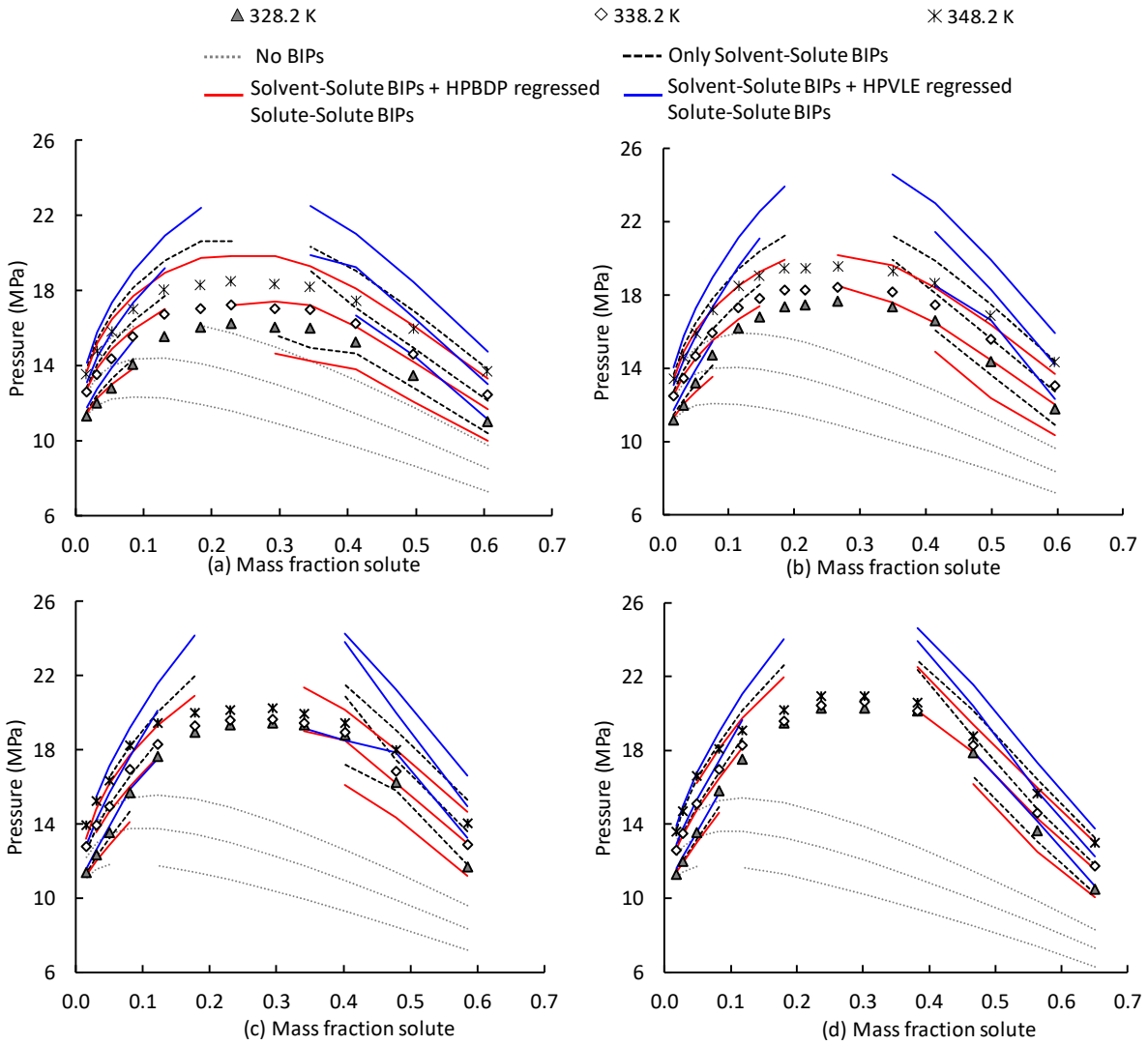

Figure 92: Pressure-composition diagrams comparing experimental data to data generated using the RK-SOAVE model for (a) Mixture 4: 75 wt% 37DM1O + 25 wt% $C_{10}OH$, (b) Mixture 5: 50 wt% 37DM1O + 50 wt% $C_{10}OH$, (c) Mixture 6: 25 wt% 37DM1O + 75 wt% $C_{10}OH$ and (d) Mixture Z6: 12.5 wt% 37DM1O + 87.5 wt% $C_{10}OH$ [5] at temperatures above 328.2 K

High pressure vapour-liquid-equilibrium data

Figure 93 analyses the accuracy with which the RK-SOAVE model can correlate VLE data for this system. From this figure it is noted that, except for the vapour phase correlations at 308 K, the inclusion of the solvent-solute BIPs generally improves model accuracy. The addition of a solute-solute BIP does not improve model accuracy at 308 K and at this temperature the reported %AAD values are large. The poor performance at this temperature has been addressed previously. The incorporation of the solute-solute BIP regressed from HPBDP data at 328 K

and 348 K is seen to either improve the liquid or the vapour phase correlations at a specific temperature, but not both. Analysis of the effect of incorporating the solute-solute BIP regressed from HPVLE at 328 K and 348 K reveals that, with the exception of the liquid phase correlations at 328 K, the inclusion of this BIP generally decreases model accuracy.

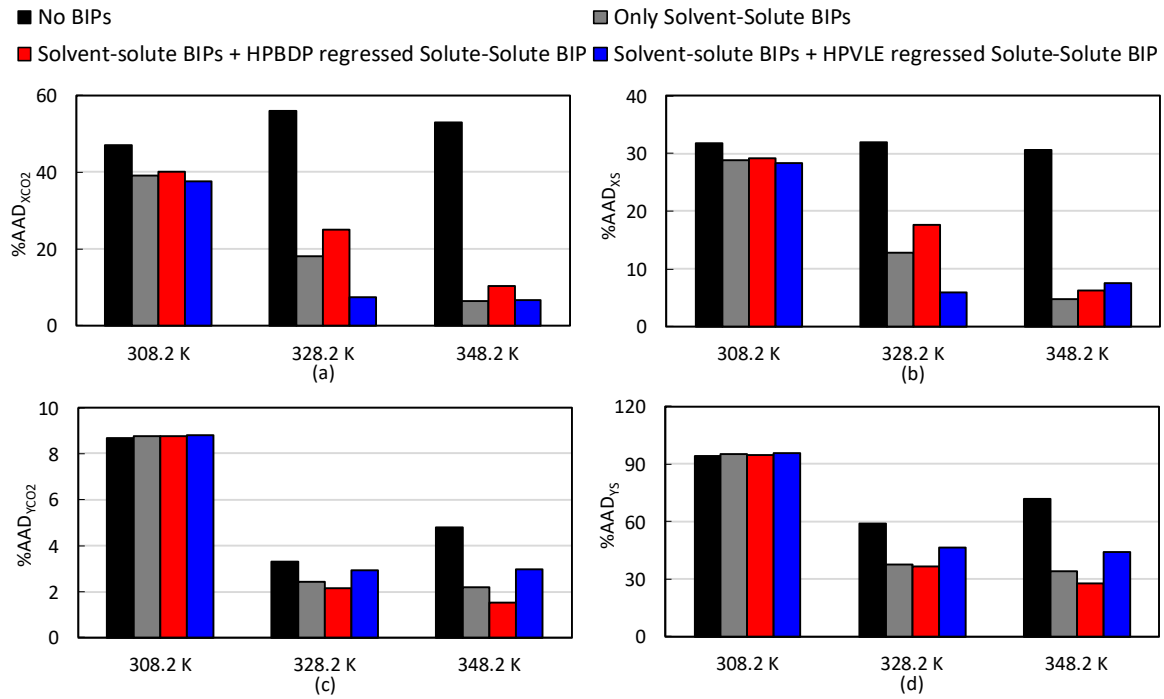

Figure 93: Evaluation of the accuracy with which the RK-SOAVE model can correlate VLE data by comparing the %AAD values for the correlation of (a) liquid and (c) vapour phase CO_2 composition and (b) liquid and (d) vapour phase solute composition (average %AAD for C_{10}OH and 37DM1O)

The model fit is analysed in Figures 94 and 95. Similar to the previous systems, the diagrams reveal that the RK-SOAVE model can generate fairly accurate tie-lines slopes. At the lower pressures, the inclusion of the solute-solute BIP regressed from HPBDP data decreases the accuracy with which the liquid phase compositions are correlated, whilst the BIP regressed from HPVLE data improves it. At moderate pressures, the incorporation of the solute-solute BIP regressed from HPBDP data generally decreases the accuracy with which the model correlates the liquid and vapour phase compositions. At these pressures, the incorporation of the solute-solute BIP regressed from HPVLE data improves the liquid phase composition correlations at 328 K, but it decreases the accuracy of the vapour phase composition correlations at 328 K and 348 K. It also misrepresents the curvature of the vapour phase boundary at these temperatures. At the highest pressures, the inclusion of the solute-solute BIP generally does not seem to improve the model's ability to correlate VLE data, regardless of the

data type used to regress it. The inclusion of a solute-solute BIP is therefore not recommended, regardless of the type of data used to regress it.

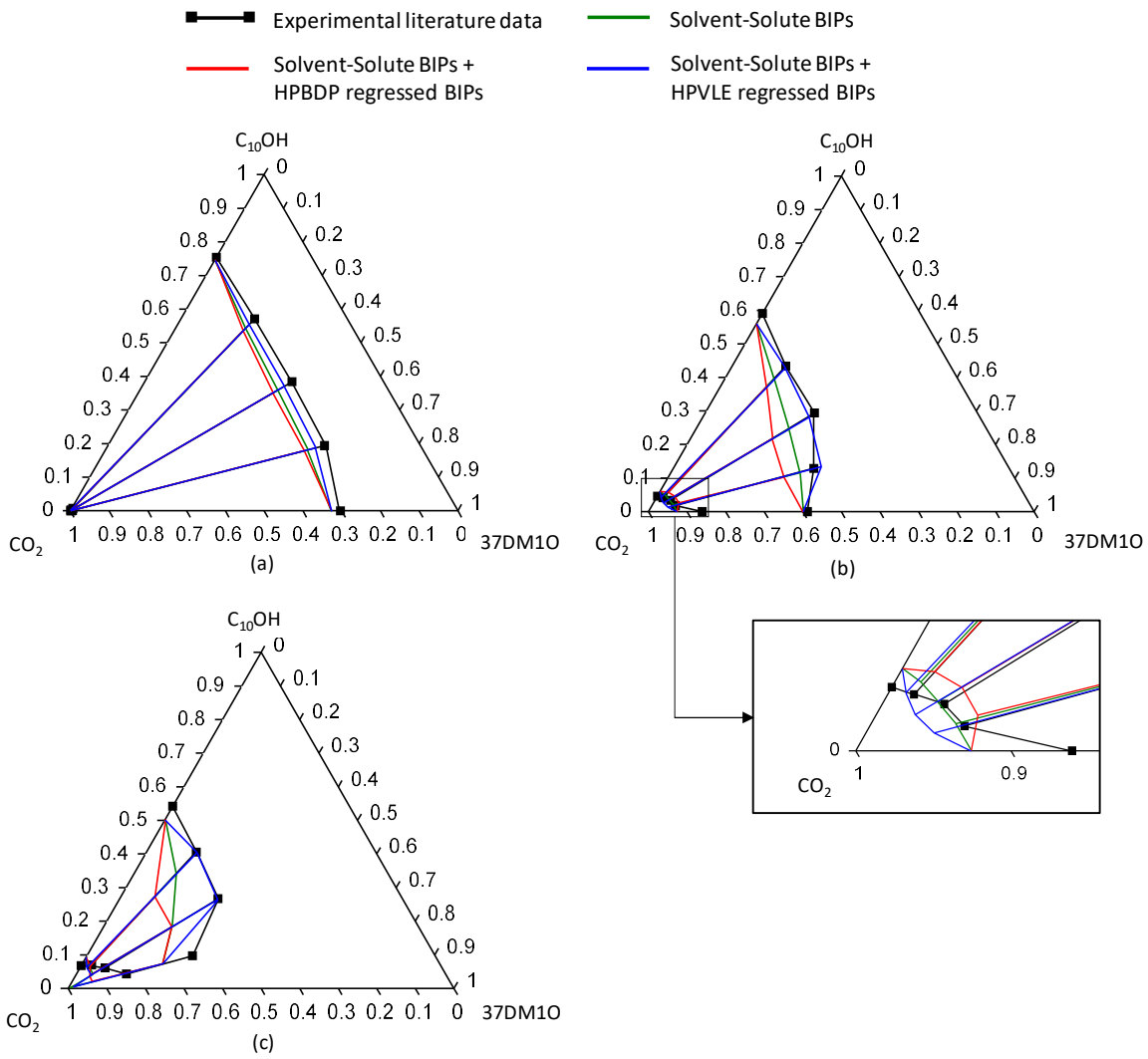

Figure 94: Gibbs phase diagram constructed at 328.2 K and (a) 8.3 MPa, (b)14.0 MPa and (c) 15.7 MPa, comparing experimental literature data [5, 14] to RK-SOAVE correlations obtained when using incorporating different parameters

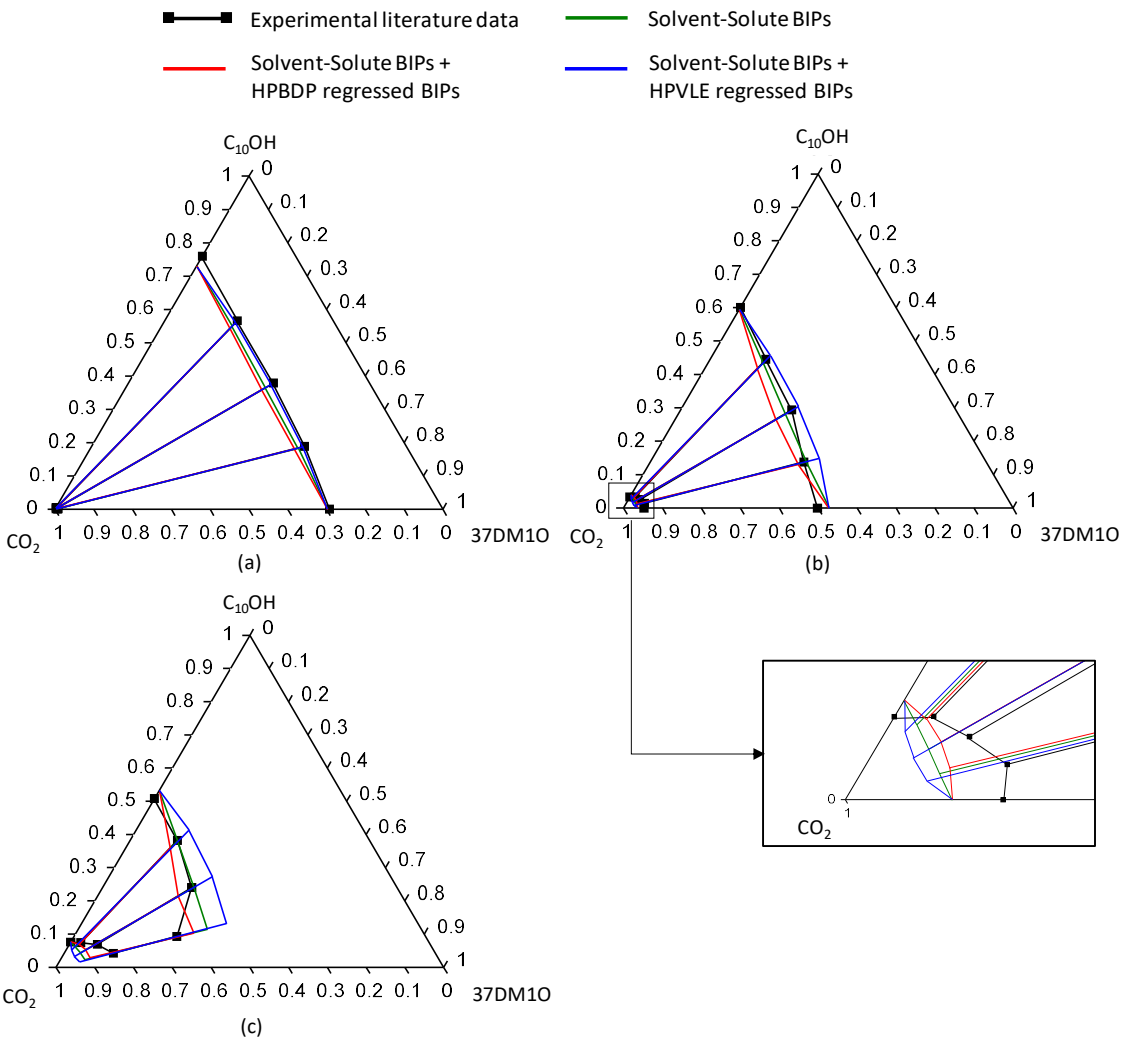

Figure 95: Gibbs phase diagram constructed at 348.2 K and (a) 10.4 MPa, (b) 15.7 MPa and (c) 18.2 MPa, comparing experimental literature data [5, 14] to RK-SOAVE correlations obtained when using incorporating different parameters

Conclusion

The RK-SOAVE model which only incorporates solvent-solute BIPs is the most suited model version. The incorporation of a solute-solute BIP is not recommended, regardless of the type of data used to regress it, as its contribution to model accuracy does not justify reducing the model robustness. Furthermore, the results indicate that the RK-SOAVE model does not generate accurate equilibrium (bubble- and dew-point and VLE) data for this ternary system, regardless of the interaction parameters included.

8.1.3.2 RK-ASPEN

High pressure bubble- and dew-point data

Figure 96 illustrates the ability of the RK-ASPEN model to generate bubble- and dew-point data for this system. Similar to the RK-SOAVE correlations, the RK-ASPEN model cannot

correlate representative bubble- and dew-point data for this system at temperatures below 328 K, therefore these temperatures were excluded from Figure 96.

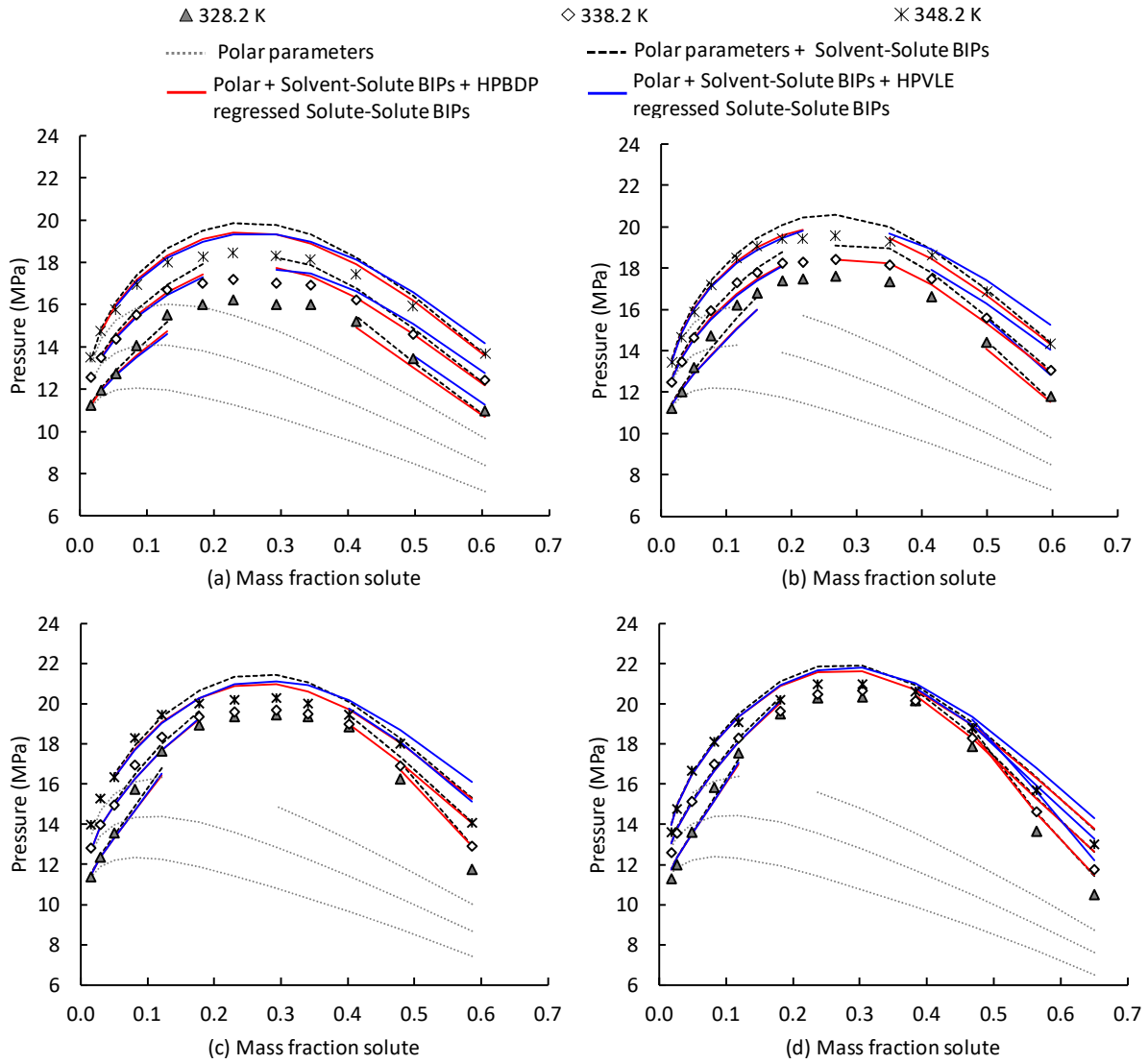

Figure 96: Pressure-composition diagrams comparing experimental data to data generated using the RK-ASPEN model for (a) Mixture 4: 75 wt% 37DM1O + 25 wt% $C_{10}OH$, (b) Mixture 5: 50 wt% 37DM1O + 50 wt% $C_{10}OH$, (c) Mixture 6: 25 wt% 37DM1O + 75 wt% $C_{10}OH$ and (d) Mixture Z6: 12.5 wt% 37DM1O + 87.5 wt% $C_{10}OH$ [5] at temperatures above 328.2 K

As seen previously, the incorporation of the solvent-solute BIPs significantly improves the model fit. The inclusion of the solute-solute BIPs generally only improves the model correlations within the mixture critical region. In this region, the incorporation of the solute-solute BIPs reduces the degree of overprediction. Within the low solute concertation region, the model correlations obtained when including only the solvent-solute BIPs is generally more accurate. When analysing the high solute concentration region it is noted that for the mixtures containing 25 wt% and 50 wt% 1-decanol, the model correlations obtained when using only

the solute-solvent BIPs is generally fairly accurate and the inclusion of the solute-solute BIPs regressed from HPBDP data is only seen to slightly improve the model correlations at some points closer to the mixture critical region. In these diagrams, a decrease in model accuracy within the high solute concentration region is generally observed due to the inclusion of the solute-solute BIP regressed from HPVLE data. Analysis of the high solute concentration region for the mixtures consisting of 75 wt% and 87.5 wt% 1-decanol indicates that the model cannot accurately correlate phase transitions pressures in this region, regardless of the type of BIPs incorporated. The model fit analysis suggests that with the inclusion of the different BIPs either the mixture critical region or the vapour- and liquid regions can be improved, but not all three regions can be improved at the same time. This trade off in model accuracy between certain regions when including different BIPs has also been reported in work done by Schwarz, et al., [126]. For supercritical fluid fractionation focus is on the low solute concentration (vapour phase) region and therefore it is recommended that the solute-solute BIPs not be included in the model.

High pressure vapour-liquid-equilibrium data

The accuracy of the VLE correlations obtained for this system when using the RK-ASPEN model, is analysed in Figure 97.

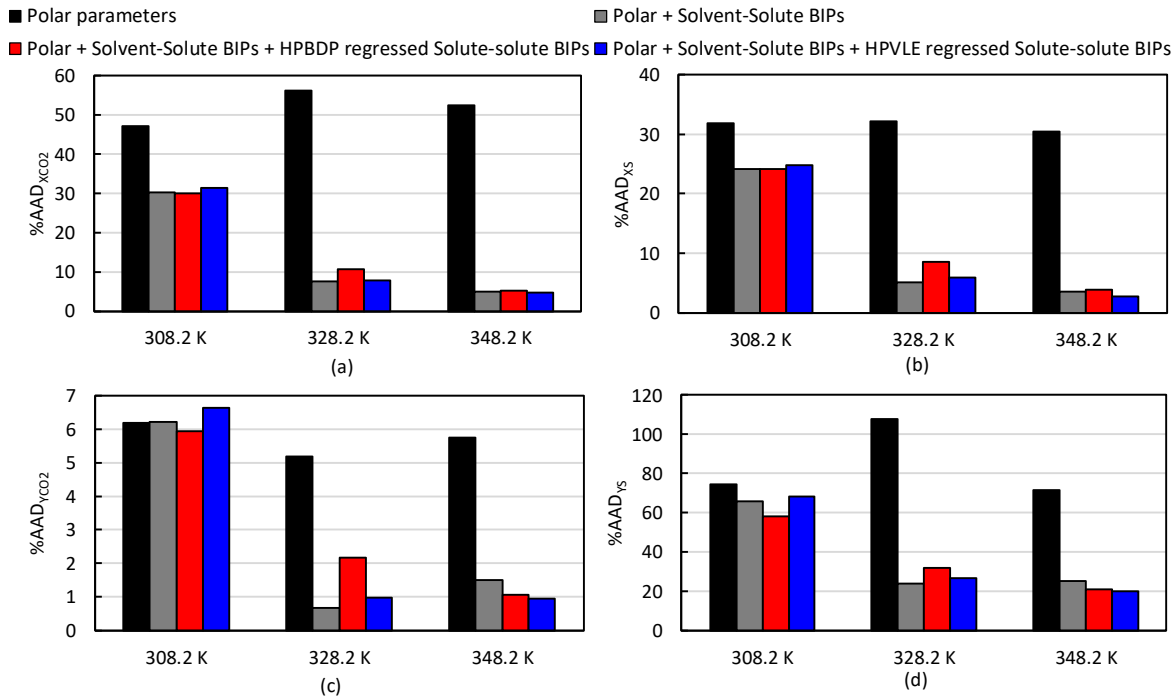

Figure 97: Evaluation of the accuracy with which the RK-ASPEN model can correlate VLE data by comparing the %AAD values for the correlation of (a) liquid and (c) vapour phase CO_2 composition and (b) liquid and (d) vapour phase solute composition (average %AAD for $C_{10}OH$ and 37DM1O)

The incorporation of the solvent-solute BIPs improves the accuracy with which the model can generate VLE data at all three temperatures. The degree of improvement observed at 308 K is however less and the %AAD values are generally larger, this has been addressed previously. The inclusion of the solute-solute BIPs tends to negatively impact the model's ability to correlate VLE data. Based on the %AAD analysis incorporation of this parameter is not recommended.

In order to analyse the effect of including these parameters on the model fit, the Gibbs phase diagrams, presented in Figure 98 and 99, were constructed. It is seen that similar to the previous systems, the model is capable of generating fairly accurate tie-lines slopes.

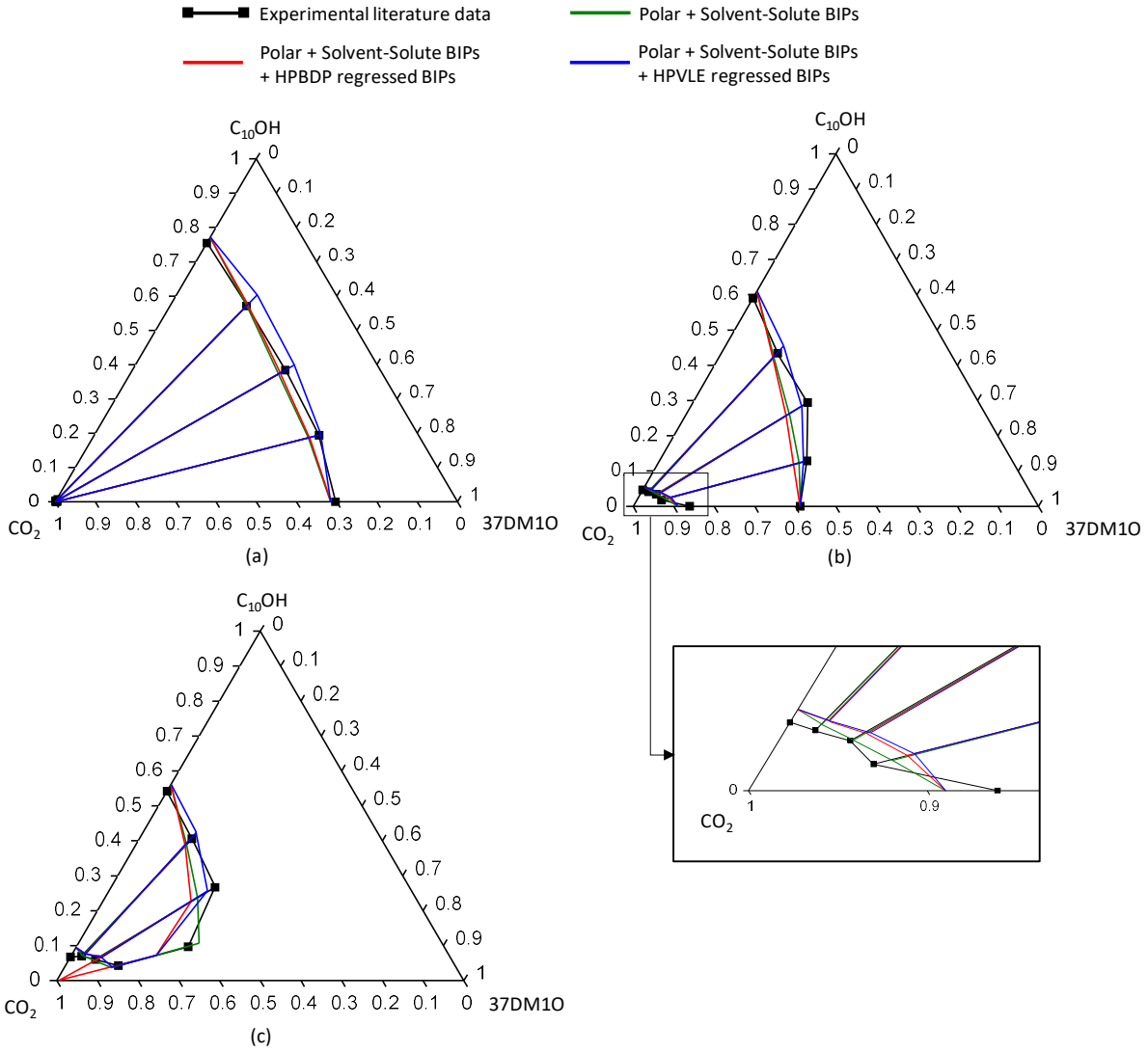

Figure 98: Gibbs phase diagram constructed at 328.2 K and (a) 8.3 MPa, (b)14.0 MPa and (c) 15.7 MPa, comparing experimental literature data [5, 14] to RK-ASPEN correlations obtained when using incorporating different parameters

Comparison of the model fit obtained with and without the inclusion of the solute-solute BIP regressed from HPBDP data indicates that the correlations are generally fairly similar at low and moderate pressures. At 328 K, the incorporation of this BIP significantly decreases the model's ability to correlate VLE data at the highest pressure. At moderate and high pressures at 348 K, the incorporation of this BIP slightly increases the accuracy with which the model correlates vapour phase composition data, but this is usually accompanied by a slight decrease in the accuracy of corresponding liquid phase compositions correlations. Based on the model fit analysis, incorporation of this parameter is not recommended.

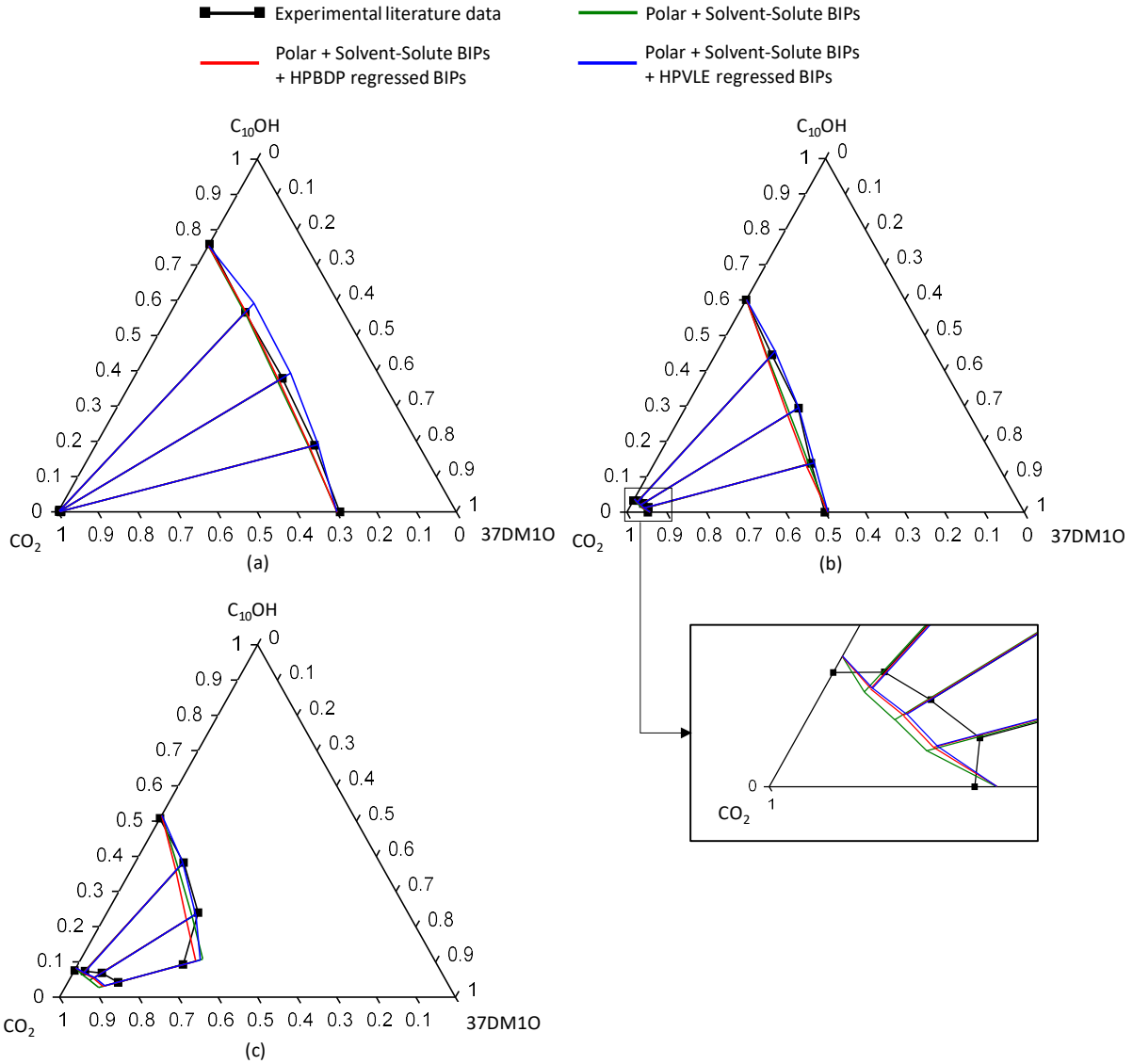

Figure 99: Gibbs phase diagram constructed at 348.2 K and (a) 10.4 MPa, (b) 15.7 MPa and (c) 18.2 MPa, comparing experimental literature data [5, 14] to RK-ASPEN correlations obtained when using incorporating different parameters.

Analysis of the effect of incorporating the solute-solute BIP regressed from HPVLE data reveals that at low pressures, inclusion of this parameter tends to decrease model accuracy. At slightly higher pressures, the incorporation of this BIP allows the model to better correlate the curvature of the liquid phase curve. This improvement is however accompanied by a decrease in the accuracy of the vapour phase composition correlations at 328 K. At the highest pressures, the incorporation of this BIP slightly improves the model fit at 348 K, but it significantly decreases the accuracy with which the model correlates liquid phase data in the low 1-decanol region at 328 K. Due to the fact that this parameter does not have a consistent positive impact on the model fit, the incorporation thereof is not recommended, as it will decrease model robustness with little/no gain in general accuracy.

Conclusion

The RK-ASPEN model, with the inclusion of polar parameters and solvent-solute BIPs, can correlate bubble- and dew-point data for the ternary system at temperatures above 328 K. The model accuracy within the high solute concentration region does however decrease if 1-decanol is present in significant amounts. Furthermore, the model cannot correlate the exact composition of co-existing equilibrium phases, but it can generate fairly accurate tie-line slopes. The incorporation of a solute-solute BIPs is not recommended, regardless of the type of data used to regress it.

8.1.3.3 CPA

High pressure bubble- and dew-point data

The accuracy with which the CPA model can correlate data for this system, at temperatures above 328 K (exclusion of low temperature discussed previously), is analysed in Figure 100. The inclusion of the solvent-solute BIPs is seen to improve the correlated phase behaviour trends. It also improves the model fit in the low- and high solute concentration regions. These improvements are however accompanied by a significant overprediction of the phase transition pressures within/or close to the mixture critical region. The inability of the model to correlate transition pressures within the mixture critical region has been discussed previously.

The addition of the solute-solute BIP regressed from HPBDP data generally reduces the degree of overprediction within/close to the mixture critical region. This improvement is however accompanied by a decrease in the accuracy with which the model correlates phase transition

pressures in the low- and high solute concentration regions at 328 K and 338 K. Incorporation of this solute-solute BIP therefore only consistently improves the model fit at 348 K. Analysis of the effect of including the solute-solute BIP regressed from HPVLE data reveals that it significantly decreases model fit and results in a general overestimation of the phase transition pressures. Seeing as the solute-solute BIP regressed from HPBDP data does not consistently improve model accuracy and the solute-solute BIP regressed from HPVLE decreases it, the incorporation of these parameters is not recommended.

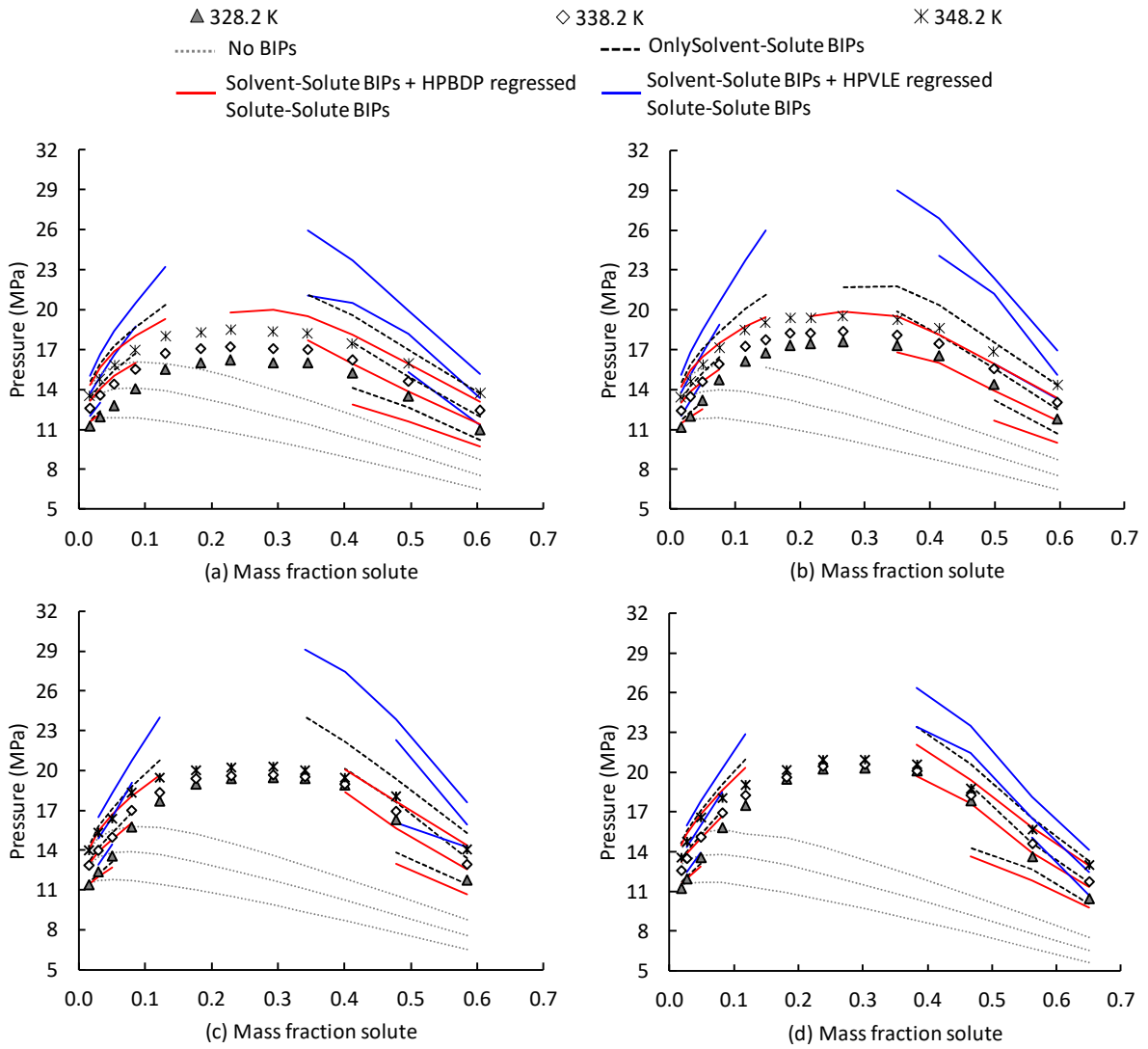

Figure 100: Pressure-composition diagrams comparing experimental data to data generated using the CPA model for (a) Mixture 4: 75 wt% 37DM1O + 25 wt% $C_{10}OH$, (b) Mixture 5: 50 wt% 37DM1O + 50 wt% $C_{10}OH$, (c) Mixture 6: 25 wt% 37DM1O + 75 wt% $C_{10}OH$ and (d) Mixture Z6: 12.5 wt% 37DM1O + 87.5 wt% $C_{10}OH$ [5] at temperatures above 328.2 K

High pressure vapour-liquid-equilibrium data

Figure 101 illustrates the accuracy with which the CPA model can generate VLE data for this system. The inclusion of the solvent-solute BIPs generally improves model accuracy, with the

only exception being the vapour phase correlations at the low temperatures. The poor performance at low temperatures has been addressed previously.

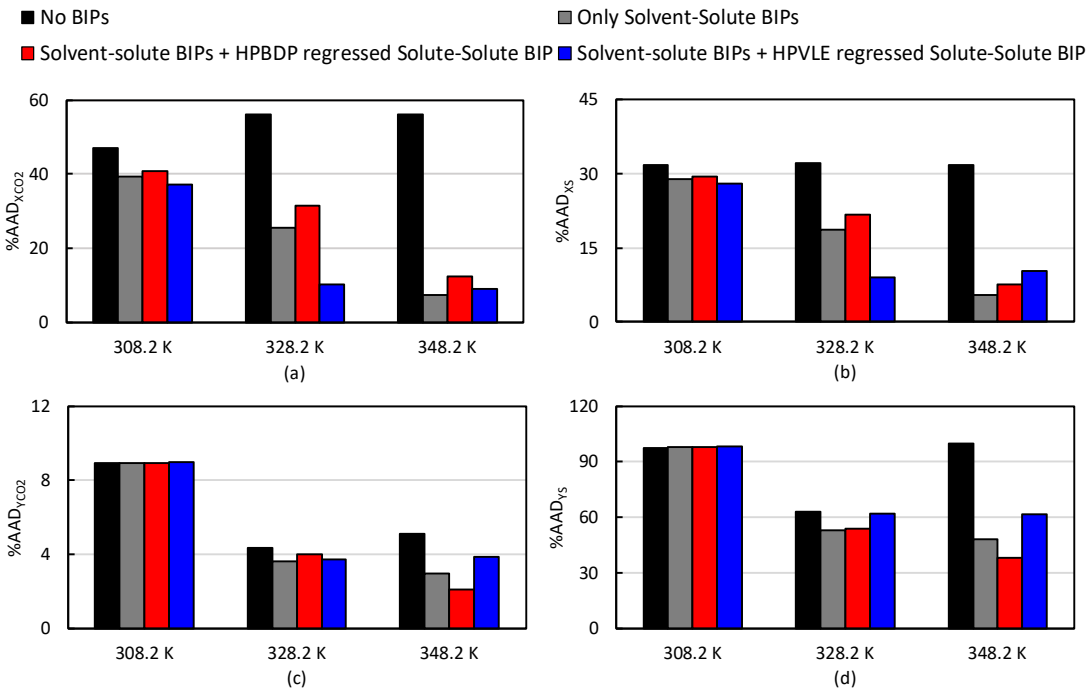

Figure 101: Evaluation of the accuracy with which the CPA model can correlate VLE data by comparing the %AAD values for the correlation of (a) liquid and (c) vapour phase CO_2 composition and (b) liquid and (d) vapour phase solute composition (average %AAD for $C_{10}OH$ and 37DM1O)

The addition of a solute-solute BIP generally reduces the model's ability to correlate VLE data for the system, regardless of the type of data used to regress it. To further analyse this the Gibbs phase diagrams, presented in Figures 102 and 103, were constructed. As seen previously, the CPA model is capable of generating fairly accurate tie-line slopes.

At the lowest pressures, the incorporation of the solute-solute BIP regressed from HPBDP data decreases the model fit. The inclusions the solute-solute BIP regressed from HPVLE data however improves the liquid phase curve correlated by the model. At slightly higher pressures, the incorporation of the solute-solute BIP regressed from HPBDP data is seen to decrease the model's ability to correlate liquid phase composition data, but it slightly improves the accuracy of the vapour phase correlations. The opposite holds true for the solute-solute BIP regressed from HPVLE data. At this pressure the inclusion of the solute-solute BIP regressed from HPVLE data also misrepresents the curvature of the vapour phase boundary. At the highest pressures the inclusion of a solute-solute BIP does not improve model accuracy, regardless of

the type of data used to regress it. Based on this, the inclusion of a solute-solute BIP is discouraged, regardless of the type of data used to regress it.

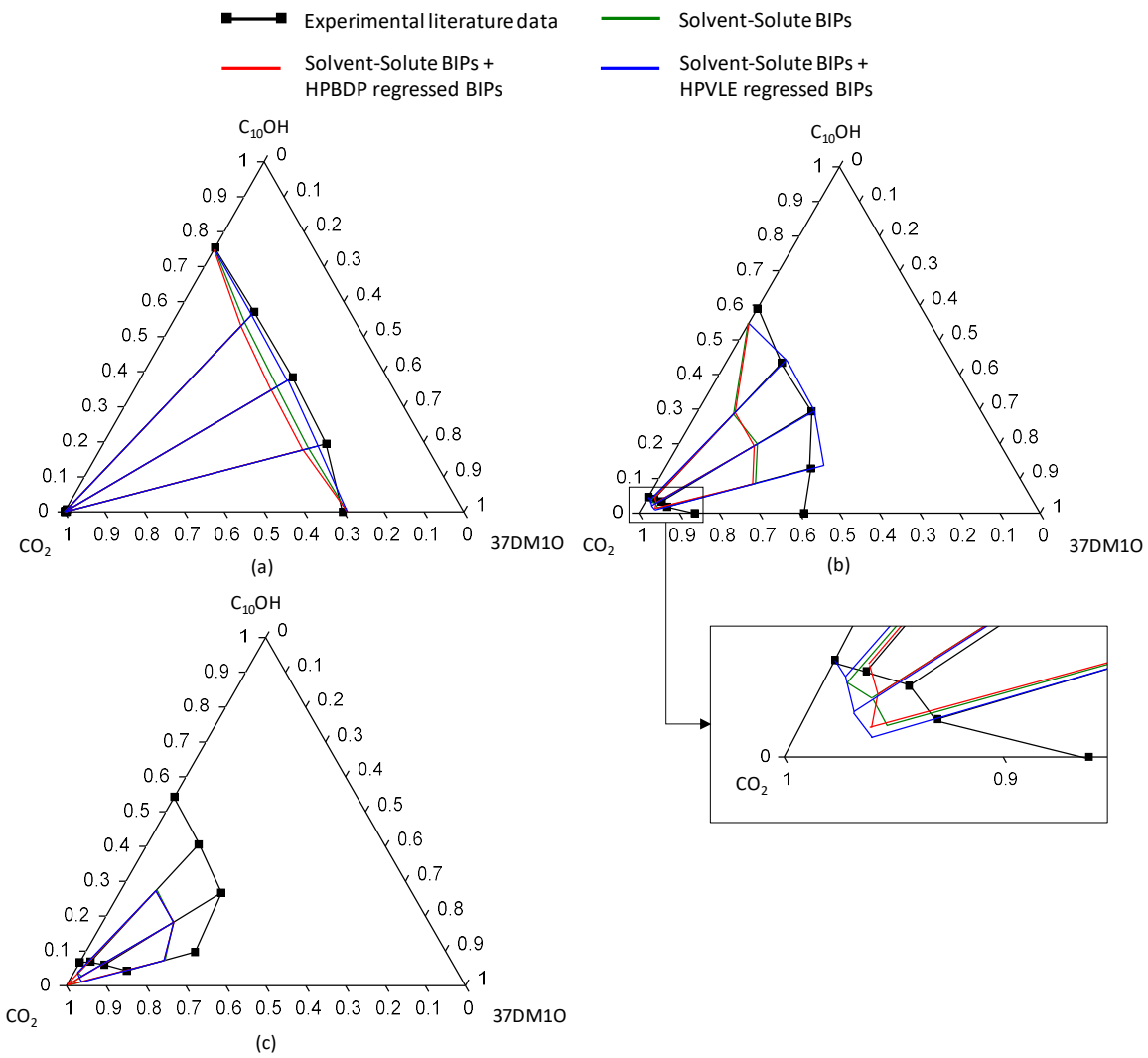

Figure 102: Gibbs phase diagram constructed at 328.2 K and (a) 8.3 MPa, (b)14.0 MPa and (c) 15.7 MPa, comparing experimental literature data [5, 14] to CPA correlations obtained when using incorporating different parameters

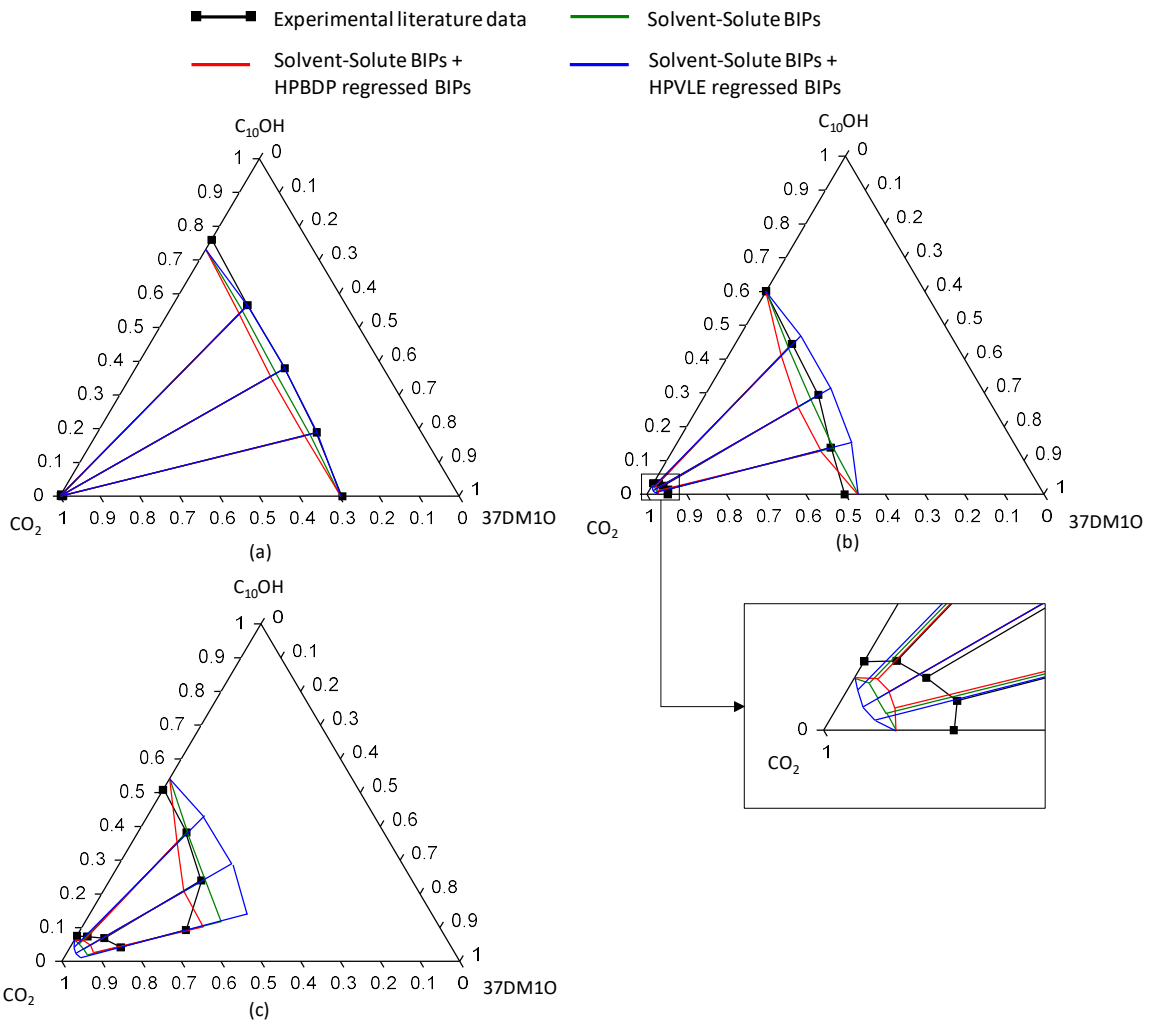

Figure 103: Gibbs phase diagram constructed at 348.2 K and (a) 10.4 MPa, (b) 15.7 MPa and (c) 18.2 MPa, comparing experimental literature data [5, 14] to CPA correlations obtained when using incorporating different parameters

Conclusion

Even with the inclusion of solvent-solute and solute-solute BIPs, the CPA model struggles to correlate accurate phase equilibrium data for this system. The incorporation of a solute-solute BIP is not recommended, regardless of the type of data used to regress it, as it tends to reduce model accuracy.

8.1.3.4 PSRK

High pressure bubble- and dew-point data

Table 39 illustrates the accuracy with which the PSRK model can predict bubble- and dew-point data for this system. It is noted that below 328 K, the %AAD values are large. The accuracy is seen to improve with an increase in temperature, but there still remains a noticeable

deviation between the experimental and predicted data. To investigate the deviations, the pressure-composition diagrams presented in Figure 104 were constructed.

Table 39: Analysis of the accuracy with which the PSRK model can predict phase transitions pressures between 308.2 K and 348.2 K

Mix no	Mixture solute composition	%AAD between experimental and PSRK predicted phase transition pressures				
		Temperature (K)				
		308.2	318.2	328.2	338.2	348.2
4	75 wt% 37DM1O + 25 wt% $C_{10}OH$	24.2	10.3	8.0	3.8	3.7
5	50 wt% 37DM1O + 50 wt% $C_{10}OH$	23.6	12.7	8.8	4.6	3.9
6	25 wt% 37DM1O + 75 wt% $C_{10}OH$	21.7	13.3	7.8	3.9	2.5
Z6	12.5 wt% 37DM1O + 66.7 wt% $C_{10}OH$	15.4	12.0	8.1	5.2	4.3

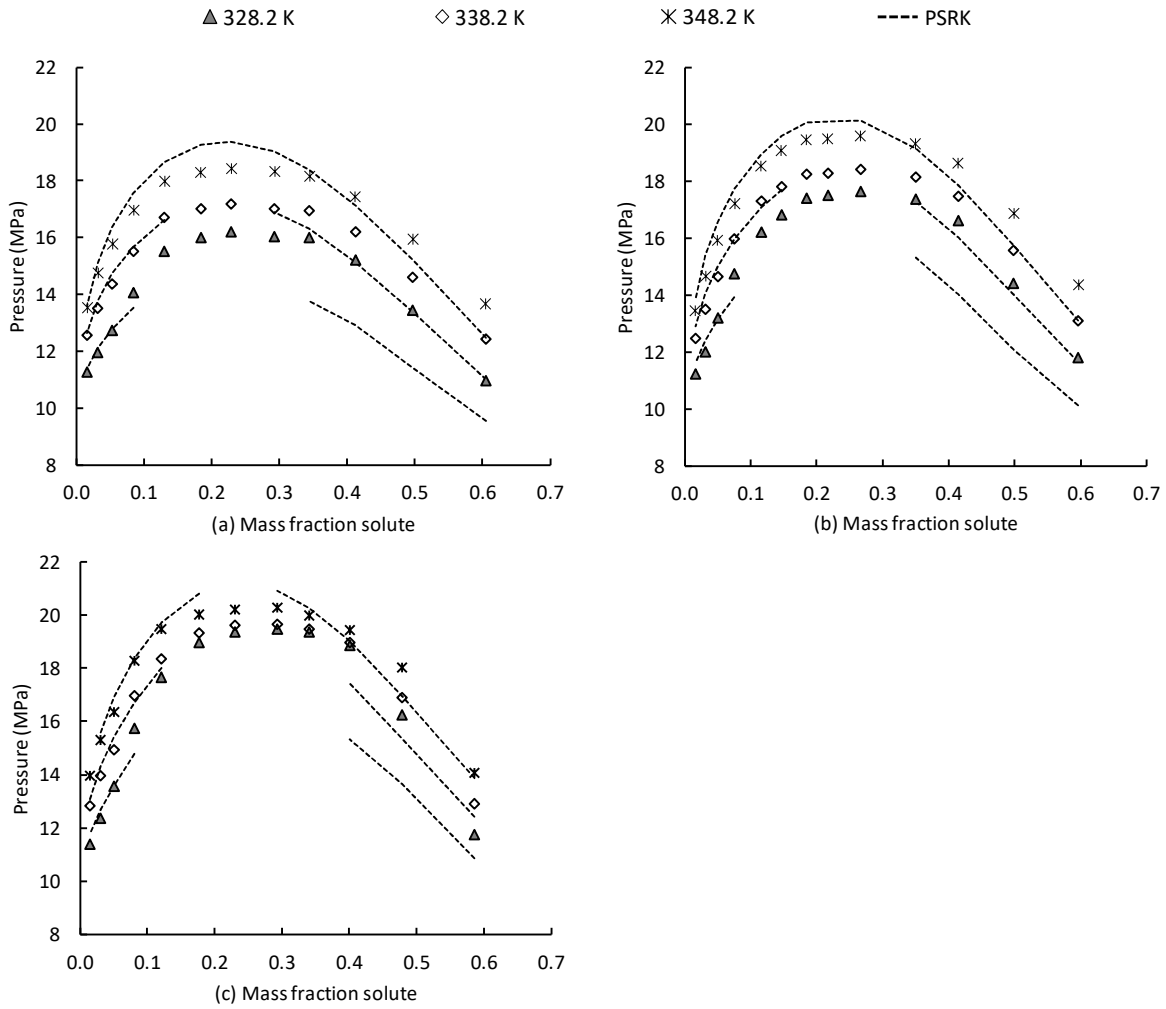

Figure 104: Pressure-composition diagrams comparing experimental data to predicted data generated using the PSRK model for (a) Mixture 4: 75 wt% 37DM1O + 25 wt% $C_{10}OH$, (b) Mixture 5: 50 wt% 37DM1O + 50 wt% $C_{10}OH$, (c) Mixture 6: 25 wt% 37DM1O + 75 wt% $C_{10}OH$ and (d) Mixture Z6: 12.5 wt% 37DM1O + 87.5 wt% $C_{10}OH$ [5] at temperatures above 328.2 K

The model generally predicts fairly accurate phase transition pressures within the low solute concentration region. The model however struggles to predict data within the mixture critical region and if the data can be predicted, the model generally overestimates the phase transition pressures. Significant deviation between the experimental and predicted data is also seen within the high solute concentration region. Within this region the model noticeably underestimates the phase transition pressures for all the mixtures. This indicates that the predictive model based on low pressure data cannot account for the strong solute-solute interactions which occur in these regions or the complex phase behaviour which occurs at high pressure.

High pressure vapour-liquid-equilibrium data

Results indicating the accuracy with which the model can predict VLE data for this system, is presented in Table 40. The %AAD values reported at 308 K are very large, due to reasons explained previously. Although the model accuracy is seen to increase with temperature, the %AAD values remain very large, particularly for the vapour phase solute composition, indicating that the model cannot predict accurate VLE data. This is deemed to be due to the fact that both solutes are polar and therefore significant interactions exist within the mixture at all temperatures.

Table 40: Analysis of the accuracy with which the PSRK model can predict VLE data the between 308.2 K and 348.2 K

Temperature (K)	%AAD			
	x_{CO2}	x_s^*	y_{CO2}	y_s^*
308.2	40.4	29.3	8.8	95.7
328.2	29.6	20.3	2.1	35.2
348.2	16.6	9.9	1.9	31.3

*Average %AAD of the 3,7-dimethyl-1-octanol and 1-decanol mass fractions in the phase

The model fit is analysed in Figures 105 and 106. From these diagrams it is seen that although the model can predict fairly accurate tie-line slopes, there is generally a significant deviation between the experimental and predicted data. At all the temperature-pressure combinations, the model is seen to underestimate the CO_2 content in the liquid phase. With the exception of the predictions at 328 K and 14 MPa the model also generally underestimates the CO_2 content in the vapour phase.

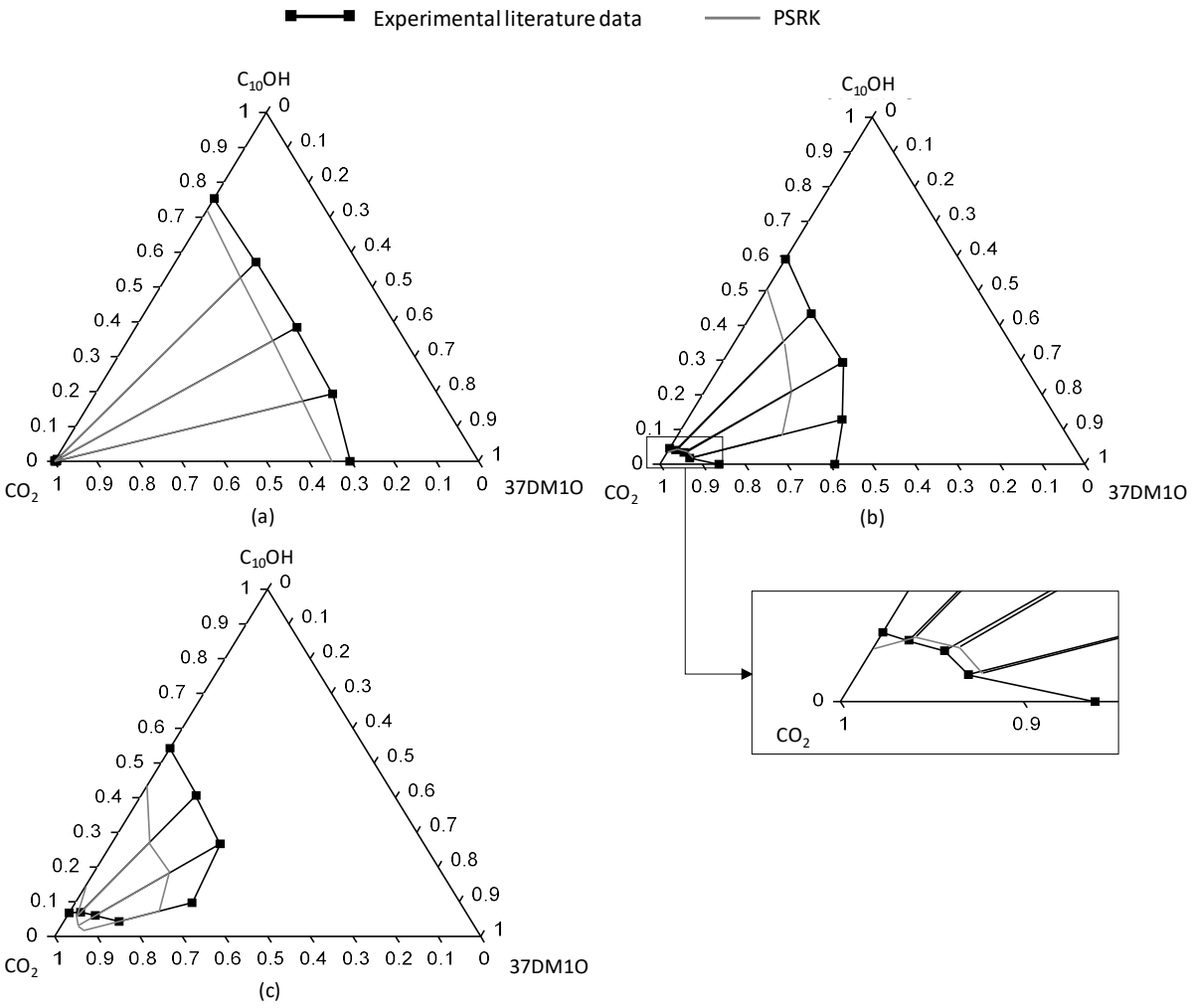

Figure 105: Gibbs phase diagram constructed at 328.2 K and (a) 8.3 MPa, (b)14.0 MPa and (c) 15.7 MPa, comparing experimental literature data [5, 14] to PSRK predictions

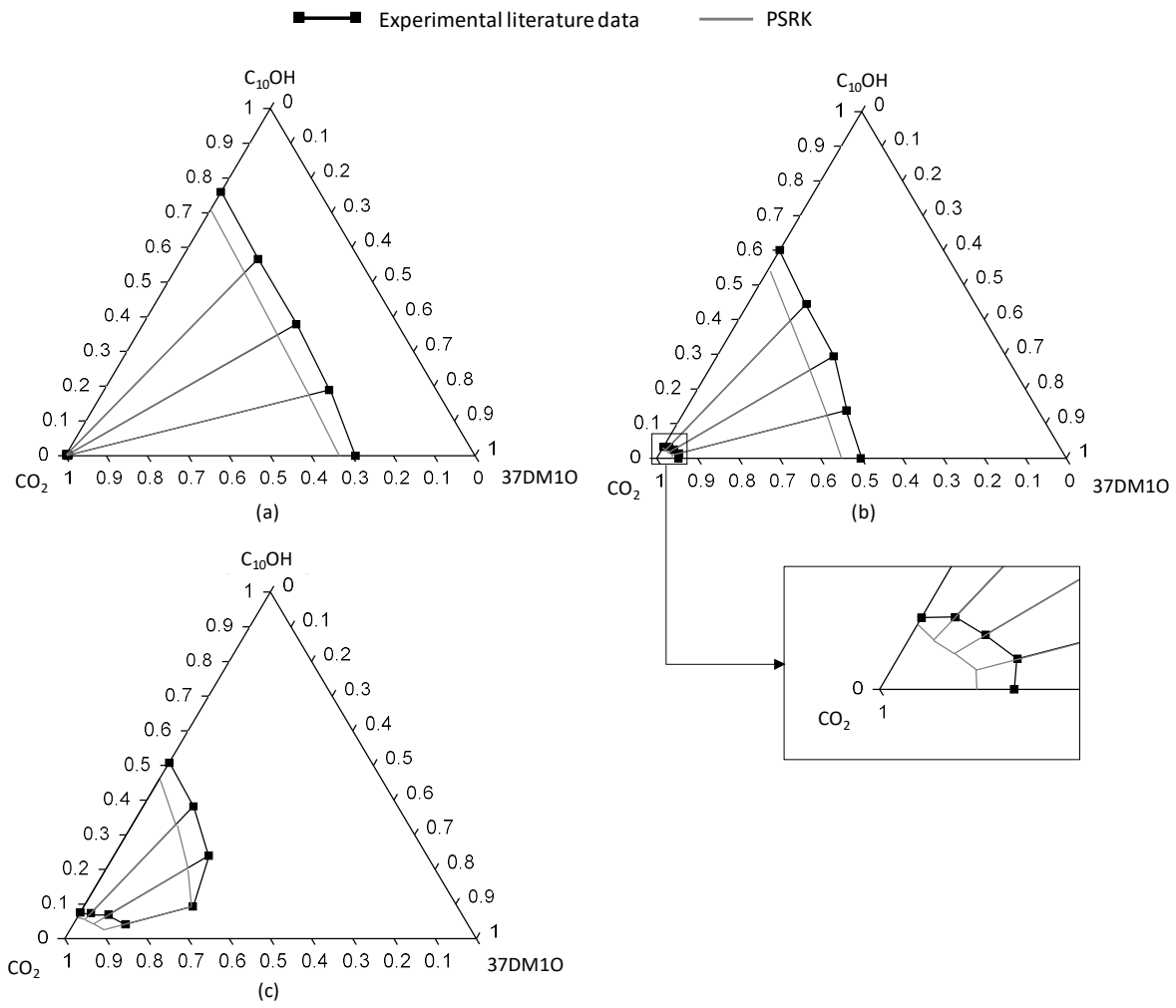

Figure 106: Gibbs phase diagram constructed at 348.2 K and (a) 10.4 MPa, (b) 15.7 MPa and (c) 18.2 MPa, comparing experimental literature data [5, 14] to PSRK predictions

Conclusion

It is clear that the PSRK model is struggles to predict phase equilibrium data for this system and the need for BIPs regressed from high pressure data to allow accurate predictions is evident.

8.1.3.5 Model comparison

The performance of the different models at temperatures above 328 K will be compared in this section. Only the optimum BIPs, as identified in the previous section, will be included in the models in this section. The fitted models used for the comparison are therefore as follows:

Bubble- and dew-point data:	Vapour-liquid-equilibrium data:
• RK-SOAVE + solvent-solute BIPs	• RK-SOAVE + solvent-solute BIPs
• RK-ASPEN + solvent-solute BIPs	• RK-ASPEN + solvent-solute BIPs

- CPA + solvent-solute BIPs
- PSRK

- CPA + solvent-solute BIPs
- PSRK

It is interesting to note that none of the models include a solute-solute BIP and this is because the incorporation of such a parameter was found to generally reduce model accuracy. The fact that an additional fitted parameter reduces accuracy is counter-intuitive. A possible explanation for this is that the incorporation of this parameter in fact overfits the model. The 1-decanol and 3,7-dimethyl-1-octanol compounds are both polar and therefore the interaction between them is less disruptive than the interaction with non-polar n-dodecane. The 3,7-dimethyl-1-octanol also does not enhance/impede the multimer formation of the 1-decanol molecules. Therefore, by adding a solute-solute BIP, the interaction between these components are exaggerated, resulting in decreased model accuracy.

High pressure bubble- and dew-point data

The accuracy with which the models can generate bubble- and dew-point data for this system is compared in Figure 107. It is clear that the correlations obtained from the RK-ASPEN model are generally more accurate than the correlations/predictions obtained from the other models. The RK-ASPEN model is also capable of generating phase transition pressures over a wider composition range. The correlations obtained from the RK-ASPEN model within the low solute concentration region also generally outperforms the other models. Based on these facts, it is concluded that the RK-ASPEN model is the best/only model that can be implemented to correlate fairly accurate bubble- and dew-point data for this system. When only considering the lower solute concentration regions ($x_s < 0.2$), the PSRK model is the second-best model. The model however fails within the higher solute concentration region. In this region the PSRK model is the least accurate model, as it significantly underestimates the phase transition pressures, highlighting the inability of the model to account for the interactions and the need for BIPs regressed from high pressure data.

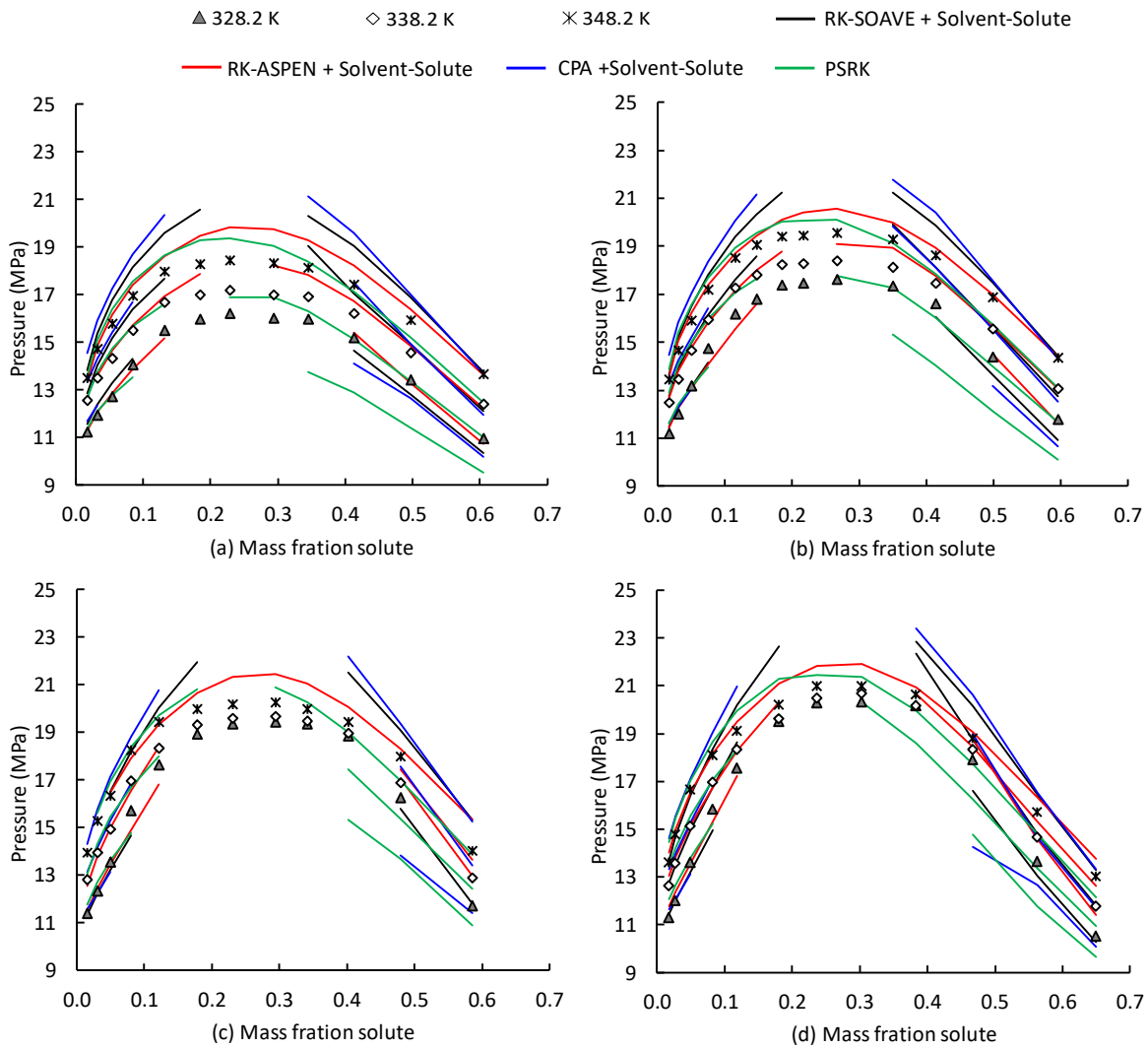

Figure 107: Pressure-composition diagrams comparing experimental data to predicted data for (a) Mixture 4: 75 wt% 37DM1O + 25 wt% $C_{10}OH$, (b) Mixture 5: 50 wt% 37DM1O + 50 wt% $C_{10}OH$, (c) Mixture 6: 25 wt% 37DM1O + 75 wt% $C_{10}OH$ and (d) Mixture Z6: 12.5 wt% 37DM1O + 87.5 wt% $C_{10}OH$ [5]

High pressure vapour-liquid-equilibrium data

The accuracy with which the models correlate/predict VLE data for this system is compared in Figures 108 and 109.

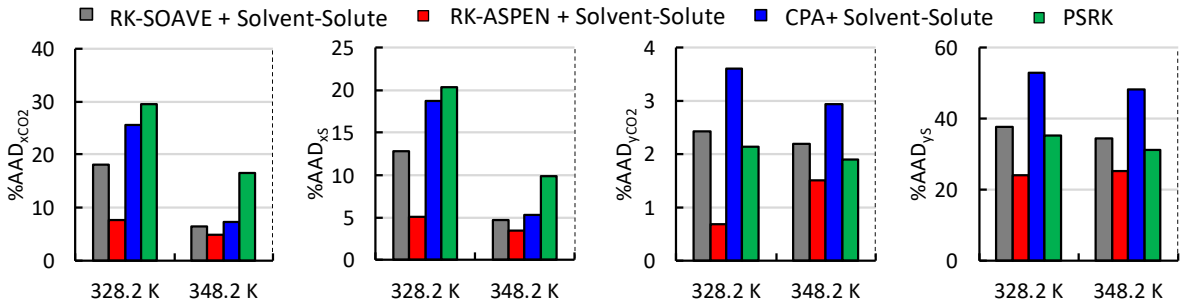

Figure 108: Comparison of the accuracy with which the four models can correlate/predict the liquid and vapour phase CO_2 composition as well as the liquid and vapour phase solute composition (average %AAD for $C_{10}OH$ and 37DM1O)

The RK-ASPEN model has the lowest %AAD values for the vapour and liquid compositions correlations/predictions, indicating that it is the most accurate model. Furthermore, the model fit obtained from the RK-ASPEN model is generally more accurate than the fit obtained by the other models. There is still however deviation between the measured and modelled data, indicating that the model cannot correlate the exact composition of co-existing equilibrium phases and can only approximate it.

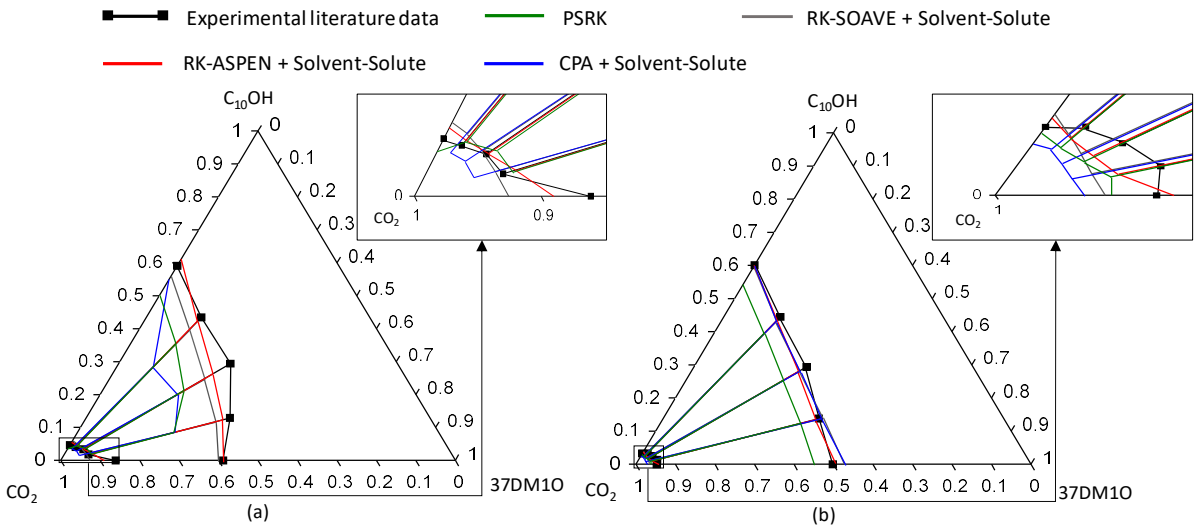

Figure 109: Gibbs phase diagram constructed at (a) 328.2 K and 14 MPa and (b) 348.2 K and 15.7 MPa comparing experimental literature data [5, 14] to modelled data

8.1.3.6 Section outcomes

The main outcomes of this section are:

- The modelling results indicated that the RK-ASPEN can correlate fairly accurate bubble- and dew-point data for the system above 328 K, but the accuracy of the correlations decreased with an increase in 1-decanol. The other models were however found to struggle to generate accurate bubble- and dew-point data for this system.
- None of the models were capable of correlating the exact composition of the co-existing equilibrium phases and could only generate accurate tie-line slopes.
- The incorporation of the 1-decanol + 3,7-dimethyl-1-octanol solute-solute BIP was cautioned/discouraged for all the models, regardless of the type of data used to regress it. It is postulated that the inclusion of the solute-solute BIP exaggerates the interaction between the two polar components, thereby decreasing model accuracy.
- The RK-ASPEN model including only the fitted solvent-solute BIPs was found to the best suited model to generate equilibrium data for this system.

8.2 Modelling quaternary phase equilibrium data

The ability of the RK-SOAVE, RK-ASPEN, CPA and PSRK models to predict equilibrium data for quaternary system is evaluated and compared in this section. The equilibrium data measured in this work, along with bubble- and dew-point data obtained from literature (Mixture Z7) [5], were used to evaluate the predictive capability of the models. Similar to the previous section, the bubble- and dew-point data were predicted using a flash drum and the VLE data were predicted using the built-in evaluation function in Aspen Plus®. The accuracy of the models were evaluated and compared by performing %AAD analyses as well as constructing and analysing pressure-composition diagrams for the bubble- and dew-point data and parity plots for the VLE data.

8.2.1 RK-SOAVE

The quaternary equilibrium data is predicted using the RK-SOAVE model which incorporates all the regressed solvent-solute BIPs and the n-dodecane + 1-decanol and n-dodecane + 3,7-dimethyl-1-octanol solute-solute BIPs, regressed from HPBDP and HPVLE data. The 1-decanol + 3,7-dimethyl-1-octanol solute-solute BIP was not included in the model, regardless of the type of data used to regress it. This is due to the fact that the ternary correlations cautioned the use of this parameter and investigation into the effect of including it when predicting quaternary data (presented in Appendix G.1) also showed that it either does not significantly improve model accuracy or decreases it.

High pressure bubble- and dew-point data

The ability of the RK-SOAVE model to predict bubble- and dew-point data for the quaternary mixtures is illustrated in Figure 110. The RK-SOAVE model is well suited to predict bubble- and dew-point data for the n-dodecane rich mixture. The model can also generally predict fairly accurate phase transition pressures within the low solute concentration region. The model accuracy is however seen to decrease when predicting data within the mixture critical and high solute concentration region for the mixtures containing larger quantities of 1-decanol. This indicates that the model cannot quantitatively account for the interactions which exist in these mixtures, which is to be expected as the model is best suited for non-polar, to slightly polar systems [16]. The inability of the model to predict data within the mixture critical region and temperatures below 328 K has been discussed previously.

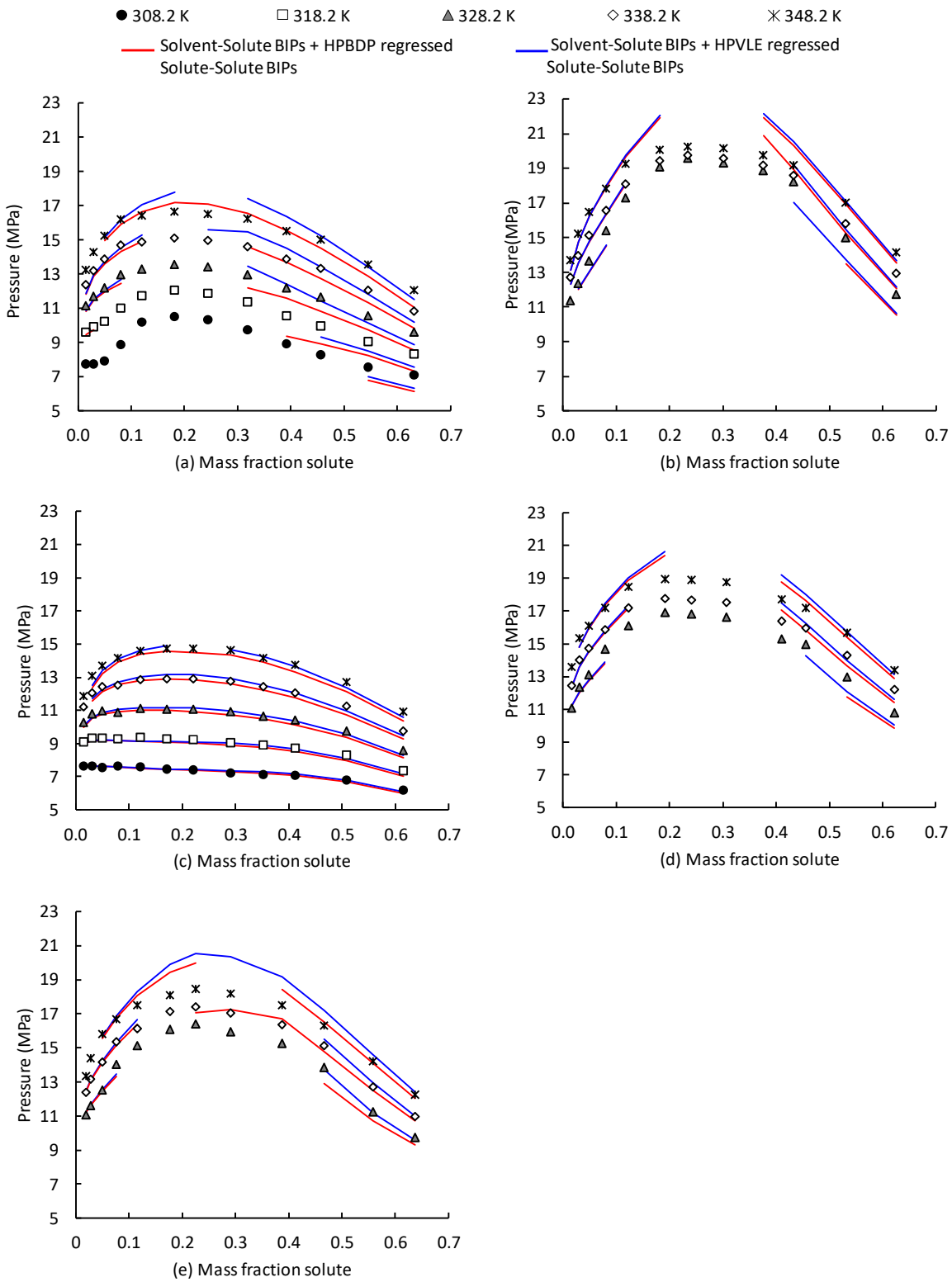

Figure 110: Comparison of experimental data and RK-SOAVE predicted data for (a) Mixture 7: 33.3 wt% nC_{12} +33.3 wt% 37DM1O +33.3 wt% $C_{10}OH$, (b) Mixture 8: 5 wt% nC_{12}+ 10 wt% 37DM1O + 85 wt% $C_{10}OH$, (c) Mixture 9: 84.2 wt% nC_{12}+ 10.5 wt% 37DM1O + 5.3 wt% $C_{10}OH$, (d) Mixture 10: 10.1 wt% nC_{12}+ 30 wt% 37DM1O + 59.9 wt% $C_{10}OH$ and (e) Mixture Z7: 20 wt% nC_{12}+ 10 wt% 37DM1O + 70 wt% $C_{10}OH$ [5]

There is generally little difference between the predictions obtained when using the solute-solute BIPs regressed from different types of data. Two exceptions are the mixture critical and

high solute concentration regions for Mixtures 7 and Z7. In the high solute concentration region, predictions obtained using the solute-solute BIP regressed from HPVLE data are more accurate for Mixture 7, whilst the opposite holds true for Mixture Z7 (except at 328 K). Within/closer to the mixture critical region, the model which incorporates the solute-solute BIP regressed from HPVLE data however tends to overestimate the phase transition pressures of both mixtures to a greater extent than the model which incorporates the BIP regressed from HPBDP data. The BIP regressed from HPVLE data only shows constant superiority in fit at 328 K. Considering the lower general accuracy and smaller range of the data points predicted at 328 K, the solute-solute BIP regressed from HPBDP data is deemed to be better suited to predict phase transition pressures for this system.

High pressure vapour-liquid-equilibrium data

The accuracy with which the RK-SOAVE model can predict the VLE data for the quaternary system, is analysed in Table 41. It is clear that the model cannot predict VLE data at 308 K, due to reasons discussed previously, and therefore this temperature is excluded from the average %AAD values ($\overline{\%AAD}$).

Table 41: Accuracy with which the RK-SOAVE model can predict VLE data for the quaternary system when including solute-solute BIPs regressed from different data types

Temperature (K)	Absolute Average Deviation (%AAD)							
	RK-SOAVE with solvent-solute and solute-solute BIPs regressed from HBDPD data – without 37DM1O + 1-decanol BIP				RK-SOAVE with solvent-solute and solute-solute BIPs regressed from HPVLE data – without 37DM1O + 1-decanol BIP			
	x_{CO2}	x_s[2]	y_{CO2}	y_s[2]	x_{CO2}	x_s[2]	y_{CO2}	y_s[2]
308.6	31.8	28.2	14.2	93.5	30.4	27.2	14.2	94.1
328.8	13.0	10.1	1.2	31.4	11.1	9.0	2.1	40.0
348.9	5.1	4.4	1.0	21.3	3.3	3.5	1.1	24.6
$\overline{\%AAD}$[1] $_{@328K, 348 K}$	10.9				11.8			

[1]Total average %AAD values excludes data 308 K due to high inaccuracy

[2] Average %AAD of the n-dodecane, 3,7-dimethyl-1-octanol and 1-decanol mass fractions in the phase

At 328 K and 348 K, the liquid phase compositions obtained when incorporating the solute-solute BIP regressed from HPVLE data are more accurate, whilst the vapour phase compositions predicted using the solute-solute BIP regressed from HPBDP data are more accurate. Furthermore, the average %AAD values indicate that although there is generally little difference in accuracy when incorporating the different solute-solute BIPs, the model which is incorporates the solute-solute BIP regressed from HPBDP data has a slightly lower %AAD value. Based on this and the fact that this model provides the most accurate vapour phase

predictions, the model which incorporates the solute-solute BIP regressed from HPBDP is deemed to be better suited to predict VLE data for the quaternary system.

Due to the difficulties plotting quaternary phase equilibrium data, the model fit at 328 K and 348 K was analysed using the parity plots presented in Figures 111 and 112. Linear trendlines were fitted to the different data sets. The model goodness-of-fit was evaluated by comparing the fitted trendline to the 1:1 line (y = x) and the coefficient of determination (R^2) was used to determine how well the linear trendline fits the data [131, 132, 133].

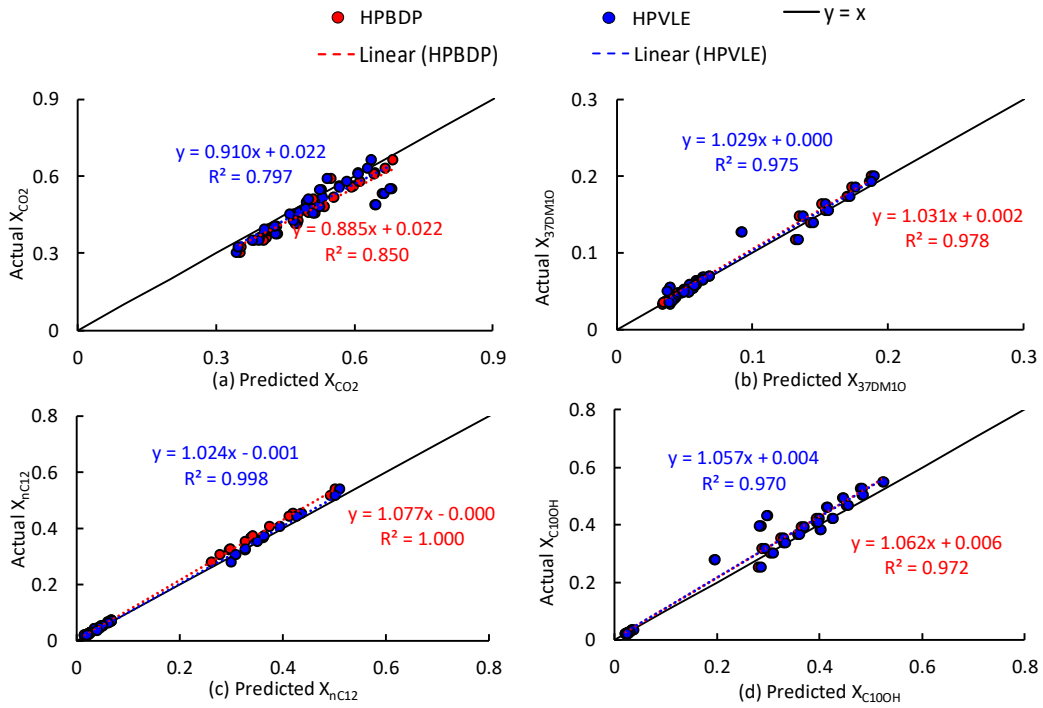

Figure 111: Parity plots for the liquid phase CO_2, 3,7-dimethyl-1-octanol, n-dodecane and 1-decanol mass fractions at 328 K and 348 K

The liquid phase composition predictions are more accurate than the vapour phase composition predictions, as the trendlines for the liquid phase predictions correspond much better to the 1:1 line. Furthermore, there is generally little difference between the trendlines fitted to the data obtained using different data types. For the vapour phase solute composition predictions, there is generally a significant deviation between the 1:1 line and the trendlines fitted to the model predictions, illustrating deviation between the experimental and predicted data. Furthermore, it is noted that when using the solute-solute BIP regressed from HPVLE data the predicted data shows some significant outliers (reflected by the lower R^2 values), which explains the weaker performance of this model compared to the model which incorporates the solute-solute BIP regressed from HPBDP data.

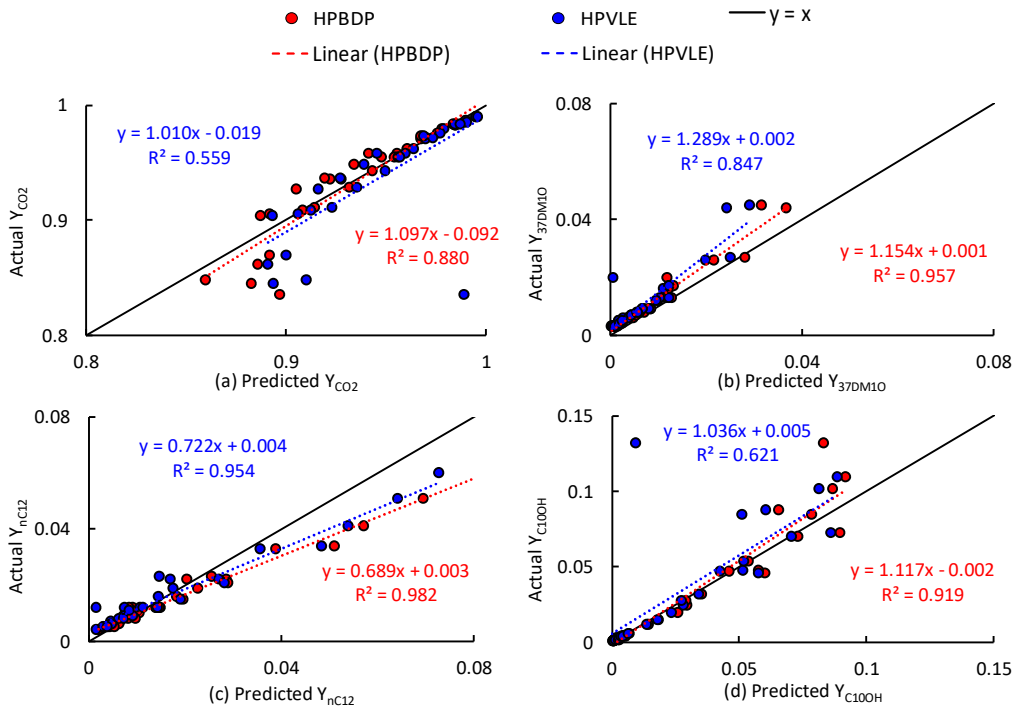

Figure 112: Parity plots for the vapour phase CO_2, 3,7-dimethyl-1-octanol, n-dodecane and 1-decanol mass fractions at 328 K and 348 K

Conclusion

The fitted RK-SOAVE model can predict fairly accurate bubble- and dew-point data for n-dodecane rich mixtures, but the model accuracy in the mixture critical and high solute concentration region decreases for mixtures containing larger quantities of 1-decanol. Furthermore, the model cannot predict the exact composition of co-existing equilibrium phases. The model which incorporates the HPBDP regressed BIP was found to be better suited to predict phase equilibrium data for this system.

8.2.2 RK-ASPEN

The RK-ASPEN model which incorporates all the regressed solvent-solute BIPs and the n-dodecane + 1-decanol and n-dodecane + 3,7-dimethyl-1-octanol solute-solute BIPs is used to predict the quaternary data. Similar to the RK-SOAVE model, the 1-decanol + 3,7-dimethyl-1-octanol solute-solute BIP is excluded from the model (details and proof for the exclusion of this parameter is provided in Appendix G.2.).

High pressure bubble- and dew-point data

Figure 113 illustrates the accuracy with which the RK-ASPEN model can predict bubble- and dew-point data for the quaternary system.

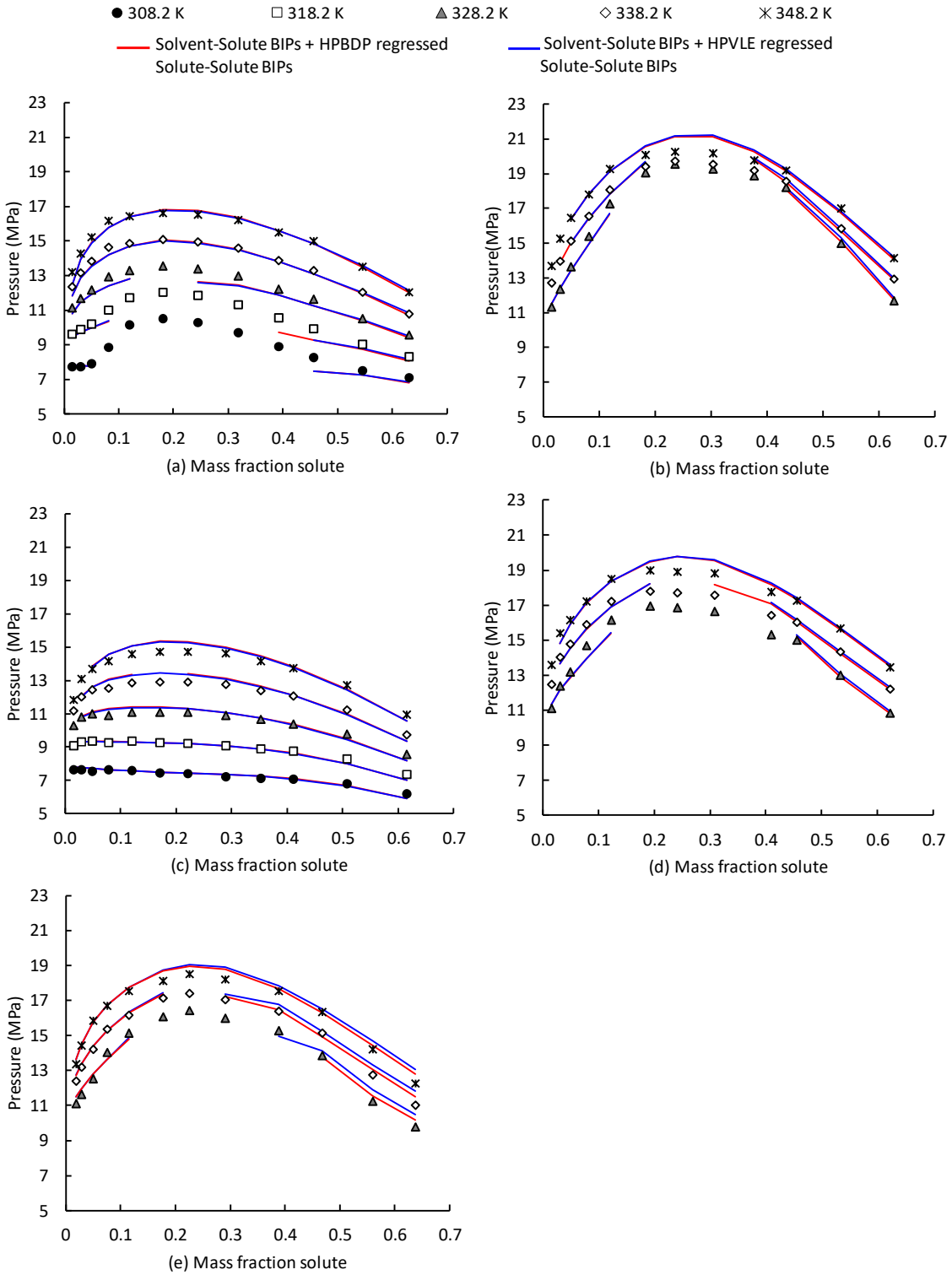

Figure 113: Comparison of experimental data and RK-ASPEN predicted data for (a) Mixture 7: 33.3 wt% nC_{12} +33.3 wt% 37DM1O +33.3 wt% $C_{10}OH$, (b) Mixture 8: 5 wt% nC_{12}+ 10 wt% 37DM1O + 85 wt% $C_{10}OH$, (c) Mixture 9: 84.2 wt% nC_{12}+ 10.5 wt% 37DM1O + 5.3 wt% $C_{10}OH$, (d) Mixture 10: 10.1 wt% nC_{12}+ 30 wt% 37DM1O + 59.9 wt% $C_{10}OH$ and (e) Mixture Z7: 20 wt% nC_{12}+ 10 wt% 37DM1O + 70 wt% $C_{10}OH$ [5]

It is seen that the RK-ASPEN model predicts fairly accurate phase transition pressures for all the mixtures. Furthermore, there is generally little difference between the predictions obtained when using the solute-solute BIPs regressed from HPBDP and HPVLE data. The only noticeable deviation is seen in the high solute concentration region for Mixture Z7, where the model which incorporates the solute-solute BIP regressed from HPBDP data is slightly more accurate. The inability of the model to predict data within the mixture critical region and temperatures below 328 K has been discussed previously.

High pressure vapour-liquid-equilibrium data

The accuracy with which the RK-ASPEN model can predict the VLE data for the quaternary system is analysed in Table 42. From the average %AAD ($\overline{\%AAD}$) values it is seen that there is little difference in the accuracy attained when using the different solute-solute BIPs, but the model incorporating the solute-solute BIP regressed from HPVLE data is slightly more accurate. Closer analysis of the data however reveals that, with the exception of the vapour phase predictions at 348 K, the model which incorporates the solute-solute BIP regressed from HPBDP data is generally more accurate.

Table 42: Accuracy with which the RK-ASPEN model can predict VLE data for the quaternary system when including solute-solute BIPs regressed from different data types.

Temperature (K)	Absolute Average Deviation (%AAD)							
	RK-ASPEN with solvent-solute and solute-solute BIPs regressed from HBDPD data – without 37DM1O + 1-decanol BIP				RK-ASPEN with solvent-solute and solute-solute BIPs regressed from HPVLE data – without 37DM1O + 1-decanol BIP			
	x_{CO2}	x_s[2]	y_{CO2}	y_s[2]	x_{CO2}	x_s[2]	y_{CO2}	y_s[2]
308.6	31.7	28.0	11.5	68.8	31.9	28.2	11.9	77.0
328.8	4.4	4.5	1.1	31.3	8.1	6.9	1.2	32.1
348.9	2.7	2.7	0.6	14.8	3.3	3.0	0.5	12.8
$\overline{\%AAD}$[1]$_{@328K, 348 K}$	7.8				7.3			

[1]Total average %AAD values excludes data 308 K due to high inaccuracy

[2] Average %AAD of the n-dodecane, 3,7-dimethyl-1-octanol and 1-decanol mass fractions in the phase

The model fit is analysed in Figures 114 and 115. From these figures it is seen that the trendlines fitted to the liquid composition data generally better corresponds to the 1:1 line than the trendlines fitted to the vapour phase composition data, indicating that the liquid phase predictions are more accurate.

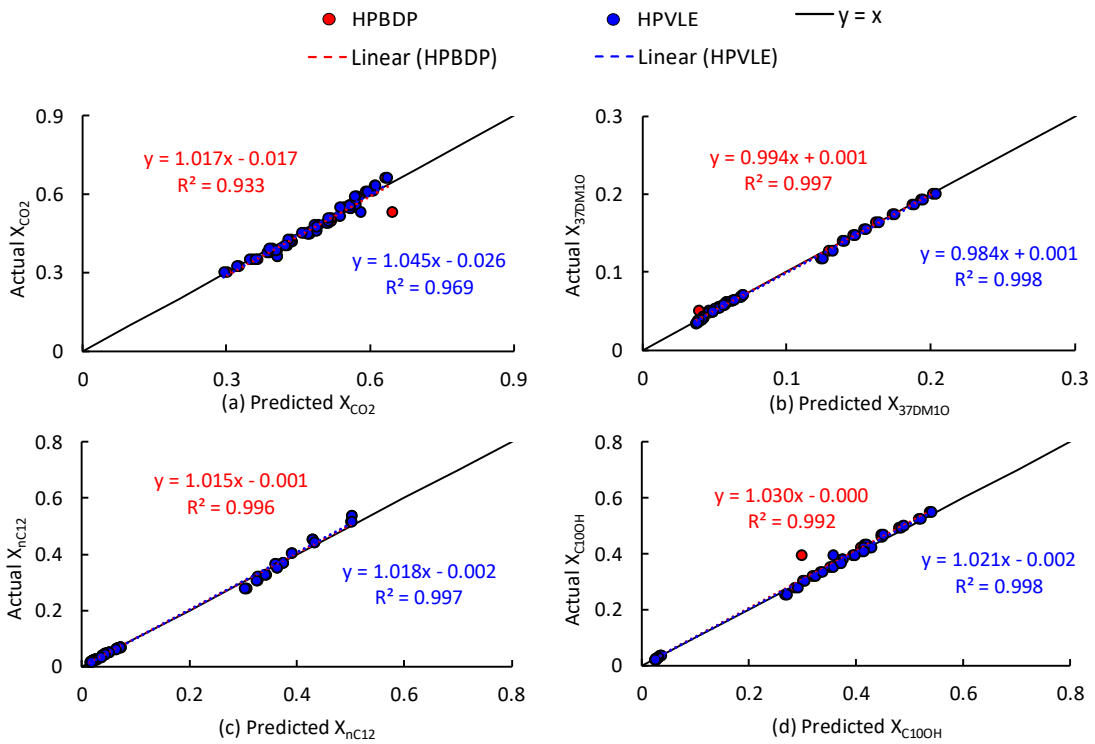

Figure 114: Parity plots for the liquid phase CO_2, 3,7-dimethyl-1-octanol, n-dodecane and 1-decanol mass fractions at 328 K and 348 K.

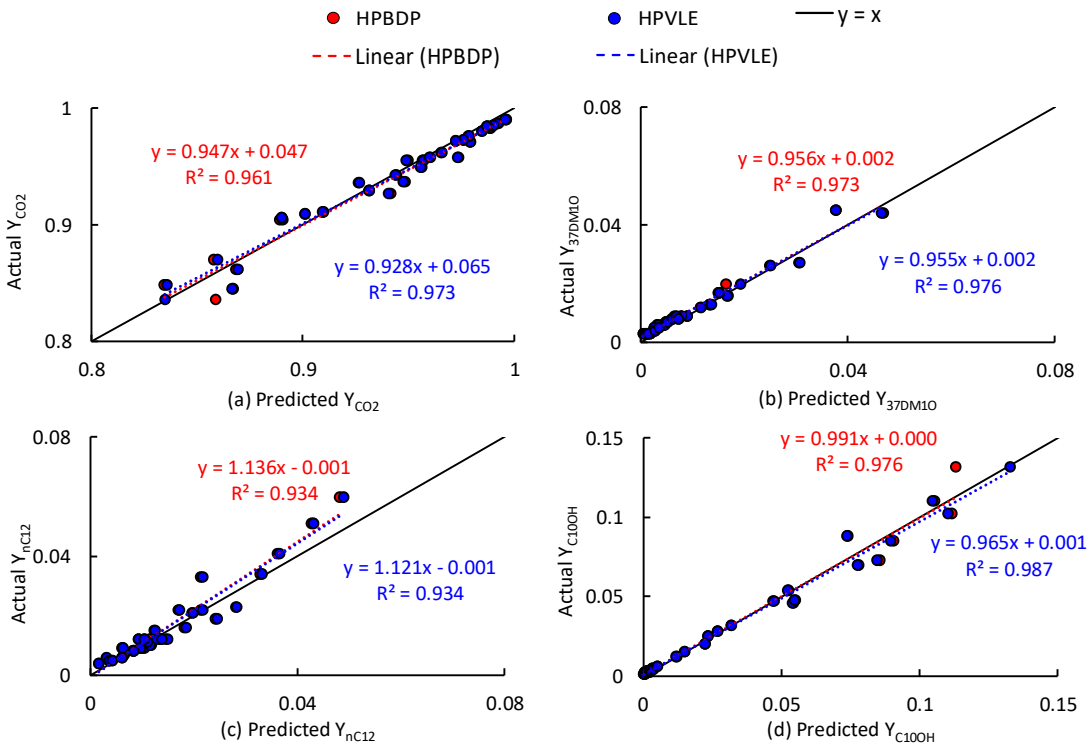

Figure 115: Parity plots for the vapour phase CO_2, 3,7-dimethyl-1-octanol, n-dodecane and 1-decanol mass fractions at 328 K and 348 K.

Comparison of the trendlines fitted to the data obtained when using the different solute-solute BIPs reveal that there is generally little difference between the fitted trendlines. The model

which incorporates the solute-solute BIPs regressed from HPBDP data does however have a few outliers, which explains the slight decrease in accuracy compared to the model which incorporates the solute-solute BIP regressed from HPVLE data, detected in the %AAD analysis. With the exception of the vapour phase n-dodecane composition predictions, the trendline slope and intercept values for the data predicted by the model which incorporates the solute-solute BIP regressed from HPBDP data better corresponds to the 1:1 line than the model which incorporates the solute-solute BIP regressed from HPVLE data. Indicating that even with the outliers (decreases R^2), where the model presumably fails, the model which incorporates the solute-solute BIP regressed from HPBDP data is generally more accurate.

Conclusion

The fitted RK-ASPEN model can predict fairly accurate bubble- and dew-point data at temperatures above 328 K and it can approximate the composition of co-existing equilibrium phases. Furthermore, the HPBDP regressed solute-solute BIP was found to be better suited to predict phase equilibrium data for the system.

8.2.3 CPA

The quaternary equilibrium data is modelled using the CPA model incorporating all the solvent-solute BIPs and only the n-dodecane + 3,7-dimethyl-1-octanol solute-solute BIP. The n-dodecane + 1-decanol and 1-decanol + 3,7-dimethyl-1-octanol solute-solute BIPs were not included, regardless of the type of data used to regress it (details and proof for the exclusion of these parameters is provided in Appendix G.3.).

High pressure bubble- and dew-point data

Figure 116 illustrates the ability of the fitted CPA model to predict bubble- and dew-point data for the quaternary system. It is clear that the CPA model can predict fairly accurate phase transition pressures for the mixture consisting largely of n-dodecane. The model is also seen to predict fairly accurate data within the low solute concentration region, regardless of the solute mixture composition. The phase diagrams for the mixtures consisting of significant 1-decanol fractions shows decreased model accuracy when compared to the n-dodecane rich mixture predictions. The model is seen to particularly struggle to predict accurate phase transition pressures within/close to the mixture critical these mixtures. The inability of the model to

predict data within the mixture critical region and temperatures below 328 K has been discussed in section 8.1.

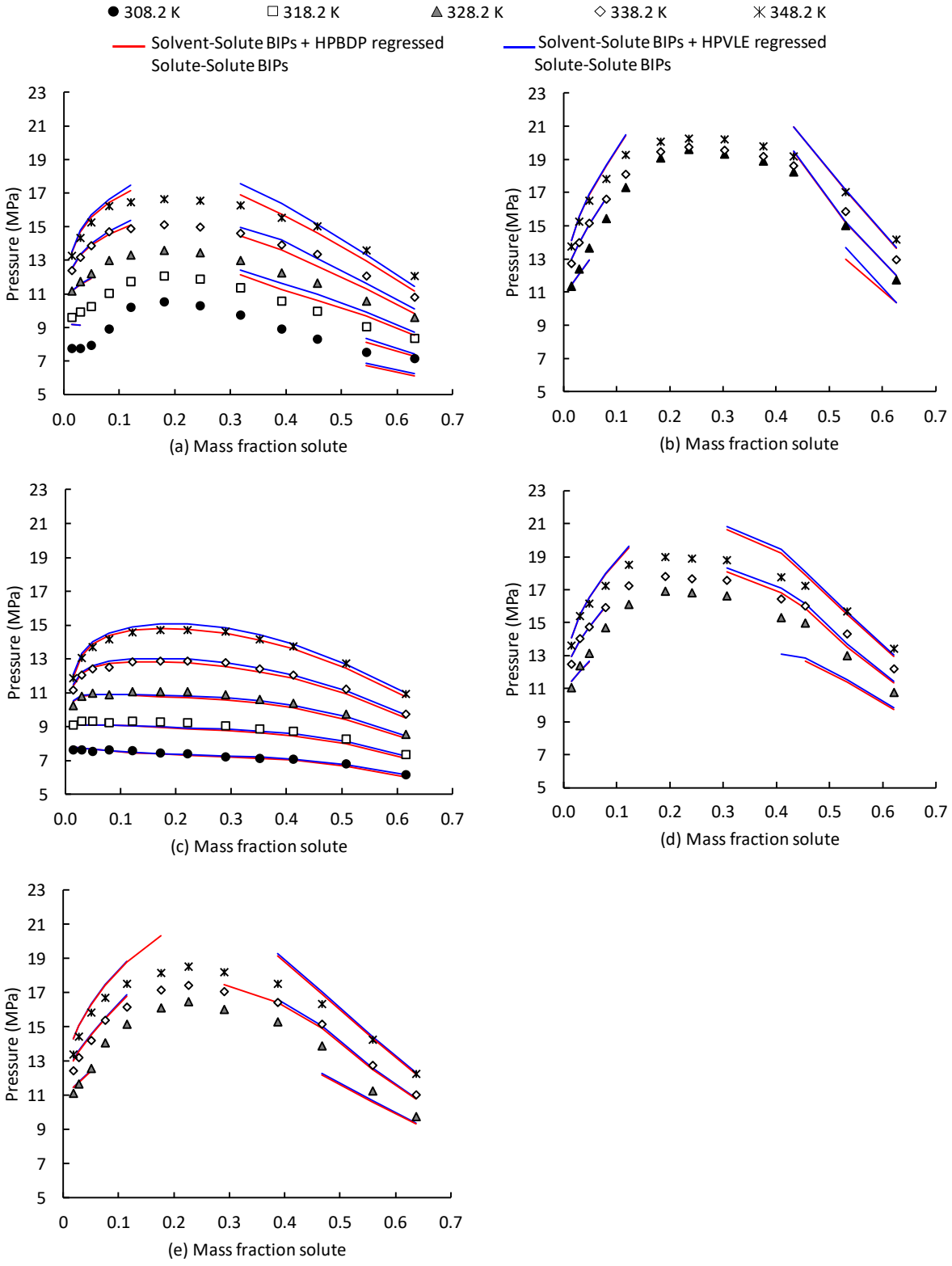

Figure 116: Comparison of experimental data and CPA predicted data for (a) Mixture 7: 33.3 wt% nC_{12} +33.3 wt% 37DM1O +33.3 wt% $C_{10}OH$, (b) Mixture 8: 5 wt% nC_{12}+ 10 wt% 37DM1O + 85 wt% $C_{10}OH$, (c) Mixture 9: 84.2 wt% nC_{12}+ 10.5 wt% 37DM1O + 5.3 wt% $C_{10}OH$, (d) Mixture 10: 10.1 wt% nC_{12}+ 30 wt% 37DM1O + 59.9 wt% $C_{10}OH$ and (e) Mixture Z7: 20 wt% nC_{12}+ 10 wt% 37DM1O + 70 wt% $C_{10}OH$ [5]

With the exception of Mixture 7, there is generally little difference between the phase transition pressures predicted when using the solute-solute BIPs regressed from HPBDP and HPVLE data. For Mixture 7, the predictions obtained when using the different solute-solute BIP deviates from one another in the higher solute concentration region. In this region the model which incorporates the solute-solute BIP regressed from HPVLE data is generally slightly more accurate.

High pressure vapour-liquid-equilibrium data

Table 43 indicates the accuracy with which the CPA model can predict quaternary VLE data for this system. According to the average %AAD values, there is little difference in the overall accuracy attained when using the different solute-solute BIPs, but the predictions obtained using the solute-solute BIP regressed from HPBDP data is slightly more accurate. Closer analysis of the %AAD values reported for each mass fraction reveals that, with the exception of the liquid phase composition data at 328 K, the model which incorporates the solute-solute BIP regressed from HPBDP data is more accurate than the model incorporating the solute-solute BIP regressed from HPVLE data.

Table 43: Accuracy with which the CPA model can predict VLE data for the quaternary system when including solute-solute BIPs regressed from different data types.

Temperature (K)	Absolute Average Deviation (%AAD)							
	CPA with solvent-solute and nC_{12} + 37DM1O solute-solute BIPs regressed from HBDPD data				CPA with solvent-solute and nC_{12} + 37DM1O solute-solute BIPs regressed from HBVLE data			
	x_{CO2}	x_s[2]	y_{CO2}	y_s[2]	x_{CO2}	x_s[2]	y_{CO2}	y_s[2]
308.6	32.2	28.8	14.5	96.9	30.9	27.5	14.5	97.0
328.8	18.7	15.3	3.4	55.8	16.3	12.1	3.4	56.2
348.9	3.4	3.2	1.7	32.3	4.0	4.9	1.9	36.4
$\overline{\%AAD}^{1}_{@328K,\ 348\ K}$	16.7				16.9			

[1]Total average %AAD values excludes data 308 K due to high inaccuracy

[2] Average %AAD of the n-dodecane, 3,7-dimethyl-1-octanol and 1-decanol mass fractions in the phase

The model fit is analysed in Figures 117 and 118. From the diagrams it is clear that the model is generally capable of predicting more accurate liquid phase data than vapour phase data. Furthermore, except for the vapour phase n-dodecane mass fraction prediction, the trendline slopes fitted to the vapour phase mass fraction predictions differ significantly from the 1:1 line. This indicates that there is a substantial deviation between the predicted and actual mass fractions. Furthermore, the R^2 values are low and this is due to the outliers which are present in the results. Comparison of the predictions obtained using the BIPs regressed from different

data types reveals there is generally little difference between the fitted trendlines and both sets of data show a similar degree of deviation in the model fit (similar R^2 values).

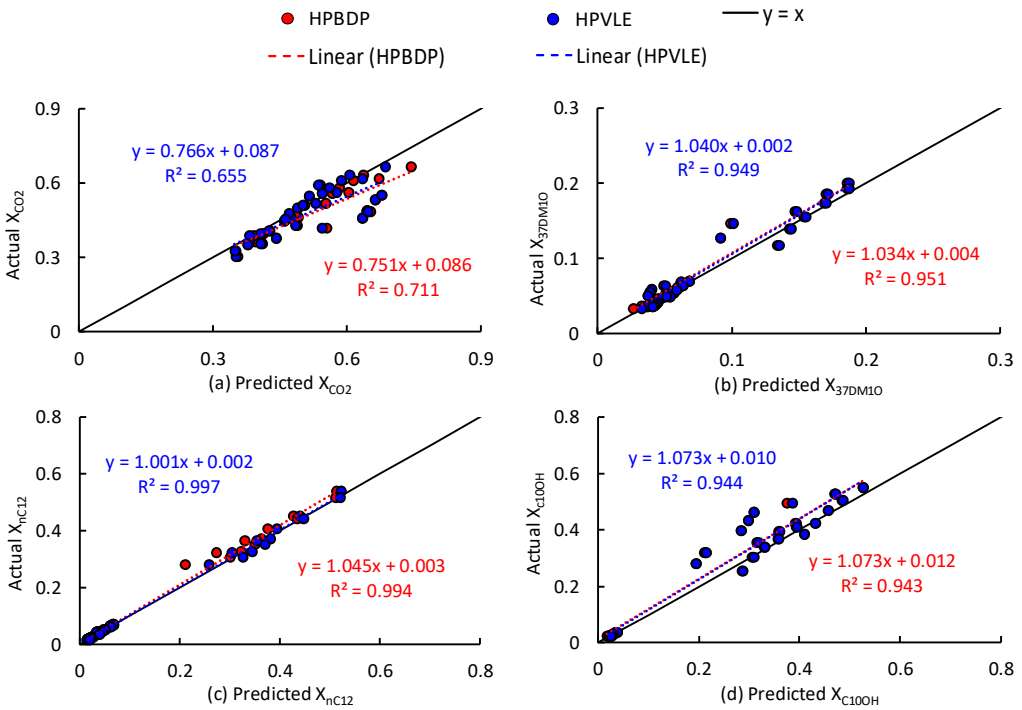

Figure 117: Parity plots for the liquid phase CO_2, 3,7-dimethyl-1-octanol, n-dodecane and 1-decanol mass fractions at 328 K and 348 K.

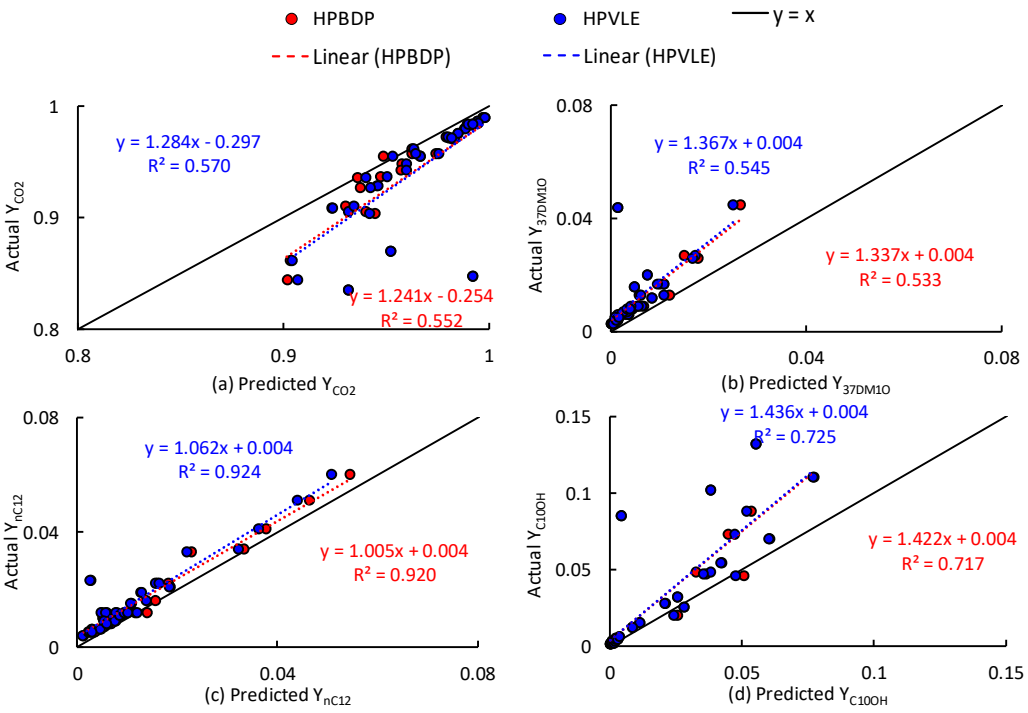

Figure 118: Parity plots for the vapour phase CO_2, 3,7-dimethyl-1-octanol, n-dodecane and 1-decanol mass fractions at 328 K and 348 K.

Conclusion

The fitted CPA model can be successfully applied to predict bubble- and dew-point data for n-dodecane rich mixtures, but it cannot predict accurate data over the entire solute composition and temperature range investigated for mixtures containing larger quantities of 1-decanol. The model can also not predict accurate VLE data for the quaternary system. The investigation into the effect of using different data types to regress the solute-solute BIPs revealed that the solutes-solute BIP regressed from HPVLE data is better suited for the bubble- and dew-point prediction, whilst the HPBDP regressed solute-solute BIP can predict slightly more accurate VLE data for the system.

8.2.4 PSRK

High pressure bubble- and dew-point data

The accuracy with which the PSRK model can predict phase transition pressures for the quaternary mixtures is presented in Table 44. It is noted that the %AAD values for the n-dodecane rich mixture are the lowest at all the temperatures, indicating that the model is most accurate for this mixture. Larger quantities of 1-decanol is seen to decrease model accuracy.

Table 44: Analysis of the accuracy with which the PSRK model can predict phase transitions pressures between 308.2 K and 348.2 K.

Mix no	Mixture solute composition	%AAD between experimental and PSRK predicted phase transition pressures				
		Temperature (K)				
		308.2	318.2	328.2	338.2	348.2
7	33.3wt% nC_{12}+ 33.3wt% 37DM1O+33.3wt% $C_{10}OH$	5.9	5.2	3.8	2.6	3.5
8	5wt% nC_{12}+10wt% 37DM1O+85wt% $C_{10}OH$	9.7	8.6	8.4	5.2	4.0
9	84.2wt% nC_{12}+10.5wt% 37DM1O+5.3wt% $C_{10}OH$	0.9	2.1	1.9	1.0	1.3
10	10.1wt% nC_{12}+30wt% 37DM1O+59.9wt% $C_{10}OH$	6.3	5.9	7.3	4.1	3.6
Z7	20wt% nC_{12}+10wt% 37DM1O+70wt% $C_{10}OH$	5.7	7.2	6.0	3.9	4.4

The model fit analysis, presented in Figure 119, illustrates that the model can predict fairly accurate phase transition pressures for the mixture consisting largely of n-dodecane. Furthermore, the vapour phase predictions for all the mixtures are also seen to be fairly accurate. The predictions for the mixtures consisting largely of 1-decanol are however seen to deviate from the experimental data within the higher solute concentration region. This indicates that the predictive model struggles to accurately account for the interactions which occur in the system. The inability of the model to predict data within the mixture critical region and temperatures below 328 K has been discussed previously.

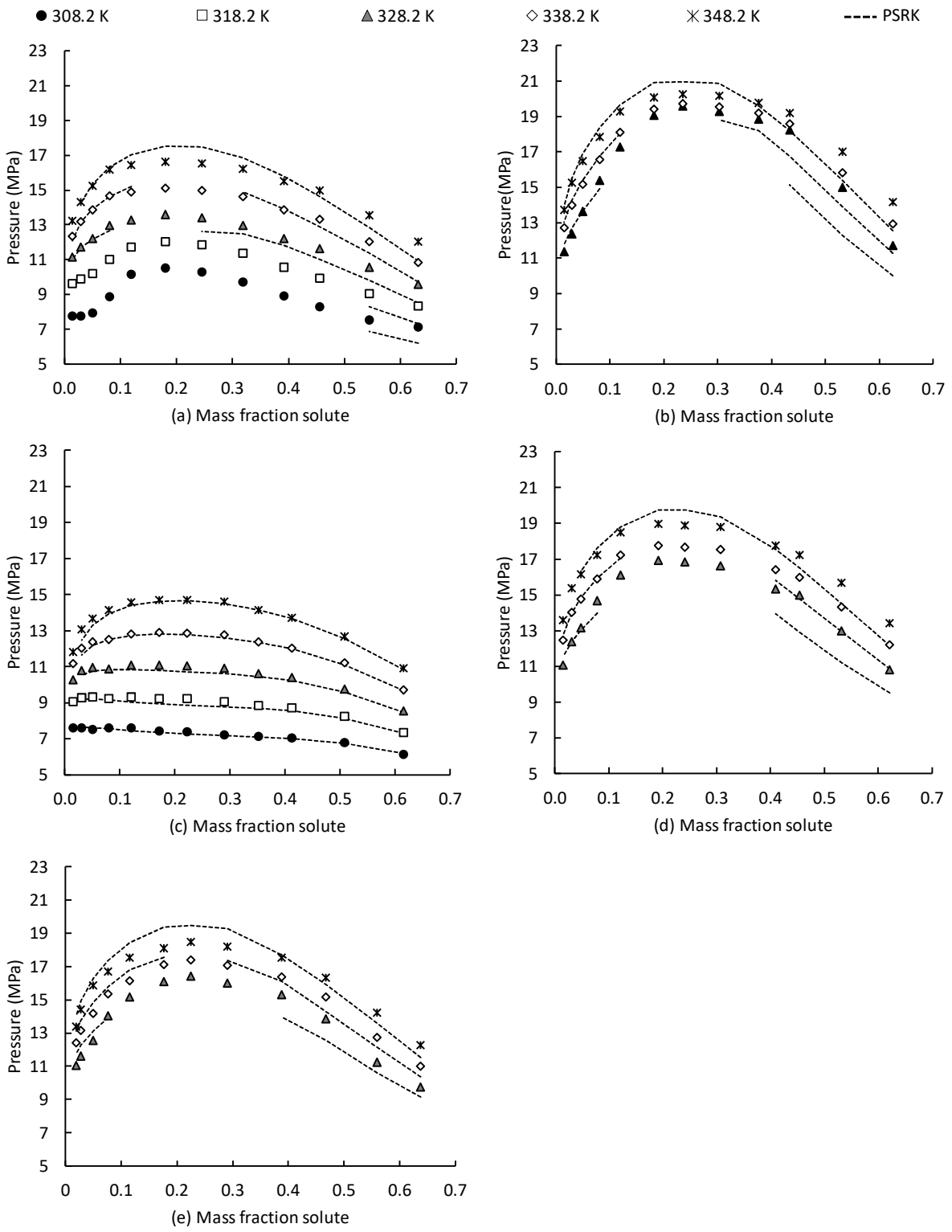

Figure 119: Comparison of experimental data and PSRK predicted data for (a) Mixture 7: 33.3 wt% nC_{12} +33.3 wt% 37DM1O +33.3 wt% $C_{10}OH$, (b) Mixture 8: 5 wt% nC_{12}+ 10 wt% 37DM1O + 85 wt% $C_{10}OH$, (c) Mixture 9: 84.2 wt% nC_{12}+ 10.5 wt% 37DM1O + 5.3 wt% $C_{10}OH$, (d) Mixture 10: 10.1 wt% nC_{12}+ 30 wt% 37DM1O + 59.9 wt% $C_{10}OH$ and (e) Mixture Z7: 20 wt% nC_{12}+ 10 wt% 37DM1O + 70 wt% $C_{10}OH$ [5]

High pressure vapour-liquid-equilibrium data

Table 45 presents an analysis of the accuracy with which the PSRK model can predict VLE data for this system. The large %AAD values reported at 308 K and the inability of the model to predict data at this temperature has been discussed previously. The model accuracy is seen to increase with an increase in temperature. This is similar to previous findings. Although the accuracy increases with temperature, the %AAD values remain large, indicating a significant degree of deviation between the experimental and predicted data, especially for the vapour phase solute composition predictions.

Table 45: Analysis of the accuracy with which the PSRK model can predict VLE data for the quaternary system at 3 temperatures between 308.6 K and 348.9 K

Temperature (K)	%AAD			
	x_{CO2}	x_s^*	y_{CO2}	y_s^*
308.6	31.3	28.3	14.3	93.8
328.8	16.6	12.3	2.3	41.9
348.9	8.0	6.8	1.7	27.6

*Average %AAD of the n-dodecane, 3,7-dimethyl-1-octanol and 1-decanol mass fractions in the phase

The model fit is analysed in Figures 120 and 121. Analysis of the diagrams reveal that the model can predict more accurate liquid phase data than vapour phase data, as the trendline fitted to the liquid phase data corresponds better to the 1:1 line and the scatter in the data is generally less (higher R^2 values). Although the liquid phase composition predictions are more accurate, the trendlines fitted to the data generally show significant deviation from the 1:1 in terms of slope, indicating weak correlation between the experimental and predicted data.

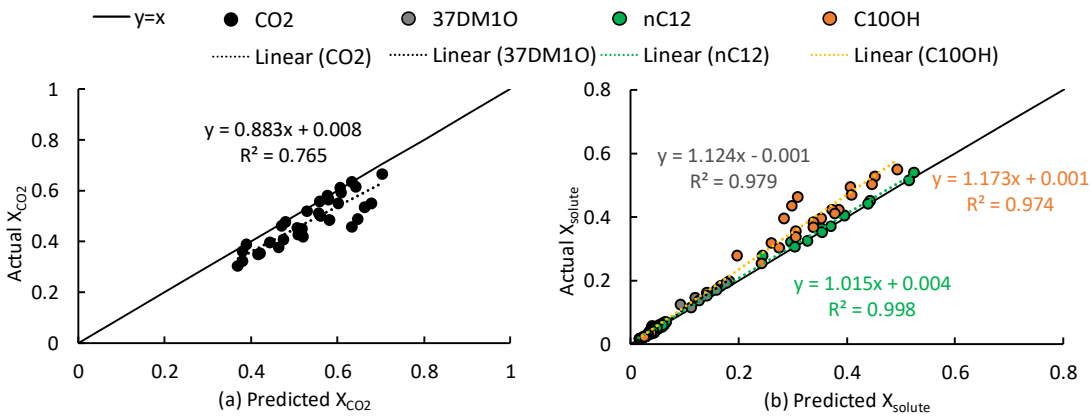

Figure 120: Parity plots for the liquid phase (a) CO_2 and (b) solutes [3,7-dimethyl-1-octanol, n-dodecane and 1-decanol] mass fractions at temperatures at 328 K and 348 K

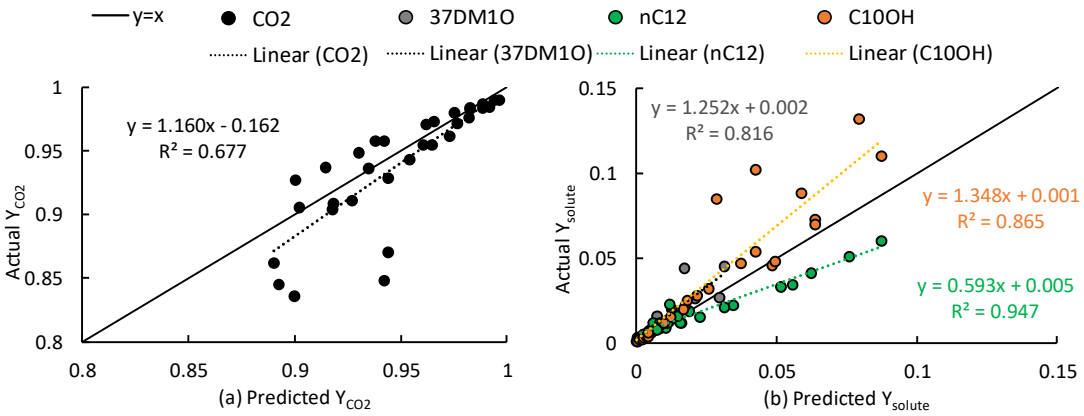

Figure 121: Parity plots for the vapour phase (a) CO_2 and (b) solutes [3,7-dimethyl-1-octanol, n-dodecane and 1-decanol] mass fractions at 328 K and 348 K

Conclusion

The PSRK model cannot predict accurate bubble- and dew-point or VLE data for the quaternary system over the entire composition and temperature range investigated.

8.2.5 Model comparison

In this section, the performance of the different models will be compared at temperatures above 328 K. Only the optimum BIPs, as identified in the previous section, will be included in the models in this section. The fitted models used for the comparison are therefore as follows:

Bubble- and dew-point data:

- RK-SOAVE + solvent-solute BIPs + solute-solute BIPs regressed from HPBDP data (no 37DM1O + C_{10}OH BIP)
- RK-ASPEN + solvent-solute BIPs + solute-solute BIPs regressed from HPBDP data (no 37DM1O + C_{10}OH BIP)
- CPA + solvent-solute BIPs + solute-solute BIPs regressed from HPVLE data (only nC_{12} + 37DM1O BIP)
- PSRK

Vapour-liquid-equilibrium data:

- RK-SOAVE + solvent-solute BIPs + solute-solute BIPs regressed from HPBDP data (no 37DM1O + C_{10}OH BIP)
- RK-ASPEN + solvent-solute BIPs + solute-solute BIPs regressed from HPBDP data (no 37DM1O + C_{10}OH BIP)
- CPA + solvent-solute BIPs + solute-solute BIPs regressed from HPBDP data (only nC_{12} + 37DM1O BIP)
- PSRK

It is noted that, with the exception of the CPA model used to predict bubble- and dew-point data, all the optimum models are based on solute-solute BIPs regressed from HPBDP data. As stated previously, this is desired due to the simpler nature of bubble- and dew-point

experiments compared to VLE experiments. It is postulated that the BIPs regressed from HPBDP data are better suited for extrapolation (predicting quaternary data) due to the more robust nature of the manual regression method.

High pressure bubble- and dew-point data

The ability of the four models to predict bubble- and dew-point data for the quaternary system is compared in Figure 122. It is clear that the RK-ASPEN model generally outperforms the other models. The predictions for Mixture 9, is the only exception where the RK-ASPEN model is not the best performing model. A possible explanation for this could be linked to the fact that the mixture consists largely of n-dodecane and the RK-ASPEN possibly overestimates the degree of solute-solute interactions in the mixture. The deviation between the RK-ASPEN model and the other models for this mixture is however minor and generally only noticeable in the mixture critical region. For the other mixtures consisting of larger quantities of 1-decanol all the models perform similarly within the low solute concentration region, but as the solute mass fraction increases (the degree of interactions increases), significant deviations between the models are evident. In the higher solute concentration region, the RK-ASPEN model predicts more accurate phase transition data than the other models, indicating that the model is better suited to account for the interactions which exist in the mixtures.

The ranking of the general ability of the models to predict bubble- and dew-point data is as follows: RK-ASPEN > RK-SOAVE > CPA > PSRK. It should be noted that within the vapour phase region the PSRK model is generally more accurate than the CPA model, but at the highest measured solute concentrations, the PSRK model is generally the least accurate model, as it noticeably underestimates the phase transition pressures. This indicates that the predictive model based on low pressure data cannot correctly account for the interactions when the solute molecules dominate the mixture composition. This highlights a need for solute-solute BIPs regressed from high pressure data to allow accurate prediction over the entire composition range.

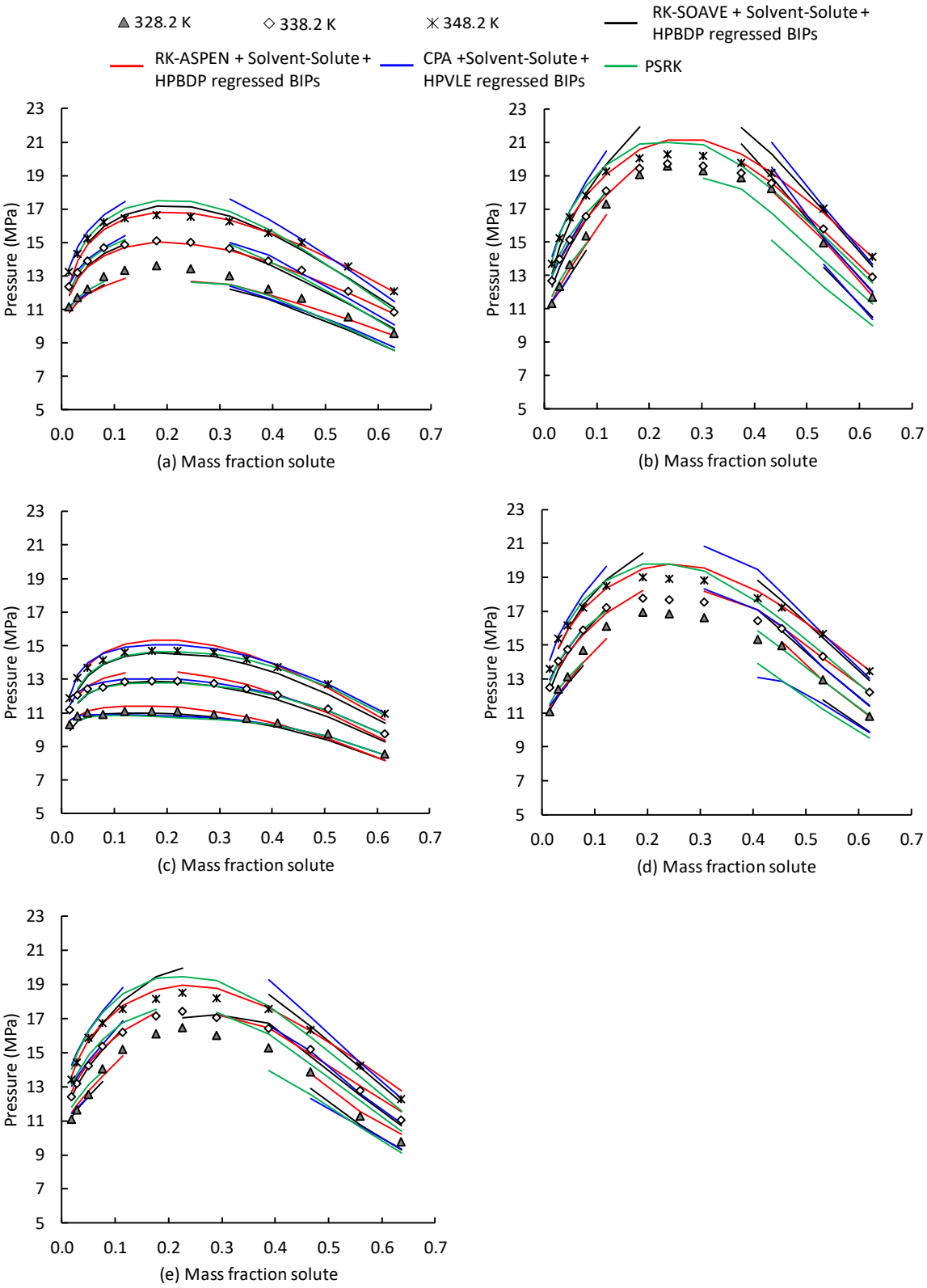

Figure 122: Pressure-composition diagrams comparing experimental data to predicted data for (a) Mixture 7: 33.3 wt% nC_{12} +33.3 wt% 37DM1O +33.3 wt% $C_{10}OH$, (b) Mixture 8: 5 wt% nC_{12}+ 10 wt% 37DM1O + 85 wt% $C_{10}OH$, (c) Mixture 9: 84.2 wt% nC_{12}+ 10.5 wt% 37DM1O + 5.3 wt% $C_{10}OH$, (d) Mixture 10: 10.1 wt% nC_{12}+ 30 wt% 37DM1O + 59.9 wt% $C_{10}OH$ and (e) Mixture Z7: 20 wt% nC_{12}+ 10 wt% 37DM1O + 70 wt% $C_{10}OH$ [5]

High pressure vapour-liquid-equilibrium data

The accuracy with which the four models can predict VLE data for this system is compared in Figure 123. It is seen that the general ability of the models to predict VLE data is as follows: RK-ASPEN > RK-SOAVE > PSRK > CPA. The RK-ASPEN model is best suited to predict VLE data for the quaternary system, as the %AAD values reported for this model are generally the lowest. Similar to the bubble- and dew-point predictions discussed previously, the PSRK and CPA models are seen the be the worst performing models. A reason contributing to the poorer performance of the CPA model could be the fact that the model is newly added to Aspen Plus® and it does not include a term to account for the quadrupole moment of CO_2. A contributing factor to the lower accuracy of the PSRK model could be that it does not include interaction parameters regressed from high pressure data, as stated previously.

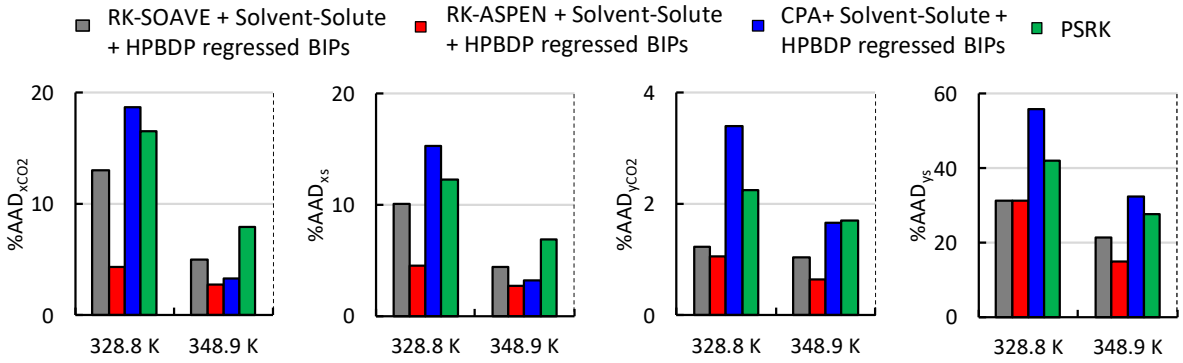

Figure 123: Comparison of the accuracy with which the four models can predict the liquid and vapour phase CO_2 composition as well as the liquid and vapour phase solute composition (average %AAD for nC_{12}, $C_{10}OH$ and 37DM1O)

Although the RK-ASPEN model is best suited to predict the VLE data for this system, there still exist significant deviation between the experimental and predicted data, indicated by the large %AAD values, particularly for the solute vapour phase composition predictions. The model can therefore only approximate the VLE data.

Figures 124 and 125 compare the experimental and RK-ASPEN predicted relative solubility results. From these diagrams it is seen that there is generally noticeable deviation between the experimental and predicted values. Although the model cannot quantitatively predict accurate relative solubility values, it can qualitatively predict accurate relative solubility trends for the 1-decanol rich mixtures (that is the relative solubility of the components in the 1-decanol rich mixtures are negatively correlated with pressure). Incorrect trends are however predicted for the n-dodecane rich mixture.

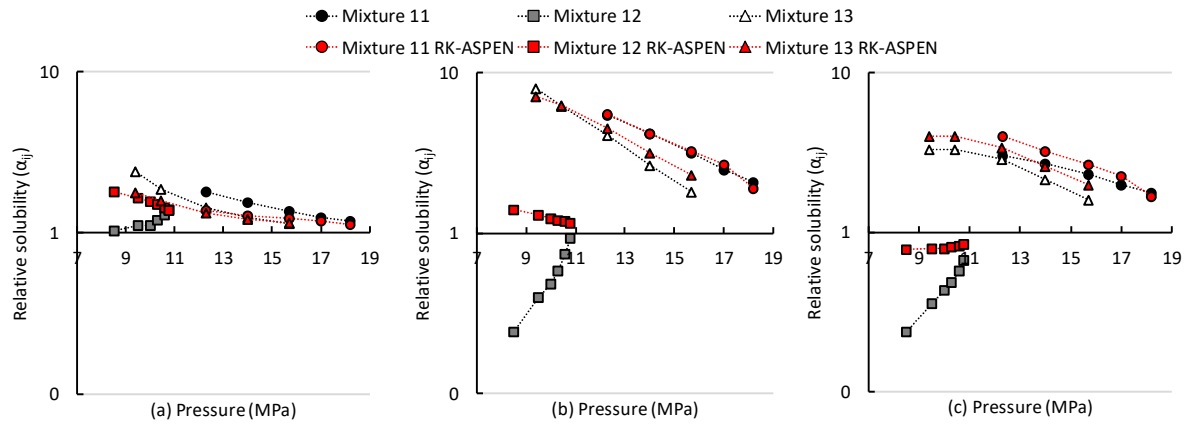

Figure 124: Log scale diagram comparing the experimental and predicted relative solubility data at 328 K for (a) $\alpha_{37DM1O,C10OH}$, (b) $\alpha_{nC12,C10OH}$ and (c) $\alpha_{nC12,37DM1O}$

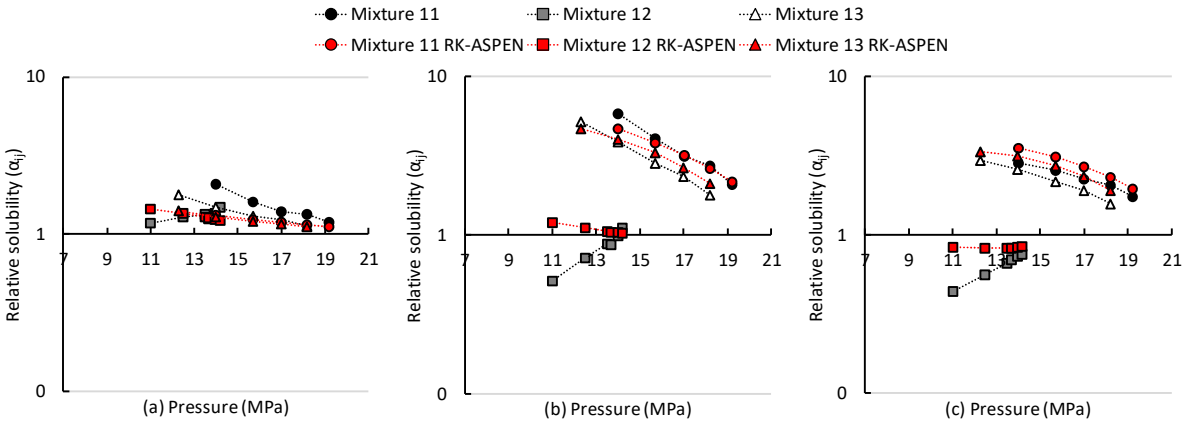

Figure 125: Log scale diagram comparing the experimental and predicted relative solubility data at 348 K for (a) $\alpha_{37DM1O,C10OH}$, (b) $\alpha_{nC12,C10OH}$ and (c) $\alpha_{nC12,37DM1O}$

8.2.6 Section outcomes

The main outcomes of this section are:

- The RK-SOAVE, CPA and PSRK models struggled to predict accurate data over the entire solute composition range. The RK-ASPEN model was however found to generally predict fairly accurate phase transition pressures at temperatures above 328 K.
- None of the models were capable of predicting the exact composition of the co-existing equilibrium phases for the system. The RK-ASPEN model can however be used to approximate VLE data for the system.
- The RK-ASPEN model which includes the solvent-solute BIPs and solute-solute BIPs regressed from HPBDP data was found to be the best suited to predict bubble- and dew-point and VLE data for the quaternary system.

- The PSRK model was found to predict fairly accurate bubble- and dew-point data in the low solute concentration region, but it was the least accurate model in the high solute concentration region, as it underestimated the phase transition pressures. This highlighted a need for solute-solute BIPs regressed from high pressure data to allow accurate prediction over the entire composition range.

8.3 Outcome of this chapter

This chapter addressed sub-objectives 3.3 and 3.4, as it aimed to (i) evaluate the accuracy with which the models can generate phase equilibrium data when incorporating the regressed BIPs, (ii) investigate how model accuracy is influenced when using different data types to regress the solute-solute BIPs and (iii) compare the performance of the models to determine which is best suited to predict equilibrium data for the systems.

The main outcomes of this chapter are:

- The inclusion of solvent-solute BIPs generally significantly improve the accuracy of the RK-SOAVE, RK-ASPEN and CPA models, as it partially accounts for the large quadruple moment of CO_2 which is not accounted for by the model structure itself.
- The incorporation of a solute-solute BIP to account for interactions between 1-decanol and 3,7-dimethyl-1-octanol was found to negatively impact model accuracy, regardless of the type of data used to regress it. Inclusion of this parameter was therefore discouraged from the RK-SOAVE, RK-ASPEN and CPA models as it is postulated that the BIP exaggerates the interaction between the two polar components, thereby overfitting the model to an extent.
- None of the models were able to correlate/predict the exact composition of co-existing phases for the ternary systems, but accurate tie-line slopes could generally be modelled. This indicates that the models can accurately describe the ratio of the solutes in the phases, but it cannot correlate the total solubility in CO_2 correctly.
- The models could not account for the temperature inversion which occurred in systems containing significant amounts of 1-decanol and correlation/predictions at low temperatures (below 328 K), where this phenomenon occurs, were generally incomplete and inaccurate.
- The RK-ASPEN model was found to be the best suited model to correlate phase equilibrium data for the ternary systems. For the CO_2 + n-dodecane + 1-decanol system,

the optimum data type used to regress the solute-solute BIP was found to correspond to the type of data being predicted. For the CO_2 + n-dodecane + 3,7-dimethyl-1-octanol system however the solute-solute BIP regressed from HPBDP data was found to be the optimum parameter to predict bubble- and dew-point and VLE data. No clear conclusion as to how the type of data used to fit the BIPs influences model accuracy could be made based on the ternary systems.

- The RK-ASPEN model which incorporated all the solvent-solute BIPs and the n-dodecane + 1-decanol and n-dodecane + 3,7-dimethyl-1-octanol solute-solute BIPs regressed from HPBDP data was found to be the best suited model to predict bubble- and dew-point data and approximate VLE data for the quaternary system. Therefore, when using this model, bubble- and dew-point data is sufficient to predict both bubble- and dew-point and VLE data for this system.
- The quaternary bubble- and dew-point predictions obtained from the PSRK model were found to be comparable to the high pressure models in the low solute concentration region. At higher solute concentrations the accuracy of the PSRK model however decreased. The model also struggled to predict accurate VLE data for the quaternary system. This highlights the need for BIPs regressed from high pressure data to allow accurate predictions.

Based on these findings it can be concluded that the aims of the chapter have been achieved and therefore the final objective of the project, namely Objective 3, was reached. The following chapter provides the conclusions of the study.

Significant contributions

- Comparison of the ability of four different variations of the Soave-Redlich-Kwong (SRK) model to describe the phase equilibrium of systems containing CO_2 with n-dodecane, 1-decanol and 3,7-dimethyl-1-octanol was conducted. This provided an outcome as to which approach is best suited for this application.
- The CPA model was used to correlate/predict data for systems containing CO_2 with n-dodecane, 1-decanol and 3,7-dimethyl-1-octanol. To date this model has not been used to predict/correlate data for such systems.
- An outcome as to how the type of data used to fit the model parameters influences the model accuracy was provided. This indicated whether a model fitted using bubble- and

dew-point data, can generate phase equilibrium data and if VLE data is required. It also provided a comparison of the degree of accuracy which can be obtained when using a predictive model based on low pressure group contribution data opposed to models regressed from high pressure data.

Publications

The modelling presented in this section formed/will form part of all the publications as all articles presenting measured data (4 articles) includes modelling.

9. CONCLUSIONS AND RECOMMENDATIONS

9.1 Conclusions

This study had two main aims, the primary aim was to experimentally ***characterise the solute-solute interactions*** which occur in mixtures containing CO_2 with detergent range alkanes and alcohols, particularly ***in the quaternary system containing CO_2 with n-dodecane, 3,7-dimethyl-1-octanol and 1-decanol***. The secondary aim was to select and fit thermodynamic models within the Aspen Plus® software to determine and compare their ability to account for the interactions which occur in this system to allow accurate prediction of phase equilibrium data for the quaternary system. Evaluation of the effect that fitting the model parameters using different types of data has on the model's ability to predict phase equilibrium data formed part of the secondary aim. A brief overview of the approach followed to achieve these aims, along with the main findings obtained from this study is provided in this chapter.

9.1.1 Aim 1: Experimentally characterise the solute-solute interactions

Objectives to be achieved

The solute-solute interactions which occur in mixtures containing CO_2 with n-dodecane, 3,7-dimethyl-1-octanol and 1-decanol were characterised by analysing literature and experimentally obtained phase behaviour data of binary, ternary and quaternary systems comprising of these components. The objectives, outlined in Chapter 1, which needed to be met to achieve this aim are:

1. *Measure bubble- and dew-point data for the binary, ternary and quaternary systems to compliment/complete literature data and analyse the measured data to determine how the solute-solute interactions influences the solubility of these mixtures.*
2. *Measure VLE data for the ternary and quaternary systems to compliment/complete literature data and analyse the measured data to determine the effect of the solute-solute interactions on the composition of co-existing equilibrium phases.*

Outcome of Objective 1

Due to a lack of published bubble- and dew-point data for the ternary CO_2 + n-dodecane + 3,7-dimethyl-1-octanol and CO_2 + 3,7-dimethyl-1-octanol + 1-decanol systems as well as the quaternary system, additional high pressure bubble- and dew-point experiments were required. The bubble- and dew-point data were measured using a static synthetic visual phase detection

method and the experiments were conducted using two previously constructed variable volume view cells.

The phase equilibrium data of the systems revealed that significant solute-solute interactions occur and these interactions result in complex phase behaviour phenomena. The bubble- and dew-point data measured for the quaternary system indicated the occurrence of ***co-solvency in mixtures consisting largely of n-dodecane***. The ternary bubble- and dew-point data however suggested that the co-solvency which occurs in these systems does not result in phenomena such as miscibility windows and liquid-liquid gas holes, within the temperature and composition ranges investigated in this work. Furthermore, the experimental bubble- and dew-point data of quaternary ***mixtures consisting largely of 1-decanol*** indicated that these mixtures ***exhibit a temperature inversion***. The bubble- and dew-point data measured for the CO_2 + 1-decanol + 3,7-dimethyl-1-octanol system also indicated the occurrence of this phenomenon and it was found that an increase in 1-decanol content drives the phase behaviour towards that of the CO_2 + 1-decanol system. Furthermore, the data revealed that 3,7-dimethyl-1-octanol disrupts the 1-decanol multimer formation, but it does not impede it as much as n-dodecane does. Based on the findings it was concluded that in quaternary mixtures where the composition consists largely of one component, the solute-solute interactions which occur in the mixture will result in the formation of complex phase behaviour phenomena associated with that component.

Outcome of Objective 2

Due to the absence of VLE data for the quaternary system, high pressure experiments were conducted to quantify the composition of co-existing phases in quaternary mixtures containing CO_2 with n-dodecane, 3,7-dimethyl-1-octanol and 1-decanol. The VLE data were measured using an analytic-sampling method and the experiments were conducted using a previously constructed static-analytic setup.

Analysis of the VLE data also indicated the occurrence of complex phase behaviour due to solute-solute interactions. The data measured for the ***1-decanol rich mixtures showed signs of a temperature inversion*** and the ***mixture consisting largely of n-dodecane hinted at complex phase behaviour*** at low temperatures, but the data could not be used to confirm co-solvency. The relative solubility analysis indicated that the components in 1-decanol rich mixtures can be separated with greater ease than the components in the n-dodecane rich mixture. Separation

of the components in the n-dodecane rich mixture were found to be temperature and pressure specific and the component which will preferentially be extracted also varies. The difficulty separating the components in the n-dodecane rich mixture is likely linked to the co-solvency which occurs in the system that may lead to pinches in separation. The separation difficulties could be resolved by incorporating a pressure-temperature swing setup.

The outcomes of Objectives 1 and 2 indicated that the phase equilibrium of mixtures containing CO_2 with n-dodecane, 1-decanol and 3,7-dimethyl-1-octanol is influenced by significant solute-solute interactions. The bubble- and dew-point and VLE data revealed that these interactions result in the occurrence of complex phase behaviour, that is temperature inversions and co-solvency. The VLE data also indicated how the separability of the components are influenced by these interactions. Both objectives therefore contributed to characterising the solute-solute interactions which occur in the quaternary system, thereby achieving Aim 1.

9.1.2 Aim 2: Thermodynamic modelling in Aspen Plus®

Objective to be achieved

In order to achieve the second aim and present a thermodynamic model capable of predicting phase equilibrium data for the quaternary system the following objective, as outlined in Chapter 1, needed to be achieved:

3. *Evaluate the ability of models available within Aspen Plus® to predict phase equilibrium data for systems containing detergent range alkanes and alcohols by:*
   - *3.1. Selecting thermodynamic models within the Aspen Plus® database.*
   - *3.2. Fitting the model parameters.*
   - *3.3. Analysing the effect that incorporating different interaction parameters and using different types of data to fit these parameters has on model accuracy.*
   - *3.4. Comparing the different models to determine which is best suited to predict phase equilibrium data for the quaternary system.*

Outcome of Objective 3

The RK-SOAVE, RK-ASPEN, CPA and PSRK models in Aspen Plus® were selected for the thermodynamic modelling performed in this work. The reason for selecting these models is that they are all based on the SRK equation of state, but they differ with regards to mixing rules and approaches to accounting for solute interactions. Comparison of these models allowed investigation into which model is best suited to generate phase equilibrium data for the system

investigated in this work (*sub-objective 3.1*). Where applicable, the models were fitted with pure component parameters and interaction parameters regressed from literature and experimental data (*sub-objective 3.2*).

In order to determine how the regressed parameters influenced the performance of the models, ternary phase equilibrium data were modelled and analysed. This analysis along with the evaluation of the effect of using different types of data to regress the model parameters yielded the following optimum parameters for each quaternary model:

Bubble- and dew-point data:

- RK-SOAVE + solvent-solute BIPs + solute-solute BIPs regressed from HPBDP data (no 37DM1O + C_{10}OH BIP)
- RK-ASPEN + solvent-solute BIPs + solute-solute BIPs regressed from HPBDP data (no 37DM1O + C_{10}OH BIP)
- CPA + solvent-solute BIPs + solute-solute BIPs regressed from HPVLE data (only nC_{12} + 37DM1O BIP)
- PSRK

Vapour-liquid-equilibrium data:

- RK-SOAVE + solvent-solute BIPs + solute-solute BIPs regressed from HPBDP data (no 37DM1O + C_{10}OH BIP)
- RK-ASPEN + solvent-solute BIPs + solute-solute BIPs regressed from HPBDP data (no 37DM1O + C_{10}OH BIP)
- CPA + solvent-solute BIPs + solute-solute BIPs regressed from HPBDP data (only nC_{12} + 37DM1O BIP)
- PSRK

Except for the CPA model used to predict bubble- and dew-point data, all the optimum models are based on solute-solute BIPs regressed from HPBDP data. It was postulated that the BIPs regressed from HPBDP data are better suited to predict quaternary data due to the more robust nature of the manual regression method. Furthermore, due to poor performance, none of the models incorporated the 1-decanol + 3,7-dimethyl-1-octanol solute-solute BIP. It was suggested that the inclusion of the solute-solute BIP exaggerates the interaction between the two polar components, thereby decreasing model accuracy (*sub-objective 3.3*).

Evaluation of the accuracy of the above listed models revealed that the RK-SOAVE, CPA and PSRK models struggled to predict bubble- and dew-point data over the entire solute composition range investigated. These models could also not predict the exact composition of the co-existing equilibrium phases. The RK-ASPEN model was however found to predict fairly accurate phase transition pressures above 328 K and the model could approximate VLE data

for the system. It was therefore concluded that the ***RK-ASPEN model with solvent-solute and solute-solute BIPs regressed from HPBDP data (no 1-decanol + 3,7-dimethyl-1-octanol BIP) is the best suited model to predict equilibrium data for the quaternary system***. When using this model, bubble- and dew-point and VLE data for the quaternary system, can be predicted using model parameters regressed from HPBDP data. This is desired as the measurement technique used to obtain bubble- and dew-point data is much easier, cheaper and faster than the method used to measure VLE data. The RK-SOAVE model was found to be the second best model and the PSRK and CPA models were the worst performing models. The poorer performance of the CPA model could likely be attributed to the fact that the model available in Aspen Plus® does not include a term to account for the quadrupole moment of CO_2 and therefore CO_2 was modelled as a self-associating component, which could have introduced error. The lower accuracy of the PSRK model (based on low pressure VLE data) highlighted the need for BIPs regressed from high pressure phase behaviour data (*sub-objective 3.4*).

9.2 Recommendations

Based on the findings presented in this work it can be concluded that the solute-solute interactions which exist in mixtures containing CO_2 with n-dodecane, 3,7-dimethyl-1-octanol and 1-decanol have been well described. Further experiments to analyse the phase behaviour of systems containing these components are therefore not required.

The thermodynamic modelling results, particularly for the VLE data, indicates room for improvement. Recommendations for further work to improve thermodynamic modelling of systems containing CO_2 with detergent range alkanes and alcohols are as follows:

- The CPA model applied in this work was newly added to the Aspen Plus® database and did not incorporate a term to account for the large quadrupole moment of CO_2. The modelling approach was then adapted to model CO_2 as a self-associating compound which could have introduced error. In future modelling attempts the CPA model which incorporates the quadrupole term must be investigated.
- In order to determine the impact of the numerical methods and algorithms employed by Aspen Plus® on model accuracy, the accuracy of using other modelling tools such as the thermodynamic software package, VLXE, should be investigated.

REFERENCES

[1] J. C. Crause, Production of detergent range alcohols, US 7,652,173 B2, 2010.

[2] M. B. O. Andersson, J. W. King and L. G. Blomberg, Synthesis of fatty alcohol mixtures from oleochemicals in supercritical fluids, Green Chemistry 2 (2000) 230-234.

[3] J. Falbe, H. Bahrmann, W. Lipps and D. Mayer, Alcohols,Aliphatics in: W. Gerhartz, Y. S. Yamamoto, F. T. Campbell, R. Pfefferkorn and J. F. Rounsaville (Eds.) Ullmann's Encyclopedia of Industrial Chemistry, VCH Publishers, Wurzburg, 1985, pp. 279-301.

[4] H. Bahrmann and H. Bach, Oxo Synthesis, in: B. Elvers, S. Hawkins and G. Schulz (Eds.) Ullmann's Encyclopedia of Industrial Chemistry, VCH Publishers, Wurzburg, 1991, pp. 321-326.

[5] M. Zamudio, The Separation of Detergent Range Alkanes and Alcohol Isomers with Alkanes and Alcohol Isomers with Supercritical Carbon Dioxide, PhD Dissertation, University of Stellenbosch, 2014.

[6] J. J. Scheibel, Production of Alcohols and Alcohol Sulfates, in: U. Zoller and P. Sosis (Eds.) Handbook of Detergents Part F: Production, CRC Press Taylor & Francis Group, Florida, 2009, pp. 117-135.

[7] G. J. K. Bonthuys, C. E. Schwarz, A. J. Burger and J. H. Knoetze, Separation of alkanes and alcohols with supercritical fluids. Part 1: Phase equilibria and viability study, The Journal of Supercritical Fluids 57 (2011) 101-111.

[8] I. P. Greager and J. C. Crause , Production of detergent range alcohols, US 7,728,178, 2010.

[9] M. Zamudio, C. E. Schwarz and J. H. Knoetze, Methodology for process modelling of supercritical fluid fractionation processes illustrated for the separation of alkane/alcohol isomer mixtures using CO_2, The Journal of Supercritical Fluids 104 (2015) 272-280.

[10] C.E. Schwarz, The Phase Euilbirium of Alkanes and Supercritical Fluids, Masters Thesis, University of Stellenbosch, 2001.

[11] G. E. Barker, G. F. Schaefer and D. Forster, Detergent range aldehyde and alcohol mixtures and derivatives, and process therefor, World Intellectual Property Organization International Bureau, WO 85/02175, 1985.

[12] C. L. Edwards, Polyoxyethylene Alcohols, in: N. M. van Os (Ed.) Nonionic Surfactants Organic Chemistry, Marcel Dekker Inc., New York, 1998, pp. 87-117.

[13] S. A. M. Smith and C. E. Schwarz, High pressure phase behaviour of the CO_2 + 1-decanol + n-dodecane system, Fluid Phase Equilbria 406 (2015) 1-9.

[14] F. C. v. N. Fourie, The high pressure phase behaviour of detergent ranges alcohols and alkanes, PhD Dissertation, University of Stellenbosch, 2018.

[15] R. Dohrn, S. Peper and J. M. S. Fonesca, High-pressure fluid-phase equilibria: Experimental methods and systems investigated (2000–2004), Fluid Phase Equilibria (2010) 288 1-54.

[16] Aspen Technology Inc., Aspen Plus V8.8, 2015.

[17] T. Clifford, Fundamentals of supercritical fluids, Oxford University Press Inc., New York, 1999.

[18] J. E. Lombard, Thermodynamic modelling of hydrocarbon-chains and light-weight supercritical solvents, Masters Thesis, University of Stellenbosch, 2015.

[19] C. Mantell, L. Casas, M. Rodriquez and E. M. Ossa, Supercritical Fluid Extraction in: S. Ramaswamy, H. Huang, B.V. Ramarao (Eds.) Separation and Purification Technologies in Biorefineries, John Wiley & Sons, Ltd., Chichester, 2013.

[20] M. Sihvonen, E. Jarvenpaa, V. Hietaniemi and R. Huopalahti, Advances in supercritical carbon dioxide technologies, Trends in Food Science and Technology 10 (1999) 217-222.

[21] D. W. Green and R. H. Perry, Perry's Chemical Engineers' Handbook, 8th ed., McGraw-Hill Companies, Inc., 2008.

[22] Y. A. Cengel and J. M. Cimbala, Fluid Mechanics Fundamentals and Application, 2nd ed., McGraw-Hill Companies Inc., New York, 2010.

[23] Y. A. Cengel and A. J. Ghajar, Heat and Mass Transfer Fundamentals and Applications, 4th ed., McGraw-Hill Companies, Inc., New York, 2011.

[24] M. A. McHugh and V. J. Krukonis, Supercritical Fluid Extraction Principles and Practice, Butterworth Publishers, Boston, 1986.

[25] G. Brunner, Supercritical fluids: technology and application to food processing, Journal of Food Engineering 67 (2005) 21-33.

[26] G. J. K. Bonthuys, Separation of 1-dodecanol and n-tetradecane through supercritical extraction, Masters Thesis, University of Stellenbosch, 2008.

[27] C. E. Schwarz, G. J. K. Bonthuys, R. F. van Schalkwyk, D. L. Laubscher, A. J. Burger and J.H. Knoetze, Separation of alkanes and alcohols with supercritical fluids. Part II: Influence of process parameters and size of operating range, The Journal of Supercritical Fluids 58 (2011) 352-359.

[28] M. Ferreira, Phase equilibria and thermodynamic modelling of the ternary system CO_2 + 1-decanol + n-tetradecane, PhD Thesis, University of Stellenbosch, 2018.

[29] U. K. Dieters and T. Kraska, High-Pressure Fluid Phase Equilibria Phenomenology and Computation, 1st ed., Elsevier, Oxford, 2012.

[30] J. M. Smith, H. C. Van Ness and M. M. Abbott, Introduction to Chemical Engineering Thermodynamics, 7th ed., McGraw-Hill Education, New York, 2005.

[31] P. H. Van Konynenburg and R. L. Scott, Critical lines and phase equilibria in binary van der waals mixtures, Philosophical Transactions of the Royal Society of London 298 (1980) 495-540.

[32] T. W. de Loos, Understanding Phase Diagrams, in: E. Kiran and J. M. H. Levelt Sengers (Eds.) Supercritical Fluids: Fundamentals for Application, Kluwer Academic Publisher, Dordrecht, 1994, pp. 65-89.

[33] C. E. Schwarz, High Pressure Phase Behavior of the Homologous Series CO_2 + 1-Alcohols, Journal of Chemical and Engineering Data 63 (2018) 2451-2466.

[34] G. Brunner, Gas Extraction. An introduction to Fundamentals of Supercritical Fluids and the Application to Separation Processes, Springer-Verlag Berlin Heidelberg, 1994.

[35] A. L. Scheidgen and G. M. Schneider, Complex phase equilibria phenomena in fluid ternary mixtures up to 100 MPa: cosolvency, holes,windows and islands - review and new results, Fluid Phase Equilibria 194-197 (2002) 1009-1028.

[36] A. L. Scheidgen and G. M. Schneider, Fluid phase equilibria of (carbon dioxide + a 1-alkanol + an alkane) up to 100 MPa and T =393 K: cosolvency effect, miscibility windows, and holes in the critical surface, The Journal of Chemical Thermodynamics, 32 (2000) 1183-1201.

[37] M. Bluma and U. K. Deiters, A classificication of phase diagrams of ternary fluid systems, Physical Chemistry Chemical Physics 1 (1999) 4307-4313.

[38] K. Gauter, C. J. Peters, A. L. Scheidgen and G. M. Schneider, Cosolvency effects, miscibility windows and two-phase lg holes in three-phase llg surfaces in ternary systems: a status report, Fluid Phase Equilibria 171 (2000) 127-149.

[39] A. Kordikowski and G. M. Schneider, Fluid phase equilibria of binary and ternary mixtures of supercritical carbon dioxide with low-volatility organic substances up to 100 MPa and 393 K: cosolvency effects and miscibility windows, Fluid Phase Equilibria 90 (1993)149-162.

[40] H. Phöler, A. L. Scheidgen and G. M. Schneider, Fluid phase equilibria of binary and ternary mixtures of supercritical carbon dioxide with a 1-alkanol and an n-alkane up to 100 MPa and 393 K- cosolvency effect and miscibility windows (Part II), Fluid Phase Equilibria 115 (1996) 165-177.

[41] M. Zamudio, C. E. Schwarz and J. H. Knoetze, Experimental measurement and modelling with Aspen Plus® of the phase behaviour of supercritical CO_2 + (n-dodecane

+ 1-decanol + 3,7-dimethyl-1-octanol), The Journal of Supercritical Fluids 84 (2013) 132-145.

[42] J. M. S. Fonseca, R. Dohrn and S. Peper, High-pressure fluid-phase equilibria: Experimental methods and systems investigated (2005-2008), Fluid Phase Equilibria 300 (2011) 1-69.

[43] M. Zamudio, C. E. Schwarz and J. H. Knoetze, Phase equilibria of branched isomers of C10-alcohols and C10-alkanes in supercritical carbon dioxide, The Journal of Supercritical Fluids 59 (2011) 14-26.

[44] G. M. Kontogeorgis and G. K. Folas, Thermodynamic models for industrial application: From classical and advanced mixing rules to association theories, 1st ed., John Wiley & Sons Ltd, Chichester, 2010.

[45] B. E. Poling, J. M. Prausnitz and J. P. O'Connell, The properties of gases and liquids, 5th ed., McGraw-Hill Education, 2001.

[46] G. M. Wilson, Vapor-Liquid Equilibrium. XI. A New Expression for the Excess Free Energy of Mixing, Journal of the Americal Chemical Society 86 (1964) 127-130.

[47] H. Renon and J. M. Prausnitz, Local Compositions in Thermodynamic Excess Functions for Liquid Mixtures, American Institute of Chemical Engineers Journal 14 (1968) 135-144.

[48] D. S. Abrams and J. M. Prausnitz, Statistical thermodynamics of liquid mixtures: A new expression for the excess Gibbs energy of partly or completely miscible systems, American Institute of Chemical Engineers Journal 21 (1975) 116-128.

[49] C. Tsonopoulos and J. L. Heidman, High pressure vapor-liquid equilibria with cubic equations of state, Fluid Phase Equilibria 29 (1986) 391-414.

[50] J. O. Valderrama, The State of the Cubic Equations of State, Industrial and Engineering Chemistry Research 42 (2003) 1603-1618.

[51] Y. S. Wei and R. J. Sadus, Equation of state for the calculation of fluid-phase equilibria, American Institute of Chemical Engineers Journal 46 (2000) 169-196.

[52] O. Redlich and J. N. S. Kwong, On the Thermodynamics of Solutions. V. An Equation of State. Fugacities of Gaseous Solutions, Chemical Reviews 44 (1949) 233-244.

[53] G. Soave, Equilibrium constants from a modified Redlich-Kwong equation of state, Chemical Engineering Science 27 (1972) 1197-1203.

[54] D. Y. Peng and D. B. Robinson, A New Two-Constant Equation of State, Industrial and Engineering Chemistry Fundamentals 15 (1976) 59-64.

[55] C. Chen and P. M. Mathias, Applied Thermodynamics for Process Modelling, American Institute of Chemical Engineers Journal 48 (2002) 194-200.

[56] G. M. Kontogeorgis and I. G. Economou, Equations of state: From the ideas of van der Waals to association theories, The Journal of Supercritical Fluids 55 (2010) 421-437.

[57] E. Voutsas, K. Magoulas and D. Tassios, Universal Mixing Rule for Cubic Equations of State Applicable to Symmetric and Asymmetric Systems: Results with the Peng-Robinson Equation of State, Industrial and Engineering Chemistry Research 43 (2004) 6238-6246.

[58] G. M. Kontogeorgis and P. Coutsikos, Thirty Years with EoS/G^E Models—What Have We Learned?, Industrial and Engineering Chemistry Research 51 (2012) 4119-4142.

[59] M-J. Huron and J. Vidal, New Mixing Rules in Simple Equation of State for Representing Vapour-Liquid Equilibria of Strongly Non-ideal Mixtures, Fluid Phase Equilibria 3 (1979) 255-271.

[60] D. S. H. Wong and S. I. Sandler, A theoretically correct mixing rule for cubic equations of state, American Institute of Chemical Engineers Journal 38 (1992) 671-680.

[61] S. Dahl and M. L. Michelsen, High-pressure vapor-liquid equilibrium with a UNIFAC-based equation of state, American Institute of Chemical Engineers Journal 36 (1990) 1829-1836.

[62] T. Holderbaum and J. Ghemling, PSRK: A Group Contribution Equation of State Based on UNIFAC, Fluid Phase Equilibria 70 (1991) 251-265.

[63] A. Fredenslund, R. L. Jones and J. M. Prausnitz, Group-contribution estimation of activity coefficients in nonideal liquid mixtures, American Institute of Chemical Engineers Journal 21 (1975) 1086-1099.

[64] I. G. Economou and M. D. Donohue, Equations of State for Hydrogen Bonding Systems, Fluid Phase Equilibria 116 (1996) 518 - 529.

[65] N. I. Diamantonis, G. C. Boulougouris, E. Mansoor, D. M. Tsangaris and I. G. Economou, Evaluation of Cubic, SAFT, and PC-SAFT Equations of State for the Vapor–Liquid Equilibrium Modeling of CO_2 Mixtures with Other Gases, Industrial and Engineering Chemistry Research 52 (2013) 3933-3942.

[66] S. H. Huang and M. Radosz, Equation of State for Small, Large, Polydisperse and Associating Molecules, Industrial and Engineering Chemistry Research 29 (1990) 2284-2294.

[67] W. G. Chapman, K. E. Gubbins, G. J. Jackson and M. Radosz, SAFT: Equation-of-State Solution Model for Associating Fluids, Fluid Phase Equilibria 52 (1989) 31-38.

[68] M. S. Wertheim, Fluids with highly directional attractive forces. I. Statistical thermodynamics, Journal of Statistical Physics 35 (1984) 19-34.

[69] M. S. Wertheim, Fluids with highly directional attractive forces. II. Thermodynamic perturbation theory and integral equations, Journal of Statistical Physics 35 (1984) 35-47.

[70] M. S. Wertheim, Fluids with highly directional attractive forces. III. Multiple attraction sites, Journal of Statitical Physics 42 (1986) 459-476.

[71] M. S. Wertheim, Fluids with highly directional attractive forces. IV. Equilibrium polymerization, Journal of Statistical Physics 42 (1986) 477-492.

[72] J. Gross and G. Sadowski, Perturbed-Chain SAFT: An Equation of State Based on a Perturbation Theory for Chain Molecules, Industrial and Engineering Chemistry Research 40 (2001) 1244-1260.

[73] G. M. Kontogeorgis, E. C. Voutsas, I. V. Yakoumis and D. P. Tassios, An Equation of State for Associating Fluids, Industrial and Engineering Chemistry Research 35 (1996) 4310-4318.

[74] I. V. Yakoumis, G. M. Kontogeorgis, E. C. Voutsas and D. P. Tassios, Vapor-liquid equilibria for alcohol/hydrocarbon systems using the CPA Equation of State, Fluid Phase Equilibria 130 (1997) 31-47.

[75] M. B. Oliveira, A. J. Queimada, G. M. Kontogeorgis and J. A. P. Coutinho, Evaluation of the CO_2 behaviour in binary mixtures with alkanes, alcohols, acids and esters using the Cubic-Plus-Association Equation of State, The Journal of Supercritical Fluids 55 (2011) 876-892.

[76] I. Tsivintzelis , G. M. Kontogeorgis, M. L. Michelsen and E. H. Stenby, Modeling phase equilibria for acid gas mixtures using the CPA equation of state. Part II: Binary mixtures with CO_2, Fluid Phase Equilibria 306 (2011) 38-56.

[77] I. Tsivintzelis and G. M. Kontogeorgis, Modelling phase equilibria for acid gas mixtures using the CPA equation of state. Part V: Multircomponent mixtures containing CO_2 and alcohols, The Journal of Supercritical Fluids 104 (2015) 29-39.

[78] I. Tsivintzelis, S. Ali and G. M. Kontogeorgis, Modeling phase equilibria for acid gas mitures using the CPA equation of state. Part IV. Application to mixtures of CO_2 with alkanes, Fluid Phase Equilibria 397 (2015) 1-17.

[79] J. Li, K. Fischer and J. Ghemling, Prediction of vapor-liquid equilibria for asymmetric systems at low and high pressures with the PSRK model, Fluid Phase Equilibria 143 (1998) 71-82.

[80] I. Nieuwoudt and M. du Rand, Measurement of phase equilibria of supercritical carbon dioxide and paraffins, The Journal of Supercritical Fluids 22 (2002) 185-199.

[81] H. Gardeler, K. Fischer and J. Gmehling, Experimental Determination of Vapor-Liquid Equilibrium Data for Asymmetric Systems, Industrial and Engineering Chemistry Research 41 (2002) 1051-1056.

[82] W. Hayduk, E. B. Walter and P. Simpson, Solubility of Propane and Carbon Dioxide in Heptane, Dodecane, and Hexadecane, Journal of Chemical and Engineering Data 17 (1972) 59-61.

[83] J. D. Hottovy, K. D. Luks and J. P. Kohn, Three-phase liquid-liquid-vapor equilibriums behavior of certain binary carbon dioxide-n-paraffin systems, Journal of Chemical and Engineering Data 26 (1981) 256-258.

[84] G. Schneider, Druckeinflub auf die Entmischung flüssiger Systeme IV. Entmischung flüssiger n-Alkan-CO_2-Systeme bis -60℃ und 1500 bar, Berichte der Bunsengesellschaft 70 (1966) 10-16.

[85] A. Henni, S. Jaffer and A. E. Mather, Solubility of N_2O and CO_2 in *n*-dodecane, The Canadian Journal of Chemical Engineering 74 (1996) 554-557.

[86] W. Weng, J. Chen and M. Lee, High Pressure Vapour-Liquid Equilibria for Mixtures Containing a Supercritical Fluid, Industrial and Engineering Chemistry Research 33 (1994) 1955-1961.

[87] C. Chang, C. Kou-Lung and D. Chang-Yih, A new apparatus for the determination of P-x-y diagrams and Henry's constants in high pressure alcohols with critical carbon dioxide, The Journal of Supercritical Fluids 12 (1998) 223-237.

[88] M. J. Lee and J. Chen, Vapor-liquid equilibrium for carbon dioxide/alcohol systems, Fluid Phase Equilibria 92 (1994) 215-231.

[89] H. Gardeler and J. Gmehling, Experimental determination of phase equilibria and comprehensive examination of the predictive capabilities of group contribution equations of state with a view of the synthesis of supercritical extraction processes in: G. Brunner (Ed.) Supercritical Fluids as Solvents and Reaction Media, Elsevier B.V., Amsterdam, 2004, pp. 3-38.

[90] D. H. Lam, A. Jangkamolkulchai and K. D. Luks, Liquid-liquid-vapour phase equilibrium behaviour of certain binary carbon dioxide + n-alkanol mixtures, Fluid Phase Equilibria 60 (1990) 131-141.

[91] R. J. Wilcock, R. Battino, W. F. Danforth and E. Wilhelm, Solubilities of gases in liquids II. The solubilities of He, Ne, Ar, Kr, O_2, N_2, CO, CO_2, CH_4, CF_4, and SF_6 in n-octane, 1-octanol, n-decane and 1-decanol, The Journal of Chemical Thermodynamics 10 (1978) 817-822.

[92] H. Pöhler, Fluidphasengleichgewichte Binärer und Ternärer Kolhendioxidmischungen mit Schwerflüchtgen Organischen Substanzen Bei Temperaturen von 303 K bis 393 K

und Drücken von 10 MPa bis 100 MPa, Disseration, der Ruht-Universität Bochum, 1994.

[93] A. Schneidgen, Fluidphasengleichgewichte binärier und ternärier Kohlendioxidmischungen mit schwerfküchtigen organischen Substanzen bis 100 MPa, Dissertation, der Fukaltät für Chemie der Ruhr-Universität Bochum, 1997.

[94] H. S. Ghaziaskar, A. Daneshfar and M. Rezayat, The co-solubility of 2-ethylhexanoic acid and some liquid alcohols in supercritical carbon dioxide, Fluid Phase Equilibria 238 (2005) 106-111.

[95] S. Ioniță, V. Feroiu and D. Geană, Phase Equilibria of the Carbon Dioxide + 1-Decanol System at High Pressures, Journal of Chemical and Engineering Data 58 (2013) 3069-3077.

[96] C. L. Patton and K. D. Luks, Multiphase equilibria of the binary mixture xenon + 1-decanol, Fluid Phase Equilibria 98 (1994) 201-211.

[97] M. Cismondi, S. B. Rodriquez-Reartes, J. M. Milanesio and M. S. Zabaloy, Phase Equilibria of CO_2 + n-Alkane Binary Systems in Wide Ranges of Conditions: Development of Predictive Correlations Based on Cubic Mixing Rules, Industrial and Engineering Chemistry Research 51 (2012) 6232-6250.

[98] M. Ferreira and C. E. Schwarz, Super- and near-critical fluid phase behavior and phenomena of the ternary system CO_2 + 1-decanol + n-tetradecane, The Journal of Chemical Thermodynamics 111 (2017) 88-99.

[99] X. Gui, Z. Tang and W. Fei, Solubility of CO_2 in Alcohols, Glycols,Ethers, and Ketones at High Pressures from (288.15 to 318.15) K, Journal of Chemical and Engineering Data 56 (2011) 2420-2429.

[100] J. D. Seader, E. J. Henley and D. K. Roper, Separation Process Principles. Chemical and Biochemical Operations,JohnWiley & Sons, Inc., New Jersey 2011.

[101] M. Goral, P. Oracz, A. Skrzecz, A. Bok and A. Maczynski, Recommended Vapour-Liquid Equilbrium Data. Part 1: Binary n-Alkanol-n-Alkane Systems, Journal of Physical and Chemical Rereference Data, vol. 31, no. 2002, pp. 701-748, 2002.

[102] M. Góral, P. Oracz, A. Skrzecz, A. Bok and A. Mączyński, Recommended Vapor-Liquid Equilibrium Data. Part 2: Binary Alkanol-Alkane Systems, Journal of Physical and Chemical Reference Data 32 (2003) 1429-1472.

[103] F. C. v. N. Fourie, C. E. Schwarz and J. H. Knoetze, CO_2 + n-dodecane + 3,7-dimethyl-1-octanol: High pressure experimental phase equilibria data and thermodynamic modelling, The Journal of Supercritical Fluids 130 (2017) 105-117.

[104] F. C. v. N. Fourie, C. E. Schwarz and J. H. Knoetze, Phase equilibria of alcohols in supercritical fluids Part I. The effect of the position of the hydroxyl group for linear C8

alcohols in supercritical carbon dioxide, The Journal of Supercritical Fluids 47 (2008) 161-167.

[105] C. E. Schwarz and I. Nieuwoudt, Phase equilibrium of propane and alkanes Part 1. Experimental procedures, dotriacontane equilibrium and EOS modelling, The Journal of Supercritical Fluids 27 (2003) 133-144.

[106] C. J. Peters, H. J. Van Der Kooi and J. De Swaan Arons, Measurements and calculations of phase equilibria for (ethane + tetracosane) and (p, V_m^*, T) of liquid tetracosane, The Journal of Chemical Thermodyamics 19 (1987) 395-405.

[107] C. J. Peters, J. Spiegelaar and J. De Swaan Arons, Phase equilibria in binary mixtures of ethane + docosane and molar volumes of liquid docosane, Fluid Phase Equilibria 41 (1988) 245-256.

[108] J. Gregorowicz, T. W. De Loos and J. De Swaan Arons, The system propane + eicosane: P, T, and x measurements in the temperature range 288-358 K, Journal of Chemical and Enigneering Data 37 (1992) 356-358.

[109] C. E. Schwarz, G. J. K. Bonthuys, J. H. Knoetze and A. J. Burger, The influence of functional end groups on the high-pressure phase equilibria of long chain molecules in supercritical propane, The Journal of Supercritical Fluids 46 (2008) 233-237.

[110] A. Kramer and G. Thodos, Solubility of 1 -Hexadecanol and Palmitic Acid in Supercritical Carbon Dioxide," Journal of Chemical and Engineering Data 33 (1988) 230-234.

[111] F. C. v. N. Fourie, C. E. Schwarz and J. H. Knoetze, Analytic Setup For Multicomponent High-Pressure Phase Equilibria via Dual Online Gas Chromatography, Chemical Engineering and Technology 38 (2015) 1165-1172.

[112] F. C. v. N. Fourie, C. E. Schwarz and J. H. Knoetze, Analytic High-Pressure Phase Equilbria Part II: Gas Chromatoggraphy and Sampling Method Development, Chemical Engineering and Technology 39 (2016) 1475-1482.

[113] Bureau International des Poids et Mesures, Evaluation of measurement data - Guide to the expression of uncertainty in measurement, Joint Committee for Guides in Metrology, 2008.

[114] A. R. H. Goodwin, J. V. Sengers and C. J. Peters, Applied Thermodynamics of Fluids, Royal Society of Chemistry, Cambridge, 2010.

[115] S. K. Shibata and S. I. Sandler, Critical Evaluation of Equation of State Mixing Rules for the Predictions of High-Pressure Phase Equilibria, Industrial and Engineering Chemistry Research 28 (1989) 1893-1898.

[116] P. M. Mathias, A versatile phase equilibrium equation of state, Industrial and Engineering Chemistry Process Design and Development 22 (1983) 385-391.

[117] G. M. Kontogeorgis, M. L. Michelsen, G. K. Folas, S. Derawi, N. von Solms and E. H. Stenby, Ten Years with the CPA (Cubic-Plus-Association) Equation of State. Part 1. Pure Compounds and Self-Associating Systems, Industrial and Engineering Chemistry Research 45 (2006) 4855-4868.

[118] P. M. Mathias and T. W. Copeman, Extension of the Peng-Robinson equation of state to complex mixtures: Evaluation of the various forms of the local composition concept, Fluid Phase Equilibria 13 (1983) 91-108.

[119] P. Kolář and K. Kojima, Predictions of critical points in multicomponent systems using the PSRK group contribution equation of state, Fluid Phase Equilibria 118 (1996) 175-200.

[120] S. Horstmann, A. Jabloniec, J. Krafczyk, K. Fischer and J. Gmehling, PSRK group contribution equation of state: comprehensive revision and extension IV, including critical constants and a-function parameters for 1000 components, Fluid Phase Equilibria 227 (2005) 157-164.

[121] C. L. Yaws and P. K. Narasimhan, Chapter 1 - Critical properties and acentric factor—Organic compounds, in: C. L. Yaws (Ed.) Thermophysical Properties of Chemicals and Hydrocarbons, William Andrew Publishing, New York, 2009, pp. 1-95.

[122] C. L. Yaws and P. K. Narasimhan, Critical properties and acentric factor—Inorganic compounds, in: C. L. Yaws (Ed.) Thermophysical Properties of Chemicals and Hydrocarbons, William Andrew Publishing, New York, 2009, pp. 96-105.

[123] M. Zamudio, C. E. Schwarz and J. H. Knoetze, Phase equilibria of branched isomers of C10-alcohols and C10-alkanes in supercritical ethane, The Journal of Supercritical Fluids 58 (2011) 330-342.

[124] C. Pienaar, Evaluation of Entrainers for the Dehydration of C2 and C3 Alcohols via Azeotropic Distillation, Masters Thesis, University of Stellenbosch, 2012.

[125] M. G. Bjørner and G. M. Kontogeorgis, Modeling derivative properties and binary mixtures with CO_2 using the CPA and the quadropular CPA equations of state, Fluid Phase Equilibria 408 (2016) 151-169.

[126] C. E. Schwarz, A. J. de Villier, C. B. McClune, G. J. K. Bonthuys, A. J. Burger and J. H. Knoetze, High pressure phase equilibrium measurements of long chain alcohols in supercritical ethane, The Journal of Supercritical Fluids 55 (2010) 554-565.

[127] J. Cai and J. M. Prausnitz, Thermodynamics for fluid mixtures near to and far from the vapor–liquid critical point, Fluid Phase Equilibria 219 (2004) 205-217.

[128] G. M. Kontogeorgis, M. L. Michelsen, G. K. Folas, S. Derawi, N. von Solms and E. H. Stenby, Ten Years with the CPA (Cubic-Plus-Association) Equation of State. Part 2. Cross-Associating and Multicomponent Systems, Industrial and Engineering Chemistry Research 45 (2006) 4869-4878.

[129] E. Forte, F. Llovell, L. F. Vega, J. P. Trusler and A. Galindo, Application of renormalization-group treatment to the statistical associating fluid theory for potentials of variable range (SAFT-VR), The Journal of Chemical Physics 134 (2011) 1-155.

[130] J. E. Gutiérreza, A. Bejaranoa and J. C. de la Fuente, Measurement and modeling of high-pressure (vapour + liquid) equilibria of (CO_2 + alcohol) binary systems, The Journal of Chemical Thermodynamics 42 (2010) 591-596.

[131] F. Mesple, M. Troussellier, C. Casellas and P. Legendre, Evaluation of simple statistical criteria to qualify a simulation, Ecological Modelling 88 (1996) 9-18.

[132] G. Pineiro, S. Perelman, J. P. Geurschman and J. M. Paruelo, How to evaluate models: Observed vs. predicted or predicted vs. observed?, Ecological Modelling 216 (2008) 316-322.

[133] E. P. Smith and K. A. Rose, Model goodness-of-fit analysis using regression and related techniques, Ecological Modelling 77 (1995) 49-64..

APPENDICES

A. Bubble- and Dew-points Experimental Setup

A.1. Detailed experimental procedure

This section provides a detailed breakdown of the loading, measuring and unloading procedures followed when conducting the bubble- and dew-point experiments. The procedures are the same for both the small and large variable volume cells. The experimental method presented here is based on the procedure developed by Schwarz [10].

LOADING

1. The piston section of the equilibrium cell is removed to load the solute.
2. A known amount of solute, weighed accurately to 0.001g, is loaded into the cell using a dropper.
3. The magnetic stirrer bar is added to the cell.
4. The cell is closed and the shaft is tightened to ensure that the Teflon seal does not leak.
5. The loading equipment, presented in Figure 126, is now connected to the equilibrium cell and a check is conducted to ensure that all valves on the fitting are closed.

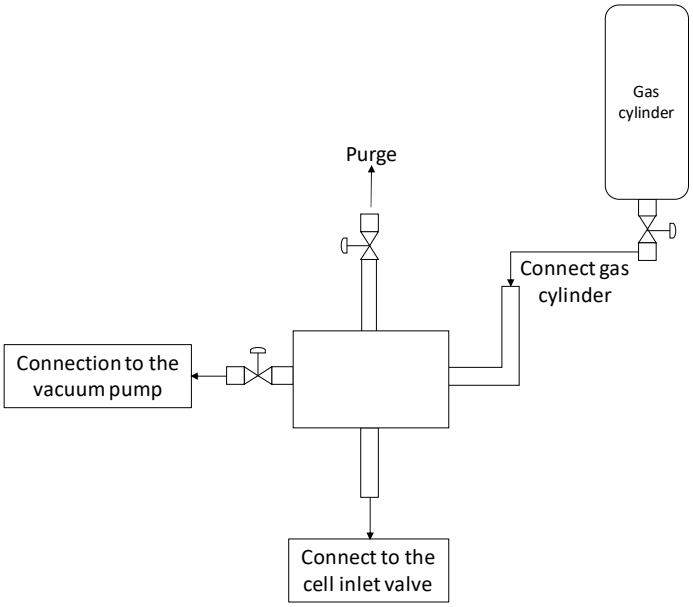

Figure 126: Schematic of the three-way valve which provides connections points for the vacuum pump, gas cylinder and purge vent required during the loading procedure (Adapted from [33])

6. The gas cylinder is loaded with CO_2 and connected to the loading equipment, as shown in Figure 126.

7. The cell is evacuated by opening the vacuum pump valve and the valve to the cell. The camera should be used during this step to ensure that no solute is removed from the cell during evacuation. Once the air is removed the vacuum pump valve and the valve to the cell are closed.
8. To remove the remaining air, the cell is flushed six times with CO_2. During the flushing procedure, small amounts of CO_2 is introduced into the cell. The purge valve, indicated on Figure 80, is then opened to release the CO_2. The purge valve is closed once the pressure inside the cell is near atmospheric pressure. Upon completion of the flushing processes care must be taken to ensure that most of the CO_2 is removed from the cell. Once all the CO_2 is removed the cell valve is closed [10].
9. The gas cylinder is removed and weighed accurate to 0.01g.
10. The required amount of CO_2 is calculated. The excess CO_2 in the gas cylinder is then vented to ensure that the gas cylinder contains the exact amount of CO_2 which is to be loaded into the cell [10].
11. The gas cylinder, containing the required amount of CO_2, is reconnected to the loading equipment.
12. The piping of the loading equipment is then evacuated by opening the vacuum pump valve. Once the air is removed the vacuum pump valve is closed.
13. The gas cylinder is heated up and then the CO_2 is loaded to the cell by opening the gas cylinder and the cell inlet valve fully.
14. Once the CO_2 has been loaded the gas cylinder valve is closed and the piping leading to the cell inlet is heated.
15. Once all the CO_2 in the piping has been loaded into the cell the inlet valve to the cell is closed.
16. The gas cylinder is then removed and weighed to ensure that the required amount of CO_2 has been loaded. The composition of the material loaded to the cell is then calculated to determine whether the cell has been loaded correctly. If the amount of CO_2 loaded to the cell is not correct, the CO_2 in the cell must be purged and the loading procedure from step 11 must be repeated [10].
17. The loading equipment is removed and the lock nut is used to close off the inlet valve to the cell.
18. The thermocouple is inserted, thermostat bath is turned on and the set point temperature is set to achieve the first measuring temperature.
19. Insulation is added to reduce heat losses.

20. The magnetic stirrer is turned on.
21. The Vernier scale is then connected.
22. The nitrogen gas line is connected to the cell.
23. The cell content is pressurised into the one phase region.

MEASURING THE DATA

1. Once the cell reaches thermal equilibrium the measuring procedure can begin.
2. The cell pressure is slowly reduced by opening the release valve on the nitrogen gas cylinder, until a second phase starts to form. The transition point is visually observed on the monitor and the pressure, temperature, piston position and the number of phases is recorded. The cell content is then pressurised into the one phase region by adjusting the regulator on the nitrogen gas cylinder. The process is repeated and the bisection method is used to measure the transition point accurately to within 0.02 MPa [10].
3. Once the transition point has been determined the set point of the thermostatic bath is adjusted to achieve the next measuring temperature and the cell pressure is increased to ensure that the cell contents remain in the one phase region.
4. After 30 to 45 minutes the measuring procedure is repeated at the new temperature.

CLEANING AND UNLOADING

1. Once the final measurement has been made the pressure in the cell is released by fully opening the release valve on the nitrogen cylinder and closing the regulator.
2. The magnetic stirrer and thermostat bath are turned off, the insulation is removed and the cell is allowed to cool.
3. The nitrogen gas line is disconnected from the cell and the Vernier is removed.
4. Once the cell has cooled the thermocouple is removed and the cell is orientated so that the cell inlet valve points downwards.
5. The cell inlet valve is carefully opened and the cell content is drained into a clean flask.
6. Once the content has been drained the inlet valve of the cell is completely opened and the cell is position so the piston section can be removed.
7. Prior to removing the piston section there are three checks:
    a. The cell inlet valve must be completely open.
    b. The pressure reading must be close to atmospheric pressure.
    c. The shaft must be loosened.

8. The piston section is removed and the cell is adjusted so that the opening of the cell points downward.
9. Whilst turning the cell into the downward facing position care must be taken not to lose the magnetic stirrer bar.
10. The cell is then cleaned with isopropanol and methanol.
11. Compressed air is used to remove traces of the cleaning agents.

A.2. Safety and risk assessment

In order to ensure safe operation of the equipment, task risk assessments forms were completed to identify possible hazards associated with the equipment and to evaluate the mitigating strategies which are in place to reduce the risk thereof. The template and risk assessment method were developed by the Department of Process Engineering and completion thereof was compulsory prior to commencing with experiments. The forms were completed in conjunction with other researchers using the same or similar equipment.

The risk calculator used is presented in Table 46 and the task risk assessment forms for the different steps in the operating procedure is presented in Tables 47 to 49.

Table 46: Risk calculator used in the task risk assessment forms, as prescribed by the Department of Process Engineering.

					Consequence				
				OHS, HR	Injury report &/or 1st aid only; substantial stress, reducing work effectiveness without lost time.	Medical treatment injury (MTI); Substantial stress, requiring professional clinical support.	Hospitalisation (less than 3 days lost time); serious temporary disability; minor permanent disability.	Hospitalisation (longer-term); single death; permanent disabilities (multiple persons).	Multiple deaths &/or permanent disability (5 plus persons).
				Environment, Community	Brief pollution: No discernable impact; internal report, liability <ZAR 10k	Transient harm: minor effects on environ, minor localised short-medium term damage; liability ZAR10k-ZAR100k	Moderate harm: Measurable environ impairment but not on ecosystem; short-med term impacts; liability ZAR 100k-1m	Significant harm: Serious environ effects, some ecosystem impairment; med-long term impacts, recovery once clean up complete; liability ZAR 1m-ZAR 10m	Long term harm: Serious environ widespread effects, significant impairment of ecosystem function; remediation required; liability > ZAR 10m
				Political, Reputation & Image	Issue resolved internally by day-to-day processes; little or no stakeholder interest.	Issue raised by students / local press; minor adverse public / media attention & complaints.	Student/Community concern; heavy local media coverage; criticism by NGOs; reputation affect with some stakeholders.	Significant adverse media coverage (national/public); reputation impacted with significant no. of stakeholders; breakdown in business partnership	Reputation affected national & international, & with majority of key stakeholders; serious public / media outcry; significant breakdown in business partnerships
				Business, Quality & Infrastructure	Negligible business interruption, brief loss of service; <10 recommendations from compliance body; event absorbed through normal activity; loss of >1 days research/work	Minor delivery delays; loss of 1-5 days research/ work; event requires management attention to minimise impact; >2 statutory non-compliances	Significant event; 2+ non-compliances & license under threat; loss of 5 days – 6wks research/work; critical service interruption.	Major event; limited accreditation/ licensing; loss of 6-13wks research/work; critical infrastructure service loss for <1 month	Extreme event – potential for collapse of part of business; school viability threatened (loss of students / clients); limited accreditation; loss of 13+wks research/work; critical infrastructure loss >1 month
				Legal	Adverse regulatory action unlikely	Regulatory action not likely; minor legislative breach	Serious legislative breach; potential for regulatory action e.g. fine, prosecution	Major legislative breach; possible investigation, prosecution &/or major fine	Significant prosecution / fines likely; "wilful" / "negligent"; potential significant litigation e.g. class action
				Financial	<ZAR 10k for Department/Faculty	ZAR 10k – 100k for Department/Faculty	ZAR 100k-1m for Department/Faculty	ZAR 1m-ZAR 10m for Department/Faculty	>ZAR 10m for Department/Faculty
					Insignificant	**Minor**	**Moderate**	**Major**	**Catastrophic**
	Probability:	**Historical:**			**1**	**2**	**3**	**4**	**5**
Likelihood	Occurs weekly	Expected to occur in most circumstances	**5**	**Almost Certain**	**M (11)**	**H (13)**	**E (20)**	**E (23)**	**E (25)**
	Occurs monthly	Will probably occur in most circumstances	**4**	**Likely**	**M (7)**	**H (12)**	**H (17)**	**E (21)**	**E (24)**
	Yearly; 1 in 20 chance	Might occur at some time	**3**	**Possible**	**L (4)**	**M (8)**	**H (16)**	**E (18)**	**E (22)**
	Once in every 10 years; 1 in 100 chance	Could occur at some time	**2**	**Unlikely**	**L (2)**	**L (5)**	**M (9)**	**H (15)**	**E (19)**
	Less than 1% chance of occurring	May occur but in exceptional circumstances	**1**	**Rare**	**L (1)**	**L (3)**	**M (6)**	**M (10)**	**H (14)**

Table 47: Task risk assessment form completed to determine the hazards and risks related to loading the variable volume cells.

Ref No.	SPECIFIC TASK / ACTIVITY STEPS	IDENTIFY POTENTIAL HAZARDS	RISK RANKING			RISK CONTROL MEASURES • *Hierarchy of Control – Elimination, Substitution, Isolation, Engineering, Administration, Personal Protection.* • *Additional information can be attached.*	RESIDUAL RISK			Actioner / Initials
			Consequence	Likelihood	Risk Rating		Consequence	Likelihood	Residual Risk	
LOADING										
1	Lifting or moving the heavy cell or low pressure chamber	Heavy load – injury.	2	1	L3	Proper training. Use platforms provided. Ask for assistance.	2	1	L3	**CL**
2	Inspecting the setup for impurities	Chemical exposure to solutes – 3,7-dimethyl-1-octanol + 1-decanol + n-dodecane	2	3	M8	Proper training. Foreknowledge of the chemicals concerned. Consult MSDS sheets attached. Adequate ventilation. Correct PPE.	2	1	L3	**CL**
3	Loading the solute	Chemical exposure to solutes – 3,7-dimethyl-1-octanol + 1-decanol + n-dodecane	2	3	M8	Proper training. Foreknowledge of the chemicals concerned. Consult MSDS sheets attached. Adequate ventilation. Correct PPE.	2	1	L3	**CL**
4	Cleaning the setup prior to loading	Chemical exposure to cleaning agents – methanol and isopropanol	2	3	M8	Proper training. Foreknowledge of the chemicals concerned. Consult MSDS sheets attached. Adequate ventilation. Correct PPE.	2	1	L3	**CL**
5	Working with tools [e.g. spanners]	Incorrect tool use / tool failure - Injury	2	1	L3	Proper training. Using the correct tool for the job. Correct PPE.	2	1	L3	**CL**
6	Using the gas bomb to flush the cell and load the solvent	High pressure –Leak	3	2	M9	Proper training and regular inspection. Regular testing of the equipment. Correct PPE.	2	1	L3	**CL**
7	Using the gas bomb to flush the cell and load the solvent	High Pressure – Equipment Failure Causing Explosive Decompression	3	1	M6	Proper training and inspection. Regular testing (every 6 months). Safety in design (up to 300 bar). Correct PPE.	3	1	M6	**CL**
8	Using the gas bomb to flush the cell and load the solvent	High Pressure – Uncontrolled Rapid Expansion.	2	3	M8	Proper training. Correct PPE.	2	1	L3	**CL**
9	Flushing the cell with CO_2	Chemical exposure to solutes – 3,7-dimethyl-1-octanol + 1-decanol + n-dodecane	2	3	M8	Proper training. Foreknowledge of the chemicals concerned. Consult MSDS sheets attached. Adequate ventilation. Correct PPE.	2	1	L3	**CL**

Table 47 continued: Task risk assessment form completed to determine the hazards and risks related to loading the variable volume cells.

Ref No.	SPECIFIC TASK / ACTIVITY STEPS	IDENTIFY POTENTIAL HAZARDS	RISK RANKING			RISK CONTROL MEASURES • *Hierarchy of Control – Elimination, Substitution, Isolation, Engineering, Administration, Personal Protection.* • *Additional information can be attached.*	RESIDUAL RISK			Actioner / Initials
			Consequence	Likelihood	Risk Rating		Consequence	Likelihood	Residual Risk	
10	Flushing the cell with CO_2	Chemical exposure to solvent – CO_2	1	3	M6	Proper training. Foreknowledge of the chemicals concerned. Consult MSDS sheets attached. Adequate ventilation. Correct PPE.	1	1	L1	**CL**
11	Using the gas bomb to load the solvent	High Heat – Light Burns.	2	2	L5	Equipment has built in safety. Proper training. Correct PPE.	2	1	L3	**CL**
12	Pressurising the cell	High Pressure – Equipment Failure Causing Explosive Decompression	3	1	M6	Proper training and inspection. Regular testing (every 6 months). Safety in design (up to 300 bar). Correct PPE.	3	1	M6	**CL**
13	Pressurising the cell	High pressure –Leak	3	2	M9	Proper training and inspection. Regular testing (every 6 months). Safety in design (up to 300 bar). Correct PPE.	2	1	L3	**CL**
14	Plug in the hairdryer	Electrocution	1	2	L3	Correct PPE.	1	1	L1	**CL**
15	Using the hairdryer to heat gas bomb	Fire due to open element and contact with flammable solutes	3	1	M6	Ensure the room is well ventilated before making use of the hairdryer. Do not use if there is a high concentration of flammable solvent present. Correct PPE	2	1	L3	**CL**

Table 48:Task risk assessment form completed to determine the hazards and risks related to measuring bubble- and dew-point data using the variable volume cells.

Ref No.	SPECIFIC TASK / ACTIVITY STEPS	IDENTIFY POTENTIAL HAZARDS	RISK RANKING			RISK CONTROL MEASURES • *Hierarchy of Control – Elimination, Substitution, Isolation, Engineering, Administration, Personal Protection.* • *Additional information can be attached.*	RESIDUAL RISK			Actioner / Initials
			Consequence	Likelihood	Risk Rating		Consequence	Likelihood	Residual Risk	
EXPERIMENTAL MEASUREMENTS										
1	Frequently increase or decreasing the pressure in the cell. Measuring under high pressure conditions	High pressure –Leak	3	2	M9	Proper training and inspection. Regular testing (every 6 months). Safety in design (up to 300 bar). Correct PPE.	2	1	L3	**CL**
2	Frequently increase or decreasing the pressure in the cell. Measuring under high pressure conditions	High Pressure – Equipment Failure Causing Explosive Decompression	3	1	M6	Proper training and inspection. Regular testing (every 6 months). Safety in design (up to 300 bar). Correct PPE.	3	1	M6	**CL**
3	Frequently increase or decreasing the pressure in the cell. Measuring under high pressure conditions	High Pressure – Uncontrolled Rapid Expansion.	2	3	M8	Proper training. Correct PPE.	2	1	L3	**CL**
4	Frequently increase or decreasing the pressure in the cell. Measuring under high pressure conditions	High Heat – Light Burns	2	2	L5	Equipment has built in safety. Proper training. Correct PPE.	2	1	L3	
5	In case of risks [1,2]	Chemical exposure to solutes –3,7-dimethyl-1-octanol + 1-decanol + n-dodecane	2	3	M8	Proper training. Foreknowledge of the chemicals concerned. Consult MSDS sheets attached. Adequate ventilation. Correct PPE.	2	1	L3	**CL**
6	In case of risks [1,2]	Chemical exposure to solvent – CO_2	1	3	M6	Proper training. Foreknowledge of the chemicals concerned. Consult MSDS sheets attached. Adequate ventilation. Correct PPE.	1	1	L1	**CL**

Table 49: Task risk assessment form completed to determine the hazards and risks related to unloading and cleaning the variable volume cells.

Ref No.	SPECIFIC TASK / ACTIVITY STEPS	IDENTIFY POTENTIAL HAZARDS	RISK RANKING			RISK CONTROL MEASURES • *Hierarchy of Control – Elimination, Substitution, Isolation, Engineering, Administration, Personal Protection.* • *Additional information can be attached.*	RESIDUAL RISK			Actioner / Initials
			Consequence	Likelihood	Risk Rating		Consequence	Likelihood	Residual Risk	
UNLOADING AND CLEANING										
1	Lifting or moving the heavy cell or low pressure chamber	Heavy loads – injury.	2	1	L3	Proper training. Use platforms provided. Ask for assistance.	2	1	L3	**CL**
2	Opening the cell to remove the solute and solvent	Chemical exposure to solvent – CO_2	1	3	M6	Proper training. Foreknowledge of the chemicals concerned. Consult MSDS sheets attached. Adequate ventilation. Correct PPE.	1	1	L1	**CL**
3	Opening the cell to remove the solute	Chemical exposure to solutes – 3,7-dimethyl-1-octanol + 1-decanol + n-dodecane	2	3	M8	Proper training. Foreknowledge of the chemicals concerned. Consult MSDS sheets attached. Adequate ventilation. Correct PPE.	2	1	L3	**CL**
4	Working with tools [e.g. spanners]	Incorrect tool use / tool failure - Injury	2	1	L3	Proper training. Using the correct tool for the job. Correct PPE.	2	1	L3	**CL**
5	Releasing pressure and opening the cell	High pressure – Gas leak	3	2	M9	Proper training and regular inspection. Regular testing of the equipment. Correct PPE.	2	1	L3	**CL**
6	Releasing pressure and opening the cell	High Pressure – Equipment Failure Causing Explosive Decompression	4	1	M10	Proper training and inspection. Regular testing. Safety in design. Correct PPE.	4	1	M10	**CL**
7	Releasing pressure and opening the cell	High Pressure – Uncontrolled Rapid Expansion.	2	3	M8	Proper training. Correct PPE.	2	3	M8	**CL**
8	Cool the cell and remove insulation + other equipment	High Heat – Burns.	2	2	L5	Equipment has built in safety. Proper training. Correct PPE.	2	1	L3	**CL**
9	Clean the cell and stirrer with isopropanol and methanol	Chemical exposure to cleaning agents – methanol and isopropanol	2	3	M8	Proper training. Foreknowledge of the chemicals concerned. Consult MSDS sheets attached. Adequate ventilation. Correct PPE.	2	1	L3	**CL**

A.3. Pressure calibration data

Pressure calibrations were performed every six months, using a dead weigh tester and the data gathered from the calibrations were used to correct the deviation between the actual and the displayed pressure. The pressure calibration data used to correct the data presented in this work is provided in Tables 50 to 52. From these tables, it is noted that the calibration data is dependent on temperature and pressure and therefore double linear interpolation was used to determine the pressure correction factor.

Table 50:Pressure calibration data set 1 for the large cell with temperature (T) in ºC and pressure (P) in bar [Calibrated in March 2016]

Dead Weight	T_{set} 1 = 34°C			T_{set} 2 = 45°C			T_{set} 3 = 53°C			T_{set} 4 = 62°C			T_{set} 5 = 71°C			T_{set} 6 = 80°C			T_{set} 7 = 90°C		
Pressure (bar)	P_{read}	T_{actual}	ΔP	P_{read}	T_{actual}	ΔP	P_{read}	T_{actual}	ΔP	P_{read}	T_{actual}	ΔP	P_{read}	T_{actual}	ΔP	P_{read}	T_{actual}	ΔP	P_{read}	T_{actual}	ΔP
35.0	28.2	32.8	6.8	28.0	42.9	7.0	29.5	50.4	5.5	28.7	58.6	6.3	30.6	67.3	4.4	31.0	75.7	4.0	31.3	85.1	3.7
50.0	42.9	32.8	7.1	42.8	42.9	7.2	44.2	50.3	5.8	43.7	58.6	6.3	44.7	67.3	5.3	45.7	75.7	4.3	46.2	85.1	3.8
65.0	56.8	32.8	8.2	57.0	42.9	8.0	58.7	50.3	6.3	58.5	58.6	6.5	59.7	67.3	5.3	60.2	75.7	4.8	60.9	85.1	4.1
79.9	72.0	32.8	7.9	71.9	42.9	8.0	73.3	50.3	6.6	73.2	58.6	6.7	74.3	67.3	5.6	74.8	75.7	5.1	75.5	85.1	4.4
94.9	86.6	32.8	8.3	86.2	42.9	8.7	87.9	50.3	7.0	88.0	58.6	6.9	88.7	67.4	6.2	89.6	75.7	5.3	90.3	85.1	4.6
109.9	101.3	32.8	8.6	101.5	42.9	8.4	102.7	50.3	7.2	102.9	58.6	7.0	103.9	67.4	6.0	104.4	75.7	5.5	105.1	85.1	4.8
124.9	115.7	32.8	9.2	116.4	42.9	8.5	117.5	50.4	7.4	117.8	58.6	7.1	118.8	67.4	6.1	119.3	75.7	5.6	120.0	85.1	4.9
139.9	130.6	32.8	9.3	131.2	42.9	8.7	132.5	50.3	7.4	132.8	58.7	7.1	133.8	67.4	6.1	134.3	75.7	5.6	135.0	85.1	4.9
154.9	146.0	32.8	8.9	146.2	42.9	8.7	147.5	50.3	7.4	147.9	58.6	7.0	148.8	67.4	6.1	149.3	75.7	5.6	150.0	85.1	4.9
169.9	161.0	32.8	8.9	161.6	42.9	8.3	162.4	50.3	7.5	163.0	58.6	6.9	163.6	67.4	6.3	164.4	75.7	5.5	165.1	85.1	4.8
184.8	175.9	32.8	8.9	176.6	42.9	8.2	177.5	50.3	7.3	178.1	58.6	6.7	178.7	67.4	6.1	179.5	75.7	5.3	180.2	85.1	4.6
199.8	191.1	32.8	8.7	191.8	43.0	8.0	192.7	50.3	7.1	193.2	58.7	6.6	194.1	67.4	5.7	194.6	75.7	5.2	195.3	85.1	4.5
214.8	206.1	32.8	8.7	206.9	43.0	7.9	207.7	50.3	7.1	208.4	58.7	6.4	209.2	67.4	5.6	209.8	75.8	5.0	210.4	85.1	4.4
229.8	221.1	32.8	8.7	222.0	43.0	7.8	222.9	50.3	6.9	223.5	58.7	6.3	224.4	67.4	5.4	224.9	75.8	4.9	225.6	85.1	4.2
244.8	236.3	32.8	8.5	237.3	43.0	7.5	238.0	50.3	6.8	238.7	58.7	6.1	239.5	67.4	5.3	240.1	75.8	4.7	240.8	85.1	4.0
259.8	251.5	32.8	8.3	252.5	43.0	7.3	253.2	50.3	6.6	253.9	58.7	5.9	254.7	67.4	5.1	255.3	75.8	4.5	256.0	85.1	3.8
274.7	266.7	32.8	8.0	267.7	43.0	7.0	268.4	50.3	6.3	269.2	58.7	5.5	269.9	67.4	4.8	270.5	75.8	4.2	271.2	85.1	3.5
289.7	281.8	32.8	7.9	282.9	43.0	6.8	283.6	50.3	6.1	284.4	58.7	5.3	285.1	67.4	4.6	285.7	75.8	4.0	286.4	85.1	3.3

Table 51: Pressure calibration data set 2 for the large cell with temperature (T) in ºC and pressure (P) in bar [Calibrated in October 2016]

Dead Weight	T_{set} 1 = 36°C			T_{set} 2 = 46°C			T_{set} 3 = 56°C			T_{set} 4 = 66°C			T_{set} 5 = 76°C			T_{set} 6 = 86°C			T_{set} 7 = 91°C		
Pressure (bar)	P_{read}	T_{actual}	ΔP	P_{read}	T_{actual}	ΔP	P_{read}	T_{actual}	ΔP	P_{read}	T_{actual}	ΔP	P_{read}	T_{actual}	ΔP	P_{read}	T_{actual}	ΔP	P_{read}	T_{actual}	ΔP
35.0	28.5	35.4	6.5	27.5	45.0	7.5	28.7	54.8	6.3	28.0	64.4	7.0	29.3	74.1	5.7	29.3	83.6	5.7	29.9	88.4	5.1
50.0	43.7	35.4	6.3	42.7	45.0	7.3	43.7	54.8	6.3	43.4	64.4	6.6	44.6	74.1	5.4	44.6	83.6	5.4	45.1	88.4	4.9
64.9	58.4	35.4	6.5	57.6	45.0	7.3	58.6	54.8	6.3	58.6	64.4	6.3	59.8	74.1	5.1	59.8	83.6	5.1	60.3	88.4	4.6
79.9	72.9	35.4	7.0	72.4	45.0	7.5	73.4	54.8	6.5	73.6	64.4	6.3	74.8	74.1	5.1	74.9	83.7	5.0	75.3	88.4	4.6
94.9	87.5	35.4	7.4	87.2	45.0	7.7	88.3	54.8	6.6	88.7	64.4	6.2	89.7	74.1	5.2	89.9	83.7	5.0	90.4	88.4	4.5
109.9	102.3	35.4	7.6	102.2	45.0	7.7	103.1	54.8	6.8	103.7	64.4	6.2	104.6	74.1	5.3	105.0	83.7	4.9	105.4	88.4	4.5
124.9	117.2	35.4	7.7	117.1	45.1	7.8	118.0	54.8	6.9	118.8	64.4	6.1	119.6	74.1	5.3	120.0	83.7	4.9	120.5	88.4	4.4
139.9	132.0	35.4	7.9	132.1	45.1	7.8	133.1	54.8	6.8	133.8	64.4	6.1	134.7	74.1	5.2	135.1	83.7	4.8	135.5	88.4	4.4
154.9	147.0	35.4	7.9	147.2	45.1	7.7	148.1	54.8	6.8	149.0	64.4	5.9	149.7	74.1	5.2	150.2	83.7	4.7	150.6	88.4	4.3
169.8	162.0	35.4	7.8	162.3	45.1	7.5	163.3	54.8	6.5	164.2	64.4	5.6	164.8	74.1	5.0	165.3	83.7	4.5	165.7	88.4	4.1
184.8	177.1	35.4	7.7	177.5	45.1	7.3	178.3	54.8	6.5	179.3	64.4	5.5	179.9	74.1	4.9	180.3	83.7	4.5	180.9	88.4	3.9
199.8	192.1	35.5	7.7	192.6	45.1	7.2	193.5	54.8	6.3	194.5	64.4	5.3	195.1	74.1	4.7	195.6	83.7	4.2	196.0	88.4	3.8
214.8	207.3	35.5	7.5	207.8	45.1	7.0	208.7	54.8	6.1	209.6	64.4	5.2	210.2	74.1	4.6	210.7	83.7	4.1	211.2	88.4	3.6
229.8	222.3	35.5	7.5	223.0	45.1	6.8	223.9	54.8	5.9	224.9	64.4	4.9	225.4	74.1	4.4	226.0	83.7	3.8	226.4	88.4	3.4
244.8	237.5	35.5	7.3	238.2	45.1	6.6	239.1	54.8	5.7	240.1	64.4	4.7	240.6	74.1	4.2	241.2	83.7	3.6	241.5	88.4	3.3
259.7	252.6	35.5	7.1	253.4	45.1	6.3	254.3	54.8	5.4	255.3	64.4	4.4	255.8	74.1	3.9	256.4	83.7	3.3	256.7	88.4	3.0
274.7	267.8	35.5	6.9	268.6	45.1	6.1	269.5	54.8	5.2	270.5	64.4	4.2	271.0	74.1	3.7	271.6	83.7	3.1	271.9	88.4	2.8
289.7	283.0	35.5	6.7	283.8	45.1	5.9	284.7	54.8	5.0	285.8	64.4	3.9	286.2	74.1	3.5	286.9	83.7	2.8	287.2	88.4	2.5

Table 52: Pressure calibration data set 1 for the small cell with temperature (T) in ºC and pressure (P) in bar [Calibrated in August 2016]

Dead Weight	T_{set} 1 = 35°C			T_{set} 2 = 45°C			T_{set} 3 = 55°C			T_{set} 4 = 65°C			T_{set} 5 = 73°C			T_{set} 6 = 83°C			T_{set} 7 = 89°C		
Pressure (bar)	P_{read}	T_{actual}	ΔP	P_{read}	T_{actual}	ΔP	P_{read}	T_{actual}	ΔP	P_{read}	T_{actual}	ΔP	P_{read}	T_{actual}	ΔP	P_{read}	T_{actual}	ΔP	P_{read}	T_{actual}	ΔP
35.0	36.2	34.0	-1.2	36.1	43.8	-1.1	36.7	53.5	-1.7	37.6	63.1	-2.6	38.1	70.9	-3.1	38.2	80.3	-3.2	38.5	86.2	-3.5
50.0	51.0	34.1	-1.0	51.1	43.8	-1.1	51.9	53.5	-1.9	52.7	63.1	-2.7	38.1	70.9	-11.9	53.3	80.3	-3.3	53.6	86.2	-3.6
65.0	65.7	34.1	-0.7	66.2	43.8	-1.2	66.9	53.5	-1.9	67.7	63.1	-2.7	38.1	70.9	-26.9	68.4	80.4	-3.4	68.7	86.2	-3.7
79.9	80.8	34.1	-0.9	81.2	43.8	-1.3	81.9	53.5	-2.0	82.7	63.2	-2.8	38.1	70.9	-41.8	83.4	80.4	-3.5	83.7	86.2	-3.8
94.9	95.7	34.1	-0.8	96.2	43.8	-1.3	96.9	53.5	-2.0	97.8	63.2	-2.9	38.1	70.9	-56.8	98.4	80.4	-3.5	98.7	86.2	-3.8
109.9	110.7	34.1	-0.8	111.2	43.9	-1.3	112.0	53.5	-2.1	112.8	63.2	-2.9	38.1	70.9	-71.8	113.4	80.4	-3.5	113.6	86.2	-3.7
124.9	125.8	34.2	-0.9	126.3	43.9	-1.4	126.9	53.5	-2.0	127.8	63.2	-2.9	38.1	70.9	-86.8	128.4	80.4	-3.5	128.6	86.2	-3.7
139.9	140.7	34.1	-0.8	141.3	43.9	-1.4	141.9	53.5	-2.0	142.8	63.2	-2.9	38.1	70.9	-101.8	143.4	80.4	-3.5	143.7	86.2	-3.8
154.9	155.7	34.2	-0.8	156.3	43.9	-1.4	157.0	53.5	-2.1	157.8	63.2	-2.9	38.1	70.9	-116.8	158.4	80.4	-3.5	158.7	86.2	-3.8
169.9	170.7	34.2	-0.8	171.4	43.9	-1.5	172.1	53.5	-2.2	172.8	63.2	-2.9	38.1	70.9	-131.8	173.5	80.4	-3.6	173.7	86.2	-3.8
184.8	185.8	34.2	-1.0	186.4	43.9	-1.6	187.1	53.5	-2.3	187.9	63.2	-3.1	38.1	70.9	-146.7	188.5	80.4	-3.7	188.8	86.2	-4.0
199.8	200.8	34.2	-1.0	201.5	43.9	-1.7	202.1	53.5	-2.3	202.9	63.2	-3.1	38.1	70.9	-161.7	203.5	80.4	-3.7	203.8	86.2	-4.0
214.8	215.0	34.3	-0.2	216.6	43.9	-1.8	217.2	53.5	-2.4	218.0	63.2	-3.2	38.1	70.9	-176.7	218.6	80.4	-3.8	218.8	86.2	-4.0
229.8	230.9	34.3	-1.1	231.6	43.9	-1.8	232.3	53.5	-2.5	233.0	63.2	-3.2	38.1	70.9	-191.7	233.6	80.4	-3.8	233.9	86.2	-4.1
244.8	245.9	34.3	-1.1	246.7	43.9	-1.9	247.3	53.5	-2.5	248.1	63.2	-3.3	38.1	70.9	-206.7	248.7	80.4	-3.9	248.9	86.2	-4.1
259.8	260.9	34.3	-1.1	261.7	43.9	-1.9	260.5	53.5	-0.7	263.1	63.2	-3.3	38.1	70.9	-221.7	263.7	80.4	-3.9	263.9	86.2	-4.1
274.7	276.0	34.3	-1.3	276.7	43.9	-2.0	277.4	53.5	-2.7	278.1	63.2	-3.4	38.1	70.9	-236.6	278.7	80.4	-4.0	279.0	86.2	-4.3
289.7	291.0	34.3	-1.3	291.7	43.9	-2.0	292.4	53.6	-2.7	293.1	63.2	-3.4	38.1	70.9	-251.6	293.7	80.4	-4.0	293.9	86.2	-4.2

A.4. Temperature calibration data

The temperature probes were calibrated by Thermon South Africa (Pty) Ltd., which is a South African National Accreditation System (SANAS) approved institute. The calibrations were performed at five temperatures between 30ºC and 200ºC. The calibration certificates for the three Pt100 probes used in the experiments, along with the temperature correction correlations developed using the data are presented in this appendix.

Pt100-large connected to the small equilibrium cell

Thermon
South Africa (Pty) Ltd.

unitemp

Calibration certificate CAL-UC-S-T-160301X04
certificate number

sanas Calibration Laboratory
1573, 373

Lab measurement equipment with certified traceability to international standards

Description	Cert. No.	Equipment. Number
Testo 400 with PT100 probe	TH\DG-6754	Unitemp4

Ambient conditions.

Temperature: 23 °C ± 5 °C

Measuring procedure (P0051)

The measurements read on this test item, in a thermostatic bath, were obtained while placed in very close proximity of a reference probe.

The result is calculated from an average of ***6*** *readings @* ***30*** *seconds intervals*

Measurement results for hi-accuracy digital thermometer with 1/10 4-wire-Pt100 external probe

Indication from reference in °C	Indication from your measuring instrument in °C	**Deviation in °C**	Manufacture's allowed tolerance in °C	Expanded uncertainty of measurement in °C	Probe insertion depth in mm	Reference Equipment Used
30.110	29.24	**-0.87**	n/a	± 0.05	118	Unitemp4
60.108	59.27	**-0.84**	n/a	± 0.05	72	Unitemp4
90.192	89.38	**-0.81**	n/a	± 0.05	75	Unitemp4
140.163	138.96	**-1.20**	n/a	± 0.05	121	Unitemp4
200.077	198.76	**-1.32**	n/a	± 0.05	60	Unitemp4

Validity of Certificate

The measurement results recorded in this certificate relate only to the instrument & attachments specified, and were correct at the time. Only the above points have been checked & performance at other points is not certain. Subsequent accuracy will depend on factors such as care, handling and frequency of use. It is recommended that recalibration be undertaken at an interval that will ensure that the instrument remains within the desired limits.

CALIBRATION LABORATORY
THERMON SA (Pty) Ltd.
2016 -03- 0 3
CAPE TOWN

page 2 of 2

END

Calibration • Validation • Training

Email: sales.za@thermon.com **Web:** www.thermon.co.za

Thermon South Africa (Pty) Ltd. Reg. No. 2015/020118/07, VAT No. 4750268387, **Directors**: G.P. Alexander, R.L. Bingham, J.C. Peterson

Temperature correction correlation for 30ºC < T < 90 ºC:

$T_{actual}(^0C) = 0.999T_{read}(^0C) + 0.897$

Pt100-small connected to the large equilibrium cell

Thermon
South Africa (Pty) Ltd.

unitemp

Calibration certificate CAL-UC-S-T-160301X05
certificate number

sanas Calibration Laboratory
1573, 373

Lab measurement equipment with certified traceability to international standards

Description	Cert. No.	Equipment. Number
Testo 400 with PT100 probe	TH\DG-6754	Unitemp4

Ambient conditions.
Temperature: 23 °C ± 5 °C

Measuring procedure (P0051)
The measurements read on this test item, in a thermostatic bath, were obtained while placed in very close proximity of a reference probe.

The result is calculated from an average of ***6*** *readings @* ***30*** *seconds intervals*

Measurement results for hi-accuracy digital thermometer with 1/10 4-wire-Pt100 external probe

Indication from reference in °C	Indication from your measuring instrument in °C	Deviation in °C	Manufacture's allowed tolerance in °C	Expanded uncertainty of measurement in °C	Probe insertion depth in mm	Reference Equipment Used
30.102	29.9	**-0.2**	n/a	± 0.2	70	Unitemp4
60.108	60.1	**0.0**	n/a	± 0.2	72	Unitemp4
90.192	90.2	**0.0**	n/a	± 0.2	75	Unitemp4
140.077	139.9	**-0.2**	n/a	± 0.2	73	Unitemp4
200.095	199.7	**-0.4**	n/a	± 0.2	60	Unitemp4

Validity of Certificate
The measurement results recorded in this certificate relate only to the instrument & attachments specified, and were correct at the time. Only the above points have been checked & performance at other points is not certain. Subsequent accuracy will depend on factors such as care, handling and frequency of use. It is recommended that recalibration be undertaken at an interval that will ensure that the instrument remains within the desired limits.

CALIBRATION LABORATORY
THERMON SA (Pty) Ltd.
2016 -03- 03
CAPE TOWN

page 2 of 2

END

Calibration • Validation • Training

Email: sales.za@thermon.com **Web**: www.thermon.co.za

Thermon South Africa (Pty) Ltd. Reg. No. 2015/020118/07, VAT No. 4750268387, **Directors**: G.P. Alexander, R.L. Bingham, J.C. Peterson

Temperature correction correlation for 30ºC < T < 90 ºC:
$T_{actual}\,(^0C) = 0.997T_{read}(^0C) + 0.277$

Handheld Pt100-probe

Thermon
South Africa (Pty) Ltd.

unitemp

Calibration certificate CAL-UC-S-T-160301X03
certificate number

sanas Calibration Laboratory
1573, 373

Lab measurement equipment with certified traceability to international standards

Description	Cert. No.	Equipment. Number
Testo 400 with PT100 probe	TH\DG-6754	Unitemp4

Ambient conditions.

Temperature: 23 °C ± 5 °C

Measuring procedure (P0051)

The measurements read on this test item, in a thermostatic bath, were obtained while placed in very close proximity of a reference probe.

The result is calculated from an average of ***6*** *readings @* ***30*** *seconds intervals*

Measurement results for hi-accuracy digital thermometer with 2-wire-Pt100 probe

Indication from reference in °C	Indication from your measuring instrument in °C	Deviation in °C	Manufacture's allowed tolerance in °C	Expanded uncertainty of measurement in °C	Probe insertion depth in mm	Reference Equipment Used
30.106	30.4	**0.3**	n/a	± 0.2	105	Unitemp4
60.149	60.5	**0.4**	n/a	± 0.2	108	Unitemp4
90.197	90.6	**0.4**	n/a	± 0.2	110	Unitemp4
140.169	140.7	**0.5**	n/a	± 0.2	100	Unitemp4
200.090	200.5	**0.4**	n/a	± 0.2	60	Unitemp4

Validity of Certificate

The measurement results recorded in this certificate relate only to the instrument & attachments specified, and were correct at the time. Only the above points have been checked & performance at other points is not certain. Subsequent accuracy will depend on factors such as care, handling and frequency of use. It is recommended that recalibration be undertaken at an interval that will ensure that the instrument remains within the desired limits.

CALIBRATION LABORATORY
THERMON SA (Pty) Ltd.
2016 -03- 03
CAPE TOWN

page 2 of 2

END

Calibration • Validation • Training

Email: sales.za@thermon.com **Web**: www.thermon.co.za

Thermon South Africa (Pty) Ltd. Reg. No. 2015/020118/07, VAT No. 4750268387, **Directors**: G.P. Alexander, R.L. Bingham, J.C. Peterson

Temperature correction correlation for 30ºC < T < 90 ºC:

$T_{actual}\,(^0C) = 0.998T_{read}(^0C) - 0.240$

B. Bubble- and Dew-points Experimental Data

The experimental bubble- and dew-point data for the following ternary and quaternary systems is presented in this appendix:

- CO_2 + (n-dodecane + 3,7-dimethyl-1-octanol)
- CO_2 + (3,7-dimethyl-1-octanol + 1-decanol)
- CO_2 + (n-dodecane + 3,7-dimethyl-1-octanol + 1-decanol)

Table 53: Experimental bubble- and dew-point data for the CO_2 + (50 wt% n-dodecane + 50 wt% 3,7-dimethyl-1-octanol) system, measured by N.S. Mabena.

Run	Cell	Thermocouple	Mass Fraction	Pressure			Temperature		
				Measured (barg)	Correction factor	Corrected (bar abs)	Measured (°C)	Corrected (°C)	Converted (K)
1	Large	Pt100-small	0.625	56.9	8.1	66.0	35.9	36.1	309.2
				69.3	7.5	77.8	45.5	45.6	318.7
				81.9	6.9	89.8	55.0	55.1	328.2
				95.5	6.4	102.9	64.7	64.8	337.9
				105.7	5.6	112.3	74.3	74.3	347.4
2	Large	Pt100-small	0.530	62.1	8.0	71.1	36.0	36.2	309.3
				76.8	7.7	85.5	45.6	45.7	318.8
				91.3	7.0	99.3	55.3	55.4	328.5
				105.9	6.3	113.2	64.9	65.0	338.1
				120.2	5.7	126.9	74.6	74.6	347.7
3	Large	Pt100-small	0.453	62.5	8.0	71.5	35.8	36.0	309.1
				79.0	7.8	87.8	45.4	45.5	318.6
				96.0	7.0	104.0	54.9	55.0	328.1
				112.8	6.4	120.2	64.4	64.5	337.6
				128.6	5.7	135.3	74.0	74.0	347.1
4	Large	Pt100-small	0.380	62.5	8.0	71.5	35.8	36.0	309.1
				80.0	7.9	88.9	45.2	45.3	318.4
				99.1	7.1	107.2	54.8	54.9	328.0
				117.6	6.4	125.0	64.3	64.4	337.5
				134.6	5.7	141.3	73.9	73.9	347.0
5	Large	Pt100-small	0.290	65.4	8.0	74.4	35.5	35.7	308.8
				83.5	8.1	92.6	45.0	45.1	318.2
				104.6	7.1	112.7	54.6	54.7	327.8
				123.8	6.5	131.3	64.1	64.2	337.3
				141.5	5.7	148.2	73.5	73.5	346.6
6	Large	Pt100-small	0.235	65.7	8.0	74.7	35.4	35.6	308.7
				84.9	8.2	94.1	44.9	45.0	318.1
				105.9	7.1	114.0	54.4	54.5	327.6
				124.6	6.5	132.1	64.0	64.1	337.2
				142.6	5.7	149.3	73.4	73.4	346.5

Table 53 continued: Experimental bubble- and dew-point data for the CO_2 + (50 wt% n-dodecane + 50 wt% 3,7-dimethyl-1-octanol) system, measured by N.S. Mabena.

Run	Cell	Thermocouple	Mass Fraction	Pressure			Temperature		
				Measured (barg)	Correction factor	Corrected (bar abs)	Measured (°C)	Corrected (°C)	Converted (K)
7	Large	Pt100-small	0.173	65.5	8.0	74.5	35.4	35.6	308.7
				85.6	8.2	94.8	45.0	45.1	318.2
				106.6	7.1	114.7	54.5	54.6	327.7
				125.4	6.5	132.9	63.9	64.0	337.1
				141.9	5.7	148.6	73.3	73.3	346.4
8	Large	Pt100-small	0.131	67.2	8.0	76.2	35.4	35.6	308.7
				86.7	8.2	95.9	44.8	44.9	318.0
				106.9	7.2	115.1	54.2	54.3	327.4
				124.8	6.5	132.3	63.4	63.5	336.6
				140.6	5.7	147.3	73.2	73.2	346.3
9	Large	Pt100-small	0.078	67.6	8.0	76.6	35.6	35.8	308.9
				86.2	8.2	95.4	45.1	45.2	318.3
				105.9	7.1	114.0	54.6	54.7	327.8
				123.4	6.4	130.8	64.2	64.3	337.4
				138.4	5.7	145.1	73.8	73.8	346.9
10	Large	Pt100-small	0.052	68.7	8.0	77.7	35.9	36.1	309.2
				86.1	8.1	95.2	45.5	45.6	318.7
				104.0	7.1	112.1	55.1	55.2	328.3
				118.7	6.4	126.1	64.7	64.8	337.9
				132.2	5.7	138.9	74.2	74.2	347.3
11	Large	Pt100-small	0.030	69.2	8.0	78.2	35.5	35.7	308.8
				84.7	8.1	93.8	45.0	45.1	318.2
				100.7	7.1	108.8	54.5	54.6	327.7
				114.3	6.5	121.8	64.0	64.1	337.2
				125.2	5.7	131.9	73.5	73.5	346.6
12	Large	Pt100-small	0.016	68.1	8.0	77.1	35.6	35.8	308.9
				82.8	8.0	91.8	45.1	45.2	318.3
				96.5	7.0	104.5	54.6	54.7	327.8
				107.6	6.4	115.0	64.2	64.3	337.4
				114.3	5.7	121.0	73.8	73.8	346.9

Table 54: Experimental bubble- and dew-point data for the CO_2 + (75 wt% n-dodecane + 25 wt% 3,7-dimethyl-1-octanol) system, measured by N.S. Mabena.

Run	Cell	Thermocouple	Mass Fraction	Pressure			Temperature		
				Measured (barg)	Correction factor	Corrected (bar abs)	Measured (°C)	Corrected (°C)	Converted (K)
1	Large	Pt100-small	0.620	55.2	8.0	64.2	35.8	36.0	309.1
				66.7	7.5	75.2	45.3	45.4	318.5
				78.1	6.8	85.9	54.9	55.0	328.1
				89.2	6.5	96.7	64.4	64.5	337.6
				100.6	5.6	107.2	73.9	73.9	347.0
2	Large	Handheld probe	0.537	59.2	8.1	68.3	36.7	36.4	309.5
				72.5	7.4	80.9	46.5	46.2	319.3
				86.0	6.9	93.9	56.2	55.9	329.0
				98.2	6.3	105.5	65.9	65.5	338.6
				111.2	5.6	117.8	75.6	75.2	348.3
3	Large	Handheld probe	0.448	61.4	8.0	70.4	36.7	36.4	309.5
				76.2	7.6	84.8	46.4	46.1	319.2
				91.4	7.0	99.4	56.1	55.8	328.9
				106.4	6.3	113.7	65.8	65.4	338.5
				120.6	5.6	127.2	75.5	75.1	348.2
4	Large	Handheld probe	0.384	63.5	8.0	72.5	36.6	36.3	309.4
				78.5	7.7	87.2	46.5	46.2	319.3
				95.4	7.0	103.4	56.2	55.9	329.0
				112.0	6.3	119.3	65.9	65.5	338.6
				127.7	5.6	134.3	75.6	75.2	348.3
5	Small	Handheld probe	0.243	72.0	-0.9	72.1	35.6	35.3	308.4
				89.0	-1.4	88.6	45.2	44.9	318.0
				108.3	-2.2	107.1	54.9	54.6	327.7
				127.1	-2.9	125.2	64.9	64.5	337.6
				143.9	-3.1	141.8	73.6	73.2	346.3
6	Small	Handheld probe	0.197	73.0	-0.9	73.1	35.6	35.3	308.4
				90.0	-1.4	89.6	45.3	45.0	318.1
				109.9	-2.2	108.7	55.1	54.8	327.9
				129.0	-2.9	127.1	64.6	64.2	337.3
				146.4	-3.2	144.2	74.3	73.9	347.0

Table 54 continued: Experimental bubble- and dew-point data for the CO_2 + (75wt% n-dodecane + 25 wt% 3,7-dimethyl-1-octanol) system, measured by N.S. Mabena.

Run	Cell	Thermocouple	Mass Fraction	Pressure			Temperature		
				Measured (barg)	Correction factor	Corrected (bar abs)	Measured (°C)	Corrected (°C)	Converted (K)
7	Small	Handheld probe	0.135	73.9	-0.9	74.0	35.7	35.4	308.5
				90.8	-1.4	90.4	45.4	45.1	318.2
				110.6	-2.2	109.4	55.0	54.7	327.8
				128.5	-2.9	126.6	64.6	64.2	337.3
				145.8	-3.2	143.6	74.5	74.1	347.2
8	Small	Handheld probe	0.088	74.3	-0.9	74.4	35.6	35.3	308.4
				91.1	-1.4	90.7	45.2	44.9	318.0
				110.3	-2.2	109.1	55.0	54.7	327.8
				128.7	-2.9	126.8	64.6	64.2	337.3
				144.7	-3.1	142.6	74.2	73.8	346.9
9	Small	Handheld probe	0.053	75.9	-0.9	76.0	35.4	35.1	308.2
				92.1	-1.3	91.8	45.1	44.8	317.9
				110.0	-2.2	108.8	54.7	54.4	327.5
				126.6	-2.9	124.7	64.3	63.9	337.0
				139.9	-3.1	137.8	73.9	73.5	346.6
10	Small	Handheld probe	0.031	76.2	-0.9	76.3	35.4	35.1	308.2
				91.2	-1.3	90.9	44.9	44.6	317.7
				107.0	-2.1	105.9	54.8	54.5	327.6
				119.2	-2.9	117.3	64.4	64.0	337.1
				128.8	-3.0	126.8	74.1	73.7	346.8
11	Small	Handheld probe	0.015	77.0	-0.9	77.1	35.6	35.3	308.4
				90.1	-1.3	89.8	45.1	44.8	317.9
				101.8	-2.1	100.7	54.9	54.6	327.7
				109.8	-2.9	107.9	64.3	63.9	337.0
				118.9	-2.9	117.0	73.9	73.5	346.6

Table 55: Experimental bubble- and dew-point data for the CO_2 + (85 wt% n-dodecane + 15 wt% 3,7-dimethyl-1-octanol) system, measured by N.S. Mabena.

Run	Cell	Thermocouple	Mass Fraction	Pressure			Temperature		
				Measured (barg)	Correction factor	Corrected (bar abs)	Measured (°C)	Corrected (°C)	Converted (K)
1	Small	Handheld probe	0.573	62.7	-0.9	62.8	35.5	35.2	308.3
				74.2	-1.3	73.9	45.2	44.9	318.0
				86.0	-2.1	84.9	54.8	54.5	327.6
				97.2	-2.8	95.4	64.5	64.1	337.2
				106.8	-2.7	105.1	74.1	73.7	346.8
2	Small	Handheld probe	0.493	67.5	-0.8	67.7	35.5	35.2	308.3
				80.5	-1.3	80.2	44.7	44.4	317.5
				93.6	-2.0	92.6	54.0	53.7	326.8
				107.0	-2.9	105.1	63.3	62.9	336.0
				120.1	-2.7	118.4	72.6	72.2	345.3
3	Small	Handheld probe	0.363	70.9	-0.8	71.1	35.6	35.3	308.4
				86.5	-1.4	86.1	45.4	45.1	318.2
				102.9	-2.1	101.8	55.0	54.7	327.8
				120.0	-2.9	118.1	64.7	64.3	337.4
				136.4	-3.0	134.4	74.3	73.9	347.0
4	Small	Handheld probe	0.331	71.9	-0.9	72.0	35.6	35.3	308.4
				87.1	-1.3	86.8	45.2	44.9	318.0
				104.2	-2.1	103.1	54.6	54.3	327.4
				121.9	-2.9	120.0	64.3	63.9	337.0
				138.9	-3.0	136.9	74.0	73.6	346.7
5	Small	Handheld probe	0.254	71.7	-0.8	71.9	35.5	35.2	308.3
				88.8	-1.4	88.4	45.2	44.9	318.0
				107.4	-2.1	106.3	54.2	53.9	327.0
				126.7	-2.9	124.8	64.2	63.8	336.9
				144.3	-3.1	142.2	73.8	73.4	346.5
6	Small	Handheld probe	0.243	72.8	-0.9	72.9	35.7	35.4	308.5
				89.3	-1.4	88.9	45.3	45.0	318.1
				108.3	-2.2	107.1	55.0	54.7	327.8
				126.2	-2.9	124.3	64.6	64.2	337.3
				143.9	-3.1	141.8	73.6	73.2	346.3

Table 55 continued: Experimental bubble- and dew-point data for the CO_2 + (85wt% n-dodecane + 15 wt% 3,7-dimethyl-1-octanol) system, measured by N.S. Mabena.

Run	Cell	Thermocouple	Mass Fraction	Pressure			Temperature		
				Measured (barg)	Correction factor	Corrected (bar abs)	Measured (°C)	Corrected (°C)	Converted (K)
7	Small	Handheld probe	0.179	73.1	-0.9	73.2	35.8	35.5	308.6
				90.3	-1.4	89.9	45.3	45.0	318.1
				110.3	-2.2	109.1	55.0	54.7	327.8
				129.0	-2.9	127.1	64.7	64.3	337.4
				146.0	-3.1	143.9	74.3	73.9	347.0
8	Small	Handheld probe	0.120	73.5	-0.9	73.6	35.4	35.1	308.2
				90.5	-1.4	90.1	45.2	44.9	318.0
				109.9	-2.2	108.7	54.7	54.4	327.5
				128.3	-2.9	126.4	64.2	63.8	336.9
				144.9	-3.1	142.8	74.5	74.1	347.2
9	Small	Handheld probe	0.090	73.8	-0.9	73.9	35.6	35.3	308.4
				90.6	-1.4	90.2	45.2	44.9	318.0
				109.5	-2.1	108.4	54.6	54.3	327.4
				127.5	-2.9	125.6	64.0	63.6	336.7
				143.8	-3.1	141.7	73.9	73.5	346.6
10	Small	Handheld probe	0.047	75.3	-0.9	75.4	35.6	35.3	308.4
				90.6	-1.3	90.3	45.0	44.7	317.8
				107.2	-2.1	106.1	54.7	54.4	327.5
				122.2	-2.9	120.3	64.1	63.7	336.8
				134.5	-3.0	132.5	73.9	73.5	346.6
11	Small	Handheld probe	0.017	76.7	-0.9	76.8	35.6	35.3	308.4
				90.0	-1.4	89.6	45.2	44.9	318.0
				101.7	-2.1	100.6	54.8	54.5	327.6
				112.9	-2.8	111.1	64.5	64.1	337.2
				118.5	-2.8	116.7	73.6	73.2	346.3

Table 56: Experimental bubble- and dew-point data for the CO_2 + (75 wt% 3,7-dimethyl-1-octanol + 15 wt% 1-decanol) system, measured by N. Schonegevel.

Run	Cell	Thermocouple	Mass Fraction	Pressure			Temperature		
				Measured (barg)	Correction factor	Corrected (bar abs)	Measured (°C)	Corrected (°C)	Converted (K)
1	Large	Handheld probe	0.605	68.2	6.9	76.1	35.9	35.6	308.7
				85.7	7.7	94.4	45.6	45.3	318.4
				101.7	6.8	109.5	55.4	55.1	328.2
				116.8	6.1	123.9	65.1	64.7	337.8
				130.0	5.2	136.2	74.9	74.5	347.6
				141.5	4.7	147.2	84.6	84.2	357.3
2	Large	Handheld probe	0.497	110.3	7.6	118.9	35.9	35.6	308.7
				117.0	7.8	125.8	45.5	45.2	318.3
				124.6	6.8	132.4	55.3	55.0	328.1
				139.6	6.0	146.6	65.1	64.7	337.8
				154.0	5.1	160.1	74.8	74.4	347.5
				167.1	4.5	172.6	84.6	84.2	357.3
3	Large	Handheld probe	0.412	131.7	7.9	140.6	35.9	35.6	308.7
				133.8	7.7	142.5	45.6	45.3	318.4
				143.8	6.7	151.5	55.4	55.1	328.2
				156.4	5.7	163.1	65.1	64.7	337.8
				169.3	5.0	175.3	75.0	74.6	347.7
				181.5	4.4	186.9	84.7	84.3	357.4
4	Large	Handheld probe	0.345	141.4	7.9	150.3	35.9	35.6	308.7
				141.9	7.7	150.6	45.6	45.3	318.4
				151.4	6.7	159.1	55.3	55.0	328.1
				163.9	5.6	170.5	65.0	64.6	337.7
				176.6	4.9	182.5	74.9	74.5	347.6
				188.7	4.3	194.0	84.7	84.3	357.4
5	Large	Handheld probe	0.293	142.2	7.9	151.1	35.9	35.6	308.7
				142.3	7.7	151.0	45.6	45.3	318.4
				151.7	6.7	159.4	55.3	55.0	328.1
				164.4	5.6	171.0	65.0	64.6	337.7
				178.6	4.9	184.5	74.8	74.4	347.5
				191.2	4.2	196.4	84.6	84.2	357.3

Table 56 continued: Experimental bubble- and dew-point data for the CO_2 + (75wt% 3,7-dimethyl-1-octanol + 15 wt% 1-decanol) system, measured by N. Schonegevel.

Run	Cell	Thermocouple	Mass Fraction	Pressure			Temperature		
				Measured (barg)	Correction factor	Corrected (bar abs)	Measured (°C)	Corrected (°C)	Converted (K)
6	Large	Handheld probe	0.235	142.6	7.9	151.5	35.9	35.6	308.7
				142.3	7.7	151.0	45.6	45.3	318.4
				153.2	6.7	160.9	55.3	55.0	328.1
				166.1	5.6	172.7	65.0	64.6	337.7
				179.2	4.9	185.1	74.8	74.4	347.5
				191.2	4.2	196.4	84.6	84.2	357.3
7	Large	Handheld probe	0.229	143.1	7.9	152.0	35.8	35.5	308.6
				143.9	7.7	152.6	45.6	45.3	318.4
				153.9	6.6	161.5	55.3	55.0	328.1
				166.4	5.6	173.0	65.0	64.6	337.7
				179.2	4.9	185.1	74.7	74.3	347.4
				191.5	4.3	196.8	84.5	84.1	357.2
8	Large	Handheld probe	0.184	139.4	7.9	148.3	35.9	35.6	308.7
				141.3	7.7	150.0	45.6	45.3	318.4
				151.5	6.7	159.2	55.3	55.0	328.1
				164.6	5.6	171.2	65.2	64.8	337.9
				178.0	4.9	183.9	74.9	74.5	347.6
				190.3	4.3	195.6	84.7	84.3	357.4
9	Large	Handheld probe	0.131	127.3	7.8	136.1	35.9	35.6	308.7
				134.4	7.7	143.1	45.5	45.2	318.3
				146.9	6.7	154.6	55.3	55.0	328.1
				160.7	5.7	167.4	65.1	64.7	337.8
				174.5	4.9	180.4	74.9	74.5	347.6
				187.0	4.3	192.3	84.7	84.3	357.4
10	Large	Handheld probe	0.085	102.6	7.6	111.2	35.9	35.6	308.7
				117.4	7.8	126.2	45.6	45.3	318.4
				133.6	6.7	141.3	55.4	55.1	328.2
				150.1	5.8	156.9	65.1	64.7	337.8
				164.1	5.0	170.1	74.9	74.5	347.6
				175.6	4.4	181.0	84.8	84.4	357.5

Table 56 continued: Experimental bubble- and dew-point data for the CO_2 + (75 wt% 3,7-dimethyl-1-octanol + 15 wt% 1-decanol) system, measured by N. Schonegevel.

Run	Cell	Thermocouple	Mass Fraction	Pressure			Temperature		
				Measured (barg)	Correction factor	Corrected (bar abs)	Measured (°C)	Corrected (°C)	Converted (K)
11	Large	Handheld probe	0.054	82.3	7.3	90.6	35.9	35.6	308.7
				101.6	7.7	110.3	45.5	45.2	318.3
				119.6	6.9	127.5	55.3	55.0	328.1
				135.8	6.0	142.8	65.1	64.7	337.8
				151.0	5.1	157.1	74.9	74.5	347.6
				164.2	4.5	169.7	84.7	84.3	357.4
12	Large	Handheld probe	0.032	70.6	7.0	78.6	35.7	35.4	308.5
				92.4	7.7	101.1	45.4	45.1	318.2
				111.5	6.8	119.3	55.3	55.0	328.1
				127.7	6.1	134.8	64.9	64.5	337.6
				139.9	5.2	146.1	74.8	74.4	347.5
				150.7	4.6	156.3	84.6	84.2	357.3
13	Large	Handheld probe	0.017	69.6	6.9	77.5	35.7	35.4	308.5
				88.4	7.7	97.1	45.7	45.4	318.5
				105.1	6.8	112.9	55.4	55.1	328.2
				118.2	6.1	125.3	65.1	64.7	337.8
				128.5	5.2	134.7	74.7	74.3	347.4
				135.9	4.7	141.6	84.6	84.2	357.3

Table 57: Experimental bubble- and dew-point data for the CO_2 + (50 wt% 3,7-dimethyl-1-octanol + 50 wt% 1-decanol) system, measured by N. Schonegevel

Run	Cell	Thermocouple	Mass Fraction	Pressure			Temperature		
				Measured (barg)	Correction factor	Corrected (bar abs)	Measured (°C)	Corrected (°C)	Converted (K)
1	Large	Handheld probe	0.596	85.0	7.4	93.4	35.9	35.6	308.7
				95.8	7.7	104.5	45.6	45.3	318.4
				110.5	6.8	118.3	55.3	55.0	328.1
				123.7	6.0	130.7	65.2	64.8	337.9
				137.0	5.6	143.6	74.8	74.4	347.5
				148.6	4.6	154.2	84.6	84.2	357.3
2	Large	Handheld probe	0.499	130.1	7.8	138.9	35.9	35.6	308.7
				127.7	7.8	136.5	45.6	45.3	318.4
				136.6	6.7	144.3	55.3	55.0	328.1
				148.7	5.8	155.5	65.1	64.7	337.8
				161.3	5.0	167.3	74.9	74.5	347.6
				173.1	4.5	178.6	84.6	84.2	357.3
3	Large	Handheld probe	0.414	171.4	7.8	180.2	35.9	35.6	308.7
				156.6	7.6	165.2	45.6	45.3	318.4
				159.2	6.6	166.8	55.3	55.0	328.1
				168.1	5.6	174.7	65.1	64.7	337.8
				179.0	4.9	184.9	74.9	74.5	347.6
				189.9	4.3	195.2	84.7	84.3	357.4
4	Large	Handheld probe	0.350	183.9	7.7	192.6	35.9	35.6	308.7
				165.4	7.5	173.9	45.6	45.3	318.4
				166.8	6.5	174.3	55.4	55.1	328.2
				174.9	5.5	181.4	65.1	64.7	337.8
				185.6	4.8	191.4	75.0	74.6	347.7
				196.3	4.2	201.5	84.6	84.2	357.3
5	Large	Handheld probe	0.266	189.2	7.7	197.9	35.9	35.6	308.7
				169.1	7.4	177.5	45.6	45.3	318.4
				169.7	6.5	177.2	55.3	55.0	328.1
				177.7	5.5	184.2	65.1	64.7	337.8
				188.0	4.8	193.8	74.8	74.4	347.5
				199.0	4.1	204.1	84.6	84.2	357.3

Table 57 continued: Experimental bubble- and dew-point data for the CO_2 + (50 wt% 3,7-dimethyl-1-octanol + 50 wt% 1-decanol) system, measured by N. Schonegevel.

Run	Cell	Thermocouple	Mass Fraction	Pressure			Temperature		
				Measured (barg)	Correction factor	Corrected (bar abs)	Measured (°C)	Corrected (°C)	Converted (K)
6	Large	Handheld probe	0.217	186.0	7.7	194.7	35.9	35.6	308.7
				166.9	7.4	175.3	45.6	45.3	318.4
				168.1	6.5	175.6	55.3	55.0	328.1
				176.4	5.5	182.9	65.1	64.7	337.8
				187.2	4.8	193.0	75.0	74.6	347.7
				198.1	4.1	203.2	84.7	84.3	357.4
7	Large	Handheld probe	0.185	181.4	7.7	190.1	35.9	35.6	308.7
				164.6	7.5	173.1	45.6	45.3	318.4
				167.2	6.5	174.7	55.3	55.0	328.1
				175.9	5.5	182.4	65.1	64.7	337.8
				186.7	4.8	192.5	74.8	74.4	347.5
				197.8	4.1	202.9	84.6	84.2	357.3
8	Large	Handheld probe	0.147	167.2	7.8	176.0	35.9	35.6	308.7
				156.2	7.6	164.8	45.6	45.3	318.4
				161.1	6.5	168.6	55.4	55.1	328.2
				171.8	5.6	178.4	65.2	64.8	337.9
				183.0	4.9	188.9	74.8	74.4	347.5
				194.8	4.2	200.0	84.6	84.2	357.3
9	Large	Handheld probe	0.116	148.4	7.8	157.2	35.9	35.6	308.7
				146.6	7.6	155.2	45.6	45.3	318.4
				154.7	6.6	162.3	55.3	55.0	328.1
				165.8	5.6	172.4	65.1	64.7	337.8
				178.1	4.9	184.0	74.9	74.5	347.6
				189.6	4.3	194.9	84.6	84.2	357.3
10	Large	Handheld probe	0.076	116.3	7.7	125.0	35.9	35.6	308.7
				125.7	7.8	134.5	45.6	45.3	318.4
				137.9	6.7	145.6	55.4	55.1	328.2
				152.3	5.8	159.1	65.1	64.7	337.8
				166.1	5.0	172.1	74.9	74.5	347.6
				177.6	4.5	183.1	84.6	84.2	357.3

Table 57 continued: Experimental bubble- and dew-point data for the CO_2 + (50 wt% 3,7-dimethyl-1-octanol + 50 wt% 1-decanol) system, measured by N. Schonegevel.

Run	Cell	Thermocouple	Mass Fraction	Pressure			Temperature		
				Measured (barg)	Correction factor	Corrected (bar abs)	Measured (°C)	Corrected (°C)	Converted (K)
11	Large	Handheld probe	0.050	89.3	7.4	97.7	36.0	35.7	308.8
				107.0	7.7	115.7	45.6	45.3	318.4
				124.9	6.8	132.7	55.4	55.1	328.2
				139.0	6.0	146.0	65.2	64.8	337.9
				151.2	5.1	157.3	74.8	74.4	347.5
				163.5	4.5	169.0	84.6	84.2	357.3
12	Large	Handheld probe	0.031	74.5	7.1	82.6	35.8	35.5	308.6
				93.0	7.7	101.7	45.6	45.3	318.4
				112.9	6.8	120.7	55.3	55.0	328.1
				128.4	6.1	135.5	65.1	64.7	337.8
				137.6	5.1	143.7	74.9	74.5	347.6
				149.8	4.6	155.4	84.7	84.3	357.4
13	Large	Handheld probe	0.016	70.8	7.0	78.8	36.0	35.7	308.8
				89.0	7.7	97.7	45.6	45.3	318.4
				103.6	6.8	111.4	55.5	55.2	328.3
				117.5	6.1	124.6	65.1	64.7	337.8
				127.6	5.2	133.8	74.8	74.4	347.5
				134.9	4.7	140.6	84.6	84.2	357.3

Table 58: Experimental bubble- and dew-point data for the CO_2 + (25 wt% 3,7-dimethyl-1-octanol + 75 wt% 1-decanol) system, measured by N. Schonegevel.

Run	Cell	Thermocouple	Mass Fraction	Pressure			Temperature		
				Measured (barg)	Correction factor	Corrected (bar abs)	Measured (°C)	Corrected (°C)	Converted (K)
1	Large	Handheld probe	0.585	88.1	7.4	96.5	36.0	35.7	308.8
				95.4	7.7	104.1	45.7	45.4	318.5
				108.6	6.8	116.4	55.3	55.0	328.1
				121.7	6.1	128.8	65.1	64.7	337.8
				134.4	5.2	140.6	75.0	74.6	347.7
				145.6	4.6	151.2	84.7	84.3	357.4
2	Large	Handheld probe	0.479	188.5	7.7	197.2	35.9	35.6	308.7
				158.9	7.5	167.4	45.6	45.3	318.4
				156.3	6.6	163.9	55.3	55.0	328.1
				162.6	5.6	169.2	65.1	64.7	337.8
				171.9	5.0	177.9	74.8	74.4	347.5
				182.2	4.4	187.6	84.6	84.2	357.3
3	Large	Handheld probe	0.401	246.2	7.2	254.4	35.9	35.6	308.7
				193.2	7.2	201.4	45.7	45.4	318.5
				182.0	6.4	189.4	55.3	55.0	328.1
				181.9	5.5	188.4	65.2	64.8	337.9
				188.8	4.8	194.6	74.9	74.5	347.6
				197.9	4.1	203.0	84.6	84.2	357.3
4	Large	Handheld probe	0.341	256.2	7.1	264.3	35.9	35.6	308.7
				199.7	7.1	207.8	45.6	45.3	318.4
				187.1	6.4	194.5	55.3	55.0	328.1
				187.1	5.4	193.5	64.9	64.5	337.6
				194.0	4.7	199.7	74.5	74.1	347.2
				202.7	4.1	207.8	84.2	83.8	356.9

Table 58 continued: Experimental bubble- and dew-point data for the CO_2 + (25wt% 3,7-dimethyl-1-octanol + 75wt% 1-decanol) system, measured by N. Schonegevel.

Run	Cell	Thermocouple	Mass Fraction	Pressure			Temperature		
				Measured (barg)	Correction factor	Corrected (bar abs)	Measured (°C)	Corrected (°C)	Converted (K)
5	Large	Handheld probe	0.293	256.0	7.1	264.1	36.1	35.8	308.9
				200.2	7.1	208.3	45.8	45.5	318.6
				187.9	6.4	195.3	55.5	55.2	328.3
				189.2	5.4	195.6	65.0	64.6	337.7
				197.0	4.7	202.7	74.9	74.5	347.6
				206.0	4.1	211.1	84.6	84.2	357.3
6	Large	Handheld probe	0.230	256.8	7.1	264.9	35.9	35.6	308.7
				199.6	7.1	207.7	45.6	45.3	318.4
				187.0	6.4	194.4	55.3	55.0	328.1
				188.7	5.4	195.1	65.1	64.7	337.8
				196.1	4.7	201.8	74.9	74.5	347.6
				204.9	4.1	210.0	84.6	84.2	357.3
7	Large	Handheld probe	0.177	238.8	7.2	247.0	35.9	35.6	308.7
				191.4	7.2	199.6	45.6	45.3	318.4
				182.6	6.4	190.0	55.3	55.0	328.1
				186.0	5.4	192.4	65.1	64.7	337.8
				194.0	4.7	199.7	74.7	74.3	347.4
				203.4	4.1	208.5	84.4	84.0	357.1
8	Large	Handheld probe	0.121	196.0	7.6	204.6	36.0	35.7	308.8
				172.1	7.4	180.5	45.7	45.4	318.5
				169.3	6.5	176.8	55.5	55.2	328.3
				177.0	5.5	183.5	65.1	64.7	337.8
				187.3	4.8	193.1	74.9	74.5	347.6
				197.2	4.1	202.3	84.6	84.2	357.3

Table 58 continued: Experimental bubble- and dew-point data for the CO_2 + (25wt% 3,7-dimethyl-1-octanol + 75wt% 1-decanol) system, measured by N. Schonegevel.

Run	Cell	Thermocouple	Mass Fraction	Pressure			Temperature		
				Measured (barg)	Correction factor	Corrected (bar abs)	Measured (°C)	Corrected (°C)	Converted (K)
9	Large	Handheld probe	0.081	142.7	7.9	151.6	36.0	35.7	308.8
				141.1	7.7	149.8	45.7	45.4	318.5
				149.6	6.7	157.3	55.5	55.2	328.3
				163.1	5.6	169.7	65.2	64.8	337.9
				175.9	4.9	181.8	75.0	74.6	347.7
				186.8	4.3	192.1	84.7	84.3	357.4
10	Large	Handheld probe	0.050	98.0	7.6	106.6	36.0	35.7	308.8
				113.2	7.7	121.9	45.7	45.4	318.5
				129.4	6.8	137.2	55.4	55.1	328.2
				143.2	5.9	150.1	65.1	64.7	337.8
				157.0	5.1	163.1	74.8	74.4	347.5
				168.6	4.5	174.1	84.5	84.1	357.2
11	Large	Handheld probe	0.030	74.6	7.1	82.7	36.1	35.8	308.9
				96.8	7.6	105.4	45.9	45.6	318.7
				116.1	6.8	123.9	55.7	55.4	328.5
				132.2	6.0	139.2	65.2	64.8	337.9
				145.8	5.1	151.9	75.1	74.7	347.8
				157.0	4.5	162.5	85.0	84.6	357.7
12	Large	Handheld probe	0.015	69.0	6.9	76.9	36.0	35.7	308.8
				88.4	7.7	97.1	45.7	45.4	318.5
				106.5	6.8	114.3	55.4	55.1	328.2
				120.9	6.1	128.0	65.1	64.7	337.8
				131.7	5.2	137.9	74.7	74.3	347.4
				141.9	4.7	147.6	84.5	84.1	357.2

Table 59: Experimental bubble- and dew-point data for the CO_2 + (33.3 wt% n-dodecane + 33.3 wt% 3,7-dimethyl-1-octanol + 33.3 wt% 1-decanol) system, measured in this work.

Run	Cell	Thermocouple	Mass Fraction	Pressure			Temperature		
				Measured (barg)	Correction factor	Corrected (bar abs)	Measured (°C)	Corrected (°C)	Converted (K)
1	Large	Pt100-small	0.631	62.6	8.0	71.6	35.9	36.1	309.2
				75.2	7.7	83.9	45.4	45.5	318.6
				88.6	7.0	96.6	54.9	55.0	328.1
				101.5	6.3	108.8	64.8	64.9	338.0
				113.5	5.6	120.1	74.3	74.3	347.4
				124.2	5.0	130.2	84.0	84.0	357.1
2	Large	Pt100-small	0.545	66.7	8.0	75.7	35.9	36.1	309.2
				82.6	7.9	91.5	45.5	45.6	318.7
				98.3	7.1	106.4	55.2	55.3	328.4
				113.9	6.4	121.3	64.8	64.9	338.0
				128.2	5.7	134.9	74.0	74.0	347.1
				141.3	5.0	147.3	83.9	83.9	357.0
3	Large	Pt100-small	0.456	74.0	8.0	83.0	35.9	36.1	309.2
				91.5	8.0	100.5	45.6	45.7	318.8
				110.4	7.1	118.5	55.4	55.5	328.6
				127.6	6.3	134.9	65.1	65.1	338.2
				143.5	5.6	150.1	74.6	74.6	347.7
				157.5	4.9	163.4	84.3	84.3	357.4
4	Large	Pt100-small	0.392	80.8	8.3	90.1	35.9	36.1	309.2
				97.0	8.0	106.0	45.6	45.7	318.8
				114.9	7.2	123.1	55.0	55.1	328.2
				132.3	6.4	139.7	64.8	64.9	338.0
				148.3	5.7	155.0	74.3	74.3	347.4
				162.7	4.8	168.5	84.0	84.0	357.1
5	Large	Pt100-small	0.318	89.4	8.5	98.9	35.8	36.0	309.1
				104.0	8.0	113.0	45.2	45.3	318.4
				121.6	7.2	129.8	54.9	55.0	328.1
				138.7	6.4	146.1	64.3	64.4	337.5
				154.6	5.7	161.3	73.9	73.9	347.0
				169.1	4.8	174.9	83.5	83.5	356.6

Table 59 continued: Experimental bubble- and dew-point data for the CO_2 +(33.3wt% n-dodecane + 33.3wt% 3,7-dimethyl-1-octanol + 33.3wt% 1-decanol) system, measured in this work.

Run	Cell	Thermocouple	Mass Fraction	Pressure			Temperature		
				Measured (barg)	Correction factor	Corrected (bar abs)	Measured (°C)	Corrected (°C)	Converted (K)
6	Large	Pt100-small	0.245	95.2	8.5	104.7	35.7	35.9	309.0
				108.9	8.1	118.0	45.3	45.4	318.5
				125.8	7.2	134.0	54.6	54.7	327.8
				142.2	6.4	149.6	64.5	64.6	337.7
				157.8	5.6	164.4	73.9	73.9	347.0
				171.9	4.8	177.7	83.7	83.7	356.8
7	Large	Pt100-small	0.181	97.7	8.5	107.2	35.5	35.7	308.8
				110.2	8.1	119.3	44.9	45.0	318.1
				126.4	7.2	134.6	54.6	54.7	327.8
				142.7	6.4	150.1	64.0	64.1	337.2
				157.7	5.7	164.4	73.3	73.3	346.4
				171.5	4.9	177.4	82.6	82.6	355.7
8	Large	Pt100-small	0.182	98.3	8.5	107.8	35.8	36.0	309.1
				110.8	8.1	119.9	45.2	45.3	318.4
				126.4	7.2	134.6	54.8	54.9	328.0
				142.8	6.4	150.2	64.4	64.5	337.6
				158.2	5.6	164.8	74.0	74.0	347.1
				172.3	4.8	178.1	83.5	83.5	356.6
9	Large	Pt100-small	0.120	92.7	8.5	102.2	35.7	35.9	309.0
				108.5	8.1	117.6	45.3	45.4	318.5
				125.8	7.2	134.0	55.1	55.2	328.3
				142.2	6.4	149.6	64.7	64.8	337.9
				157.4	5.6	164.0	74.2	74.2	347.3
				170.7	4.8	176.5	83.9	83.9	357.0
10	Large	Pt100-small	0.081	81.6	8.3	90.9	35.7	35.9	309.0
				101.5	8.0	110.5	45.2	45.3	318.4
				120.4	7.2	128.6	54.7	54.8	327.9
				138.5	6.4	145.9	64.0	64.1	337.2
				153.4	5.7	160.1	73.9	73.9	347.0
				167.8	4.8	173.6	83.5	83.5	356.6

Table 59 continued: Experimental bubble- and dew-point data for the CO_2 +(33.3wt% n-dodecane + 33.3wt% 3,7-dimethyl-1-octanol + 33.3wt% 1-decanol) system, measured in this work.

Run	Cell	Thermocouple	Mass Fraction	Pressure			Temperature		
				Measured (barg)	Correction factor	Corrected (bar abs)	Measured (°C)	Corrected (°C)	Converted (K)
11	Large	Pt100-small	0.050	72.6	8.0	81.6	35.9	36.1	309.2
				94.6	8.0	103.6	45.4	45.5	318.6
				114.1	7.2	122.3	55.2	55.3	328.4
				130.7	6.4	138.1	64.7	64.8	337.9
				144.9	5.7	151.6	74.3	74.3	347.4
				156.5	4.9	162.4	83.9	83.9	357.0
12	Large	Pt100-small	0.030	70.0	8.0	79.0	35.6	35.8	308.9
				90.4	8.2	99.6	45.0	45.1	318.2
				108.1	7.2	116.3	54.6	54.7	327.8
				123.7	6.4	131.1	64.5	64.6	337.7
				135.4	5.7	142.1	74.1	74.1	347.2
				145.1	5.0	151.1	83.1	83.1	356.2
13	Large	Pt100-small	0.015	69.7	8.0	78.7	35.5	35.7	308.8
				87.4	8.2	96.6	45.1	45.2	318.3
				102.6	7.1	110.7	54.5	54.6	327.7
				115.2	6.5	122.7	64.0	64.1	337.2
				124.5	5.7	131.2	73.6	73.6	346.7
				131.0	5.0	137.0	82.9	82.9	356.0

Table 60: Experimental bubble- and dew-point data for the CO_2 + (5wt% n-dodecane + 10wt% 3,7-dimethyl-1-octanol + 85wt% 1-decanol) system, measured in this work.

Run	Cell	Thermocouple	Mass Fraction	Pressure			Temperature		
				Measured (barg)	Correction factor	Corrected (bar abs)	Measured (°C)	Corrected (°C)	Converted (K)
1	Large	Pt100-small	0.625	85.6	8.4	95.0	35.8	36.0	309.1
				94.6	8.1	103.7	45.3	45.4	318.5
				108.9	7.1	117.0	54.9	55.0	328.1
				122.0	6.4	129.4	64.4	64.5	337.6
				134.3	5.7	141.0	74.0	74.0	347.1
				145.0	5.0	151.0	83.4	83.4	356.5
2	Large	Pt100-small	0.531	160.8	8.7	170.5	35.8	36.0	309.1
				141.5	8.2	150.7	45.3	45.4	318.5
				142.8	7.2	151.0	54.9	55.0	328.1
				151.0	6.4	158.4	64.6	64.7	337.8
				161.5	5.6	168.1	74.1	74.1	347.2
				171.9	4.8	177.7	83.6	83.6	356.7
3	Large	Pt100-small	0.433	231.8	8.2	241.0	35.8	36.0	309.1
				184.0	7.8	192.8	45.3	45.4	318.5
				174.7	7.0	182.7	54.9	55.0	328.1
				177.6	6.4	185.0	64.1	64.2	337.3
				184.7	5.5	191.2	73.5	73.5	346.6
				193.5	4.7	199.2	83.1	83.1	356.2
4	Large	Pt100-small	0.376	253.1	7.9	262.0	35.6	35.8	308.9
				193.5	7.7	202.2	45.2	45.3	318.4
				181.5	7.0	189.5	54.7	54.8	327.9
				183.6	6.2	190.8	64.3	64.4	337.5
				190.9	5.4	197.3	73.8	73.8	346.9
				199.9	4.6	205.5	83.3	83.3	356.4

Table 60 continued: Experimental bubble- and dew-point data for the CO_2 + (5wt% n-dodecane + 10wt% 3,7-dimethyl-1-octanol + 85wt% 1-decanol) system, measured in this work.

Run	Cell	Thermocouple	Mass Fraction	Pressure			Temperature		
				Measured (barg)	Correction factor	Corrected (bar abs)	Measured (°C)	Corrected (°C)	Converted (K)
5	Large	Pt100-small	0.302	264.9	7.8	273.7	35.8	36.0	309.1
				200.6	7.7	209.3	45.3	45.4	318.5
				185.8	6.9	193.7	54.9	55.0	328.1
				187.7	6.1	194.8	64.5	64.6	337.7
				195.2	5.3	201.5	74.0	74.0	347.1
				204.2	4.6	209.8	83.6	83.6	356.7
6	Large	Pt100-small	0.235	266.0	7.8	274.8	35.7	35.9	309.0
				203.0	7.7	211.7	45.3	45.4	318.5
				188.8	6.9	196.7	54.9	55.0	328.1
				189.4	6.1	196.5	64.5	64.6	337.7
				196.3	5.3	202.6	74.1	74.1	347.2
				205.4	4.5	210.9	83.7	83.7	356.8
7	Large	Pt100-small	0.182	247.7	8.0	256.7	35.8	36.0	309.1
				194.3	7.7	203.0	45.4	45.5	318.6
				183.7	6.9	191.6	55.0	55.1	328.2
				186.3	6.2	193.5	64.6	64.7	337.8
				194.3	5.3	200.6	74.2	74.2	347.3
				203.5	4.5	209.0	83.9	83.9	357.0
8	Large	Pt100-small	0.118	192.1	8.5	201.6	35.7	35.9	309.0
				166.4	8.0	175.4	45.4	45.5	318.6
				166.1	7.1	174.2	55.0	55.1	328.2
				173.8	6.4	181.2	64.6	64.7	337.8
				184.3	5.4	190.7	74.3	74.3	347.4
				194.5	4.6	200.1	84.0	84.0	357.1

Table 60 continued: Experimental bubble- and dew-point data for the CO_2 + (5wt% n-dodecane + 10wt% 3,7-dimethyl-1-octanol + 85wt% 1-decanol) system, measured in this work.

Run	Cell	Thermocouple	Mass Fraction	Pressure			Temperature		
				Measured (barg)	Correction factor	Corrected (bar abs)	Measured (°C)	Corrected (°C)	Converted (K)
9	Large	Pt100-small	0.080	141.1	8.9	151.0	35.6	35.8	308.9
				137.9	8.3	147.2	45.3	45.4	318.5
				146.3	7.4	154.7	55.0	55.1	328.2
				158.3	6.4	165.7	64.5	64.6	337.7
				170.2	5.5	176.7	74.3	74.3	347.4
				181.0	4.7	186.7	83.7	83.7	356.8
10	Large	Pt100-small	0.049	93.6	8.5	103.1	35.6	35.8	308.9
				110.3	8.1	119.4	45.1	45.2	318.3
				127.4	7.2	135.6	54.6	54.7	327.8
				143.3	6.4	150.7	64.2	64.3	337.4
				157.6	5.7	164.3	73.8	73.8	346.9
				168.3	4.9	174.2	83.2	83.2	356.3
11	Large	Pt100-small	0.029	75.2	8.1	84.3	35.7	35.9	309.0
				96.0	8.0	105.0	45.4	45.5	318.6
				115.3	7.2	123.5	55.0	55.1	328.2
				131.8	6.4	139.2	64.3	64.4	337.5
				145.2	5.7	151.9	74.3	74.3	347.4
				155.2	4.9	161.1	84.1	84.1	357.2
12	Large	Pt100-small	0.015	69.2	8.0	78.2	35.6	35.8	308.9
				88.6	8.1	97.7	45.4	45.5	318.6
				105.8	7.1	113.9	55.1	55.2	328.3
				119.3	6.4	126.7	64.7	64.8	337.9
				129.8	5.7	136.5	74.3	74.3	347.4
				137.6	5.0	143.6	83.9	83.9	357.0

Table 61: Experimental bubble- and dew-point data for the CO_2 +(84.2wt% n-dodecane + 10.5wt% 3,7-dimethyl-1-octanol + 5.3wt% 1-decanol) system, measured in this work.

Run	Cell	Thermocouple	Mass Fraction	Pressure			Temperature		
				Measured (barg)	Correction factor	Corrected (bar abs)	Measured (°C)	Corrected (°C)	Converted (K)
1	Large	Pt100-small	0.615	53.5	7.9	62.4	35.5	35.7	308.8
				65.4	7.5	73.9	45.3	45.4	318.5
				77.4	6.8	85.2	54.8	54.9	328.0
				89.6	6.5	97.1	64.4	64.5	337.6
				101.5	5.6	108.1	74.1	74.1	347.2
				113.3	5.0	119.3	83.6	83.6	356.7
2	Large	Pt100-small	0.508	59.5	8.1	68.6	35.4	35.6	308.7
				73.9	7.7	82.6	44.9	45.0	318.1
				88.5	7.0	96.5	54.4	54.5	327.6
				103.2	6.4	110.6	63.9	64.0	337.1
				118.4	5.7	125.1	73.3	73.3	346.4
				132.0	5.1	138.1	82.8	82.8	355.9
3	Large	Pt100-small	0.412	62.8	8.0	71.8	35.7	35.9	309.0
				78.7	7.8	87.5	45.3	45.4	318.5
				95.6	7.0	103.6	54.8	54.9	328.0
				112.7	6.4	120.1	64.4	64.5	337.6
				129.4	5.7	136.1	73.9	73.9	347.0
				144.6	5.0	150.6	83.6	83.6	356.7
4	Large	Pt100-small	0.352	63.1	8.0	72.1	35.5	35.7	308.8
				79.6	7.9	88.5	45.1	45.2	318.3
				97.9	7.1	106.0	54.8	54.9	328.0
				116.4	6.4	123.8	64.4	64.5	337.6
				133.9	5.7	140.6	74.0	74.0	347.1
				149.7	5.0	155.7	83.7	83.7	356.8

Table 61 continued: Experimental bubble- and dew-point data for the CO_2 +(84.2wt% n-dodecane + 10.5wt% 3,7-dimethyl-1-octanol + 5.3wt% 1-decanol) system, measured in this work.

Run	Cell	Thermocouple	Mass Fraction	Pressure			Temperature		
				Measured (barg)	Correction factor	Corrected (bar abs)	Measured (°C)	Corrected (°C)	Converted (K)
5	Large	Pt100-small	0.290	64.2	8.0	73.2	35.7	35.9	309.0
				81.3	8.0	90.3	45.0	45.1	318.2
				100.4	7.1	108.5	54.7	54.8	327.9
				119.7	6.4	127.1	64.3	64.4	337.5
				137.4	5.7	144.1	73.5	73.5	346.6
				153.4	5.0	159.4	82.9	82.9	356.0
6	Large	Pt100-small	0.221	66.0	8.0	75.0	35.9	36.1	309.2
				83.7	8.0	92.7	45.6	45.7	318.8
				103.8	7.1	111.9	55.2	55.3	328.4
				122.9	6.4	130.3	64.8	64.9	338.0
				139.9	5.6	146.5	74.5	74.5	347.6
				155.9	4.9	161.8	84.1	84.1	357.2
7	Large	Pt100-small	0.172	64.4	8.0	73.4	34.9	35.1	308.2
				83.9	8.0	92.9	45.5	45.6	318.7
				104.2	7.1	112.3	55.2	55.3	328.4
				123.0	6.4	130.4	64.7	64.8	337.9
				139.8	5.7	146.5	74.4	74.4	347.5
				155.2	4.9	161.1	84.0	84.0	357.1
8	Large	Pt100-small	0.121	67.5	8.0	76.5	35.9	36.1	309.2
				85.1	8.0	94.1	45.6	45.7	318.8
				104.2	7.1	112.3	55.1	55.2	328.3
				122.6	6.4	130.0	64.9	65.0	338.1
				139.0	5.6	145.6	74.5	74.5	347.6
				153.5	4.9	159.4	84.0	84.0	357.1

Table 61 continued: Experimental bubble- and dew-point data for the CO_2 +(84.2wt% n-dodecane + 10.5wt% 3,7-dimethyl-1-octanol + 5.3wt% 1-decanol) system, measured in this work.

Run	Cell	Thermocouple	Mass Fraction	Pressure			Temperature		
				Measured (barg)	Correction factor	Corrected (bar abs)	Measured (°C)	Corrected (°C)	Converted (K)
9	Large	Pt100-small	0.079	66.9	8.0	75.9	35.8	36.0	309.1
				84.1	8.0	93.1	45.4	45.5	318.6
				102.0	7.1	110.1	54.9	55.0	328.1
				119.4	6.4	126.8	64.6	64.7	337.8
				134.4	5.7	141.1	74.2	74.2	347.3
				147.1	5.0	153.1	83.8	83.8	356.9
10	Large	Pt100-small	0.050	68.0	8.0	77.0	35.6	35.8	308.9
				83.9	8.1	93.0	45.2	45.3	318.4
				100.8	7.1	108.9	54.7	54.8	327.9
				116.2	6.4	123.6	64.2	64.3	337.4
				128.8	5.7	135.5	73.8	73.8	346.9
				139.5	5.0	145.5	83.3	83.3	356.4
11	Large	Pt100-small	0.030	69.1	8.0	78.1	35.7	35.9	309.0
				83.5	8.1	92.6	45.2	45.3	318.4
				99.1	7.1	107.2	54.5	54.6	327.7
				112.4	6.4	119.8	64.3	64.4	337.5
				123.0	5.7	129.7	73.8	73.8	346.9
				131.3	5.0	137.3	83.6	83.6	356.7
12	Large	Pt100-small	0.015	68.6	8.0	77.6	35.7	35.9	309.0
				82.1	7.9	91.0	45.4	45.5	318.6
				94.8	7.0	102.8	55.0	55.1	328.2
				104.3	6.3	111.6	64.6	64.7	337.8
				111.4	5.6	118.0	74.4	74.4	347.5
				115.7	5.0	121.7	83.4	83.4	356.5

Table 62: Experimental bubble- and dew-point data for the CO_2 +(10.1wt% n-dodecane + 30wt% 3,7-dimethyl-1-octanol + 59.9wt% 1-decanol) system, measured in this work.

Run	Cell	Thermocouple	Mass Fraction	Pressure			Temperature		
				Measured (barg)	Correction factor	Corrected (bar abs)	Measured (°C)	Corrected (°C)	Converted (K)
1	Large	Pt100-small	0.621	66.2	8.0	75.2	35.5	35.7	308.8
				83.1	8.1	92.2	45.0	45.1	318.2
				99.0	7.1	107.1	54.4	54.5	327.6
				113.4	6.5	120.9	63.8	63.9	337.0
				125.2	5.7	131.9	73.3	73.3	346.4
				136.7	5.0	142.7	82.8	82.8	355.9
2	Large	Pt100-small	0.533	106.6	8.7	116.3	35.9	36.1	309.2
				110.6	8.0	119.6	45.6	45.7	318.8
				122.1	7.2	130.3	55.1	55.2	328.3
				135.8	6.4	143.2	64.8	64.9	338.0
				148.8	5.6	155.4	74.4	74.4	347.5
				160.7	4.9	166.6	84.1	84.1	357.2
3	Large	Handheld probe	0.455	143.0	8.8	152.8	36.8	36.5	309.6
				136.2	8.3	145.5	45.5	45.2	318.3
				142.0	7.2	150.2	55.3	55.0	328.1
				152.8	6.4	160.2	65.0	64.6	337.7
				164.0	5.6	170.6	74.8	74.4	347.5
				176.2	4.7	181.9	84.6	84.2	357.3
4	Small	Handheld probe	0.410	163.1	-0.8	163.3	34.6	34.3	307.4
				149.7	-1.5	149.2	44.6	44.3	317.4
				154.3	-2.2	153.1	54.2	53.9	327.0
				164.4	-2.9	162.5	63.6	63.2	336.3
				176.7	-3.4	174.3	73.7	73.3	346.4
				188.5	-3.8	185.7	83.0	82.6	355.7

Table 62 continued: Experimental bubble- and dew-point data for the CO_2 +(10.1wt% n-dodecane + 30wt% 3,7-dimethyl-1-octanol + 59.9wt% 1-decanol) system, measured in this work.

Run	Cell	Thermocouple	Mass Fraction	Pressure			Temperature		
				Measured (barg)	Correction factor	Corrected (bar abs)	Measured (°C)	Corrected (°C)	Converted (K)
5	Large	Handheld probe	0.307	174.5	7.7	183.2	36.2	35.9	309.0
				157.0	7.5	165.5	45.8	45.5	318.6
				160.0	6.5	167.5	55.6	55.3	328.4
				169.1	5.6	175.7	65.2	64.8	337.9
				180.4	4.9	186.3	74.9	74.5	347.6
				192.1	4.2	197.3	84.7	84.3	357.4
6	Large	Handheld probe	0.241	179.8	7.7	188.5	36.0	35.7	308.8
				160.6	7.5	169.1	45.6	45.3	318.4
				161.7	6.5	169.2	55.3	55.0	328.1
				170.3	5.6	176.9	65.1	64.7	337.8
				181.3	4.9	187.2	74.7	74.3	347.4
				193.0	4.2	198.2	84.5	84.1	357.2
7	Large	Handheld probe	0.192	180.1	7.7	188.8	35.9	35.6	308.7
				161.3	7.5	169.8	45.5	45.2	318.3
				162.6	6.5	170.1	55.2	54.9	328.0
				171.1	5.6	177.7	64.9	64.5	337.6
				182.2	4.9	188.1	74.7	74.3	347.4
				193.4	4.2	198.6	84.5	84.1	357.2
8	Large	Handheld probe	0.122	154.4	7.8	163.2	35.9	35.6	308.7
				147.3	7.6	155.9	45.5	45.2	318.3
				154.1	6.7	161.8	55.2	54.9	328.0
				165.4	5.6	172.0	64.9	64.5	337.6
				177.2	4.9	183.1	74.6	74.2	347.3
				188.7	4.3	194.0	84.3	83.9	357.0

Table 62 continued: Experimental bubble- and dew-point data for the CO_2 +(10.1wt% n-dodecane + 30wt% 3,7-dimethyl-1-octanol + 59.9wt% 1-decanol) system, measured in this work.

Run	Cell	Thermocouple	Mass Fraction	Pressure			Temperature		
				Measured (barg)	Correction factor	Corrected (bar abs)	Measured (°C)	Corrected (°C)	Converted (K)
9	Large	Handheld probe	0.078	119.2	7.7	127.9	36.0	35.7	308.8
				125.7	7.8	134.5	45.6	45.3	318.4
				138.4	6.7	146.1	55.3	55.0	328.1
				152.6	5.8	159.4	65.0	64.6	337.7
				166.4	5.0	172.4	74.7	74.3	347.4
				178.7	4.5	184.2	84.4	84.0	357.1
10	Large	Handheld probe	0.048	85.8	7.4	94.2	35.9	35.6	308.7
				104.7	7.7	113.4	45.6	45.3	318.4
				123.3	6.8	131.1	55.3	55.0	328.1
				140.2	6.0	147.2	65.0	64.6	337.7
				154.7	5.1	160.8	74.7	74.3	347.4
				166.2	4.5	171.7	84.5	84.1	357.2
11	Large	Handheld probe	0.031	74.8	7.1	82.9	35.5	35.6	308.7
				96.4	7.7	105.1	45.5	45.3	318.4
				115.7	6.9	123.6	55.3	54.8	327.9
				132.2	6.0	139.2	65.5	64.7	337.8
				146.1	5.2	152.3	75.0	73.9	347.0
				157.0	4.6	162.6	84.6	83.2	356.3
12	Large	Handheld probe	0.015	68.2	6.9	76.1	36.2	36.3	309.4
				86.7	7.6	95.3	46.1	45.8	318.9
				103.3	6.8	111.1	55.8	55.3	328.4
				116.4	6.1	123.5	65.5	64.7	337.8
				129.9	5.2	136.1	75.3	74.2	347.3
				136.6	4.8	142.4	84.9	83.5	356.6

C. Vapour-Liquid-Equilibrium Experimental Setup

C.1. Detailed experimental procedure

This section provides a detailed breakdown of the procedures followed when conducting the VLE experiments. The experimental method presented here is based on the procedure developed by Fourie [111, 112].

LOADING

The schematic presented in Figure 127, indicates all the cell inlets/outlets which are sealed off with needle valves. These valves are numbered from 1 to 3 and in the experimental procedure, reference is made to these valves to better explain the specific steps.

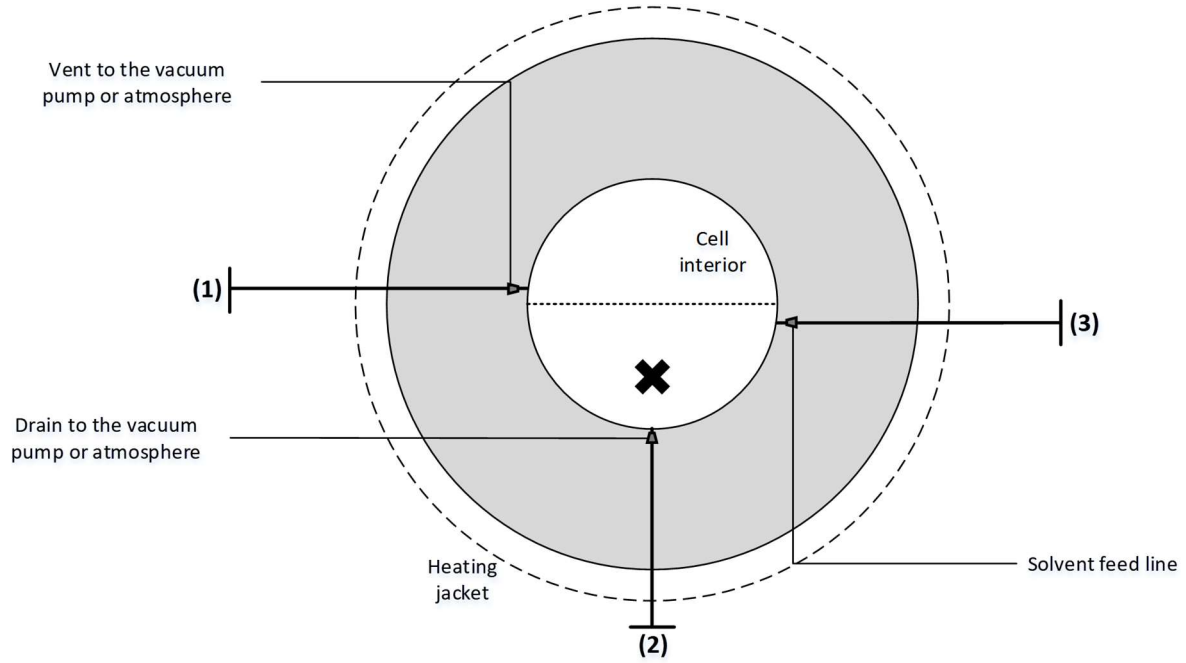

Figure 127: Simplified schematic of the variable volume cell which forms part of the analytic setup Adapted from [111])

Procedure:

1. Turn on the vacuum pump, electric plugs and the water bath.
2. Clean out the cell with compressed air.
3. Close off the cell by tightening valves (1) – (3).
4. Clean the magnetic stirrer bar and place it into the cell.
5. Slide the pressure intensifier into position.

6. Align the piston with the cell and gently push the piston into the cell.
7. Turn the cell onto the thread and continuously check the piston movement while turning.
8. Tighten the piston.
9. Set the bath temperature to 27ºC.
10. Tighten the ROLSI screws.
11. Tighten the seal around the sight glass.
12. Connect the nitrogen line.
13. Remove valve (3) to load the solute.
14. Load the solute:
    a. Weigh the syringe
    b. Measure the volume of solute to be loaded, using the syringe (usually load ± 23 ml).
    c. Weigh the loaded syringe and record the value.
    d. Inject the content of the syringe into the cell through the opening where valve (3) was removed.
    e. Re-weigh empty syringe and record the value.
15. Clean valve (3) and then place needle valve back into feed line.
16. Record loading temperature and pressure.
17. Turn on the stirrer.
18. Draw vacuum in the cell by opening valve (1) and the valve connected to the vacuum pump.
19. After approximately five minutes, close valve (1).
20. Load the solvent gas cylinder:
    a. Remove the empty cylinder from the fridge.
    b. Purge the gas cylinder connection line.
    c. Fill the cylinder with CO_2.
    d. In the lab place the CO_2 cylinder on the stand and heat whilst wiping dry.
    e. While heating, check the pressure and release if pressure increases to 250 bar.
21. Remove the stirrer to gain access to the solvent loading line.
22. Connect the CO_2 cylinder to the solvent loading line.
23. Flush the connecting line and cell with CO_2:
    a. Draw a vacuum in the cell and the connecting feed line by opening valve (1) and (3), respectively.
    b. Once the air is removed, close valves (1) and (3).

c. Slightly open the CO_2 cylinder and then close.
d. Slowly open valve (3) to allow CO_2 into the cell.
e. Release the CO_2 by opening valve (1) and purging it to the vacuum pump.
f. Close valves (1) and (3).
g. Repeat flushing steps (c - f) three times.

24. Disconnect CO_2 cylinder, weigh it and record the value.
25. Place the stirrer in position.
26. Open valve (1) to draw a vacuum and ensure that no CO_2 is dissolved in the mixture.
27. Close valve (1).
28. Heat the CO_2 cylinder, weigh it and record the value.
29. Release CO_2 until the cylinder reaches the correct weight.
30. Remove the stirrer.
31. Connect the CO_2 cylinder to the solvent loading line.
32. Draw a vacuum in the cell and the connecting feed line by opening valve (1) and (3), respectively.
33. Once the air is removed, close valves (1) and (3).
34. Open the CO_2 cylinder whilst heating it.
35. Slowly open valve (3) to load the CO_2.
36. Check the amount of liquid in the cell and once it reaches the desired level, close the CO_2 cylinder.
37. Heat the piping to the cell to allow all the CO_2 to enter the cell.
38. Close valve (3).
39. Remove the CO_2 cylinder, weigh it and record the value.
40. Record the loading temperature and pressure.
41. Turn off the vacuum pump.
42. Tighten all the valves and check that the bolt on the piston is tight.
43. Tighten the sight glass.
44. Place the insulation around the cell.
45. Place the heat distributing plates into position.
46. Place the stirrer into position.
47. Turn on the stirrer.
48. Place the oven panelling in position, except for the front panel.
49. Connect the heating tubes.
50. Place the temperature probes into position.

51. Place the camera in position.
52. Place the front oven panel into position.
53. Turn on the oven and set the temperature.
54. Set the water bath temperature to the first measuring temperature.

SAMPLING

The sampling procedure employed in this work consists of two parts, namely a slow purge run and an interchanging fast purge and analysis run. During the entire sampling procedure outlined below, the pressure is continuously monitored and adjusted to maintain it within ±0.01 MPa of the desired measuring pressure.

Slow purge run:

1. Switch on the ROLSI timers.
2. Switch on the thermal regulators.
3. Set the temperature of the transfer tube heating.
4. Turn on the camera.
5. Adjust the pressure to the desired measuring pressure.
6. Allow the different phases to settle.
7. Position the ROLSI samplers to ensure that the back ROLSI is submerged in the dense phase and the front ROLSI is able to extract a vapour sample.
8. If the adjustment of the ROLSI samplers influences the pressure, re-adjust the pressure by adding or venting nitrogen from the low pressure chamber.
9. Continue mixing until equilibrium is attained and the system is visually stable.
10. Once the system is visually stable and the transitional phase is completely developed, turn off the stirrer.
11. Allow the system to stabilize before sampling commences.
12. Turn on the computer screen and open the online sampling program.
13. Open the air, nitrogen and hydrogen gas cylinders and regulate the pressure at 400 kPa.
14. Using the computer program, switch on the FID and TCD detectors by selecting all the detector parameters available in the program, except for the negative polarity for the TCD and pressing apply.
15. Load the slow purge method.
16. Create a folder for the slow purge run.

17. Change the default method parameters by using the program to:
    a. Turn off the inlet gas saver for the back and front inlet.
    b. Turn on the inlet septum purge for the back and front inlet.
    c. Set the oven temperature to 250ºC and the runtime to 90 min.
18. Turn on data analyser.
19. Set the ROLSI timers to open every 2:30 min for 0.05 s and 0.18 s for the back and front ROLSI samplers, respectively.
20. Start the ROLSI timers and extract samples from both phases until the peak heights are stable.
21. During the sampling, continuously monitor and adjust the pressure to maintain it within ±0.01 MPa of the desired measuring pressure.
22. Once the peaks stabilize stop the timers to stop sampling.
23. Wait for the final peaks to emerge and then press stop on the GC front panel to end the run.

Sampling and fast purge series:

1. Select the fast purge method.
2. Create a folder for the fast purge run.
3. Change the default method parameters by using the program to:
    a. Turn off the inlet gas saver for the back and front inlet.
    b. Turn on the inlet septum purge for the back and front inlet.
4. Wet the bubble flow meter.
5. Set the ROLSI timers to open every 4 s for 0.05 s and 0.24 s for the back and front ROLSI samplers, respectively.
6. Start the ROLSI timers and allow 5 samples to be withdrawn, then stop the timers.
7. Using the program, turn on the gas saver for the back and front inlet.
8. Set the timer for the analysis run by changing the sampling time for the front ROLSI from 0.24 s to 0.29 s.
9. Manually stop the GC at a run time of 1.8 min and quickly load the analysis method.
10. Create folder for the analysis run.
11. Change the default method parameters by using the program to:
    a. Turn off the inlet gas saver for the back and front inlet.
    b. Turn off the inlet septum purge for the back and front inlet.
12. Also using the program, de-select the valves but do not press apply.

13. Once the oven reaches 100.5ºC press apply to switch the valves and immediately start the ROLSI timers to extract one sample from each phase.
14. Using the program, turn on the gas saver for the back and front inlet.
15. Perform three bubble flow meter tests and record the results.
16. Set the ROLSI timers back to the fast purge settings.
17. At a GC runtime of 7 min use the program to:
    a. Set the oven temperature to 250ºC.
    b. Change the run time to 10 min.
    c. Switch the valves.
18. During the sampling, continuously monitor and adjust the pressure to maintain it within ±0.01 MPa of the desired measuring pressure.
19. Repeat this sampling and fast purge series until at least three samples of acceptable repeatability are withdrawn.
20. Once sampling and fast purge series is complete, use the computer program to switch off the FID and TCD detectors by unselecting all the detector parameters available in the program, except for the heater and pressing apply.
21. Close the air, nitrogen and hydrogen gas cylinders.
22. Select the sleep method.
23. Switch off the ROLSI timers.
24. Switch off the thermal regulators.
25. Turn off the camera.
26. Release the pressure in the cell by venting the nitrogen in the low pressure chamber.

VENTING SOLVENT

It is often required to vent CO_2 from the system to measure data at lower pressures. The CO_2 venting procedure is outlined below and the valves referred to in this section is presented in Figure 127.

Procedure:

1. Turn off the oven and remove the heating tubes.
2. Remove the front and side oven panelling.
3. Turn off the stirrer.

4. Slowly cool the cell by systematically lowering the water bath set temperature. Cooling at lower temperatures can be aided by adding ice water to the water bath.
5. Once the cell is cooled, turn on the camera.
6. Ensure that the liquid line is below the vent outlet.
7. Open the line which vents to the atmosphere.
8. Slowly open valve (1) to release CO2 from the system.
9. Once the pressure reaches the desired value, close valve (1).
10. Turn on the stirrer.
11. Turn off the camera.
12. Slowly start re-heating the cell by systematically increasing the water bath set temperature.
13. Place the heating tubes and oven panelling in position.
14. Once the cell is heated to atmospheric temperature, turn on the oven and set the water bath and oven temperature to the desired measuring temperature.

ADDING SOLVENT

It is often required to add CO_2 to the system to measure data at higher pressures. The procedure to load additional CO_2, without unloading the cell, is outlined below and the valves referred to in this section is presented in Figure 127.

Procedure:

1. Turn off the oven and set the water bath to 27ºC.
2. Remove the heating tubes along with the front and side oven panelling.
3. Turn off the stirrer.
4. Once the set temperature is close to the set temperature, remove the stirrer to gain access to the solvent loading line.
5. Turn on the camera.
6. Load the solvent gas cylinder:
    a. Remove the empty cylinder from the fridge.
    b. Purge the gas cylinder connection line.
    c. Fill the cylinder with CO_2.
    d. In the lab place the CO_2 cylinder on the stand and heat whilst wiping dry.
    e. While heating, check the pressure and release if pressure increases to 250 bar.
7. When the cylinder is heated, connect it to the solvent loading line.

8. Purge the solvent loading line:
    a. Slightly open the CO_2 cylinder and then close.
    b. Release the CO_2 from the line by loosening the nut connecting the CO_2 cylinder and the cell.
    c. Repeat three times.
9. Open the CO_2 cylinder fully whilst heating it.
10. Slowly open valve (3) to load the CO_2.
11. Check the amount of liquid and pressure in the cell and once it reaches the desired level and/or value, close valve (3).
12. Close the CO_2 cylinder.
13. Relieve pressure in the solvent loading line by slowly loosening the connection between the CO_2 cylinder and the cell.
14. Remove the CO_2 cylinder.
15. Place the stirrer in position.
16. Turn on the stirrer.
17. Turn off the camera
18. Place the heating tubes and oven panelling in position.
19. Turn on the oven and set the oven and water bath temperature to the desired set temperatures.

UNLOADING AND CLEANING

Once all the measurements for a specific mixture is complete, the cell must be unloaded and thoroughly cleaned. The unloading and cleaning procedure are outlined below and the valves referred to in this section is presented in Figure 127.

Procedure:

1. Turn off the oven and water bath.
2. Release all the nitrogen in the low pressure chamber.
3. Once the system is cooled, remove the heating tubes and oven panelling.
4. Remove the insulation.
5. Remove the temperature probes.
6. Disconnect the nitrogen line.
7. Place the camera in position and turn it on.

8. Set the water bath temperature to 70ºC and turn it on.
9. Place a plastic bottle and bowl at the atmospheric vent and drain outlets, respectively.
10. Open the line which vents to the atmosphere.
11. Slowly open valve (1) to release the gas.
12. Remove the stirrer to gain access to the bottom drain valve (2).
13. Open the line which drains to the atmosphere.
14. Once all the gas is released, open the bottom valve (2) to drain the liquid.
15. Once content has drained, loosen the piston by untightening the bolts.
16. Turn off the water bath.
17. Remove the low pressure chamber and continuously check the piston movement while turning.
18. Remove the magnetic stirrer bar from the cell using a magnet.
19. Clean the stirrer with acetone and high pressure air.
20. Cover the area surrounding the cell and the GC with towels.
21. Close off the cell by tightening valves (1) – (3).
22. Rinse the inside of the cell with acetone and high-pressure air. When using high-pressure air in the cell take care not to damage the ROLSI capillaries.
23. Clean the feed, vent and drain lines:
    a. Loosen the needle valve of the respective line to allow access to the cell.
    b. Fill a needle-syringe with acetone.
    c. Place the needle in the line and inject acetone into the line.
    d. Blow high pressure air into the line.
    e. Repeat three times.
    f. Remove the needle valve and wash it with acetone and high pressure air.
    g. Place the needle valve back and tighten it to seal off the line and prevent re-contamination whilst cleaning the rest of the cell.
24. Once the feed, vent and drain lines are clean, re-wash the inside of the cell with acetone and high-pressure air.
25. Clean the piston head and Teflon seal with acetone and high pressure air.
26. Turn off the camera.

C.2. Safety and risk assessment

In order to ensure safe operation of the equipment, task risk assessments forms were completed to identify possible hazards associated with the equipment and to evaluate the mitigating strategies which are in place to reduce the risk thereof. The template and risk assessment method were developed by the Department of Process Engineering and completion thereof was compulsory prior to commencing with experiments. The forms were completed in conjunction with other researchers using the same or similar equipment.

The risk calculator presented in Table 46 in Appendix A was also used to complete the risk assessment forms presented in Tables 63 to 67.

Table 63: Task risk assessment form completed to determine the hazards and risks related to loading the analytic setup

Ref No.	SPECIFIC TASK / ACTIVITY STEPS	IDENTIFY POTENTIAL HAZARDS	RISK RANKING			RISK CONTROL MEASURES • *Hierarchy of Control – Elimination, Substitution, Isolation, Engineering, Administration, Personal Protection.* • *Additional information can be attached.*	RESIDUAL RISK			Actioner / Initials
			Consequence	Likelihood	Risk Rating		Consequence	Likelihood	Residual Risk	
LOADING										
1	Switch on electrical plugs	Electrocution	2	2	L5	Isolation – plugs placed out of harm's way; Wear correct PPE; Administrative – correct plugs/adaptors bought;	2	1	L3	CL
2	Clean magnetic stirrer and place inside cell	Skin contact with acetone (99%)	1	4	M7	Wear correct PPE	1	3	L4	CL
3	Attach low-pressure chamber	Heavy load – injury to feet	2	3	M8	Engineering – correct lifting equipment available; Wear correct PPE	2	3	M8	CL
4	Remove feed line microvalve screw And clean the pin	Skin contact with acetone (99%)	1	4	M7	Wear correct PPE	1	3	L4	CL
5	Remove gas cylinder from the freezer and fill with CO_2	Temperature (cold) - burns; Pressure (high) - Equipment Failure Causing Explosive Decompression	4 4	2 1	M7 M10	Wear correct PPE; Engineering – designed to withstands pressures up to 300 bar; Hydrostatic tests conducted every 6 months to ensure safe operating conditions; Administrative – safety training done;	1 4	1 1	L1 M10	CL
6	Load the solutes using a syringe	Skin contact with liquid solutes – n-dodecane, 1-decanol + 3,7-dimethyl-1-octanol	1	3	L4	Wear correct PPE	1	2	L2	CL
7	Connecting the gas cylinder	High pressure - Equipment Failure Causing Explosive Decompression	4	1	M10	Engineering – designed to withstands pressures up to 300 bar; Hydrostatic tests conducted every 6 months to ensure safe operating conditions; Administrative – safety training done; Wear correct PPE	4	1	M10	CL

Table 63 continued: Task risk assessment form completed to determine the hazards and risks related to loading the analytic setup

Ref No.	SPECIFIC TASK / ACTIVITY STEPS	IDENTIFY POTENTIAL HAZARDS	RISK RANKING			RISK CONTROL MEASURES • Hierarchy of Control – Elimination, Substitution, Isolation, Engineering, Administration, Personal Protection. • Additional information can be attached.	RESIDUAL RISK			Actioner / Initials
			Consequence	Likelihood	Risk Rating		Consequence	Likelihood	Residual Risk	
8	Flushing the cell	High pressure - Equipment Failure Causing Explosive Decompression	4	1	M10	Engineering – cell and gas cylinder designed to withstand pressures up to 300 bar; Hydrostatic tests conducted every 6 months to ensure safe operating conditions; Administrative – correct training undergone to work with equipment safely; Wear correct PPE	4	1	M10	CL
9	Heating the cylinder with a hairdryer	Electrocution High pressure - Equipment Failure Causing Explosive Decompression	2 4	2 1	L5 M10	Engineering – cell and gas cylinder designed to withstand pressures up to 300 bar; Hydrostatic tests conducted every 6 months to ensure safe operating conditions; Administrative – correct training undergone to work with equipment safely; Wear correct PPE Isolation – plugs placed out of harm's way; Administrative – correct plugs/adaptors bought; Elimination – when conducting experiments with flammable vapours/solvents ensure the room is well ventilated before making use of the hairdryer.	2 4	1 1	L3 M10	CL

Table 63 continued: Task risk assessment form completed to determine the hazards and risks related to loading the analytic setup

Ref No.	SPECIFIC TASK / ACTIVITY STEPS	IDENTIFY POTENTIAL HAZARDS	RISK RANKING			RISK CONTROL MEASURES • *Hierarchy of Control – Elimination, Substitution, Isolation, Engineering, Administration, Personal Protection.* • *Additional information can be attached.*	RESIDUAL RISK			Actioner / Initials
			Consequence	Likelihood	Risk Rating		Consequence	Likelihood	Residual Risk	
10	Loading the solvent into the cell whilst heating the cylinder	Electrocution High pressure - Equipment Failure Causing Explosive Decompression	2 4	2 1	L5 M10	Engineering – cell and gas cylinder designed to withstand pressures up to 300 bar; Hydrostatic tests conducted every 6 months to ensure safe operating conditions; Administrative – correct training undergone to work with equipment safely; Wear correct PPE Isolation – plugs placed out of harm's way; Administrative – correct plugs/adaptors bought; Elimination – when conducting experiments with flammable vapours/solvents ensure the room is well ventilated before making use of the hairdryer.	2 4	1 1	L3 M10	CL
11	Removing the gas cylinder and tightening all the valves	High pressure- Equipment Failure Causing Explosive Decompression	4	1	M10	Engineering – cell and gas cylinder designed to withstand pressures up to 300 bar; Hydrostatic tests conducted every 6 months to ensure safe operating conditions; Administrative – correct training undergone to work with equipment safely; Wear correct PPE	4	1	M10	CL
12	Set the oven and water bath temperatures	Temperature of water bath - burn	2	2	L5	Wear correct PPE; Isolation – water bath and oven placed out of harm's way and closed	1	1	L1	CL

Table 64:Task risk assessment form completed to determine the hazards and risks related to measuring VLE data

Ref No.	SPECIFIC TASK / ACTIVITY STEPS	IDENTIFY POTENTIAL HAZARDS	RISK RANKING			RISK CONTROL MEASURES • *Hierarchy of Control – Elimination, Substitution, Isolation, Engineering, Administration, Personal Protection.* • *Additional information can be attached.*	RESIDUAL RISK			Actioner / Initials
			Consequence	Likelihood	Risk Rating		Consequence	Likelihood	Residual Risk	
SAMPLING										
1	Increase and/or decrease cell pressure to reach the set point	High pressure - Equipment Failure Causing Explosive Decompression	4	1	M10	Engineering – regular recertification of equipment; Administrative – regular hydrostatic testing; Wear correct PPE	4	1	M10	CL
2	Switch on detectors and open air, helium and hydrogen cylinders	Hydrogen leak – flammable environment, if ignited uncontrolled fire/explosion	4	1	M10	Engineering – gas bottles and thermocouples designed to withstand high pressures; Isolate – hydrogen placed away safely from other gas bottles and secured with cables; Administrative – Hydrogen cylinder and installation in lab was conducted/specified by the fire department (correct distance from other gases and minimum exposure to risks); Remaining gas bottles also secured safely with metal chains; Wear correct PPE; Administrative – correct training with gas bottles done, safety signs placed in lab and on gas bottle, safety switch on GC to switch off Remove ignition sources	4	1	M10	CL
3	Do a pre-purge run followed by alternating fast purge and analysis runs.	High temperature - burns High pressure - Equipment Failure Causing Explosive Decompression	2 4	2 1	L4 M10	Wear correct PPE; Isolation – the water bath and GC are placed out of the way securely Administrative – correct training done before starting with experiments; Engineering – regular recertification of equipment;	1 4	1 1	L1 M10	CL

Table 64 continued: Task risk assessment form completed to determine the hazards and risks related to measuring VLE data

Ref No.	SPECIFIC TASK / ACTIVITY STEPS	IDENTIFY POTENTIAL HAZARDS	RISK RANKING			RISK CONTROL MEASURES • *Hierarchy of Control – Elimination, Substitution, Isolation, Engineering, Administration, Personal Protection.* • *Additional information can be attached.*	RESIDUAL RISK			Actioner / Initials
			Consequence	Likelihood	Risk Rating		Consequence	Likelihood	Residual Risk	
4	Switch off detectors and close hydrogen, air and helium cylinders	Hydrogen leak – flammable environment, if ignited uncontrolled fire/explosion	4	1	M10	Engineering – gas bottles and thermocouples designed to withstand high pressures; Isolate – hydrogen placed away safely from other gas bottles and secured with cables; Administrative – Hydrogen cylinder and installation in lab was conducted/specified by the fire department (correct distance from other gases and minimum exposure to risks); Remaining gas bottles also secured safely with metal chains; Wear correct PPE; Administrative – correct training with gas bottles done, safety signs placed in lab and on gas bottle, safety switch on GC to switch off Engineering – regular recertification of equipment; Remove ignition sources	4	1	M10	CL
5	Set the water bath and oven to the next isothermal condition	High temperature - burns	2	2	L4	Wear correct PPE; Isolation – water bath and oven are closed and placed out of harm's way	1	1	L1	CL

Table 65: Task risk assessment form completed to determine the hazards and risks related to venting CO_2 from the analytic setup whilst loaded

Ref No.	SPECIFIC TASK / ACTIVITY STEPS	IDENTIFY POTENTIAL HAZARDS	RISK RANKING			RISK CONTROL MEASURES • *Hierarchy of Control – Elimination, Substitution, Isolation, Engineering, Administration, Personal Protection.* • *Additional information can be attached.*	RESIDUAL RISK			Actioner / Initials
			Consequence	Likelihood	Risk Rating		Consequence	Likelihood	Residual Risk	
VENTING SOLVENT										
1	Cool the cell using ice water	Low temperature - burns	1	2	L3	Wear correct PPE; Isolation – water bath closed and placed out of harm's way	1	1	L1	CL
2	Release carbon dioxide by opening the vent valve.	Low temperature - burns High pressure- Equipment Failure Causing Explosive Decompression	1 4	2 1	L3 M10	Wear correct PPE; Isolation – water bath closed and placed out of harm's way; Elimination – ensure no open flames in the lab when venting the solvent from the cell; Room ventilation should be on when unloading any solvent/solute mixtures from the equilibrium cell to avoid inhalation of hazardous vapours; Engineering – regular recertification of equipment; Administrative – regular hydrostatic testing;	1 4	1 1	L1 M10	CL
3	Systematically re-heat cell and then set water bath and oven temperature to desired value.	High temperature - burns	2	2	L4	Wear correct PPE; Isolation – water bath and oven is closed and placed out of harm's way	1	1	L1	CL

Table 66: Task risk assessment form completed to determine the hazards and risks related to adding CO_2 to the analytic setup whilst loaded

Ref No.	SPECIFIC TASK / ACTIVITY STEPS	IDENTIFY POTENTIAL HAZARDS	RISK RANKING			RISK CONTROL MEASURES • *Hierarchy of Control – Elimination, Substitution, Isolation, Engineering, Administration, Personal Protection.* • *Additional information can be attached.*	RESIDUAL RISK			Actioner / Initials
			Consequence	Likelihood	Risk Rating		Consequence	Likelihood	Residual Risk	
ADDING SOLVENT										
1	Remove cylinder from the freezer and load it.	Cold temperature - burns High pressure - Equipment Failure Causing Explosive Decompression	2 4	2 1	L4 M10	Wear correct PPE; Engineering – designed to withstands pressures up to 300 bar; Hydrostatic tests conducted every 6 months to ensure safe operating conditions; Administrative – safety training done;	1 4	1 1	L1 M10	CL
2	Heat the cylinder using a hairdryer	Electrocution High pressure - Equipment Failure Causing Explosive Decompression	2 4	2 1	L4 M10	Engineering – cell and gas cylinder designed to withstand pressures up to 300 bar; Hydrostatic tests conducted every 6 months to ensure safe operating conditions; Administrative – correct training undergone to work with equipment safely; Wear correct PPE Isolation – plugs placed out of harm's way; Administrative – correct plugs/adaptors bought; Elimination – when conducting experiments with flammable vapours/solvents ensure the room is well ventilated before making use of the hairdryer.	1 4	1 1	L1 M10	CL

Table 66 continued: Task risk assessment form completed to determine the hazards and risks related to adding CO_2 to the analytic setup whilst loaded

Ref No.	SPECIFIC TASK / ACTIVITY STEPS	IDENTIFY POTENTIAL HAZARDS	RISK RANKING			RISK CONTROL MEASURES • *Hierarchy of Control – Elimination, Substitution, Isolation, Engineering, Administration, Personal Protection.* • *Additional information can be attached.*	RESIDUAL RISK			Actioner / Initials
			Consequence	Likelihood	Risk Rating		Consequence	Likelihood	Residual Risk	
3	Flush the solvent loading line. Whilst heating load carbon dioxide to the cell.	High pressure - Equipment Failure Causing Explosive Decompression	4	1	M10	Engineering – cell and gas cylinder designed to withstand pressures up to 300 bar; Hydrostatic tests conducted every 6 months to ensure safe operating conditions; Administrative – correct training undergone to work with equipment safely; Wear correct PPE Elimination – when conducting experiments with flammable vapours/solvents ensure the room is well ventilated before making use of the hairdryer.	4	1	M10	CL

Table 67: Task risk assessment form completed to determine the hazards and risks related to unloading and cleaning the analytic setup

Ref No.	SPECIFIC TASK / ACTIVITY STEPS	IDENTIFY POTENTIAL HAZARDS	RISK RANKING			RISK CONTROL MEASURES • *Hierarchy of Control – Elimination, Substitution, Isolation, Engineering, Administration, Personal Protection.* • *Additional information can be attached.*	RESIDUAL RISK			Actioner / Initials
			Consequence	Likelihood	Risk Rating		Consequence	Likelihood	Residual Risk	
UNLOADING AND CLEANING										
1	Vent CO_2 from the degas line	Skin contact with liquid solutes – n-dodecane, 1-decanol + 3,7-dimethyl -1-octanol High pressure- Equipment Failure Causing Explosive Decompression	1 4	3 1	L4 M10	Engineering – regular recertification of equipment; Administrative – regular hydrostatic testing; Wear correct PPE; Administrative – correct waste containers placed below the cell; Elimination – ensure no open flames in the lab when venting the solvent from the cell; Room ventilation should be on when unloading any solvent/solute mixtures from the equilibrium cell to avoid inhalation of hazardous vapours	1 4	2 1	L2 M10	CL
2	Drain the liquid components through the bottom drain line	Skin contact with liquid solutes – n-dodecane, 1-decanol + 3,7-dimethyl -1-octanol	1	3	L4	Wear correct PPE	1	2	L2	CL
3	Loosen the piston bolts and unscrew the low pressure chamber of the cell	Heavy load – injury to feet	2	3	M8	Engineering – correct lifting equipment available; Wear correct PPE	2	3	M8	CL
4	Clean the stirrer and piston with acetone	Skin contact with acetone (99%)	1	4	M7	Wear correct PPE	1	3	L4	CL
5	Wash the cell and all drain and vent valves with acetone and flush with compressed air	Skin contact with acetone (99%)	1	4	M7	Wear correct PPE	1	3	L4	CL
6	Discard the waste into the respective containers	Skin contact with acetone (99%)	1	4	M7	Wear correct PPE	1	3	L4	CL

C.3. Pressure calibration data

Pressure calibrations were performed using a dead weigh tester and the data gathered from the calibrations were used develop linear temperature-specific pressure correlation. The pressure calibration data along with the pressure correlation curves are presented Table 68.

Table 68: Pressure calibration data and temperature-specific pressure correlations for the analytic setup [Calibrated in September 2016].

Set Temperature 1		**Set Temperature 2**		**Set Temperature 3**	
$T_{calibration}$ [°C] 35	$T_{ambient}$ [°C] 18	$T_{calibration}$ [°C] 55	$T_{ambient}$ [°C] 18	$T_{calibration}$ [°C] 75	$T_{ambient}$ [°C] 18
Gefran Process	Julabo (13) EC-DIAG	Gefran Process	Julabo (13) EC-DIAG	Gefran Process	Julabo (13) EC-DIAG
T_{set} [°C] = 34.6	T_{set} [°C] = 34.37	T_{set} [°C] = 54.6	T_{set} [°C] = 54.37	T_{set} [°C] = 74.6	T_{set} [°C] = 74.37
$T_{display}$[°C] = 34.6	$T_{display}$[°C] = 34.33-34.36	$T_{display}$[°C] = 54.7	$T_{display}$[°C] = 54.64-54.59	$T_{display}$[°C] = 74.70	$T_{display}$[°C] = 74.55-74.50
$P_{applied}$ (bar)	$P_{display}$ (bar)	$P_{applied}$ (bar)	$P_{display}$ (bar)	$P_{applied}$ (bar)	$P_{display}$ (bar)
5.0	-4.1	5.0	-2.4	5.0	-0.1
20.0	9.3	20.0	11.0	20.0	13.3
34.9	23.8	34.9	25.7	34.9	28.0
49.9	38.6	49.9	40.5	49.9	42.8
64.9	53.6	64.9	55.6	64.9	57.6
79.8	68.7	79.8	70.5	79.8	72.8
94.8	83.8	94.8	85.7	94.8	87.8
109.7	99.0	109.7	100.9	109.7	103.0
124.7	114.2	124.7	116.1	124.7	118.1
139.7	129.3	139.7	131.3	139.7	133.3
154.6	144.6	154.6	146.5	154.6	148.5
169.6	159.8	169.6	161.7	169.6	163.6
184.6	175.0	184.6	176.9	184.6	178.8
199.5	190.1	199.5	192.0	199.5	194.0
214.5	205.3	214.5	207.2	214.5	209.2
229.4	220.5	229.4	222.2	229.4	224.2
244.4	235.6	244.4	237.4	244.4	239.4
259.4	250.8	259.4	252.5	259.4	254.4
274.3	265.8	274.3	267.6	274.3	269.6
289.3	280.9	289.3	282.6	289.3	284.6
294.3	286.0	294.3	287.7	294.3	289.6
299.3	290.9	299.3	292.6	299.3	294.5
303.3	294.9	303.3	296.6	303.3	298.6
$P_{display}$ = **SLOPE** × $P_{applied}$ + **INTERCEPT**		$P_{display}$ = **SLOPE** × $P_{applied}$ + **INTERCEPT**		$P_{display}$ = **SLOPE** × $P_{applied}$ + **INTERCEPT**	
SLOPE	1.0095	SLOPE	1.0091	SLOPE	1.0079
INTERCEPT	-11.3040	INTERCEPT	-9.4016	INTERCEPT	-7.1548
RSQ	1.0000	RSQ	1.0000	RSQ	1.0000

C.4. Temperature calibration data

The temperature probe used to measure the temperature within the equilibrium cell was calibrated by Thermon South Africa (Pty) Ltd., which is a South African National Accreditation System (SANAS) approved institute. The calibration was performed at four temperatures between 30ºC and 120ºC. The calibration certificates for the Pt100 probe, along with the temperature correction correlation developed using the data are presented in this appendix.

Thermon
South Africa (Pty) Ltd.

unitemp

Calibration certificate CAL-UC-S-T-160229X03

certificate number

sanas Calibration Laboratory 1573, 373

Lab measurement equipment with certified traceability to international standards

Description	Cert. No.	Equipment. Number
Testo 400 with PT100 probe	TH\DG-6754	Unitemp4

Ambient conditions.

Temperature: 23 °C ± 5 °C

Measuring procedure (P0051)

The measurements read on this test item, in a thermostatic bath, were obtained while placed in very close proximity of a reference probe.

The result is calculated from an average of ***6*** *readings @* ***30*** *seconds intervals*

Measurement results for hi-accuracy digital thermometer with 1/10 4-wire-Pt100 external probe

Indication from reference in °C	Indication from your measuring instrument in °C	**Deviation in °C**	Manufacture's allowed tolerance in °C	Expanded uncertainty of measurement in °C	Probe insertion depth in mm	Reference Equipment Used
30.015	29.43	**-0.58**	n/a	± 0.05	45	Unitemp4
60.176	59.29	**-0.89**	n/a	± 0.05	45	Unitemp4
90.078	89.52	**-0.56**	n/a	± 0.05	45	Unitemp4
120.035	119.42	**-0.61**	n/a	± 0.05	45	Unitemp4

Validity of Certificate

The measurement results recorded in this certificate relate only to the instrument & attachments specified, and were correct at the time. Only the above points have been checked & performance at other points is not certain. Subsequent accuracy will depend on factors such as care, handling and frequency of use. It is recommended that recalibration be undertaken at an interval that will ensure that the instrument remains within the desired limits.

CALIBRATION LABORATORY THERMON SA (Pty) Ltd. 2016 -03- 03 CAPE TOWN

page 2 of 2

END

Calibration • Validation • Training

Email: sales.za@thermon.com **Web**: www.thermon.co.za

Thermon South Africa (Pty) Ltd. Reg. No. 2015/020118/07. VAT No. 4750268387. **Directors**: G.P. Alexander, R.L. Bingham, J.C. Peterson

Temperature correction correlation:

$T_{actual}(^0C) = 0.9992T_{read}(^0C) + 0.7206$

C.5. GC calibration data

The component-specific calibration curves which were used to quantify the composition of the sampled phases are presented in Figures 128 to 131.

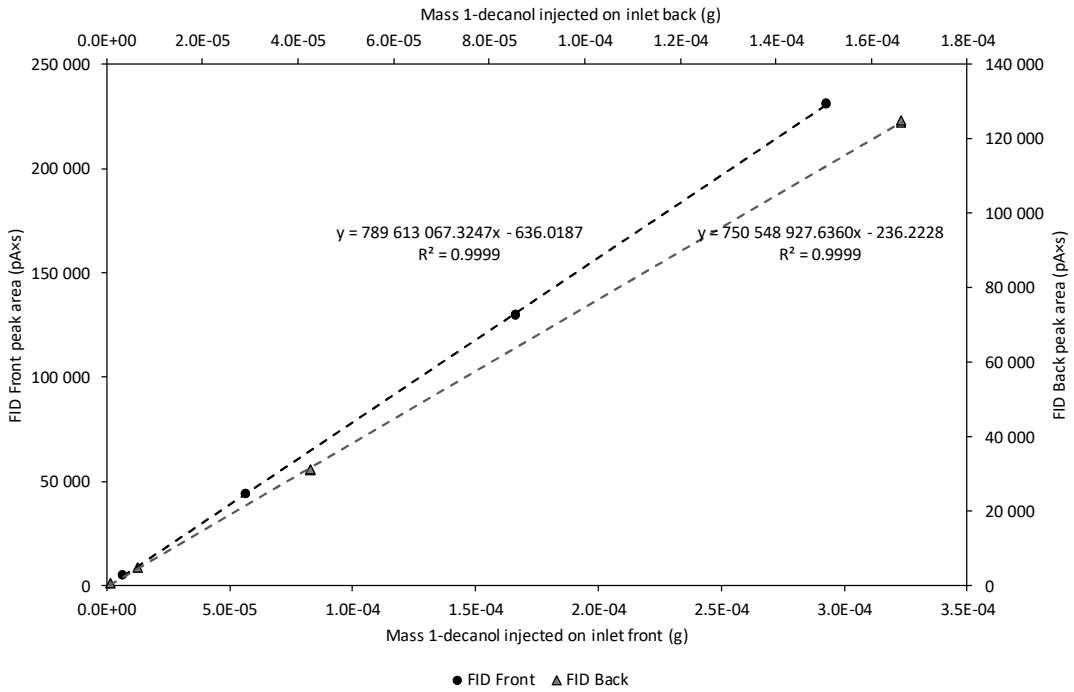

Figure 128: Calibration curves used to quantify the amount of 1-decanol present in the vapour (FID Back) and liquid (FID Front) phases.

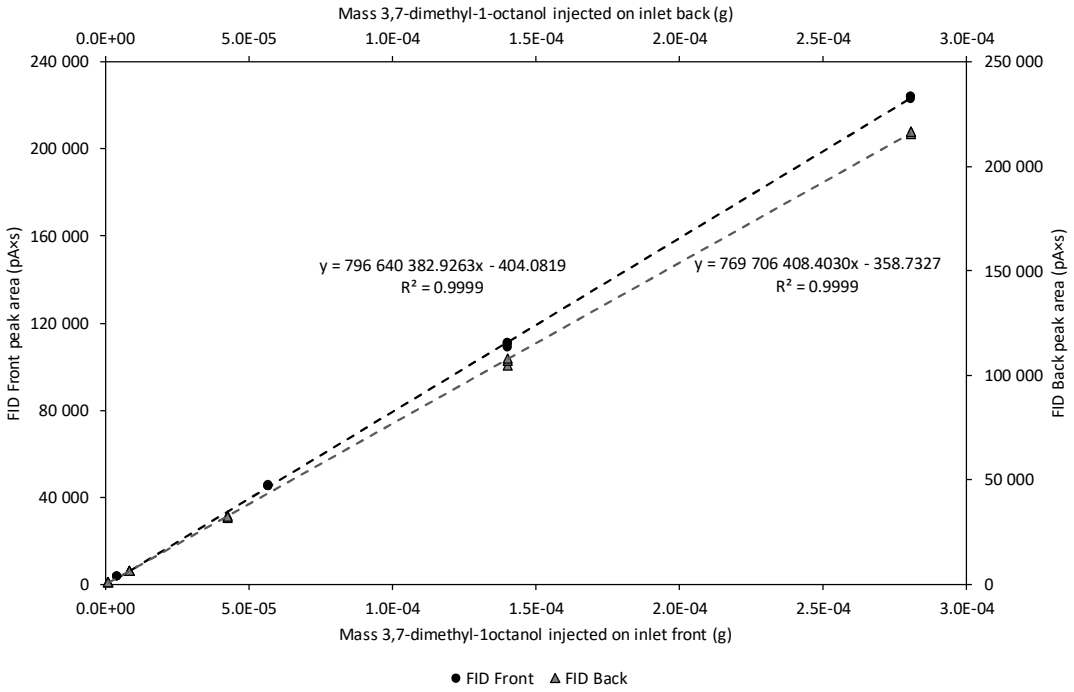

Figure 129: Calibration curves used to quantify the amount of 3,7-dimethyl-1-octanol present in the vapour (FID Back) and liquid (FID Front) phases.

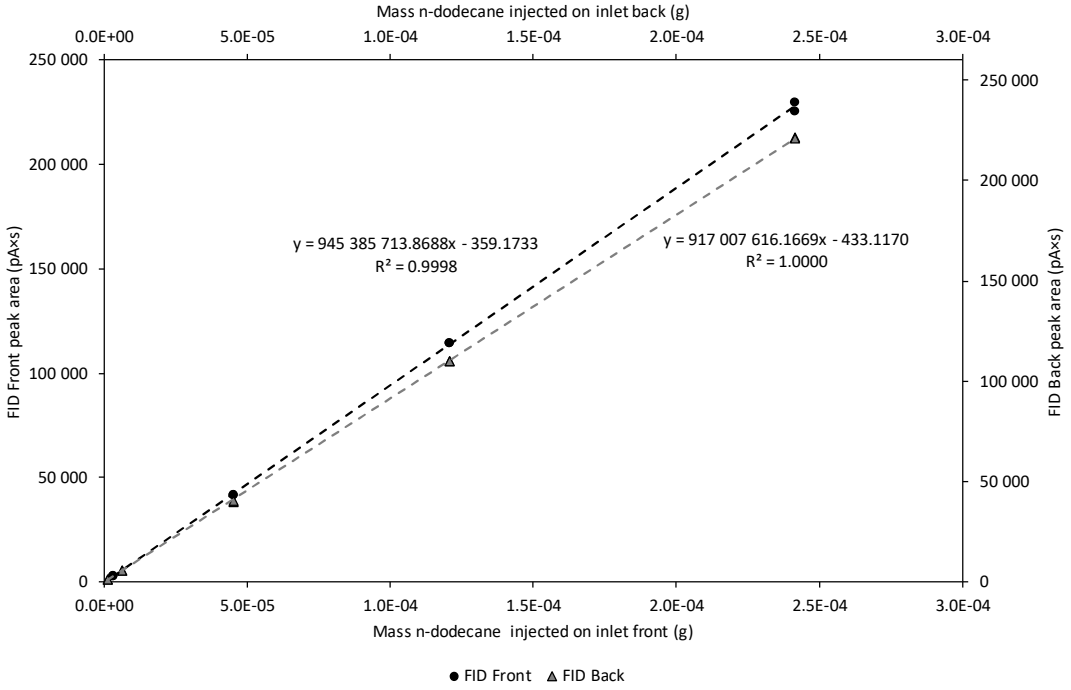

Figure 130: Calibration curves used to quantify the amount of n-dodecane present in the vapour (FID Back) and liquid (FID Front) phases.

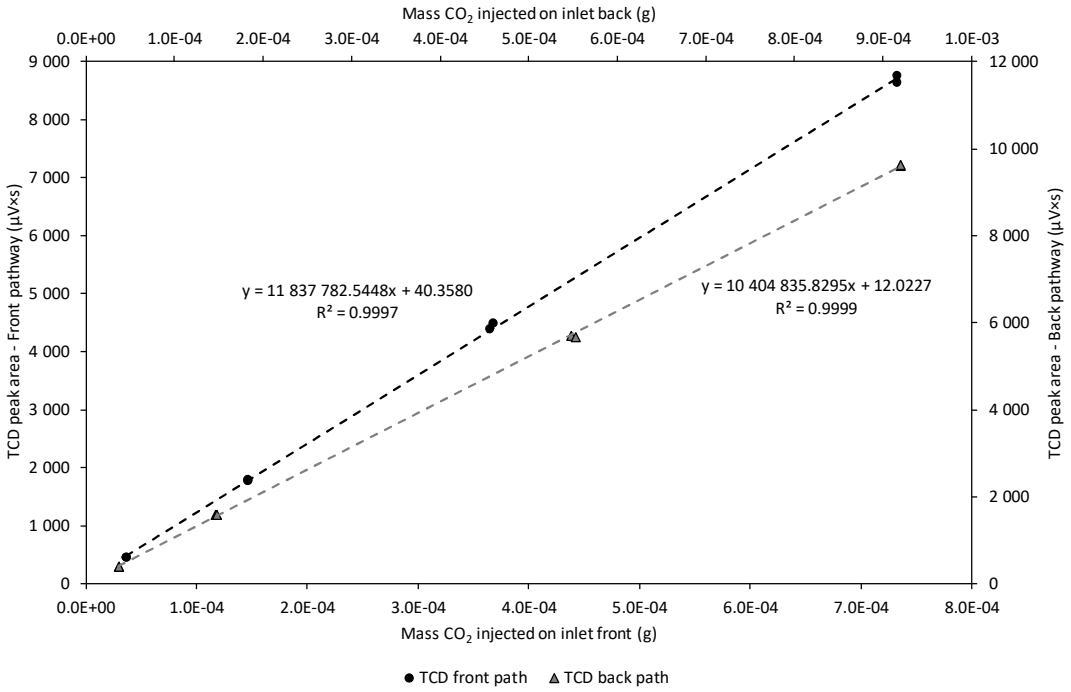

Figure 131: Calibration curves used to quantify the amount of CO_2 present in the vapour (TCD back path) and liquid (TCD front path) phases.

C.6. Accuracy analysis of co-existing compositions

In order to determine the uncertainty in the mass fractions reported in this work, the "Guide to the expression of uncertainty in measurement" [113] was used. In this guide, an 8-step procedure is outlined to evaluate and express uncertainty. In this work, the first 6 steps were used to determine the accuracy of the compositions reported in this work. These steps are described in this appendix and application thereof is illustrated. Sample calculations are also provided.

Step 1: Mathematically model the measurand Y, using its dependent input quantities X_i

The mass of each component is determined using calibration curves in which the adapted peak area (the original area x ratio of the bubble-flow-test results) is plotted against mass. Modelling the measurand i.e. mass fraction, therefore has two sections. The first is the calibration where the mass is determined using linear correlations between mass and peak area. The calibration method differs for solutes and solvents and each is outlined below. The second is determining the mass fraction.

Calibration:

$$A_i \left[\frac{C_1}{\tau_B}\right] = \alpha + \beta m_i$$

For the solutes:

$$A_i = \left[\frac{\tau_B}{C_1}\right]\alpha + \left[\frac{\tau_B\beta}{C_1}\right]m_i = \left[\frac{\tau_B}{C_1}\right]\alpha + \left[\frac{\tau_B\beta}{C_1}\right]\rho_i y_i V$$

For the solvent:

$$A_i = \left[\frac{\tau_B}{C_1}\right]\alpha + \left[\frac{\tau_B\beta}{C_1}\right]m_i = \left[\frac{\tau_B}{C_1}\right]\alpha + \left[\frac{\tau_B\beta}{C_1}\right]\frac{PVM_w}{RT}$$

Thus,

$$A_i = \alpha' + \beta' m_i$$

$$\alpha = \frac{\alpha' C_1}{\tau}$$

$$\beta = \frac{\beta' C_1}{\tau}$$

Mass fraction determination:

$$w_i = \frac{m_i}{m_1 + m_2 + m_3 + m_4}$$

With $m_i = \frac{1}{\beta}\left[\frac{A_i C_1}{\tau} - \alpha\right]$

Step 2: Determine the estimated input values, x_i

A_i → Obtained from GC

α, β → Obtained from calibration data

C_1 → Constant set at 9.73

τ → Obtained from bubble flow tests

Step 3: Determine the standard uncertainty of the input estimates

A_i → Standard deviation of the GC peak areas

α, β → Obtained from calibration data

C_1 → Obtained from bubble flow tests

τ → Obtained from bubble flow tests

Step 4: Determine covariance between input estimates

If the input quantities are correlated, the covariance between them must be taken into account in order to prevent an overestimation of the error. The correlation coefficient presented below is used to characterise the degree of correlation between the input quantities x_i and x_j [113].

$$r(x_i, x_j) = \frac{u(x_i, x_j)}{u(x_i)u(x_j)}$$

Where $-1 \leq r(x_i, x_j) \leq 1$ and if x_i and x_j are independent/uncorrelated $r(x_i, x_j) = 0$.

Co-variance can be neglected if [113]:

- The input quantities are uncorrelated e.g. measured in a different experiment or using different equipment.
- One of the input quantities is a constant.
- There is insufficient data to determine the covariance between the input variables.

The covariance of the input quantities in this work is analysed in the symmetric matrix below. From this is it seen that covariance must be accounted for between the α and β values, as they are linked in the calibration correlations.

	α	β	A_i	C_1	τ
α	-	-	-	-	-
β	YES	-	-	-	-
A_i	NO	NO	-	-	-
C_1	NO	NO	NO	-	-
τ	NO	NO	NO	NO	-

Step 5: Calculate the estimate y, using the input estimates evaluated in step 2

Input all the estimated inputs into: $m_i = \frac{1}{\beta}\left[\frac{A_i\, C_1}{\tau} - \alpha\right]$

Step 6: Evaluate the combined standard uncertainty

Determine the combined standard uncertainty by using the Law of Propagation Uncertainty [113]:

$$u_c^2\,(m_i) = \sum_{i=1}^{N}\left(\frac{\partial m_i}{\partial x_i}\right)^2 u^2(x_i) + 2\sum_{i=1}^{N-1}\sum_{j}^{N}\left(\frac{\partial m_i}{\partial x_i}\right)\left(\frac{\partial m_i}{\partial x_j}\right) u^2(x_i, x_j)$$

Application to 1-decanol:

(see GUM [113] *guidelines for formulas)*

Calibration contribution to uncertainty:

(i) *Physical calibration technique*

X_i	Step 2 x_i	Step 3 $u(x_i)$	Units	Notes
ρ_{C10OH}	0.83	**0.0012**	g/mL	
ρ_{2E1H}	0.833	**0.0012**	g/mL	
y	0.8294	**0.0003**	mL/mL	
Uncertainty in preparing the GC dilution sample for calibration (y is volume fraction solute) — Input estimates	Value	u		
m_{C10OH}	0.2596	0.0000448	g	[Scale calibration]
m_{2E1H}	1.2667	0.0000448	g	
ρ_{C10OH}	0.83	0.0012	g/mL	[NIST approximate]
ρ_{2E1H}	0.833	0.0012	g/mL	
Derivatives	Value	Uncertainty contribution		
m_{C10OH}	0.545	5.96225E-10		
m_{2E1H}	-0.112	2.50422E-11		
ρ_{C10OH}	-0.170	4.18475E-08		
ρ_{2E1H}	0.170	4.15466E-08		
$V_{Syringe}$	0.0004	**4.6188E-06**	mL	[Manufacturer certificate]
τ	9.38	**0.032787193**	s	[Repeated bubble-flow-test]
C_1	9.73	**0.032787193**	s	[Repeated bubble-flow-test]
A_1	42241	**42.66341**		[Repeated GC results]

(ii) *Correlations developed using data*

Calibration data, y = α + ßx

i	m_{C10OH} (g) x_i	*Adapted peak area* y_i	x_i^2	$x_i y_i$	$(x_i - x_{avg})^2$	R_i^2	$(y_i - y_{avg})^2$
1	5.664E-05	4.380E+04	3.208E-09	2.4808057	5.46198E-09	80642.489	3438705767
2	1.663E-04	1.299E+05	2.765E-08	21.59796	1.27776E-09	615924.09	752982813.1
3	1.663E-04	1.295E+05	2.765E-08	21.533008	1.27776E-09	1381575.2	731699056.1
4	6.531E-06	5.122E+03	4.266E-11	0.0334554	1.53788E-08	361347.75	9471136177
5	2.927E-04	2.307E+05	8.568E-08	67.542815	2.62993E-08	64176.941	16462270115
6	6.531E-06	5.044E+03	4.266E-11	0.0329414	1.53788E-08	272940.3	9486457617
7	5.664E-05	4.406E+04	3.208E-09	2.4952861	5.46198E-09	801.31181	3408786056
8	2.927E-04	2.314E+05	8.568E-08	67.730817	2.62993E-08	802109.42	16627497032
∑	0.00104434	819536.5602	2.332E-07	183.44709	9.68357E-08	3579517.5	60379534633
Avg	0.000130543	102442.07					

Uncertainty calculations for calibration using above given data (equations H.3.2 [113]):

n	8
D	7.74685E-07
α	-636.0187024
$ß$	789613067.3
s^2	596586.2527
$\boldsymbol{u(\alpha)}$	**423.7473689**
$\boldsymbol{u(ß)}$	**2482098.091**

Step 2 for α and β

Step 3 for α and β

$r(\alpha,ß)$	-0.764652225
$\boldsymbol{u(\alpha,ß)}$	**-804247855.7**

Step 4 covariance between α and β

Additional contributions to u(α) (based on H.3.2 note 2 [113]:

$$A_i = \left[\frac{\tau_B}{C_1}\right]\alpha + \left[\frac{\tau_B\beta}{C_1}\right]m_i = \left[\frac{\tau_B}{C_1}\right]\alpha + \left[\frac{\tau_B\beta}{C_1}\right]\rho_i y_i V \quad \rightarrow \quad \alpha_a = \frac{A_i\, C_1}{\tau_B}$$

$$\rightarrow \quad \alpha_b = \left[\frac{\tau_B\beta}{C_1}\right]\rho_i y_i V$$

Uncertainty for α_a using the Law of Propagation Uncertainty:

Derivatives with regards to:	Value	Contribution to u
A	1.037313433	1958.534081
C_1	4503.304904	21800.73669
τ_B	-4671.338669	23458.01033
$\boldsymbol{\alpha_a}$	**43817.15672**	**217.2953775**

Uncertainty for α_b using the Law of Propagation Uncertainty:

Derivatives with regards to:	Value	Contribution to u
ρ_{C10OH}	2.53E+05	9.18E+04
y	2.54E+05	5.40E+03
V_T	5.26E+08	5.90E+06
C_1	-21620.38571	5.02E+05
τ_B	2.24E+04	5.41E+05
$ß$	0.000266417	4.37E+05
$\boldsymbol{\alpha_b}$	**2.10E+05**	**2.73E+03**

Step 5 and 6 for area

Total uncertainty in α:

$$\boldsymbol{u_c(\alpha)} = \sqrt{u(\alpha)^2 + u(\alpha_a)^2 + u(\alpha_b)^2} = 2775.8$$

Experimental contribution to uncertainty:

X_i	***Step 2*** x_i	***Step 3*** $u(x_i)$	**Units**	**Notes**
α	-636.0187024	**2775.794692**		[Calibration curve]
β	789613067.3	**2482098.091**		[Calibration curve]
A	391283	**3951.9583**		[Repeated GC results]
C_1	9.73	**0.032787193**	s	[Repeated bubble-flow-test]
τ_B	9.168	**0.008151391**	s	[Repeated bubble-flow-test]

Covariance calculated previously: **u(α,ß) = -804247855.7** | Step 4 covariance between α and β

Using the Law of Propagation Uncertainty:

$$m_i = \frac{1}{\beta}\left[\frac{A_i\, C_1}{\tau} - \alpha\right]$$

Derivatives with regards to:	Value	Contribution to u
α	-1.26644E-09	1.23579E-11
β	-6.6706E-13	2.74137E-12
A	1.34408E-09	2.82145E-11
C_1	5.40508E-05	3.1406E-12
τ_B	-5.73641E-05	2.18647E-13
α,β	8.44794E-22	-1.35885E-12
m_i	**0.5267**	**0.0067**

Step 5 and 6 for mass of 1-decanol

Do this for all components and results are as follows:

X_i	x_i	$u(x_i)$	**Units**
m_{C10OH}	0.5267197	0.006731584	g
m_{nC12}	0.0250657	0.003901183	g
m_{37DM1O}	0.0675696	0.003578871	g
m_{CO2}	0.7649144	0.010903565	g

Calculate the uncertainty in mass fraction using the Law of Propagation Uncertainty:

$$w_i = \frac{m_i}{m_1 + m_2 + m_3 + m_4}$$

Derivative with regards to:	Value	Contribution to u
m_{C10OH}	0.4475	9.08E-06
m_{nC12}	-0.2749	1.15E-06
m_{37DM1O}	-0.2749	9.68E-07
m_{CO2}	-0.2749	8.98E-06
w_{C10OH}	**0.3805**	**0.004**

D. Vapour-Liquid-Equilibrium Experimental Data

The VLE data measured in this work for the three quaternary mixtures containing CO_2 with n-dodecane, 3,7-dimethyl-1-octanol and 1-decanol is presented in Tables 69 to 77.

Table 69: Experimental VLE data for the quaternary systems CO_2 + (5 wt% n-dodecane + 12 wt% 3,7-dimethyl-1-octanol + 83 wt% 1-decanol) at 35ºC.

SAMPLE	P_{READ}	P_{ACT}	T_{READ}	T_{ATC}	Purge Flow Split Vent (s)										FID Front (pA×s)			FID Back (pA×s)			TCD CO_2 (µV×s)		ROLSI Back$_{(Front\ Path)}$ mass fraction				ROLSI Front$_{(Back\ Path)}$ mass fraction			
	(barg)	(bar)	(°C)	(°C)	Front (ref. = 9.73)					Back (ref. = 9.56)					37DM1O	nC_{12}	$C_{10}OH$	37DM1O	nC_{12}	$C_{10}OH$	Front path	Back path	CO_2	37DM1O	nC_{12}	$C_{10}OH$	CO_2	37DM1O	nC_{12}	$C_{10}OH$
1	92.8	104.1	34.79	35.48	9.50	9.53	9.47	9.47		9.31	9.28	9.40	9.41		47218.0	19 289	371 085	830	1 252	4 743	3 799	1 998	0.365	0.069	0.024	0.542	0.950	0.008	0.009	0.033
	92.8	104.1	34.79	35.48	9.31	9.50	9.41	9.50		8.93	8.93	8.97			48452.5	19 876	378 544	850	1 249	4 757	3 929	1 955	0.369	0.069	0.024	0.539	0.949	0.008	0.009	0.034
	92.9	104.2	34.80	35.49	9.47	9.50	9.50	9.47		8.93	8.88	9.03	8.96		46568.4	19 147	364 366	838	1 225	4 737	3 788	1 954	0.369	0.069	0.024	0.538	0.949	0.008	0.009	0.034
	92.8	104.1	34.80	35.49	9.47	9.56	9.47	9.53		9.41	9.25	9.31	9.31	9.31	46390.6	19 012	365 131	854	1 252	4 833	3 782	2 014	0.368	0.068	0.024	0.540	0.950	0.008	0.009	0.033
																						AVERAGE		**0.368**	**0.069**	**0.024**	**0.540**	**0.950**	**0.008**	**0.009**	**0.033**
																						STANDARD DEVIATION		**0.002**	**0.000**	**0.000**	**0.002**	**0.001**	**0.000**	**0.000**	**0.000**
SAMPLE	P_{READ}	P_{ACT}	T_{READ}	T_{ATC}	Purge Flow Split Vent (s)										FID Front (pA×s)			FID Back (pA×s)			TCD CO_2 (µV×s)		ROLSI Back$_{(Front\ Path)}$ mass fraction				ROLSI Front$_{(Back\ Path)}$ mass fraction			
	(barg)	(bar)	(°C)	(°C)	Front (ref. = 9.73)					Back (ref. = 9.56)					37DM1O	nC_{12}	$C_{10}OH$	37DM1O	nC_{12}	$C_{10}OH$	Front path	Back path	CO_2	37DM1O	nC_{12}	$C_{10}OH$	CO_2	37DM1O	nC_{12}	$C_{10}OH$
2	111.8	122.9	34.76	35.45	9.35	9.44	9.37	9.32		8.88	8.97	8.88	8.78	8.88	52783.5	21 332	419 873	1 373	1 729	8 072	4 649	2 300	0.385	0.066	0.023	0.526	0.933	0.010	0.010	0.047
	112.0	123.1	34.76	35.45	9.37	9.47	9.32	9.35		9.19	9.22	9.25			53971.1	21 951	422 959	1 503	1 850	8 995	4 802	2 355	0.390	0.066	0.023	0.521	0.929	0.010	0.010	0.051
	112.1	123.2	34.77	35.46	9.31	9.28	9.35			9.34	9.28	9.19	9.32	9.28	51783.4	20 931	411 994	1 449	1 813	8 559	4 559	2 371	0.385	0.066	0.023	0.527	0.932	0.010	0.010	0.048
																						AVERAGE		**0.387**	**0.066**	**0.023**	**0.525**	**0.932**	**0.010**	**0.010**	**0.049**
																						STANDARD DEVIATION		**0.003**	**0.000**	**0.000**	**0.003**	**0.002**	**0.000**	**0.000**	**0.002**
SAMPLE	P_{READ}	P_{ACT}	T_{READ}	T_{ATC}	Purge Flow Split Vent (s)										FID Front (pA×s)			FID Back (pA×s)			TCD CO_2 (µV×s)		ROLSI Back$_{(Front\ Path)}$ mass fraction				ROLSI Front$_{(Back\ Path)}$ mass fraction			
	(barg)	(bar)	(°C)	(°C)	Front (ref. = 9.73)					Back (ref. = 9.56)					37DM1O	nC_{12}	$C_{10}OH$	37DM1O	nC_{12}	$C_{10}OH$	Front path	Back path	CO_2	37DM1O	nC_{12}	$C_{10}OH$	CO_2	37DM1O	nC_{12}	$C_{10}OH$
3	129.0	140.0	34.81	35.50	9.69	9.75	9.72	9.69		9.34	9.50	9.53	9.41	9.53	60207.5	24 687	472 841	2 519	2 475	16 207	5 721	2 679	0.406	0.064	0.022	0.507	0.899	0.013	0.011	0.077
	128.9	139.9	34.82	35.51	9.50	9.47	9.44	9.50		9.32	9.35	9.44	9.35	9.44	58106.5	23 495	461 354	2 409	2 377	15 512	5 427	2 602	0.400	0.064	0.022	0.514	0.900	0.013	0.011	0.076
	129.2	140.2	34.82	35.51	9.43	9.56	9.38	9.47	9.56	9.37	9.44	9.47	9.38		59181.4	24 203	462 420	2 516	2 495	16 061	5 591	2 635	0.406	0.065	0.022	0.507	0.898	0.013	0.011	0.077
	129.0	140.0	34.81	35.50	9.53	9.44	9.50	9.44		9.25	9.25	9.25			59137.6	24 127	466 925	2 345	2 362	15 009	5 584	2 560	0.403	0.064	0.022	0.510	0.901	0.013	0.011	0.075
	128.9	139.9	34.80	35.49	9.38	9.50	9.47	9.41		9.41	9.31	9.40	9.40	9.44	57125.7	23 206	453 357	2 416	2 384	15 452	5 338	2 536	0.400	0.064	0.022	0.514	0.898	0.013	0.011	0.077
																						AVERAGE		**0.403**	**0.064**	**0.022**	**0.510**	**0.899**	**0.013**	**0.011**	**0.076**
																						STANDARD DEVIATION		**0.003**	**0.000**	**0.000**	**0.003**	**0.001**	**0.000**	**0.000**	**0.001**
SAMPLE	P_{READ}	P_{ACT}	T_{READ}	T_{ATC}	Purge Flow Split Vent (s)										FID Front (pA×s)			FID Back (pA×s)			TCD CO_2 (µV×s)		ROLSI Back$_{(Front\ Path)}$ mass fraction				ROLSI Front$_{(Back\ Path)}$ mass fraction			
	(barg)	(bar)	(°C)	(°C)	Front (ref. = 9.73)					Back (ref. = 9.56)					37DM1O	nC_{12}	$C_{10}OH$	37DM1O	nC_{12}	$C_{10}OH$	Front path	Back path	CO_2	37DM1O	nC_{12}	$C_{10}OH$	CO_2	37DM1O	nC_{12}	$C_{10}OH$
4	146.1	156.9	34.75	35.44	9.12	9.09	9.10	9.12		9.09	9.09	9.03	9.12		63313.6	24 341	508 619	3 151	2 781	20 519	6 356	2 983	0.415	0.062	0.020	0.502	0.889	0.014	0.011	0.086
	146.1	156.9	34.76	35.45	9.12	9.09	9.07	9.16	9.13	9.00	8.94	9.03	9.06	9.09	62053.7	23 991	496 785	3 279	2 864	21 401	6 274	2 964	0.418	0.062	0.020	0.500	0.884	0.015	0.011	0.090
	146.1	156.9	34.74	35.43	9.06	9.03	9.15	9.09		8.28	8.31	8.32	8.34		61757.7	23 649	497 961	2 908	2 555	19 045	6 127	2 671	0.412	0.062	0.020	0.506	0.885	0.015	0.011	0.089
																						AVERAGE		**0.415**	**0.062**	**0.020**	**0.502**	**0.886**	**0.015**	**0.011**	**0.088**
																						STANDARD DEVIATION		**0.003**	**0.000**	**0.000**	**0.003**	**0.002**	**0.000**	**0.000**	**0.002**
SAMPLE	P_{READ}	P_{ACT}	T_{READ}	T_{ATC}	Purge Flow Split Vent (s)										FID Front (pA×s)			FID Back (pA×s)			TCD CO_2 (µV×s)		ROLSI Back$_{(Front\ Path)}$ mass fraction				ROLSI Front$_{(Back\ Path)}$ mass fraction			
	(barg)	(bar)	(°C)	(°C)	Front (ref. = 9.73)					Back (ref. = 9.56)					37DM1O	nC_{12}	$C_{10}OH$	37DM1O	nC_{12}	$C_{10}OH$	Front path	Back path	CO_2	37DM1O	nC_{12}	$C_{10}OH$	CO_2	37DM1O	nC_{12}	$C_{10}OH$
5	159.3	170.0	34.72	35.41	9.06	9.06	9.13	9.12	9.19	8.93	9.00	9.06	8.96	8.97	66240.3	26615	530179	4385	3897	28452	6755	3638	0.420	0.062	0.021	0.497	0.876	0.015	0.012	0.096
	159.3	170.0	34.72	35.41	9.10	9.00	9.03	9.00	8.94	8.88	8.94	8.91	8.97	8.91	66119.9	26740	529362	4044	3662	26025	6839	3619	0.423	0.062	0.021	0.494	0.885	0.015	0.011	0.089
	159.2	169.9	34.71	35.40	9.00	9.00	8.93	8.90	8.91	8.40	8.41	8.38	8.44	8.43	66722.9	26826	538403	3928	3483	25477	6811	3353	0.418	0.062	0.021	0.499	0.879	0.015	0.012	0.094
	159.3	170.0	34.71	35.40	8.85	8.88	8.87	8.88		8.81	8.78	8.72	8.85	8.81	66466.3	26962	528151	4082	3692	26210	6800	3651	0.422	0.062	0.021	0.495	0.885	0.015	0.011	0.089
																						AVERAGE		**0.421**	**0.062**	**0.021**	**0.496**	**0.881**	**0.015**	**0.012**	**0.092**
																						STANDARD DEVIATION		**0.002**	**0.000**	**0.000**	**0.002**	**0.004**	**0.000**	**0.000**	**0.003**
SAMPLE	P_{READ}	P_{ACT}	T_{READ}	T_{ATC}	Purge Flow Split Vent (s)										FID Front (pA×s)			FID Back (pA×s)			TCD CO_2 (µV×s)		ROLSI Back$_{(Front\ Path)}$ mass fraction				ROLSI Front$_{(Back\ Path)}$ mass fraction			
	(barg)	(bar)	(°C)	(°C)	Front (ref. = 9.73)					Back (ref. = 9.56)					37DM1O	nC_{12}	$C_{10}OH$	37DM1O	nC_{12}	$C_{10}OH$	Front path	Back path	CO_2	37DM1O	nC_{12}	$C_{10}OH$	CO_2	37DM1O	nC_{12}	$C_{10}OH$
6	181.6	192.1	34.78	35.47	9.66	9.59	9.59	9.71	9.69	9.25	9.31	9.31	9.28		10749.9	10 342	76 420	19 668	8 170	152 174	10 076	2 373	0.873	0.014	0.012	0.101	0.488	0.056	0.020	0.436
	181.6	192.1	34.78	35.47	9.25	9.25	9.28			9.22	9.22	9.28	9.28		10414.4	10 024	73 105	19 667	8 131	152 354	9 821	2 383	0.875	0.014	0.012	0.099	0.488	0.056	0.020	0.436
	181.6	192.1	34.76	35.45	9.18	9.16	9.28	9.29	9.31	9.13	9.10	9.19	9.22	9.22	11060.4	8 594	71 674	19 455	8 019	149 889	9 894	2 302	0.878	0.015	0.010	0.097	0.484	0.057	0.020	0.440
	181.6	192.1	34.76	35.45	9.13	9.19	9.19	9.28	9.25	8.38	8.41	8.43	8.38		10475.7	8 411	67 555	17 700	7 220	137 676	9 524	2 085	0.880	0.015	0.010	0.095	0.480	0.057	0.020	0.443
																						AVERAGE		**0.877**	**0.015**	**0.011**	**0.098**	**0.485**	**0.056**	**0.020**	**0.439**
																						STANDARD DEVIATION		**0.003**	**0.000**	**0.001**	**0.003**	**0.004**	**0.000**	**0.000**	**0.003**

Table 70: Experimental VLE data for the quaternary systems CO_2 + (5 wt% n-dodecane + 12 wt% 3,7-dimethyl-1-octanol + 83 wt% 1-decanol) at 55ºC.

SAMPLE	P_{READ}	P_{ACT}	T_{READ}	T_{ATC}	Purge Flow Split Vent (s)										FID Front (pA×s)			FID Back (pA×s)			TCD CO_2 (µV×s)		ROLSI Back$_{(Front\ Path)}$ mass fraction				ROLSI Front$_{(Back\ Path)}$ mass fraction			
	(barg)	(bar)	(°C)	(°C)	Front (ref. = 9.73)					Back (ref. = 9.56)					37DM1O	nC_{12}	$C_{10}OH$	37DM1O	nC_{12}	$C_{10}OH$	Front path	Back path	CO_2	37DM1O	nC_{12}	$C_{10}OH$	CO_2	37DM1O	nC_{12}	$C_{10}OH$
1	113.8	123.1	54.93	55.61	9.69	9.57	9.60	9.65		9.47	9.47	9.47			55610.50	25 247	430 710	837	1 234	4 899	4 591	2 615	0.374	0.068	0.026	0.531	0.961	0.006	0.007	0.026
	113.8	123.1	54.92	55.60	9.53	9.56	9.47	9.57		9.40	9.50	9.50	9.47		55851.10	25 483	432 369	849	1 256	4 939	4 663	2 687	0.377	0.068	0.026	0.529	0.961	0.006	0.007	0.026
	113.8	123.1	54.93	55.61	9.56	9.47	9.47	9.43		9.38	9.41	9.46	9.38		53987.30	24 956	414 731	806	1 207	4 646	4 616	2 611	0.384	0.068	0.027	0.522	0.962	0.006	0.007	0.025
	113.8	123.1	54.93	55.61	9.35	9.38	9.47	9.41		9.47	9.37	9.44	9.44		55427.30	25 430	423 395	791	1 192	4 502	4 703	2 597	0.383	0.068	0.027	0.522	0.963	0.006	0.007	0.024
	113.8	123.1	54.92	55.60	9.47	9.44	9.41			9.41	9.35	9.40			54220.80	24 915	418 882	794	1 208	4 544	4 589	2 661	0.380	0.068	0.026	0.526	0.963	0.006	0.007	0.024
																						AVERAGE	**0.379**	**0.068**	**0.026**	**0.526**	**0.962**	**0.006**	**0.007**	**0.025**
																						STANDARD DEVIATION	**0.004**	**0.000**	**0.000**	**0.004**	**0.001**	**0.000**	**0.000**	**0.001**
SAMPLE	P_{READ}	P_{ACT}	T_{READ}	T_{ATC}	Purge Flow Split Vent (s)										FID Front (pA×s)			FID Back (pA×s)			TCD CO_2 (µV×s)		ROLSI Back$_{(Front\ Path)}$ mass fraction				ROLSI Front$_{(Back\ Path)}$ mass fraction			
	(barg)	(bar)	(°C)	(°C)	Front (ref. = 9.73)					Back (ref. = 9.56)					37DM1O	nC_{12}	$C_{10}OH$	37DM1O	nC_{12}	$C_{10}OH$	Front path	Back path	CO_2	37DM1O	nC_{12}	$C_{10}OH$	CO_2	37DM1O	nC_{12}	$C_{10}OH$
2	131.0	140.1	54.93	55.61	9.71	9.59	9.68	9.72		9.53	9.57	9.66	9.53	9.59	55239.30	24 153	430 868	1 479	1 786	8 767	5 553	2 716	0.420	0.063	0.023	0.493	0.939	0.009	0.009	0.043
	130.9	140.0	54.92	55.60	9.53	9.60	9.59	9.60		9.41	9.37	9.37	9.44		54102.70	23 678	420 433	1 554	1 824	9 387	5 441	2 621	0.421	0.063	0.023	0.492	0.934	0.009	0.009	0.048
	131.0	140.1	54.92	55.60	9.56	9.56	9.50	9.56		8.94	8.87	8.87	8.97		55976.30	24 389	436 081	1 402	1 681	8 369	5 550	2 512	0.417	0.063	0.023	0.496	0.937	0.009	0.009	0.045
	130.9	140.0	54.92	55.60	9.59	9.56	9.66	9.56		9.44	9.40	9.37	9.38	9.47	55211.60	23 971	431 994	1 480	1 753	8 918	5 477	2 569	0.416	0.063	0.023	0.497	0.935	0.009	0.009	0.046
	130.9	140.0	54.92	55.60	9.53	9.44	9.56	9.53		8.96	9.07	9.00	9.06		55753.60	24 303	436 752	1 491	1 751	9 042	5 593	2 513	0.419	0.063	0.023	0.495	0.933	0.009	0.009	0.048
																						AVERAGE	**0.419**	**0.063**	**0.023**	**0.495**	**0.936**	**0.009**	**0.009**	**0.046**
																						STANDARD DEVIATION	**0.002**	**0.000**	**0.000**	**0.002**	**0.002**	**0.000**	**0.000**	**0.002**
SAMPLE	P_{READ}	P_{ACT}	T_{READ}	T_{ATC}	Purge Flow Split Vent (s)										FID Front (pA×s)			FID Back (pA×s)			TCD CO_2 (µV×s)		ROLSI Back$_{(Front\ Path)}$ mass fraction				ROLSI Front$_{(Back\ Path)}$ mass fraction			
	(barg)	(bar)	(°C)	(°C)	Front (ref. = 9.73)					Back (ref. = 9.56)					37DM1O	nC_{12}	$C_{10}OH$	37DM1O	nC_{12}	$C_{10}OH$	Front path	Back path	CO_2	37DM1O	nC_{12}	$C_{10}OH$	CO_2	37DM1O	nC_{12}	$C_{10}OH$
3	148.0	157.0	54.87	55.55	9.28	9.21	9.22	9.25	9.29	9.15	9.06	9.28	9.16	9.19	52033.00	21 223	420 767	2 666	2 429	17 097	6 231	2 911	0.457	0.057	0.020	0.466	0.902	0.013	0.010	0.075
	148.0	157.0	54.89	55.57	9.15	9.22	9.16	9.22		8.41	8.34	8.41	8.35		53573.30	21 719	427 367	2 417	2 229	15 531	6 344	2 677	0.457	0.058	0.020	0.465	0.903	0.013	0.010	0.074
	148.0	157.0	54.88	55.56	9.13	9.19	9.19	9.19		9.06	9.09	9.12	9.09		54820.00	22 373	435 345	2 606	2 412	16 588	6 538	2 962	0.460	0.058	0.020	0.462	0.906	0.012	0.010	0.072
	148.0	157.0	54.88	55.56	9.13	9.16	9.16	9.22	9.25	9.19	9.19	9.19	9.13		53196.70	21 550	423 139	2 748	2 503	17 662	6 240	2 959	0.455	0.058	0.020	0.466	0.901	0.013	0.010	0.076
	148.0	157.0	54.87	55.55	9.18	9.16	9.10	9.13		8.90	8.85	8.84	8.90		52635.50	21 538	417 703	2 474	2 313	15 826	6 328	2 862	0.462	0.058	0.020	0.460	0.907	0.012	0.010	0.071
																						AVERAGE	**0.458**	**0.058**	**0.020**	**0.464**	**0.904**	**0.013**	**0.010**	**0.073**
																						STANDARD DEVIATION	**0.003**	**0.000**	**0.000**	**0.003**	**0.003**	**0.000**	**0.000**	**0.002**
SAMPLE	P_{READ}	P_{ACT}	T_{READ}	T_{ATC}	Purge Flow Split Vent (s)										FID Front (pA×s)			FID Back (pA×s)			TCD CO_2 (µV×s)		ROLSI Back$_{(Front\ Path)}$ mass fraction				ROLSI Front$_{(Back\ Path)}$ mass fraction			
	(barg)	(bar)	(°C)	(°C)	Front (ref. = 9.73)					Back (ref. = 9.56)					37DM1O	nC_{12}	$C_{10}OH$	37DM1O	nC_{12}	$C_{10}OH$	Front path	Back path	CO_2	37DM1O	nC_{12}	$C_{10}OH$	CO_2	37DM1O	nC_{12}	$C_{10}OH$
4	161.3	170.2	54.79	55.47	9.10	9.12	9.13	9.15	9.09	9.12	9.09	9.16	9.15	9.19	54797.7	23 576	432 315	4 451	3 714	29 489	7 336	3 440	0.489	0.055	0.020	0.435	0.867	0.016	0.012	0.104
	161.3	170.2	54.77	55.45	9.03	9.00	9.03	9.04		8.81	8.78	8.81	8.85	8.81	54509.3	23 818	426 823	4 382	3 700	28 807	7 416	3 458	0.495	0.055	0.020	0.430	0.870	0.016	0.012	0.102
	161.3	170.2	54.79	55.47	9.06	9.00	9.03	9.04		8.94	8.94	9.00	8.97		55292.3	23 188	431 325	4 500	3 781	29 846	7 232	3 536	0.486	0.056	0.020	0.438	0.869	0.016	0.012	0.103
	161.3	170.2	54.78	55.46	8.97	9.00	9.00	8.94		8.78	8.81	8.85	8.75		54229.2	23 717	424 216	4 294	3 638	28 203	7 266	3 439	0.491	0.055	0.020	0.433	0.872	0.016	0.012	0.100
	161.3	170.2	54.78	55.46	8.94	8.91	9.03	9.03	9.03	8.91	8.97	8.87	8.90	9.03	52591.2	22 735	407 637	4 335	3 653	28 686	6 970	3 458	0.491	0.056	0.020	0.433	0.871	0.016	0.012	0.101
																						AVERAGE	**0.490**	**0.055**	**0.020**	**0.434**	**0.870**	**0.016**	**0.012**	**0.102**
																						STANDARD DEVIATION	**0.003**	**0.001**	**0.000**	**0.003**	**0.002**	**0.000**	**0.000**	**0.002**
SAMPLE	P_{READ}	P_{ACT}	T_{READ}	T_{ATC}	Purge Flow Split Vent (s)										FID Front (pA×s)			FID Back (pA×s)			TCD CO_2 (µV×s)		ROLSI Back$_{(Front\ Path)}$ mass fraction				ROLSI Front$_{(Back\ Path)}$ mass fraction			
	(barg)	(bar)	(°C)	(°C)	Front (ref. = 9.73)					Back (ref. = 9.56)					37DM1O	nC_{12}	$C_{10}OH$	37DM1O	nC_{12}	$C_{10}OH$	Front path	Back path	CO_2	37DM1O	nC_{12}	$C_{10}OH$	CO_2	37DM1O	nC_{12}	$C_{10}OH$
5	173.2	182.0	54.88	55.56	9.31	9.25	9.28	9.25		9.16	9.15	9.16			51064.00	20 969	405 101	5 440	3 828	37 589	8 174	3 417	0.533	0.050	0.018	0.399	0.839	0.019	0.012	0.129
	173.2	182.0	54.87	55.55	9.21	9.16	9.22	9.28	9.25	9.07	9.18	9.16	9.18	9.25	52214.00	21 237	411 872	5 551	3 887	38 659	8 352	3 357	0.535	0.050	0.017	0.398	0.834	0.020	0.012	0.134
	173.2	182.0	54.86	55.54	9.06	9.09	9.19	9.19	9.13	9.00	9.09	9.09			53452.90	22 182	421 991	5 716	4 008	39 357	8 534	3 426	0.534	0.050	0.018	0.398	0.834	0.020	0.012	0.134
																						AVERAGE	**0.534**	**0.050**	**0.018**	**0.398**	**0.836**	**0.020**	**0.012**	**0.133**
																						STANDARD DEVIATION	**0.001**	**0.000**	**0.000**	**0.001**	**0.003**	**0.000**	**0.000**	**0.003**

Table 71: Experimental VLE data for the quaternary systems CO_2 + (5 wt% n-dodecane + 12 wt% 3,7-dimethyl-1-octanol + 83 wt% 1-decanol) at 75ºC.

SAMPLE	P_{READ}	P_{ACT}	T_{READ}	T_{ATC}	Purge Flow Split Vent (s)										FID Front (pA×s)			FID Back (pA×s)			TCD CO_2 (µV×s)		ROLSI Back$_{(Front\ Path)}$ mass fraction				ROLSI Front$_{(Back\ Path)}$ mass fraction			
	(barg)	(bar)	(°C)	(°C)	Front (ref. = 9.73)					Back (ref. = 9.56)					37DM1O	nC_{12}	$C_{10}OH$	37DM1O	nC_{12}	$C_{10}OH$	Front path	Back path	CO_2	37DM1O	nC_{12}	$C_{10}OH$	CO_2	37DM1O	nC_{12}	$C_{10}OH$
1	132.9	140.0	74.98	75.64	9.40	9.50	9.41	9.44		9.28	9.31	9.35	9.31		64389.2	30 748	500 801	581	836	3 265	4 865	3 040	0.352	0.070	0.028	0.549	0.976	0.004	0.005	0.016
	132.9	140.0	74.98	75.64	9.32	9.28	9.31			9.31	9.35	9.34	9.29	9.31	64568.3	30 705	508 898	577	837	3 221	4 858	3 033	0.349	0.070	0.028	0.553	0.976	0.004	0.005	0.015
	132.9	140.0	74.98	75.64	9.31	9.38	9.34			9.37	9.28	9.35	9.32		65259.9	31 238	506 043	584	847	3 264	4 948	3 084	0.354	0.070	0.029	0.547	0.976	0.004	0.005	0.015
	132.9	140.0	75.00	75.66	9.34	9.31	9.28	9.35	9.34	9.25	9.19	9.32	9.22	9.25	65999.5	31 475	517 183	580	843	3 245	5 008	3 064	0.352	0.070	0.028	0.550	0.976	0.004	0.005	0.015
	132.9	140.0	74.99	75.65	9.35	9.31	9.35			8.53	8.56	8.44	8.47		65360.3	31 020	509 200	539	785	3 014	4 888	2 861	0.350	0.071	0.028	0.551	0.976	0.004	0.005	0.015
																						AVERAGE	**0.351**	**0.070**	**0.028**	**0.550**	**0.976**	**0.004**	**0.005**	**0.015**
																						STANDARD DEVIATION	**0.002**	**0.000**	**0.000**	**0.002**	**0.000**	**0.000**	**0.000**	**0.000**
SAMPLE	P_{READ}	P_{ACT}	T_{READ}	T_{ATC}	Purge Flow Split Vent (s)										FID Front (pA×s)			FID Back (pA×s)			TCD CO_2 (µV×s)		ROLSI Back$_{(Front\ Path)}$ mass fraction				ROLSI Front$_{(Back\ Path)}$ mass fraction			
	(barg)	(bar)	(°C)	(°C)	Front (ref. = 9.73)					Back (ref. = 9.56)					37DM1O	nC_{12}	$C_{10}OH$	37DM1O	nC_{12}	$C_{10}OH$	Front path	Back path	CO_2	37DM1O	nC_{12}	$C_{10}OH$	CO_2	37DM1O	nC_{12}	$C_{10}OH$
2	150.2	157.1	74.99	75.65	9.35	9.35	9.41			9.31	9.28	9.40	9.31		59860.1	27 546	468 348	1 303	1 528	7 723	5 780	3 284	0.410	0.064	0.025	0.502	0.955	0.007	0.006	0.032
	150.2	157.1	74.99	75.65	9.25	9.16	9.22	9.22		9.03	9.06	9.03	9.13		61677.2	28 329	482 697	1 304	1 534	7 732	5 897	3 304	0.407	0.064	0.025	0.504	0.955	0.007	0.006	0.032
	150.2	157.1	74.97	75.63	9.22	9.15	9.25	9.22		9.16	9.19	9.19	9.19		59905.4	27 562	468 698	1 291	1 525	7 650	5 681	3 292	0.405	0.064	0.025	0.505	0.955	0.006	0.006	0.032
	150.2	157.1	74.96	75.62	9.15	9.16	9.22	9.22		9.09	9.16	9.09	9.09	9.16	62181.9	28 711	484 959	1 342	1 584	7 951	5 964	3 439	0.409	0.064	0.025	0.502	0.956	0.006	0.006	0.032
	150.1	157.0	74.98	75.64	9.32	9.16	9.25	9.25	9.19	8.79	8.75	8.75	8.75		60353.8	27 747	473 842	1 232	1 456	7 291	5 730	3 150	0.405	0.064	0.025	0.506	0.955	0.007	0.007	0.032
																						AVERAGE	**0.407**	**0.064**	**0.025**	**0.504**	**0.955**	**0.007**	**0.006**	**0.032**
																						STANDARD DEVIATION	**0.002**	**0.000**	**0.000**	**0.002**	**0.000**	**0.000**	**0.000**	**0.000**
SAMPLE	P_{READ}	P_{ACT}	T_{READ}	T_{ATC}	Purge Flow Split Vent (s)										FID Front (pA×s)			FID Back (pA×s)			TCD CO_2 (µV×s)		ROLSI Back$_{(Front\ Path)}$ mass fraction				ROLSI Front$_{(Back\ Path)}$ mass fraction			
	(barg)	(bar)	(°C)	(°C)	Front (ref. = 9.73)					Back (ref. = 9.56)					37DM1O	nC_{12}	$C_{10}OH$	37DM1O	nC_{12}	$C_{10}OH$	Front path	Back path	CO_2	37DM1O	nC_{12}	$C_{10}OH$	CO_2	37DM1O	nC_{12}	$C_{10}OH$
3	163.3	170.1	74.91	75.57	9.22	9.22	9.19	9.29	9.25	9.09	9.13	9.12	9.16	9.10	60011.9	28 026	473 354	2 394	2 460	14 858	6 788	3 703	0.447	0.059	0.024	0.470	0.930	0.009	0.008	0.053
	163.3	170.1	74.90	75.56	9.22	9.18	9.18	9.22	9.16	8.97	8.94	8.87	9.00	9.00	59951.4	27 823	465 637	2 356	2 426	14 703	6 787	3 600	0.450	0.060	0.024	0.466	0.929	0.009	0.008	0.054
	163.3	170.1	74.88	75.54	9.12	9.19	9.28	9.28	9.25	9.06	9.09	9.03	9.12	9.19	58823.2	27 105	460 962	2 405	2 498	14 958	6 675	3 717	0.449	0.060	0.023	0.468	0.929	0.009	0.008	0.053
	163.3	170.1	74.88	75.54	9.03	9.09	9.03	9.09	9.13	8.97	9.09	8.97	9.00	9.06	59830.2	27 621	472 464	2 396	2 495	14 917	6 827	3 721	0.449	0.059	0.023	0.469	0.930	0.009	0.008	0.053
																						AVERAGE	**0.449**	**0.059**	**0.023**	**0.469**	**0.929**	**0.009**	**0.008**	**0.053**
																						STANDARD DEVIATION	**0.001**	**0.000**	**0.000**	**0.002**	**0.001**	**0.000**	**0.000**	**0.000**
SAMPLE	P_{READ}	P_{ACT}	T_{READ}	T_{ATC}	Purge Flow Split Vent (s)										FID Front (pA×s)			FID Back (pA×s)			TCD CO_2 (µV×s)		ROLSI Back$_{(Front\ Path)}$ mass fraction				ROLSI Front$_{(Back\ Path)}$ mass fraction			
	(barg)	(bar)	(°C)	(°C)	Front (ref. = 9.73)					Back (ref. = 9.56)					37DM1O	nC_{12}	$C_{10}OH$	37DM1O	nC_{12}	$C_{10}OH$	Front path	Back path	CO_2	37DM1O	nC_{12}	$C_{10}OH$	CO_2	37DM1O	nC_{12}	$C_{10}OH$
4	175.4	182.1	75.00	75.66	9.28	9.19	9.25	9.35	9.32	9.12	9.13	9.03	9.12	9.22	54117.1	23 541	430 046	3 143	2 694	20 152	7 583	3 605	0.499	0.054	0.020	0.427	0.908	0.012	0.009	0.071
	175.4	182.1	75.01	75.67	9.31	9.28	9.34	9.29	9.25	8.81	8.81	8.85	8.87		54734.5	23 426	428 612	2 971	2 560	19 015	7 694	3 474	0.503	0.054	0.020	0.423	0.909	0.012	0.009	0.070
	175.4	182.1	75.00	75.66	9.19	9.22	9.22	9.25		8.88	8.93	8.87	8.97		58055.0	25 097	456 351	3 055	2 644	19 505	8 080	3 640	0.500	0.054	0.020	0.426	0.911	0.012	0.009	0.069
																						AVERAGE	**0.501**	**0.054**	**0.020**	**0.426**	**0.909**	**0.012**	**0.009**	**0.070**
																						STANDARD DEVIATION	**0.002**	**0.000**	**0.000**	**0.002**	**0.002**	**0.000**	**0.000**	**0.001**
SAMPLE	P_{READ}	P_{ACT}	T_{READ}	T_{ATC}	Purge Flow Split Vent (s)										FID Front (pA×s)			FID Back (pA×s)			TCD CO_2 (µV×s)		ROLSI Back$_{(Front\ Path)}$ mass fraction				ROLSI Front$_{(Back\ Path)}$ mass fraction			
	(barg)	(bar)	(°C)	(°C)	Front (ref. = 9.73)					Back (ref. = 9.56)					37DM1O	nC_{12}	$C_{10}OH$	37DM1O	nC_{12}	$C_{10}OH$	Front path	Back path	CO_2	37DM1O	nC_{12}	$C_{10}OH$	CO_2	37DM1O	nC_{12}	$C_{10}OH$
5	185.4	192.0	75.02	75.68	9.22	9.15	9.15	9.13	9.19	9.00	9.03	9.06	9.03		50338.80	21 990	391 283	5 047	3 621	34 071	8 570	3 737	0.552	0.049	0.018	0.381	0.862	0.017	0.011	0.110
	185.4	192.0	75.00	75.66	9.03	9.10	9.04	9.06	9.12	8.18	8.09	8.12	8.09		51584.9	21 694	399 168	4 576	3 303	30 888	8 605	3 462	0.549	0.049	0.018	0.384	0.865	0.017	0.011	0.108
	185.6	192.2	75.00	75.66	9.15	9.06	9.12	9.12	9.06	9.06	8.97	9.09	9.03		52165.6	22 354	408 796	5 097	3 617	34 742	8 720	3 706	0.546	0.049	0.018	0.386	0.859	0.017	0.011	0.113
	185.6	192.2	75.01	75.67	8.94	9.90	9.06	9.03		8.97	9.04	8.97	9.00		49949.8	21 369	390 446	5 049	3 613	34 222	8 471	3 724	0.551	0.049	0.018	0.383	0.862	0.017	0.011	0.111
	185.6	192.2	74.99	75.65	9.00	9.03	9.12	9.03	9.09	8.81	8.90	8.93	8.82	8.88	50374.3	20 993	388 150	4 966	3 556	33 585	8 367	3 729	0.549	0.050	0.018	0.384	0.864	0.017	0.011	0.109
	185.6	192.2	75.00	75.66	9.03	9.06	9.06			8.88	8.96	9.00	8.97		50803.7	21 630	396 869	4 987	3 575	33 724	8 573	3 730	0.549	0.049	0.018	0.384	0.863	0.017	0.011	0.109
	185.6	192.2	74.98	75.64	9.06	9.03	9.03	9.06		8.78	8.78	8.72	8.87		53944.6	22 060	408 438	4 959	3 527	33 751	8 654	3 674	0.544	0.051	0.018	0.387	0.862	0.017	0.011	0.111
																						AVERAGE	**0.549**	**0.049**	**0.018**	**0.384**	**0.862**	**0.017**	**0.011**	**0.110**
																						STANDARD DEVIATION	**0.003**	**0.001**	**0.000**	**0.002**	**0.002**	**0.000**	**0.000**	**0.002**

Table 72: Experimental VLE data for the quaternary systems CO_2 + (85 wt% n-dodecane + 10 wt% 3,7-dimethyl-1-octanol + 5 wt% 1-decanol) at 35ºC.

SAMPLE	P_{READ}	P_{ACT}	T_{READ}	T_{ATC}	Purge Flow Split Vent (s)										FID Front (pA×s)			FID Back (pA×s)			TCD CO_2 (µV×s)		ROLSI Back$_{(Front Path)}$ mass fraction				ROLSI Front$_{(Back Path)}$ mass fraction			
	(barg)	(bar)	(°C)	(°C)	Front (ref. = 9.73)					Back (ref. = 9.56)					37DM1O	nC_{12}	$C_{10}OH$	37DM1O	nC_{12}	$C_{10}OH$	Front path	Back path	CO_2	37DM1O	nC_{12}	$C_{10}OH$	CO_2	37DM1O	nC_{12}	$C_{10}OH$
1	48.6	60.3	34.74	35.43	9.28	9.34	9.25	9.31	9.35	9.09	9.13	9.09	9.12		24452.50	255 910	13 376	290	3 227	149	1 880	1 309	0.327	0.066	0.570	0.037	0.959	0.006	0.031	0.004
	48.6	60.3	34.74	35.43	9.28	9.29	9.31	9.31		9.13	9.16	9.15	9.13		25537.60	268 281	14 038	271	3 135	146	1 948	1 354	0.325	0.066	0.572	0.037	0.961	0.006	0.029	0.004
	48.6	60.3	34.74	35.43	9.32	9.22	9.25	9.22	9.22	9.09	9.13	9.13	9.12		24871.90	260 644	13 625	204	2 419	111	1 956	1 346	0.332	0.065	0.566	0.037	0.968	0.006	0.023	0.003
	48.6	60.3	34.74	35.43	9.25	9.28	9.31	9.28		9.16	9.16	9.16	9.12		27575.60	290 184	15 261	202	2 351	108	2 104	1 419	0.325	0.065	0.572	0.037	0.970	0.005	0.022	0.003
	48.6	60.3	34.74	35.43	9.25	9.29	9.28	9.28		8.75	8.75	8.72	8.71		24875.90	260 532	13 595	191	2 130	101	1 924	1 302	0.328	0.065	0.569	0.037	0.969	0.006	0.022	0.004
	48.6	60.3	34.73	35.42	9.25	9.21	9.22	9.22		9.12	9.09	9.13	9.12		26853.40	281 934	14 609	321	3 177	146	2 009	1 377	0.321	0.066	0.576	0.037	0.961	0.006	0.029	0.004
																						AVERAGE	**0.326**	**0.066**	**0.571**	**0.037**	**0.965**	**0.006**	**0.026**	**0.004**
																						STANDARD DEVIATION	**0.004**	**0.000**	**0.003**	**0.000**	**0.005**	**0.001**	**0.004**	**0.000**
SAMPLE	P_{READ}	P_{ACT}	T_{READ}	T_{ATC}	Purge Flow Split Vent (s)										FID Front (pA×s)			FID Back (pA×s)			TCD CO_2 (µV×s)		ROLSI Back$_{(Front Path)}$ mass fraction				ROLSI Front$_{(Back Path)}$ mass fraction			
	(barg)	(bar)	(°C)	(°C)	Front (ref. = 9.73)					Back (ref. = 9.56)					37DM1O	nC_{12}	$C_{10}OH$	37DM1O	nC_{12}	$C_{10}OH$	Front path	Back path	CO_2	37DM1O	nC_{12}	$C_{10}OH$	CO_2	37DM1O	nC_{12}	$C_{10}OH$
2	48.4	60.1	34.72	35.41	9.28	9.25	9.22	9.19	9.19	9.13	9.16	9.15	9.19		25065.70	263 200	13 326	334	3 496	162	1 931	1 278	0.327	0.065	0.571	0.036	0.955	0.007	0.034	0.004
	48.4	60.1	34.71	35.40	9.19	9.22	9.25	9.28	9.18	9.09	9.03	9.00	9.09		24373.10	255 711	13 081	301	3 495	162	1 883	1 227	0.328	0.065	0.570	0.037	0.954	0.007	0.035	0.004
	48.4	60.1	34.71	35.40	9.25	9.28	9.22	9.28		9.12	9.12	9.16	9.10		25517.30	268 427	13 861	231	2 662	123	1 958	1 293	0.326	0.065	0.572	0.037	0.964	0.006	0.026	0.004
	48.4	60.1	34.71	35.40	9.16	9.15	9.19	9.19		9.00	8.97	8.94	9.06		26697.50	280 975	14 536	211	2 379	109	2 051	1 310	0.326	0.065	0.572	0.037	0.967	0.006	0.024	0.004
	48.4	60.1	34.73	35.42	9.09	9.12	9.13	9.10		9.06	9.03	9.00	9.00		23961.70	251 281	13 229	218	2 421	112	1 849	1 276	0.327	0.065	0.570	0.038	0.966	0.006	0.025	0.004
																						AVERAGE	**0.327**	**0.065**	**0.571**	**0.037**	**0.961**	**0.006**	**0.029**	**0.004**
																						STANDARD DEVIATION	**0.001**	**0.000**	**0.001**	**0.001**	**0.006**	**0.001**	**0.005**	**0.000**
SAMPLE	P_{READ}	P_{ACT}	T_{READ}	T_{ATC}	Purge Flow Split Vent (s)										FID Front (pA×s)			FID Back (pA×s)			TCD CO_2 (µV×s)		ROLSI Back$_{(Front Path)}$ mass fraction				ROLSI Front$_{(Back Path)}$ mass fraction			
	(barg)	(bar)	(°C)	(°C)	Front (ref. = 9.73)					Back (ref. = 9.56)					37DM1O	nC_{12}	$C_{10}OH$	37DM1O	nC_{12}	$C_{10}OH$	Front path	Back path	CO_2	37DM1O	nC_{12}	$C_{10}OH$	CO_2	37DM1O	nC_{12}	$C_{10}OH$
3	54.2	65.9	34.76	35.45	9.25	9.19	9.22	9.22	9.22	8.81	8.78	8.53	8.79	8.72	22251.70	233 077	11 943	0	109	0	2 337	1 376	0.400	0.059	0.509	0.033	0.990	0.004	0.004	0.002
	54.2	65.9	34.76	35.45	8.97	9.00	8.97	9.03		8.78	8.81	8.88	8.94	8.87	21721.70	227 310	11 726	0	119	0	2 295	1 508	0.401	0.058	0.507	0.033	0.991	0.003	0.004	0.002
	54.2	65.9	34.74	35.43	9.00	8.88	8.97	8.93	8.97	8.88	8.94	8.97	8.91	8.90	21470.50	224 728	11 601	0	121	0	2 272	1 641	0.401	0.058	0.507	0.033	0.991	0.003	0.004	0.002
	54.2	65.9	34.75	35.44	9.00	8.97	8.88	9.00	9.00	8.88	8.94	8.97	9.03	8.96	22629.90	237 079	12 435	0	122	0	2 362	1 531	0.398	0.059	0.510	0.034	0.991	0.003	0.004	0.002
	54.2	65.9	34.74	35.43	8.93	8.90	8.97	8.93		8.12	8.12	8.13	8.13		21768.90	227 808	11 916	0	109	0	2 315	1 357	0.403	0.058	0.506	0.033	0.990	0.004	0.004	0.002
	54.2	65.9	34.75	35.44	8.90	9.03	8.94	8.97		8.82	8.84	8.84	8.84	8.88	22358.80	234 345	12 328	0	122	0	2 374	1 510	0.402	0.058	0.506	0.033	0.990	0.003	0.004	0.002
																						AVERAGE	**0.401**	**0.058**	**0.507**	**0.033**	**0.990**	**0.003**	**0.004**	**0.002**
																						STANDARD DEVIATION	**0.002**	**0.000**	**0.002**	**0.000**	**0.001**	**0.000**	**0.000**	**0.000**
SAMPLE	P_{READ}	P_{ACT}	T_{READ}	T_{ATC}	Purge Flow Split Vent (s)										FID Front (pA×s)			FID Back (pA×s)			TCD CO_2 (µV×s)		ROLSI Back$_{(Front Path)}$ mass fraction				ROLSI Front$_{(Back Path)}$ mass fraction			
	(barg)	(bar)	(°C)	(°C)	Front (ref. = 9.73)					Back (ref. = 9.56)					37DM1O	nC_{12}	$C_{10}OH$	37DM1O	nC_{12}	$C_{10}OH$	Front path	Back path	CO_2	37DM1O	nC_{12}	$C_{10}OH$	CO_2	37DM1O	nC_{12}	$C_{10}OH$
4	56.5	68.2	34.76	35.45	9.21	9.28	9.34	9.31		9.15	9.22	9.16	9.25	9.22	18567.00	190 505	11 408	153	1 640	82	2 400	1 543	0.453	0.054	0.459	0.035	0.978	0.004	0.015	0.003
	56.5	68.2	34.77	35.46	9.19	9.09	9.18	9.22	9.19	8.37	8.50	8.50	8.53		19353.00	198 870	11 974	171	1 829	92	2 500	1 447	0.452	0.054	0.459	0.035	0.975	0.005	0.017	0.003
	56.5	68.2	34.76	35.45	9.31	9.28	9.22	9.31		8.75	8.85	8.75	8.85		19435.10	199 997	12 106	157	1 668	83	2 488	1 480	0.450	0.054	0.461	0.035	0.977	0.005	0.016	0.003
																						AVERAGE	**0.452**	**0.054**	**0.459**	**0.035**	**0.976**	**0.005**	**0.016**	**0.003**
																						STANDARD DEVIATION	**0.002**	**0.000**	**0.001**	**0.000**	**0.002**	**0.000**	**0.001**	**0.000**
SAMPLE	P_{READ}	P_{ACT}	T_{READ}	T_{ATC}	Purge Flow Split Vent (s)										FID Front (pA×s)			FID Back (pA×s)			TCD CO_2 (µV×s)		ROLSI Back$_{(Front Path)}$ mass fraction				ROLSI Front$_{(Back Path)}$ mass fraction			
	(barg)	(bar)	(°C)	(°C)	Front (ref. = 9.73)					Back (ref. = 9.56)					37DM1O	nC_{12}	$C_{10}OH$	37DM1O	nC_{12}	$C_{10}OH$	Front path	Back path	CO_2	37DM1O	nC_{12}	$C_{10}OH$	CO_2	37DM1O	nC_{12}	$C_{10}OH$
5	58.9	70.5	34.78	35.47	9.66	9.66	9.69			8.85	8.90	8.78	8.88		15694.00	160 434	9 820	0	208	0	2 709	1 559	0.526	0.047	0.397	0.031	0.990	0.003	0.005	0.002
	58.9	70.5	34.78	35.47	9.40	9.47	9.31	9.31	9.35	9.18	9.19	9.25	9.22	9.22	16093.80	164 656	10 380	0	226	0	2 788	1 681	0.526	0.047	0.395	0.032	0.991	0.003	0.004	0.002
	58.9	70.5	34.78	35.47	9.35	9.22	9.28	9.28	9.34	8.59	8.57	8.63	8.63		15611.60	159 501	9 814	0	208	0	2 718	1 544	0.528	0.047	0.394	0.031	0.990	0.003	0.005	0.002
	58.9	70.5	34.78	35.47	9.41	9.25	9.19	9.31	9.47	9.19	9.21	9.25	9.25		15508.00	158 411	9 431	0	224	0	2 703	1 678	0.529	0.047	0.395	0.030	0.991	0.003	0.004	0.002
	58.9	70.5	34.78	35.47	9.28	9.28	9.25	9.28		9.19	9.22	9.22	9.16	9.19	15373.30	156 721	9 776	0	224	0	2 682	1 690	0.528	0.047	0.393	0.031	0.991	0.003	0.004	0.002
																						AVERAGE	**0.527**	**0.047**	**0.395**	**0.031**	**0.991**	**0.003**	**0.005**	**0.002**
																						STANDARD DEVIATION	**0.001**	**0.000**	**0.001**	**0.001**	**0.000**	**0.000**	**0.000**	**0.000**

Table 72 continued: Experimental VLE data for the quaternary systems CO_2 + (85 wt% n-dodecane + 10 wt% 3,7-dimethyl-1-octanol + 5 wt% 1-decanol) at 35ºC.

SAMPLE	P_{READ}	P_{ACT}	T_{READ}	T_{ATC}	Purge Flow Split Vent (s)										FID Front (pA×s)			FID Back (pA×s)			TCD CO_2 (µV×s)		ROLSI Back$_{(Front Path)}$ mass fraction				ROLSI Front$_{(Back Path)}$ mass fraction			
	(barg)	(bar)	(°C)	(°C)	Front (ref. = 9.73)					Back (ref. = 9.56)					37DM1O	nC_{12}	$C_{10}OH$	37DM1O	nC_{12}	$C_{10}OH$	Front path	Back path	CO_2	37DM1O	nC_{12}	$C_{10}OH$	CO_2	37DM1O	nC_{12}	$C_{10}OH$
6	60.4	72.0	34.72	35.41	9.19	9.19	9.22	9.19	9.22	9.16	9.06	9.13	9.06		13350.70	136 391	8 133	0	238	0	2 815	1 678	0.575	0.042	0.355	0.027	0.991	0.003	0.005	0.002
	60.4	72.0	34.72	35.41	9.13	9.18	9.13	9.13	9.16	8.81	8.91	8.84	8.90		13296.30	135 664	8 239	0	238	0	2 852	1 689	0.580	0.042	0.351	0.027	0.991	0.003	0.004	0.002
	60.4	72.0	34.72	35.41	9.16	9.16	9.19	9.13		9.03	9.10	9.04	9.06		13081.20	133 382	7 947	0	238	0	2 845	1 689	0.583	0.042	0.348	0.027	0.991	0.003	0.004	0.002
	60.4	72.0	34.72	35.41	9.15	9.13	9.12	9.13		9.06	9.04	9.12	9.13	9.15	13063.80	133 125	7 932	0	241	0	2 797	1 707	0.580	0.042	0.351	0.027	0.991	0.003	0.004	0.002
																						AVERAGE	**0.579**	**0.042**	**0.351**	**0.027**	**0.991**	**0.003**	**0.004**	**0.002**
																						STANDARD DEVIATION	**0.003**	**0.000**	**0.003**	**0.000**	**0.000**	**0.000**	**0.000**	**0.000**

Table 73: Experimental VLE data for the quaternary systems CO_2 + (85 wt% n-dodecane + 10 wt% 3,7-dimethyl-1-octanol + 5 wt% 1-decanol) at 55ºC.

SAMPLE	P_{READ}	P_{ACT}	T_{READ}	T_{ATC}	Purge Flow Split Vent (s)										FID Front (pA×s)			FID Back (pA×s)			TCD CO_2 (µV×s)		ROLSI Back$_{(Front Path)}$ mass fraction				ROLSI Front$_{(Back Path)}$ mass fraction			
	(barg)	(bar)	(°C)	(°C)	Front (ref. = 9.73)					Back (ref. = 9.56)					37DM1O	nC_{12}	$C_{10}OH$	37DM1O	nC_{12}	$C_{10}OH$	Front path	Back path	CO_2	37DM1O	nC_{12}	$C_{10}OH$	CO_2	37DM1O	nC_{12}	$C_{10}OH$
1	75.5	85.1	54.96	55.64	9.10	9.13	9.09	9.09		8.88	8.84	8.90	8.85		32351.3	342 847	18 459	56	609	0	2 936	2 047	0.364	0.061	0.539	0.036	0.990	0.003	0.006	0.002
	75.4	85.0	54.97	55.65	9.10	9.06	9.10	9.06	9.06	8.75	8.75	8.79	8.75		33952.8	359 929	19 139	57	618	0	3 090	2 099	0.364	0.061	0.539	0.035	0.990	0.003	0.006	0.002
	75.4	85.0	54.94	55.62	8.91	8.90	8.90	8.91		8.81	8.91	8.91	8.81	8.88	33768.1	358 012	20 047	57	609	0	3 056	2 079	0.362	0.061	0.539	0.037	0.990	0.003	0.006	0.002
	75.4	85.0	54.96	55.64	8.93	8.84	8.85	8.88	8.87	8.84	8.78	8.84	8.94	8.93	32000.4	338 538	18 809	57	609	0	2 894	2 077	0.363	0.061	0.539	0.037	0.990	0.003	0.006	0.002
	75.4	85.0	54.96	55.64	9.05	8.91	8.87	8.81	8.97	8.88	8.85	8.94	8.94	8.84	33234.0	351 898	19 467	58	617	0	2 989	2 099	0.361	0.061	0.540	0.037	0.990	0.003	0.006	0.002
	75.4	85.0	54.97	55.65	8.85	8.94	8.97	8.91	8.91	8.56	8.66	8.71	8.79	8.62	31420.1	331 438	18 219	54	576	0	2 828	1 977	0.362	0.061	0.540	0.037	0.990	0.003	0.006	0.002
																						AVERAGE	**0.363**	**0.061**	**0.540**	**0.037**	**0.990**	**0.003**	**0.006**	**0.002**
																						STANDARD DEVIATION	**0.001**	**0.000**	**0.001**	**0.001**	**0.000**	**0.000**	**0.000**	**0.000**
SAMPLE	P_{READ}	P_{ACT}	T_{READ}	T_{ATC}	Purge Flow Split Vent (s)										FID Front (pA×s)			FID Back (pA×s)			TCD CO_2 (µV×s)		ROLSI Back$_{(Front Path)}$ mass fraction				ROLSI Front$_{(Back Path)}$ mass fraction			
	(barg)	(bar)	(°C)	(°C)	Front (ref. = 9.73)					Back (ref. = 9.56)					37DM1O	nC_{12}	$C_{10}OH$	37DM1O	nC_{12}	$C_{10}OH$	Front path	Back path	CO_2	37DM1O	nC_{12}	$C_{10}OH$	CO_2	37DM1O	nC_{12}	$C_{10}OH$
2	85.7	95.2	54.86	55.54	9.16	9.19	9.19			8.84	8.75	8.88			25812.6	270 358	16 574	146	1 458	57	3 563	2 347	0.466	0.052	0.448	0.034	0.986	0.003	0.009	0.002
	85.7	95.2	54.85	55.53	9.04	9.10	9.07	9.03		9.03	9.03	9.03	9.00		25691.3	269 251	15 715	148	1 476	57	3 474	2 398	0.461	0.052	0.454	0.033	0.987	0.003	0.009	0.002
	85.7	95.2	54.85	55.53	9.03	8.97	8.91	9.03		8.75	8.75	8.78			26225.7	275 462	17 091	143	1 423	56	3 529	2 359	0.459	0.052	0.454	0.035	0.987	0.003	0.009	0.002
	85.7	95.2	54.84	55.52	9.03	8.94	8.93	9.03		8.75	8.78	8.91	8.78		25837.8	270 263	16 938	143	1 427	56	3 500	2 357	0.461	0.052	0.452	0.035	0.987	0.003	0.009	0.002
	85.7	95.2	54.84	55.52	9.00	8.91	8.94	8.94		8.88	8.81	8.91	8.91		25751.2	269 593	16 970	143	1 427	56	3 441	2 368	0.457	0.052	0.455	0.036	0.987	0.003	0.009	0.002
																						AVERAGE	**0.461**	**0.052**	**0.453**	**0.035**	**0.987**	**0.003**	**0.009**	**0.002**
																						STANDARD DEVIATION	**0.003**	**0.000**	**0.003**	**0.001**	**0.000**	**0.000**	**0.000**	**0.000**
SAMPLE	P_{READ}	P_{ACT}	T_{READ}	T_{ATC}	Purge Flow Split Vent (s)										FID Front (pA×s)			FID Back (pA×s)			TCD CO_2 (µV×s)		ROLSI Back$_{(Front Path)}$ mass fraction				ROLSI Front$_{(Back Path)}$ mass fraction			
	(barg)	(bar)	(°C)	(°C)	Front (ref. = 9.73)					Back (ref. = 9.56)					37DM1O	nC_{12}	$C_{10}OH$	37DM1O	nC_{12}	$C_{10}OH$	Front path	Back path	CO_2	37DM1O	nC_{12}	$C_{10}OH$	CO_2	37DM1O	nC_{12}	$C_{10}OH$
3	90.5	100.0	54.90	55.58	9.38	9.31	9.28	9.34		9.10	9.10	9.07	9.16	9.15	23641.1	248 893	14 113	231	2 239	85	3 995	2 475	0.517	0.047	0.408	0.029	0.983	0.003	0.012	0.002
	90.5	100.0	54.90	55.58	9.13	9.18	9.22	9.25	9.19	9.09	9.07	9.03	9.06		22813.7	240 682	13 999	233	2 249	85	3 874	2 490	0.517	0.047	0.407	0.030	0.983	0.003	0.012	0.002
	90.5	100.0	54.91	55.59	9.19	9.22	9.16	9.12	9.22	9.12	9.16	9.00	9.03	9.03	23305.0	244 915	13 170	228	2 200	83	3 989	2 472	0.521	0.046	0.405	0.027	0.983	0.003	0.012	0.002
	90.5	100.0	54.90	55.58	9.19	9.13	9.12	9.18	9.12	8.97	9.00	8.97	8.97		21995.3	230 760	13 043	229	2 206	83	3 737	2 501	0.519	0.047	0.406	0.029	0.983	0.003	0.012	0.002
	90.5	100.0	54.91	55.59	9.12	9.16	9.12	9.12	9.16	9.10	9.03	8.97	9.00	9.06	22199.4	233 074	13 483	227	2 186	86	3 745	2 501	0.516	0.047	0.407	0.029	0.983	0.003	0.012	0.002
																						AVERAGE	**0.518**	**0.047**	**0.407**	**0.029**	**0.983**	**0.003**	**0.012**	**0.002**
																						STANDARD DEVIATION	**0.002**	**0.000**	**0.001**	**0.001**	**0.000**	**0.000**	**0.000**	**0.000**

Table 73 continued: Experimental VLE data for the quaternary systems CO_2 + (85 wt% n-dodecane + 10 wt% 3,7-dimethyl-1-octanol + 5 wt% 1-decanol) at 55ºC.

SAMPLE	P_{READ}	P_{ACT}	T_{READ}	T_{ATC}	Purge Flow Split Vent (s)										FID Front (pA×s)			FID Back (pA×s)			TCD CO_2 (µV×s)		ROLSI Back$_{(Front\ Path)}$ mass fraction				ROLSI Front$_{(Back\ Path)}$ mass fraction			
	(barg)	(bar)	(°C)	(°C)	Front (ref. = 9.73)					Back (ref. = 9.56)					37DM1O	nC_{12}	$C_{10}OH$	37DM1O	nC_{12}	$C_{10}OH$	Front path	Back path	CO_2	37DM1O	nC_{12}	$C_{10}OH$	CO_2	37DM1O	nC_{12}	$C_{10}OH$
4	93.6	103.1	54.93	55.61	9.25	9.41	9.32	9.32	9.44	9.04	9.00	9.04	9.12	9.06	20140.3	211 843	12 493	300	2 859	112	4 088	2 543	0.562	0.042	0.369	0.027	0.980	0.003	0.014	0.002
	93.6	103.1	54.92	55.60	9.47	9.60	9.53	9.59		9.16	9.16	9.22	9.12	9.18	22663.1	238 805	14 161	304	2 885	114	4 664	2 559	0.565	0.042	0.366	0.027	0.980	0.003	0.014	0.002
	93.6	103.1	54.92	55.60	9.18	9.22	9.19	9.22		9.13	9.18	9.12	9.15		21119.9	221 729	13 298	309	2 924	115	4 322	2 591	0.564	0.042	0.366	0.028	0.980	0.003	0.014	0.002
	93.6	103.1	54.91	55.59	9.22	9.25	9.22	9.19	9.28	9.09	9.00	9.16	9.09	9.13	20693.3	217 356	12 559	311	2 940	115	4 232	2 580	0.564	0.042	0.367	0.027	0.980	0.003	0.015	0.002
	93.6	103.1	54.91	55.59	9.13	9.22	9.15	9.12	9.18	9.12	9.09	9.03	9.10	9.10	19814.5	207 800	12 431	315	2 972	116	4 080	2 580	0.566	0.042	0.365	0.027	0.980	0.003	0.015	0.002
																						AVERAGE	**0.564**	**0.042**	**0.367**	**0.027**	**0.980**	**0.003**	**0.015**	**0.002**
																						STANDARD DEVIATION	**0.002**	**0.000**	**0.001**	**0.000**	**0.000**	**0.000**	**0.000**	**0.000**
SAMPLE	P_{READ}	P_{ACT}	T_{READ}	T_{ATC}	Purge Flow Split Vent (s)										FID Front (pA×s)			FID Back (pA×s)			TCD CO_2 (µV×s)		ROLSI Back$_{(Front\ Path)}$ mass fraction				ROLSI Front$_{(Back\ Path)}$ mass fraction			
	(barg)	(bar)	(°C)	(°C)	Front (ref. = 9.73)					Back (ref. = 9.56)					37DM1O	nC_{12}	$C_{10}OH$	37DM1O	nC_{12}	$C_{10}OH$	Front path	Back path	CO_2	37DM1O	nC_{12}	$C_{10}OH$	CO_2	37DM1O	nC_{12}	$C_{10}OH$
5	96.5	106.0	54.89	55.57	9.34	9.19	9.25	9.25		8.87	8.97	8.88	9.00	8.97	17665.3	184 748	11 293	487	4 589	193	4 452	2 492	0.615	0.037	0.323	0.025	0.971	0.004	0.022	0.002
	96.5	106.0	54.89	55.57	9.25	9.16	9.25	9.16		8.93	9.04	9.03	9.09		17877.2	186 703	11 521	489	4 598	193	4 547	2 515	0.617	0.037	0.321	0.025	0.971	0.004	0.022	0.002
	96.5	106.0	54.87	55.55	9.22	9.21	9.28	9.31	9.31	8.88	8.91	8.93	8.97	9.03	17733.5	185 122	11 624	465	4 373	184	4 486	2 412	0.616	0.037	0.322	0.025	0.971	0.004	0.022	0.002
	96.5	106.0	54.89	55.57	9.06	9.09	8.97	9.06		8.43	8.50	8.43	8.40		17932.5	186 560	11 605	463	4 339	182	4 530	2 417	0.616	0.037	0.321	0.025	0.971	0.004	0.022	0.002
																						AVERAGE	**0.616**	**0.037**	**0.322**	**0.025**	**0.971**	**0.004**	**0.022**	**0.002**
																						STANDARD DEVIATION	**0.001**	**0.000**	**0.001**	**0.000**	**0.000**	**0.000**	**0.000**	**0.000**
SAMPLE	P_{READ}	P_{ACT}	T_{READ}	T_{ATC}	Purge Flow Split Vent (s)										FID Front (pA×s)			FID Back (pA×s)			TCD CO_2 (µV×s)		ROLSI Back$_{(Front\ Path)}$ mass fraction				ROLSI Front$_{(Back\ Path)}$ mass fraction			
	(barg)	(bar)	(°C)	(°C)	Front (ref. = 9.73)					Back (ref. = 9.56)					37DM1O	nC_{12}	$C_{10}OH$	37DM1O	nC_{12}	$C_{10}OH$	Front path	Back path	CO_2	37DM1O	nC_{12}	$C_{10}OH$	CO_2	37DM1O	nC_{12}	$C_{10}OH$
6	98.5	107.9	54.84	55.52	9.44	9.34	9.37	9.40	9.41	8.44	8.43	8.44	8.44		15046.9	156 621	10 811	670	6 413	284	4 702	2 215	0.663	0.033	0.280	0.024	0.957	0.006	0.034	0.003
	98.5	107.9	54.84	55.52	9.12	9.06	9.16	9.09	9.13	8.97	8.94	9.00	9.06	9.00	15080.5	156 312	10 871	722	7 069	313	4 725	2 421	0.665	0.033	0.278	0.024	0.957	0.006	0.034	0.003
	98.5	107.9	54.83	55.51	9.10	9.13	9.06	9.15	9.13	9.06	9.03	9.09	9.12	9.06	14887.2	153 997	9 342	730	7 023	310	4 607	2 445	0.664	0.033	0.281	0.022	0.958	0.006	0.033	0.003
	98.5	107.9	54.84	55.52	9.00	9.12	9.03	9.03	9.06	9.09	9.06	8.97	9.00	9.07	15643.1	162 224	10 972	769	7 355	326	4 867	2 565	0.663	0.033	0.280	0.024	0.958	0.006	0.033	0.003
	98.5	107.9	54.82	55.50	9.06	9.12	9.15	9.12	9.15	8.63	8.47	8.63	8.50	8.56	14942.2	154 625	10 097	698	6 654	293	4 651	2 342	0.664	0.033	0.280	0.023	0.958	0.006	0.033	0.003
																						AVERAGE	**0.664**	**0.033**	**0.280**	**0.024**	**0.958**	**0.006**	**0.033**	**0.003**
																						STANDARD DEVIATION	**0.001**	**0.000**	**0.001**	**0.001**	**0.000**	**0.000**	**0.000**	**0.000**

Table 74: Experimental VLE data for the quaternary systems CO_2 + (85 wt% n-dodecane + 10 wt% 3,7-dimethyl-1-octanol + 5 wt% 1-decanol) 75ºC.

SAMPLE	P_{READ}	P_{ACT}	T_{READ}	T_{ATC}	Purge Flow Split Vent (s)										FID Front (pA×s)			FID Back (pA×s)			TCD CO_2 (µV×s)		ROLSI Back$_{(Front\ Path)}$ mass fraction				ROLSI Front$_{(Back\ Path)}$ mass fraction			
	(barg)	(bar)	(°C)	(°C)	Front (ref. = 9.73)					Back (ref. = 9.56)					37DM1O	nC_{12}	$C_{10}OH$	37DM1O	nC_{12}	$C_{10}OH$	Front path	Back path	CO_2	37DM1O	nC_{12}	$C_{10}OH$	CO_2	37DM1O	nC_{12}	$C_{10}OH$
1	102.9	110.2	75.03	75.69	9.44	9.47	9.53	9.47		8.72	8.69	8.69	8.78		38653.50	419 812	24 785	265	2 451	103	3 987	2 765	0.388	0.057	0.517	0.037	0.984	0.003	0.012	0.002
	102.9	110.2	75.04	75.70	9.19	9.06	9.16			9.06	8.97	8.97	8.91		38706.40	419 495	24 504	276	2 558	108	3 975	2 865	0.388	0.057	0.518	0.037	0.984	0.003	0.012	0.002
	102.9	110.2	75.05	75.71	9.12	9.07	9.16	9.09		9.03	8.97	9.09	9.10		37206.80	401 788	23 848	285	2 648	112	3 807	2 954	0.387	0.057	0.518	0.038	0.984	0.003	0.012	0.002
	102.9	110.2	75.04	75.70	9.04	9.09	9.06			9.03	9.06	9.09	9.00	9.03	36139.80	390 535	23 385	272	2 533	107	3 721	2 793	0.388	0.057	0.516	0.038	0.983	0.003	0.012	0.002
																						AVERAGE	**0.388**	**0.057**	**0.517**	**0.038**	**0.984**	**0.003**	**0.012**	**0.002**
																						STANDARD DEVIATION	**0.000**	**0.000**	**0.001**	**0.000**	**0.000**	**0.000**	**0.000**	**0.000**
SAMPLE	P_{READ}	P_{ACT}	T_{READ}	T_{ATC}	Purge Flow Split Vent (s)										FID Front (pA×s)			FID Back (pA×s)			TCD CO_2 (µV×s)		ROLSI Back$_{(Front\ Path)}$ mass fraction				ROLSI Front$_{(Back\ Path)}$ mass fraction			
	(barg)	(bar)	(°C)	(°C)	Front (ref. = 9.73)					Back (ref. = 9.56)					37DM1O	nC_{12}	$C_{10}OH$	37DM1O	nC_{12}	$C_{10}OH$	Front path	Back path	CO_2	37DM1O	nC_{12}	$C_{10}OH$	CO_2	37DM1O	nC_{12}	$C_{10}OH$
2	117.7	124.9	75.08	75.74	9.50	9.41	9.47	9.47		8.56	8.60	8.60	8.59		32992.80	361 301	20 713	556	5 070	215	4 924	2 889	0.477	0.049	0.443	0.031	0.973	0.004	0.021	0.002
	117.7	124.9	75.05	75.71	9.09	9.13	9.12	9.09		8.90	8.94	8.88	8.94		31664.60	345 328	19 825	593	5 408	229	4 681	3 071	0.476	0.049	0.444	0.031	0.973	0.004	0.021	0.002
	117.7	124.9	75.05	75.71	9.00	9.10	9.03	9.10	9.12	8.96	9.03	9.04	9.09	9.06	32156.70	350 782	19 631	603	5 495	232	4 776	3 129	0.477	0.049	0.443	0.031	0.973	0.004	0.021	0.002
	117.7	124.9	75.06	75.72	9.03	9.12	9.12	9.03		8.94	9.03	9.00	9.09	9.06	31576.10	342 674	20 210	566	5 158	219	4 689	2 960	0.478	0.049	0.441	0.032	0.973	0.004	0.021	0.002
	117.7	124.9	75.05	75.71	9.07	9.03	9.00	9.03		8.97	9.09	8.88	9.00	9.00	32561.10	354 573	20 878	576	5 248	223	4 826	3 019	0.477	0.049	0.443	0.032	0.973	0.004	0.021	0.002
																						AVERAGE	**0.477**	**0.049**	**0.443**	**0.032**	**0.973**	**0.004**	**0.021**	**0.002**
																						STANDARD DEVIATION	**0.001**	**0.000**	**0.001**	**0.001**	**0.000**	**0.000**	**0.000**	**0.000**

Table 74 continued: Experimental VLE data for the quaternary systems CO_2 + (85 wt% n-dodecane + 10 wt% 3,7-dimethyl-1-octanol + 5 wt% 1-decanol) at 75°C.

SAMPLE	P_{READ}	P_{ACT}	T_{READ}	T_{ATC}	Purge Flow Split Vent (s)										FID Front (pA×s)			FID Back (pA×s)			TCD CO_2 (µV×s)		ROLSI Back$_{(Front\ Path)}$ mass fraction				ROLSI Front$_{(Back\ Path)}$ mass fraction			
	(barg)	(bar)	(°C)	(°C)	Front (ref. = 9.73)					Back (ref. = 9.56)					37DM1O	nC_{12}	$C_{10}OH$	37DM1O	nC_{12}	$C_{10}OH$	Front path	Back path	CO_2	37DM1O	nC_{12}	$C_{10}OH$	CO_2	37DM1O	nC_{12}	$C_{10}OH$
3	128.0	135.1	75.03	75.69	9.68	9.53	9.47	9.47	9.40	9.31	9.31	9.25	9.28		28070.50	306 112	16 923	1 119	10 176	456	5 849	3 477	0.562	0.041	0.371	0.025	0.959	0.006	0.033	0.003
	127.8	134.9	75.06	75.72	9.25	9.34	9.22	9.31	9.31	9.16	8.97	8.94	9.16	9.06	26907.80	291 806	17 435	1 025	9 335	419	5 549	3 138	0.560	0.041	0.372	0.028	0.958	0.006	0.034	0.003
	128.0	135.1	75.04	75.70	9.22	9.19	9.28	9.22	9.19	9.19	9.10	9.13	9.18		26296.10	284 795	18 387	1 070	9 757	438	5 394	3 257	0.557	0.041	0.372	0.030	0.957	0.006	0.034	0.003
	128.0	135.1	75.05	75.71	9.28	9.16	9.03	9.16	9.04	9.22	9.15	9.25	9.22		27047.80	292 911	14 304	1 090	9 932	445	5 534	3 305	0.561	0.042	0.375	0.023	0.957	0.006	0.034	0.003
	128.0	135.1	75.05	75.71	9.16	9.16	9.25	9.19	9.25	9.15	9.22	9.13	9.12		27594.90	298 223	18 120	1 093	9 951	447	5 645	3 280	0.558	0.041	0.372	0.028	0.957	0.006	0.035	0.003
																						AVERAGE	**0.560**	**0.041**	**0.372**	**0.027**	**0.958**	**0.006**	**0.034**	**0.003**
																						STANDARD DEVIATION	**0.002**	**0.000**	**0.001**	**0.003**	**0.001**	**0.000**	**0.000**	**0.000**
SAMPLE	P_{READ}	P_{ACT}	T_{READ}	T_{ATC}	Purge Flow Split Vent (s)										FID Front (pA×s)			FID Back (pA×s)			TCD CO_2 (µV×s)		ROLSI Back$_{(Front\ Path)}$ mass fraction				ROLSI Front$_{(Back\ Path)}$ mass fraction			
	(barg)	(bar)	(°C)	(°C)	Front (ref. = 9.73)					Back (ref. = 9.56)					37DM1O	nC_{12}	$C_{10}OH$	37DM1O	nC_{12}	$C_{10}OH$	Front path	Back path	CO_2	37DM1O	nC_{12}	$C_{10}OH$	CO_2	37DM1O	nC_{12}	$C_{10}OH$
4	129.8	136.9	75.05	75.71	9.28	9.41	9.34	9.31	9.28	9.03	9.03	9.03	9.09	9.12	26660.10	289 626	16 664	1 353	12 381	565	5 981	3 350	0.581	0.039	0.355	0.025	0.949	0.007	0.041	0.003
	129.8	136.9	75.05	75.71	9.09	9.06	9.12	9.13	9.12	8.93	8.97	8.97	8.97	9.00	26212.60	284 699	15 725	1 351	12 454	569	5 967	3 344	0.585	0.039	0.352	0.024	0.949	0.007	0.042	0.003
	129.8	136.9	75.05	75.71	9.00	9.00	9.07	9.13	9.13	9.03	9.00	8.94	9.06	9.10	26404.70	286 216	17 019	1 331	12 155	554	5 910	3 322	0.580	0.039	0.355	0.026	0.949	0.007	0.041	0.003
	129.7	136.8	75.05	75.71	9.03	9.04	9.13	9.06	9.10	9.03	8.97	8.97	9.03		26880.30	291 452	14 302	1 354	12 384	566	6 069	3 346	0.585	0.039	0.354	0.022	0.949	0.007	0.041	0.003
	129.8	136.9	75.05	75.71	8.93	8.97	9.03	9.00	9.00	8.37	8.34	8.35	8.34	8.38	25818.80	278 721	13 606	1 211	11 076	507	5 757	3 010	0.582	0.040	0.356	0.022	0.949	0.007	0.041	0.003
																						AVERAGE	**0.582**	**0.039**	**0.354**	**0.024**	**0.949**	**0.007**	**0.041**	**0.003**
																						STANDARD DEVIATION	**0.002**	**0.000**	**0.001**	**0.002**	**0.000**	**0.000**	**0.000**	**0.000**
SAMPLE	P_{READ}	P_{ACT}	T_{READ}	T_{ATC}	Purge Flow Split Vent (s)										FID Front (pA×s)			FID Back (pA×s)			TCD CO_2 (µV×s)		ROLSI Back$_{(Front\ Path)}$ mass fraction				ROLSI Front$_{(Back\ Path)}$ mass fraction			
	(barg)	(bar)	(°C)	(°C)	Front (ref. = 9.73)					Back (ref. = 9.56)					37DM1O	nC_{12}	$C_{10}OH$	37DM1O	nC_{12}	$C_{10}OH$	Front path	Back path	CO_2	37DM1O	nC_{12}	$C_{10}OH$	CO_2	37DM1O	nC_{12}	$C_{10}OH$
5	132.8	139.9	75.08	75.74	9.35	9.37	9.32	9.38		9.19	9.19	9.12	9.13	9.15	24913.60	270 130	17 343	1 703	15 688	731	6 317	3 367	0.609	0.036	0.329	0.026	0.937	0.008	0.051	0.004
	132.9	140.0	75.07	75.73	9.13	9.18	9.18	9.25	9.22	8.91	8.87	8.90	8.97	8.87	23388.70	251 851	15 631	1 611	14 809	690	5 934	3 179	0.611	0.037	0.327	0.025	0.937	0.008	0.051	0.004
	132.9	140.0	75.03	75.69	9.12	9.03	9.10	9.16	9.12	8.93	8.97	9.06	9.06	9.00	23195.10	249 126	14 449	1 673	15 400	714	5 912	3 298	0.613	0.037	0.326	0.024	0.937	0.008	0.051	0.004
	132.9	140.0	75.05	75.71	9.12	9.12	9.16	9.12	9.10	9.09	9.10	9.13	9.09	9.07	23871.40	257 213	12 582	1 707	15 690	731	6 055	3 357	0.614	0.037	0.329	0.020	0.937	0.008	0.051	0.004
	132.8	139.9	75.06	75.72	9.19	9.22	9.25	9.19	9.18	9.13	9.13	9.03	9.10	9.09	23070.80	247 441	14 583	1 686	15 496	721	5 889	3 322	0.614	0.037	0.326	0.024	0.937	0.008	0.051	0.004
																						AVERAGE	**0.612**	**0.037**	**0.327**	**0.024**	**0.937**	**0.008**	**0.051**	**0.004**
																						STANDARD DEVIATION	**0.002**	**0.000**	**0.001**	**0.002**	**0.000**	**0.000**	**0.000**	**0.000**
SAMPLE	P_{READ}	P_{ACT}	T_{READ}	T_{ATC}	Purge Flow Split Vent (s)										FID Front (pA×s)			FID Back (pA×s)			TCD CO_2 (µV×s)		ROLSI Back$_{(Front\ Path)}$ mass fraction				ROLSI Front$_{(Back\ Path)}$ mass fraction			
	(barg)	(bar)	(°C)	(°C)	Front (ref. = 9.73)					Back (ref. = 9.56)					37DM1O	nC_{12}	$C_{10}OH$	37DM1O	nC_{12}	$C_{10}OH$	Front path	Back path	CO_2	37DM1O	nC_{12}	$C_{10}OH$	CO_2	37DM1O	nC_{12}	$C_{10}OH$
6	134.9	141.9	75.07	75.73	9.03	9.15	9.12	9.06	9.18	8.50	8.53	8.47	8.53		22629.10	243 089	15 061	1 905	17 691	827	6 342	3 181	0.635	0.034	0.307	0.024	0.927	0.009	0.060	0.004
	135.0	142.0	75.03	75.69	8.96	9.09	9.03	9.03	9.09	8.91	8.85	8.97	8.88	8.94	22427.80	240 637	15 987	1 924	17 793	836	6 229	3 244	0.632	0.035	0.308	0.025	0.928	0.009	0.059	0.004
	134.9	141.9	75.05	75.71	9.07	9.03	9.10	9.03		8.94	8.97	9.00	9.00		24841.90	266 615	18 056	1 957	18 129	852	7 004	3 294	0.635	0.034	0.305	0.026	0.927	0.009	0.060	0.004
	135.0	142.0	75.04	75.70	9.16	9.19	9.03	9.16	9.00	9.00	9.00	8.91	8.93	9.03	21513.90	229 952	13 829	1 894	17 564	822	5 980	3 151	0.634	0.035	0.308	0.023	0.926	0.009	0.060	0.004
	134.9	141.9	75.03	75.69	9.00	9.00	9.00	9.00		8.38	8.41	8.35	8.43		22936.00	245 146	16 366	1 879	17 432	821	6 395	3 155	0.634	0.035	0.306	0.025	0.927	0.009	0.060	0.004
																						AVERAGE	**0.634**	**0.035**	**0.307**	**0.025**	**0.927**	**0.009**	**0.060**	**0.004**
																						STANDARD DEVIATION	**0.001**	**0.000**	**0.001**	**0.001**	**0.000**	**0.000**	**0.000**	**0.000**

Table 75: Experimental VLE data for the quaternary systems CO_2 + (10 wt% n-dodecane + 30 wt% 3,7-dimethyl-1-octanol + 60 wt% 1-decanol) at 35ºC.

SAMPLE	P_{READ}	P_{ACT}	T_{READ}	T_{ATC}	Purge Flow Split Vent (s)										FID Front (pA×s)			FID Back (pA×s)			TCD CO_2 (µV×s)		ROLSI Back$_{(Front\ Path)}$ mass fraction				ROLSI Front$_{(Back\ Path)}$ mass fraction			
	(barg)	(bar)	(°C)	(°C)	Front (ref. = 9.73)					Back (ref. = 9.56)					37DM1O	nC_{12}	$C_{10}OH$	37DM1O	nC_{12}	$C_{10}OH$	Front path	Back path	CO_2	37DM1O	nC_{12}	$C_{10}OH$	CO_2	37DM1O	nC_{12}	$C_{10}OH$
1	82.6	94.0	34.77	35.46	9.22	9.25	9.28	9.31	9.31	9.00	9.09	9.13	9.07		96764.2	33 086	207 647	1 866	2 078	3 050	3 494	1 731	0.409	0.171	0.050	0.370	0.943	0.016	0.016	0.025
	82.5	93.9	34.78	35.47	9.25	9.21	9.22	9.22		9.03	9.03	9.13	9.09	9.15	101096.0	34 413	217 403	1 841	2 068	3 004	3 600	1 836	0.406	0.172	0.050	0.373	0.947	0.015	0.015	0.023
	82.6	94.0	34.78	35.47	9.32	9.31	9.25	9.31	9.25	9.07	9.10	9.07	9.13	9.00	99368.1	33 937	212 869	1 904	2 133	3 046	3 583	1 724	0.409	0.171	0.050	0.370	0.942	0.017	0.016	0.025
	82.6	94.0	34.75	35.44	9.31	9.25	9.31	9.31	9.31	9.13	9.10	9.06	9.00	9.09	97227.5	33 373	208 008	1 797	2 064	2 875	3 525	1 778	0.411	0.171	0.050	0.369	0.946	0.016	0.015	0.023
	82.6	94.0	34.76	35.45	9.28	9.19	9.09	9.13	9.13	9.03	9.07	9.12	9.16	9.12	97915.7	33 140	209 753	1 720	1 954	2 819	3 475	1 835	0.406	0.172	0.050	0.372	0.949	0.015	0.014	0.022
																						AVERAGE	**0.408**	**0.172**	**0.050**	**0.371**	**0.945**	**0.016**	**0.015**	**0.024**
																						STANDARD DEVIATION	**0.002**	**0.001**	**0.000**	**0.002**	**0.003**	**0.001**	**0.001**	**0.001**
SAMPLE	P_{READ}	P_{ACT}	T_{READ}	T_{ATC}	Purge Flow Split Vent (s)										FID Front (pA×s)			FID Back (pA×s)			TCD CO_2 (µV×s)		ROLSI Back$_{(Front\ Path)}$ mass fraction				ROLSI Front$_{(Back\ Path)}$ mass fraction			
	(barg)	(bar)	(°C)	(°C)	Front (ref. = 9.73)					Back (ref. = 9.56)					37DM1O	nC_{12}	$C_{10}OH$	37DM1O	nC_{12}	$C_{10}OH$	Front path	Back path	CO_2	37DM1O	nC_{12}	$C_{10}OH$	CO_2	37DM1O	nC_{12}	$C_{10}OH$
2	92.8	104.1	34.72	35.41	9.31	9.28	9.28	9.31		8.78	8.75	8.78	8.78		106872.0	33 596	235 550	2 486	2 505	4 037	4 075	1 980	0.421	0.166	0.044	0.369	0.938	0.018	0.016	0.028
	92.8	104.1	34.72	35.41	9.00	9.04	9.03	9.03		8.90	8.94	8.94	8.90		102611.0	32 606	224 937	2 606	2 553	4 227	3 977	2 021	0.425	0.165	0.045	0.365	0.937	0.019	0.016	0.029
	92.8	104.1	34.74	35.43	9.07	9.10	9.07	9.03	9.09	8.94	9.00	8.93	8.97		102069.0	32 047	224 395	2 642	2 617	4 315	3 918	2 065	0.422	0.166	0.044	0.367	0.937	0.019	0.016	0.029
	92.8	104.1	34.75	35.44	9.06	9.06	9.04	9.00	9.03	8.97	8.96	9.03	9.03	9.03	106463.0	33 487	234 462	2 805	2 716	4 685	4 104	1 977	0.423	0.165	0.044	0.367	0.931	0.020	0.017	0.032
																						AVERAGE	**0.423**	**0.166**	**0.044**	**0.367**	**0.935**	**0.019**	**0.016**	**0.030**
																						STANDARD DEVIATION	**0.002**	**0.000**	**0.000**	**0.002**	**0.003**	**0.001**	**0.001**	**0.002**
SAMPLE	P_{READ}	P_{ACT}	T_{READ}	T_{ATC}	Purge Flow Split Vent (s)										FID Front (pA×s)			FID Back (pA×s)			TCD CO_2 (µV×s)		ROLSI Back$_{(Front\ Path)}$ mass fraction				ROLSI Front$_{(Back\ Path)}$ mass fraction			
	(barg)	(bar)	(°C)	(°C)	Front (ref. = 9.73)					Back (ref. = 9.56)					37DM1O	nC_{12}	$C_{10}OH$	37DM1O	nC_{12}	$C_{10}OH$	Front path	Back path	CO_2	37DM1O	nC_{12}	$C_{10}OH$	CO_2	37DM1O	nC_{12}	$C_{10}OH$
3	112.0	123.1	34.71	35.40	9.38	9.37	9.34	9.40		9.06	9.09	9.10	9.07		115955.0	38 006	258 498	5 895	4 649	10 448	5 053	2 455	0.451	0.156	0.043	0.350	0.894	0.031	0.021	0.054
	112.0	123.1	34.71	35.40	9.03	9.06	9.00	9.06		8.85	8.94	8.94	8.91	8.97	116858.0	40 839	258 607	6 531	5 058	11 783	5 122	2 413	0.453	0.155	0.046	0.346	0.882	0.034	0.023	0.061
	112.0	123.1	34.71	35.40	9.22	9.09	9.00	9.07	9.00	8.97	9.00	8.94	8.97	9.06	115000.0	37 514	248 980	6 082	4 823	10 830	5 050	2 404	0.458	0.157	0.043	0.342	0.889	0.032	0.022	0.057
	112.0	123.1	34.71	35.40	9.07	8.94	9.10	8.97	9.06	8.78	8.91	8.87	8.90	8.84	113543.0	37 177	251 698	6 080	4 731	10 916	4 978	2 399	0.454	0.156	0.043	0.348	0.888	0.032	0.022	0.058
																						AVERAGE	**0.454**	**0.156**	**0.044**	**0.346**	**0.888**	**0.032**	**0.022**	**0.057**
																						STANDARD DEVIATION	**0.003**	**0.001**	**0.001**	**0.003**	**0.005**	**0.001**	**0.001**	**0.003**
SAMPLE	P_{READ}	P_{ACT}	T_{READ}	T_{ATC}	Purge Flow Split Vent (s)										FID Front (pA×s)			FID Back (pA×s)			TCD CO_2 (µV×s)		ROLSI Back$_{(Front\ Path)}$ mass fraction				ROLSI Front$_{(Back\ Path)}$ mass fraction			
	(barg)	(bar)	(°C)	(°C)	Front (ref. = 9.73)					Back (ref. = 9.56)					37DM1O	nC_{12}	$C_{10}OH$	37DM1O	nC_{12}	$C_{10}OH$	Front path	Back path	CO_2	37DM1O	nC_{12}	$C_{10}OH$	CO_2	37DM1O	nC_{12}	$C_{10}OH$
4	129.2	140.2	34.75	35.44	9.09	9.03	9.06	9.07		8.90	8.97	8.91	9.03	9.09	122490.0	40 011	268 910	9 389	6 290	17 513	5 951	2 731	0.481	0.149	0.041	0.329	0.857	0.042	0.024	0.078
	129.2	140.2	34.74	35.43	9.03	9.03	9.90	9.09	9.06	8.88	8.90	8.97	8.97	9.00	121278.0	39 955	268 115	9 408	6 173	17 609	5 947	2 698	0.482	0.148	0.041	0.329	0.855	0.042	0.024	0.079
	129.2	140.2	34.73	35.42	8.94	9.03	8.97	8.91		8.91	8.88	9.00	8.90	9.00	123951.0	40 567	271 220	9 622	6 489	18 075	6 063	2 795	0.483	0.148	0.041	0.327	0.856	0.042	0.024	0.078
	129.2	140.2	34.73	35.42	9.03	9.00	9.00	8.97		8.69	8.72	8.68	8.69		124377.0	40 581	272 703	9 229	6 169	17 359	6 042	2 703	0.481	0.149	0.041	0.329	0.857	0.041	0.024	0.078
	129.2	140.2	34.72	35.41	8.94	8.97	9.00	8.97		8.81	8.81	8.82	8.84		121108.0	39 629	264 586	9 802	6 546	18 364	5 931	2 713	0.484	0.148	0.041	0.327	0.851	0.043	0.025	0.081
																						AVERAGE	**0.482**	**0.148**	**0.041**	**0.328**	**0.855**	**0.042**	**0.024**	**0.079**
																						STANDARD DEVIATION	**0.001**	**0.000**	**0.000**	**0.001**	**0.003**	**0.001**	**0.000**	**0.001**
SAMPLE	P_{READ}	P_{ACT}	T_{READ}	T_{ATC}	Purge Flow Split Vent (s)										FID Front (pA×s)			FID Back (pA×s)			TCD CO_2 (µV×s)		ROLSI Back$_{(Front\ Path)}$ mass fraction				ROLSI Front$_{(Back\ Path)}$ mass fraction			
	(barg)	(bar)	(°C)	(°C)	Front (ref. = 9.73)					Back (ref. = 9.56)					37DM1O	nC_{12}	$C_{10}OH$	37DM1O	nC_{12}	$C_{10}OH$	Front path	Back path	CO_2	37DM1O	nC_{12}	$C_{10}OH$	CO_2	37DM1O	nC_{12}	$C_{10}OH$
5	146.2	157.0	34.74	35.43	9.03	8.97	8.94	9.03		9.00	8.97	8.97	9.00		125146.0	45 841	275 409	11 909	7 201	22 628	6 989	2 975	0.514	0.138	0.043	0.306	0.839	0.047	0.025	0.090
	146.2	157.0	34.74	35.43	8.87	9.03	8.94	8.97	8.94	8.81	8.79	8.87	8.91	8.94	124108.0	45 896	272 125	11 917	7 228	22 630	6 918	2 991	0.513	0.138	0.043	0.305	0.839	0.047	0.024	0.089
	146.2	157.0	34.73	35.42	8.94	8.94	9.03	9.00	9.03	8.96	8.91	8.97	8.97		125065.0	42 459	275 240	12 150	7 369	23 040	6 928	3 037	0.513	0.139	0.040	0.308	0.839	0.047	0.025	0.090
	146.2	157.0	34.73	35.42	8.91	8.97	9.03	8.97	9.03	8.57	8.66	8.63	8.63		129951.0	47 784	283 695	11 979	7 257	22 668	7 340	2 978	0.518	0.137	0.043	0.302	0.838	0.047	0.025	0.090
	146.1	156.9	34.73	35.42	9.00	8.97	9.03	9.00		8.88	8.84	8.81	8.87		127287.0	47 030	278 982	12 179	7 386	23 199	7 139	2 956	0.515	0.138	0.043	0.304	0.835	0.048	0.025	0.092
																						AVERAGE	**0.515**	**0.138**	**0.042**	**0.305**	**0.838**	**0.047**	**0.025**	**0.090**
																						STANDARD DEVIATION	**0.002**	**0.001**	**0.001**	**0.002**	**0.002**	**0.001**	**0.000**	**0.001**

Table 75 continued: Experimental VLE data for the quaternary systems CO_2 + (10 wt% n-dodecane + 30 wt% 3,7-dimethyl-1-octanol + 60 wt% 1-decanol) at 35ºC.

SAMPLE	P_{READ}	P_{ACT}	T_{READ}	T_{ATC}	Purge Flow Split Vent (s)										FID Front (pA×s)			FID Back (pA×s)			TCD CO_2 (µV×s)		ROLSI Back$_{(Front Path)}$ mass fraction				ROLSI Front$_{(Back Path)}$ mass fraction			
	(barg)	(bar)	(°C)	(°C)	Front (ref. = 9.73)					Back (ref. = 9.56)					37DM1O	nC_{12}	$C_{10}OH$	37DM1O	nC_{12}	$C_{10}OH$	Front path	Back path	CO_2	37DM1O	nC_{12}	$C_{10}OH$	CO_2	37DM1O	nC_{12}	$C_{10}OH$
6	159.4	170.1	34.73	35.42	9.00	9.06	9.07	9.10	9.06	9.00	9.03	8.97	9.03	9.00	123291.0	45 985	271 696	14 565	8 084	28 074	7 790	3 145	0.544	0.129	0.041	0.286	0.819	0.053	0.025	0.103
	159.4	170.1	34.74	35.43	8.94	8.94	9.00	9.03	9.00	8.97	8.94	8.93	8.94		123653.0	41 659	272 438	15 211	8 338	29 531	7 917	3 164	0.549	0.129	0.037	0.285	0.814	0.054	0.026	0.106
	159.4	170.1	34.72	35.41	9.03	9.10	9.06	9.07	9.13	8.34	8.41	8.37	8.47	8.44	126153.0	42 706	277 807	14 274	7 806	27 617	8 092	3 029	0.550	0.128	0.037	0.285	0.817	0.054	0.025	0.105
																						AVERAGE	**0.548**	**0.129**	**0.038**	**0.286**	**0.817**	**0.054**	**0.025**	**0.105**
																						STANDARD DEVIATION	**0.003**	**0.000**	**0.002**	**0.001**	**0.003**	**0.001**	**0.000**	**0.002**

Table 76: Experimental VLE data for the quaternary systems CO_2 + (10 wt% n-dodecane + 30 wt% 3,7-dimethyl-1-octanol + 60 wt% 1-decanol) at 55ºC.

SAMPLE	P_{READ}	P_{ACT}	T_{READ}	T_{ATC}	Purge Flow Split Vent (s)										FID Front (pA×s)			FID Back (pA×s)			TCD CO_2 (µV×s)		ROLSI Back$_{(Front Path)}$ mass fraction				ROLSI Front$_{(Back Path)}$ mass fraction			
	(barg)	(bar)	(°C)	(°C)	Front (ref. = 9.73)					Back (ref. = 9.56)					37DM1O	nC_{12}	$C_{10}OH$	37DM1O	nC_{12}	$C_{10}OH$	Front path	Back path	CO_2	37DM1O	nC_{12}	$C_{10}OH$	CO_2	37DM1O	nC_{12}	$C_{10}OH$
1	84.5	94.1	54.88	55.56	9.21	9.31	9.22	9.35	9.25	9.00	9.07	9.03	9.06	9.09	137287	60 026	286 926	130	251	178	3 189	1 924	0.307	0.199	0.074	0.420	0.990	0.003	0.004	0.003
	84.5	94.1	54.88	55.56	9.25	9.22	9.22	9.25		8.25	8.50	8.19	8.28	8.25	140344	57 962	295 105	117	232	166	3 160	1 764	0.301	0.202	0.070	0.427	0.989	0.004	0.004	0.003
	84.5	94.1	54.88	55.56	9.15	9.09	9.06	9.06		8.93	8.88	8.88	8.94		140276	58 290	293 470	132	260	188	3 219	1 996	0.305	0.201	0.071	0.423	0.990	0.003	0.004	0.003
	84.5	94.1	54.87	55.55	8.97	9.03	9.06	9.00	9.07	8.97	8.97	8.97	9.04		131722	54 354	277 751	121	239	177	3 004	1 877	0.303	0.201	0.070	0.426	0.989	0.003	0.004	0.003
	84.5	94.1	54.89	55.57	8.94	9.06	9.00	9.09	9.03	8.87	8.94	8.87	8.88	8.93	137948	57 562	288 905	127	248	185	3 196	1 979	0.307	0.200	0.071	0.422	0.990	0.003	0.004	0.003
																							0.305	**0.200**	**0.071**	**0.424**	**0.990**	**0.003**	**0.004**	**0.003**
																							0.003	**0.001**	**0.001**	**0.003**	**0.000**	**0.000**	**0.000**	**0.000**
SAMPLE	P_{READ}	P_{ACT}	T_{READ}	T_{ATC}	Purge Flow Split Vent (s)										FID Front (pA×s)			FID Back (pA×s)			TCD CO_2 (µV×s)		ROLSI Back$_{(Front Path)}$ mass fraction				ROLSI Front$_{(Back Path)}$ mass fraction			
	(barg)	(bar)	(°C)	(°C)	Front (ref. = 9.73)					Back (ref. = 9.56)					37DM1O	nC_{12}	$C_{10}OH$	37DM1O	nC_{12}	$C_{10}OH$	Front path	Back path	CO_2	37DM1O	nC_{12}	$C_{10}OH$	CO_2	37DM1O	nC_{12}	$C_{10}OH$
2	94.9	104.4	54.85	55.53	9.06	9.06	9.03	9.06		8.85	8.84	8.90	8.85		127886	52 635	268 591	405	613	637	3 721	2 177	0.358	0.185	0.065	0.392	0.984	0.005	0.005	0.005
	94.9	104.4	54.85	55.53	8.97	9.00	8.94	9.00	8.97	8.94	9.00	8.97	9.00	9.00	128263	52 467	271 391	408	614	629	3 654	2 198	0.352	0.186	0.064	0.397	0.985	0.005	0.005	0.005
	94.9	104.4	54.86	55.54	9.00	9.00	8.93	9.03		8.94	9.06	8.94	8.97	9.03	125214	51 566	264 182	395	603	600	3 625	2 190	0.356	0.185	0.065	0.394	0.985	0.005	0.005	0.005
	94.9	104.4	54.85	55.53	8.90	8.88	8.93	9.00	9.06	8.91	9.00	8.94	8.97		130724	53 286	277 623	395	607	593	3 728	2 220	0.352	0.186	0.064	0.398	0.985	0.005	0.005	0.005
	94.9	104.4	54.85	55.53	9.00	8.94	8.87	8.94	8.97	7.81	7.87	7.87	7.97	7.93	127450	54 593	269 715	347	531	517	3 622	1 920	0.350	0.186	0.067	0.396	0.984	0.005	0.006	0.005
																							0.354	**0.186**	**0.065**	**0.396**	**0.985**	**0.005**	**0.005**	**0.005**
																							0.003	**0.000**	**0.001**	**0.002**	**0.000**	**0.000**	**0.000**	**0.000**
SAMPLE	P_{READ}	P_{ACT}	T_{READ}	T_{ATC}	Purge Flow Split Vent (s)										FID Front (pA×s)			FID Back (pA×s)			TCD CO_2 (µV×s)		ROLSI Back$_{(Front Path)}$ mass fraction				ROLSI Front$_{(Back Path)}$ mass fraction			
	(barg)	(bar)	(°C)	(°C)	Front (ref. = 9.73)					Back (ref. = 9.56)					37DM1O	nC_{12}	$C_{10}OH$	37DM1O	nC_{12}	$C_{10}OH$	Front path	Back path	CO_2	37DM1O	nC_{12}	$C_{10}OH$	CO_2	37DM1O	nC_{12}	$C_{10}OH$
3	113.7	123.0	54.82	55.50	8.94	9.03	8.94	8.94	9.03	8.40	8.43	8.50	8.47	8.50	121118	46 940	263 347	2 287	2 498	3 755	4 844	2 578	0.430	0.162	0.053	0.355	0.954	0.013	0.012	0.021
	113.7	123.0	54.81	55.49	8.84	9.00	8.88	9.00	8.93	8.62	8.72	8.81	8.84	8.75	118814	45 784	259 110	2 330	2 575	3 760	4 638	2 708	0.424	0.163	0.053	0.359	0.955	0.013	0.012	0.020
	113.7	123.0	54.79	55.47	8.00	8.91	8.97	8.93	9.00	8.87	8.90	8.96	8.90	8.91	118762	45 901	258 742	2 410	2 651	3 877	4 694	2 750	0.427	0.163	0.053	0.357	0.955	0.013	0.012	0.020
	113.7	123.0	54.79	55.47	8.87	8.90	8.90	8.88		8.66	8.66	8.84	8.69	8.81	120672	46 605	261 769	2 447	2 698	3 899	4 761	2 844	0.428	0.163	0.053	0.356	0.956	0.013	0.012	0.019
	113.7	123.0	54.80	55.48	8.81	8.88	8.85	8.88		8.82	8.78	8.81	8.87	8.84	118169	45 988	256 482	2 390	2 650	3 893	4 731	2 788	0.431	0.162	0.053	0.354	0.955	0.013	0.012	0.020
																							0.428	**0.163**	**0.053**	**0.356**	**0.955**	**0.013**	**0.012**	**0.020**
																							0.003	**0.001**	**0.000**	**0.002**	**0.001**	**0.000**	**0.000**	**0.000**

Table 76 continued: Experimental VLE data for the quaternary systems CO_2 + (10 wt% n-dodecane + 30 wt% 3,7-dimethyl-1-octanol + 60 wt% 1-decanol) at 55ºC.

SAMPLE	P_{READ}	P_{ACT}	T_{READ}	T_{ATC}	Purge Flow Split Vent (s)										FID Front (pA×s)			FID Back (pA×s)			TCD CO_2 (µV×s)		ROLSI Back$_{(Front\ Path)}$ mass fraction				ROLSI Front$_{(Back\ Path)}$ mass fraction			
	(barg)	(bar)	(°C)	(°C)	Front (ref. = 9.73)					Back (ref. = 9.56)					37DM1O	nC_{12}	$C_{10}OH$	37DM1O	nC_{12}	$C_{10}OH$	Front path	Back path	CO_2	37DM1O	nC_{12}	$C_{10}OH$	CO_2	37DM1O	nC_{12}	$C_{10}OH$
4	130.9	140.0	54.78	55.46	8.78	8.87	8.87	8.84		8.31	8.32	8.28	8.34		116403	43 798	250 919	5 976	4 725	10 744	5 794	2 698	0.487	0.147	0.047	0.319	0.901	0.029	0.020	0.051
	130.9	140.0	54.80	55.48	8.78	8.91	8.94	8.88	8.84	8.72	8.71	8.68	8.75		114426	43 242	247 408	6 005	4 595	10 839	5 697	2 783	0.486	0.147	0.047	0.320	0.903	0.028	0.019	0.050
	130.9	140.0	54.79	55.47	8.75	8.78	8.90	8.78	8.75	8.84	8.85	8.81	8.84		117208	44 050	254 280	5 995	4 637	10 742	5 762	2 871	0.483	0.148	0.047	0.323	0.906	0.027	0.018	0.048
	131.0	140.1	54.80	55.48	8.79	8.82	8.87	8.85	8.87	8.22	8.25	8.25	8.22		118401	43 967	256 893	5 465	4 452	9 685	5 798	2 691	0.482	0.148	0.046	0.323	0.908	0.027	0.019	0.047
	130.9	140.0	54.80	55.48	8.78	8.78	8.78	8.84		8.75	8.78	8.81	8.78		111263	41 933	241 332	5 496	4 443	9 653	5 499	2 805	0.484	0.147	0.047	0.322	0.911	0.026	0.018	0.045
																							0.485	**0.147**	**0.047**	**0.321**	**0.906**	**0.027**	**0.019**	**0.048**
																							0.002	**0.000**	**0.000**	**0.002**	**0.004**	**0.001**	**0.001**	**0.003**
SAMPLE	P_{READ}	P_{ACT}	T_{READ}	T_{ATC}	Purge Flow Split Vent (s)										FID Front (pA×s)			FID Back (pA×s)			TCD CO_2 (µV×s)		ROLSI Back$_{(Front\ Path)}$ mass fraction				ROLSI Front$_{(Back\ Path)}$ mass fraction			
	(barg)	(bar)	(°C)	(°C)	Front (ref. = 9.73)					Back (ref. = 9.56)					37DM1O	nC_{12}	$C_{10}OH$	37DM1O	nC_{12}	$C_{10}OH$	Front path	Back path	CO_2	37DM1O	nC_{12}	$C_{10}OH$	CO_2	37DM1O	nC_{12}	$C_{10}OH$
5	148.0	157.0	54.85	55.53	9.22	9.21	9.28	9.22	9.16	8.97	9.00	8.97	9.03		111787	43 310	243 339	11 938	7 287	22 718	7 283	3 218	0.552	0.127	0.042	0.279	0.849	0.044	0.023	0.084
	148.0	157.0	54.80	55.48	8.94	8.97	8.94	8.94		8.78	8.72	8.78	8.78		111393	42 706	243 391	11 739	7 096	22 629	7 255	3 175	0.552	0.127	0.041	0.280	0.848	0.044	0.023	0.085
	148.0	157.0	54.81	55.49	8.87	8.94	8.88	8.94	8.97	8.90	8.90	8.85	8.93		107692	42 084	234 541	12 051	7 218	23 051	6 928	3 176	0.549	0.128	0.042	0.281	0.846	0.045	0.023	0.086
	148.0	157.0	54.81	55.49	8.84	8.81	8.78	8.81	8.88	8.75	8.81	8.78	8.81	8.78	104944	40 861	228 588	11 184	6 806	21 381	6 839	3 119	0.552	0.127	0.042	0.279	0.852	0.043	0.023	0.082
	148.0	157.0	54.80	55.48	8.75	8.85	8.78	8.75		8.78	8.78	8.85	8.84		107853	41 817	235 304	12 137	7 278	23 278	6 984	3 183	0.550	0.127	0.042	0.280	0.845	0.045	0.023	0.087
																							0.551	**0.127**	**0.042**	**0.280**	**0.848**	**0.044**	**0.023**	**0.085**
																							0.001	**0.000**	**0.000**	**0.001**	**0.003**	**0.001**	**0.000**	**0.002**

Table 77: Experimental VLE data for the quaternary systems CO_2 + (10 wt% n-dodecane + 30 wt% 3,7-dimethyl-1-octanol + 60 wt% 1-decanol) at 75ºC.

SAMPLE	P_{READ}	P_{ACT}	T_{READ}	T_{ATC}	Purge Flow Split Vent (s)										FID Front (pA×s)			FID Back (pA×s)			TCD CO_2 (µV×s)		ROLSI Back$_{(Front\ Path)}$ mass fraction				ROLSI Front$_{(Back\ Path)}$ mass fraction			
	(barg)	(bar)	(°C)	(°C)	Front (ref. = 9.73)					Back (ref. = 9.56)					37DM1O	nC_{12}	$C_{10}OH$	37DM1O	nC_{12}	$C_{10}OH$	Front path	Back path	CO_2	37DM1O	nC_{12}	$C_{10}OH$	CO_2	37DM1O	nC_{12}	$C_{10}OH$
1	115.8	123.0	75.05	75.71	9.37	9.50	9.35	9.41	9.43	9.09	9.06	9.06	9.09		167670	72 450	355 361	624	812	914	4 278	2 748	0.326	0.192	0.070	0.411	0.984	0.005	0.005	0.006
	115.8	123.0	75.03	75.69	9.50	9.56	9.50	9.50	9.44	8.32	8.35	8.31	8.35		177749	76 393	376 558	608	786	889	4 490	2 638	0.324	0.193	0.070	0.412	0.984	0.005	0.005	0.006
	115.8	123.0	75.03	75.69	9.13	9.09	9.15	9.22	9.12	8.96	8.91	9.00	9.00	9.00	167156	69 823	353 308	635	817	929	4 247	2 755	0.327	0.193	0.068	0.412	0.984	0.005	0.005	0.006
	115.8	123.0	75.02	75.68	9.12	9.03	9.00	9.09	9.16	9.10	9.00	9.12	9.03	9.10	175639	75 638	371 447	655	844	953	4 469	2 851	0.326	0.193	0.070	0.411	0.985	0.005	0.005	0.006
	115.8	123.0	75.01	75.67	9.06	9.00	9.07	8.97	9.00	8.97	8.97	9.00	8.97		169531	72 399	359 943	638	822	928	4 215	2 780	0.321	0.194	0.070	0.415	0.984	0.005	0.005	0.006
																							0.325	**0.193**	**0.070**	**0.412**	**0.984**	**0.005**	**0.005**	**0.006**
																							0.002	**0.001**	**0.001**	**0.002**	**0.000**	**0.000**	**0.000**	**0.000**
SAMPLE	P_{READ}	P_{ACT}	T_{READ}	T_{ATC}	Purge Flow Split Vent (s)										FID Front (pA×s)			FID Back (pA×s)			TCD CO_2 (µV×s)		ROLSI Back$_{(Front\ Path)}$ mass fraction				ROLSI Front$_{(Back\ Path)}$ mass fraction			
	(barg)	(bar)	(°C)	(°C)	Front (ref. = 9.73)					Back (ref. = 9.56)					37DM1O	nC_{12}	$C_{10}OH$	37DM1O	nC_{12}	$C_{10}OH$	Front path	Back path	CO_2	37DM1O	nC_{12}	$C_{10}OH$	CO_2	37DM1O	nC_{12}	$C_{10}OH$
2	132.9	140.0	74.99	75.65	9.13	9.03	9.03	9.06	9.09	9.07	9.06	9.06	9.06		157843	68 346	330 600	1 748	1 923	2 718	5 512	3 292	0.401	0.172	0.063	0.364	0.972	0.008	0.008	0.012
	132.9	140.0	74.99	75.65	9.09	9.00	8.97	8.97	9.00	8.90	8.90	8.88	8.87		150884	65 014	320 726	1 653	1 828	2 563	5 178	3 138	0.395	0.173	0.063	0.370	0.972	0.008	0.008	0.012
	132.9	140.0	74.99	75.65	9.10	9.00	9.00	9.00	9.03	8.93	8.96	8.97	8.94		147005	62 875	312 996	1 677	1 860	2 599	5 001	3 199	0.392	0.173	0.063	0.372	0.972	0.008	0.008	0.012
	132.9	140.0	74.97	75.63	8.94	9.03	9.00	9.06	9.07	8.50	8.56	8.59	8.65	8.65	155692	66 832	330 933	1 656	1 840	2 597	5 316	3 159	0.394	0.173	0.063	0.371	0.972	0.008	0.008	0.012
	132.9	140.0	74.97	75.63	9.04	8.97	8.91	9.00	9.00	8.87	8.91	8.87	8.84	8.90	153470	65 958	325 284	1 691	1 879	2 618	5 281	3 237	0.396	0.173	0.063	0.369	0.972	0.008	0.008	0.012
																							0.395	**0.173**	**0.063**	**0.369**	**0.972**	**0.008**	**0.008**	**0.012**
																							0.003	**0.000**	**0.000**	**0.003**	**0.000**	**0.000**	**0.000**	**0.000**

Table 77 continued: Experimental VLE data for the quaternary systems CO_2 + (10 wt% n-dodecane + 30 wt% 3,7-dimethyl-1-octanol + 60 wt% 1-decanol) at 75ºC.

SAMPLE	P_{READ}	P_{ACT}	T_{READ}	T_{ATC}	Purge Flow Split Vent (s)										FID Front (pA×s)			FID Back (pA×s)			TCD CO_2 (µV×s)		ROLSI Back$_{(Front Path)}$ mass fraction				ROLSI Front$_{(Back Path)}$ mass fraction			
	(barg)	(bar)	(°C)	(°C)	Front (ref. = 9.73)					Back (ref. = 9.56)					37DM1O	nC_{12}	$C_{10}OH$	37DM1O	nC_{12}	$C_{10}OH$	Front path	Back path	CO_2	37DM1O	nC_{12}	$C_{10}OH$	CO_2	37DM1O	nC_{12}	$C_{10}OH$
3	150.1	157.0	74.98	75.64	9.28	9.21	9.25	9.28		8.87	8.90	8.96	8.88		152430	60 245	330 117	4 712	3 913	8 137	6 555	3 691	0.449	0.157	0.052	0.342	0.940	0.018	0.013	0.030
	150.1	157.0	74.97	75.63	8.94	8.91	8.94	8.94		8.69	8.72	8.69	8.66		147439	58 747	318 922	4 529	3 818	7 673	6 508	3 693	0.456	0.155	0.052	0.337	0.943	0.017	0.012	0.028
	150.1	157.0	74.97	75.63	8.87	8.87	8.88	8.87		8.81	8.88	8.81	8.84		138213	55 383	298 806	4 356	3 713	7 343	6 121	3 613	0.456	0.155	0.052	0.337	0.943	0.017	0.012	0.028
	150.1	157.0	74.98	75.64	8.91	8.81	8.75	8.93	8.88	8.84	8.78	8.87	8.84	8.87	143193	57 284	307 369	4 531	3 887	7 733	6 365	3 753	0.458	0.155	0.052	0.335	0.943	0.017	0.012	0.028
	150.1	157.0	74.96	75.62	8.81	8.84	8.81	8.87	8.88	7.97	7.97	8.03	8.03	8.03	144539	58 150	311 366	4 168	3 568	7 009	6 392	3 472	0.456	0.155	0.053	0.336	0.944	0.017	0.012	0.027
																							0.455	**0.155**	**0.052**	**0.337**	**0.943**	**0.017**	**0.012**	**0.028**
																							0.004	**0.001**	**0.000**	**0.003**	**0.001**	**0.000**	**0.000**	**0.001**
SAMPLE	P_{READ}	P_{ACT}	T_{READ}	T_{ATC}	Purge Flow Split Vent (s)										FID Front (pA×s)			FID Back (pA×s)			TCD CO_2 (µV×s)		ROLSI Back$_{(Front Path)}$ mass fraction				ROLSI Front$_{(Back Path)}$ mass fraction			
	(barg)	(bar)	(°C)	(°C)	Front (ref. = 9.73)					Back (ref. = 9.56)					37DM1O	nC_{12}	$C_{10}OH$	37DM1O	nC_{12}	$C_{10}OH$	Front path	Back path	CO_2	37DM1O	nC_{12}	$C_{10}OH$	CO_2	37DM1O	nC_{12}	$C_{10}OH$
4	163.2	170.0	74.95	75.61	9.06	9.00	8.97	9.00	9.06	8.87	8.96	8.88	8.88	9.00	135361	52 847	294 251	7 931	5 556	14 292	7 459	3 789	0.511	0.139	0.046	0.304	0.908	0.027	0.016	0.048
	163.2	170.0	74.96	75.62	8.87	8.96	8.88	8.88	9.00	8.84	8.81	8.88	8.90	9.00	135249	48 957	294 708	7 536	5 520	13 383	7 346	3 867	0.509	0.140	0.043	0.308	0.914	0.025	0.016	0.045
	163.2	170.0	74.96	75.62	8.97	8.85	8.84	8.93	8.97	8.88	8.91	8.81	8.88	8.94	135871	49 219	295 776	7 902	5 560	14 160	7 614	3 853	0.517	0.138	0.042	0.303	0.910	0.026	0.016	0.047
	163.2	170.0	74.95	75.61	9.00	8.97	8.91	8.97		8.90	8.91	8.90	8.85		141965	55 361	308 047	7 747	5 451	13 714	7 983	3 843	0.516	0.138	0.045	0.301	0.912	0.026	0.016	0.046
	163.2	170.0	74.95	75.61	8.87	8.91	8.94	8.91		8.47	8.50	8.47	8.50		138255	54 064	301 850	7 562	5 318	13 614	7 553	3 629	0.508	0.139	0.046	0.307	0.909	0.027	0.016	0.048
																							0.512	**0.139**	**0.045**	**0.305**	**0.911**	**0.026**	**0.016**	**0.047**
																							0.004	**0.001**	**0.002**	**0.003**	**0.002**	**0.001**	**0.000**	**0.002**
SAMPLE	P_{READ}	P_{ACT}	T_{READ}	T_{ATC}	Purge Flow Split Vent (s)										FID Front (pA×s)			FID Back (pA×s)			TCD CO_2 (µV×s)		ROLSI Back$_{(Front Path)}$ mass fraction				ROLSI Front$_{(Back Path)}$ mass fraction			
	(barg)	(bar)	(°C)	(°C)	Front (ref. = 9.73)					Back (ref. = 9.56)					37DM1O	nC_{12}	$C_{10}OH$	37DM1O	nC_{12}	$C_{10}OH$	Front path	Back path	CO_2	37DM1O	nC_{12}	$C_{10}OH$	CO_2	37DM1O	nC_{12}	$C_{10}OH$
5	175.3	182.0	74.99	75.65	9.06	9.06	9.03	9.00		8.97	9.00	9.00	8.94		105758	38 064	228 027	14 874	8 377	28 585	7 977	3 784	0.591	0.118	0.036	0.255	0.842	0.046	0.022	0.089
	175.3	182.0	74.99	75.65	9.03	8.96	8.97	9.04		8.91	8.84	8.81	8.88		110513	40 122	241 564	14 394	8 084	27 498	8 432	3 734	0.592	0.116	0.036	0.256	0.845	0.045	0.022	0.087
	175.3	182.0	74.99	75.65	9.10	9.03	9.00	8.97	8.94	8.93	9.03	8.94	8.91	8.88	109871	39 846	239 169	14 872	8 323	28 432	8 334	3 789	0.591	0.117	0.036	0.256	0.843	0.046	0.022	0.089
	175.3	182.0	74.98	75.64	9.00	8.93	8.97	8.94		8.91	8.97	8.88	8.84	8.90	108359	39 204	235 783	14 466	8 141	27 609	8 296	3 810	0.593	0.116	0.036	0.255	0.847	0.045	0.022	0.086
																							0.592	**0.117**	**0.036**	**0.256**	**0.845**	**0.045**	**0.022**	**0.088**
																							0.001	**0.001**	**0.000**	**0.001**	**0.002**	**0.001**	**0.000**	**0.001**

E. Thermodynamic Modelling: Model Parameters

E.1. Saturated vapour pressures and liquid densities

The parameters required to calculate saturation vapour pressures and liquid densities, obtained from Aspen Plus®, are provided in Tables 78 and 79.

Table 78: Parameters for the extended Antoine and NIST Wagner 25 correlations with input temperatures in K and vapour pressure calculated in MPa [16].

Component	Correlation parameters								
	C_1	C_2	C_3	C_4	C_5	C_6	C_7	C_8	C_9
n-dodecane	123.654	-11976	0	0	-16.698	8.09E-06	2	263.57	658
1-decanol	142.424	-15212	0	0	-18.424	8.50E-18	6	280.05	688
3,7-dimethyl-1-octanol	-8.715	-1.539	0	0	210	667	-	-	-
CO_2	33.2015	-2839	0	0	-3.8639	2.81E-16	6	216.58	304
Ethane*	38.0415	-2598.7	0	0	-5.1283	1.49E-05	2	90.35	305

*Required for CPA pure component parameter fitting

Table 79: Parameters for the DIPPR 105 and NIST TDE Expansion correlations with input temperatures in K and liquid molar density calculated in mol/l [16].

Component	Correlation parameters							
	ρ_c (mol/l)	C_1	C_2	C_3	C_4	C_5	C_6	C_7
n-dodecane	-	0.33267	0.24664	658	0.28571	0	264	658
1-decanol	-	0.38208	0.24645	688	0.26125	0	280	688
3,7-dimethyl-1-octanol	1.45845	4.12263	0.0949489	3.30074	-3.60581	0	0	-
CO_2	-	2.768	0.26212	304.21	0.2908	0	217	304
Ethane*	-	1.9122	0.27937	305.32	0.29187	0	90.4	305

*Required for CPA pure component parameter fitting

E.2. Binary Solvent-Solute Interaction Parameters

The effect of incorporating temperature dependence for the CO_2 + 1-decanol and CO_2 + 3,7-dimethyl-1-octanol solvent-solute interaction parameters on model accuracy is analysed in Figure 132. It should be noted that in Figure 132 (c) and (d), the %AAD reported for the composition deviations ($\%AAD_x$ and $\%AAD_y$), represents an average of the CO_2 and solute deviation in the respective phases.

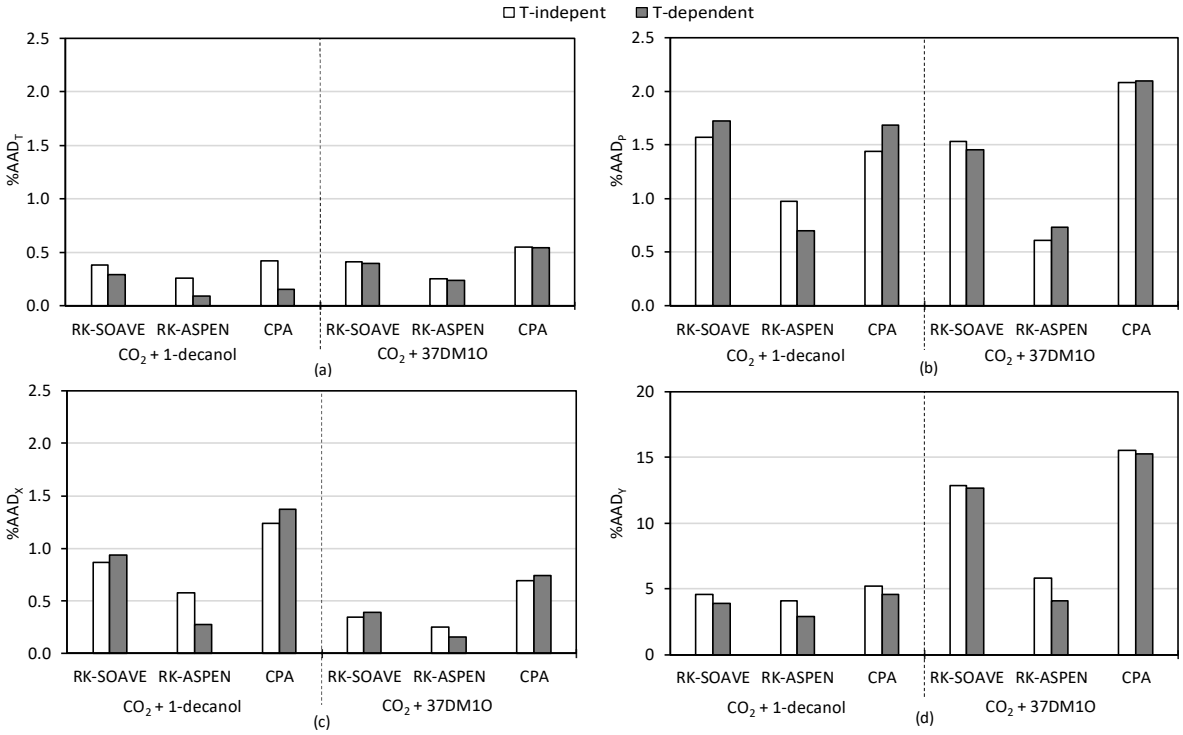

Figure 132: %AAD results for the 4 data sets, namely (a) temperature, (b) pressure, (c) liquid composition and (d) vapour composition, used in the regression of the CO_2 + 1-decanol [5] and CO_2 + 3,7-dimethyl-1-octanol [5] interaction parameters with the RK-SOAVE, RK-ASPEN and CPA models

When analysing the diagrams presented in Figure 132 it is noted that the model fit for the CO_2 + 1-decanol interaction parameter, when regressing the parameter using the RK-SOAVE and CPA models, does not show clear improvement for all 4 regression data sets when incorporating temperature dependence, thus it is neglected from the model parameter. Temperature dependence is however seen to improve the regression results for all 4 regression data sets for the CO_2 + 1-decanol parameter when using the RK-ASPEN model and it is therefore incorporated.

Referring to the regression results for the CO_2 + 3,7-dimethyl-1-octanol interaction parameter it is noted that the model fit with and without the inclusion of temperature dependency for the RK-SOAVE and CPA models is generally similar (similar %AAD values), therefore these models are not unnecessarily complicated by incorporating temperature dependency in the CO_2 + 3,7-dimethyl-1-octanol parameter. When viewing the regression results for the RK-ASPEN CO_2 + 3,7-dimethyl-1-octanol parameter it is noted that the inclusion of temperature

dependence generally improves the model accuracy, particularly the accuracy of the vapour phase results. This motivates the inclusion of temperature dependency in this parameter.

E.3. Binary Solute-Solute Interaction Parameters

Interaction parameters regressed from bubble- and dew-point data

Results of the manual regressions performed to determine the solute-solute BIPs for each model, along with the limits within which the regressions were performed, are presented in Tables 80 to 82.

Table 80: Regressed solute-solute interaction parameters for the RK-SOAVE model, along with the regression limits imposed for each system

Mixture containing CO_2+...	**Mixture component ratio (1):(2)**	**Regression limits**	**BIP resulting in the lowest %AAD for a specific mixture**
		$k_{a,ij}^0$	$k_{a,ij}^0$
(1) n-dodecane + (2) 37DM1O	50:50	0.000 – 0.070	0.040
	75:25		0.050
	85:15		0.060
(1) n-dodecane + (2) 1-decanol	40:60	-0.020 – 0.060	0.040
	80:20		0.030
	90:10		0.020
(1) 37DM1O + (2) 1-decanol	25:75	0.000 – 0.060	0.010
	50:50		0.010
	75:25		0.020

Table 81: Regressed solute-solute interaction parameters for the CPA model, along with the regression limits imposed for each system

Mixture containing CO_2+...	**Mixture component ratio (1):(2)**	**Regression limits**	**BIP resulting in the lowest %AAD for a specific mixture**
		$k_{a,ij}^0$	$k_{a,ij}^0$
(1) n-dodecane + (2) 37DM1O	50:50	0.000 – 0.100	0.050
	75:25		0.060
	85:15		0.070
(1) n-dodecane + (2) 1-decanol	40:60	-0.020 – 0.060	0.040
	80:20		0.010
	90:10		0.000
(1) 37DM1O + (2) 1-decanol	25:75	-0.020 – 0.060	0.020
	50:50		0.010
	75:25		0.030

Table 82: Regressed solute-solute interaction parameters for the RK-ASPEN model, along with the regression limits imposed for each system

Mixture containing CO_2+...	**Mixture component ratio (1):(2)**	**Regression limits**		**BIP pair resulting in the lowest %AAD for a specific mixture**	
		$k_{a,ij}^0$	$k_{b,ij}^0$	$k_{a,ij}^0$	$k_{b,ij}^0$
(1) n-dodecane + (2) 37DM1O	50:50	0.000 – 0.240	-0.045 – 0.330	0.015	0.150
	75:25			0.180	0.240
	85:15			0.210	0.210
(1) n-dodecane + (2) 1-decanol	40:60	0.000 – 0.210	0.000 – 0.300	0.075	0.075
	80:20			0.150	0.210
	90:10			0.180	0.270
(1) 37DM1O + (2) 1-decanol	25:75	-0.030 – 0.060	-0.090 – 0.060	-0.015	-0.060
	50:50			0.015	0.015
	75:25			0.030	0.030

Interaction parameters regressed from vapour-liquid-equilibrium data

In order to analyse the effect of neglecting temperature dependency from the solute-solute BIPs regressed from VLE data on model accuracy, the model fit obtained with and without temperature dependency for all three models are compared in Figure 133.

When analysing the diagrams in Figure 133 it is noted that there is no clear indication that the incorporation of temperature dependency significantly and/consistently improves the model fit for either of the models. In some instances, it is even seen that the model fit without the incorporation of temperature dependency is more accurate. Generally, there are small differences in the %AAD values with and without temperature dependency and in the cases where temperature dependency is seen to improve model accuracy, the improvement is small. The minor increase or even decrease in accuracy in the regression results presented in Figure 133, can be attributed to the limited number of temperature sets that were used to perform the regressions. Fourie [14] only measured data at 308 K, 328 K and 348 K and as stated previously, the 308 K data sets were excluded from the regression procedure. The regressions were therefore performed only using data measured at two temperatures and thus temperature dependency could not accurately be accounted for. The limitation imposed by neglecting temperature dependency for the VLE solute-solute interaction parameters will therefore not have a significant impact on model accuracy in this work, but if the VLE data used for the regression are measured over a wider temperature range it might be beneficial to incorporate temperature dependency.

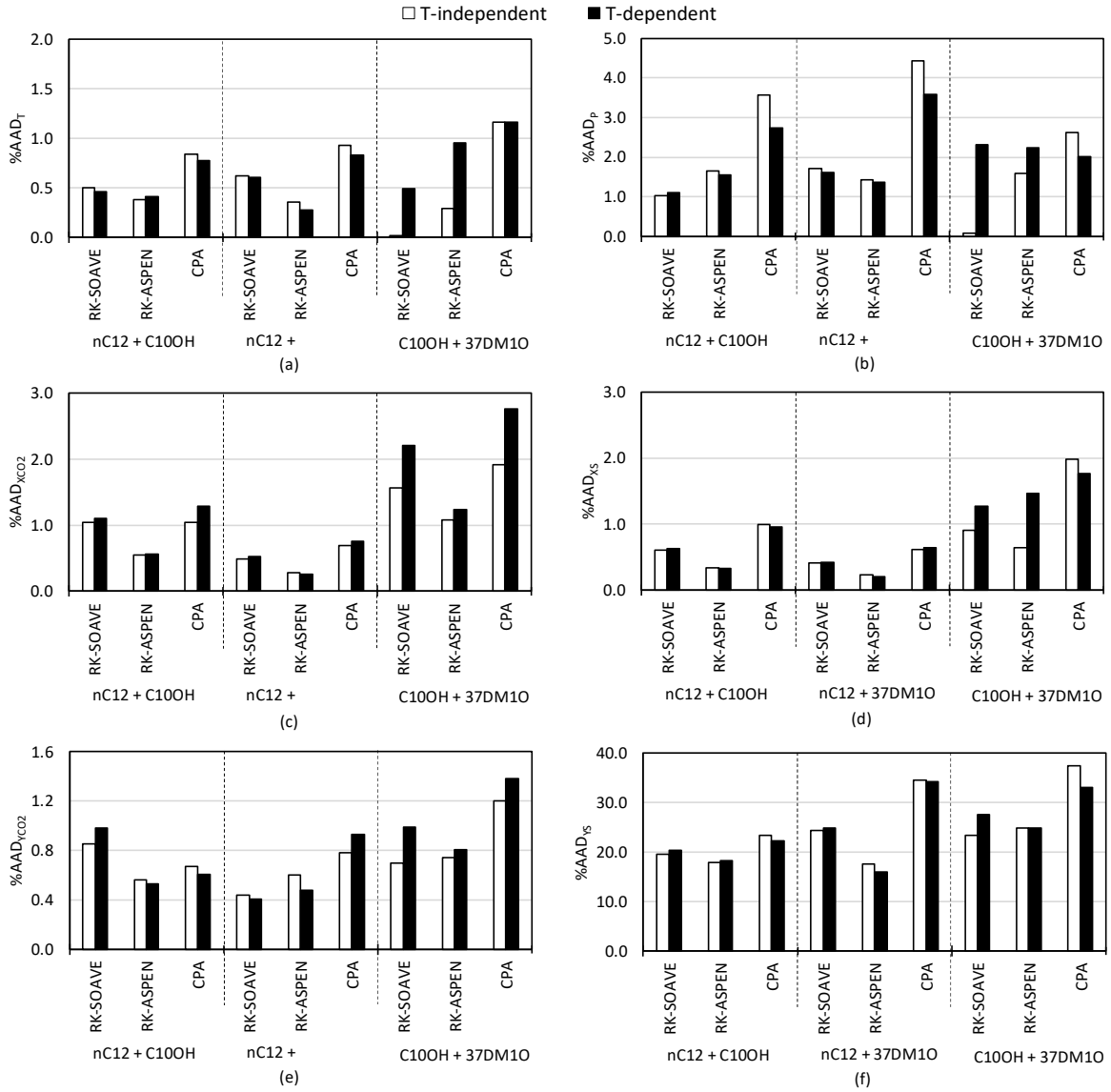

Figure 133: %AAD values comparing the model fit with and without the incorporation of temperature dependency for the 6 data sets, namely (a) temperature, (b) pressure, (c) liquid CO_2 composition and (d) average liquid solute composition, (e) vapour CO_2 composition and (f) average vapour solute composition, used in the regression of the HPVLE solute-solute interaction parameters for the RK-SOAVE, RK-ASPEN and CPA models

F. Thermodynamic Modelling: Binary Systems

In Chapter 8, the inability of the models to accurately correlate/predict the curvature of the phase boundaries was partially attributed to the accuracy with which the models can correlate/predict binary phase equilibrium data. The modelled data for the CO_2 + 1-decanol [5], CO_2 + n-dodecane [5] and CO_2 + 3,7-dimethyl-1-octanol [5] systems at 328 K and 348 K (temperatures at which the ternary diagrams were constructed) is therefore analysed and compared in Figure 134.

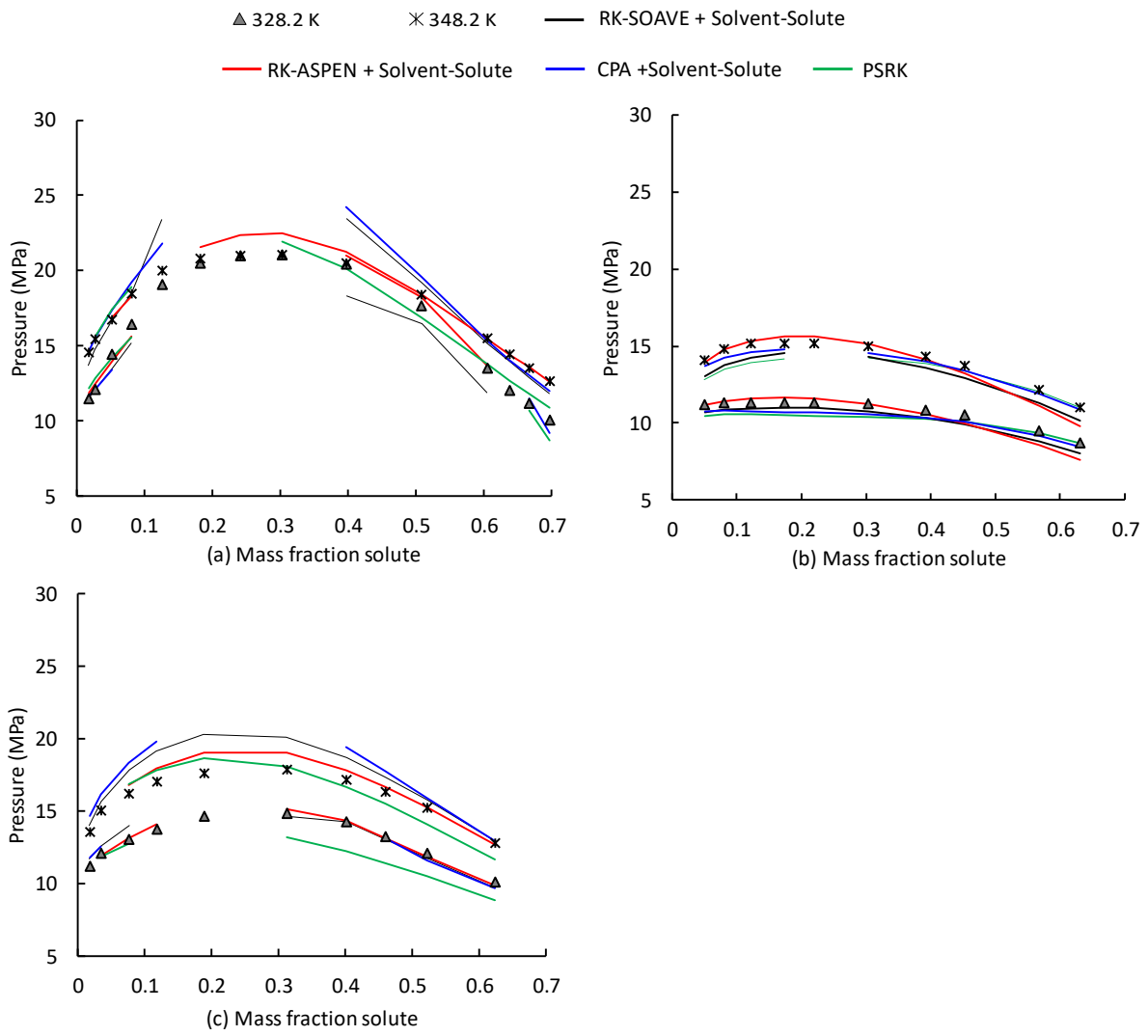

Figure 134: Pressure-composition diagram comparing experimental data at 328 K and 348 K to data obtained from the RK-SOAVE, RK-ASPEN, CPA and PSRK models for the (a) CO_2 + 1-decanol, (b) CO_2 + n-dodecane and (c) CO_2 + 3,7-diemthyl-1-octanol systems [5].

CO_2 + 1-decanol:

All of the models are capable of modelling fairly accurate phase transition pressures within the low solute concentration region. Within/close to the mixture critical region the models are seen to be incapable of correlating/predicting data over a wide range of compositions and the data which can be modelled generally deviates significantly from the experimental data. In this region, the RK-ASPEN model is generally the most accurate. At 328 K, the modelled data within the high solute concentration region is also inaccurate, regardless of the model used to correlate/predict it. Except for the PSRK predictions, the accuracy improves at 348 K, with the RK-ASPEN model again being the most accurate.

CO_2 + n-dodecane:

All of the models tend to correlate/predict the correct trends, but noticeable deviation between the experimental and modelled data exist in certain regions. The RK-ASPEN model is generally fairly accurate within the low solute concentration and mixture critical region (slight overestimation), but underestimates the pressures in the high solute concentration region. The RK-SOAVE model generally underestimates the phase transition pressures and the deviation between the experimental and modelled data becomes more apparent at 348 K. The data modelled using the CPA and PSRK models only correlate with the experimental data in the high solute concentration region. At lower solute concentrations these models generally underestimate the phase transition pressures.

CO_2 + 3,7-dimethyl-1-octanol:

The RK-ASPEN model is generally the most accurate, but there are still regions in which the model is incapable of correlating data and it tends to slightly overestimate pressures within/close to the mixture critical region at 348 K. The RK-SOAVE and CPA models are seen to perform similarly. At 328 K, these models correlate fairly accurate data in the high solute concentration region, but noticeable deviations are present in the low solute concentration region. At 348 K, these models tend to overestimate the phase transition pressures with the deviations becoming more apparent as the mixture critical region is approached. Except for the low solute concentration predictions at 328 K, the PSRK model predictions generally deviate from the experimental data, with the largest deviations seen in the high solute concentration region where the model significantly underestimates the phase transition pressures.

Conclusion:

It is clear that there is generally noticeable deviation between the experimental and modelled binary data, particularly in the mixture critical and high solute concentration regions. Generating VLE data would therefore result in inaccuracy in the vapour and liquid compositions.

G. Thermodynamic Modelling: Quaternary Systems

G.1. RK-SOAVE

The ternary predictions highlighted that the inclusion of the 1-decanol + 3,7-dimethyl-1-octanol solute-solute BIP regressed from either HPBDP or HPVLE data could negatively impact the accuracy of the RK-SOAVE model when predicting equilibrium data for the quaternary system. The effect of incorporating this parameter when predicting bubble- and dew-point and VLE data is therefore analysed in this section.

High pressure bubble- and dew-point data

Results indicating the effect of incorporating the 3,7-dimethyl-1-octanol + 1-decanol solute-solute BIP on model accuracy when predicting the quaternary bubble- and dew-point data is presented in Tables 83 and 84. In order to reduce the inaccuracy introduced at lower temperatures, due to reasons explained previously, the average %AAD values presented in these tables are based on results at temperatures above 328 K.

Table 83: Analysis of the impact of including the 3,7-dimethyl-1-octanol + 1-decanol regressed from HPBDP data on the model

Mix	Absolute Average Deviation (%AAD)									
	RK-SOAVE with solvent-solute and all solute-solute BIPs regressed from HPBDP data					RK-SOAVE with solvent-solute and solute-solute BIPs regressed from HPBDP data without 37DM1O + 1-decanol BIP				
	Pressure (MPa)					Pressure (MPa)				
	308.2 K	318.2 K	328.2 K	338.2 K	348.2 K	308.2 K	318.2 K	328.2 K	338.2 K	348.2 K
7	6.9	9.0	6.8	4.8	3.6	6.3	7.7	5.2	3.2	3.2
8	9.9	7.0	7.4	4.3	3.8	9.5	6.1	6.8	3.5	4.3
9	1.0	2.1	2.1	1.9	2.8	1.0	2.0	2.0	1.9	2.8
10	6.7	6.3	7.6	5.5	3.5	6.0	5.2	5.3	2.7	3.3
Z7	6.1	4.9	5.2	2.5	3.0	5.6	4.6	3.3	1.5	3.2
$\overline{\%AAD}^*$			4.3					3.5		

*Average %AAD for temperatures above 328 K

When analysing the data presented in Tables 83 and 84, it is seen that the inclusion of the 3,7-dimethyl-1-octanol + 1-decanol BIP slightly decreases model accuracy. It is therefore justified to remove it from the model when predicting bubble- and dew-point data.

Table 84: Analysis of the impact of including the 3,7-dimethyl-1-octanol + 1-decanol regressed from HPVLE data on the model

Mix	Absolute Average Deviation (%AAD)									
	RK-SOAVE with solvent-solute and all solute-solute BIPs regressed from HPVLE data					RK-SOAVE with solvent-solute and solute-solute BIPs regressed from HPVLE data without 37DM1O + 1-decanol BIP				
	Pressure (MPa)					Pressure (MPa)				
	308.2 K	318.2 K	328.2 K	338.2 K	348.2 K	308.2 K	318.2 K	328.2 K	338.2 K	348.2 K
7	3.9	2.6	3.6	6.4	6.6	6.2	5.7	2.8	2.9	3.6
8	8.7	4.6	2.3	3.6	7.7	9.3	5.8	6.2	2.7	4.5
9	1.0	1.1	1.3	1.7	1.5	1.0	1.2	1.3	1.7	1.5
10	4.0	2.9	2.1	5.3	11.0	5.5	4.7	4.4	2.5	3.7
Z7	3.8	2.7	2.7	3.0	6.8	4.5	3.3	1.4	1.1	5.8
$\overline{\%AAD}^{*}$	4.4					3.1				

*Average %AAD for temperatures above 328 K

High pressure vapour-liquid-equilibrium data

An accuracy analysis illustrating the effect of including the 3,7-dimethyl-1-octanol + 1-decanol BIP on the model's ability to predict quaternary VLE data is presented in Tables 85 and 86. Similar to the bubble- and dew-point predictions discussed previously, the average %AAD values reported in the tables are only based on the result obtained at 328 K and 348 K.

When analysing the data presented in Table 85 it is clear that the inclusion of the 3,7-dimethyl-1-octanol + 1-decanol BIP regressed from HPBDP data reduces the model accuracy and the exclusion of this parameter is justified when predicting quaternary VLE data using BIPs regressed from HPBDP data.

Table 85: Analysis of the impact of including the 3,7-dimethyl-1-octanol + 1-decanol regressed from HPBDP data on the model

Temperature (K)	Absolute Average Deviation (%AAD)							
	RK-SOAVE with solvent-solute and all solute-solute BIPs regressed from HPBDP data				RK-SOAVE with solvent-solute and solute-solute BIPs regressed from HPBDP data without 37DM1O + 1-decanol BIP			
	x_{CO2}	x_s^*	y_{CO2}	y_s^*	x_{CO2}	x_s^*	y_{CO2}	y_s^*
308.6	31.8	28.2	14.2	93.4	31.8	28.2	14.2	93.5
328.8	17.9	13.7	2.8	39.3	13.0	10.1	1.2	31.4
348.9	6.4	4.9	0.9	18.2	5.1	4.4	1.0	21.3
$\overline{\%AAD}_{@328K,\ 348\ K}$	13.0				10.9			

*Average %AAD of the n-dodecane, 3,7-dimethyl-1-octanol and 1-decanol mass fractions in the phase

The results presented in Table 86 reveals that the inclusion of the 3,7-dimethyl-1-octanol parameter slightly improves model accuracy. However, when considering the degree of

deviation between the experimental and predicted data the improvement is deemed minor and it does not justify decreasing the model robustness by incorporating another BIP. The exclusion of this parameter is therefore justified when predicting quaternary VLE data using BIPs regressed from HPVLE data. This also allows for consistency with regard to the number of model parameters incorporated in the model when predicting equilibrium data.

Table 86: Analysis of the impact of including the 3,7-dimethyl-1-octanol + 1-decanol regressed from HPVLE data on the model

Temperature (K)	Absolute Average Deviation (%AAD)							
	RK-SOAVE with solvent-solute and all solute-solute BIPs regressed from HPVLE data				RK-SOAVE with solvent-solute and solute-solute BIPs regressed from HPVLE data without 37DM1O + 1-decanol BIP			
	x_{CO2}	x_s^*	y_{CO2}	y_s^*	x_{CO2}	x_s^*	y_{CO2}	y_s^*
308.6	30.3	27.1	14.3	94.3	30.4	27.2	14.2	94.1
328.8	7.0	6.0	1.4	37.9	11.1	9.0	2.1	40.0
348.9	4.6	5.8	1.5	28.4	3.3	3.5	1.1	24.6
$\overline{\%AAD}_{@328K,\ 348\ K}$	11.6				11.8			

*Average %AAD of the n-dodecane, 3,7-dimethyl-1-octanol and 1-decanol mass fractions in the phase

G.2. RK-ASPEN

The ternary predictions highlighted that the inclusion of the 1-decanol + 3,7-dimethyl-1-octanol solute-solute BIP regressed from either HPBDP or HPVLE data could negatively impact the accuracy of the RK-ASPEN model when predicting equilibrium data for the quaternary system. The effect of incorporating this parameter when predicting equilibrium data is therefore analysed in this section.

High pressure bubble- and dew-point data

The accuracy with which the RK-ASPEN model can predict phase transition pressures for the quaternary mixtures, with and without the inclusion of the 3,7-dimethyl-1-octanol + 1-decanol solute-solute BIP is analysed in Tables 87 and 88.

When analysing the %AAD values, presented in Tables 87 and 88, it is seen that the inclusion of the 3,7-dimethyl-1-octanol + 1-decanol solute-solute BIP slightly reduces model accuracy, regardless of the type of data used to regress it. It is therefore justified to remove it from the model based on HPBDP and HPVLE data, when predicting bubble- and dew-point data.

Table 87: Analysis of the impact of including the 3,7-dimethyl-1-octanol + 1-decanol regressed from HPBDP data on the model

Mix	Absolute Average Deviation (%AAD)									
	RK-ASPEN with polar, solvent-solute and all solute-solute BIPs regressed from HPBDP data					RK-ASPEN with polar, solvent-solute and solute-solute BIPs regressed from HPBDP data without 37DM1O + 1-decanol BIP				
	Pressure (MPa)					Pressure (MPa)				
	308.2 K	318.2 K	328.2 K	338.2 K	348.2 K	308.2 K	318.2 K	328.2 K	338.2 K	348.2 K
7	3.8	4.8	3.8	2.5	1.8	3.7	4.0	3.1	1.5	1.5
8	4.4	4.4	1.8	1.3	1.7	4.3	4.0	1.4	1.2	1.8
9	1.6	1.0	2.2	2.8	2.7	1.6	1.0	2.2	2.6	2.8
10	5.3	4.8	3.1	1.9	1.7	5.5	3.8	2.3	1.9	2.0
Z7	3.7	3.7	2.8	1.5	1.3	3.6	3.8	2.6	1.7	1.7
$\overline{\%AAD}^{*}$	2.2					2.0				

*Average %AAD for temperatures above 328 K

Table 88: Analysis of the impact of including the 3,7-dimethyl-1-octanol + 1-decanol regressed from HPVLE data on the model

Mix	Absolute Average Deviation (%AAD)									
	RK-ASPEN with polar, solvent-solute and all solute-solute BIPs regressed from HPVLE data					RK-ASPEN with polar, solvent-solute and solute-solute BIPs regressed from HPVLE data without 37DM1O + 1-decanol BIP				
	Pressure (MPa)					Pressure (MPa)				
	308.2 K	318.2 K	328.2 K	338.2 K	348.2 K	308.2 K	318.2 K	328.2 K	338.2 K	348.2 K
7	3.7	3.5	3.1	1.5	1.5	3.5	3.3	3.1	1.5	1.5
8	2.8	6.1	3.2	2.1	2.2	3.9	4.2	1.7	1.3	1.9
9	1.6	1.0	2.0	2.4	2.5	1.6	1.0	2.1	2.6	2.6
10	7.7	5.6	5.6	3.6	2.8	7.5	3.9	2.5	2.0	2.2
Z7	4.1	5.6	4.2	2.4	2.3	3.8	5.1	3.4	2.3	2.3
$\overline{\%AAD}^{*}$	2.8					2.2				

*Average %AAD for temperatures above 328 K

High pressure vapour-liquid-equilibrium data

The effect of including the 3,7-dimethyl-1-octanol + 1-decanol solute-solute BIP, regressed from HPBDP and HPVLE data, on the model's ability to predict quaternary VLE data is analysed in Tables 89 and 90, respectively.

Table 89: Analysis of the impact of including the 3,7-dimethyl-1-octanol + 1-decanol regressed from HPBDP data on the model

Temperature (K)	Absolute Average Deviation (%AAD)							
	RK-ASPEN with polar, solvent-solute and all solute-solute BIPs regressed from HPBDP data				RK-ASPEN with polar, solvent-solute and solute-solute BIPs regressed from HPBDP data without 37DM1O + 1-decanol BIP			
	x_{CO2}	x_s^{*}	y_{CO2}	y_s^{*}	x_{CO2}	x_s^{*}	y_{CO2}	y_s^{*}
308.6	31.8	28.1	12.6	76.7	31.7	28.0	11.5	68.8
328.8	6.3	6.3	1.1	32.0	4.4	4.5	1.1	31.3
348.9	3.0	2.9	0.5	13.3	2.7	2.7	0.6	14.8
$\overline{\%AAD}_{@328K,\ 348\ K}$	8.2				7.8			

*Average %AAD of the n-dodecane, 3,7-dimethyl-1-octanol and 1-decanol mass fractions in the phase

Table 90: Analysis of the impact of including the 3,7-dimethyl-1-octanol + 1-decanol regressed from HPVLE data on the model

Temperature (K)	Absolute Average Deviation (%AAD)							
	RK-ASPEN with polar, solvent-solute and all solute-solute BIPs regressed from HPVLE data				RK-ASPEN with polar, solvent-solute and solute-solute BIPs regressed from HPVLE data without 37DM1O + 1-decanol BIP			
	x_{CO2}	x_s^*	y_{CO2}	y_s^*	x_{CO2}	x_s^*	y_{CO2}	y_s^*
308.6	31.9	28.2	11.9	77.0	31.5	28.0	12.4	73.2
328.8	8.1	6.9	1.2	32.1	3.5	3.7	0.9	30.3
348.9	3.3	3.0	0.5	12.8	2.4	2.4	0.6	14.2
$\overline{\%AAD}_{@328K,\ 348\ K}$	8.5				7.3			

*Average %AAD of the n-dodecane, 3,7-dimethyl-1-octanol and 1-decanol mass fractions in the phase

When analysing the average %AAD values presented in Tables 89 and 90 it is clear that the model which excludes the 3,7-dimethyl-1-octanol + 1-decanol solute-solute BIP is more accurate, regardless of the type of data used to regress it. Closer analysis of the data reported for the different mass fractions reveals that with the exception of the vapour phase predictions at 348 K, the exclusion of the 3,7-dimethyl-1-octanol + 1-decanol BIP improves the accuracy of the model whether HPBDP or HPVLE data is used to regress the solute-solute BIP. It is therefore justified to exclude the HPBDP and HPVLE regressed 3,7-dimethyl-1-octanol + 1-decanol solute-solute BIPs from the model when predicting VLE data for the quaternary system.

G.3. CPA

The ternary predictions highlighted that the inclusion of the n-dodecane + 1-decanol and 3,7-dimethyl-1-octanol + 1-decanol solute-solute BIPs regressed from either HPBDP or HPVLE data could negatively impact the accuracy of the CPA model when predicting equilibrium data for the quaternary system. The effect of incorporating these parameters is therefore analysed in this section.

High pressure bubble- and dew-point data

The effect of excluding the n-dodecane + 1-decanol and 3,7-dimethyl-1-octanol + 1-decanol BIPs on model accuracy when predicting bubble- and dew-point data for the quaternary system is analysed in Tables 91 and 92. Due to the low accuracy of the model at temperatures below 328 K, these temperatures were excluded from the tables.

From Table 91 it is seen that, based on the average %AAD values, the model which incorporates only the n-dodecane + 3,7-dimethyl-1octanol BIP regressed from HPBDP data is slightly more accurate than the other two fitted versions. When analysing the %AAD values reported for each temperature, it is noted that the model which only incorporates the n-dodecane + 3,7-dimethyl-1octanol BIP generally outperforms the other models and is only slightly less accurate than the other two models at 348 K. This justifies using the model which only incorporates the n-dodecane + 3,7-dimethyl-1octanol BIP regressed from HPBDP data (no 3,7-dimethyl-1-octanol + 1-decanol and n-dodecane + 1-decanol BIPs included).

Table 91: Analysis of the impact of excluding the 3,7-dimethyl-1-octanol + 1-decanol and n-dodecane + 1-decanol BIPs regressed from HPBDP data on the model

Mix	Absolute Average Deviation (%AAD)								
	CPA with solvent-solute and all solute-solute BIPs regressed from HPBDP data			CPA with solvent-solute and nC_{12} + 37DM1O solute-solute BIPs regressed from HPBDP data			CPA with solvent-solute and nC_{12} + 37DM1O and nC_{12} + $C_{10}OH$ solute-solute BIPs regressed from HPBDP data		
	Pressure (MPa)			Pressure (MPa)			Pressure (MPa)		
	328.2 K	338.2 K	348.2 K	328.2 K	338.2 K	348.2 K	328.2 K	338.2 K	348.2 K
7	8.5	5.6	3.3	5.8	2.8	3.2	7.7	3.1	3.1
8	8.4	4.3	3.5	6.7	2.7	3.9	6.8	2.3	4.7
9	2.3	1.5	1.0	2.4	1.3	1.0	2.3	1.3	1.0
10	10.9	6.5	2.7	7.9	2.7	4.3	8.1	3.3	4.2
Z7	6.0	3.4	4.1	4.6	2.3	5.1	5.2	2.8	4.9
$\overline{\%AAD}$		4.8			3.8			4.1	

Table 92: Analysis of the impact of excluding the 3,7-dimethyl-1-octanol + 1-decanol and n-dodecane + 1-decanol BIPs regressed from HPVLE data on the model

Mix	Absolute Average Deviation (%AAD)								
	CPA with solvent-solute and all solute-solute BIPs regressed from HPVLE data			CPA with solvent-solute and nC_{12} + 37DM1O solute-solute BIPs regressed from HPVLE data			CPA with solvent-solute and nC_{12} + 37DM1O and nC_{12} + $C_{10}OH$ solute-solute BIPs regressed from HPVLE data		
	Pressure (MPa)			Pressure (MPa)			Pressure (MPa)		
	328.2 K	338.2 K	348.2 K	328.2 K	338.2 K	348.2 K	328.2 K	338.2 K	348.2 K
7	3.8	8.2	11.5	4.1	2.4	3.8	2.8	2.7	4.7
8	2.9	5.4	9.4	5.7	2.7	3.9	6.1	2.7	5.5
9	1.1	1.7	2.5	1.4	1.2	1.7	1.2	1.5	2.3
10	3.9	12.4	13.3	8.3	2.8	4.6	7.6	2.6	5.8
Z7	4.3	9.3	12.2	4.3	2.3	4.7	2.9	4.2	6.7
$\overline{\%AAD}$		6.8			3.6			4.0	

Analysis of the average %AAD values reported in Table 92 indicates that the model which only incorporates the n-dodecane + 3,7-dimhethyl-1-octanol regressed from HPVLE data is the most accurate fitted model. There is however little difference in accuracy between this model

and the model which also includes the n-dodecane + 1-decanol BIP. Closer analysis of %AAD values reveals that the model which also includes the n-dodecane + 1-decanol BIP only has two %AAD values which are slightly smaller than that of the model which only includes the n-dodecane + 3,7-dimhethyl-1-octanol BIP. Using the model which only incorporates the n-dodecane + 3,7-dimethyl-1octanol BIP regressed from HPVLE data is therefore justified (no 3,7-dimethyl-1-octanol + 1-decanol and n-dodecane + 1-decanol BIPs included).

High pressure vapour-liquid-equilibrium data

The accuracy with which the model can predict VLE data when excluding the 3,7-dimethyl-1-octanol + 1-decanol and n-dodecane + 1-decanol BIPs is analysed in Tables 93 and 94.

Table 93: Analysis of the impact of excluding the 3,7-dimethyl-1-octanol + 1-decanol and n-dodecane + 1-decanol BIPs regressed from HPBDP data on the model

Temperature (K)	Absolute Average Deviation (%AAD)											
	CPA with solvent-solute and all solute-solute BIPs regressed from HPBDP data				CPA with solvent-solute and nC_{12} + 37DM1O solute-solute BIPs regressed from HPBDP data				CPA with solvent-solute and nC_{12} + 37DM1O and nC_{12} + $C_{10}OH$ solute-solute BIPs regressed from HPBDP data			
	x_{CO2}	x_s^*	y_{CO2}	y_s^*	x_{CO2}	x_s^*	y_{CO2}	y_s^*	x_{CO2}	x_s^*	y_{CO2}	y_s^*
308.6	32.5	29.1	14.4	96.7	32.2	28.8	14.5	96.9	32.4	29.0	14.4	96.8
328.8	22.4	18.0	3.8	57.1	18.7	15.3	3.4	55.8	19.4	16.0	3.3	54.1
348.9	5.6	3.9	1.1	24.9	3.4	3.2	1.7	32.3	3.7	3.2	1.6	30.1
$\overline{\%AAD}_{@328K,\ 348\ K}$	17.1				16.7				16.4			

*Average %AAD of the n-dodecane, 3,7-dimethyl-1-octanol and 1-decanol mass fractions in the phase

When analysing the average %AAD values presented in Table 93, it is noted that the model which includes both the n-dodecane + 3,7-dimethyl-1-octanol and n-dodecane + 1-decanol BIPs, regressed from HPBDP data, is slightly more accurate than the other models. However, when considering the degree of deviation between the experimental and predicted data this improvement is deemed minor compared to the model which only incorporates the n-dodecane + 3,7-dimethyl-1-octanol BIP and it does not justify decreasing the model robustness by incorporating another BIP. Based on this only the n-dodecane + 3,7-dimethyl-1-octanol BIP regressed from HPBDP data is to be included in the CPA model when predicting bubble- and dew-point and VLE data. This also allows for consistency with regard to the number of model parameters incorporated in the model when predicting equilibrium data.

Analysis of the average %AAD values presented in Table 94, reveals that the model which only incorporates the n-dodecane + 3,7-dimethyl-1-octanol BIP regressed from HPVLE data is

the most accurate model. The largest improvement in accuracy when using this model is seen for the predictions at 348 K, particularly the solute vapour phase composition predictions. This justifies using the model which only incorporates the n-dodecane + 3,7-dimethyl-1octanol BIP regressed from HPVLE data (no 3,7-dimethyl-1-octanol + 1-decanol and n-dodecane + 1-decanol BIPs included).

Table 94: Analysis of the impact of excluding the 3,7-dimethyl-1-octanol + 1-decanol and n-dodecane + 1-decanol BIPs regressed from HPVLE data on the model

Temperature (K)	Absolute Average Deviation (%AAD)											
	CPA with solvent-solute and all solute-solute BIPs regressed from HPVLE data				CPA with solvent-solute and nC_{12} + 37DM1O solute-solute BIPs regressed from HPVLE data				CPA with solvent-solute and nC_{12} + 37DM1O and nC_{12} + $C_{10}OH$ solute-solute BIPs regressed from HPVLE data			
	x_{CO2}	x_s^*	y_{CO2}	y_s^*	x_{CO2}	x_s^*	y_{CO2}	y_s^*	x_{CO2}	x_s^*	y_{CO2}	y_s^*
308.6	30.2	26.9	14.5	97.3	30.9	27.5	14.5	97.0	30.4	27.1	14.5	97.2
328.8	9.0	8.1	3.3	58.8	16.3	12.1	3.4	56.2	14.8	11.4	3.4	58.3
348.9	7.8	10.5	2.6	46.3	4.0	4.9	1.9	36.4	4.4	6.3	2.1	40.9
$\overline{\%AAD}_{@328K,\ 348\ K}$	18.3				16.9				17.7			

*Average %AAD of the n-dodecane, 3,7-dimethyl-1-octanol and 1-decanol mass fractions in the phase